A study of interparticle adhesion in pharmaceutical powder mixtures

Laycock, Steven

Award date:
1987

Awarding institution:
University of Bath

A study of interparticle adhesion in pharmaceutical powder mixtures.

submitted by Steven Laycock

for the degree of PhD

of the University of Bath

September 1987

ProQuest LLC
789 East Eisenhower Parkway
P.O. Box 1346
Ann Arbor, MI 48106-1346

A study of interparticle adhesion in pharmaceutical powder mixtures.

by Steven Laycock

submitted for the degree of Doctor of Philosophy, September 1987.

A technique used to produce thermoelectrets and test for their presence is described and its operation verified by the use of carnauba wax, a material known to produce thermoelectrets. The ability of cellulose based tableting excipients, Avicel PH102 and Elcema G250, to form thermoelectrets is demonstrated.

The magnitude of the electret charge in Avicel PH102 and Elcema G250 has been measured using thermally stimulated discharge current (TSDC) and maximum discharge currents of approximately $4x10^{-11}$ amperes recorded compared to base line currents of less than $5x10^{-13}$ amperes. The electret charge in Elcema G250 is shown to be measurable, using TSDC, for a period approaching sixty days using samples wrapped in aluminium foil, in very low humidity atmospheres. The adsorption of atmospheric moisture destroyed the electret charge within a two hour period.

An image analysis system was developed, based around a slow scan video digitising interface and a BBC model "B" microcomputer with additional memory. An image analysis technique was developed which overcame the depth of field limitation of conventional light microscopy. A sequence of digitised images, at different levels of focus through an Elcema G250 particle with (UV) fluorescing adherent triamterene particles, was used to construct a digitised image in which all the adherent particles were focused. This 'focused' image allowed the size, location and distribution of the adherent particles to be recorded.

A centrifugation technique was used to apply a separating force to the adherent particles in single ordered units of a binary powder mixture of Elcema G250 and triamterene. Elcema G250 was processed in four different ways and the effect of the processing examined by determining the particle adhesion profiles. The image analysis method above was used to record the number and size of adherent particles before and after centrifugation. The particle adhesion profiles generated showed that the adhesion of triamterene particles was significantly greater for electrised Elcema G250 than for standard, moist or dried Elcema G250.

Keywords

Electret, Thermoelectret, Thermally Stimulated Discharge Current, TSDC, Image Analysis, Interparticle Ahesion Forces, Ordered Mixing, Centrifugation, Electrostatic Charging.

Acknowledgments

I would like to extend my thanks to Dr. John Staniforth for his help, guidance and friendship and also for his supervision of this work.

My thanks are also due to the University of Bath for providing the grant which allowed this work to be carried out.

I would like to thank Mr N. Park for his ability to obtain equipment and his intimate knowledge of the facilities available within the University departments. I am also indebted to the Microprocessor Unit of the University of Bath and in particular Dr. Adrian Bowyer who provided access to the experimental graphics workstation and discussions on computing in general.

I would also like to thank the technical services department of the University of Bath for manufacturing the electrodes and separating rings of the TSDC cell, the perspex inserts for the centrifuge tube and the punches and die used to prepare compacts of Avicel PH102 and Elcema G250.

In addition I would like to thank the staff of the School of Pharmacy and Pharmacology, Academic, Secretarial and Technical, who were always willing to provide assitance in times of need.

My thanks are also due to the Upjohn Company Ltd who extended my grant for a three month period to allow this thesis to be written up and for the continuing support of Mr B. S. Johnson, Dr. C. A. Hampson and Dr. K. J. Thrower, of Upjohn Ltd, whilst the job was completed.

Finally I am deeply grateful to my wife, Sarah, who performed near miracles to provide the photographs presented in this thesis and who never let me give up.

List of Contents

List of Tables

List of Figures

List Of Plates

List of Symbols

A number of symbols have been used to refer to more than one measured quantity. This has been done when the symbols are commonly used to describe the quantity to which they refer. The definition of any symbol in the text is always given on its first usage and it should be noted that the quantity referred to will be redefined locally if its definition changes.

A	Cross sectional area (metre^2)
A	Hamaker constant.
c	Speed of light in vacuum (metre second^{-1}).
C	Capacitance (Farad).
d	Distance between two bodies (metre).
d_0	Minimum distance between two bodies (metre).
d_{fd}	Depth of field of a microscope (metres).
$D(r)$	Displacement, electrical flux density at a distance, r, from the source of the displacement (Coulomb metre^{-2})
E	Energy (Joule).
E_k	Kinetic energy (Joule).
E_p	Potential energy (Joule).
E_t	Total energy (Joule).
$E(t)$	Time dependent Young's modulus of the softer of two surfaces in contact (Pascal).
F	Force (Newton).
F_{el}	Force between two bodies due to electrostatic attraction or repulsion (Newton).
F_g	Force between two bodies due to gravitational attraction (Newton).
F_{im}	Force of attraction between a real charge and the induced image charge in an earthed conducting plane (Newton).
F_{lb}	Force between two particles due to the presence of a liquid bridge (Newton).
F_{ST}	Force between a surface and a liquid due to the surface tension of the liquid (Newton).
F^0	Force between two adhering particles prior to deformation at the point of contact (Newton).

$F(\delta)_{el}$ Force between two bodies due to an electrostatic charge layer, δ, at the surface of one or both of the particles (Newton).

F^{0}_{vdW} Force due to the van der Waals attraction between a sphere and a plane surface (Half space) (Newton).

G Universal constant of gravitation (Newton metre^{2} kilogramme^{-2}).

H(t) Time dependent hardness of the softer of two surfaces in contact.

λ Plank's constant (Joule second).

I Brightness of an image or of a point in an image.

I_n Brightness of a pixel in a digitised image after contrast enhancement.

I_c Current brightness value of a pixel in a digitised image. Often used to refer to the value of the pixel after digitisation and prior to image manipulation.

I_{tmax} Theoretical maximum brightness possible for a pixel in a digitised image.

I_{max} Maximum brightness value found in a digitised image.

I_{min} Minimum brightness value found in a digitised image.

$I_{x,y}$ Brightness of the pixel at location X,Y in a digitised image.

K Electric moment per unit volume due to spontaneous electric dipoles (Coulomb metre^{-2}).

l Distance between the plates of a parallel plate capacitor (Metre).

L Magnetic moment per unit volume due to spontaneous magnetic dipoles (Ampere metre^{-1}).

L(a) Langevin function.

$L(I_{x,y})$ Laplacian transform of the brightness of the pixel with brightness of $I_{x,y}$ in a digitised image.

m Mass of a body (kilogramme).

m_e Mass of an electron (kilogramme).

m_p Mass of a photon (kilogramme).

n Number of particles in a sample from a binary random powder mixture.

n	Refractive index of the medium between the objective lens of a microscope and the object being viewed.
N	Avogadro's number.
NA	Numerical aperture of a microscope objective.
p	Momentum (kilogramme metre second^{-1}).
P	Polarisation density (Coulomb metre^{-2}).
P^-	Force of attraction per unit area across the contact area between two surfaces (Newton metre^{-2}).
P^-_{vdW}	Pressure over the contact area between two plane surfaces (half spaces) due to van der Waals interactions (Newton metre^{-2}).
P^-_{ed}	Pressure over the contact area between two plane surfaces (half spaces) due to an electrostatic double layer (Newton metre^{-2}).
q	Quantity of electrostatic charge on a particle (Coulomb).
Q	Quantity of electrostatic charge (Coulomb).
r	Radius of a body (metre)
R	Resolution of a microscope (metre).
R	Electrical resistance (Ohm).
s_{ox}	Thickness of the oxide layer on a surface (metre).
T	Temperature (Kelvin).
u	Half the angle subtended by the objective lens of a microscope.
$U(r)$	Electric potential of a test charge at a distance , r, from an electrostatic charge of q (Joule).
v	Velocity of an electron (metre second^{-1}).
v_p	Poissons's ratio.
V	Electrical potential difference (Volt).
$V(r)$	Potential energy of a test charge at a distance,r , from an electric charge of q (Volt).
W	Work (Joule).
α_e	Electric polarisation density due to the opposite displacement of electrons and protons in an electric field (Coulomb metre^{-2})

α_i Electric polarisation density due to opposite displacements of poitive and negative ions in a dielectric (Coulomb metre^{-2}).

$\bar{\alpha}$ Mean proportion of particles of the first type in a sequence of samples from a binary random powder mixture as defined by Lacey (11).

$\bar{\beta}$ Mean proportion of particles of the second type in a sequence of samples from a binary random powder mixture as defined by Lacey (11).

γ Euler's constant.

γ Surface tension (Newton metre^{-1}).

δ Thickness of a charge layer at a surface (metre).

δ_H Depth of an electrostatic charge layer located at a plane surface (metre).

δ_s Depth of an electrostatic charge layer located at the surface of a particle (metre).

θ Angular measurement (degrees).

ϵ Electric permittivity of a material (Farad metre^{-1})

ϵ_0 Electric permittivity of free space (Farad metre^{-1}).

ϵ_r Relative permittivity of a material.

λ Wavelength of light (metre).

μ Magnetic permittivity (or permeability) of a material (Henry metre^{-1}).

μ Eectric polarisation density due to the alignment of permanent dipoles in an electric feld (Coulomb metre^{-2}).

μ_0 Magnetic permittivity (or permeability) of free space (Henry metre^{-1})

μ_r Relative magnetic permittivity (or permeability) of a material.

ξ Electric field intensity (Volt metre^{-1})

$\xi(r)$ Electric field intensity at a distance, r, from an electric charge of q (Volt metre^{-1}).

σ_r root mean square deviation or standard deviation of a random powder mixture as defined by Lacey (11).

σ_{el} Electrostatic charge density (Displacement) at a surface (Coulomb metre^{-2})

χ_e Electric susceptiblity of a dielectric.

ω Angular velocity (Radians second^{-1}).

$\bar{\omega}$ Mean angular frequency.

Chapter 1.

1. Introduction.

1.1. Pharmaceutical powder technology.

1.1.1. Content uniformity in solid dosage forms.

During the formulation exercise necessary for the production of a solid dosage form, such as a compressed tablet or hard gelatin capsule, a significant amount of effort is made to ensure that the drug is stable in the formulation, that it is released in a suitable manner and that each dose unit contains the stated amount of drug (1, 2). However, even when solid dosage formulations have been rigorously tested, the potential still exists for variations in drug content to occur both within and between batches. Where potent pharmaceuticals are involved, any variations in the active constituent of capsules or tablets within a batch may prove to be harmful. For this reason, every batch of tablets or capsules manufactured is subject to regulatory tests which are designed to test both physical and chemical characteristics.

The test used to examine the variability of drug content between dosage units within a batch is usually referred to as the 'Uniformity of content' test and such a test for tablets or capsules can be found in most pharmacopoeias (for example 3, 4). In general, a 'Uniformity of content' test involves combining together a number of dose units (reduced to the powder form in the case of tablets), determining the total drug content and then calculating the average. For example, the British Pharmacopoeia (3) requires that twenty tablets be ground together to provide a suitable sample for assay. This technique allows the average drug content of the dose units to be readily determined but gives no information regarding the variability of drug content between the dose units. It is therefore possible for a uniformity of content test to produce acceptable results for the average value of the dose content when a significant variation is present between the individual dose units (5, 6). For this reason it is becoming increasingly more common for potent drugs to be subject to more stringent 'Uniformity of Content' tests based on individual tablet assays (7, 8).

1.1.2. Homogeneity of powder mixes.

Solid dosage forms, such as tablets and capsules, are prepared by mixing together a number of different particulate solids to form a

powder mixture which is processed to produce the final dose unit. These particlulate solids are the pharmacologically active, or drug component and a number of excipients that are generally pharmacologically inactive at the concentrations used. Excipients can be defined as materials which have been included in a formulation for their physical rather than pharmacological properties (9).

If the mixing of the active constituent and excipients is not carried out to completion or other physical factors prevent complete mixing, some regions within the body of the powder mix will contain more of the drug than others. Thus, when the bulk of the powder mix is split into the sublots representing a single dose unit, there will be a degree of variation in the amount of drug included. In this manner, the variation in the drug content between individual dose units is dependent on the quality of the 'parent' powder mix.

When a sequence of samples are taken from a powder bed and are found to contain very nearly the same content of drug they can be described as being homogeneous (10). The quality of a powder mixture could therefore be defined by its homogeneity, which, for powder mixes, could be defined as being a measure of the difference between the actual amount of active ingredient contained within a number of samples and the amount that should be theoretically present. A powder mix with a good homogeneity will therefore exhibit little inter sample variation of the active constituent(s) whereas a powder mix with poor homogeneity will exhibit large inter sample variations.

For pharmaceutical powders this definition of homogeneity can be further qualified by making the sample size used to determine the homogeneity of a powder mixture, equivalent to, or smaller than, the total quantity of powder used to manufacture the number of unit dosage forms required for the 'Uniformity of content' test employed. This extra qualification ensures that the homogeneity measured can be confidently used as an indication of the average concentration of the active ingredient throughout the powder mixture. It should be noted that this definition of homogeneity is very simple and has implicitly assumed that the powder bed has been adequately mixed prior to the removal of samples for homogeneity testing.

If the homogeneity of a powder mixture is one of the major factors that determine the content uniformity of the dose units produced then it is clear that an understanding of how particulate materials behave when being mixed together will allow powder mixtures

with the desired homogeneity to be manufactured. One theory that has been developed to describe how particulate materials behave when being mixed together is based on the random (stochastic) movement of particles within a powder bed.

1.1.3. Powder mixing due to random processes.

The theoretical description of powder mixing by random processes was formalised by Lacey (11, 12) and can, for practical purposes, be considered as the 'classical' powder mixing theory which has been used as the basis for the development of more complex theoretical considerations. The requirements for random mixing, are very simple and can be summarised as two basic premises.

1. The particles to be mixed must be indistinguishable by size, weight or density.
2. The movement of particles within the mixing container are affected only by chance collisions with other particles or the walls of the mixing container.

When a powder bed consisting of two sets of particles, distinguished only by colour, is considered, then in its initial state the location of the particles can be very accurately described (Figure 1.1). If a sample is removed from this powder bed, then, provided the location from which the sample was taken is known, the concentration of either type of particle in the sample can be calculated very precisely. When this powder bed is mixed the two types of particle will distribute themselves throughout the body of the powder bed in a random manner according to the arguments given above. If mixing is continued for a sufficiently long period then a state of equilibrium will be reached where further mixing will not increase the randomness of the distribution of the two sets of particles (Figure 1.2). A powder mixture in this condition can be described as being an 'ideal random mixture' (11).

When an ideal mixture is attained it is not possible to calculate precisely the concentration of one type of particle in a sample because the exact distribution of the two sets of particles is not known. It is possible, however, using a sample of known size, to calculate the probability of obtaining the same relative proportion of the two types of particles that was present in the parent mixture. This was the approach used by Lacey (11) to derive a mathematical relationship that allowed the variability of a number of samples to

be related to the proportion of the two types of particle in the powder mixture and the size of the sample.

$$\sigma_r = \sqrt{\left(\frac{\bar{\alpha}\bar{\beta}}{n}\right)} \qquad (1.1)$$

where $\bar{\alpha}$ = Mean proportion of particles of the first type in the powder mixture.

$\bar{\beta}$ = Mean proportion of particles of the second type in the powder mixture.

n = number of particles in the sample.

σ_r = root mean square deviation or standard deviation of a random mix.

In the expression above, α and β are the proportions of the two types of particle in the sample of the powder mixture (where $\beta=1-\alpha$). The values $\bar{\alpha}$ and $\bar{\beta}$ are the mean proportions of the two types of particle where the powder mixture has been split into a number of samples (each containing n particles) of equal size and shape.

Equation 1.1 shows that the degree of dispersion of a set of samples is inversely proportional to the size of the sample used. This theoretical prediction can be verified by taking samples from Figure 1.2. If small square areas are used very large differences from the mean value can be obtained whereas if large squares are used the effect of a slight excess of one type of particle has a less significant effect (Table 1.1).

The practical aspect of equation 1.1 is that if the size of the sample and the proportion of the two types of particle in the powder bed are known then it is possible to calculate a theoretical standard deviation against which the measured standard deviation can be compared. Thus, if the best attainable standard deviation possible can be calculated in advance it becomes possible to assess the time it will take to mix a powder bed by measuring the standard deviation of a number of samples at increasing mixing times.

1.1.4. Powder mixing mechanisms.

The theoretical consideration of powder mixing used by Lacey (11, 12) states that the particles in a powder bed move in a random manner and are only constrained by chance collisions with other particles or the wall of the mixing vessel. However, unlike molecules of gas, particles in a powder bed will not move unless they are deliberately agitated. Lacey(12) described three distinct mechanisms

by which particles in an agitated powder bed could be dispersed. These mechanisms are convection, diffusion and shear.

A detailed description of these mechanisms is beyond the scope of this discussion and may be obtained elsewhere (13-15) if desired, however, a brief example of each of these mixing mechanisms is useful as they can illustrate a significant deficiency of the mixing theory described above. Shear mixing occurs when a slip plane is formed in the powder bed and the bulk of powder on either side of the plane moves as a body (Figure 1.3). Diffusive mixing occurs when an interchange of particles takes place across an interface in the powder bed. This interface is usally a slip plane (Figure 1.4). Convective mixing involves the movement of groups of particles from one place in the powder bed to another. The exact mechanism appears to be unclear although it seems to be a cross between shear and diffusive mixing. An example of convective mixing would be the distribution of particles over the surface of a tumbling powder bed (Figure 1.5).

Although these mechanisms can be discussed in isolation they must occur concurrently in any mixing operation (16). By considering Figures 1.3-1.5 it can be deduced that the possibility exists that sections of the powder bed will move as a discrete body. If this is the case than the individual particles cannot be moving in a random manner and the mixing theory described above no longer describes the powder mixing process.

1.1.5. Application of randomness to powder mixing.

The theory described above, for describing the mixing of powders by random processes, can only be applied under a very specific set of circumstances. The application of such a theory to real pharmaceutical powder systems would be invalid because such powder mixtures usually consist of more than two components each of which has a unique particle size distribution and true density.

It is possible to derive mathematical descriptions of the state of a powder mixture more complex than that used above, whilst still employing the random movement of particles as the process by which an ideal mixture is reached(17-27). Several of these descriptions can be shown to be related to each other (28).

The concept of random movement has also been utilised in computer models of powder mixing (29, 30) which have shown that

random mixing theories can give good estimates of measured parameters, specifically the rate of mixing where the process of random particle movement is dominated by the diffusion mechanism (30).

1.1.6. Segregation during mixing.

When free flowing particles of different sizes are mixed together the attainment of an ideal random mixture is prevented by the presence of unmixing mechanisms. That this is so can be demonstrated by considering the effect of adding a third set of particles to the system used above (1.1.3). If this third set of particles is made sufficiently small then they will be able to pass through the interstices formed by the other two types of particle. If only a few of these smaller particles are present then they will form a layer at the bottom of the powder bed where thay have filled any available gaps between particles.

When this powder bed is mixed, the smaller particles will be distributed in a random manner throughout the the bulk of the bed along with the other particles present. However, when the mixing operation is stopped the small particles will fall through the interstices of the larger particles due to the effects of gravity and will again form a layer at the bottom of the powder bed. When this effect occurs during a mixing operation the unmixing process of segregation can be said to be occurring. The process of random mixing in the presence of different sized free flowing particles can therefore be viewed as a competition between the mixing and unmixing mechanisms (31).

Three mechanisms for segregation have been described (15, 32, 33).

1. Trajectory segregation. Particles which are projected horizontally, as when being spread over the surface of a powder bed, will only travel a distance that is proportional to the square root of the particle diameter.
2. Percolation. When a void is created in a powder bed due to particle re-arrangement, small particles have a greater probability of filling the void than do large particles. Thus small particles will demonstrate a tendency to sink in an agitated powder bed.
3. Vibration. This mechanism is sometimes referred to as

densification segregation (15) and occurs when a powder bed is vibrated. The vibrations cause an increase in the packing density of the powder bed and as a result large particles are forced to the surface. This occurs even when there is a significant difference in density between the large and small particles.

Real pharmaceutical powder mixtures consist of particles which have very wide size distributions. It is therefore highly probable that segregation in pharmaceutical powder mixtures should be a major problem, particularly where a small amount of a finely ground material is being added to a relatively large bulk. It is interesting to note therefore that, for many pharmaceutical powder mixtures, such segregation is not readily observed.

1.1.7. Particle interaction in powder mixtures.

Powder mixing theories based on random movement of particles generally assume that the particles do not interact with each other. That is, particles cannot influence the movement of other particles except by chance collision. It is, however, well known that finely ground particles are cohesive and that, in general, pharmaceutical powders are of a size range where the effect of surface forces are significant. Consequently it should be expected that individual particles of a pharmaceutical powder mixture will interact during the mixing process (34, 35).

The presence of particle interaction has been used to explain the poor flow properties and other anomalous behaviour of bulk powders (36-39). In addition, the mode of action of pharmaceutical excipients, such as lubricants, glidants and anti-agglomerating agents, have been shown to be a result of these particles coating other particles within the body of the mix (40-44).

Particle interaction can also be influenced by forces other than those due to the intrinsic surface properties of the particles themselves. The most common effect observed here is due to the presence of moisture at the surface of the particle (45-48).

With such a prominent degree of interaction between particles documented, the mixing of pharmaceutical powders cannot reasonably be described by using theories which do not include the possibility of interaction between particles.

1.1.8. Ordered powder mixing.

A theoretical description of powder mixing based on particle interaction was given by Hersey (49, 50). Here interactions between particles were invoked as a deliberate mechanism to describe how powder mixtures with good homogeneity were possible when random mixing theory clearly did not apply. The main premise of Hersey's theory was that surface forces of particles produced agglomerates where fine particles coated larger particles (Figure 1.6). This type of mixing was called 'Ordered mixing'.

With ordered mixing, homogeneity is attained through the formation of structured agglomerates (ordered units). Ordered mixtures can therefore be readily distinguished from random mixtures where homogeneity is a property of the lack of structure and order.

A perfect ordered mixture can be defined as one which consists of monosized carrier particles uniformly coated with monosized adherent particles. In such a system the ratio of the carrier to the adherent is the same in every ordered unit and, as a consequence, any sequence of samples taken will exhibit zero variance with regard to the content of the adherent particles provided that the sample consists of whole ordered units.

The formation of a perfect ordered mixture from real pharmaceutical materials is highly improbable as these are composed of particles which are not monosized. Pharmaceutical powder mixtures have, however, been prepared that are composed of discrete units of adhering particles similar to those described for a perfect ordered mix (51-55). It has also also been demonstrated that the sample size variance of such powder mixes behaves in a manner similar to that described for a perfect ordered mixture (54).

The property of ordered mixtures which allow the homogeneity of a powder mix to be independent of the size of the sample used for its assessment has been employed by several authors to demonstrate that a highly agglomerated powder mixture, similar to an ordered mixture, had been formed (54, 56, 57). This method of determining the formation of an ordered mixture has been criticised (58) because the degree of error of the sample size variance were very large compared to the measured variance of drug content.

The principles outlined by Hersey's concept of ordered mixing has also been criticised (59) on the basis that the adherence of fine particles to a carrier substrate procedes due to random contact. Any

powder mix so produced could not be described as being ordered because the best possible homogeneity that could be obtained would be equivalent to the maximum homogeneity attainable for a random powder mixture (52-54).

The basis for this criticism is that the adherent particles are collected by the carrier particle as a result of the random collisions which occur throughout the mixing process. The distribution of the adherent particles on the carrier particles will not therefore be uniform but will vary around a mean value. Variations in the amount of drug bound by the individual carrier particles means that the homogeneity of the mix is not independent of sample size (60). Such an ordered mix will behave in a similar manner to a random mix where the homogeneity of a number of samples is dependent on the sample size although not to the same degree. It should be noted, however, that the term 'ordered mixing' was only used by Hersey (50, 51) to distinguish between powder mixtures in which the particles did interact and those in which particles did not interact.

1.1.9. Segregation in ordered powder mixtures.

The most important implication of ordered mixing is the observation that particle interactions occur which help to stabilise the distribution of the active fine particles (61). Thus, for ordered powder mixtures, segregation of the active material would not be expected to occur either during mixing or any subsequent processing. However, as most powder mixtures are not formulated to take advantage of the adhesive forces available for particle interaction, or the concept of ordered mixing, segregation still occurs, even in supposed ordered mixes (51, 58, 60, 62-71). The patterns of segregation of these 'near' ordered mixes are more complicated than those observed in random mixes and proceed via several mechanisms.

When ordered units are formed the interaction is between the adherent particles and the carrier particles. In a pharmaceutical powder mixture the particles of each constituent will not be monosized but will have a unique size distribution. These particles will interact to produce ordered units which can be regarded as being discrete stable entities, with their own unique size distribution, and which have little ability to interact with each

other. This reduction in interaction has been shown to be responsible for the improvement in the flow properties of powder mixes that have had glidants, lubricants or anti-agglomerating agents added to them (40-44).

The lack of interaction between ordered units enables each ordered unit to be treated as a single particle and consequently the mixing mechanisms at the ordered unit level once again proceed by stochastic processes. It is therefore possible to envisage segregation patterns similar to those observed for random mixes where the only differences between particles (ordered units) are those of size and density. As small carrier particles are able to carry more drug per unit volume than the larger particles it would be expected that any separation into distinct carrier size fractions due to flow, vibration or other processing stresses would lead to some areas of the mix becoming rich in drug content and other areas being correspondingly poorer. This effect is called 'ordered unit' segregation and has been observed experimentally (65, 66). Ordered unit segregation can be minimised by using carrier excipients with similar, narrow size ranges (61, 62) and similar densities.

The second mechanism by which segregation occurs in ordered mixtures is called 'constituent particle' segregation and occurs when free fine particles are found in the mixture. The causes of constituent particle segregation are threefold.

1. Excess adherent particles (61-63, 66, 70). If the number of adherent particles present in a mix is greater than that which can be bound by the carrier particles then the free adherent particles mix by stochastic processes. Free movement of drug particles leads to localised concentrations of adherent fines within the mixture and hence reduces the homogeneity which can be attained.
2. Inadequate adhesion forces (66, 67, 69). This form of constituent particle segregation occurs when the interparticle adhesion forces are insufficient to prevent the removal of the adherent fines due to external stresses. The result is the same as that described above, where the unbound fine particles can move independently through the powder bed. It is not always possible to distinguish between constituent particle segregation due to excess fines or due to inadequate adhesion forces.
3. Effect of additional fine particles (61, 63, 69). The third

variety of constituent particle segregation that has been observed occurs when additional fine particles, eg a lubricant, are added to an otherwise stable ordered powder mixture. Again, this type of segregation is largely dependent on the magnitude of the interparticle forces and hence the ease and frequency with which adherent particles can become detached from their carrier substrate.

If bound adherent particles are detached from the carrier substrate then the added fines can compete for those sites which have been temporarily vacated. The final distribution of the two species of fine particle will, therefore, be determined by their relative affinities for the carrier substrate. If the carrier particles do not have sufficient free binding sites to adsorb the additonal quantity of fine particles added then free active fines will be present thereby allowing constituent particle segregation to occur.

Constituent particle and ordered unit segregation are fundamentally different from the segregation observed in non interacting powder mixtures because they are due to phenomena that can be measured and therefore controlled. Placing a restriction on the size distribution of the carrier particles has already been referred to as a method for reducing ordered unit segregation (61, 62). The elimination of constituent particle segregation would require the ability to detemine the availability and magnitude of interparticle forces available so that the quantity of fines added to a powder mixture could be suitably adjusted. Alternatively the surfaces forces involved in particle interaction could be enhanced by suitable processing of either the carrier or adherent particles or by modifying the environment in which mixing occurs. The application of any of these options allows the possibility of producing ordered mixtures that are both homogeneous and resistant to segregation.

1.2. Interparticle forces and interactions.

The interactions which cause small particles to adhere to larger carrier particles can be split into two categories. The long range forces, gravity, magnetism and electrostatics, where the degree of interaction varies as the inverse of the square of the distance between the interacting particles, and the short range forces due to van der Waals-London interactions, electrostatic double layers,

dipole and hydrogen bonding, liquid bridging, chemical and physical bonding which require the interacting particles to be very close together or in contact before their effect becomes significant.

1.2.1. Long range interparticle forces.

In ordered mixtures, long range forces act on particles in two ways. At a distance, their effect is to attract two particles together so that the smaller particles impinge on the larger. After collision, the long range forces also contribute to the complex adhesion force that may bind the smaller particle to the surface of the carrier particle.

1.2.1.1 Gravitational attraction.

Gravitational forces occur as a direct consequence of a particle or body having mass and always results in the bodies or particles involved being attracted to each other. The magnitude of the gravitational force is related to the mass of the bodies involved in the interaction according to the relationship,

$$F_g = \frac{Gm_1m_2}{d^2} \qquad (1.2)$$

where F_g = force of gravitational attraction between two bodies.

G = universal constant of gravitation.

$= 6.672 \times 10^{-11}\ Nm^2Kg^{-2}$.

m_1 = mass of first body.

m_2 = mass of second body.

d = distance between the two bodies.

Gravitational forces between the particles in pharmaceutical powders mixes are invariably overwhelmed by the much greater gravitational attraction between the Earth and the particles. For this reason gravitational forces are much more likely to promote segregation in a powder mixture rather than promote the formation of ordered units.

1.2.1.2. Electrostatic charge.

Electrostatic forces between particles occur when either or both particles are electrically charged due to an excess or deficit of electrons (Appendix 1). A particle with an excess of electrons is said to be negatively charged whereas one with a deficit of electrons is said to be positively charged. When two charged particles are

exposed to each other they will experience a force of attraction if one particle has a positive charge and the other a negative charge, or a force of repulsion if the particles are both negatively or both positively charged.

In the simplest case of two point electric charges, the magnitude of the electrostatic force, F_{el}, between them can be described by Coulomb's law (Appendix 1).

$$F_{el} = \frac{q_1 q_2}{4\pi\varepsilon_0\varepsilon_r d^2} \qquad (1.3)$$

where F = force of attraction or repulsion (N).

q_1 = electric charge on the first particle in Coulomb (q).

q_2 = electric charge on the second particle in Coulomb (q).

ε_0 = permittivity of free space (Fm^{-1}).

ε_r = relative permittivity (dielectric constant, no units).

NB. The product of ε_0 and ε_r is, ε, and is referred to as permittivity (Fm^{-1}).

d = distance between the point charges in meters (m).

4π = constant of proportionality.

For a single charged particle near a flat (plane) earthed conducting surface (Appendix 1) this relationship becomes.

$$F_{el} = \frac{q_1^2}{16\pi\varepsilon d^2} \qquad (1.4)$$

This relationship is important because it shows that a charged particle will always be attracted to an uncharged conducting surface. If the plane surface above is replaced by a second uncharged particle then the image charge induced is reduced from q to q' (72).

$$q' = -q\left(1 - \frac{d}{\sqrt{(r^2+d^2)}}\right) \qquad (1.5)$$

where r = radius of the uncharged particle.

d = distance between the charged particle and the uncharged particle.

Thus the force between a point charge and an uncharged particle can be written as follows,

$$F_{el} = \frac{q^2\left(1 - \frac{d}{\sqrt{(r^2+d^2)}}\right)}{16\pi\varepsilon_0\varepsilon_r d^2} \qquad (1.6)$$

This relationship approximates to equation 1.3 above as the radius of the uncharged sphere increases.

When charged particles approach each other very closely the

nature of the surface and the distribution of the charge within the particles become important. For a charged particle resting on a plane conductor coated with a thin non conducting oxide layer, the effective force can be approximately expressed (73) as

$$F_{el} = \frac{q^2}{4\pi\epsilon_0\epsilon_r r^2} \cdot \left(\frac{r}{3s_{ox}}\right)^{0.7} \qquad (1.7)$$

where r = radius of the particle.

s_{ox} = thickness of the oxide layer on which the particle is resting.

This relationship shows that the presence of a very thin oxide layer can significantly increase the electrostatic force experienced by a particle attached to or resting on a surface. An alternative form of this relationship (74) only requires the particle to be separated by a small distance rather than resting on an insulating layer. For a charged, conducting particle, and an earthed conducting plane, the electrostatic force can be expressed as,

$$F_{el} = \frac{q^2}{16\pi\epsilon_0\epsilon_r rd} \cdot \frac{1}{\left(\gamma + \frac{1}{2}\ln\left(\frac{2r}{d}\right)\right)^2} \qquad (1.8)$$

where γ = Euler's constant (0.5772).

d = distance between the sphere and the plane surface.

r = radius of the sphere.

This relationship assumes that there will be no charge transfer between the charged particle and the earthed conducting plane as the particle approaches. In addition, it is also assumed that the material of the particle or the plane do not deform when they are in close proximity.

If, in the above example, the materials concerned are not conductors then any charge carrying species present in the particle will be fixed in position within the bulk of the body and not evenly distributed over the surface, as in a conductor. The immobilisation of the charge carrying species in the body of the particle has the effect of reducing the electric field of charges further from the surface. Consequently only those charges within a specific region at the surface of the particle will be involved in the induction of an image charge in the nearby plane. In this case the electrostatic force, $F(\delta)_{el}$, (74) due to the layer of charge, δ, than can interact is given by,

$$F(\delta)_{el} = \frac{q^2}{16\pi\varepsilon r\delta} \cdot \frac{\ln\left(1 + \frac{\delta}{d}\right)}{\left(\frac{\delta+1}{2}\ln\left(\frac{2r}{d}\right)\right)\left(\frac{\delta+1}{2}\ln\left(\frac{2r}{(d+\delta)}\right)\right)} \qquad (1.9)$$

where $\varepsilon = \varepsilon_0\varepsilon_r$

$\delta = \delta_H + \delta_S$

δ_H = depth of charge layer in the plane.

δ_S = depth of charge layer in the particle.

It should be noted that equation 1.9 overestimates the force due to assumptions made in its derivation (74). This error does not exceed 25% if δ is within the range 0 to 1×10^{-6}m, d is within the range 4×10^{-10}m to 1×10^{-7}m and r is in the range 1×10^{-6}m to 50m. If the plane surface is a second particle then the radius term in equations 1.8 and 1.9 should be replaced with $r_1r_2/(r_1+r_2)$ where r_1 and r_2 are the radii of the two particles involved (74).

1.2.1.3 Magnetic forces.

Magnetic forces, F_m, are the result of two types of magnetic effect, paramagnetism and diamagnetism (75, 76). A material is said to exhibit paramagnetism when the atoms or molecules of that material exhibit a magnetic dipole which can be aligned to obtain a gross magnetic field in the absence of external electric and magnetic fields. A material that is diamagnetic is one whose atoms or molecules exhibit a magnetic dipole which can only be aligned to produce a gross magnetic field in the presence of an external magnetic or electric field. Most materials have the ability to be diamagnetic under the correct conditions.

For the usual range of pharmaceutical materials, paramagnetism is not present to any significant degree, if at all. Furthermore, as mixing is not usually carried out in the presence of strong electric or magnetic fields there are no effects due to diamagnetism.

At the macroscopic level, magnetic effects can be considered to be nonexistent with regard to pharmaceutical materials and can therefore be dismissed as a mechanism for the long range attraction of particles during mixing.

1.2.2. Short range forces.

Short range forces can be defined as those forces which only act when particles are in very close proximity or are actually touching.

These forces are van der Waals' forces, electrical double layer forces, capillary or surface tension forces, hydrogen bonding, chemical bonding, and crystal bonding and all result in an increase in the energy required to separate the objects involved. These types of forces are not forces of attraction in the manner of the force between electric charges and are better viewed as conferring a surface 'stickiness' which can only be felt if the particles are brought within a finite small distance which would certainly be less than 1×10^{-6}m (74).

1.2.2.1. Forces due to van der Waals interactions.

Van der Waals' forces can be described by using either macroscopic methods (77, 78) where the interactions between groups of particles are considered, or by microscopic methods (79) where the interactions of individual atoms and molcules are considered and then added together. The microscopic approach to van der Waals' interactions is based upon the fact that the movement of electrons in atoms or molecules cause electric and magnetic dipoles whose orientation fluctuates very rapidly and in a random manner. This state can be represented by two equations,

$$D = \varepsilon_0 \varepsilon_r \mathcal{E} + K \qquad (1.10)$$

$$B = \mu_0 \mu_r H + L \qquad (1.11)$$

where D = dielectric displacement due to the spontaneous electric polarisation.

$\mathcal{E}$ = electric field due to the spontaneous electric polarisation.

B = magnetic flux density due to the spontaneous magnetic polarisation.

H = magnetic field strength due to the spontaneous magnetic polarisaton.

μ_0 = magnetic permittivity (or permeability) of free space $4\pi \times 10^{-7}$ (Hm^{-1}).

μ_r = relative magnetic permittivity (or permeability) of a material.

L = magnetic moment per unit volume due to spontaneous magnetic dipoles (Im^2).

K = electric moment per unit volume due to spontaneous electric dipoles in (qm).

Although the effect of the spontaneous electric and magnetic dipoles may be very pronounced when measured in close proximity to an atom, when the same effect is measured at a distance for a large number of atoms, the random fluctuation of the dipoles causes the net effect to be zero. It is for this reason that van der Waals forces can only act over a very short distance.

The strength of the van der Waals' forces can be calculated using both the microscopic and macroscopic theories. From the macroscopic theory an adhesional pressure, P^{-}_{vdW}, can be obtained.

$$P^{-}_{vdW} = \frac{\lambda\bar{\omega}}{8\pi^2(d_0)^3} \qquad (1.12)$$

where P^{-}_{vdW} = van der Waals' force of attraction per unit area.

λ = Plank's constant.

$\bar{\omega}$ = mean angular frequency.

$\lambda\bar{\omega}$ = Lifshitz-van der Waals' constant(74)(units are electron volts, eV).

d_0 = distance at which the adhesional force between the two surfaces is at its maximum (assumed to be 4×10^{-10}m (74)).

From microscopic considerations the van der Waals' pressure can be shown given as

$$P^{-}_{vdW} = \frac{A}{6\pi(d_0)^3} \qquad (1.13)$$

where A = Hamaker constant (78).

$= 3\lambda\bar{\omega}/(4\pi)$ (74).

This relationship (equation 1.13) was derived for two plane surfaces. The van der Waals force' between a sphere and a plane surface (78) is given by.

$$F^{0}_{vdW} = \frac{Ar}{6(d_0)^2} \qquad (1.14)$$

where r = radius of the sphere.

Equations 1.12, 1.13 and 1.14 can be combined (74) to give

$$F^{0}_{vdW} = \frac{\lambda\bar{\omega}r}{8\pi(d_0)^2} \qquad (1.15)$$

Equation 1.15 combines both the microscopic and macroscopic estimates of the van der Waals' forces between an undeformed sphere and a plane surface. The superscripted 0 in the force term indicates that the van der Waals' force is being measured when it is at its maximum. The inverse square relationship of the force to the

separation distance between the sphere and the surface only applies when d is much smaller than r. As the separation distance between the sphere and the plane is increased this relationship changes to an inverse fifth law ($F_{vdW} \propto d^{-5}$ (74)).

When the van der Waals interaction is between two spheres Equation 1.15 can be modified as follows

$$F^{0}_{vdW} = \frac{\lambda\bar{\omega}}{8\pi d_0^{2}} \frac{r_1 r_2}{(r_1+r_2)} \qquad (1.16)$$

where r_1 and r_2 are the radii of the two spheres involved (74).

1.2.2.2. Electric double layer or contact potential.

When two dissimilar materials are brought into contact there is a possibility that electric charge will be transferred from one body to another (75, 76, 80, Appendix 1). If a transfer of electric charge does occur, then a potential difference is created between the two surfaces in contact which is referred to as the 'contact potential'. The term 'electric double layer', in relation to the contact potential of two materials, refers to the fact that the portion of the surfaces in contact each have a layer of charge which is located close to the surface so that there is a double layer of electric charges (Figure 1.7).

The adhesional pressure generated by the double layer of charge is relatively easy to calculate (74) for the case where two plane surfaces are involved as the system approximates very closely to a capacitor whose conducting plates are separated by a vacuum (75, 76, 80, Appendix 1).

$$P^{-}_{ed} = \frac{\epsilon_0 \mathcal{E}^2}{2} = \frac{\epsilon_0 U^2}{2(d_0)^2} = \frac{\sigma_{el}^{2}}{2\epsilon_0} \qquad (1.17)$$

where U = Potential difference between the two surfaces (V).

σ_{el} = Electric charge density (displacement) at the surfaces (qm^{-2}).

If one or more of the surfaces is a dielectric (74) then the relative permittivity of the two surfaces must be considered

$$P^{-}_{ed} = \frac{\sigma_{el}^{2}}{2\epsilon_0\epsilon_r} \qquad (1.18)$$

where ϵ_r = a weighted mean value for the relative permittivity of the two surfaces.

Once created, the forces generated by the electric double layer are as long ranging as those discussed above

when considering electrostatically charged particles. The equations for electrically charged particles, derived above, cannot be correctly applied here because the charge generated only exists in the immediate environs of the contact area and not over the whole surface.

1.2.2.3. Liquid bridging forces.

The presence of an adsorbed surface liquid, eg water, on a spherical particle and a plane surface will result in an adhesional force. This force occurs because the molecules of the adsorbed liquid are attracted to the surfaces of the plane and the sphere by short range adhesional forces and, for the same reasons, other molecules of the liquid. As a result, the two adsorbed surface layers will tend to merge on contact and form a liquid bridge joining the particle and the plane.

The force required to remove a particle from a surface due to the presence of a liquid bridge (81) is given by.

$$F_{ST} = 4\pi\gamma r_m \qquad (1.19)$$

where F_{ST} = Adhesional force due to surface tension of the surface liquid at the point of contact.

γ = Surface tension of the liquid forming the bridge.

r_m = radius of the narrowest part of the liquid bridge.

Where the contact is between two spheres this relationship must be modified (82, 84) to account for the curvature of both surfaces.

$$F_{lb} = \frac{4\pi\gamma r_m}{(1 + \tan(\theta/2))} \qquad (1.20)$$

where θ = angle produce by a line from the center of the particle to the most narrow part of the meniscus and a line from the center of the particle to the lip of the meniscus on the particle

The presence of a liquid bridge will affect the magnitude of van der Waals, electrostatic and electric double layer forces (74) because these interactions will take place with the liquid in the bridge rather than between the surfaces of the particles. In cases where van der Waals' and electrostatic forces are effectively zero due to the presence of the liquid bridge and where the internal attractive forces of the liquid are greater than the short range forces between the particle and the liquid, it is possible for the adhesional force between the particle and the surface to be reduced

rather than increased. Such an interaction could be expected when the adherent particle is very hydrophobic and the liquid forming the bridge is very hydrophilic.

1.2.2.4. Hydrogen bonding, permanent and induced dipole interactions.

Hydrogen bonding and permament dipole interactions occur because of an uneven distribution of the charge density of electrons involved in a chemical bond (84). A permanent dipole will always exist when two atoms in a chemical bond have different electronegativities (or electron affinity). When this phenomenon occurs, the charge distribution describing the electrons in the bond will be biased towards the atom with the greater electronegativity, thus creating a region of negative charge. As a result of this, the other atom involved in the bond will become positively charged. The effective electric charge due to the polarisation, or permanent dipole, so produced is small compared to the charge on an electron but when summed over a large number of dipoles can give rise to a significant adhesional pressure.

If permanent dipoles on two surfaces in very close proximity are arranged so that opposite charges are aligned then a force of attraction will be experienced which will be similar to that due to the electric double layer. The difference between the dipole-dipole interaction and contact potential is that no charge is transferred between the two surfaces. The strength of permanent dipole interactions are such that the energies involved in bonding can be as great as 42 kJ $mole^{-1}$ of dipoles (85).

Induced dipole interactions occur when the normal distribution of electrons in a chemical bond are polarised due to the presence of an external dipole, electric or magnetic field. In these cases a dipole is created which only exists whilst the inducing agent is present. Again the energies involved in such bonding can be as high as 42 kJ $mole^{-1}$ (85).

Hydrogen bonding can be viewed as a special case of the permanent dipole interaction and occurs when a hydrogen atom is chemically bonded to a strong electron withdrawing atom, such as oxygen. Hydrogen has a stable state when two electrons are in its bonding orbital. It is therefore possible for an atom which has a lone pair of electrons to become involved in an electron sharing

arrangement with the positively polarised hydrogen atom.

The acceptance of a lone pair of electrons by a positively polarised hydrogen atom stabilises both the donor atom, by reducing the charge density at the donor atom due to the lone pair, and the electronegative atom bonded to the hydrogen, by allowing it to gain a greater share of the electrons shared with the hydrogen atom. The bond energies involved in hydrogen bonding average around 27 KJ $mole^{-1}$ (84, 85). It should be noted that hydrogen bonding only occurs when a lone pair of electrons are shared by the hydrogen atom and that the lone pair always remains chemically bonded to the donor atom. When a polarised hydrogen atom is associated with another dipole, a dipole-dipole interaction occurs and not a hydrogen bond.

1.2.2.5. Chemical bonding.

An adhesive bond will occur if actual chemical bonding occurs between surfaces which are in contact. Whilst it is feasible for such bonds to occur they are, in the short term, very improbable in the case of most pharmaceutical excipients and actives. The contribution of chemical bonding to interparticle adhesion forces is very likely to be negligible and therefore will not be considered any further.

1.2.2.6. Mechanical bonding.

Mechanical bonding between two surfaces can occur due to recrystallisation, surface diffusion and evaporation and recondensation (74). Recrystallisation may occur where soluble materials are dissolved in the liquid of a liquid bridge which subsequently dries out thereby depositing dissolved material at the interface. Alternatively one or both of the surfaces may be crystalline and have water associated with the crystal structure. An applied compressive force may do sufficient work on the surfaces to raise their temperature above the melting point of the crystal (self solubilisation). The liquid formed would cool and consequently recrystallise forming a mechanical bond.

Surface diffusion occurs when the materials involved at the contact point are able to diffuse into each other to form a continuous matrix. It is unlikely that the conditions for such an event would occur at normal temperature with the common range of pharmaceutical materials (74). Evaporation and recondensation

implies that the temperature at the interface between two surfaces is such that one is able to melt or vaporise and then, at a subsequent time, condense or solidify. Again it is unlikely that the temperature necessary for this phenomenon to occur would be available in pharmaceutical powder systems.

1.2.3. Effect of contact deformation on interparticle adhesion.

During the discussion of the long and short range forces that may act between two particles (sections 1.2.1 and 1.2.2) it has been assumed that the particles have either been separated by a small distance or that they are touching. Thus far no consideration has been given to the effect of deformation of the surfaces at the point of contact (74, 86-88).

The deformation that occurs when a spherical particle approaches a plane surface depends upon the relative hardness of the two surfaces. If the material of the particle is harder than that of the plane surface then the plane surface will be deformed. However, if the plane surface is harder than the material of the spherical particle then the spherical particle will be deformed. In cases where the hardnesses of the two materials are comparable the deformation experienced on contact will be between these two extremes.

When contact deformation occurs the mechanism of deformation will be either elastic (recoverable) or plastic (non recoverable or permanent), or a combination of both (74, 86-88) and, in addition, may also exhibit a time dependent component, creep, where the deformed area increases slowly with time (74). Where creep occurs the increase in the contact area between the two surfaces in contact produces a corresponding increase in the adhesive bond. However, in the case of elastic deformation, the increase in the adhesive bond is due to the electrostatic double layer formed and not to van der Waals' interactions as these are reversible (86, 87, 89). Conversely, where the deformation is due to plastic deformation the van der Waals' component of the adhesive bond will not be reversible. Materials that suffer plastic deformation, when in contact, will be subject to a greater adhesive bond for the same area of contact if it is assumed that all other aspects of bond formation are equal.

1.2.4 General adhesion equation.

Krupp (74) derived a general equation which describes the adhesive force between a perfectly smooth sphere and a perfectly smooth plane where the radius of the contact area was much smaller than that of the contacting sphere.

$$F = F^0\left(1+\frac{P^-}{H(t)}+\begin{pmatrix}1/3\\-2/3\end{pmatrix}\left(\frac{\pi^{3/2}(1-v_p{}^2)rH(t)}{2E(t)}\right)^2\frac{P^-}{F^0}\right) \qquad (1.21)$$

where

F^0 = force acting on the adherents at the point of contact (eg electrostatic and van der Waals') prior to deformation.

P^- = force due to the attractive forces across the area of adhesion (eg dipole interaction, van der Waals', Electric double layer effects but not mechanical or chemical effects).

$H(t)$ = Time dependent hardness of the softer of the two contacting materials.

$E(t)$ = Time dependent Young's modulus of the softer of the two contacting materials.

v_p = Poisson number of the softer of the two contacting materials

r = radius of the sphere.

The values of 1/3 and -2/3 are used for deformation without elastic recovery and deformation with elestic recovery respectively.

The strict application of this relationship is difficult as the microscopic values for $H(t)$, $E(t)$ and v_p are very difficult to obtain as they cannot be asssumed to be similar to the values obtained for the bulk material. In view of these difficulties, this relationship is included here for the sake of completeness rather than any real practical application.

1.2.5. Comparison of the contributions of the long and short range forces involved in interparticle adhesion.

When a fine particle adheres to a larger carrier particle the adhesive force must be greater than the separating force applied due to gravity. The maximum separation force due to gravity occurs when the adherent particle is suspended underneath the carrier particle and is equivalent to the mass of the adherent particle times the acceleration due to gravity (9.81 ms^{-2}). If it is assumed that

the carrier and adherent particles are perfectly smooth spheres each with a density of 1000 kgm^{-3} and diameters of 200μm and 5μm respectively then the maximum separation force that can be applied by gravity is ($9.80665 \times 6.5450 \times 10^{-14}$) 6.4185×10^{-13} N. Thus for a particle to adhere to the surface of the carrier particle the adhesive force must be greater than 6.4185×10^{-13} N.

The force of gravitational attraction between the two particles can be calculated using equation 1.2 and is $\approx 2 \times 10^{-27}$ N. This figure assumes that the two particles are touching so that the distance between their centres of gravity is 102.5μm. The adhesional gravitational force is therefore $\approx 3 \times 10^{-12}$ times less than the gravitational force between the particle and the Earth and can, therefore, be considered to be non existent for practical particle systems.

The force exerted on an uncharged particle due to an electrostatic charge on a second particle can be calculated using equation 1.6. The maximum surface charge density that can be practically attained by a spherical particle (in air) before the magnitude of the electric field causes ionisation of the surrounding air is given by $8.18 \times 10^{-6} r^{-0.3}$ coulomb m^{-2} (72). Thus if the charged particle is the 200μm diameter carrier particle (surface area 1.2566×10^{-7} m^2) the maximum sustainable surface charge density can be calculated as $\approx 1 \times 10^{-4}$ qm^{-2}. This charge density is equivalent to an electrostatic charge of $\approx 2 \times 10^{-11}$ q. The force exerted on the 5μm diameter uncharged particle due to this charge exceeds that due to gravity up to a maximum distance of $\approx 1 \times 10^{-3}$m. Whilst this distance may appear to be small compared to the potential size of a powder bed it is in fact sufficient to ensure that any fine particle moving in the interstices of a packed powder bed will be attracted to and bound to a carrier particle surface.

When the uncharged particle above is adhered to the carrier particle the force of adhesion will be described by either equation 1.8 if the particles are conductors or equation 1.9 if at least one of the particles is a dielectric. In the case of pharmaceutical materials it is probable that both materials will effectively be dielectrics (non conductors) so that equation 1.9 will apply, suitably modified for the case of two spheres rather than a sphere and a plane surface.

If it is assumed that the charge layer, δ, is the maximum

allowed (1×10^{-6}m), that the particles are at the distance of maximum force ($d_0 = 0{\cdot}4\times10^{-9}$ m), that they are effectively separated by vacuum ($\epsilon_r = 1$), no surface deformation occurs on either particle and that no charge transfer takes place then the adhesive force, $F(\delta)_{el}$, is $\approx 0{\cdot}3$ N. In comparison, the gravitational force required to pull the adherent particle from the surface of the carrier particle would need to be 4×10^{11} greater than that due to the earth's gravity. Whilst the attainment of this magnitude of adhesion force is unlikely due purely to electrostatic effects the calculation does serve to show that electrostatic charging of particles can play a very significant role in particle adhesion.

Using equation 1.9 the minimum charge required to cause particle adhesion between the 200 μm diameter carrier particle and the 5μm diameter particle can be calculated as $\approx 2\times10^{-17}$ q. This magnitude of charge is equivalent to that of 160 electrons and could be readily accommodated by the material of the carrier particle.

From equation 1.16 the magnitude of the Lifshitz-van der Waals[1] constant (photon energy) required for the minimum adhesion force can be calculated as $\approx 1{\cdot}\times10^{-24}$ J or $\approx 7{\cdot}\times10^{-6}$ eV. This is very small compared to other published results (74). If a more realistic figure of 2 eV is used for the Lifshitz-van der Waals' constant in equation 1.16 then the adhesion force can be calculated as $\approx 2\times10^{-7}$ N. The van der Waals') adhesion force, assuming that the Lifshitz-van der Waals') constant is 2 eV, is thus $\approx 3{\cdot}\times10^{5}$ times that due to gravitational attraction. This calculation suggests that van der Waals') interactions will always have a significant contribution to particle adhesion in pharmaceutical particle systems.

When two particles are brought into contact electric charge may be transferred to create a double layer which creates an adhesive bond (74). If it is assumed that sufficient charge is transferred to prevent the 5μm diameter particle (as above) from being removed from the carrier particle surface, that the mean weighted dielectric constant of the two materials is at least 3 (cellulose acetate for example is 3.8 (80)), and that the transferred charge has the maximum charge density permitted for a 200μm diameter sphere ($\approx 1{\cdot}\times10^{-4}$ qm^{-2} (72)) then the contact area can be calculated. From equation 1.18 the contact area can be calculated as $\approx 2\times10^{-15}$ m^2. The cross sectional area of the 5μm diameter sphere is 2×10^{-11} m^2 which is 1×10^{4} times the diameter of the contact area and implies that this

situation is feasible. Perhaps the most surprising aspect of this hypothetical situation comes from a consideration of the amount of charge transferred to cause adhesion. If the maximum possible charge density for the 200μm diameter sphere is assumed (as it was above) to be $\approx 1 \times 10^{-4}$ qm^{-2} and the calculated contact area is $\approx 2 \times 10^{-15}$ m^2 then the total charge transferred is $\approx 2 \times 10^{-19}$ q which is equivalent to ≈ 2 electrons!

The effect of the presence of an electric double layer is difficult to gauge because of the problems associated with accurately measuring the contact area. The calculations above have been used to illustrate that the presence of an electric double layer can significantly contribute to the interparticle adhesion force and that this is true even when the contact area is relatively small.

When the surfaces of the two particles are covered by an adsorbed molecule, such as water, the force of adhesion can be described by equation 1.20 (or 1.19 if the angle subtended by the contact area is very small). If it is assumed that the two particles are held together purely by the water bridge (where the surface tension of water is 728×10^{-3} Nm^{-1}) then, for the minimum adhesion force, the radius of the narrow part of the meniscus can be calculated as $\approx 7 \times 10^{-13}$ m which corresponds to an area of $\approx 2 \times 10^{-24}$ m^2. This area is significantly less than that required for the generation of an electric double layer with an equivalent force. If the radius of the contact area obtained for the electric double layer is used in place of the radius of the meniscus then the force of adhesion, F_{lb}, can be estimated, using equation 1.20, as $\approx 2 \times 10^{-11}$ N, approximately 30 times the separation force due to gravity. It should however be noted that the adhesion at the water/triamterene or water/cellulose interface may be much less than that between the water molecules nd this would decrease the strength of the liquid bridge bond accordingly.

The energy required by dipole or hydrogen bonds to overcome the separating force of gravity can be obtained by realising that the work per unit time done on the adherent particle must be equivalent to the energy involved in the bond in order for it to be broken. The energy equivalent to the minimum adhesion force necessary to prevent the adherent particle from being removed from the carrier particle surface can therefore be calculated as $\approx 1 \times 10^{-12}$ J. If it is assumed that the bond energy of the dipole or hydrogen bond is 29 kJ

$mole^{-1}$ then the number of dipole or hydrogen bonds required can be calculated as $\approx 2 \times 10^{7}$. If the molecules involved in hydrogen bonding are water (molecular volume of water = 18.018×10^{-6} m^3 $mole^{-1}$) then the cross sectional area involved, assuming one hydrogen bond per molecule, would be $\approx 2 \times 10^{-12}$ m^2.

The calculations above have been made to establish a comparative measure of their potential contribution to the adhesional force between a 200μm diameter particle and a 5μm diameter particle. In order to perform some of these calculations it has been necessary to make assumptions concerning local conditions so it may be that inaccuracies of several orders of magnitude in any of the calculated estimates have been introduced. Despite this uncertainty the comparisons indicate that most of the mechanisms outlined above are capable of contributing significantly, if not wholly, to the interparticle adhesion force. However, as real surfaces are not smooth or homogeneous, it is highly probable that the adhesion forces in a real particle system will be a complex combination of some or all of the above mechanisms. The relationships defined above should be applied with discretion if a meaningful interpretation of particle adhesion data is required.

1.3. Interparticle forces and ordered powder mixtures.

It was stated above that an increase in the degree of particle interaction in an ordered powder mixture should contribute towards improving homogeneity by reducing the potential for component particle segregation. Testing such a hypothesis requires some method for measuring the degree of adhesion in a powder bed so that the effect of enhancing the interparticle forces can be quantified in a usable manner.

1.3.1. Measurement of interparticle adhesion forces.

The assessment of the degree of particle interaction has been reported by a number of authors who have examined either the bulk behaviour of powders (51, 58, 66, 71, 90-94) or the adhesion forces present in single ordered units (95, 96). The former approach allows the stability of the bulk mixture to be assesed and can be used to discriminate between ordered powder mixtures where the interparticle adhesion forces are poor from those where the interparticle adhesion forces are strong. However, no information is provided about the

range or magnitude of the separating forces that prevail so that it can be difficult to distinguish between the presence of weak adhesion and an excess of fine particles (65).

The latter approach allows detailed information about the adhesion forces between individual adherent particles and carrier particles to be collected but cannot describe the behaviour of the bulk powder. In simple cases it is possible to calculate the adhesion forces acting on individual (96) or groups (95) of adherent particles as has been done in more fundamental particle adhesion studies (74, 97-99). Examining individual adherent particles in this manner allows the quantity of the adherent component removed to be directly related to the applied separating force. This method will be discussed in detail in Chapter 4.

1.3.1.1. Determination of the stability of bulk samples of an ordered mixture.

The determination of the stability of a bulk sample of an ordered mixture by sieving has been reported by a number of workers (51, 90, 91, 93, 94). Generally, a sample of the powder to be examined is placed on a sieve whose aperture is less than the diameter of the carrier particles but larger than the diameter of the adherent particles. Sieving is then carried out for a known period using a mechanical sieving system (ie vibrating sieve shaker or air jet) and the material passing through the sieve collected. The quantity of the adherent fines passing through the sieve mesh is then measured as a function of time or degree of sieving thereby allowing the stability of the ordered mixture to be assessed.

However, whist sieving does stress a powder bed, the forces applied are very dependent on the sieving conditions used. It is, for example, highly likely that the total amount of adherent particles dislodged in an air jet sieve will be significantly greater than the amount of adherent particles dislodged by a gyratory or vibrating sieve shaker. In addition, a disadvantage of sieving is that the process can be different to the conditions usually encountered during the preparation of the final dosage form, the exception being powder in the feed frame of a rotary tablet press. Conventionally, prior to processing, the bulk powder is held in a hopper which is subject to vibration from the processing equipment. For this reason a number of workers have used vibrated powder beds to

simulate storage in a hopper during processing (58, 66, 71, 92, 93 100).

The determination of the stability of bulk samples of an ordered mixture by vibration of a powder bed has been performed using two methods. In both cases the powder bed is placed in a container and subjected to vibration of known frequency for a specific duration. One method employed has been to remove small samples from within the bulk of the powder bed (73, 93). This allows the concentration of the adherent material to be estimated at specific points in the powder bed but is subject to the sampling errors usually associated with this method. An alternative method, used by Staniforth (58, 66, 92, 100) utilised a powder hopper that could be dismantled a layer at a time. This allowed the total concentration of drug in a layer of the powder bed to be estimated. This procedure has less error asssociated with it because the whole of the powder bed is analysed, however, the distribution of the adherent particles within each section is unknown.

1.3.2. Determination of interparticle adhesion forces in ordered units.

The measurement of the adhesion forces between the individual adherent particles and the carrier particles requires some means of applying a separating force to the adherent system. A method for achieving this has been described by Krupp (74) who used a centrifuge to apply a separating force to different types of small particle which were adhering to a plane metal substrate (ie flat surface).

This method has the advantage that relatively large separating forces can be applied to small particles in a non invasive manner and, as a consequence, has been widely used and adapted by a number of workers (73, 81, 96-99, 101-103) to measure interparticle adhesion forces in a number different systems. Of particular interest are the applications where this method has been used to examine the effects of electrostatic forces (73, 103) and humidity(78, 101, 102) on the magnitude of the adhesion forces between small particles and plane surfaces.

The centrifugal method for determining interparticle adhesion forces utilises test particles which have been scattered onto, dusted on or otherwise placed onto the adherent surface. The distribution of the adherent particles is then recorded, usually photographically,

then exposed to a separating force by applying centrifugation. After centrifugation, the distribution of the remaining adherent particles is again recorded so that the distribution before and after can be compared.

The adherent particles are then subjected to a second, larger, separating force by centrifuging at a higher rotational speed. After centrifugation the distribution of the adherent particles is again recorded. This process is repeated at known and increasing centrifugation speeds thereby providing a range of separating forces. Comparison of the records of the adherent particle distributions made between each period of centrifugation allows the identification of any particles that were dislodged. Then, as the centrifugation speed necessary to dislodge a particle, its density and diameter are known, the separating force which removed the particle from the adherent surface can be calculated.

This technique allows an adhesion force profile to be constructed for a particluar type of adherent material and surface using known conditions. A number of different profiles can be obtained for different materials so that it becomes possible to compare the behaviour of adherent particles applied to different adherent surfaces or under a variety of atmospheric conditions.

The application of a centrifugation method for measuring adhesion force profiles has been applied to ordered mixtures (69, 95, 96, 104-106) with varying degrees of success. Staniforth et al (69, 95, 105, 106) applied centrifugal separating forces to samples of an ordered mixture which were supported by a steel mesh. During centrifugation any fine adherent particles that were dislodged were able to fall through the mesh and were collected. After centrifugation the dislodged fines were measured using a spectrophotometric assay. Using this method it was shown that it was possible to derive adhesion profiles for the adherent particles in ordered mixtures and that the different mixtures employed had different adhesion profiles (69, 95, 105, 106).

Laycock et al (96) were able to examine the adhesion force profiles of single ordered units using a logical extension of the method used by Staniforth. Here single ordered units were trapped at one end of a very fine hole drilled through a brass plate. The ordered units were back illuminated by an intense, cold, fibre optic light source. Photomicrographs were then taken from the other side

of the brass plate before and after centrifugation. Using this technique it was possiblle to generate adhesion force profiles for an ordered mixture of a red food dye and Elcema G250 in a similar manner to that of Staniforth et al(96). This method of examining the adhesion force profiles of the adherent particles in a single ordered unit was found to have problems (104). The forces applied to remove adherent particles were also found to deform the carrier particles so that the area examined photomicrographically changed with increasing centrifugation speed. In some cases the ordered units were extruded through the hole in the brass plate and as a consequence could not be examined any further. A second, more serious problem, was that the depth of field available for photomicrography was less than the depth of the surface of the ordered units being examined. Consequently some areas of the photomicrographs used were out of focus and the accurate determination of the position or presence of the adherent particles was consequently difficult. This latter problem represented an absolute physical limitation because the depth of field and resolution requirements were at or beyond the limits of conventional light microscopy (104).

1.3.3. Enhancement of particle interactions.

The enhancement of particulate interaction can be achieved either by changing the physical structure of the materials involved or by increasing the magnitude and type of the naturally occurring cohesive forces already present at the surface. The modification of the materials involved to improve interaction between particles is probably the least desirable of these measures although it has been employed in attempts to improve the dissolution rate of materials (107) and the compression properties of tableting excipients (106, 107). The enhancement of the surface forces involved in particle interaction already occurs during some processing methods although it is not done by deliberate intention(107, 108).

It has already been observed that the presence of high levels of humidity increases the amount of particle interaction in powder mixes (45-48). A similar effect has also been observed by other workers (101, 102, 109, 110) who have measured the effect of atmospheric moisture on the strength of adhesion of small particles to plane surfaces. In contrast, adhesion measurements have also been made using particles adhered under a vacuum (98). The mixing of metal

powder in a vacuum has also been found to improve the homogeneity of the powder mixture (111).

Pharmaceutical processes, such as milling, sieving and mixing, often produce high levels of electrostatic charge (100, 112-114). The generation of an electrostatic charge is due to the formation of new surfaces, during milling, or the triboelectric generation of an excess of free electrons during the mixing operation itself through interparticle friction. The presence of electrostatic charges on small particles has also been shown to increase the degree of adhesion between those particles and the surfaces to which they adhere (73, 103).

The degree of particle interaction present in a powder mixture could be manipulated by using either humidity or electrostatic charges, particularly as it has been demonstrated that these two already implicated in modifying particle interaction. There are however problems associated with the use of both humidity and electrostatic forces that preclude their use in certain circumstances.

Increasing the ambient humidity during mixing would not be possible if the drug or any other constituent in the powder mix was adversely affected by the presence of atmospheric or surface moisture, eg moisture labile drugs, or readily water soluble powders such as sugar based tableting excipients. Electrostatic discharges in the presence of dust clouds of fine particles is a common cause of industrial explosions (115). The potential for powder explosions has not, however, prevented a number of attempts at mixing powders by the application of electrostatic charges (100, 106, 116-120).

1.3.4. Application of electrostatic forces.

When applied to everyday objects, electrostatic forces appear very weak in comparison to gravitational forces. However, when electrostatic forces are applied to very small objects, as demonstrated above, they can overcome both gravitational and aerodynamic forces and become the predominant factor when considering the movement of such particles. The strength of electrostatic forces in such situations has led to their widespread use in industrial applications (121, 122) in fields as diverse as the control of air pollution, air filtration, xerography (photocopying), mineral processing and efficient powder coating processes used to replace

conventional spray painting (123-130). All of these processes use electrostatic forces either to cause the capture of fine particles onto a surface (123-125, 127, 129) or to separate particles with different charge/mass ratios (126, 128, 130).

1.4. Electrets.

All of the applications for electrostatic charges described above depend upon the use of electrostatic charges produced by an excess of free electrons or ions. The use of mobile electrostatic charges is very common but is not the only method by which electrostatic forces can be employed. In certain circumstances it is possible to induce a quasi-permanent electrostatic field in a material which is not dependent on the presence of a mobile electrostatic charge but is a result of the electronic properties of the material itself. Such a material would be the electrostatic equivalent of a permanent magnet. This concept was first used by Heaviside (131, 132) who used the term 'electret' to describe a body that exhibited a permanent electrostatic charge.

The ability of materials to form electrets when exposed to suitable conditions is a function of both the macroscopic and quantum behaviour of groups of atoms and molecules. Appendix 1 has been included as an introduction to electrostatic and quantum behaviour of materials which emphasises the theoretical concepts related to the formation of electrets.

1.4.1. Applications of electrets.

Electret research is extensive (133, 134), and electrets have found a wide range of applications, some of which are the logical development of those processes mentioned above and others which are the direct result of the special properties of the electret itself. For example, the inclusion of electrised materials in filters can improve their efficiency without introducing the hazards involved with the use of mobile electrostatic charge (135, 136). Electrets in the form of thin films are used in the manufacture of microphones (137) and dosimeters for measuring exposure to radiation (137, 138).

The advantage of using an electric field produced by an electret is that it removes the danger of electrostatic discharge due to the fundamental difference in the way the electric field is generated. The application of electrostatic attraction to the problem of

increasing the degree of particle interaction in powder mixes has not been totally successful as the electrostatic charges used are dissipated too rapidly (100, 106, 116-120). However, if the electrostatic attraction between particles in a powder mixture was provided by an electric field due to an electret, then the electrostatic charge would not dissipate rapidly nor would there be the inherent danger of a powder explosion.

The induction of the electret effect in cellulose and cellulose related or derived compounds (cellophane and Avi-cel (sic)) has been reported by several authors (139-150). This evidence for the electret effect in cellulosic materials would indicate that cellulose based compression excipients, such as Avicel and Elcema, should have their electret forming potential investigated. The successful induction of the electret effect in these materials would, of course, lead to an investigation of their use in the formation of stabilised ordered powder mixtures.

1.4.2. The classical thermoelectret.

The first practical work into the deliberate manufacture of electrets was performed by Eguchi (151-158), who investigated the change in the conductivity of naturally occurring waxes and rosins with temperature (156). This work led Eguchi to the conclusion that it should be possible to obtain a permanently polarised dielectric by allowing these waxes to solidify in the presence of a strong electric field.

The original method used by Eguchi (151) to manufacture electrets employed a sample of wax which was melted and then exposed to a strong electric field. The wax was then allowed to cool and solidify whilst still under the influence of the electric field. When cool, the samples of wax used were found to exhibit a permanent electric field which was present throughout the volume of the wax (151), and which persisted despite attempts to remove it (152-155, 157). By manufacturing wax electrets using a variety of methods, Eguchi was able to determine that the electret effect observed was due to the presence of polarised elements throughout the body of the observed electret (156).

Electrets formed by the simultaneous application of heat and an electric field are now called thermoelectrets and thermoelectrets manufactured from organic waxes or rosins (such as carnauba wax) are

said to be 'classical' thermoelectrets (159). The charge stored in carnauba wax thermoelectrets has been studied extensively (160-169) and been found to be caused by the alignment of polar molecules and the presence of a space charge component.

1.4.3. Measurement of charge storage in electrets.

The charge stored in an electret can be a complex combinaton of a number of charge storage mechanisms depending upon the method used to manufacture the electret. The measurement of the charge stored in an electret can be done using two methods each of which has advantages and disadvantages.

The magnitude of the electric field produced by the net charge on an electret can be assessed by measuring the charged induced in a conducting body placed in that electric field, that is, the measurement of the induced charge. This method of measuring the charge of an electret was used by Eguchi (155). One problem associated with this type of measurment is ensuring that the induced charge is due solely to the electric field of the electret and not due to transient electrostatic charges generated during handling (168). A more fundamental problem is that the measurement of the electric field generated by an electret does not give any indication of the mechanisms by which the charge is stored.

Alternative techniques, the frequency dependence of the electric field (170) or the electric field respone to high intensity light pulses (171), have been developed for measuring the electric field generated by an electret. However, these procedures still rely on measuring an induced charge and still produce little or no information concerning the mechanisms by which the electric field is generated. The measurement of the electric field of an electret using charge inductance has the advantage of preserving the charge on the electret thereby making it possible to monitor the electric field generated by an electret over long periods.

The main alternative method used to measure the charge stored in an electret is based on heating the electret in a controlled manner and measuring the changes in the external electric field with time. This method destroys the charge stored in the electret but does produce information on the different types of charge storage mechanisms. The measurement of the charge stored in an electret in this manner is called 'thermally stimulated discharge current'

(TSDC) and was first used to investigate charge storage in electrets by Bucci (172, 173).

The term 'TSDC' is taken here to mean the measurement of an electric current produced by the decay of a deliberately induced charge. The terminology used to refer to TSDC as described above is somewhat confused in the literature as different names are used to descibe the same process in many cases and, in equally as many cases, different processes use the same name (174).

1.4.4. Measurement of charge storage using TSDC.

The application of TSDC to the measurement of the charge stored in an electret involves techniques very similar to those used to manufacture thermoelectrets (174). An electret is placed between the plates of a capacitor and these are then connected across a very sensitive galvanometer. Initially the galvanometer will not register any charge since no current will flow in the circuit after the initial induction of an image charge on the capacitor. The sample electret is then heated at a constant linear rate to a temperature greater than that used to form the electret. As the temperature is increased the stored charge gains energy until the point is reached where it becomes free to dissipate (Appendix 1).

The dissipation of the stored charge, on heating, is due to aligned dipoles becoming disorientated due to random thermal agitation, separated charges recombining and trapped space charges being free to move out of the body of the electret. All of these changes are reflected in variations in the strength of the external electric field of the electret. As a result of this variation, the induced charge on the capacitor will change causing a net flow of charge into or out of the capacitor. It is the flow of charge (electric current) which is measured by the galvanometer (174) and used to produce the traces typical of TSDC.

1.5. Limitations in microscopy.

The measurement of the adhesion force between individual adherent particles and the carrier surface in ordered units has been performed using photomicrography. (96). One of the problems associated with this method was that the surfaces being examined were very deep in comparison with the depth of field of a microscope. As a consequence it was usually impossible for the whole surface of the

ordered unit to be examined in focus simultaneously (104). This limitation was due to the physical nature of microscopy and could not be resolved using conventional photomicrographic techniques.

1.5.1. Resolution.

The resolution of a microscope is a measure of its ability to distinguish fine detail in a specimen. This, in turn, is dependent on the numerical aperture of the lens system used to produce the image (Figure 1.8) and the wavelength of the light used to illuminate the specimen (175, 176).

$$R = \frac{0.5\lambda}{n \sin(u)} = \frac{0.5\lambda}{NA} \qquad (1.22)$$

where R = smallest distance that can be seen between two features.

λ = wavelength of the illuminating light.

n = refractive index of medium between the object being examined and the objective lens of the microscope.

u = half the angle subtended by the objecive lens (Figure 1.8).

NA = numerical aperture, n sin(u).

High quality images require that the resolution be as small as possible. An objective lens should therefore aim to have as large a numerical aperture as possible. In addition, the wavelength of the light used to illuminate the sample should be as small as possible. For calculations using white light, the wavelength of green light, 0.55μm, is used, since this is in the middle of the visible (to humans) range of wavelengths.

1.5.2. Depth of field.

The term, depth of field, describes the distance between the nearest and farthest object planes that are in focus (176). When objects are a considerable distance from the lens, the depth of field is large; however, as the object approaches the lens, the depth of field rapidly decreases. For a microscope, the distance between the object and the lens is very small and as a result the depth of field, d_{fd}, is very small. The equation relating the depth of field to a particular objective lens is given by,

$$d_{fd} = \frac{\lambda\sqrt{(n^2 - (NA)^2)}}{NA^2} \qquad (1.23)$$

The depth of field can therefore be increased by illuminating the sample with a long wavelength of light, by using a medium with a large refractive index between the objective lens and the sample and by using an objective lens with a small numerical aperture. The requirements for producing a large depth of field can therefore be seen to be precisely the opposite of those required for a high quality image with good resolution.

1.5.3. Photomicrography of deep surfaces.

Examination of the relationship between resolution and depth of field demonstrates why Laycock and Staniforth (96, 104) were not able to obtain completely focused photomicrographs of the ordered units used. If, however, the requirement for depth of field in such a situation were relaxed, it would be possible to obtain high quality photomicrographs where a small section of the image would be in focus. A series of photomicrographs could then be made, each of which contains a slightly different area in focus. Combining these photomicrographs would provide all the information necessary to determine the position and size of every adherent particle and consequently the adhesion force profiles of the adherent particles.

The application of this method of photomicrographing deep surfaces would be both expensive and time consuming. Some improvements could be made and costs could be reduced by using a multiple exposure technique and automating the movement of the focus position during photomicrography. The increase in the quality of the images obtained by these improvements would be small because the small dark areas marking the adherent particles (96, 104) would be affected by out of focus glare from other exposures. The problem of glare could be reduced by the use of confocal imaging (177, 178). However, confocal imaging with microscopes requires high intensity illumination, usually provided by a laser, and surfaces which reflect a significant proportion of the incident light. This latter requirement means that most pharmaceutical excipients cannot be used as their surface reflectivity is too low.

An alternative approach to recording images in a photographic emulsion would be to use an image analyser to capture a video image of the surface. A sequence of images could then be recorded on reusable magnetic media using the same process as above. This technique offers a number of advantages over photomicrography as it

would be possible to process the images to produce a single image with all areas in focus. This image could then be used to automatically document the position and size of the adherent particles after each period of centrifugation.

The ability of an image analyser to record and process images eliminates many of the problems encountered by Laycock and Staniforth (96, 104) when measuring the adhesion force profiles of adherent particles in single ordered units. The application of image analysis techniques should, therefore, allow a practical attempt to be made at measuring interparticle adhesion forces in ordered units.

1.6. Image analysis and processing.

Modern image analysers/processors are instruments that can manipulate digitised images stored in the memory of a computer using specially written programs (179, 181). These systems are much more flexible than early systems which processed real time video signals by simple grey level thresholding (182, 183). A digitised image or sequence of images can be repeatedly manipulated until a satisfactory result is obtained because both the raw and processed images can be stored on conventional magnetic media (disc drives, tape). The facility to store images so that they can be recalled and re-examined as required is one of the main requirements of any image analysis system that is to be used to analyse adherent particles in ordered units as described above.

The advent of powerful microprocessor based image analysis sytems such as the Magiscan 2A (179), the IBAS 2000 and the Quantimet 900 (181), has allowed image analysis techniques to be applied to a broad base of tasks, most of which would be difficult or extremely tedious to perform manually. The type of tasks that can now routinely undertaken by image analysers are the examination of particulate contaminants (184-186) for the rapid identification and classification of the types of particles involved with the minimum of operator involvment and Chromosome analysis (187-189) which allows automatic karyotyping (pairing) and hence the identification of abnormalities and other changes to be performed rapidly and reliably.

Image analysis can be applied to the examination of mammalian cells (190-194) for counting purposes in cell cloning (190), the identification of cancerous changes (191) and the identification of morphological features (192, 193). The comparison of consecutive

tissue slices has been used to reconstruct the three dimensional structure of neurones (194, 195), a similar application to that required for the examination of the adherent particles on a carrier particle. Other applications (196, 197) are the examination of the effect of processes on particle size in areas such as the stability of artificial blood (196), to optimising the combustion of coal particles (197) and the determination of dimensional characteristics of particles (197-201).

A wide range of mathematical techniques have been developed to assist in processing (202-205). Many of these techniques have been developed for the enhancement or reconstruction of degraded or poor quality images whereas others have been developed to allow the identification of features or objects in an image. Where the image to be analysed is of high quality the analysis techniques required to extract information concerning the position of objects can be very simple therby eliminating the need to use computationally intensive (time consuming) fourier transforms and similar methods.

The simplicity of the processes used to perform basic image analysis is such that very low cost image analysis systems available for microcomputers designed for the home would be satisfatory in many cases (206, 207). This observation holds true even if an external graphics displays is required so that digitised images can be viewed with the same (or greater) grey scale resolution they were originally captured with (208).

1.6.1. Digitisation of the image.

The most convenient method for obtaining digitised images is to convert the signal from a standard video camera into a numeric form that can be understood by the computer being used to process the image (202-205). For a video signal this conversion is usually done by passing the analogue voltage signal through an analogue to digitial convertor (ADC). Using this system the quality of the digitised image depends on the horizontal, vertical and grey scale resolutions used.

The horizontal resolution of a digitised image is dependent upon the speed at which the ADC can sample the video signal. An ADC with a short sample and hold time allows a scan line of a video image to be divided into a larger number of discrete points than a slow sample and hold time. This is true even when the time taken to convert the

sampled voltage to a digital value is long compared to sample and hold time. If an ADC cannot process the video signal rapidly enough to allow real time digitisation then multiple scans of the image can be used to create the digitised version but only if the object being viewed is stationary.

The vertical resolution of the digitised image is dependent on the number of scan lines used by the camera. Increasing the number of scan lines will increase the vertical resolution. Common vertical resolutions are 256 or 512 for 50Hz video signals but resolutions up to 4096 vertical lines are available on professional systems.

The number of bits used by the ADC to quantify the brightness of the digitised image will affect the tonal quality. In general terms, however, the higher the number of bits required the slower the ADC. For most 'flash' ADC's (those converting the video signal in real time) the number of bits is usually 6 or 7. For a monochrome system this is quite adequate as the human eye is unable to distinguish more than 64 (2^6) distinct grey levels (204).

When an image has been digitised it can be treated as a two dimensional array of numbers, each of which corresponds to a point in the original image. Increasing the horizontal or vertical resolution of the digitised image allows greater detail but also increases the size of the array necessary to store the image in memory.

The tonal quality of a digitised image is dependent on the maximum value allowable for the numbers in the array describing the image. Monochrome systems can have as little as 2^6 grey levels of tonal quality and be perfectly satisfactory however high quality colour images images may have as many as 2^{32} levels (2^8 for red, green and blue components of the image and 2^8 for brightness or luminance) to describe each pixel adequately.

1.6.2. Contrast enhancement.

When an image is digitised the maximum brightness recorded may not be equivalent to the maximum allowable value. In a bad case, the total range of brightnesses may only occupy a small fraction of the available range. In these cases it becomes possible to utilise the fact that the digitised image is represented as an array of numbers which can readily be manipulated so that all of the available brightness range is occupied. This process is known as contrast enhancement (202-205). The simplest contrast stretching algorithm

that can be used is the linear mapping of the recorded brightness range onto the whole brightness range available.

$$I_n = \frac{(I_c - I_{min})\ I_{tmax}}{(I_{max} - I_{min})} \qquad (1.24)$$

where I_n = pixel value after contrast enhancement.

I_c = current pixel value.

I_{tmax} = Maximum pixel value that is allowed.

I_{max} = Maximum pixel value in image before contrast enhancement.

I_{min} = Minimum pixel value in image before contrast enhancement.

The effect of applying this transformation to a digitised image (Figure 1.9) is to stretch the recorded range of grey levels so that they occupy the full grey level range available (Figure 1.10).

More sophisticated applications of this type of enhancement (202-205) may use a non-linear transformation, apply the transform to only part of recorded range of grey levels, or may apply different transforms to different sections of the recorded brightness range. The particular transform used on a digitised image depends greatly on the type of processing and information required. However, for many applications a simple linear transformation is satisfactory.

1.6.3. Removal of noise.

When an image is digitised it is possible that image degradation can occur due to the presence of noise. Noise can be defined as non picture information being superimposed on the picture information. This type of degradation can be in the form of a structured distortion of the image such as that obtained due to uneven illumination or in correct focusing or a random distortion where a degree of white noise has been introduced into the image (202-205). This latter effect is easily demonstrated by adding noise with a grey level range of 0 to 3 to Figure 1.9 (Figure 1.11).

The restoration of a digitised image with a structured degradation may require a significant amount of processing and the use of advanced mathematical techniques. This type of processing is usually beyond the capacity of home computers to perform on a realistic time scale and consequently will not be considered further.

The effects of random noise can be dealt with effectively by averaging over a number of frames. For each succesive frame the

white noise superimposed on the image will have a different distribution whereas the picture information will remain constant. When the series of digitised images are added together and averaged the effect of the random noise will be significantly reduced in comparison to the picture information. This process can be demonstrated using a sequence of 32 images based on Figure 1.9 which have had a low level of white noise added to them. When the average of this sequence of images is obtained (Figure 1.12) the effect of the noise is significantly reduced compared to the individual images. If any changes occur in the image between successive digitised frames then averaging cannot easily be applied to remove noise. In cases such as this, alternative techniques have been developed to reduce the effect of noise.

1.6.4 Smoothing transformations.

Smoothing transformations can be used to remove or reduce the effects of random noise when only a single digitised image is available for processing (202-205). One of the simplest smoothing filters is the three by three weighted average filter. When this filter is used each pixel in the image is replaced by the weighted average of that pixel plus the surrounding eight pixels. The weighted average employed may vary, the most common being

$$I_{x,y} = \frac{I_{x,y}}{2} + \frac{I_{x+1,y+1}}{16} + \frac{I_{x+1,y}}{16} + \frac{I_{x+1,y-1}}{16} + \frac{I_{x,y+1}}{16} \cdot\cdot \qquad (1.25)$$

$$+ \frac{I_{x,y-1}}{16} + \frac{I_{x-1,y+1}}{16} + \frac{I_{x-1,y}}{16} + \frac{I_{x-1,y-1}}{16}$$

The effectiveness of this filter can be demonstrated by applying it to Figure 1.11 (Figure 1.9 with added noise) on four occasions (Figure 1.13). A comparison of Figures 1.11 and 1.13 shows that the the added noise has been significantly reduced. The smoothing transformation also has some unwanted side effects, however, as the height of peaks in the digitised image are reduced and edge information is less prominant. This effect is easily observed by comparing Figures 1.9 and 1.13. If this type of image degradation produces problems then it is possible to use other types of transformations which re-emphasise edges and peaks.

1.6.5. Sharpening transformations.

As demonstrated in 1.6.4 it is possible to reduce the effect of noise by using a smoothing transform. This does have the side effect that peaks in the image also become less sharp and edge infomation less well defined. One method of overcoming these disadvantages are by the application of another transformation which will re-emphasise peaks and edges, a sharpening transform. One sharpening transform that is relatively simple to implement is the Laplacian transform (202, 203).

$$L(I_{x,y}) = 5I_{x,y} - (I_{x-1,y} + I_{x+1,y} + I_{x,y-1} + I_{x,y+1}) \quad (1.26)$$

where $L(I_{x,y})$ = Laplacian transform of the brightness of the point $I_{x,y}$ using the vertical and horizontal neighbours of that point.

$I_{x,y}$ = Brightness of the point at x,y in the original digitised image.

If $L(I_{x,y})$ is outside the allowable range for the brightness then it is clipped to the nearest limit, ie -2 becomes 0 and 300 become 255 for a system with 8 grey levels.

When this transformation is applied to an area of constant brightness $I_{x,y}$ and all its neighbours have the same values and consequently no change occurs and $L(I_{x,y})$ stays the same as $I_{x,y}$. On uniform slopes the changes around the $I_{x,y}$ are again cancelled completely or very nearly cancelled so that $L(I_{x,y})$ again remains the same as $I_{x,y}$ or changes by a small amount. When applied acoss an edge some of the values surrounding $I_{x,y}$ will be less than $I_{x,y}$ so that the value of $L(I_{x,y})$ will be greater or less than $I_{x,y}$ depending on whether $I_{x,y}$ is brighter or darker than the pixels at the edge. The application of the Laplacian transform described by equation 1.26 caused undershoot at the bottom of slopes and overshoot at the top of slopes.

The effect of this transform can be demonstrated (Figure 1.14) by applying it to Figure 1.13 (a image smoothed after adding low level noise). A comparison of Figures 1.11 and 1.14 shows that the peaks are approximately the same height and the these areas have been affected to a greater extent than any low level noise present.

1.6.6 Measurement and determination of features.

Frequently it is unnecessary to enhance the digitised image but simply to extract information from it. A typical application

requiring the extraction of information from an image is the determination of the cross sectional area and perimeter of an object. This is a relatively simple procedure providing the object to be measured can be distinguished from the background (objects with the different colours may have the same brightness when viewed with a monochrome video camera and therefore be difficult to distinguish). Thus if the objects to be measured are darker than the background, as is usually the case with transmitted light microscopy, the sections of the image corresponding to adherent particles, for example, could be isolated and then measured. As an example of this process the image in Figure 1.9 will be processed using two different methods to isolate the areas of interest which are the peaks.

Contrast enhancement followed by five applications of the smoothing transform described above produces an image (Figure 1.15) where the areas of interest have been emphasised. The peaks can then be isolated by setting any pixel less than a specific value eg 40 to zero (Figure 1.16). This method is relatively quick, less than 2 minutes, however, consideration of Figure 1.16 does illustrate one of the problems associated with this process as objects of interest in the central area of the image have not been separated.

An alternative treatment of the original image is to again perform contrast enhancement followed by three passes of the smoothing transformation (Figure 1.17). This operation has the effect of increasing the height of the peaks in relation to the lower levels of brightness in the image. This process can be continued by repeated applications of a sequence of one pass of the sharpening transformation followed by three passes of the smoothing transformation so that the areas of interest eventually become separated. This effect can be seen after 25 passes of the above sequence (Figure 1.18). This operation produces a superior separation compared to that observed in Figure 1.16 but takes more than 30 minutes to run using the 'C' program PROFILE on the Sinclair QL (Appendix 2). Where a number of images have to be examined the time taken by this process mean that it is unlikely to be used.

The objects left in the image can be measured by searching for a non-zero pixel value. When a non background pixel is found, a 'grass fire burn' (209) is used to determine the area of the object (Chapter 3). In this manner, the number of objects in the processed image and

their cross sectional areas are easily obtained.

The image processing methods described above represent a very simplistic approach to the determination of the area of objects in a digitised image because it has assumed that no objects are touching or overlapping. It does however serve to illustrate how the application of very simple processes can extract information that is useful.

1.7. Summary and objectives.

The theoretical considerations of interparticle adhesion discussed in section 1.1 and 1.2 have shown that interparticle forces can give rise to stable homogeneous powder mixtures by utilising the concepts of ordered mixing. An examination of the adhesion forces available for particle interaction, section 1.3, has shown that electrostatic forces represent a potentially useful mechanism by which interaction can be increased. The ability of some materials to form electrets was discussed in section 1.4, leading to the observation that cellulose-based materials had demonstrated this effect. The ability of cellulose-based tableting excipients to form electrets will therefore be investigated with a view to introducing electrostatic forces in powder mixtures using electrised materials.

The measurement of interparticle adhesion forces (section 1.3) has indicated that methods exist which could be adapted to the measurement of forces in single ordered units. The physical limitation of microscopy have been discussed (section 1.5) as these were the major limitations in one of the more successful methods. A consideration of the potential for image analysis to replace photomicrography has indicated that it would be possible to examine deep surfaces unavailable to conventional microscopy. The development of an image analysis package capable of analysing the deep surfaces on single ordered units and consequently producing detailed adhesion force profiles on an individual adherent particle basis will be examined.

The ultimate objective of this study is to produce a system which can be used to measure interparticle adhesion forces in ordered units on an individual adherent particle basis and to demonstrate the effects of processing (electrised materials) and environmental conditions (humidity) on the adhesion force profiles of a model powder system.

Number of samples taken	Number of particles in sample	mean proportion of white particles in sample	mean proportion of black particles in sample	Lacey's standard deviation
1024	16	0.4990234	0.5009766	0.1249998
655	25	0.4969160	0.5030840	0.0999981
455	36	0.5030525	0.4969475	0.08333178
334	49	0.5087987	0.4912013	0.07141751
256	64	0.5046997	0.4953003	0.06249724
202	81	0.4952329	0.5047671	0.05555303
163	100	0.4990798	0.5009202	0.04999992
135	121	0.5075605	0.4924395	0.04544935
113	144	0.4966184	0.5033186	0.04166575
96	169	0.5031435	0.4968565	0.03846078
83	196	0.4906565	0.5093435	0.03570805
72	225	0.5016667	0.4983333	0.03333315
64	256	0.5024414	0.4975586	0.03124963
56	289	0.5093302	0.4906698	0.02940664
50	324	0.5058642	0.4941358	0.02777587
45	361	0.4998461	0.5001539	0.02631579
40	400	0.497625	0.502375	0.02499972
37	441	0.4949439	0.5050561	0.02380831
33	484	0.5055732	0.4944277	0.02272586
30	529	0.5003781	0.4996219	0.02173912
28	576	0.4988839	0.5011161	0.02083328
26	625	0.4944615	0.5055385	0.01999877
24	676	0.5022806	0.4977194	0.01923057
22	729	0.4980671	0.5019329	0.01851838
20	784	0.4996173	0.5003827	0.01785714
19	841	0.499781	0.500219	0.01724138
18	900	0.4977778	0.5022222	0.0166665
17	961	0.4949501	0.5050499	0.01612821
16	1024	0.5089111	0.4910889	0.01562252
15	1089	0.4988655	0.5022345	0.01515136
14	1156	0.5022862	0.4977138	0.01470573
13	1225	0.5021036	0.4978964	0.01428559
12	1296	0.5019933	0.4980067	0.01388878
11	1369	0.4956504	0.5043496	0.013513
11	1444	0.4993075	0.5006924	0.0135788
10	1521	0.5052597	0.4947402	0.0128198
10	1600	0.50275	0.49725	0.01249981

Table 1.1. Effect of sample size on the number of samples that can be taken, the number of particles in each sample, the mean proportions of the two types of particle in the set of samples and the standard deviation as defined by Lacey (11). Data calculated using Figure 1.2.

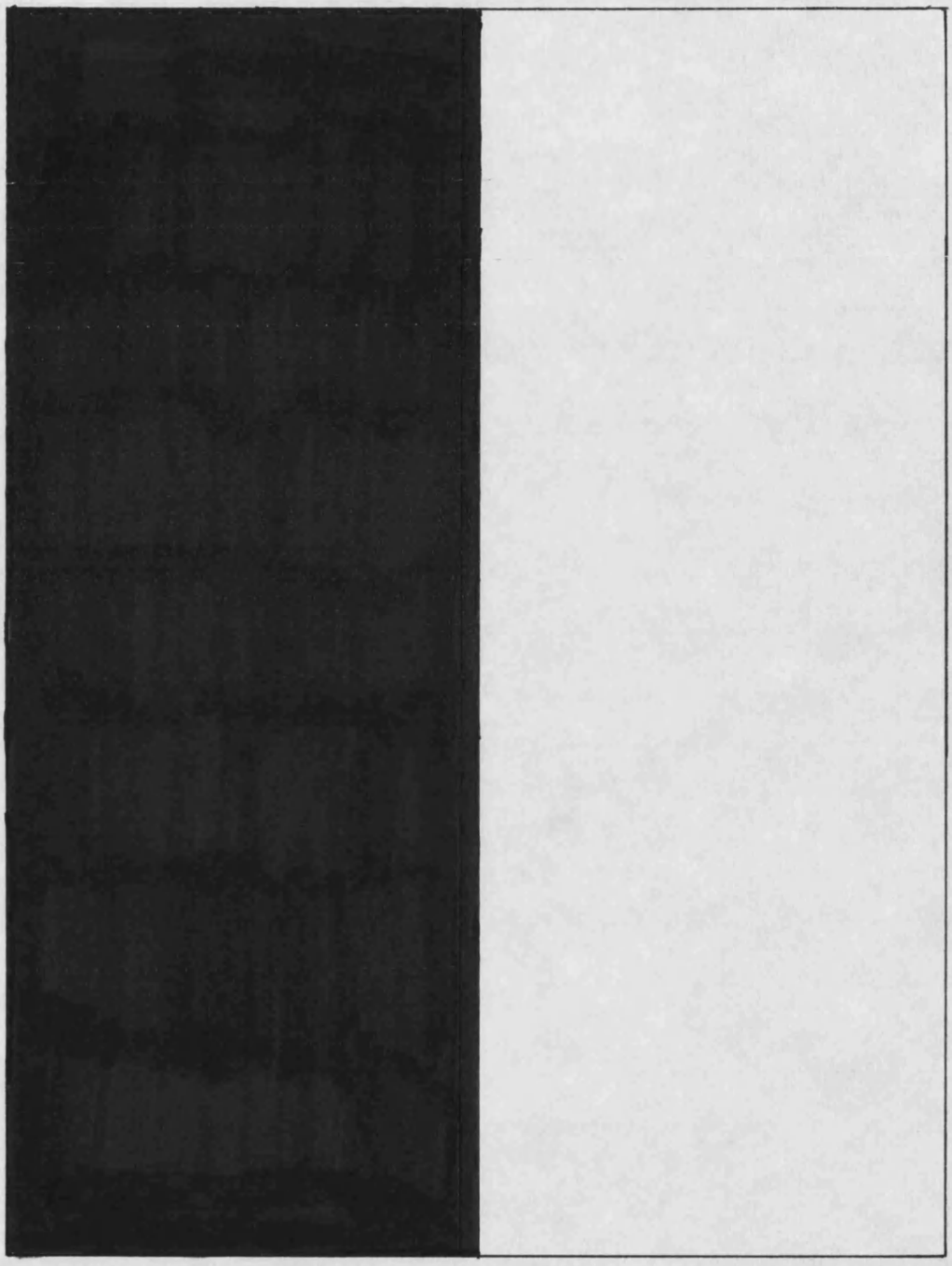

Figure 1.1. Schematic representation of an unmixed powder bed. The composition of samples from this bed can be predicted exactly if it is known where the sample was taken from.

Figure 1.2. Schematic representation of the powder bed shown in Figure 1.1 after prolonged mixing by random processes. The composition of a sample from this powder bed cannot be exactly known, however, the probability of a sample containing a given ratio of the two types of particle can be calculated.

Figure 1.3. Schematic representation of the mechanism of shear mixing.

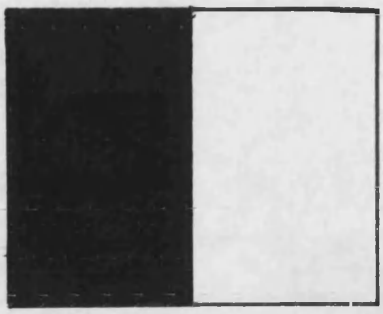

Powder bed in its original state prior to mixing.

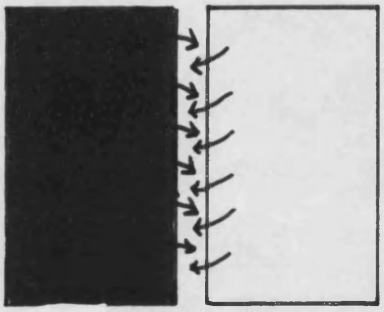

During mixing particles are free to move where shear planes form.

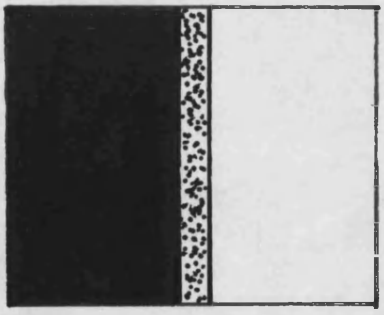

Particles are therefore mixed at the shear interface.

Figure 1.4. Schematic representation of the mechnism of diffusive powder mixing.

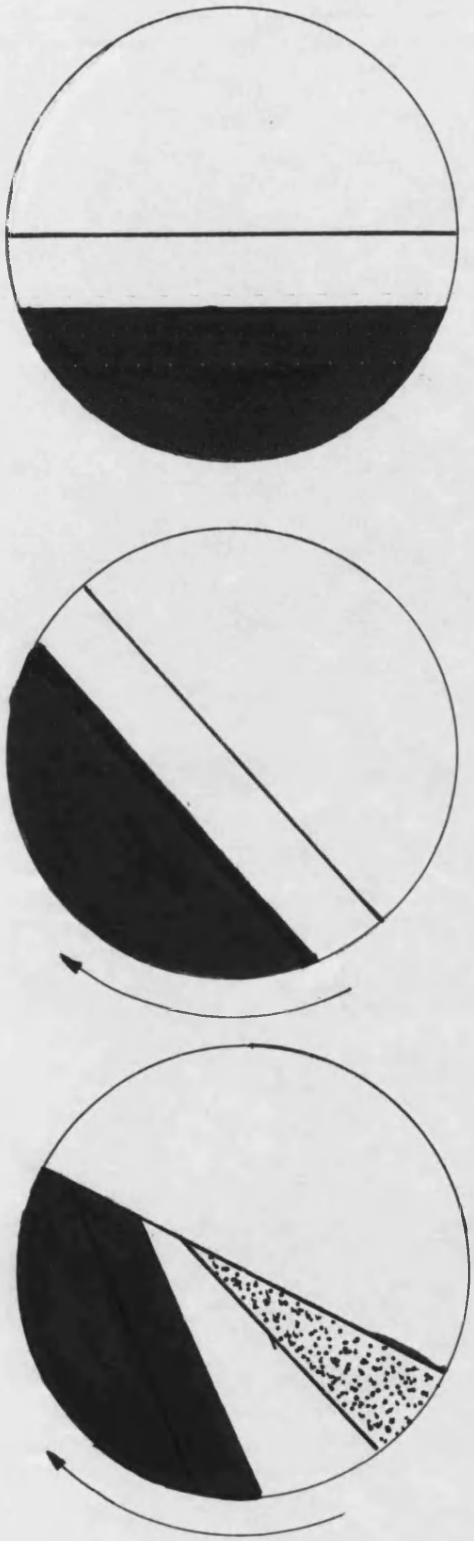

Figure 1.5. Schematic representation of the mechanism of convective mixing.

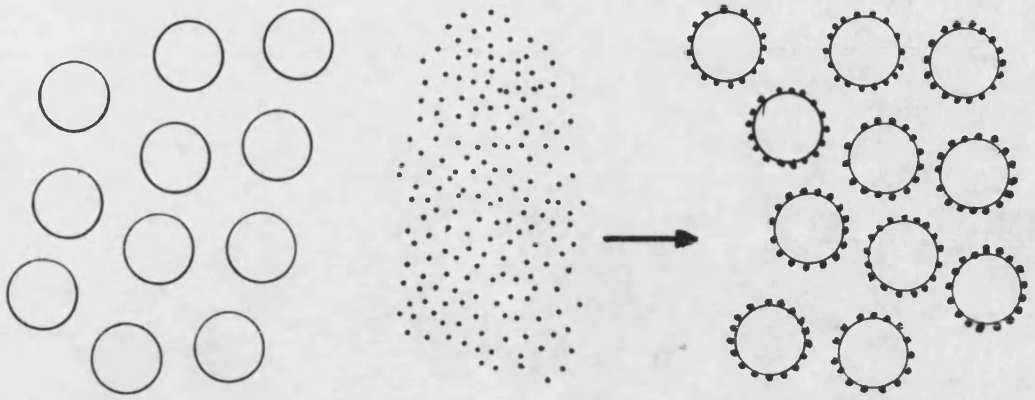

Figure 1.6. Formation of an ordered powder mixture due to fine particles adhering to the surface of larger 'Carrier' particles.

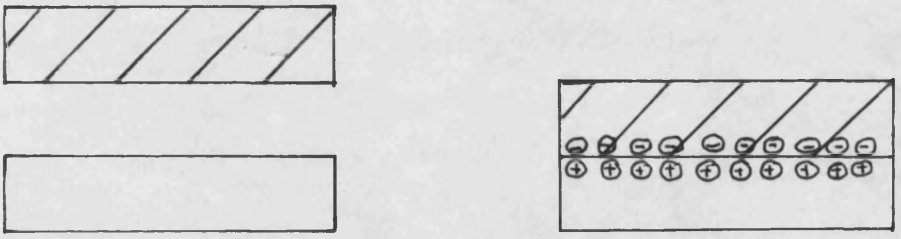

Figure 1.7. Formation of an electric double layer in solid dielectrics. Before contact, no electrostatic charge is present. After contact, electric charge has been transferred from one body to the other. The charge is located at the interface because the materials are not conductors.

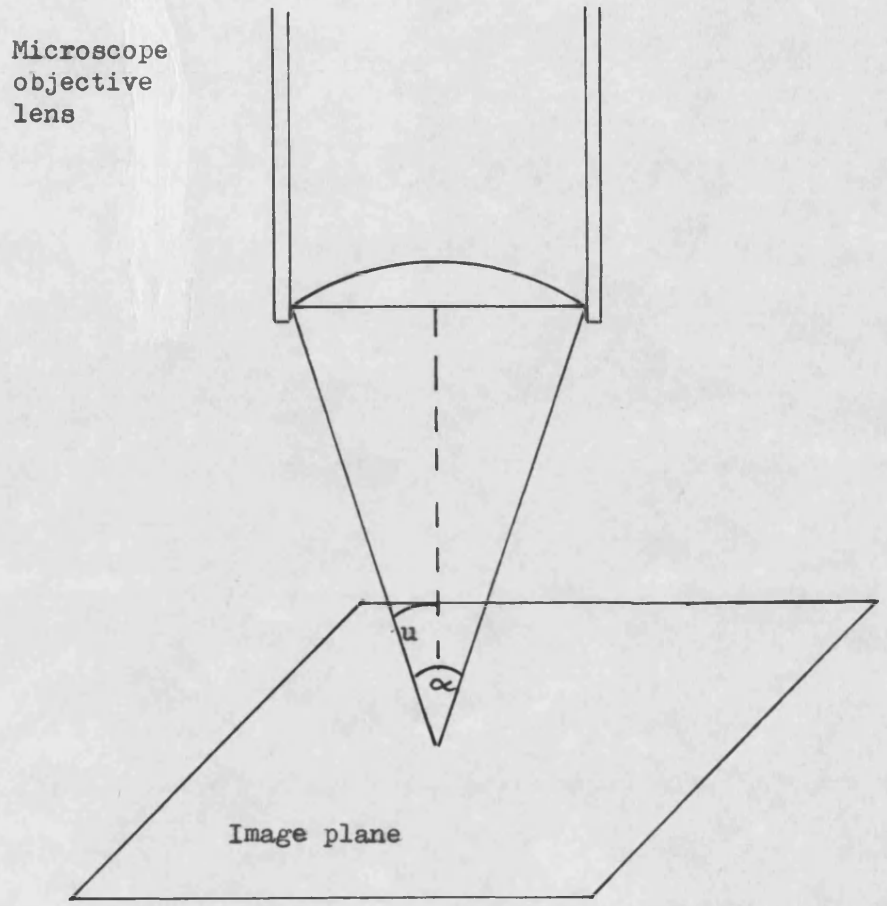

Figure 1.8. Maximum cone of light that can be collected by the objective lens of a microscope.

α Angle subtended by the objective lens.
u Half the subtended angle, α.

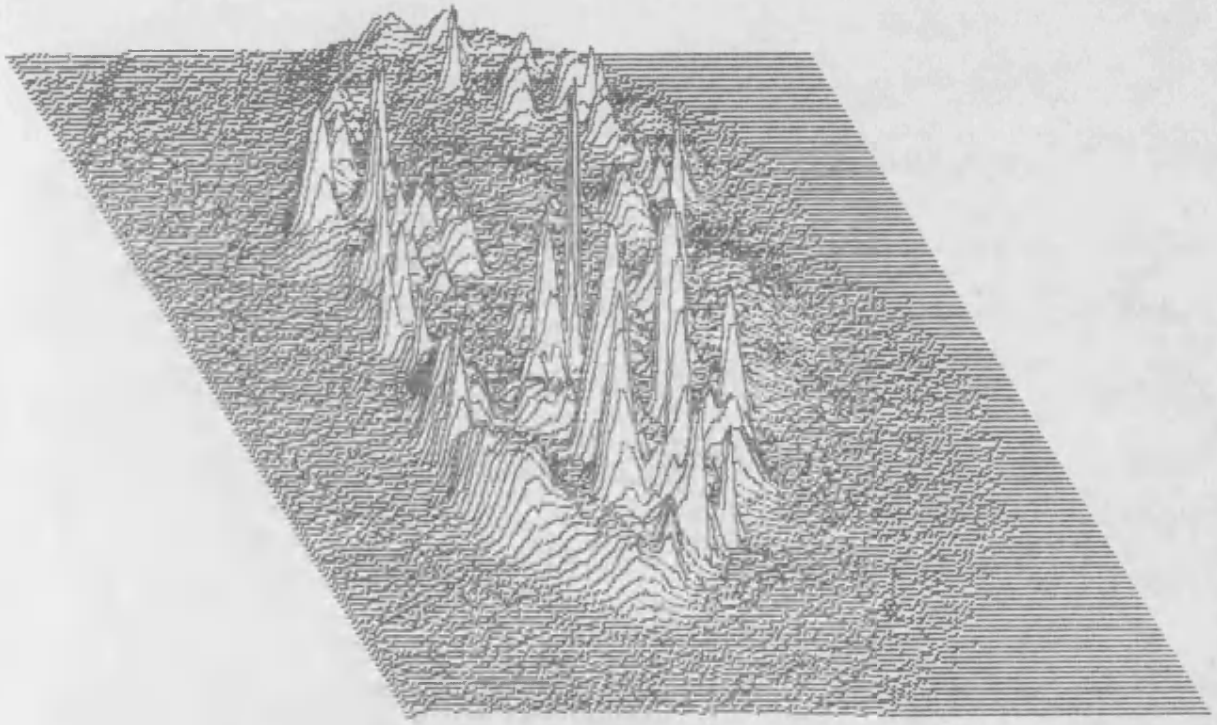

Figure 1.9. Isometric projection of the brightness of a digitised image of an Elcema G250 particle with adherent, fluorescing Triamterene particles. The bright areas in the image are represented by the peaks and correspond to adherent particles which are in focus. The less bright areas are due to Triamterene particles which are not fully focussed and the background fluorescence of the Elcema G250.

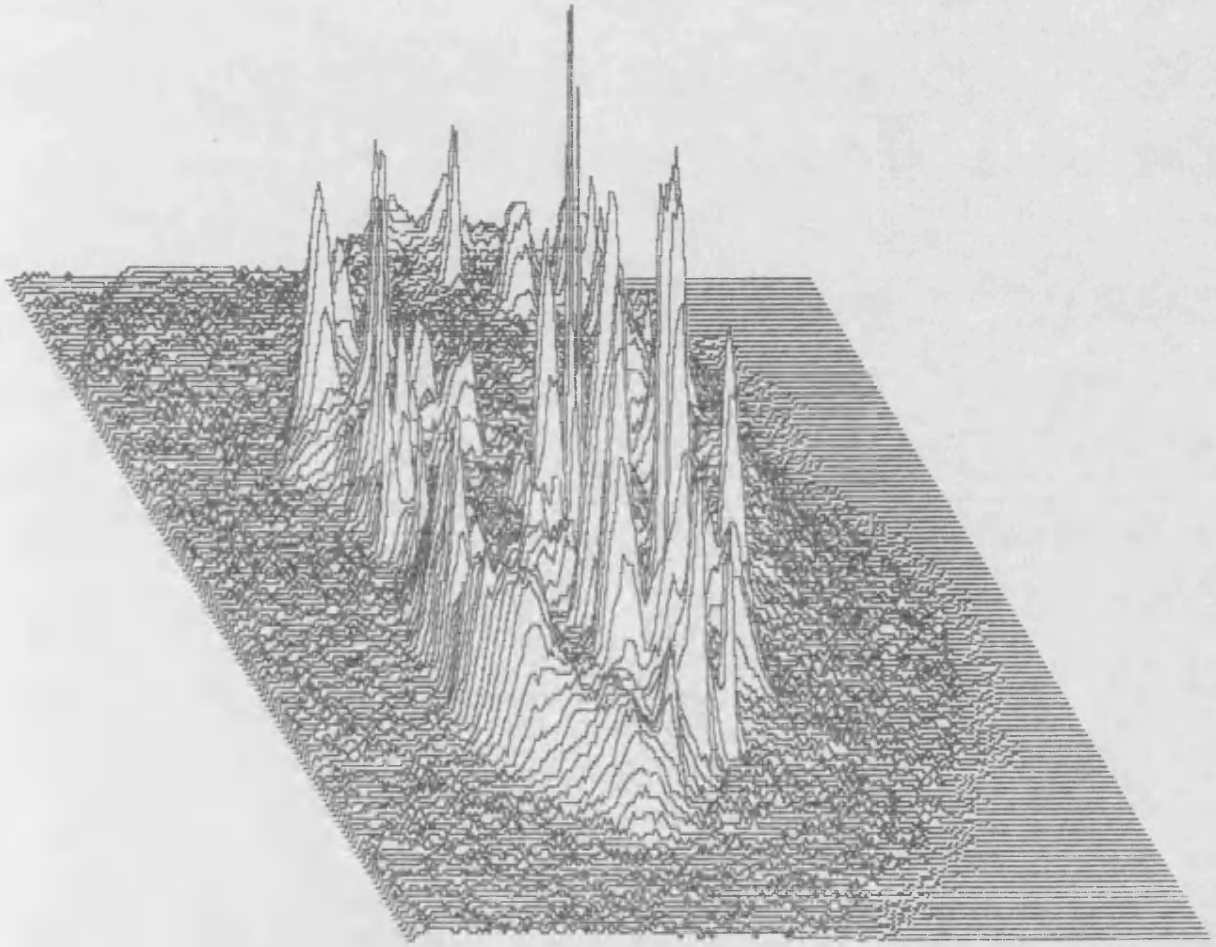

Figure 1.10. Isometric projection of the digitised image shown in Figure 1.9 after the application of contrast enhancement as described in Chapter 1, 1.6.2.

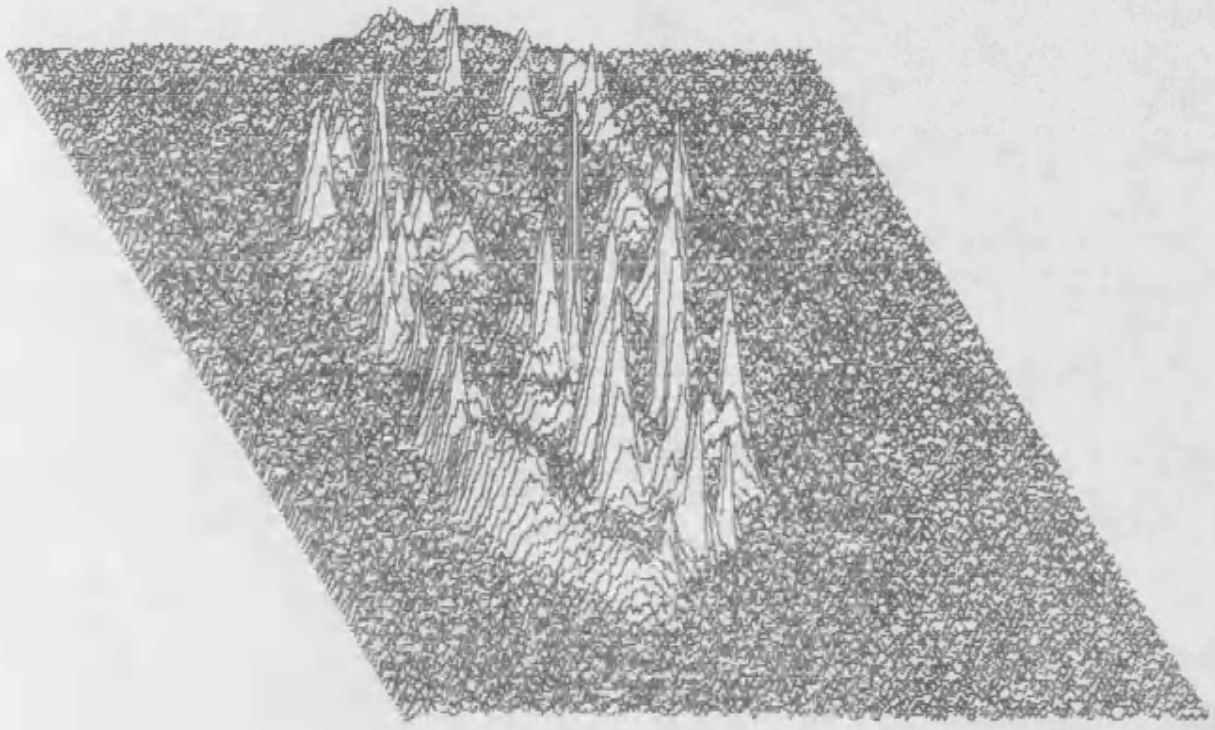

Figure 1.11. Effect of low level white noise. Isometric projection of the brightness of the digitised image shown in Figure 1.9 after the addition of low level noise in the range 0 - 3 grey levels.

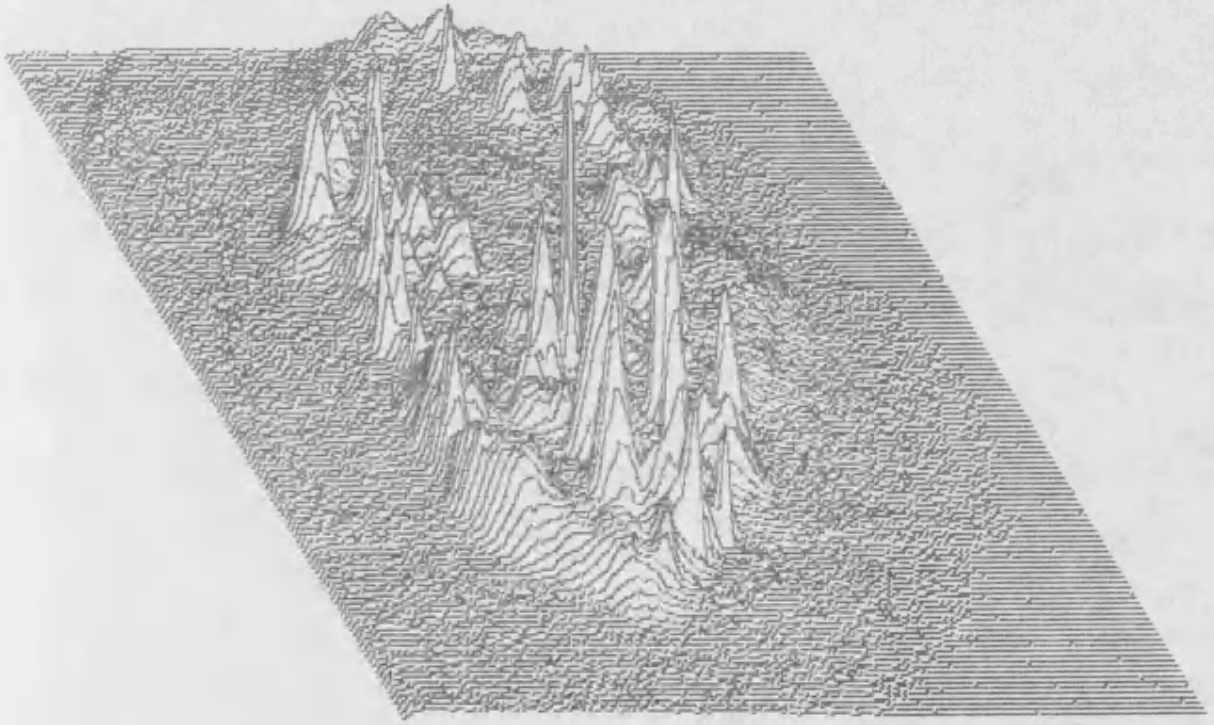

Figure 1.12. Effect of averaging over a number of frames. Isometric projection of a digitised image produced by averaging 32 images of Figure 1.9 each with a different pattern of low level noise as in Figure 1.11.

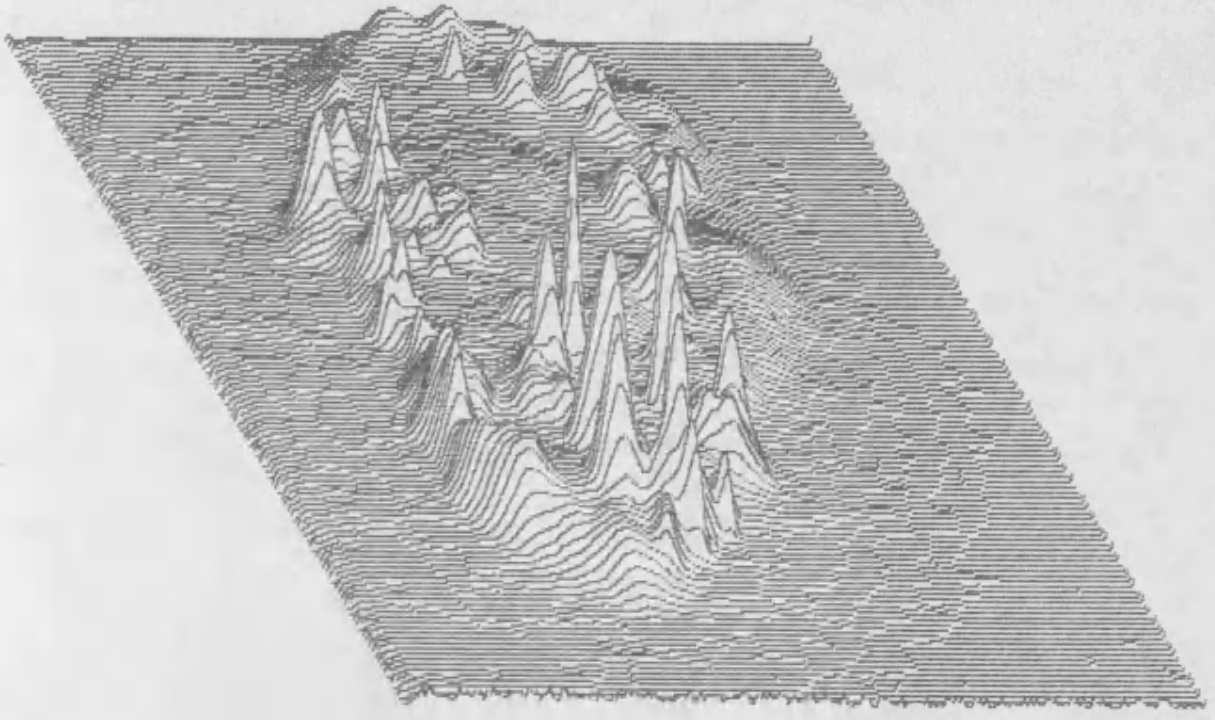

Figure 1.13. Effect of a smoothing transformation. Isometric projection of the digitised image shown in Figure 1.11 (Figure 1.9 with added noise) after four passes of the smoothing transformation described in Chapter 1, 1.6.4. This image should be compared with Figure 1.12.

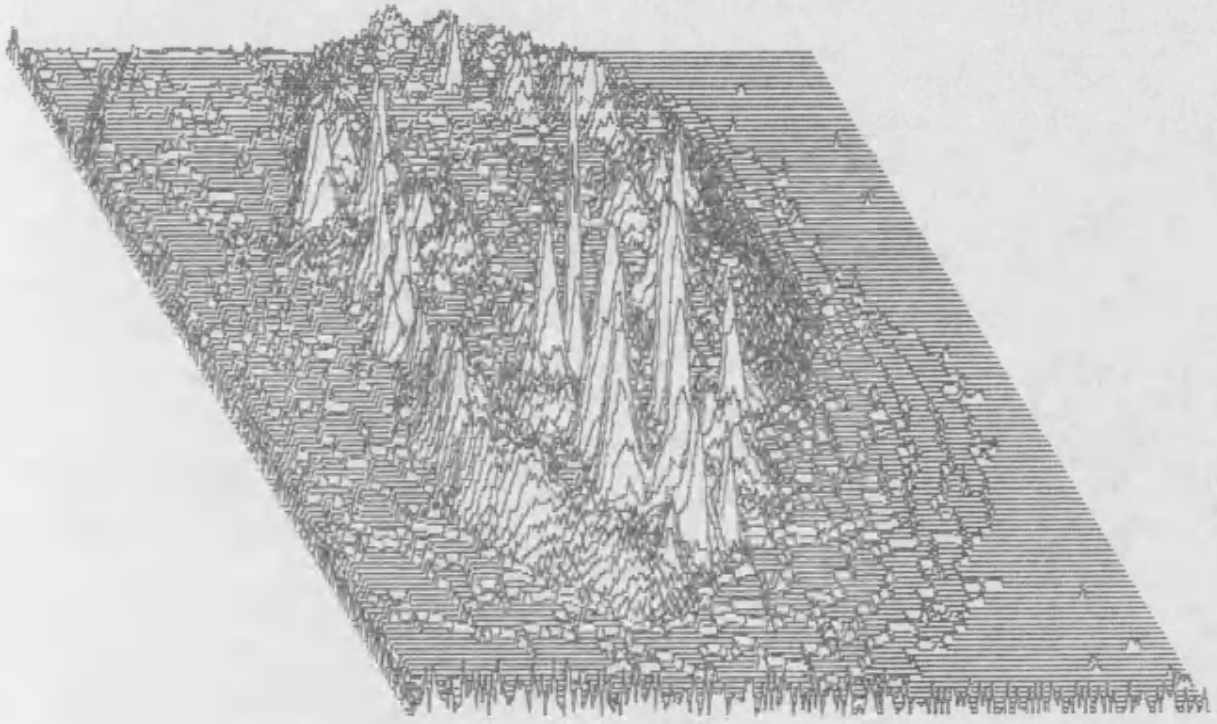

Figure 1.14. Effect of a sharpening transformation. Isometric projection of the smoothed digitised image shown in Figure 1.13 after the application of the Laplacian sharpening transformation described in Chapter 1, 1.6.5

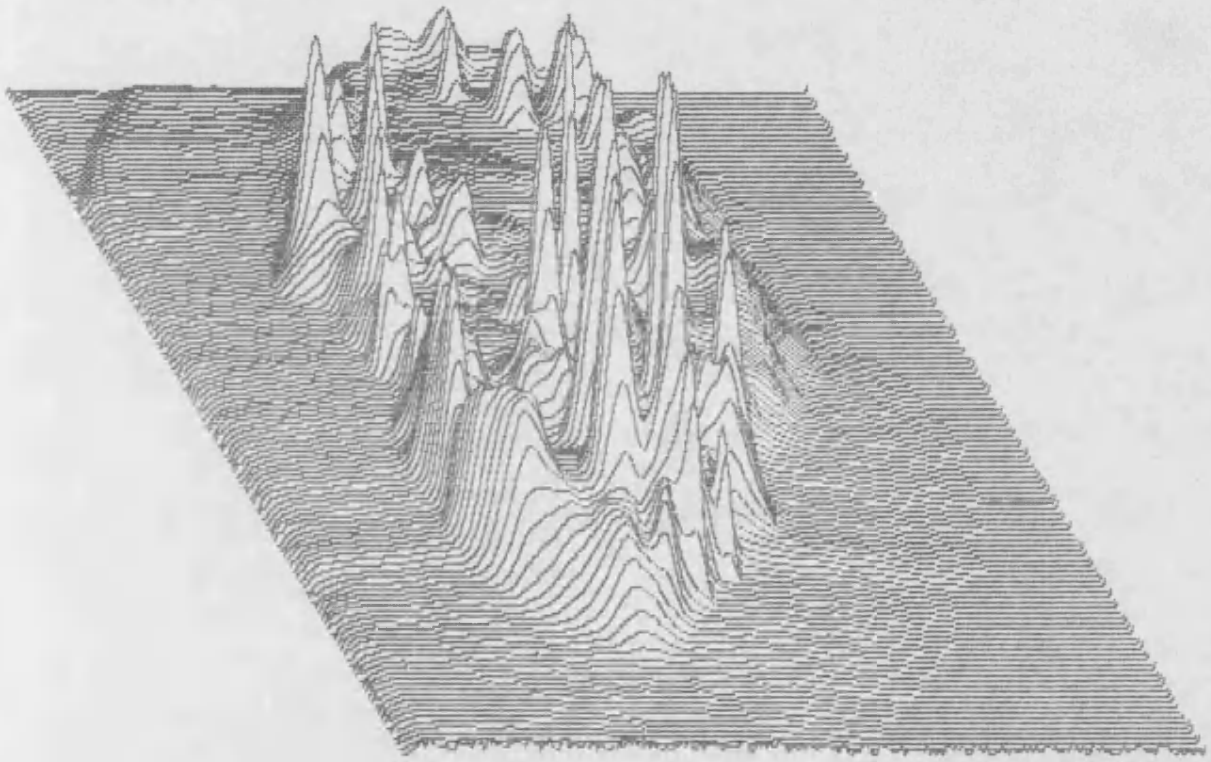

Figure 1.15. Determination of features (method 1). Isometric projection of the image shown in Figure 1.9 after contrast enhancement followed by five application of the smoothing transformation.

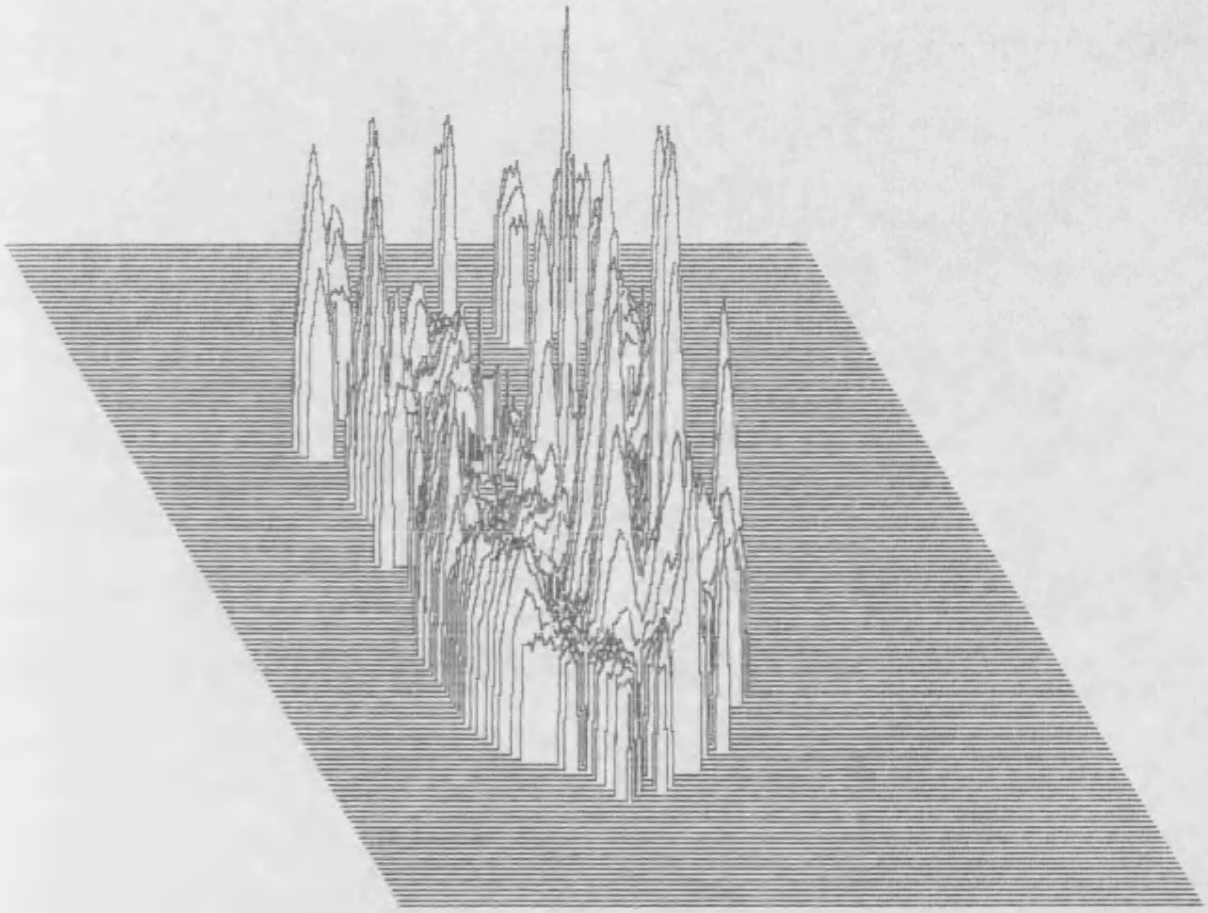

Figure 1.16. Determination of features (method 1). Isometric projection of the digitised image shown in Figure 1.15 after clipping at 40, ie any pixel with a grey level less than 40 has been set to zero. This operation separates the peak areas.

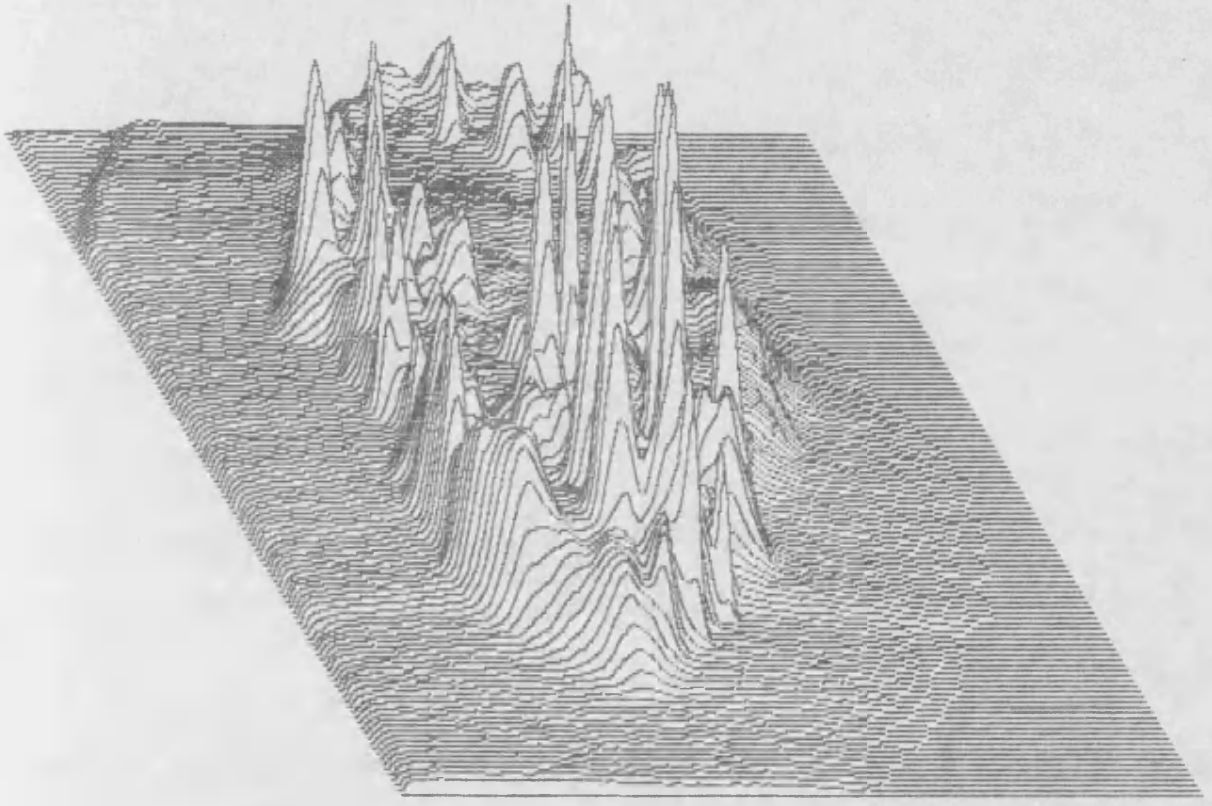

Figure 1.17. Determination of features (method 2). Isometric projection of the image shown in Figure 1.9 after contrast enhancement followed by three passes of the smoothing transformation.

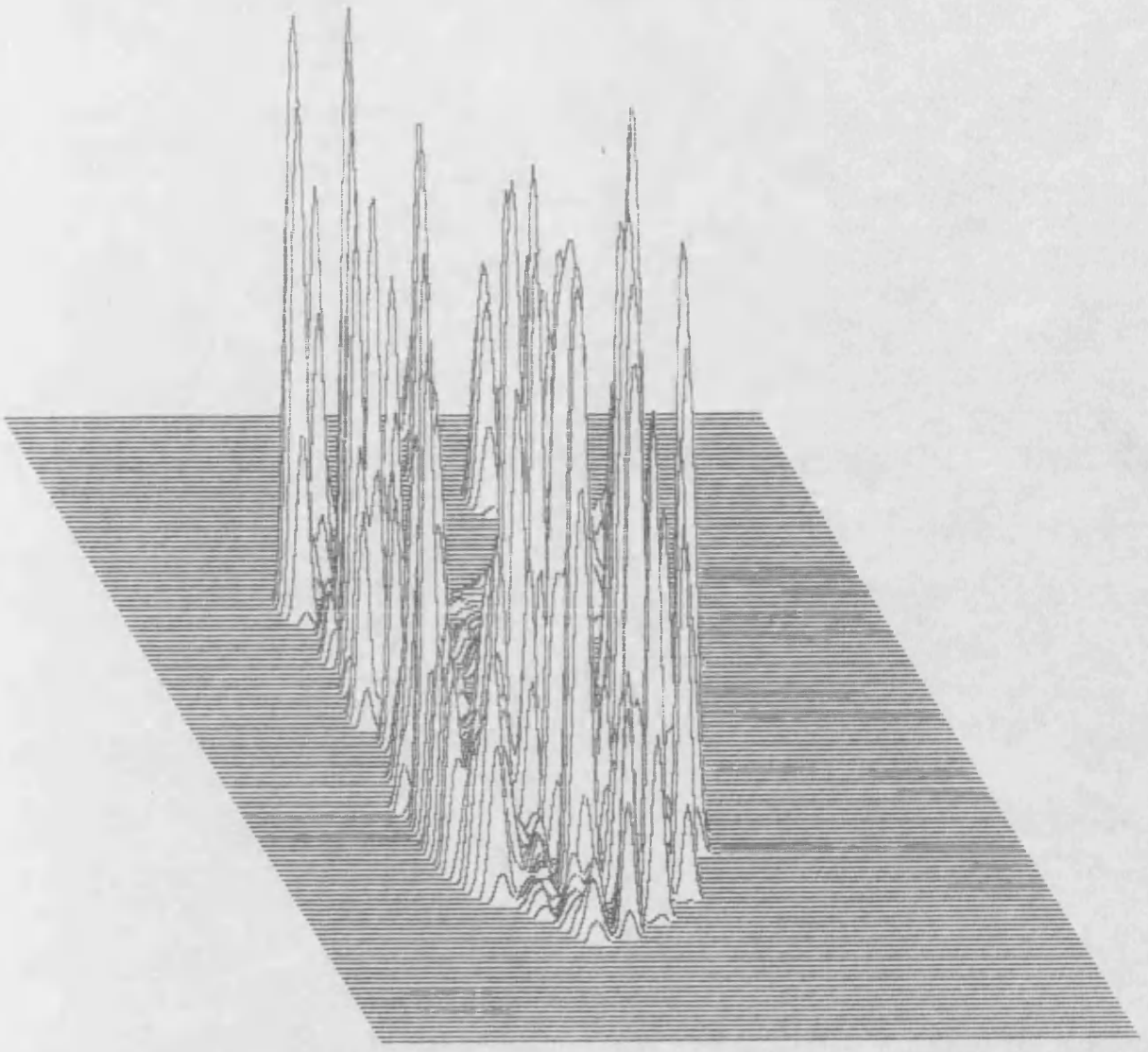

Figure 1.18. Determination of features (method 2). Isometric projection of the digitised image shown in Figure 1.17 after 25 applications of the sequence one pass of the sharpening filter followed by three passes of the smoothing filter. This image should be compared with that in Figure 1.16.

Chapter 2

2. The preparation and stability of thermoelectrets produced from tableting excipients based on cellulose.

The ability to induce a quasi-permanent electrostatic force in a tableting excipient has been proposed as a mechanism for enhancing the adhesion of fine particles to coarse particles during mixing so that formation of stable ordered units can be guaranteed (Chapter 1, 1.4.1). To this end the feasibility of inducing quasi-permanent electrostatic forces in cellulose-based tableting excipients, such as Avicel PH102 and Elcema G250, by means of the thermoelectret effect was studied.

2.1. Materials, apparatus and methods.

2.1.1. Materials.

The materials used for the preparation and investigation of the thermoelectret properties of cellulose based tableting excipients were as follows.

1. Carnauba wax, a material known to produce thermoelectrets and first described for such use by Eguchi (151-158).
2. Avicel PH102, lot 7242, FMC Corporation, Philadelphia, U.S.A., through Honeywill and Stein, London, U.K..
3. Elcema G250, BN D/409165, Degussa GmbH, Frankfurt, FRG.

Carnauba wax was selected as the material for testing the specially constructed apparatus for the production and analysis of thermoelectrets because of its well documented thermoelectret behaviour (151-158, 160-169). Avicel PH102 was chosen for the investigation because it has previously been described as exhibiting thermoelectret properties (as Avi-cel, 144). Elcema G250 was chosen because it was a cellulose based tableting excipient and also for its large particle size (approx 250μm diameter) and regular spheroidal shape. These latter properties were chosen to facilitate the isolation of single ordered units from binary powder mixes. The ability to isolate individual ordered units with relative ease was needed for subsequent investigations of the thermoelectret effect on the interaction between carrier excipients and adherent drug.

2.1.2. Apparatus.

The apparatus used for the manufacture of thermoelectrets and their subsequent analysis was specially designed and constructed for

the production of thermoelectrets using pharmaceutical materials.

2.1.2.1. Apparatus used for preparing thermoelectrets.

The equipment used to prepare thermoelectrets from Carnuaba wax, Avicel PH102 and Elcema G250 consisted of an oven, an extra high tension (EHT) generator (Telemax, insulation test set, IOS/16498, type 115, Telemechanics Ltd), a mercury thermometer and a specially designed and constructed charging cell. A second EHT generator (type HVT 699, Volstatic Ltd, London U.K.) was used to provide an negative charging potential to the charging cell for a small number of experiments.

The charging cell (Figures 2.1-2.3) comprised two identical brass electrodes (Figure 2.1) for air gap charging, an upper brass electrode (Figure 2.2) for contact electrode charging and a PTFE separating ring (Figure 2.3). The inner surface of the brass electrodes (Figure 2.1) was recessed to allow the separating ring to be located accurately when the cell was assembled for use. The separating ring was designed to prevent electrostatic discharge occurring between the brass electrodes when the the high voltage electric field necessary for the charging process was applied.

During the manufacture of thermoelectrets the charging cell was mounted on a cork ring to provide electrical insulation. The lower electrode of the cell was fitted into a recess which prevented the cell from moving off the cork ring due to vibration (Figure 2.4).

The EHT generator was connected to the electrodes of the charging cell by passsing the connecting cables through an air vent in the roof of the oven (Figure 2.5). The insulation of the wires connecting the electrodes of the cell to the EHT generator was propyl rubber. This material was selected because it had the heat and electrical resistance required for use at high temperatures and voltage. The lower electrode of the charging cell was connected to the earthed terminal of the EHT generator and the upper electrode to the positive terminal. The upper electrode of the cell was used to apply the electric field to minimise the possibility of accidental discharge of high voltage electricity to the metal shelves and walls of the oven.

The EHT generator used allowed a maximum measurable electrical potential of +14 kilovolts (kV) with respect to earth to be applied to the upper electrode. Due to the induction of image charge on the

lower, earthed electrode this implies a total potential difference between the upper and lower electrodes of approximately 28kV. A switch mounted on the front panel of the EHT generator allowed a meter to indicate either the applied voltage in kilovolts or the leakage current in microamperes, (μa), due to the applied electric potential.

The mercury thermometer was suspended through the air vent of the oven and used to monitor the temperature of the oven in addition to the oven's built in thermometer. The oven was of a type designed for the heat sterilisation of pharmaceuticals and was therefore capable of maintaining a constant and even temperature thoughout its internal volume. Heat uniformity was assisted by an air-circulating fan built into the oven. Temperature control was provided by an adjustable thermostat mounted outside the oven.

2.1.2.2. Apparatus used for measuring the charge stored in a thermoelectret.

The apparatus used to measure the charge stored in a thermoelectret (Figure 2.6) included a gas chromatograph oven (Perkin Elmer serial no A2310), a temperature programmer (Perkin Elmer, Type 4540040, serial no 24432), an XY/t chart recorder (Type PL4, JJ Lloyd Instruments, Southampton, England), an electrometer (type 610C, Keithley Instruments Inc., Cleveland, Ohio, USA), two thermocouples (type k, chromel-alumel), a discharge cell (specially constructed), metal tripod, cork ring, mercury thermometer, a melting ice/water bath and temperature resistant cable with low impedance which was used to connect the discharge cell to the electrometer.

The discharge cell used to measure the charge stored in any thermoelectrets produced was identical to the standard charging cell (Figures 2.1-2.3). The discharge cell was mounted on a cork ring in the same manner as the charging cell (Figure 2.4). The cork ring and discharge cell were, however, also mounted on the metal tripod to raise the assembly above the air circulating fan of the gas chromatograph oven.

The gas chromatagraph oven used was controlled by a temperature programmer. This arrangement allowed the temperature of the oven to be accurately controlled during the measurement of the charge stored in a thermoelectret, a process which could take several hours. The temperature programmer was used to provide an initial equilibration

period at a known temperature and then a linear temperature rise at a known rate to a predetermined upper limit. This control of the rate of sample heating was necessary to obtain reproducible discharge currents from the thermoelectrets being measured.

The temperature of the discharge cell was monitored using two type k thermocouples. The thermocouples were used in opposition, one junction inserted into the wall of the separating ring of the discharge cell and the other into a melting ice/distilled water mixture. The melting ice/distilled water mixture was used to provide a known reference voltage so that the temperature of the sample could be measured accurately. The output of the pair of thermocouples was checked against reference values (210) by measuring the voltage output of the pair with one junction immersed in a melting ice/distilled water mixture and the other in boiling distilled water.

The electrometer used was capable of measuring several electrical parameters, including voltage and resistance, but was used here in current (electrical) mode as a nanoammeter. The sensitivity of the instrument in current mode was such that it was capable of measuring a current of $1x10^{-14}$ ampere for a full scale deflection of the meter. In general the following settings were used during TSDC measurements:

Mode	:	Fast
Meter	:	Centre Zero
Range	:	$1x10^{-10}$ or $1x10^{-11}$ ampere f.s.d.
Multiplier	:	x1 or x3

The electrometer was used in 'fast' mode as this was suitable for the low currents being measured. In this mode, increases in the capacitance of the system due to transient voltage changes were neutralised very rapidly and did not therefore affect the current being measured and the traces thus obtained.

The use of the metre in 'centre zero' mode allowed the meter to register positive and negative current flows as opposed to only positive or only negative current flows. The magnitude of the electrical parameter being measured, necessary to produce a full scale deflection of the meter, were obtained by multiplying the value of the multiplier switch by that of the range switch. The example setting values given above therefore gave full scale deflections of $1x10^{-11}$ amps, $3x10^{-11}$ amps, $1x10^{-10}$ amps and $3x10^{-10}$ amps, although the latter range was not used.

A full scale deflection of the meter produced a 3 volt signal at the 'output' socket at the rear of the electrometer. This output signal was fully proportional to the value indicated by the meter producing negative voltages when negative values were obtained and even when the meter indicated overrange values.

The XY/t plotter was used in its XY mode to record the output voltages of the thermocouples and electrometer. The scales used by the plotter were given in voltages for a 100mm distance on the plotter bed. The output from the electrometer was connected to the Y input of the plotter and a scale of 2.5 Volt per 100 mm was used. This meant that a full scale deflection of the electrometer produced a pen displacement of 120mm. The thermocouples were connected to the X input of the plotter and utilised scales of 2.5 mV per 100 mm or 5mV per 100 mm depending upon whether Carnauba wax was being measured or Avicel PH102 or Elcema G250. The input signals were arranged so that increasing the temperature (X) produced a pen displacement to the right and a positive movement of the meter needle of the electrometer (Y) produced an upward pen displacement.

The cables used to connect the electrodes of the discharge cell to the electrometer were chosen to minimise problems due to the internal capacitance of the wires, vibration and external electrical fields which would otherwise introduce a high degree of noise into the signal being measured. The insulating material betweeen the signal core and the outer shielding of the cable was PTFE and therefore had excellent electrical insulating properties even at elevated temperatures. The cable itself was taped to firm non-vibrating surfaces to reduce internal triboelectric charging caused by friction due to vibration. The outer shielding braids of the signal cables were connected together and then to an earthing post on the electrometer to provide the same shielding characteristics for both the input signal and its reference. These measures substantially reduced the degree of noise present in the signal over the current ranges used to measure the discharge of thermoelectrets.

2.1.2.3 Punch and die assembly for preparing compressed sample discs from Avicel PH102 and Elcema G250.

The Avicel PH102 and Elcema G250 powders used were compressed into sample discs using a punch and die constructed from mild steel

(Figure 2.7). The die was constructed to the same dimensions as the separating ring used in the charging and discharging cells. The punch and base plate used with the die had flat surfaces on both sides so that the Avicel PH102 and Elcema G250 compacts could be prepared using a hand operated hydraulic press. The reason for manufacturing compacts was solely to allow the powdered material to be handled conveniently. The pressures used during compression were relatively low so that the compacts formed could be repowdered by mild mechanical stress, such as that applied by gently rubbing between thumb and fingers.

2.1.3. Methods.

2.1.3.1. Preparation of blank samples.

Thermoelectrets of carnauba wax, Avicel PH102 and Elcema G250 were produced from discs of the material or powder. When discs were used the method of preparation varied depending upon the material in question.

Carnauba wax discs were formed by pouring the molten wax into a discharge cell that had previously had several layers of aluminium foil sandwiched between the separating ring and the lower electrode to prevent leaks. The molten wax was then placed in a preheated oven at 80°C to 90°C which was then allowed to cool naturally to room temperature. When cool the wax disc was removed and the upper and lower surfaces smoothed. This smoothing was performed by rubbing the wax disc on a sheet of carborundum paper placed on the benchtop. This procedure was necessary to remove the meniscus ring and curvature of the disc induced during cooling thereby promoting better contact between the wax disc and the charging or discharge electrode(s).

Discs of Avicel PH102 and Elcema G250 were prepared by compression in the specially constructed punch and die. The die was mounted on the base plate and then filled with the material to be compressed (a level fill of the die, rather than a weiged amount, was used to assure consistency of fill for each type of material used). The upper punch was then placed on the powder bed and pressed down by hand to partially consolidate the powder bed. The prepared punch and die were then placed in a hand operated hydrualic press, a large, solid, metal cylinder placed on the upper punch to act as a spacer (Figure 2.8), and compressed. The force used to compress the

material was monitored using a loading gauge built into the press. A measured load of approximately one ton was sufficient to produce discs of desired properties using Avicel PH102 whereas five tons was necessary for Elcema G250 (approximately 1 and 5 tonnes). The degree of compression utilised was only sufficient to form discs which could easily be disrupted using very mild mechanical pressure as described above.

When it was necessary to prepare thermoelectrets from powdered Avicel PH102 and Elcema G250 the powder was bulk filled into the discharge cell and then pressed down manually using the upper punch of the punch and die described above. This manual compression was carried out to expel air from the powder bed and prevented spouting during the charging and discharging procedures.

2.1.3.2. The electret forming procedure.

The method used for manufacturing thermoelectrets from carnauba wax was very similar to that used by Eguchi (152, 158). In this case, however, the carnauba wax was softened but not allowed to melt as the construction of the charging cell allowed molten wax to leak. The compressed discs and powder samples of Avicel PH102 and Elcema G250 were charged in the same manner as Carnauba wax, the only differences being the duration of the equilibration period and the charging temperature used.

The blank sample to be charged was placed in the charging cell which was then mounted inside the oven used. The temperature required for the charging procedure was set on the thermostat of the oven and the sample left to heat up. When at the charging temperature, the sample was allowed to equilibrate; for carnauba wax this was a five minute period whereas for Avicel PH102 and Elcema G250 a minimum of thirty minutes was used. In the latter case the upper electrode was not placed on the charging cell until after the equilibration period. This delay was necessary to allow water desorbed from the cellulose substrate (211, 212) to disperse.

The temperature and electric potential were then maintained for one hour. After the hour had elapsed the oven and sample were allowed to cool to room temperature whereupon the electric potential was turned off and the charged sample tested or stored for later use.

When using airgap charging (Figure 2.9) the maximum electric potential applied to charge the sample without inducing corona

dicharge around or onto the sample varied between 10 kV and 14kV. These electric potentials convert to electric field strengths of 1000 kVm^{-1} and 1400 kVm^{-1} (assuming that the earthed electrode has no induced charge).

When using contact charging electrodes (Figure 2.9), the maximum electric potential used to discharge the sample without inducing corona discharge around or onto the sample was lower and much more variable. The electric field strength, however, was dependent upon the thickness of the sample. Thus a 7kV potential applied across a sample whose thickness was 0.4 cm would have been equivalent to an electric field of 1750 kV m^{-1} (7kV/0.004m), again assuming that there was no induced charge on the lower electrode.

2.1.3.3. Measurement of the charge stored in a thermoelectret.

The electrical charge stored in a prepared thermoelectret was measured using thermally stimulated discharge (or depolarising) current (TSDC). The charged sample to be assessed was mounted in the discharge cell which was then placed in the gas chromatograph oven as described above (2.1.2.2.). The sample and discharge cell were then allowed to equilibrate at 25°C (room temperature) for approximately 10 minutes. After the equilibration period, the temperature of the oven was raised at a constant rate of 2°C min^{-1} to the predetermined upper limit (a maximum of 80°C for carnauba wax and 140°C or higher for Avicel PH102 and Elcema G250). The duration and temperature of the equilibration period, heating rate and upper temperature limit were controlled by the temperature programmer. The upper temperature limit was maintained for approximately twenty minutes to allow the contents of the discharge cell to equilibrate. The temperature of the discharging sample was monitored using a thermocouple, so as to allow accurate discharge current vs temperature traces to be obtained.

2.1.3.4. Linearity of the heating rate in the TSDC oven and discharge cell.

The linearity of the heating rate of the chromatograph oven used for TSDC measurements was checked by recording the temperature increase at a rate of 2°C min^{-1} using the XY/t chart recorder in Y/t mode. The temperature of the oven was monitored by the same thermocouple arrangement as that used during TSDC measurements.

To ensure that the temperature within the discharge cell was also linear the same procedure was carried out using the thermocouple inserted inside the empty discharge cell.

The temperature range over which the linearity of the heating rate was measured was 25°C to 140°C. The heating rate, temperature limits and initial equilibration period were also determined using appropriate settings on the temperature controller.

2.1.3.5. Initial testing of the TSDC apparatus.

The baseline stability and sensitivity of the apparatus used for measuring the TSDC of charged samples was determined using an empty discharge cell, PTFE discs similar in size to the sample discs, blank carnauba wax samples and charged carnuaba wax samples.

TSDC was performed on an empty discharge cell (airgap electrodes only) to determine the linearity of the baseline and to determine the response of the empty discharge cell.

TSDC was performed on a blank PTFE disc using both airgap and contact electrodes to determine the effect of the presence of a sample in the discharge cell.

TSDC was performed on carnauba wax discs that had been deliberately discharged by exposure to the electret forming procedure whilst omitting the application of an electric potential. The discharged discs were used within thirty minutes of their cooling to room temperature. Blank carnauba wax discs were used to examine the effect on the baseline of a discharged sample of a known thermoelectret. Both air gap and contact electrodes were used during TSDC.

TSDC was performed on carnuaba wax discs that had been exposed to the full electret charging procedure. This was done to check the response of the TSDC apparatus using a known thermoelectret and to provide traces that could be compared against those presented in the literature (166, 168).

2.1.3.6. Manufacture and TSDC of thermoelectrets manufactured from Avicel PH102 and Elcema G250.

Samples of Avicel PH102 and Elcema G250 were subjected to the electret forming procedure in a number of distinct ways.

1. A sample of the powder was placed in the discharge cell and the resulting powder bed compressed by hand as described above.

TSDC was then performed on the uncharged powder.

2. A sample of the powder was placed in the discharge cell and the resulting powder bed compressed by hand as described above. The powder bed was then exposed to the electret forming procedure in the discharge cell. When cool, the discharge cell assembly was transferred intact to the TSDC apparatus to prevent any disturbance of the charged powder bed and TSDC performed.
3. A sample of the unprocessed powder was placed in the charging cell and the resulting powder bed compressed by hand. The powder bed was then exposed to the electret forming procedure in the charging cell. When cool, the powder was transferred to the discharge cell, ensuring that the charged powder bed was thoroughly disturbed in the process to randomise the orientation of any aligned dipoles present. The transferred powder was then compressed by hand in the discharge cell and TSDC performed.
4. An uncharged compact was placed in the discharge cell and TSDC performed.
5. Compacts were charged using the electret forming procedure described above. The charged compact was then reduced to powder using a glass pestle and mortar. The resulting powder was placed in the discharge cell and compressed by hand. TSDC was performed on the resulting powder bed.
6. Compacts were charged using the electret forming procedure described above. TSDC was performed on the charged thermoelectrets immediately they had cooled to room temperature and also after storage.

TSDC was carried out using both air gap and contact electrodes so that differences, if any, between the two techniques could be differentiated.

2.1.3.7. The effect of low relative humidity on the charge stability of thermoelectrets manufactured from Elcema G250.

Environments with very low relative humidities were provided by using desiccators that either contained activated silica gel in vacuo or in which air was dried by phosphorous pentoxide. The stored thermoelectrets were also tightly wrapped in aluminium foil to reduce the possibility of accidental contamination with atmospheric moisture when the desiccators were opened to remove a sample for testing. Samples were removed from the low relative humidity atmosphere at

known intervals and subjected to TSDC to determine the charge stored.

2.1.3.8. The effect of humidity on the stability of thermoelectrets manufactured from Elcema G250.

Environments of 55% relative humidity were provided using desiccators containing a reservoir of a saturated solution of sodium nitrate (213). The relative humidity of the atmosphere generated at 30°C was measured using a hair hygrometer. The stored samples were not wrapped in aluminium foil so that atmospheric moisture in the desiccator could equilibrate with the stored thermoelectrets. Samples were removed at known intervals and TSDC performed to determine the charge stored.

2.2. Results.

2.2.1. Calibration of the thermocouples used to measure temperature inside the TSDC oven.

The voltage produced by the thermocouple was measured using the XY/t recorder with ranges of 2.5mV $100mm^{-1}$ and 5.0mV $100mm^{-1}$. The pen displacements measured for an effective temperature difference of 100°C were 164 mm for the former range and 82mm for the latter. Both of these displacements corresponded to voltages of 4.1mV for the 0°C-100°C temperature range. This was in very good agreement with the literature values (210).

2.2.2. Fluctuations in the applied electric field during the electret charging procedure.

Measurement of the applied electric field during the manufacture of a thermoelectret showed that the voltage reduced to a minimum value after approximately 20 minutes and then increased to slightly more than than the preset value as the temperature increased (Table 2.1, Figure 2.10). This phenomenon was observed only when using cellulose based samples for the thermoelectret forming procedure that had not been previously dried and where the electric field used was applied immediately rather than when the sample had equilibrated to the charging temperature.

The changes in the applied charging potential were correlated with the temperatures within the oven and sample by measuring the temperature of the sample and oven with an electronic thermometer (hand held electronic thermometer with electronic cold junction).

Plotting the change in the applied voltage with time for Avicel PH102 compacts (Tables 2.1, Figure 2.10) showed that a minimum period of 30 minutes was necessary to allow the applied voltage to return to its initial value. A sample of Avicel PH102 that had been dried at 120°C for two hours prior to charging (Table 2.2, Figure 2.11) did not exhibit any significant drop in the applied voltage during charging. Plotting the sample temperature and oven temperature against time showed that the sample temperature lagged significantly behind that of the oven (Table 2.3, Figure 2.12).

Plotting the change in the applied potential against the temperature of the oven and the sample (Table 2.3, Figure 2.12) confirms the hypothesis that the change in the applied voltage is due to the release of water bound physically to the cellulose molecule.

2.2.3. Linearity of the heating rate of the TSDC oven.

The heating rate of the gas chromatograph oven used for the TSDC measurements and a test sample were measured using the reverse biased thermocouple pair referenced against a distilled water/melting ice mixture. The heating rate of the oven was found to be very linear when controlled by the temperature programmer (Table 2.4, Figure 2.14). The temperature rise inside the discharge cell was also found to be acceptably linear, the only deviation occurring during the inital and final heating period (Table 2.4, Figure 2.14). The initial non linear response of the discharge cell relative to the oven temperature meant that the temperature inside the discharge cell was always lower than that of the oven. The upper limit of the temperature programmer had been set for 140°C, in both cases this was the maximum temperature reached. It should be noted that the temperatures inside the oven and the sample were not measured simultaneously but on two separate occasions as only one thermocouple pair was available.

2.2.4. Initial testing of TSDC apparatus.

The initial testing of the TSDC discharge cell was carried out using air gap electrodes and an empty cell. The typical trace obtained from this arrangement (Figure 2.15) was very flat with a small amount of random noise. This noise was attributed to the cell and connecting cables vibrating slightly due to the action of the air circulating fan within the oven.

The effect of a known blank sample (a PTFE disc) was examined by performing TSDC using airgap electrodes and contact electrodes. Typical traces obtained (Figures 2.16, 2.17) were very simiar to the empty cell, the traces obtained being very flat with a small amount of random noise due to the vibration of the discharge cell and connecting cables.

TSDC was performed on carnauba wax blanks, using both air gap and contact electrodes, to assess the response of the discharge cell to a non charged sample of a material with known thermoelectret properties. Typical traces obtained (Figures 2.18, 2.19) were not as flat as those obtained for the empty cell or the PTFE blank, an upward displacment of the trace being obtained in both cases. The deviation from the flat base line was observed to be very severe for the contact electrode traces as the temperature increased.

TSDC of charged samples of carnauba wax were obtained using only air gap electrodes to avoid the excessive tailing observed when using contact electrodes. The typical trace obtained (Figure 2.20) consisted of two peaks, the first being a positive displacement and the second being a negative displacement. These two peaks indicate that current flow in opposite directions has occured during discharge of the thermoelectret.

The traces obtained using charged carnauba wax samples confirmed that the apparatus assembled for measuring the charge stored in thermoelectrets functioned correctly and was sufficiently sensitive to allow the measurment of discharge currents greater than $5x10^{-13}$ amperes. The type of TSDC trace obtained for the charged samples of carnauba wax and the magnitude of the discharge currents obtained were in good agreement with reported values (166, 168).

2.2.5 Initial examination of the thermoelectret properties of Avicel PH102.

The response of the TSDC apparatus to a cellulose based material, Avicel PH102, with known thermoelectret properties (144) was tested using air gap electrodes. Samples of fresh, dried and charged Avicel PH102 were used for this investigation.

Examination of Avicel PH102 in the powdered form in which it was supplied (Figure 2.21) produced a very flat trace showing no detectable current flow.

Examination of Avicel PH102 powder that had been dried (Figure

2.22) and had TSDC performed on the undisturbed powder bed generally produced a small positive peak. This observation was difficult to reproduce consistently, although its magnitude and duration imply that it is unlikely to be a random event.

Examination of Avicel PH102 powder that had been charged and discharged with no disturbance of the powder bed produced a small positive displacement (Figure 2.23). This event was again difficult to reproduce consistently.

Examination of Avicel PH102 powder that had been charged and then had the powder bed disturbed before TSDC produced a flat trace indicating little or no discharge currrent (Figure 2.24).

Examination of Avicel PH102 compacts that had dried prior to TSDC again produced a flat trace indicating little or no discharge current (Figure 2.25).

Examination of Avicel PH102 compacts that had been charged (ie Avicel PH102 thermoelectrets) produced traces very similar to those obtained for Carnauba wax thermoelectrets. A typical trace (Figure 2.26) consisted of two peaks, the first, a positive displacement, occurring around 45°C-55°C and the second, a negative displacement, occurring at around 72°C-82°C.

Examination of charged compacts that had been repowdered in a glass pestle and mortar produced flat TSDC traces showing little or no discharge current (Figure 2.27).

2.2.6. Effect of compact thickness on the TSDC of Avicel PH102 using air gap electrodes.

The magnitude of the two peaks obtained during TSDC of Avicel PH102 appeared to be variable. In an attempt to eliminate one possible variable a series of samples of differing thickness were charged using approximately the same electric field. The compact thicknesses used were 1.3mm, 2.95mm, 4.3mm and 5.8mm and the corresponding electric fields applied during the charging process were 1540 kVm^{-1}, 1360 kVm^{-1}, 1400kV m^{-1} and 1380kV m^{-1}. The traces obtained for these compacts (Figures 2.28-2.31) show that as the thickness of the compact increases so does the magnitude of the discharge peaks. A second effect that was observed was that the position of the peaks were shifted to the right, that is, as the thickness of the compacts were increased the temperature at which the peak was obtained was increased.

2.2.7. Initial examination of the thermoelectret properties of Elcema G250.

The initial thermoelectret properties of Elcema G250 were examined using both air gap electrodes and contact electrodes during TSDC.

TSDC of Elcema G250 compacts produced very different results for the two types of electrode arrangement. The contact electrodes (Figures 2.32, 2.33) produced a massive positive displacement which remained off scale for a considerable period of time. TSDC of Elcema G250 compacts that had been previously dried produced very flat traces with contact electrodes (Figure 2.34), a small positive displacement appearing only at the extreme upper end of the temperature range used.

TSDC of unprocessed Elcema G250 using air gap electrodes (Figure 2.35) produced a very flat trace indicating the presence of little or no discharge current.

Air gap TSDC of charged Elcema G250 thermoelectrets that had been repowdered using a glass pestle and mortar produced a relatively flat trace indicating little or no discharge current (Figure 2.36).

Elcema G250 thermoelectrets were charged using either a positive or a negative potential applied to the upper electrode whilst the lower electrode was earthed. Air gap TSDC of the thermoelectrets formed, using the negative potential, were found to have reversed profiles (Figure 2.37) when compared to thermoelectrets formed using the positive potential (Figure 2.38).

Themoelectrets formed from Elcema G250 using either a positive or a negative applied potential as above were produced and then stored under ambient conditions, wrapped in aluminium foil, for approximately 15 hours. TSDC of these thermoelectrets, using air gap electrodes, again showed that peaks obtained using a negative forming potential (Figure 2.39) were opposite to those obtained using a positive forming potential(Figure 2.40). A further effect observed was that the traces obtained after storage showed only a single peak rather than a peak in both positive and negative regions as had previously been obtained.

TSDC was performed on thermoelectrets that had been exposed to ambient atmospheric conditions for a minimum of 20 hours. The trace obtained for the thermoelectret (exposed 20 hours) examined using

contact electrodes (Figure 2.41) produced a massive positive displacement similar to that obtained using unprocessed Elcema G250 (Figures 2.32, 2.33). The trace obtained for the thermoelectret (exposed 30-40 hours) examined using air gap electrodes (Figure 2.42) was very flat indicating very little or no discharge current.

2.2.8. TSDC of Elcema G250 thermoelectrets stored in a low humidity environment.

Thermoelectrets made from Elcema G250 were stored wrapped in aluminium foil in one of two low humidity environments. Samples were stored for known intervals and then examined using TSDC with contact electrodes. This method was chosen because it produced discharge peaks that were less likely to be affected by the thickness of the thermoelectret being examined. Furthermore, the emergence of a tailing peak could be used to assess the extent to which moisture adsorption had occurred.

The first low humidity environment was provided by drying air with phosphorous pentoxide in a desiccator. Samples exposed to this environment were examined after 1, 25, 72, 114, 408, 499, 503, 576, 957 and 1370 hours (Figures 2.43-2.52). The magnitude and position of the two peaks for these thermoelectrets are given in Table 2.5. The TSDC traces showed that there was a slow decline in the size of the discharge current with time. This observation implies that the amount of charge stored by the thermoelectret decreased with time. No attempt was made during storage to indicate the orientation in which the thermoelectrets were charged. Consequently it was possible for the TSDC traces obtained to have either positive or negative first peaks with the second peak being opposite to that of the first. A further point to note is that the tailing peak is also orientation sensitive. This effect is contrary to that expected from observations of the uncharged material.

The second low humidity environment was provided by storage over silica gel in a vacuum. Samples exposed to this environment were examined after 0, 70, 107, 214 and 663 hours (Figures 2.53-2.57). The magnitude and position of the two peaks obtained are given in Table 2.5. The TSDC traces obtained again showed that the magnitude of the peaks decreased with time, however, the appearance of a tailing peak, presumed to be due to the adsorption of moisture, was more pronounced than that obtained for thermoelectrets stored over

phosphorous pentoxide.

2.2.9. TSDC of Elcema G250 stored in an environment of 55% relative humidity.

Thermoelectrets of Elcema G250 were stored exposed to a relative humidity of 55% at a temperature of 30°C. Samples were removed at known intervals and TSDC performed using contact electrodes. The first sample examined after storage for 2 hours 30 minutes (Figure 2.58) showed that the stored charge had been completely removed, the trace obtained being similar to that of the original material.

2.3. Discussion.

2.3.1. Fluctuations in the applied electric field during charging.

When compacts of Avicel PH102 were first used to produce thermoelectrets, the procedure followed was exactly the same as that used for carnauba wax, apart from the higher temperature employed. During the early stage of the charging procedure, as the sample was being heated up, it was noted that the applied electric potential was reduced significantly. When the oven, and hence the sample being charged, reached the maximum operating temperature the reduced electric potential gradually increased until it was slightly greater than the original starting electric potential. This is the effect demonstrated in Figures 2.10 and 2.13. If the Avicel PH102 compact was dried before use, by exposing it to a temperature of 120°C for several hours, the above effect disappeared (Figure 2.11). In addition, the minimum value attained by the electric potential was found to occur when the temperature of the sample in the cell was in the approximate range of 90°C to 100°C.

The reduction in the applied potential during the heating period is due to a number of electrical and physical effects caused by the release of adsorbed water. In cellulose based materials the desorption of physically bound water can occur up to 150°C (211, 212) and is therefore certain to occur during the heating up period experienced during the production of a thermoelectret. The most common effects likely to occur due to the release of bound water are condensation and consequently droplet charging, changes in the conductivity of the cellulose substrate due to the presence of unbound moisture and an increase in the number of water molecules in the atmosphere inside the cell.

The presence of free moisture in the atmosphere, on the surface of the cellulose matrix and on internal surfaces of the discharge cell would provide the paths necessary for conduction through the cell. This conduction would reduce the maximum potential attainable as observed. The sustained heating would certainly be sufficient to vapourise any free or bound moisture present in the cell which would then leak out of the cell. If applied for a sufficiently long period most of the freed water present in the cell would escape therby removing the mechanisms for current flow through the cell. Eventually, when equilibrium is reached, the leakage current will be reduced to a minimum because most of the available water molecules will have left the charging cell. This corresponds to a recovery in the maximum applied electric potential as observed. It should be noted that a small leakage current will persist even when equilibrium is reached due to the presence of very low levels of atmospheic moisture ramaining in the cell and also due to ionic conduction within the cellulose matrix itself (214).

2.3.2 Initial testing of TSDC apparatus.

TSDC involves the measurement of electrical currents that are typically less than $1x10^{-9}$ amps. When measuring electrical currents of this, or lower, magnitude it is necessary to take steps to ensure that the apparatus is effectively screened from changes in external electric fields. Furthermore, any junctions in the measuring circuit that are heated (ie the connections to the brass electrodes of the discharge cell) should not act as thermocouples as a resut of the Seebeck effect (75). It was for these reasons that a very low impedance cable was used, the shielding of the cables connected to earth and the cables secured to reduce electrostatic charging due to friction inside the cable.

TSDC of the empty discharge cell (Figure 2.15) showed that the precautions that had been taken were sufficient to produce a flat response from the apparatus used. A low level of noise was present on the signal which was due either to the alternating current in the heating coils of the oven or due to vibration caused by the air circulating fan of the chromatograph oven. The response of the chart recorder to these sources of electrical noise was evident as a very small amount of pen vibration. For the sake of clarity, this noise is not reproduced in the TSDC traces shown.

A more severe source of noise on the TSDC signal was vibration of the oven due to an incorrectly balanced air circulating fan. Vibration of the oven caused both the electrodes and the connecting cables to vibrate with a corresponding increase in signal noise. This problem was resolved by replacing the fan rotor with one that caused less vibration.

The flatness of the TSDC response measured with a full scale deflection of $1x10^{-11}$ amps (Figure 2.15) showed that the apparatus assembled was acceptable. The use of a PTFE disc was designed to test the discharge cell for any thermoelectric response when the contacts with the electrodes of the discharge cell were asymmetric. The presence of the PTFE sample in contact with only one of the electrodes (Figure 2.16) and then in contact with both electrodes (Figure 2.17) showed that the the presence of an insulator did not change the response of the discharge cell. The TSDC traces obtained using blank carnauba wax samples (Figures 2.18, 2.19) were similar to those obtained for the PTFE disc.

The main difference between carnauba wax and the empty discharge cell and discharge cell with PTFE blank (using air gap charging) was that a very slight degree of curvature was noted in the TSDC trace for carnauba wax. Furthermore a very rapid rise in the discharge current at the upper end of the temperature range used was noted in the case of contact electrode TSDC. It was assumed that this effect was due to the release of water from the wax matrix or surface melting, however, these hypotheses were not tested.

TSDC of carnauba wax thermoelectrets produced the classical response. The ability to compare the TSDC behaviour of carnauba wax in the TSDC apparatus used here with that reported by other workers (156-166) was the main reason for using this material. This comparison was successful as it showed that the apparatus assembled for performing TSDC on thermoelectrets was functioning as required.

2.3.3. The thermoelectret response of Avicel PH102.

The use of powdered and compressed Avicel PH102 was an attempt to discover if the thermoelectret charge induced was due to the alignment of dipoles, the introduction of a space charge or both. Samples of Avicel PH102 that had been compressed, charged and then examined using TSDC (Figures 2.26, 2.28-2.31) showed that it was possible to form thermoelectrets and measure the discharge current.

The assumption was made that if the thermoelectret charge was

due to the presence of oriented dipoles then disruption of the powder bed would produce a random alignment of the individual particles. TSDC of such a sample would then show no evidence of a peak because the dipoles would no longer be aligned in a uniform manner. If however the TSDC peak was due to the presence of a trapped space charge then disruption of the powder bed would not affect the peak as its appearance would not be dependant on the orientation of the particles in the powder bed.

Air gap TSDC of unprocessed Avicel PH102 showed that the discharge current was negligible as expected ((Figure 2.21). When the Avicel PH102 was dried and TSDC performed on the dried sample without the powder bed being disturbed a small peak around 50°C to 60°C appeared (Figure 2.22). This effect was also observed for charged samples where TSDC was performed without disturbing the powder bed (Figure 2.23). If the powder bed was disturbed after charging the peak at 50°C to 60°C was not observed (Figure 2.24). These observations indicate that a component of the electret effect in Avicel PH102 was due to the presence of an aligned dipole.

All of the above TSDC experiments were performed using air gap electrodes and performed prior to the study which showed that atmospheric moisture could affect the charge stored in a thermoelectret. For this reason, the above data is only meaningful when used to demonstrate that cellulose based tableting excipients can form thermoelectrets, thereby proving the hypothesis which the experiments were designed to test. It is also worth noting that several authors have reported peaks in the 50°C to 60°C temperature range for other types of cellulose (142, 143, 144, 148).

2.3.4. Effect of thermoelectret thickness on the discharge current measured during air gap TSDC.

The repeatability of air gap TSDC traces obtained from samples used immediately after charging was poor. It was considered that this effect may have been due to differences in sample thickness. This hypothesis was investigated by producing thermoelectrets from Avicel PH102 compacts with different thicknesses. The results (Figures 2.28-2.31) demonstrated that varying the thickness of the sample affected the magnitude of the discharge currents obtained in a proportional manner (assuming that the electric field used to charge the thermoelectrets was maintained at a constant magnitude). This

result was probably due to the inverse relationship between sample thickness and the distance of the upper surface of the sample from the upper electrode of the air gap discharge cell.

The electret/conductor system can be considered to be a form of a capacitor. Such a system differs from a true capacitor because the circuit is 'open' on the side of the conductor, this being connected to ground potential rather than a source of e.m.f. such as a battery. The presence of a fixed charge on the electret will cause a charge of opposite sign to be induced in the electrode of the TSDC cell. Consequently, changes in the charge on the electret will be reflected by a change in the charge on the electrode of the TSDC cell, although the converse is not true. The potential difference between the electret and the electrode of the TSDC cell can thus be seen to be partially dependent on the amount of charge induced on the electrode.

The capacitance of a true parallel plate capacitor can be defined by two equations (Appendix 1),

$$C = Q/V \qquad (2.1)$$

and

$$C = \varepsilon A/l \qquad (2.2)$$

where C = capacitance of the capacitor.

Q = charge on the upper surface of the electret.

V = potential difference between the plates of the capacitor.

ε = product of the relative permittivity of the medium between the plates of the capacitor and the permittivity of free space.

A = cross sectional area of the capacitor.

l = distance between the plates of the capacitor.

Eliminating C from equations 2.1 and 2.2 gives

$$Q = \varepsilon AV/l \qquad (2.3)$$

As the potential differnce across the electret/electrode system is partially dependent on the charge induced on the electrode it can be deduced from equation 2.3 that increasing l will decrease both Q and V and that increasing decreasing l will increase Q and V.

As the total amount of charge induced in the electrode of the TSDC cell is reduced with increasing distance from the electret any changes in the charge on the electret will produce correspondingly smaller changes in the charge on the electrode and

hence a smaller current flow. Thus, for a given change in the charge on the electret, the further away the electrode is from the electret, the smaller will be the current flow generated by that change.

Thus, for the air gap discharge cell, the discharge current measured during TSDC will be inversely proportional to the distance between the upper surface of the thermoelectret and the lower surface of the upper electrode of the discharge cell. This was the effect observed (Figures 2.28-2.31).

2.3.6. Thermoelectret response of Elcema G250.

Elcema G250 was used because its relatively large particle size and spheroidal shape allowed individual ordered units to be handled more easily during the investigation of the effect of the thermoelectret charge on interparticle adhesion (Chapter 4). Figures 2.32 to 2.34 show the difference between air gap TSDC and contact TSDC for unprocessed compacts of Elcema G250. The extremely large peaks observed in Figures 2.32 and 2.33 were considered to be due to the desorption of physically bound water. However, it is also possible that the presence of high levels of water vapour at elevated temperatures might chemically react with the brass of the electrodes to provide the current detected. This hypothesis is supported to some extent by the observation that the inner surfaces of the electrodes were always badly discoloured after using unprocessed Avicel PH102 or Elcema G250 (hence the reason for regularly cleaning the electrodes with Duraglit). This effect, however, was not investigated, merely controlled, as most of the Elcema G250

thermoelectrets produced had been severely dried due to the heating during the thermoelectret production process.

TSDC of non-dried Elcema G250 using air gap electrodes showed little or no discharge current during TSDC (Figure 2.35). Repowdered charged thermoelectrets (Figure 2.36) also showed little or no discharge current when examined by air gap TSDC.

Elcema G250 compacts were charged using upper electrodes with either positive or negative potentials relative to earth potential. When these compacts were examined using air gap TSDC those samples charged using the negative potential were found to have peaks in the same places but with opposite sign to those samples charged using a positive potential (Figures 2.37, 2.38). This effect was maintained after storage for approximately 15 hours even though the shape of the traces had changed from a double to a single peak.

Thermoelectrets of Elcema G250 that were exposed to atmospheric conditions overnight or longer completely lost any charge stored in them. This was demonstrated for both contact electrode TSDC (Figure 2.41) and airgap electrode TSDC (Figure 2.42). This observation supports the hypothesis that atmospheric moisture can affect the charge stored in a thermoelectret as discussed above. The effect of atmospheric moisture on cellulose charging suggests that hydrogen bonding between the cellulose molecules may play some part in the formation of the thermoelectret (215). In addition the dependence of the sign of the TSDC peaks on the orientation of the electret during TSDC further supports the hypothesis that there is an aligned dipole component associated with the electret effect in cellulose.

2.3.7. Charge storage in Elcema G250 thermoelectrets exposed to low humidity environments.

To test the hypothesis that the adsorption of atmospheric moisture by the cellulose substrate of Avicel PH102 and Elcema G250 was the cause of charge loss, thermoelectrets were stored in atmospheres very low in humidity. To further reduce the risk of accidental contamination by moisture the charged thermoelectrets were also tightly wrapped in aluminium foil. Two low humidity environments were used, the first provided by air at standard temperature and pressure dried by phosphorous pentoxide and the second created by evacuating a desiccator containing activated silica gel.

In both cases the duration of charge storage was significantly increased (Figures 2.43 - 2.52 for electrets stored in air dried by phosphorous pentoxide, Figures 2.53 - 2.57 for electrets stored under vacuum), the longest period measured being 1370 hours (approx 57 days) for a thermoelectret stored in air dried by phosphorous pentoxide (Figure 2.52).

Charge storage did not remain constant throughout the storage period but slowly diminished as demonstrated by the reduction in the magnitude of the discharge peaks observed (Table 2.5). The reduction in the stored charge was matched by the slow emergence of the tailing peak due to the adsorption of atmospheric moisture, the source of which was due to probably leakage through the seal of the desiccator.

The data obtained for the two dry atmospheres further supports the hypothesis that the adsorption of atmospheric moisture caused a reduction in the stored charge of thermoelectrets directly exposed to normal atmospheric conditions.

A further point to note is that the charging orientation of the thermoelectrets used for the above analyses were not deliberately recorded. TSDC was therefore carried out on thermoelectrets that had the same orientation as when charged and also on some which would have been "upside down". When TSDC was obtained from an "upside down" thermoelectret the trace obtained was inverted (eg Figure 2.48 in Figures 2.43 to 2.52). Furthermore the tailing peak, presumed due to the adsorption of atospheric moisture, also shows sign reversal. This result is unexpected and no attempt was made to investigate the effect in detail.

2.3.8. Charge storage in Elcema G250 thermoelectrets exposed to a relative humidity of 55%.

The relative humidity used in this series of experiments was provided by storage over a saturated solution of sodium nitrate at 25°C to 30°C (213). Samples stored in this environment were not wrapped in aluminium foil to assist the penetration of atmospheric moisture into the body of the thermoelectrets. The result of such storage was invariably a rapid loss in the charge stored in the thermoelectret as shown in Figure 2.58 (storage for 2.5 hours). Again this result supports the hypothesis that the adsorption of atmospheric moisture can affect the charge stored in a cellulose based thermoelectret. The rapid discharge of the electret due to the

presence of high levels of atmospheric moisture would seem to definitely indicate that the electret effect in cellulose is associated with hydrogen bonding within or between the cellulose molecules.

2.3.9. Mechanisms for charge storage in cellulose thermoelectrets based on pharmaceutical tableting excipients.

The experiments carried out above were primarily designed to determine if it was possible to induce a thermoelectret effect in Avicel PH102 and Elcema G250, to measure the persistence of the thermoelectret effect and to examine the susceptibility of the stored charge to the presence of atmospheric moisture. These aims produced experiments different to those which would have been undertaken if it had been the mechanisms of charge storage that were being investigated. This discussion is therefore based on the theoretical background for electrets (Appendix 1), on storage mechanisms reported in the literature and observations made on the data presented above.

Electrets can be formed in many ways (135-137, 139, 141) however the fundamental physical nature of an electret can be described using only two basic concepts.

1. The alignment of dipolar molecules, the electric field thus generated being the summation of the charge present on each dipole.
2. The presence of charge carriers with either a positive or negative sign, the electric field generated being due to the charge carrier in excess. The importance of this statement is that both positive and negative charge carriers can be present simultaneously in the body of the electret.

Using these two effects it is possible to construct three different basic charging patterns (Figure 2.59). Electrets formed due to the alignment of molecular or atomic dipoles will always have surfaces that exhibit charges opposite to that of the adjacent electrode. The term, dipolar electret, can be used to describe such electrets although it is more correctly used to describe electrets whose faces have opposite charges.

Where the electret formed is a result of the presence of charge carriers the charge on the surface can either be of opposite sign to the forming electrode or the same sign. In the former case the charge carriers are already present in the material and all the

charging electric field has done is to separate them. In the latter case the charge carriers have been injected from the polarising electrode and have been captured by traps (Appendix 1).

The three possible types of charge formation above have thus far been discussed in isolation. In practice, however, the electric field of a thermoelectret may be due to the presence of any combination of the above.

The use of TSDC to measure or assess the charge storage mechanism of an electret implies that given a certain degree of thermal energy, the aligned dipoles or trapped charges will be free to move. It is therefore possible to envisage an electret with several dipole alignments, and hence several TSDC peaks due to the different activation energies involved. Where the energies required to 'free' aligned dipoles are spread over a large range the resulting TSDC peaks may merge producing a single, very broad peak. This is particularly the case where complex organic molecules such as polymers are the host material for the electret charge (174).

In order to determine the cause of the electret mechanism in Avicel PH102 and Elcema G250 it is necessary to consider what happens to the charge induced on the upper electrode of the discharge cell as the electric field of the electret disappears during TSDC. Figure 2.60 shows the change in the charge induced on the upper electrode, and current generated as a result of that change when a single charging species is present. As can be seen only a single TSDC peak can be obtained. If, however, two charging species are present with different activation energies then two possibilities can occur. Figure 2.61 shows the changes in the charge induced in the electrode of the discharge cell and the current generated when the charging species have the same sign and Figure 2.62 when the charge carrying species are of different sign.

Figure 2.61 has two TSDC peaks of the same sign whereas Figure 2.62 has two TSDC peaks of opposite sign. It is the latter case which is representative of the type of TSDC trace obtained for both Avicel PH102 and Elcema G250 and it is therefore assumed that the electret mechanism in both of these materials must be the result of the presence of at least two charge carrying species with opposite signs.

The two possibilities that can be used to produce two peaks with opposite signs are first, that there are aligned dipoles and injected

space charge components or second that there are injected and separated space charge components present. The third possibility, involving the presence of a dipole alignment and separated space charge, would produce two charge carrying species of the same sign and can therefore be discounted.

Cellulose is a biological polymer formed from β D-glucose molecules that are linked through carbon atoms 1 and 4 (Figure 2.63). This β(1-4)-glycosidic link between the D-glucose molecules combined with their ring structure confers a high degree of rigidity to the cellulose polymer. The high level of hydroxyl groups present on each glucose unit makes it highly probable that a significant amount of hydrogen bonding will occur between cellulose molecules. X ray diffraction studies of cellulose (216) has shown that the molecules are linked through hydrogen bonds with the primary hydroxyl group of the $-CH_2OH$ group.

The ability to form an extensive network of hydrogen bonds between molecules plus the rigidity of the polymer itself means that cellulose molecules can align themselves in such a way that the bulk material can be considered as being ordered. Cellulose can in fact be shown to consist of a mixture of small longitudinal micelles (217) between which there is a parallel alignment of charge. The existence of such micelles allows the trapping of a space charge within the micelle to be considered as they may provide the traps or holes necessary.

The complexity of the cellulose molecule means that crystalline regions (presumed to be areas with aligned micelles) are restricted in scope, ie not continuous throughout the body of the material. Furthermore, the orientation of the crystalline regions and hence the dipoles on the micelles involved in the intermolecular bonding are unlikely to be consistent so that no electret effect is seen in the unprocessed material even though spontaneous dipole alignment exists.

The cellulose present in Avicel PH102 and Elcema G250 is obtained from natural sources and is therefore likely to be more complicated than that shown in simple structural diagrams of the molecule, ie molecules of cellulose could be cross linked through the primary hydroxyl bonds. The exact mechanism of dipole alignment is therefore extremely difficult to determine. The presence of other molecules, side groups and even cross linking does however allow for the possibility of charge trapping due to discontinuities in the

electronic structure of the polymer.

The reported data for cellulose and cellulose derivatives (142-150) indicate that TSDC peaks may be obtained from around 25°C to 90°C. This is a consequence of the variety of materials used and not a problem with identification of the TSDC peaks. One difference between the data presented above and that found in the literature is that the dual peaks observed above with Avicel PH102 and Elcema G250 are not reported elsewhere, with one exception (142), where peaks were obtained for a regenerated cellulose film at around 25°C and around 90°C. Even in this case, however, a TSDC trace of both peaks was not shown.

The lack of results exactly like those obtained above should not be considered as an indication that the techniques used were incorrect. The term TSDC has been used here to describe the technique used for quantifying charge storage, however, a number of other methods have been reported which use similar terminology whilst being significantly different in practice (174).

In general TSDC peaks for cellulose and cellulose derivatives have been observed over a much wider temperature range than employed above. It is generally considered that a dipole charge for the primary hydroxyl group occurs around -70°C, well below the temperature range used above (142, 144, 145). For the peaks observed within the temperature range used in the present study there is no firm concensus of opinion within the literature as to the mechanism. It is thought however that the peak around 25°C-40°C may be due to the second order phase change (glass-rubber transition) associated with amorphous cellulose (142, 218). This type of effect is known to be a source of the electret effect in other materials (174), charge separation occurring between the different phases present by virtue of the Maxwell-Wagner effect (174 pp165-170).

The TSDC peak at the higher temperature is considered to be due to the release of the trapped charge injected from the electrodes (142). This observation could be explained by locating the injected charge component of the electret inside micelles of cellulose molecules. However, this effect does require the primary hydroxyl hydrogen bonds to have a significantly higher resistance to thermal energy as it has already been stated that this bond becomes free to rotate at around -70°C. This may be possible if the presence of the injected charge stabilises the micelle to the extent that the amount

of thermal energy required to break the primary hydroxyl hydrogen bonds binding the cellulose molecules in the micelles becomes greater than that required to disrupt hydrogen bonds due to the secondary hydroxyl hydrogen bonds. The possibility of this mechanism actually occurring is not known. If it did occur it would allow aligned dipoles due to the secondary hydroxyl hydrogen bonds or charge separated due to the orientation of the micelles to be released before charge held within the micelle.

If the electret effect is not partly due to the alignment of secondary hydroxyl hydrogen bonds, then it may still be related to the behaviour of non-aligned hydrogen bonding between individual cellulose molecules. This hydrogen bonding could cause the separation of charge between different phases in response to a glass-rubber transition or Maxwell-Wagner effect where charge separation occurs across amorphous-crystalline phase boundaries. Charge separation across liquid-solid phase boundaries, the Costa-Ribeiro effect (219), are unlikely to occur in dried cellulose.

In all of these cases free atmospheric moisture would almost certainly hydrogen bond to the hydroxyl groups present in the D-glucose molecules of the cellulose polymer. This hydrogen bonding will compete for sites with intermolecular hydrogen bonds between the cellulose molecules. If the atmospheric water molecules compete successfully, then any aligned dipoles producing the electret charge will be lost or phase boundaries will change or disappear. The probability of this occurring should be relatively high as a significant proportion of the intermolecular hydrogen bonds should be strained to some degree so that their replacement by water is energetically favourable. Such a mechanism would help to explain the extreme sensitivity to atmospheric moisture observed for the electret charge in both Avicel PH102 and Elcema G250.

The TSDC traces obtained for Avicel PH102 and Elcema G250 have generally shown two peaks although in a number of cases one of these peaks has been relatively small. The only firm evidence for two charge carrying species being present are Figures 2.39 and 2.40. Here only a single large peak was obtained after exposure to atmospheric conditions for approximately 15 hours whilst wrapped in aluminium foil. The significance of these traces are that one of the charge carrying species contributing to the electret effect has been eliminated whereas the other has not.

If the assumption is made that the charge component lost is that due to dipole alignment then the mechanism of adsorption of atmospheric moisture can be used to explain the disappearance of the electret charge. Furthermore, if the dipole alignment is assumed to be due to the systematic orientation of hydroxyl groups it becomes possible to advance an explanation for the very small peak observed in Figure 2.22.

These very small peaks were only obtained where the compressed disc or powder bed were heated and allowed to cool before TSDC was carried out on the sample. When such a sample was heated it would be possible for the hydroxyl groups involved in hydrogen bonding to have been freed. More importantly, the hydrogen end of the hydroxyl group would have become free to change its orientation at random until cooled and fixed in position. If during these random movements the hydrogen atom approached the earthed electrode then it would experience a small attraction to the electrode due to an induced image charge.

Whilst this attraction is small, it should bias the orientation of the hydroxyl group. When sufficient numbers of such events are taken into consideration it is possible for a number of such alignments to be frozen in when the sample is cooled. The number of aligned dipoles would be small but could be sufficient to produce an effect similar to that observed in Figure 2.22.

As stated earlier no attempt was made to investigate the mechanism of charge storage in thermoelectrets manufactured from Avicel PH102 and Elcema G250. However, a working hypothesis would be that a dipole alignment involving the hydroxyl groups available on the D-glucose units of the cellulose is responsible for the low temperature peak. This is supported by the presence of a glass-rubber phase change observed in cellulose at that point (218). The high temperature peak must therefore be due to an injected space charge to account for its opposite sign. The hypothesis here is that the charge is localised within cellulose micelles although the presence of foreign molecules or atoms could provide the holes and traps to produce these charges.

Time (minute)	Applied potential (kiloVolt)	Time (minute)	Applied potential (kilovolt)
0	10.	15	3.0
1	9.2	16	2.9
2	8.8	17	2.8
3	-	18	2.8
4	7.6	19	2.6
5	7.0	20	2.6
6	6.3	21	2.8
7	5.6	22	3.0
8	-	23	3.4
9	4.4	24	4.0
10	4.0	25	4.9
11	3.6	27	6.1
12	3.4	27	7.6
13	-	28	9.1
14	3.1	29	10.4

Table 2.1. Change in the applied electric potential with time during the manufacture of a thermoelectret using unprocessed Avicel PH102.

Time (minute)	Applied potential (kiloVolt)	Time (minute)	Applied potential (kiloVolt)
0	10.0	19	9.8
1	9.9	20	9.8
2	9.9	21	9.8
3	-	22	-
4	9.85	23	9.8
5	9.9	24	9.8
6	9.9	25	-
7	9.9	26	9.8
8	-	27	9.8
9	9.9	28	-
10	9.9	29	9.8
11	9.9	30	-
12	9.9	31	9.8
13	9.9	32	-
14	9.9	33	9.8
15	9.9	34	9.8
16	-	35	9.9
17	9.85	36	9.9
18	9.8		

Table 2.2. Change in the applied electric potential with time during the manufacture of a thermoelectret using Avicel PH102 that had previously been dried at 120°C for two hours.

Time (minute)	Applied potential (kiloVolt)	Oven temperature (°C)	Sample temperature (°C)
0	10	40	27.6
1	9.5	42	28.6
2	9.2	47	30.0
3	8.7	53	31.7
4	8.2	60	33.7
5	7.6	68	36.4
6	7.0	75	39.1
7	6.4	83	42.2
8	5.9	90	45.5
9	5.2	97	49.1
10	4.6	98	52.8
11	4.2	111	56.9
12	3.8	115	60.6
13	3.5	119	64.6
14	3.3	122	68.3
15	3.2	124	72.1
16	3.0	127	75.6
17	3.0	129	79.1
18	3.0	129	83.5
19	3.0	129	85.9
20	3.0	130	89.0
21	3.2	131	91.6
22	3.3	131	94.3
23	3.5	131	96.9
24	3.9	132	99.5
25	4.4	132	101.9
26	5.0	132	104.4
27	6.1	132	106.6
28	7.4	132	108.9
29	8.8	132	110.9
30	>10	132	112.1
31		133	114.0
32		133	115.4
33		133	116.5
34		133	117.5
35		133	118.5
36		134	119.5
37		134	120.5
38		134	121.4
39		134	122.2
40		134	123.0
41		134	123.8
42		135	124.4
43		135	125.1
44		135	125.8
45		135	126.4

Table 2.3. Change in the applied voltage, oven temperature and sample temperature with time for a thermoelectret prepared using unprocessed Avicel PH102.

Table continued below.

Table continued from above.

Time (minute)	Applied potential (kiloVolt)	Oven temperature (°C)	Sample temperature (°C)
46		135	127.0
47		135	127.6
48		135	128.0
49		135	128.5
50		135	129.0
51		135	129.5
52		135	129.9

Table 2.3. Change in the applied voltage, oven temperature and sample temperature with time for a thermoelectret prepared using unprocessed Avicel PH102.

Time (minutes)	Oven temperature (°C)	Sample temperature (°C)	Time (minutes)	Oven temperature (°C)	Sample temperature (°C)
0.0	28.0	18.9	52.5	105.5	89.6
2.5	27.4	20.1	55.0	111.0	93.9
5.0	26.8	21.3	57.5	115.9	99.4
7.5	26.5	23.2	60.0	120.7	104.3
10.0	26.2	23.2	62.5	125.6	109.8
12.5	26.8	23.2	65.0	131.1	115.2
15.0	30.8	24.4	67.5	135.4	120.1
17.5	35.4	26.2	70.0	139.6	125.0
20.0	40.2	28.7	72.5	139.6	129.9
22.5	44.5	32.6	75.0	139.6	132.3
25.0	50.0	36.6	77.5	139.6	134.8
27.5	55.1	41.5	80.0	139.6	136.0
30.0	60.4	45.7	82.5	139.6	137.2
32.5	65.2	50.0	85.0	139.6	138.4
35.0	70.7	54.9	87.5	140.2	139.0
37.5	75.6	59.8	90.0	140.2	139.0
40.0	80.5	65.2	92.5	140.2	139.6
42.5	85.4	69.5	95.0	140.2	140.2
45.0	90.9	74.4	97.5	140.2	140.2
47.5	95.7	79.3	100.0	140.2	140.2
50.0	100.6	84.1			

Table 2.4. Temperature of TSDC oven and the inside of the empty discharge cell. Temperatures were measured using the reverse biased thermocouples referenced against an ice/water bath. The heating rate of the oven was 2°C min^{-1} and the chart recorder in Y/t mode. The above data was compiled from the traces obtained (Figure 2.14).

Storage time (hour)	Conditions	First peak temperature (°C)	First Peak current ($\times 10^{-12}$ amp)	Second peak temperature (°C)	Second Peak current ($\times 10^{-12}$ amp)
1	P_2O_5/air	58.46	-37.70	86.15	35.08
25	P_2O_5/air	60.0	-24.60	86.15	32.47
72	P_2O_5/air	55.38	-6.32	81.54	31.46
114	P_2O_5/air	56.15	-5.55	84.62	>10.0
408	P_2O_5/air	55.38	-4.13	78.46	10.0
499	P_2O_5/air	53.08	-7.02	80.00	>10.0
503	P_2O_5/air	43.08	-2.30	69.23	9.58
576	P_2O_5/air	56.92	-3.40	83.08	9.27
957	P_2O_5/air	49.23	-1.36	79.23	9.21
1370	P_2O_5/air	53.08	-0.63	80.77	1.52
0	vacuum	56.92	-33.51	84.62	17.80
70	vacuum	49.23	-1.57	76.92	22.5
107	vacuum	-	-	79.23	8.68
214	vacuum	-	-	76.15	>10
663	vacuum	57.69	2.93	80.77	2.09

Table 2.5. Peak discharge currents and the temperature at which they occurred for Elcema G250 thermoelectrets stored under humid conditions. Note the first peak is always represented as a negative value even though the relevant figure indicates a positive current. This has been done to remove any confusion due to the orientation of the thermoelectrets during TSDC.

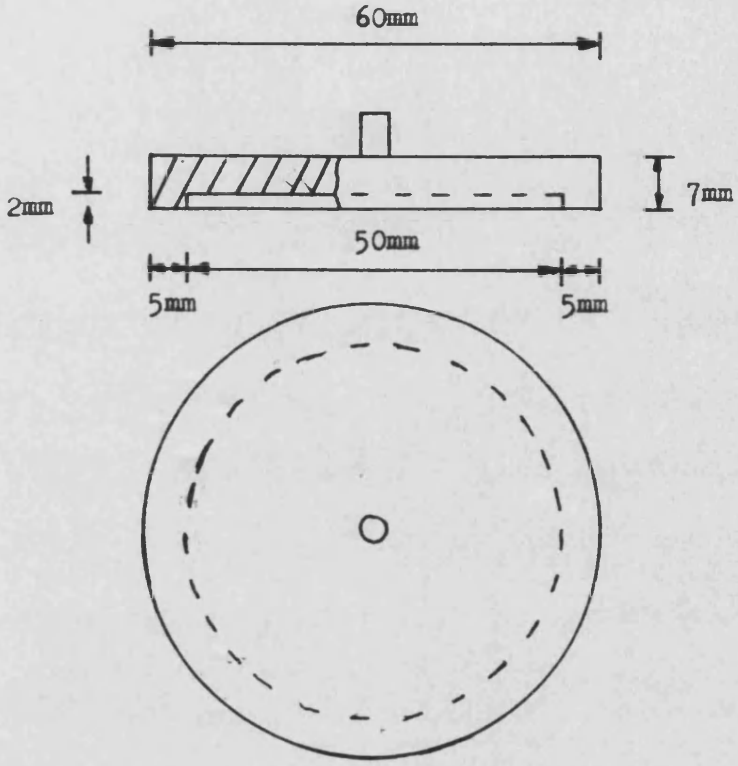

Figure 2.1. Electrode used in the standard cell for air gap charging and airgap TSDC.

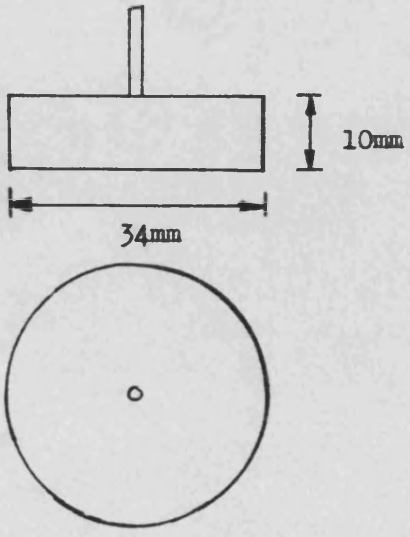

Figure 2.2. Upper electrode used in the standard cell for contact charging and contact TSDC.

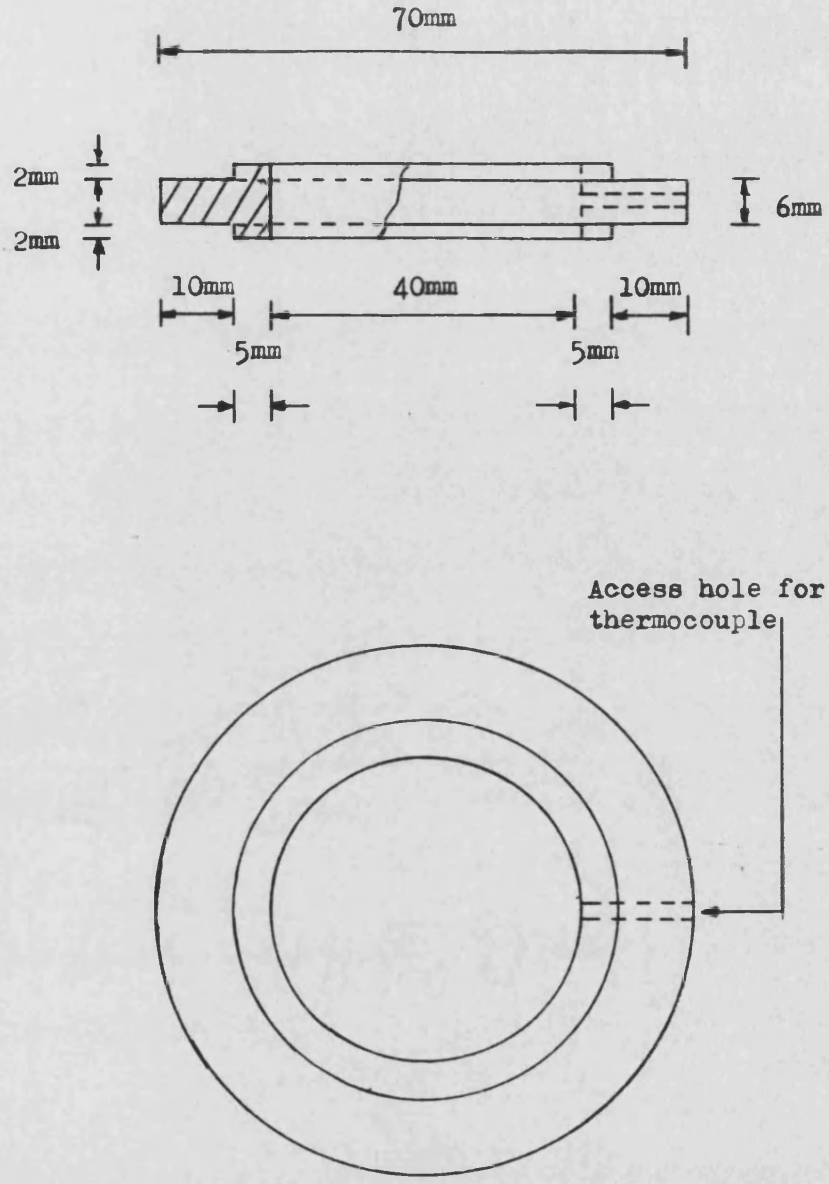

Figure 2.3. PTFE separating ring used in the standard charging cell and standard discharge (TSDC) cell.

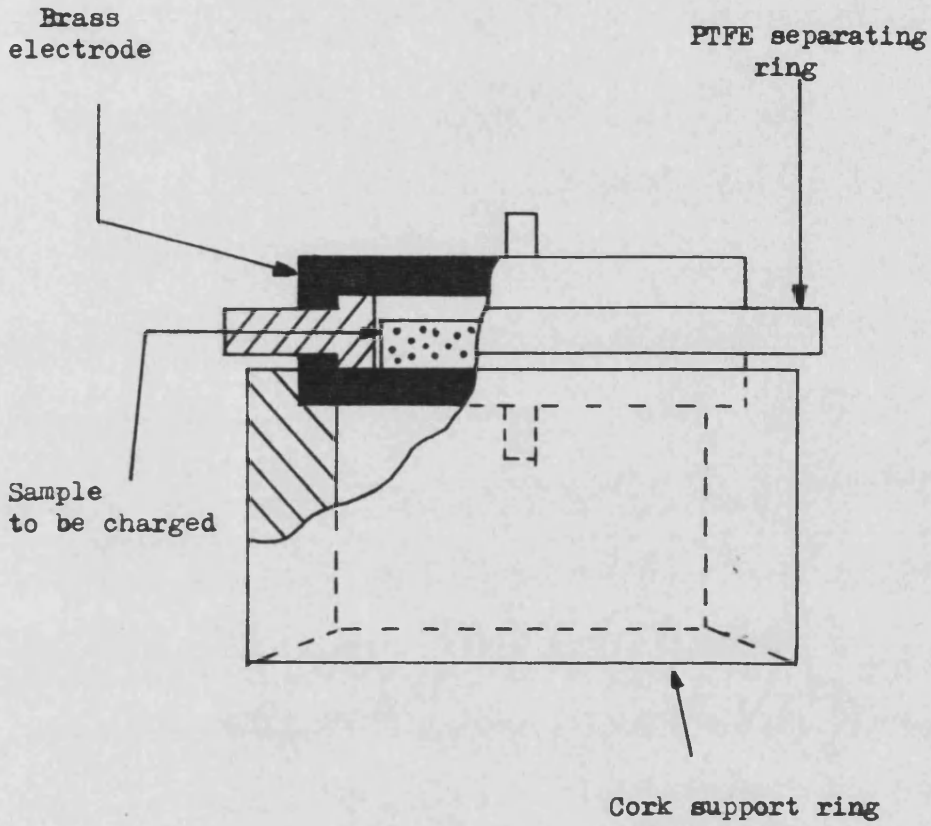

Figure 2.4. Standard cell, assembled for air gap charging, mounted on insulating cork ring. When used for contact charging, the upper electrode is replaced with that shown in Figure 2.2.

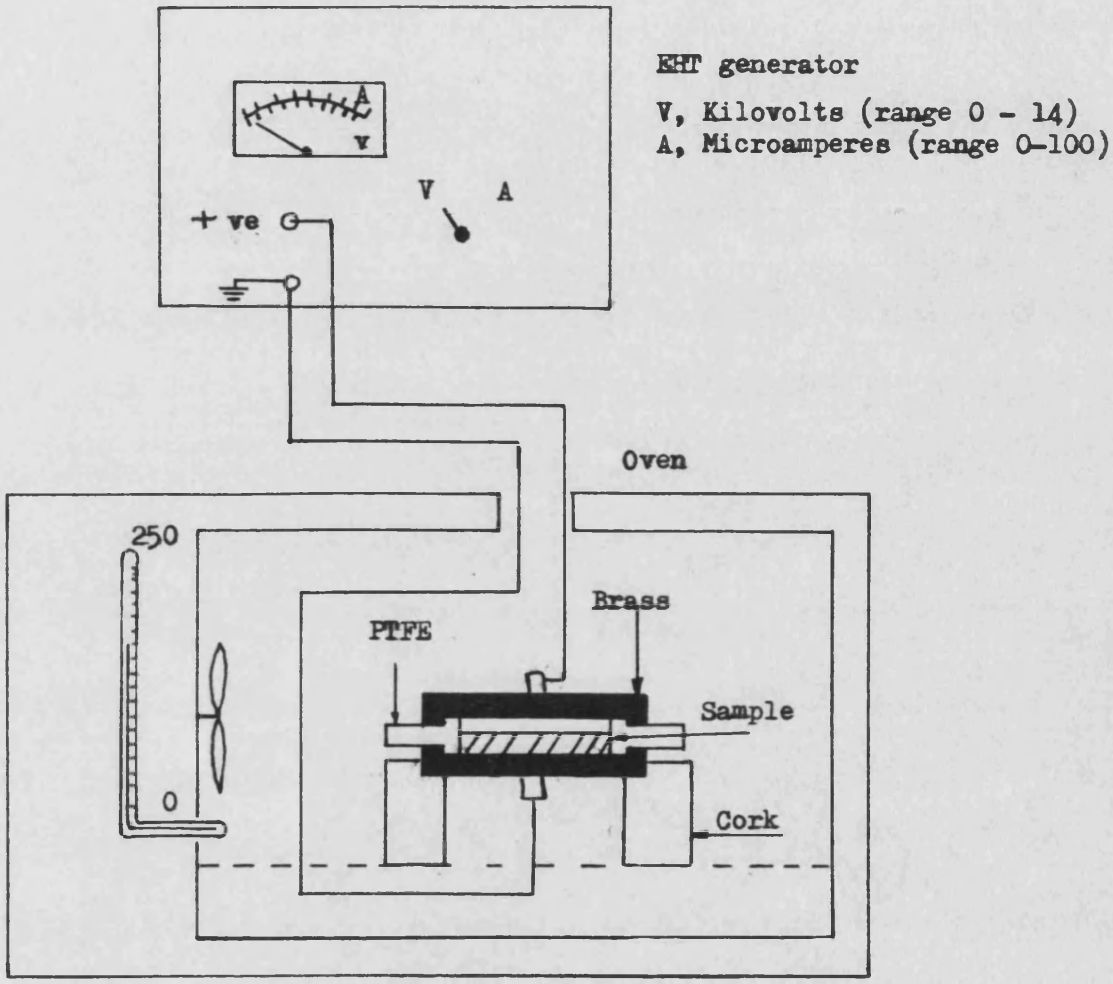

Figure 2.5. Schematic representation of the apparatus used for preparing thermoelectrets.

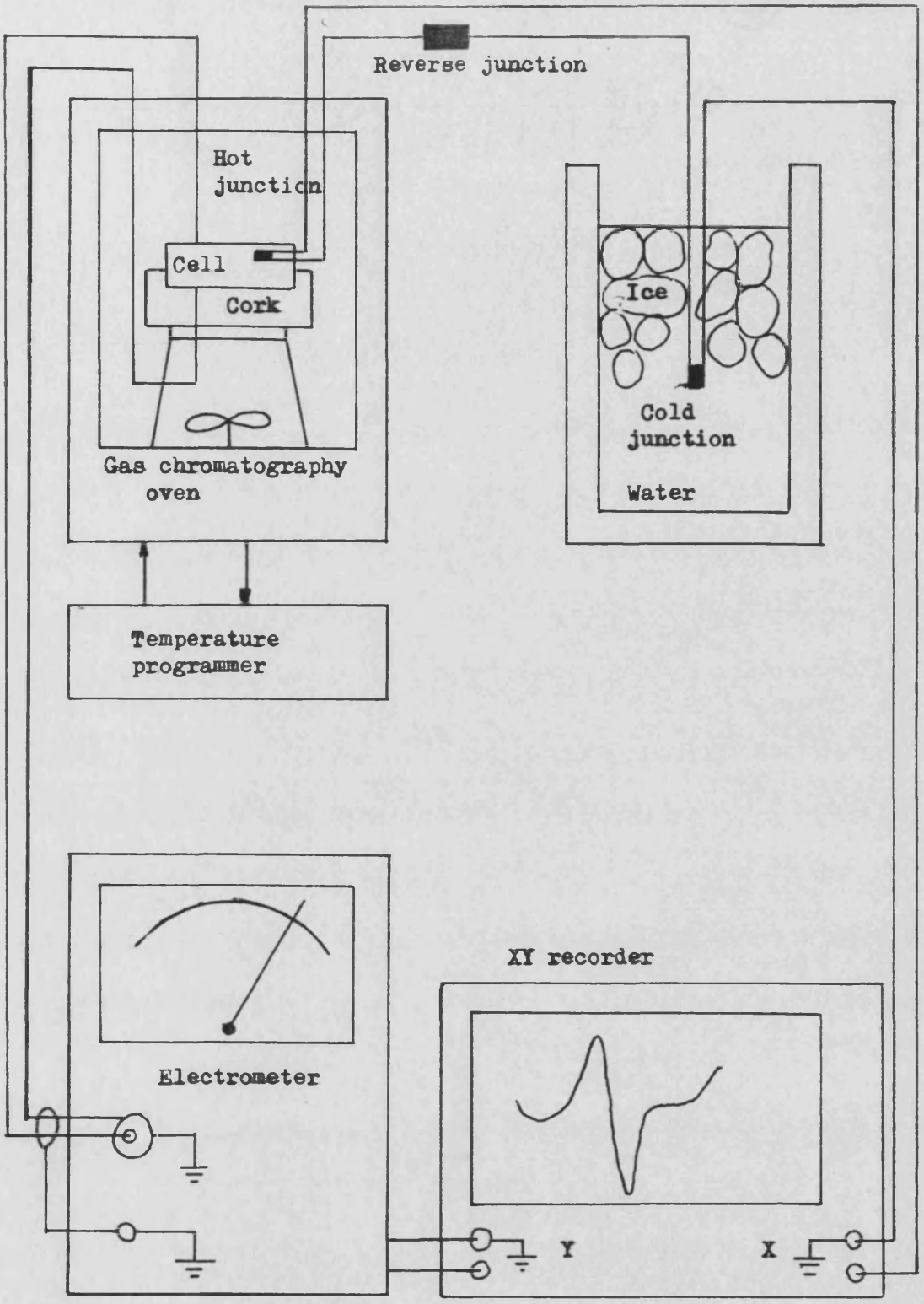

Figure 2.6. Schematic representation of the apparatus used to measure the thermally stimulated discharge current (TSDC) of thermoelectrets.

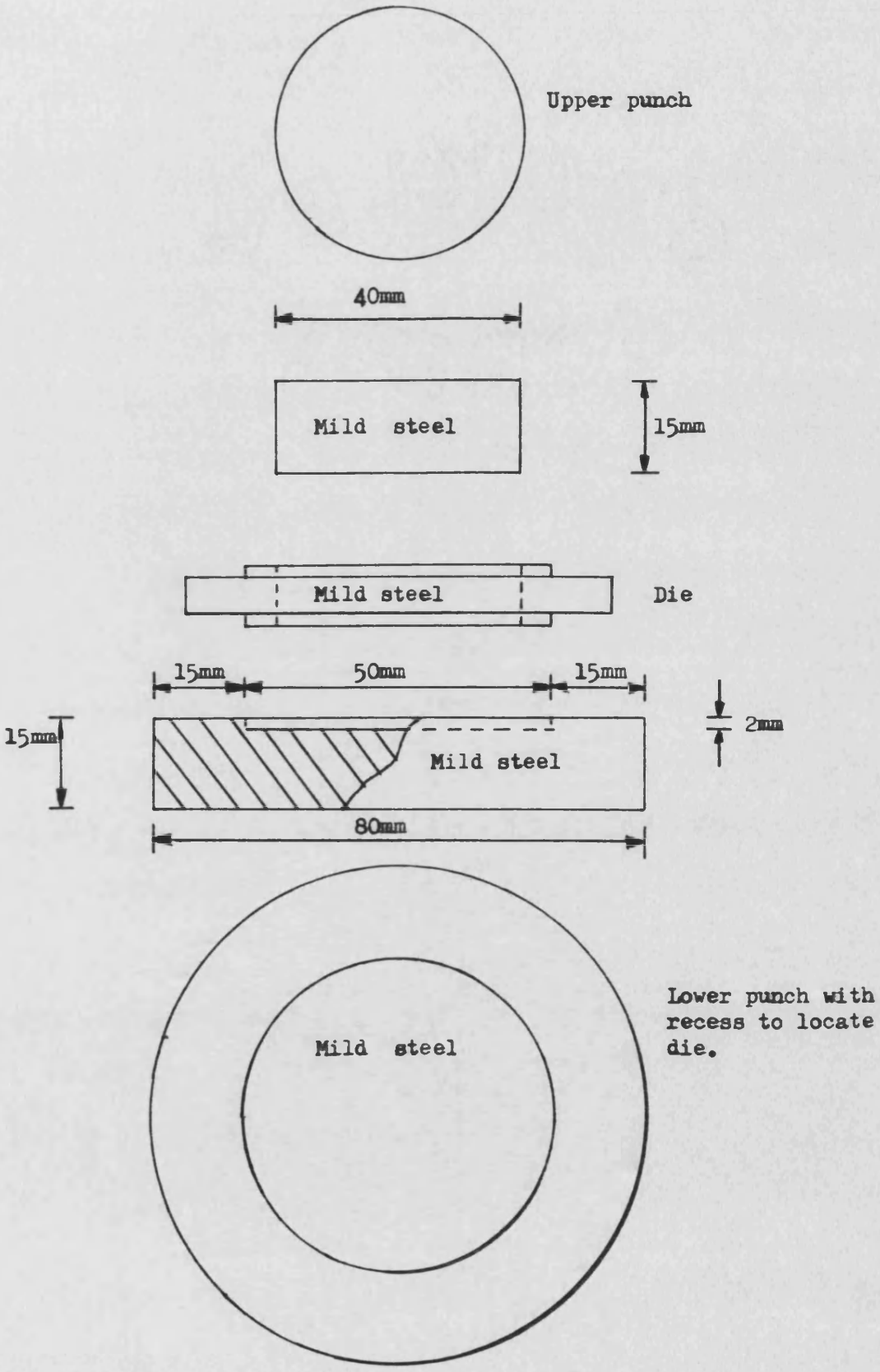

Figure 2.7. Punch and die assembly used for manufa cturing compacts from Avicel PH102 and Elcema G250.

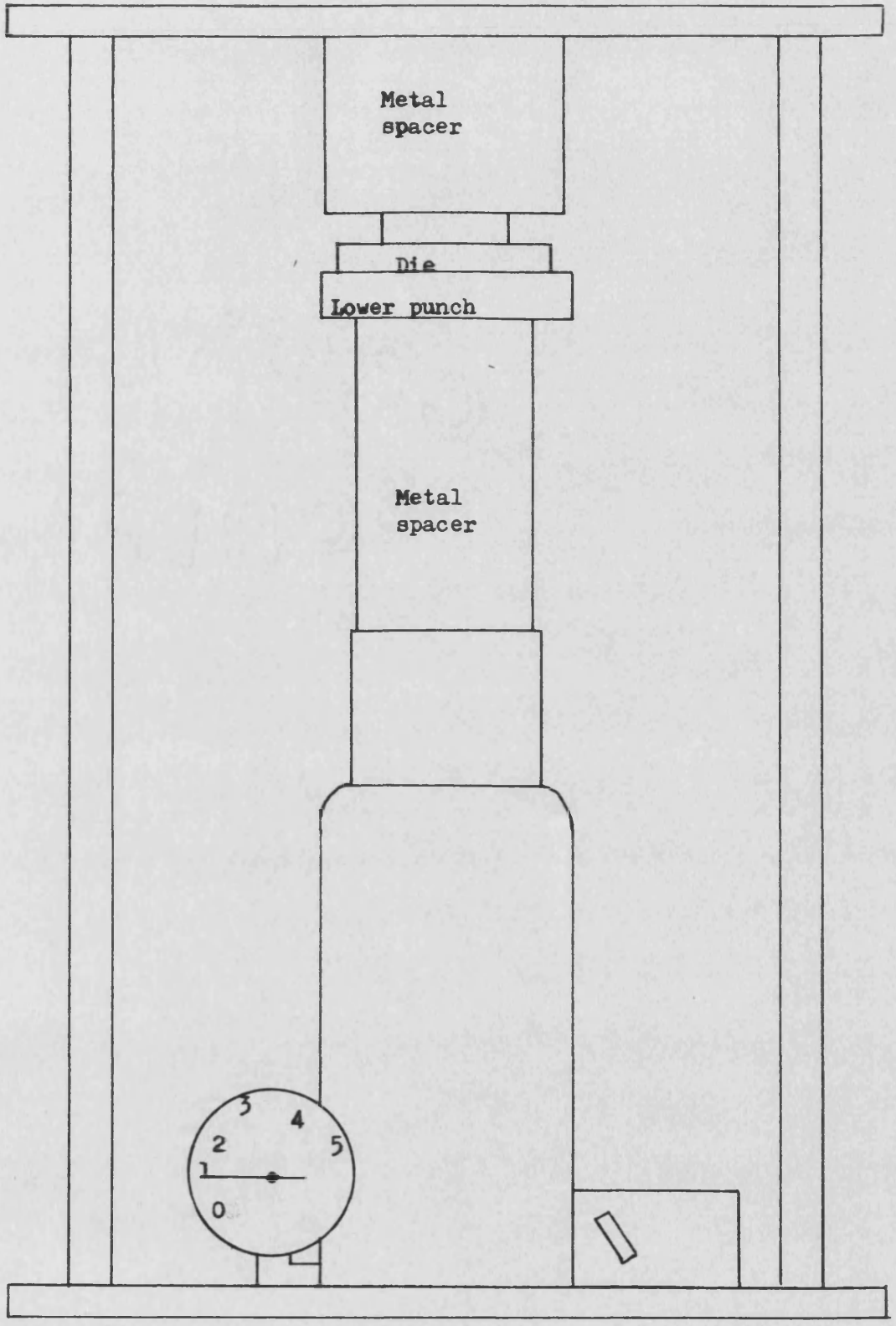

Figure 2.8. Schematic representation of the manually operated hydraulic press used to prepare compacts from Avicel PH102 and Elcema G250.

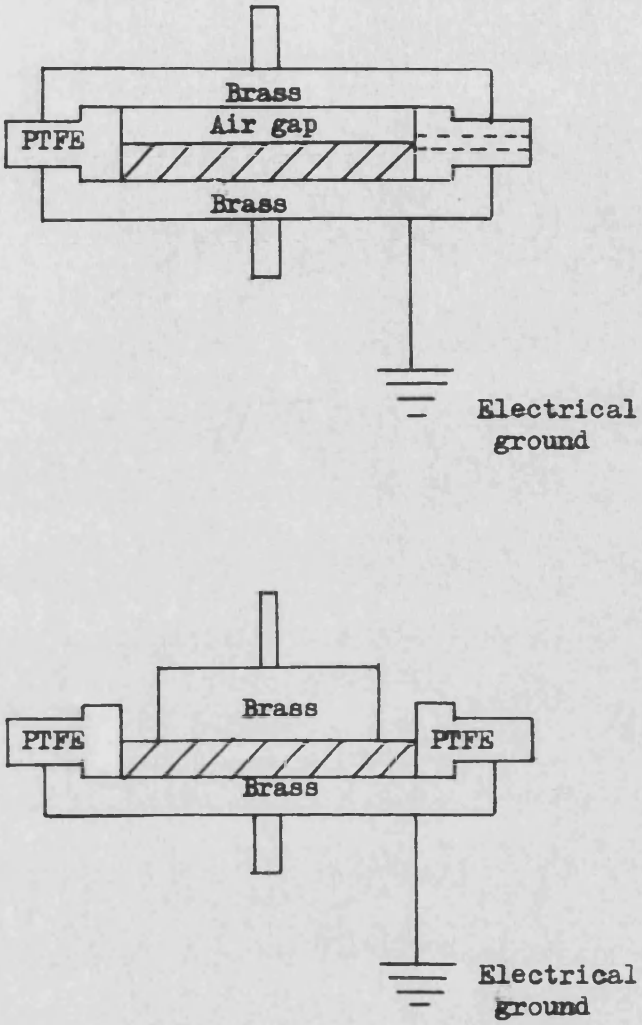

Figure 2.9. Arrangement of the electrodes for airgap charging and air gap TSDC (top) and for contact charging and contact TSDC (bottom).

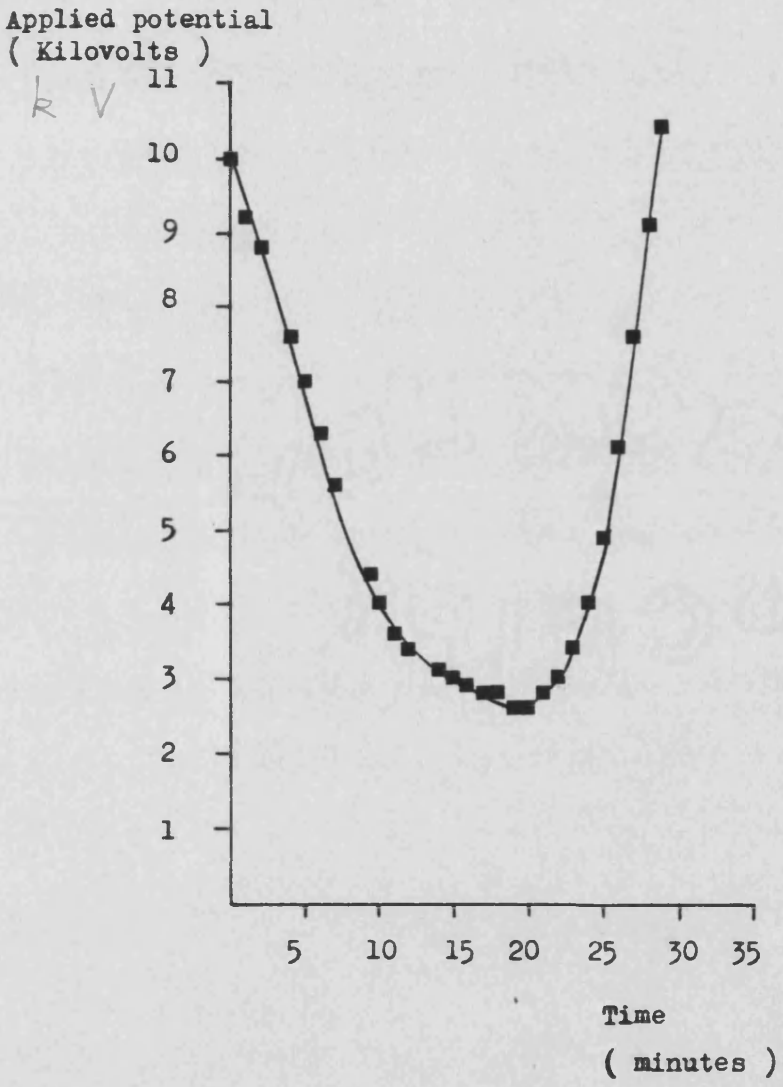

Figure 2.10. Change in applied potential with time when charging an Avicel PH102 compact prepared from the fresh material.

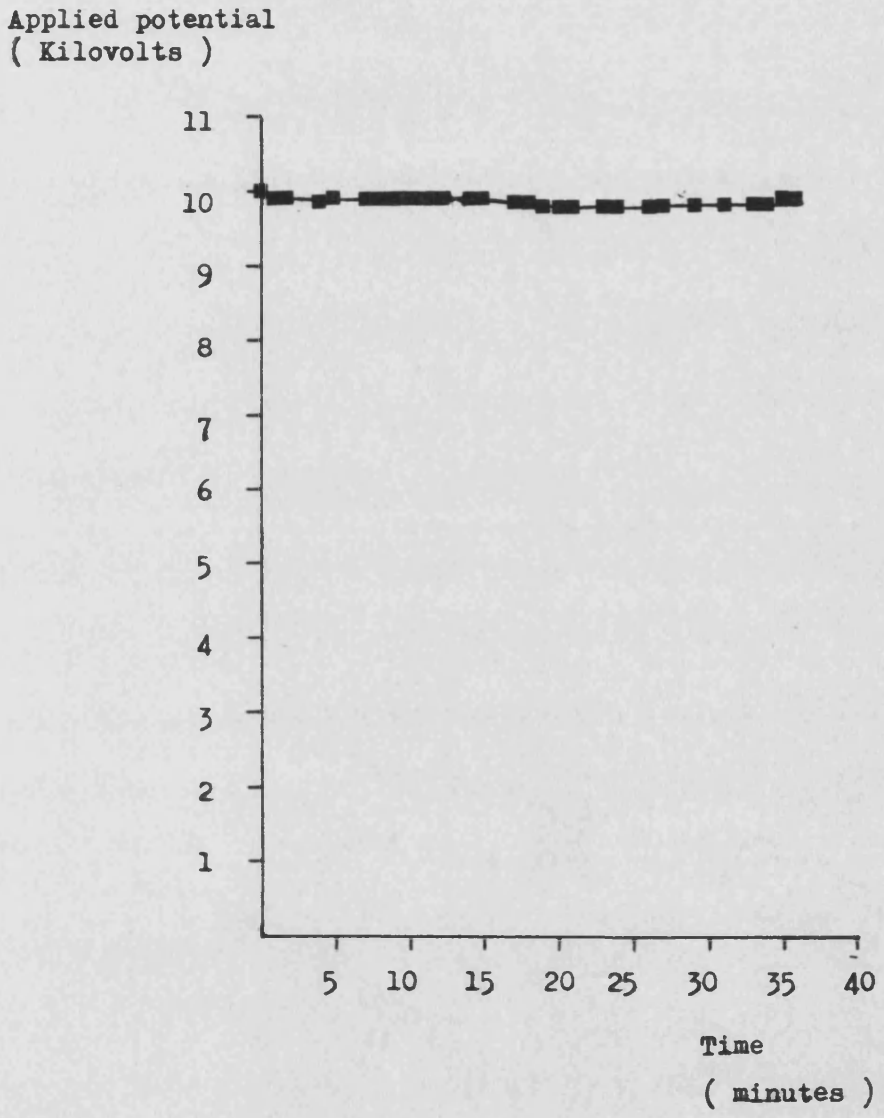

Figure 2.11. Change in applied potential with time when charging an Avicel PH102 that had previously been dried at 120°C for two hours.

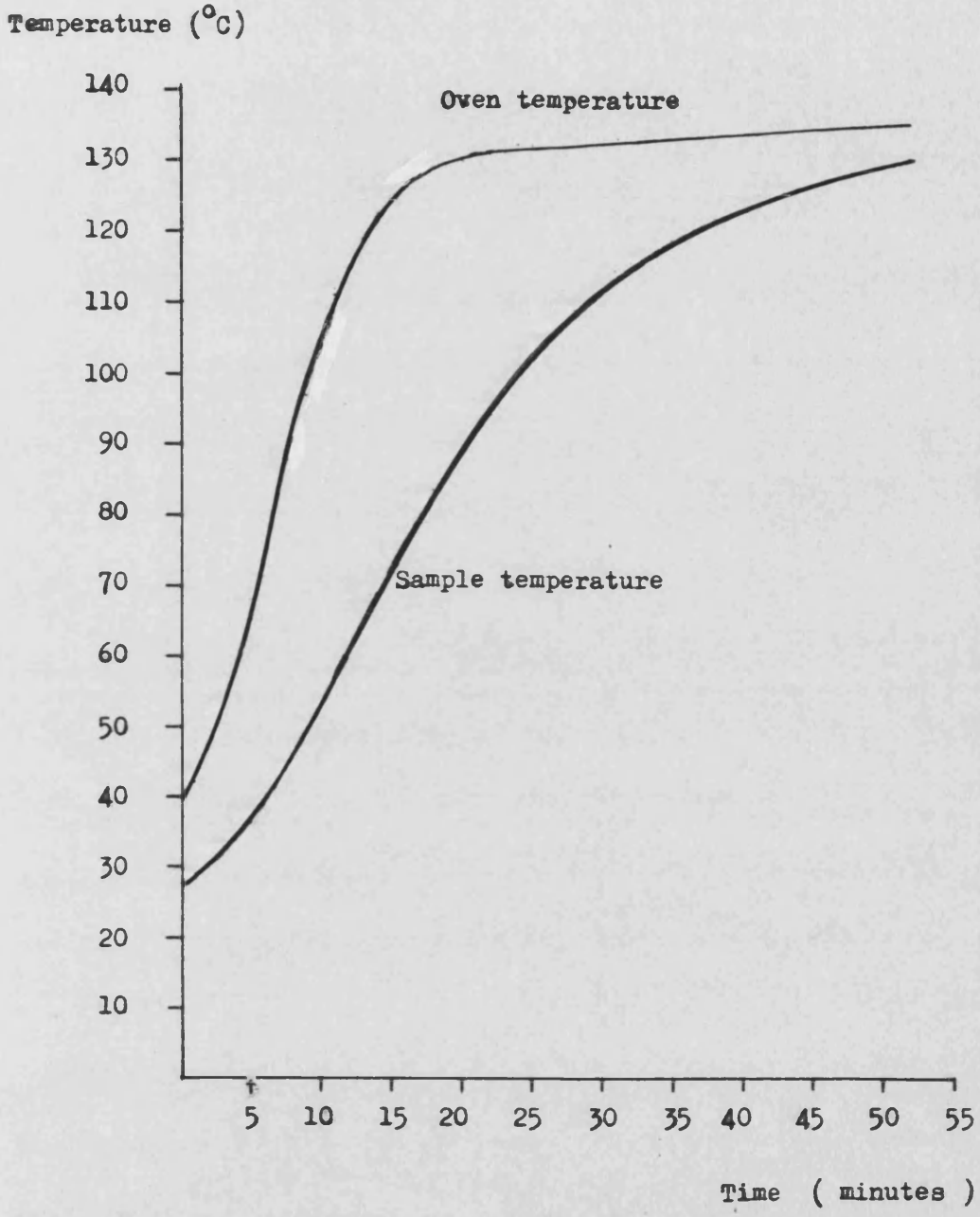

Figure 2.12. Comparison of oven temperature and sample temperature for an Avicel PH102 compact. The sample temperature lags behind the oven temperature by a significant amount.

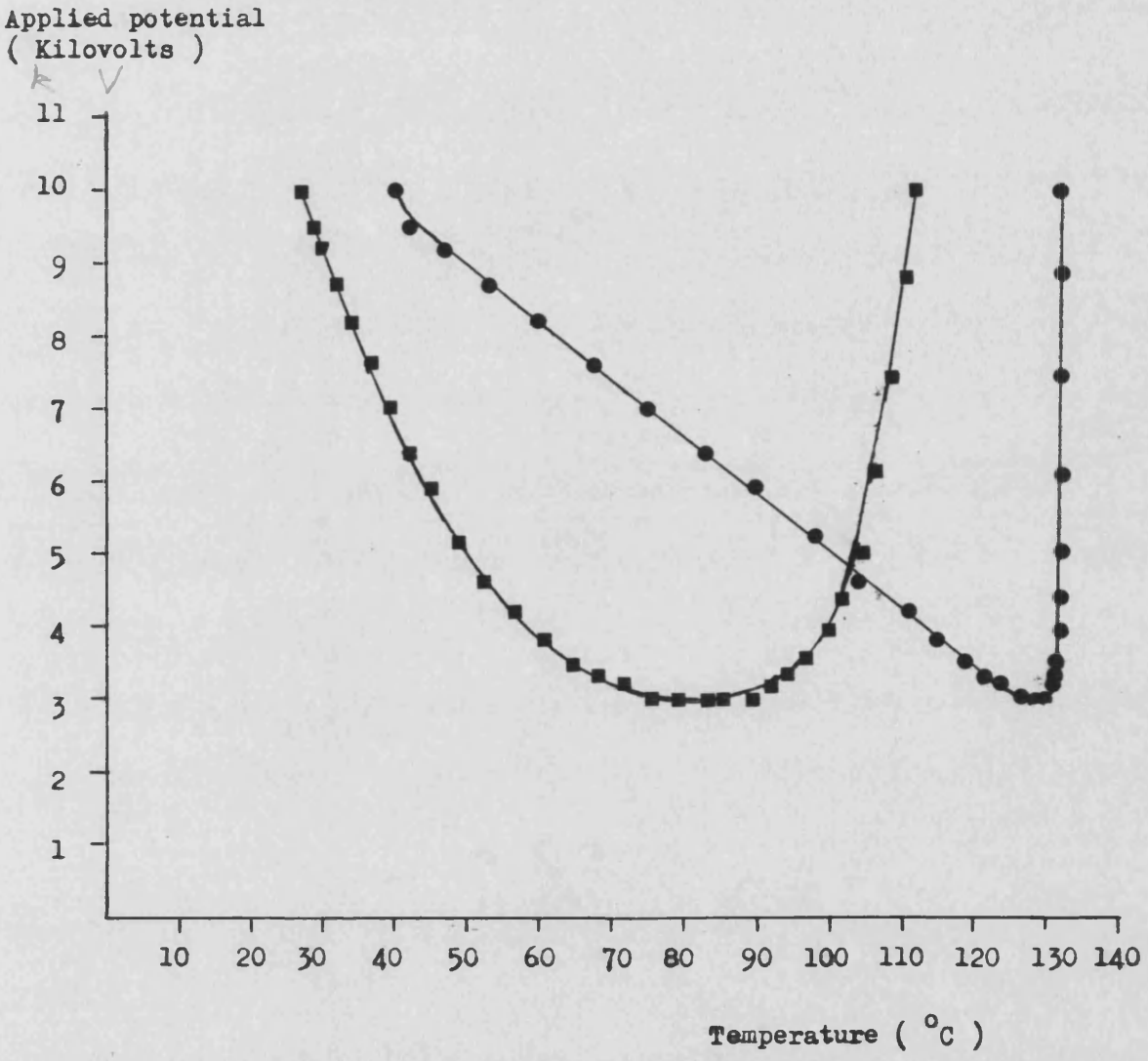

Figure 2.13. Change in the applied potential with temperature when charging an Avicel PH102 compact prepared from the fresh material.
● Oven, ■ Avicel PH102

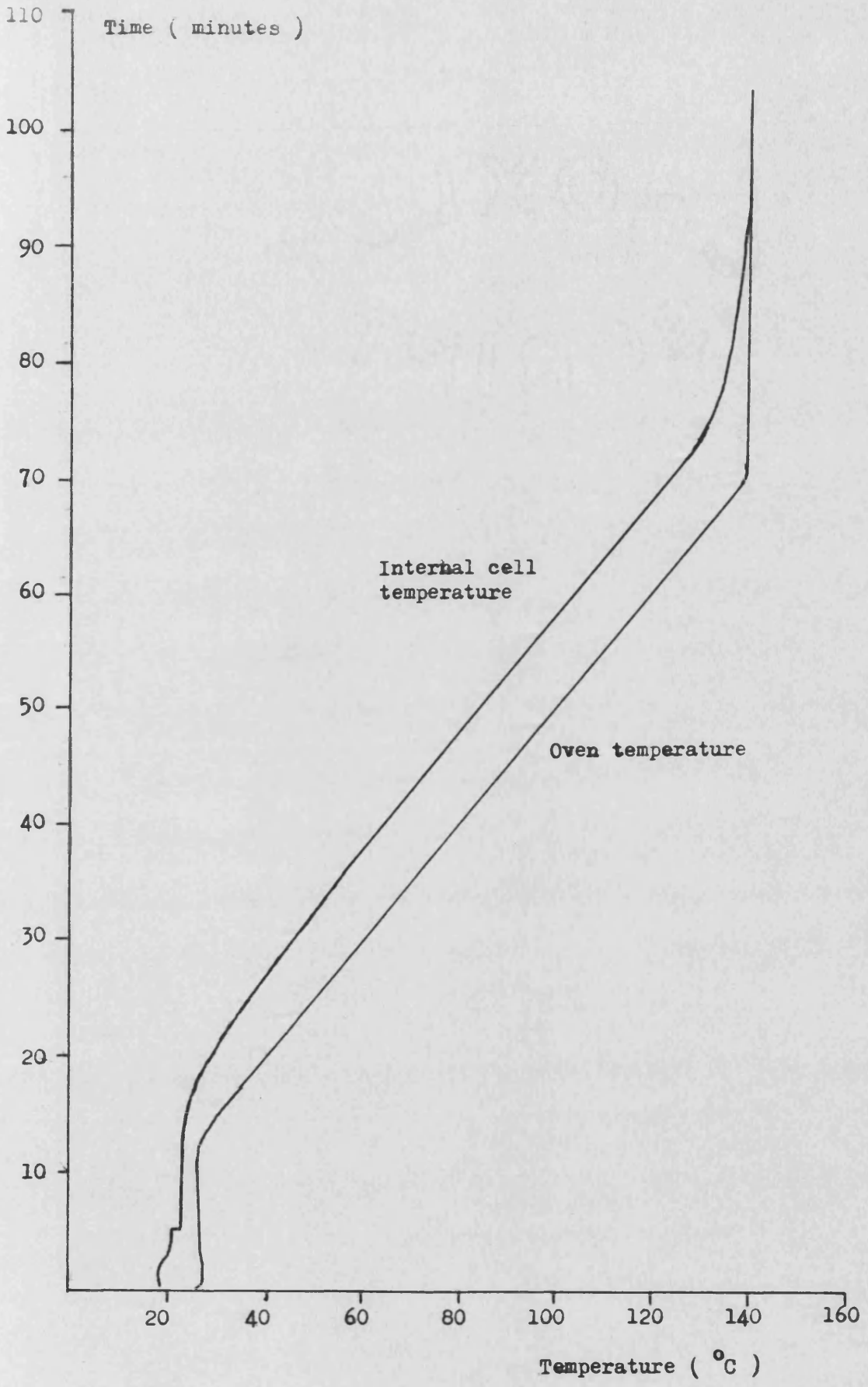

Figure 2.14. Temperature in the gas chromatography oven and inside the empty discharge cell (TSDC). Heating rate 2 °C min^{-1}.

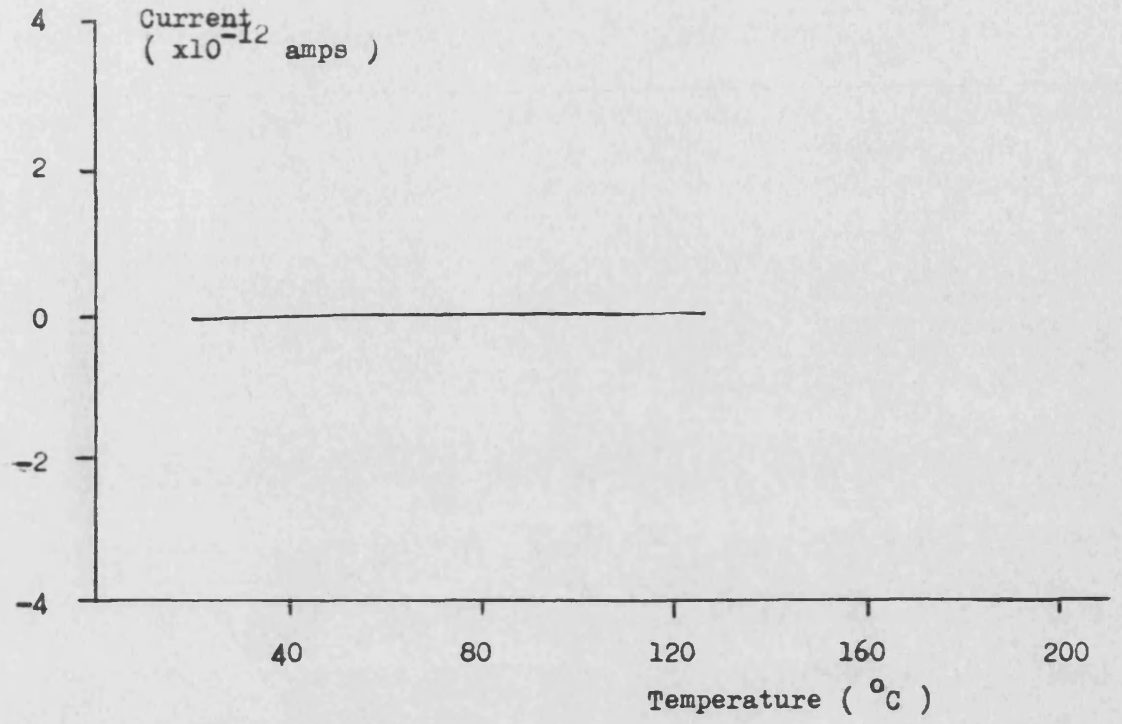

Figure 2.15. Air gap TSDC of an empty discharge cell.

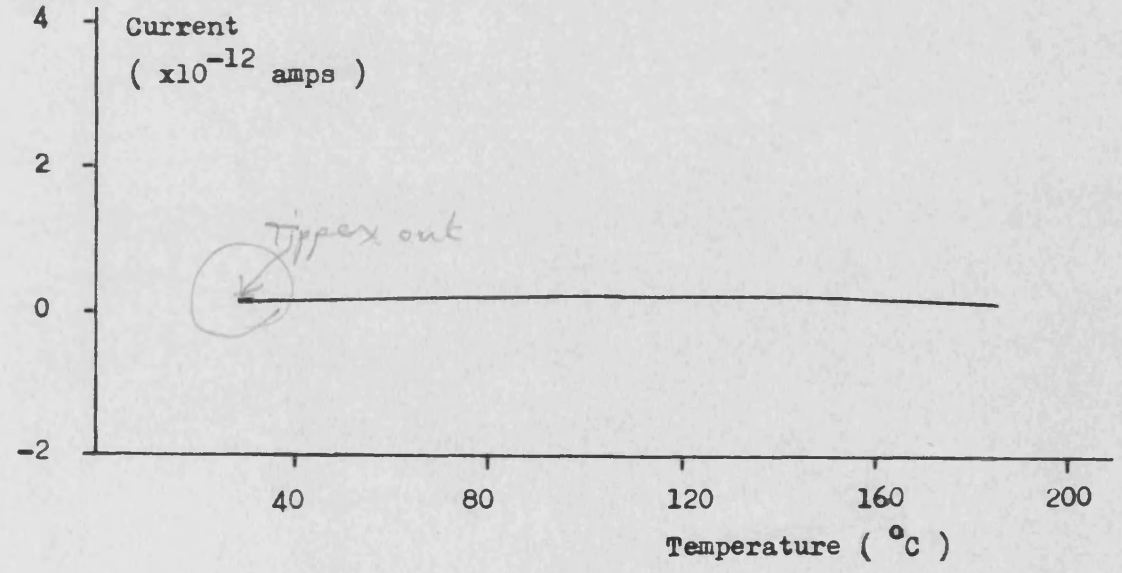

Figure 2.16. Air gap TSDC of the PTFE blank.

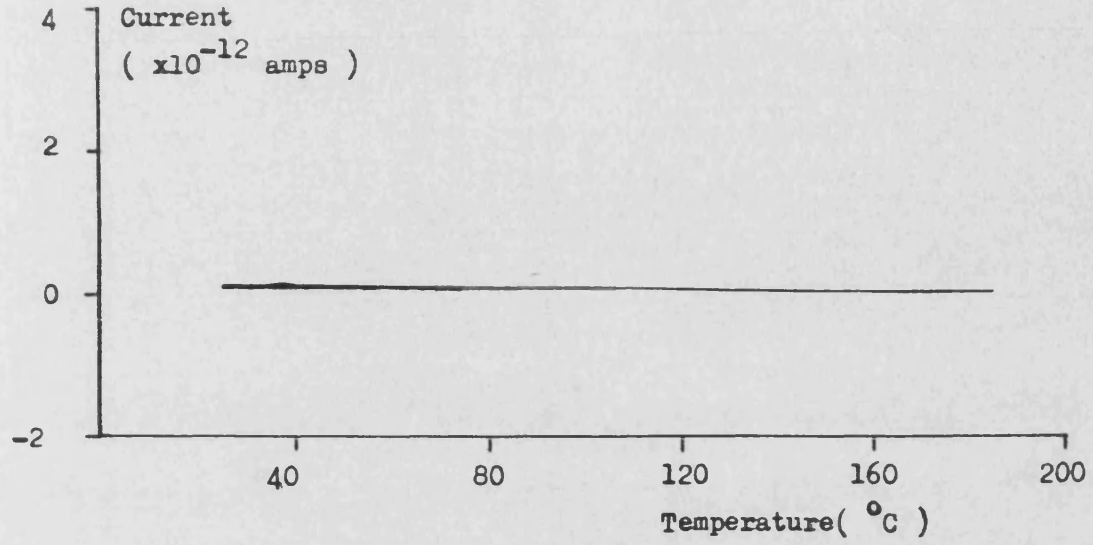

Figure 2.17. Contact TSDC of the PTFE blank.

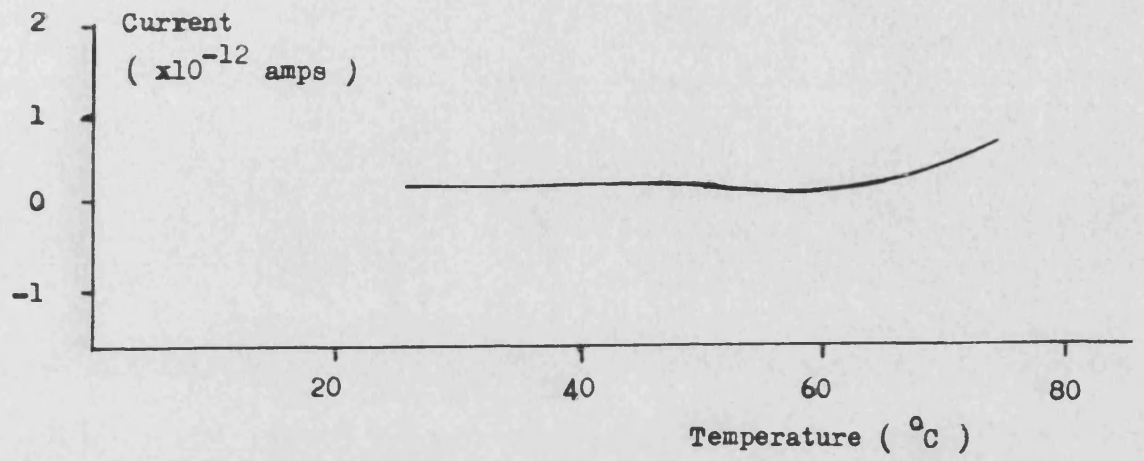

Figure 2.18. Air gap TSDC of an uncharged sample of Carnauba wax.

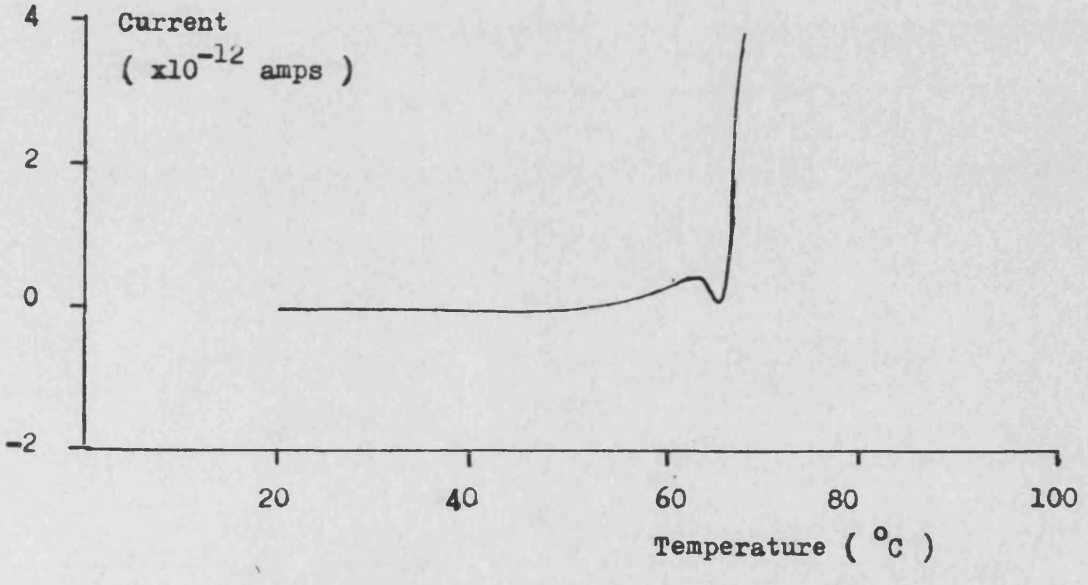

Figure 2.19. Contact TSDC of an uncharged sample of Carnauba wax.

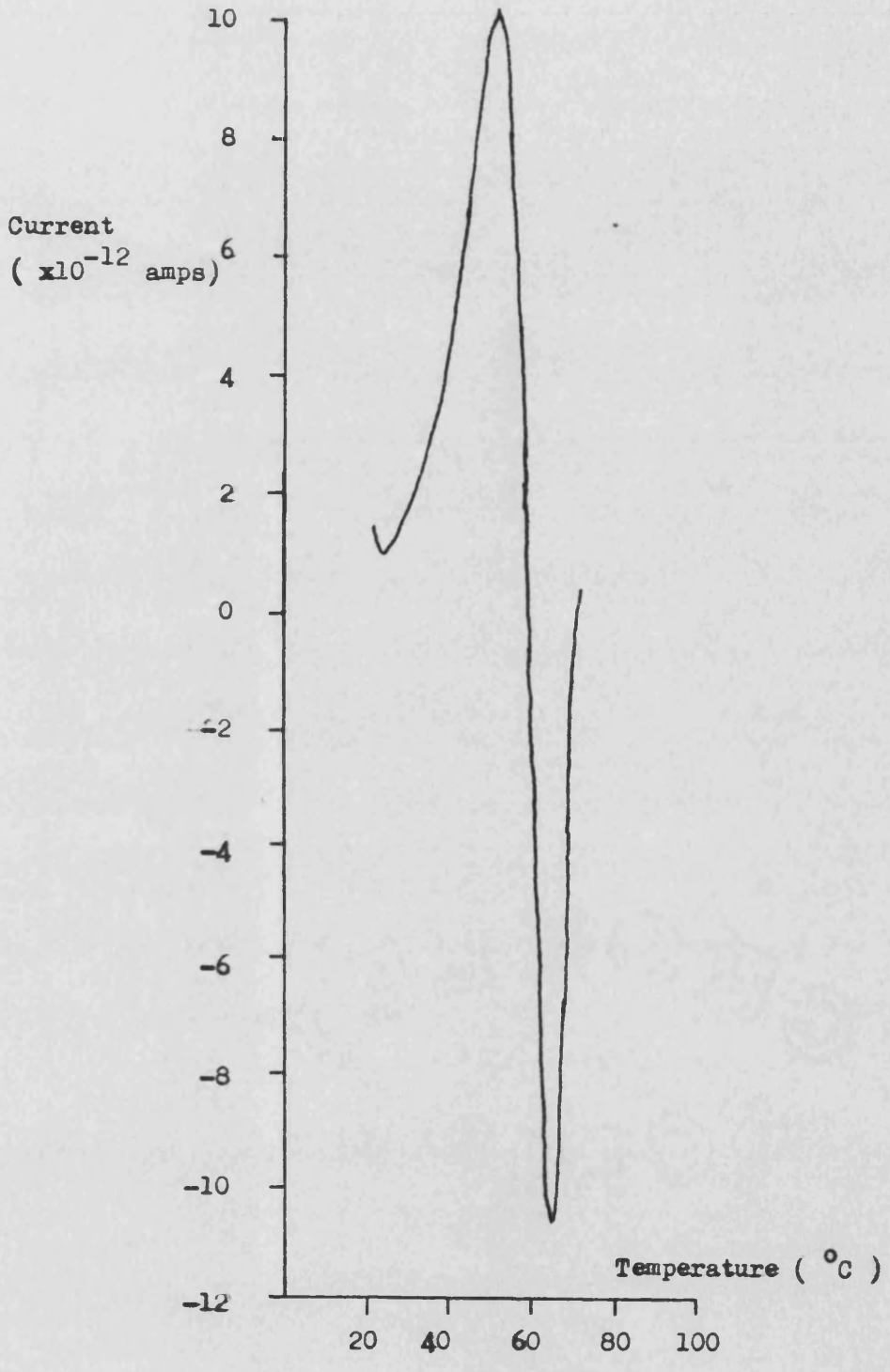

Figure 2.20. Air gap TSDC of a Carnauba wax thermoelectret.

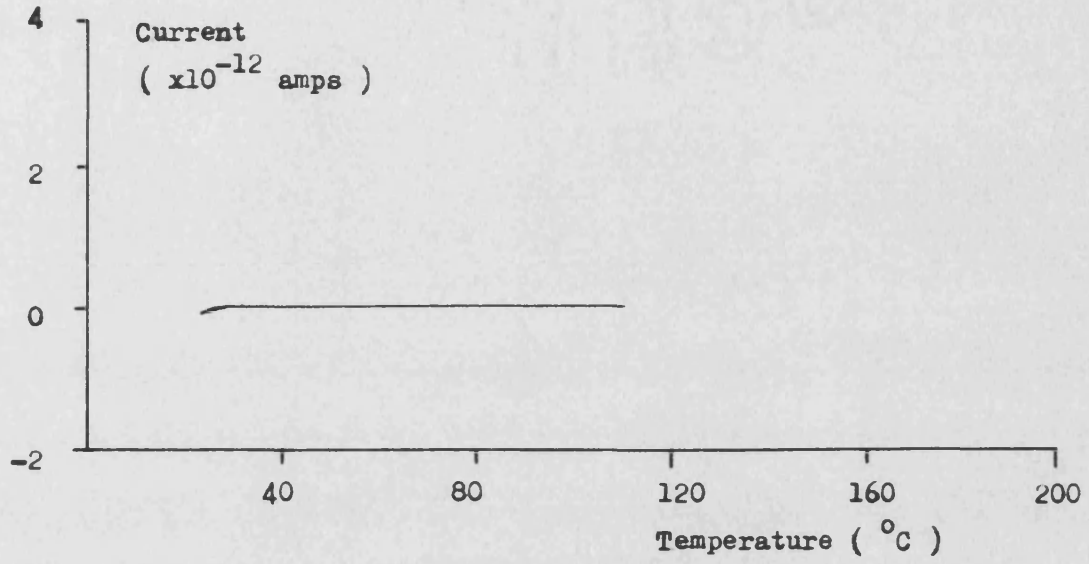

Figure 2.21. Air gap TSDC of a sample of unprocessed, Avicel PH102 powder.

Figure 2.22. Air gap TSDC of a sample of dried Avicel PH102 powder. The powder bed was preserved intact between drying and TSDC.

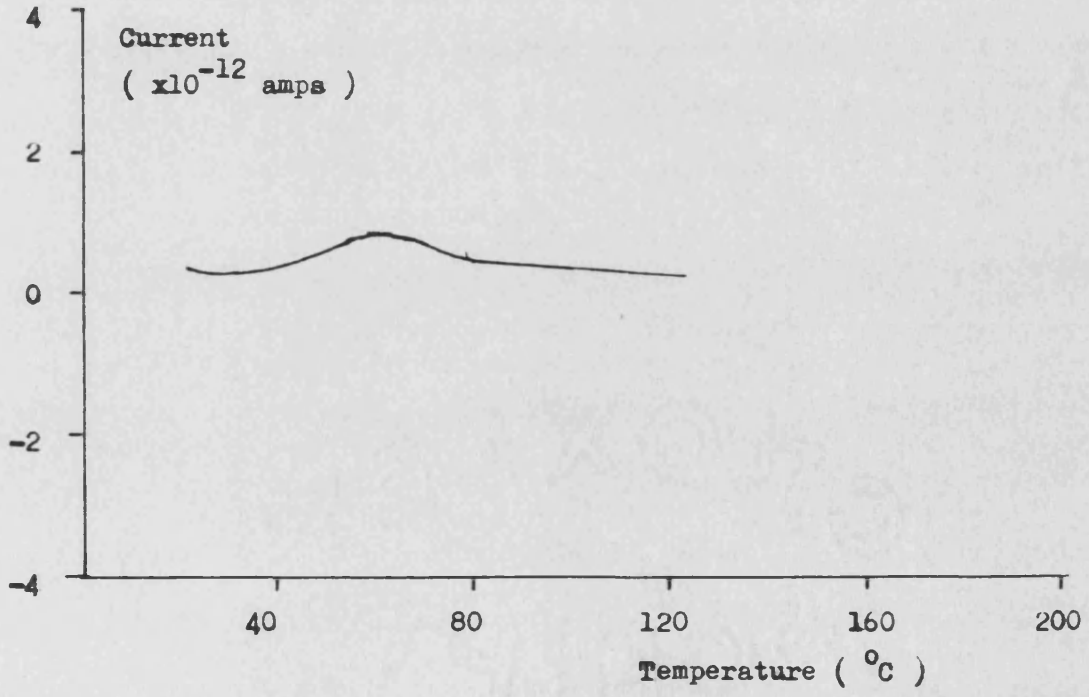

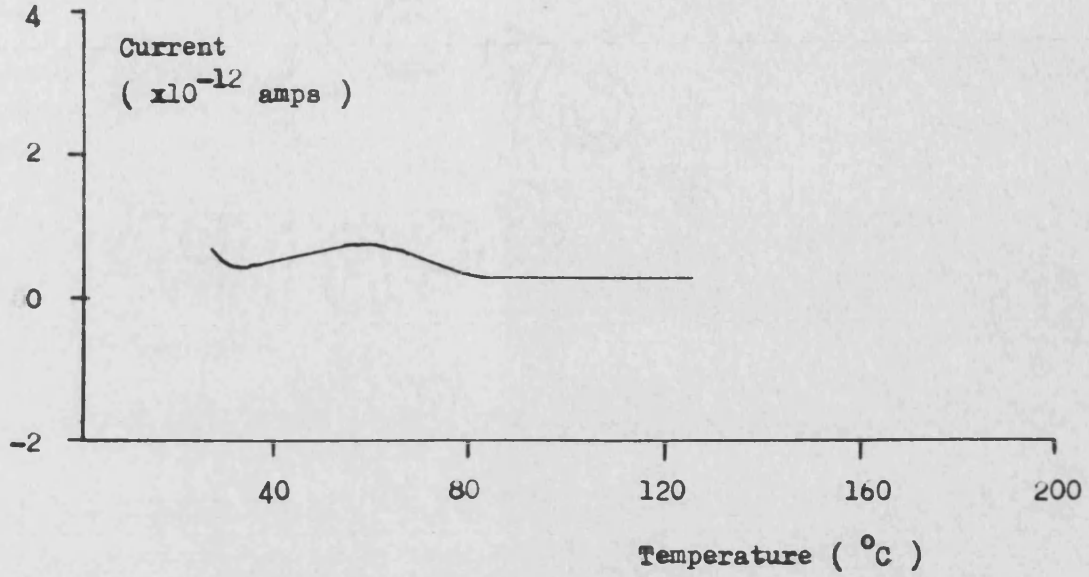

Figure 2.23. Air gap TSDC of an electrised sample of Avicel PH102 powder. As in Figure 2.22, the powder bed was undisturbed between electrising and TSDC.

Figure 2.24. Air gap TSDC of an electrised sample of Avicel PH102 powder. In this case the electrised powder bed was thoroughly disturbed prior to TSDC.

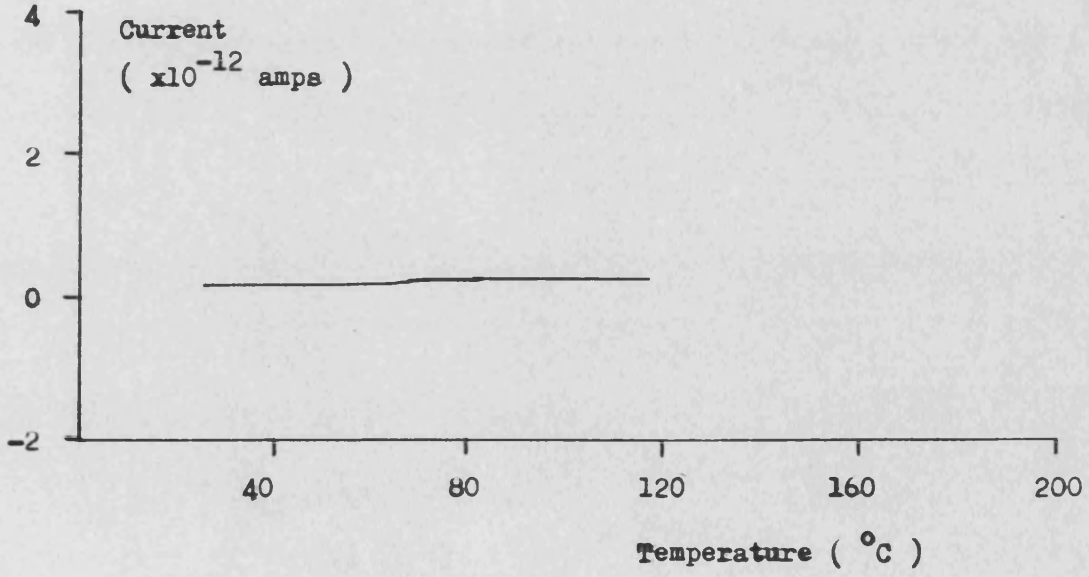

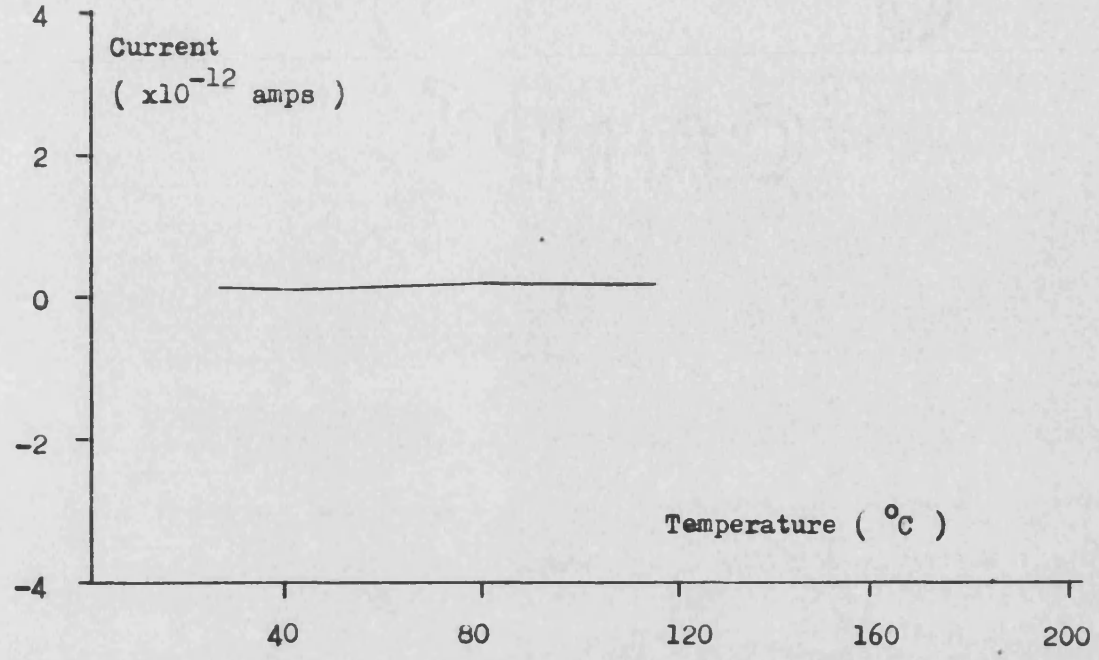

Figure 2.25. Air gap TSDC of a dried Avicel PH102 compact.

Figure 2.26. Air gap TSDC of an electrised Avicel PH102 compact.

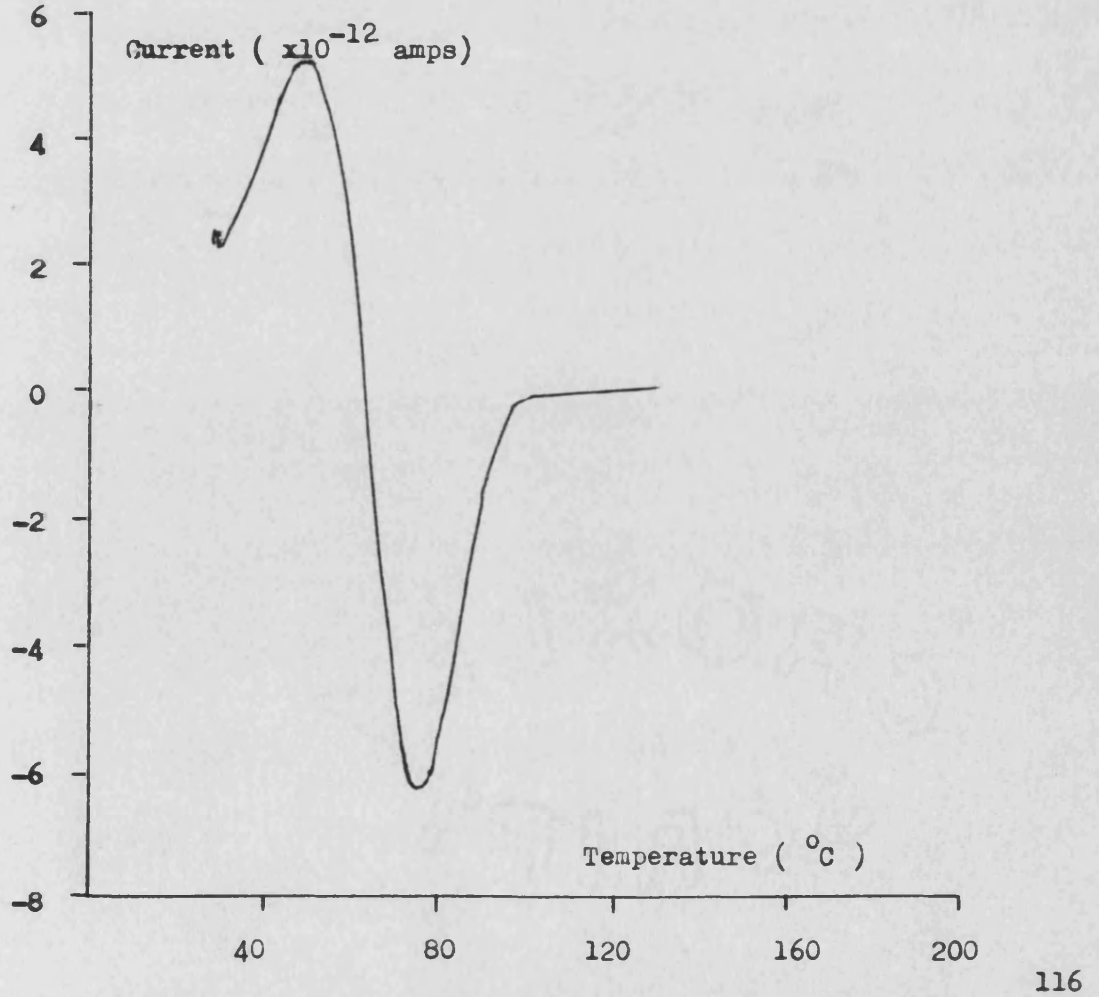

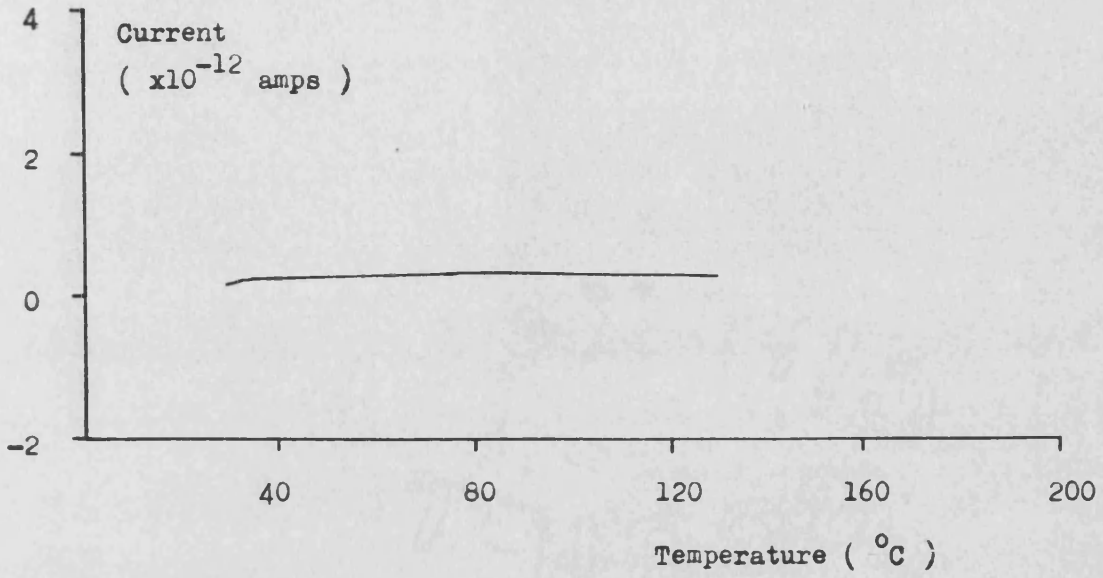

Figure 2.27. Air gap TSDC of an electrised Avicel PH102 compact. The compact was reduced to powder prior to TSDC.

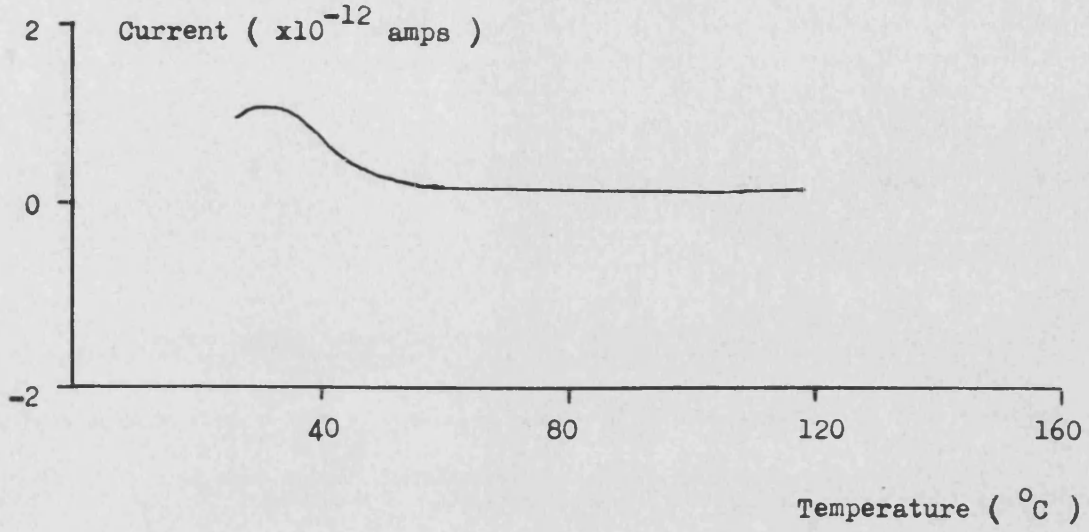

Figure 2.28. Air gap TSDC of an electrised Avicel PH102 compact. The compact was 1.3mm in thickness.

Figure 2.29. Air gap TSDC of an electrised Avicel PH102 compact. The compact was 2.95mm in thickness.

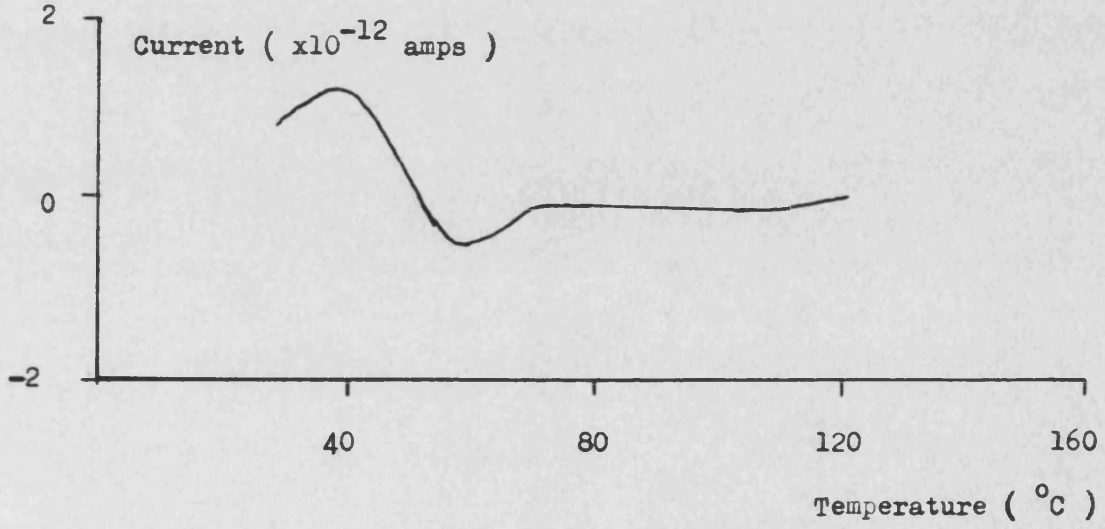

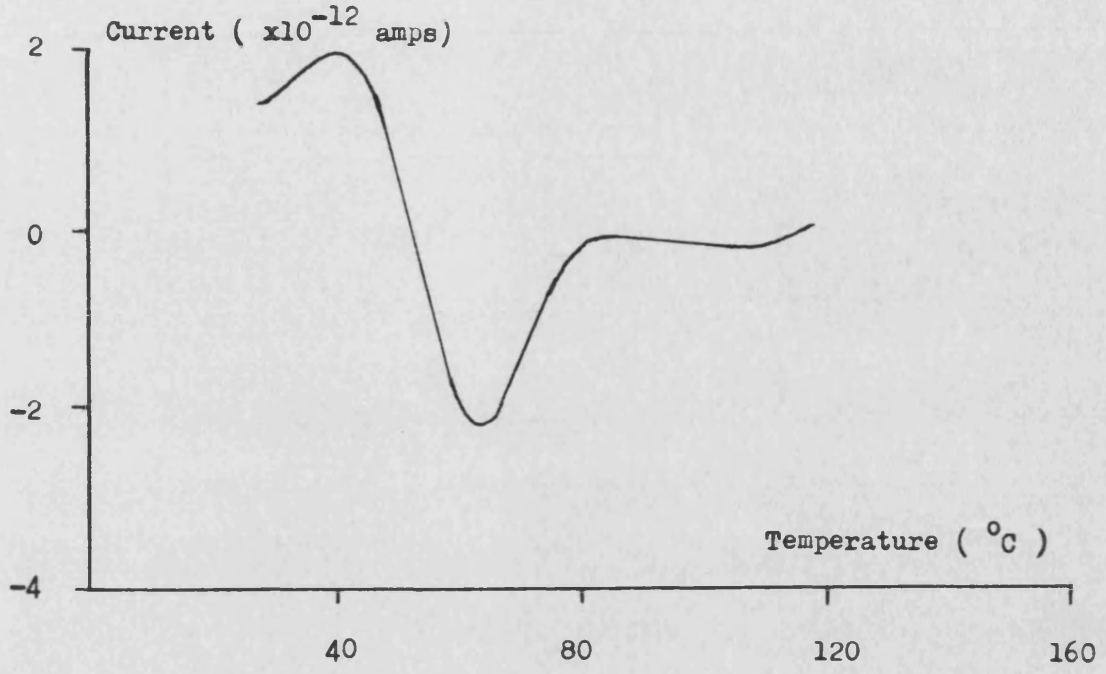

Figure 2.30. Air gap TSDC of an electrised Avicel PH102 compact. The compact was 4.3mm in thickness.

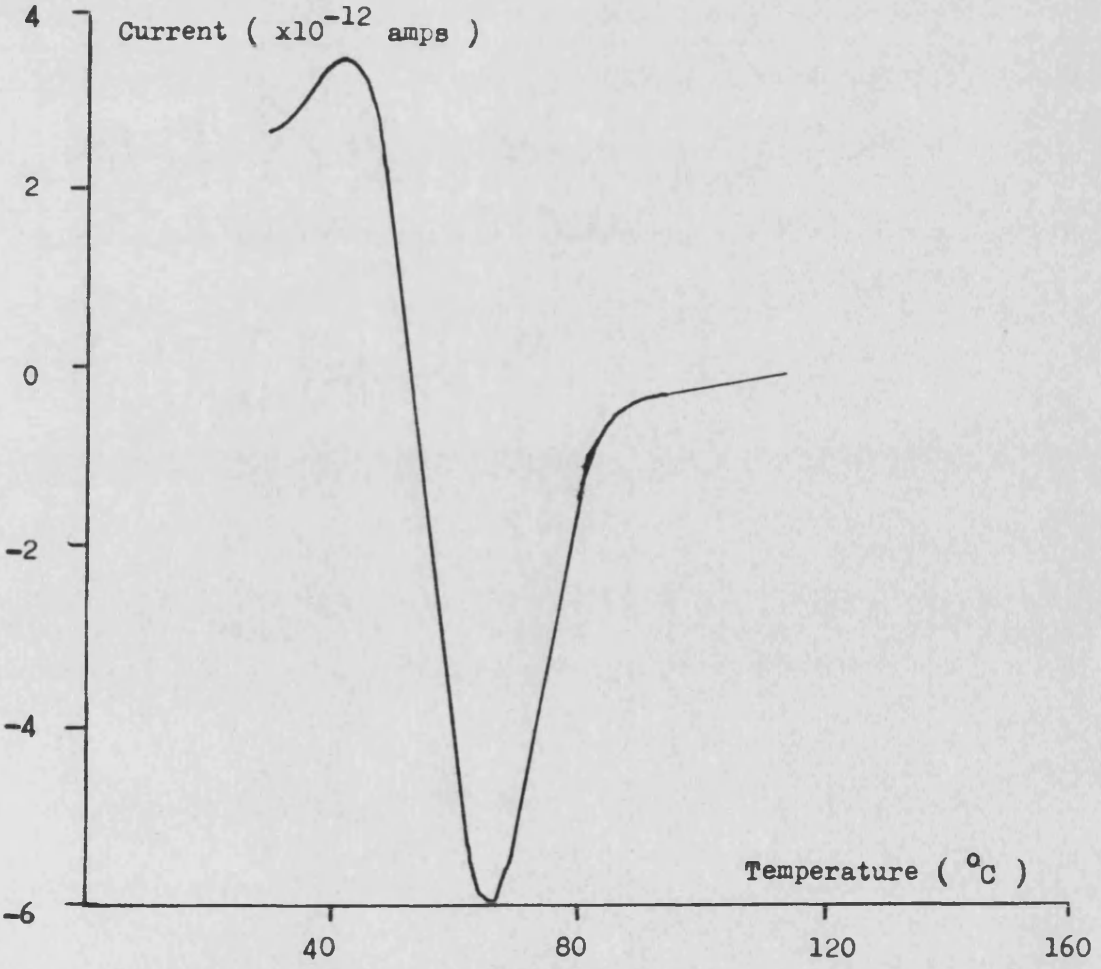

Figure 2.31. Air gap TSDC of an electrised Avicel PH102 compact. The compact was 5.8mm thick.

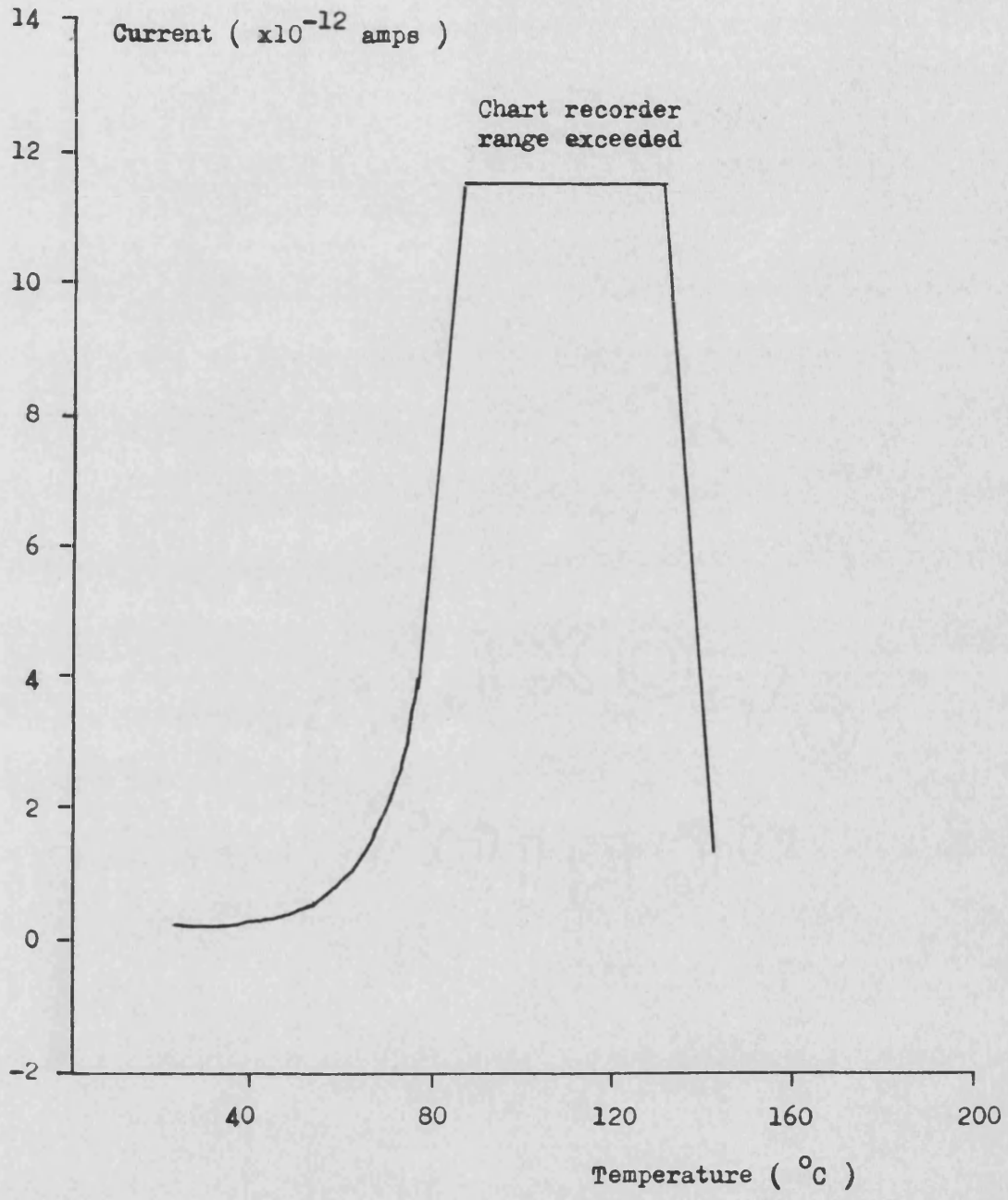

Figure 2.32. Contact TSDC of an unprocessed Elcema G250 compact.

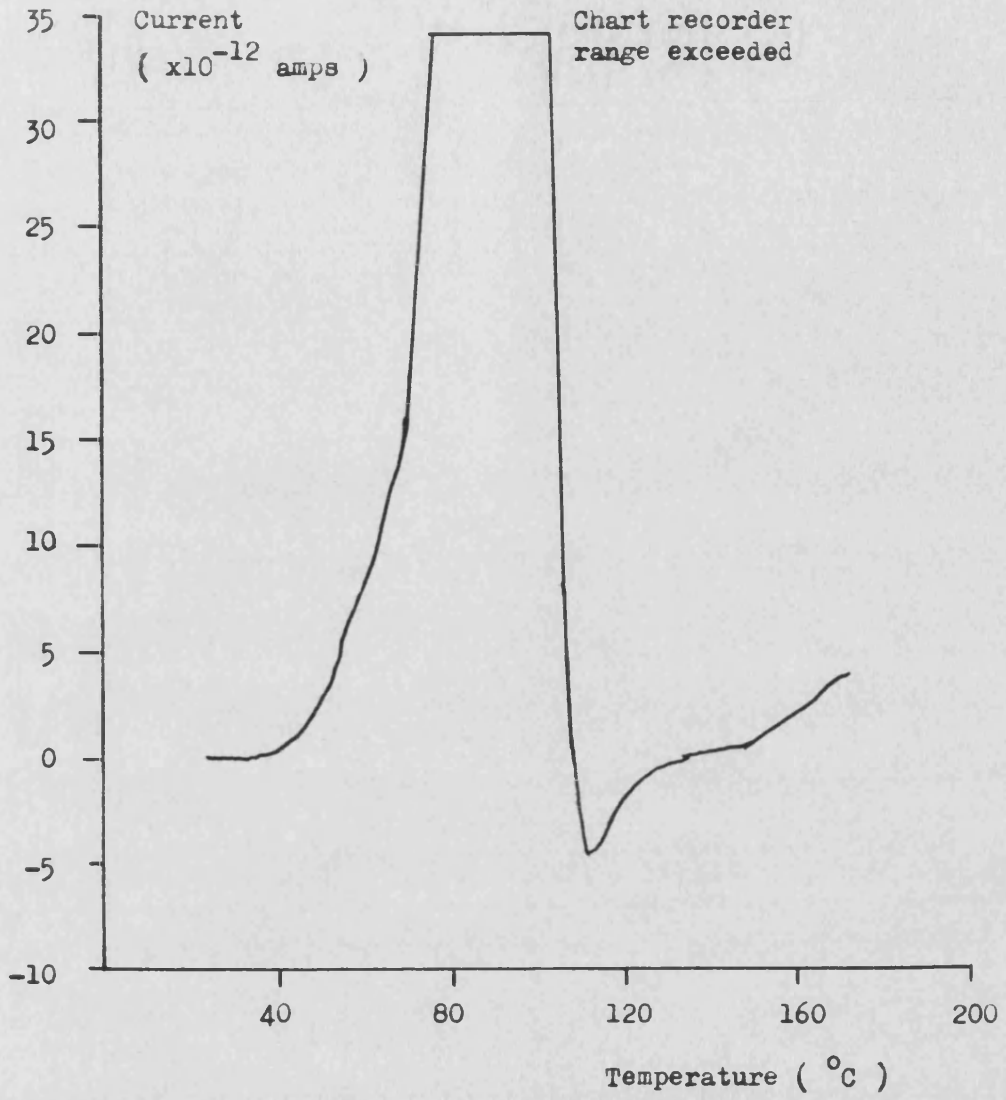

Figure 2.33. Contact TSDC of an unprocessed Elcema G250 compact.

Figure 2.34. Contact TSDC of a dried Elcema G250 compact.

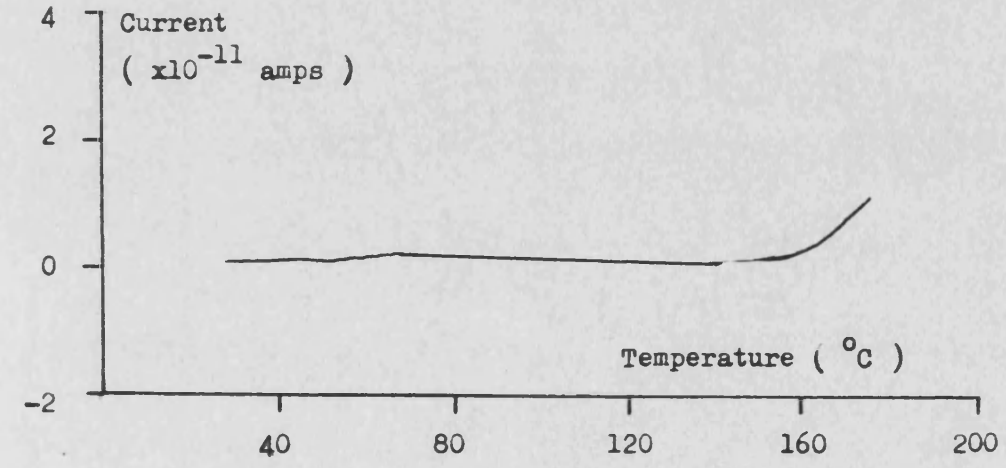

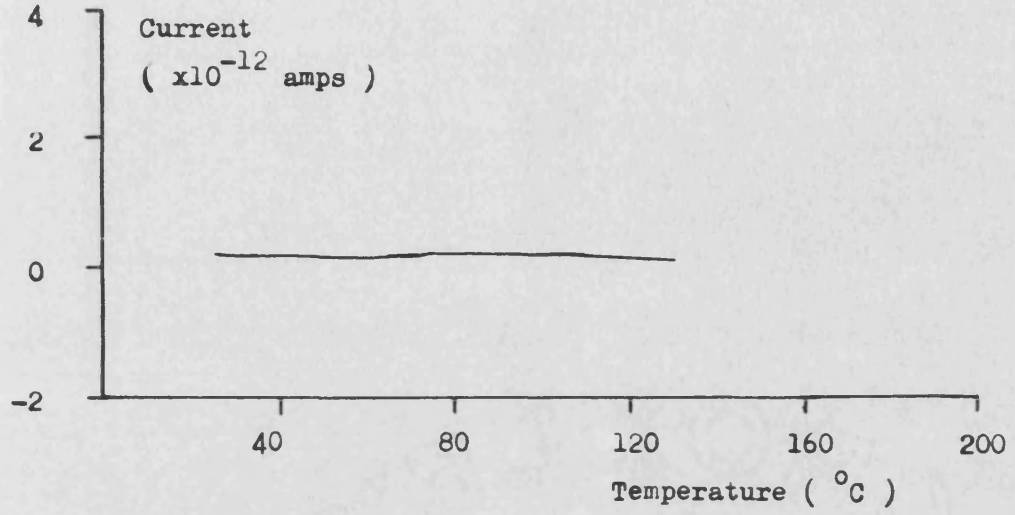

Figure 2.35. Air gap TSDC of an unprocessed Elcema G250 compact.

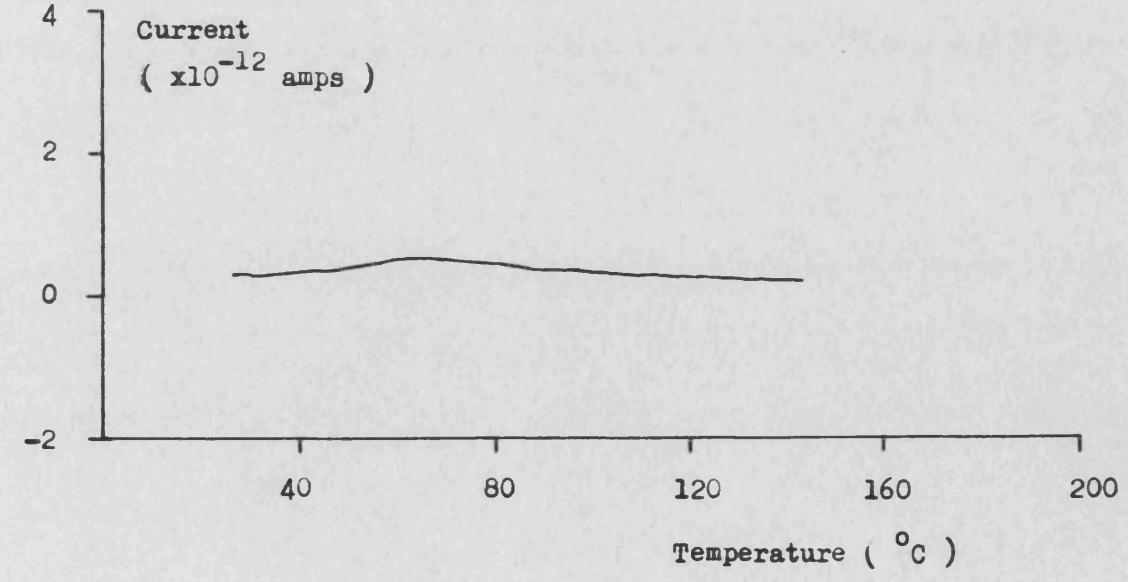

Figure 2.36. Air gap TSDC of an electrised Elcema G250 compact.
The compact was powdered before TSDC.

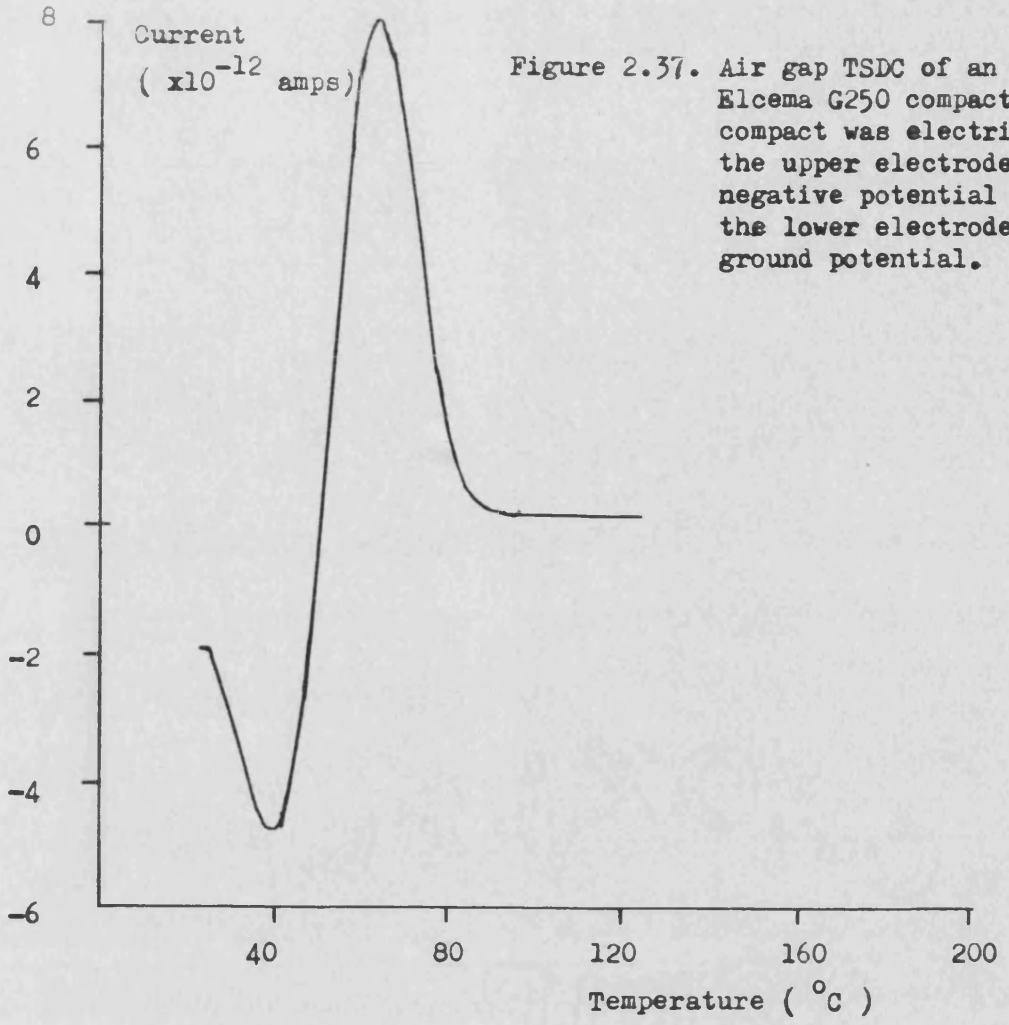

Figure 2.37. Air gap TSDC of an electrised Elcema G250 compact. The compact was electrised with the upper electrode at a negative potential and the lower electrode at ground potential.

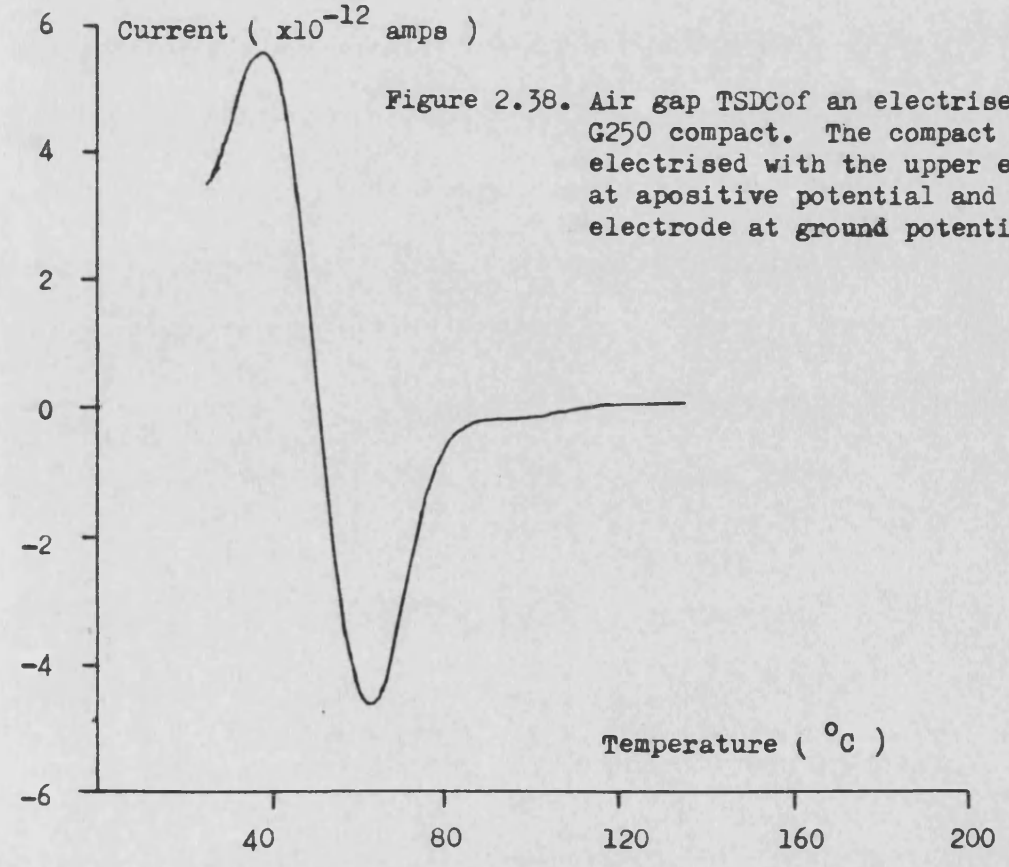

Figure 2.38. Air gap TSDCof an electrised Elcema G250 compact. The compact was electrised with the upper electrode at apositive potential and the lower electrode at ground potential.

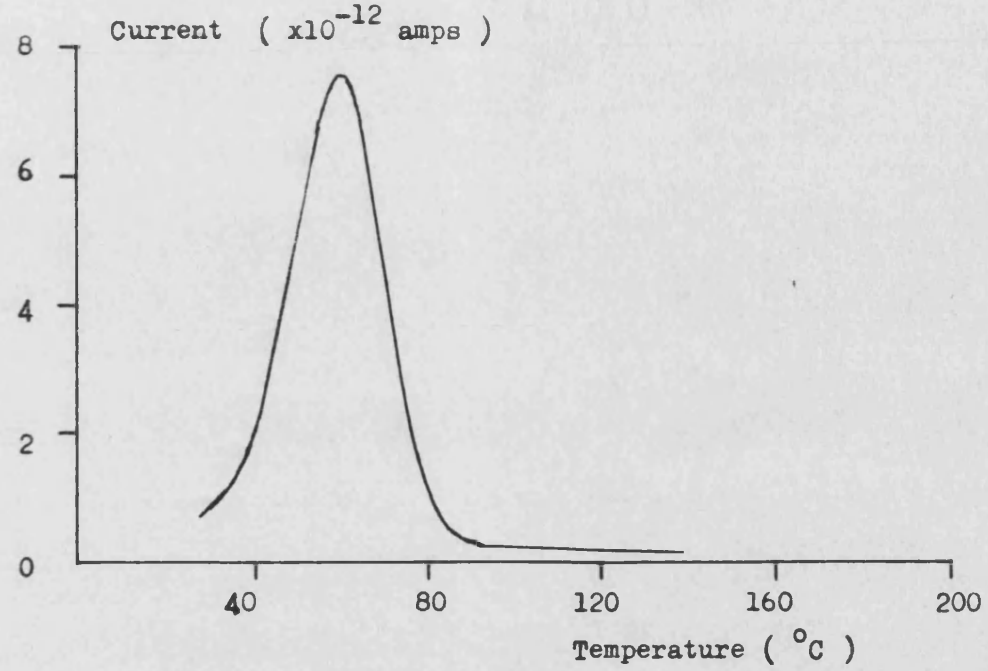

Figure 2.39. Air gap TSDC of an electrised Elcema G250 compact. The compact was electrised with the upper electrode at negative potential and the lower electrode at ground potential. The electrised compact was then wrapped in aluminium foil and stored for approximately 15 hours under ambient atmospheric conditions.

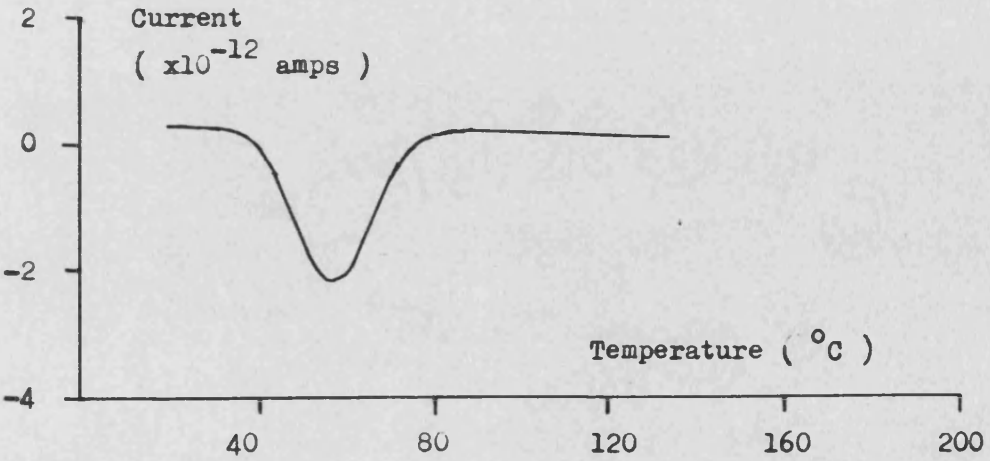

Figure 2.40. Air gap TSDC of an electrised Elcema G250 compact. The compact was electrised with the upper electrode at positive potential and the lower electrode at ground potential. The electrised compact was then wrapped in aluminium foil and stored for approximately 15 hours under ambient atmospheric conditions.

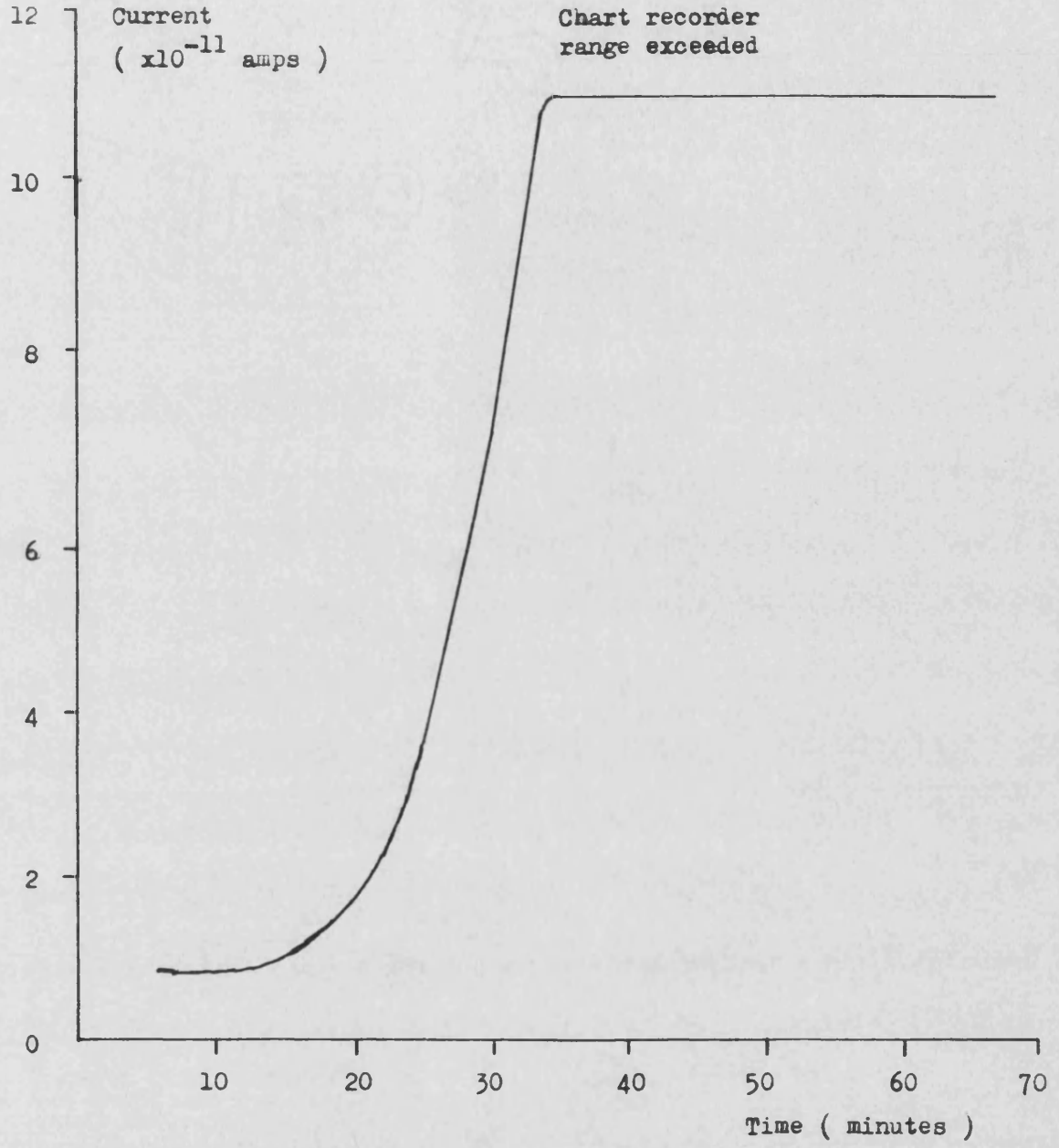

Figure 2.41. Contact TSDC of an electrised Elcema G250 compact. The compact was exposed to ambient atmospheric conditions for approximately 20 hours, without the protection of aluminium foil, prior to TSDC. Heating rate 2°C min^{-1}.

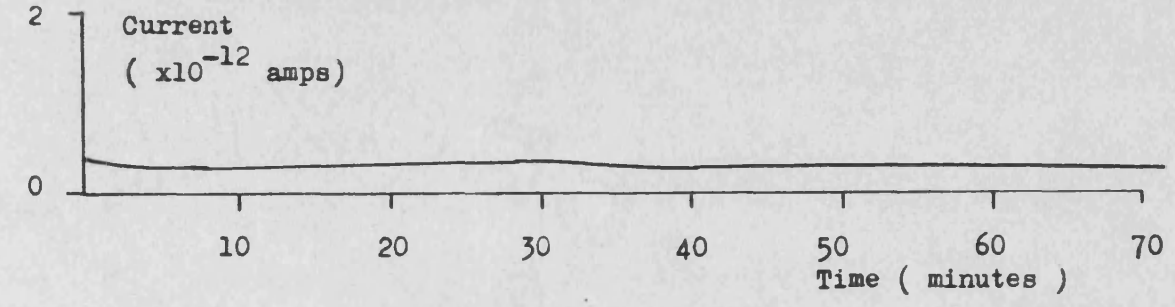

Figure 2.42. Air gap TSDC of an electrised Elcema G250 compact. The compact was exposed to ambient atmospheric conditions for approximately 40 hours, without the protection of aluminium foil, prior to TSDC. Heating rate 2°C min^{-1}.

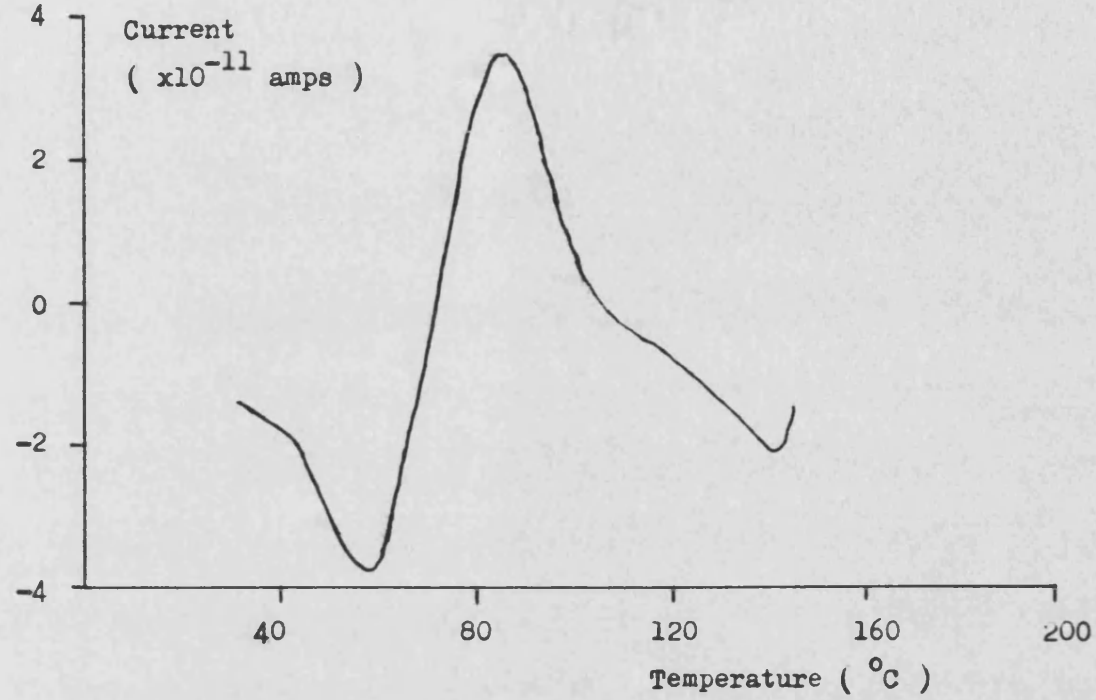

Figure 2.43. Contact TSDC of an electrised Elcema G250 compact. The compact was stored, wrapped in aluminium foil, in air dried by phosphorous pentoxide for 1 hour prior to TSDC.

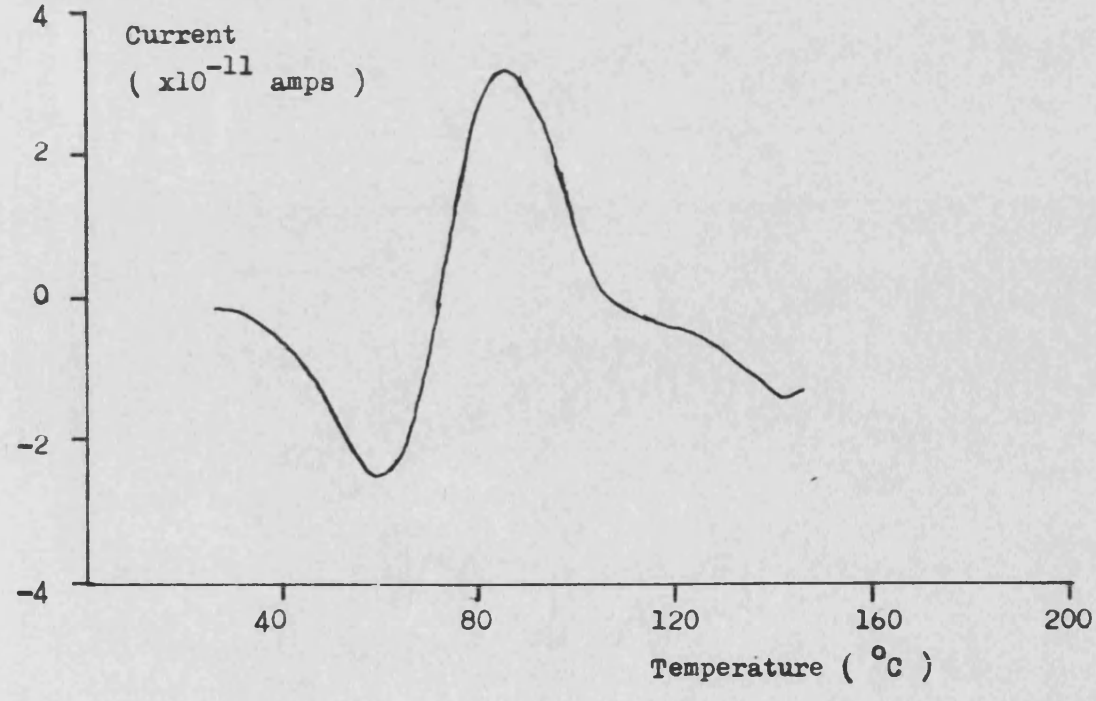

Figure 2.44. Contact TSDC of an electrised Elcema G250 compact. The compact was stored, wrapped in aluminium foil, in air dried by phosphorous pentoxide for 25 hours prior to TSDC.

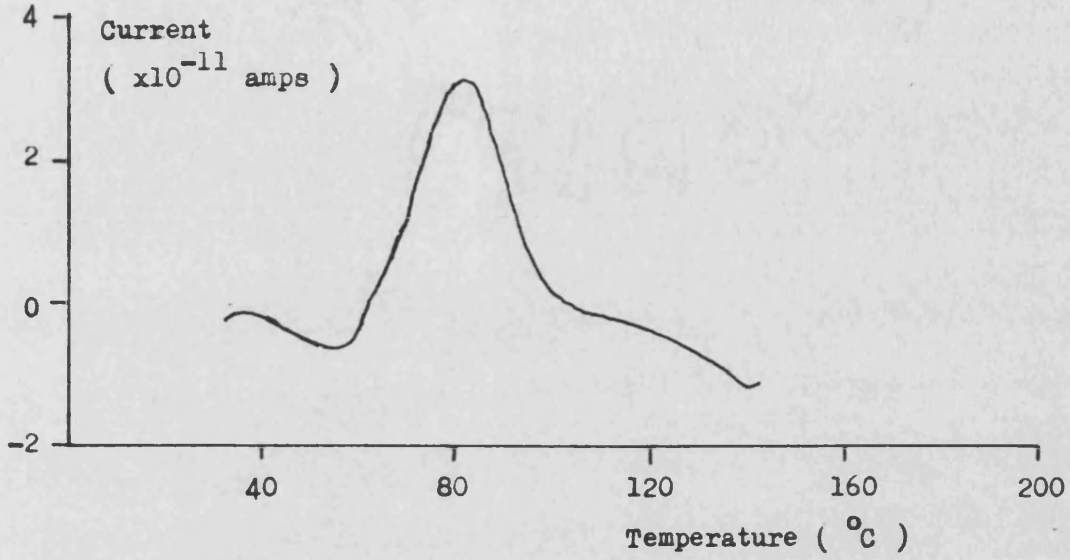

Figure 2.45. Contact TSDC of an electrised Elcema G250 compact. The compact was stored, wrapped in aluminium foil, in air dried by phosphorous pentoxide for 72 hours 20 minutes prior to TSDC.

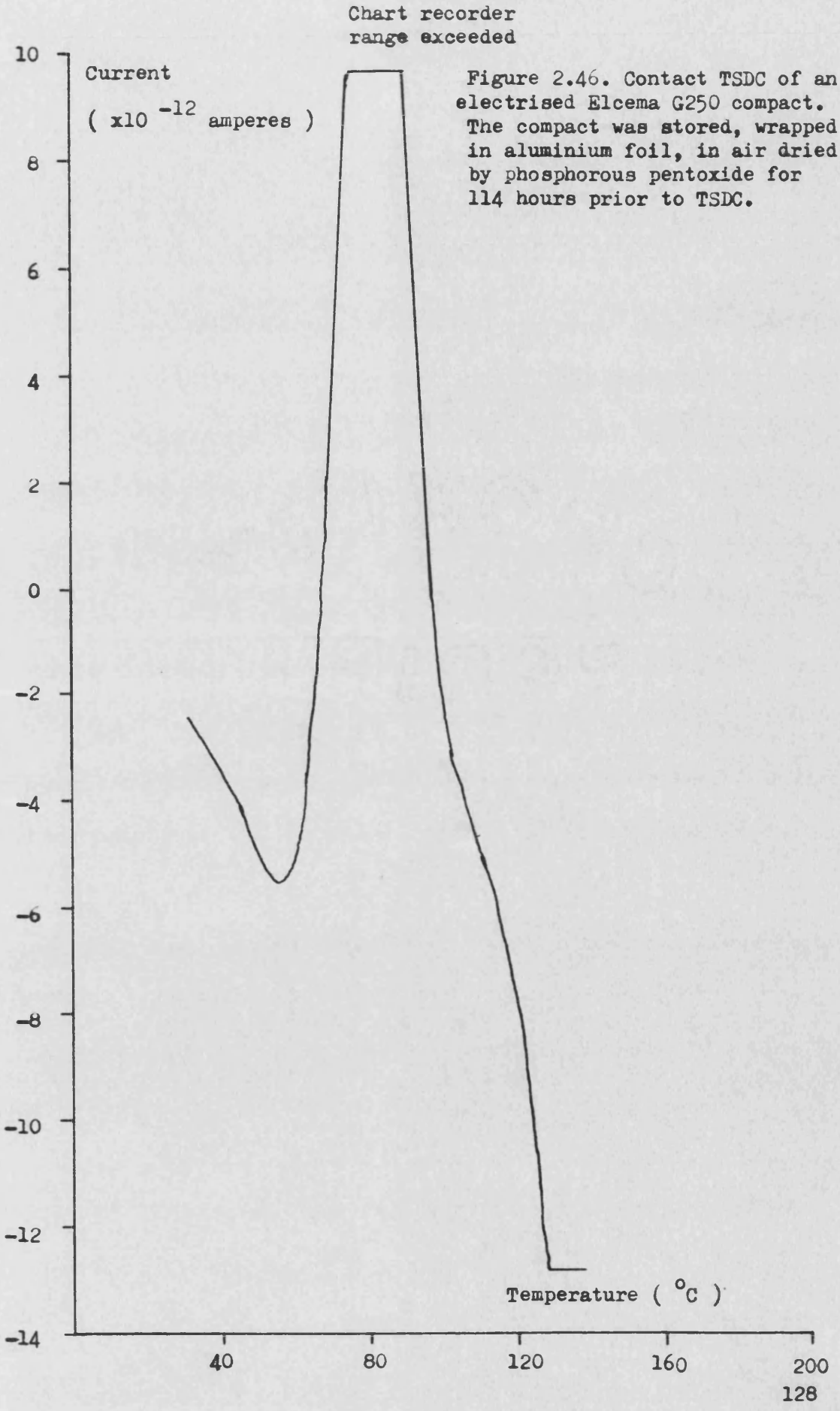

Figure 2.46. Contact TSDC of an electrised Elcema G250 compact. The compact was stored, wrapped in aluminium foil, in air dried by phosphorous pentoxide for 114 hours prior to TSDC.

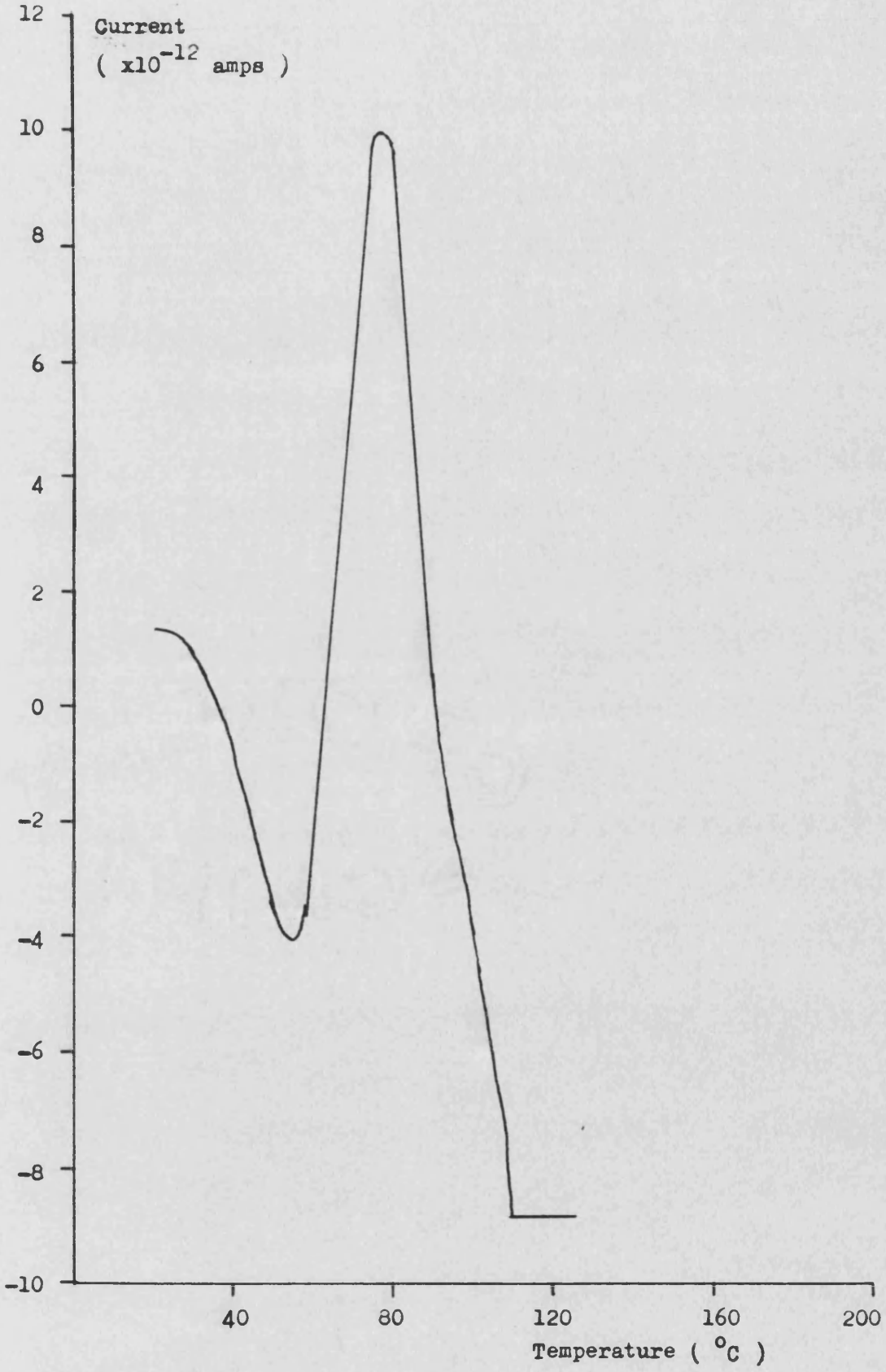

Figure 2.47. Contact TSDC of an electrised Elcema G250 compact. The compact was stored, wrapped in aluminium foil, in air dried by phosphorous pentoxide for 408 hours prior to TSDC.

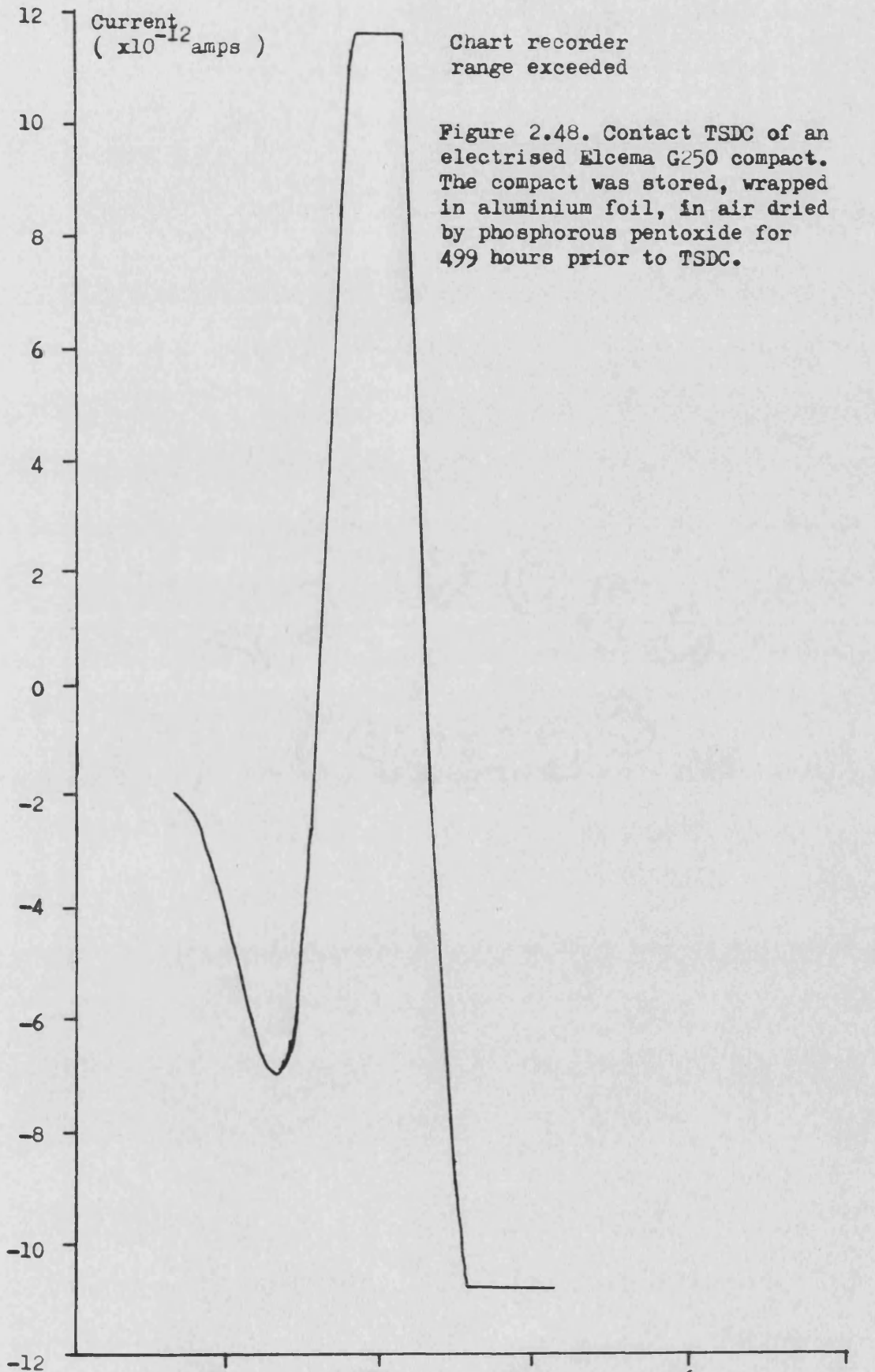

Chart recorder range exceeded

Figure 2.48. Contact TSDC of an electrised Elcema G250 compact. The compact was stored, wrapped in aluminium foil, in air dried by phosphorous pentoxide for 499 hours prior to TSDC.

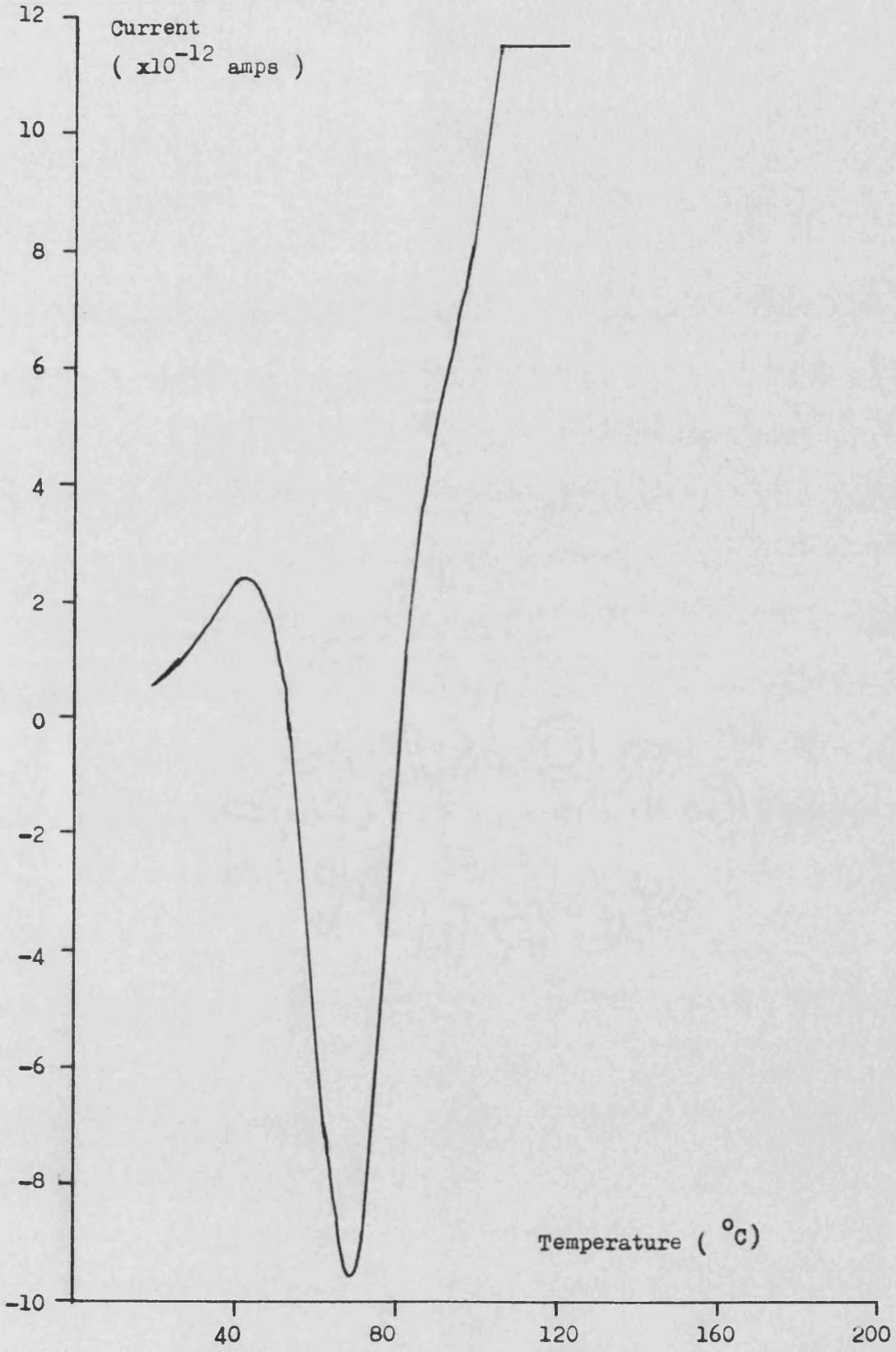

Figure 2.49. Contact TSDC of an electrised Elcema G250 compact. The compact was stored, wrapped in aluminium foil, in air dried by phosphorous pentoxide for 503 hours prior to TSDC. The inversion of this trace compared to Figures 2.43 -2.48 is due to the orientation of the compact in the discharge cell.

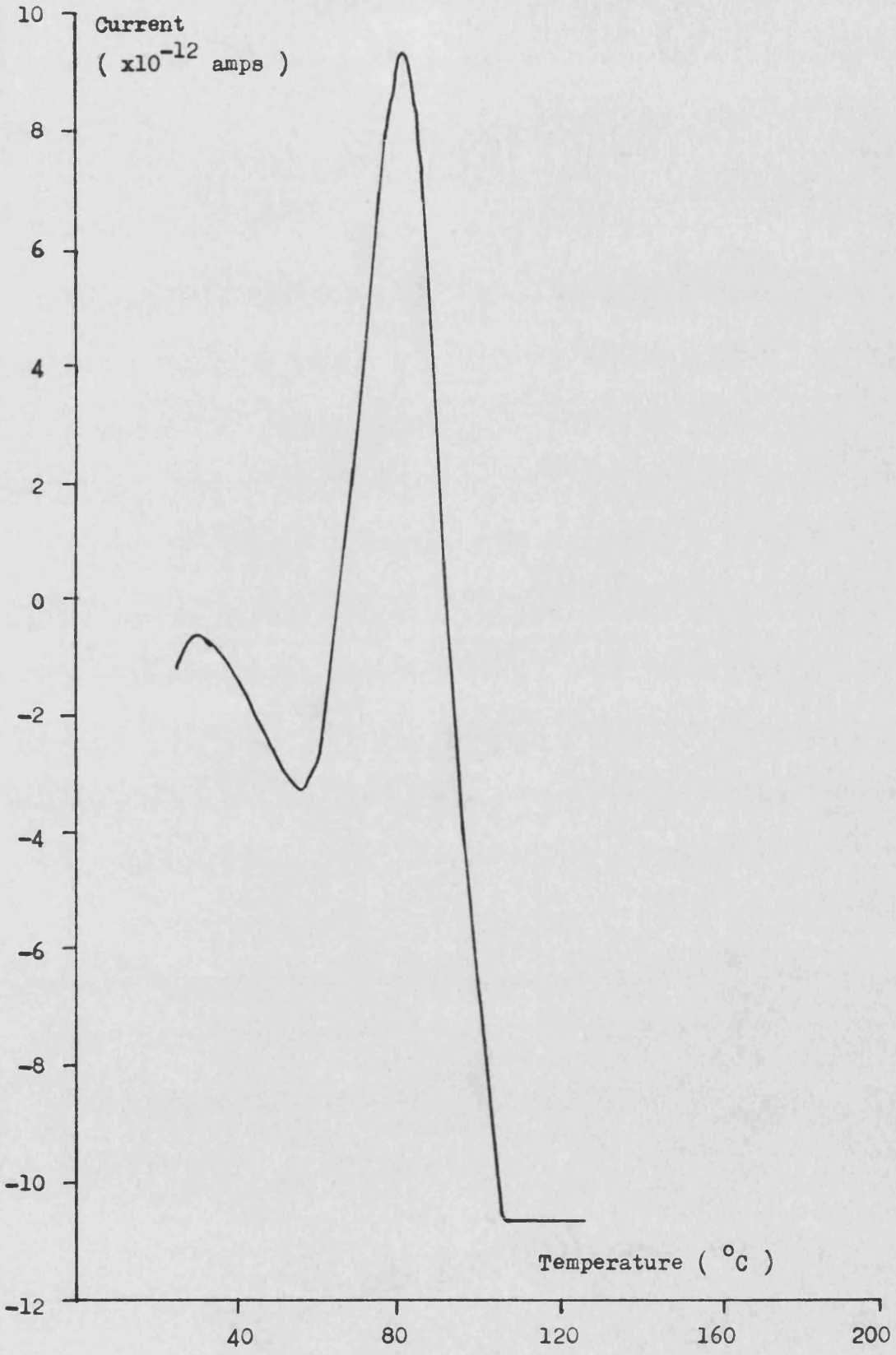

Figure 2.50. Contact TSDC of a charged Elcema G250 compact. The compact was stored, wrapped in aluminium foil, in air dried by phosphorous pentoxide for 576 hours prior to TSDC.

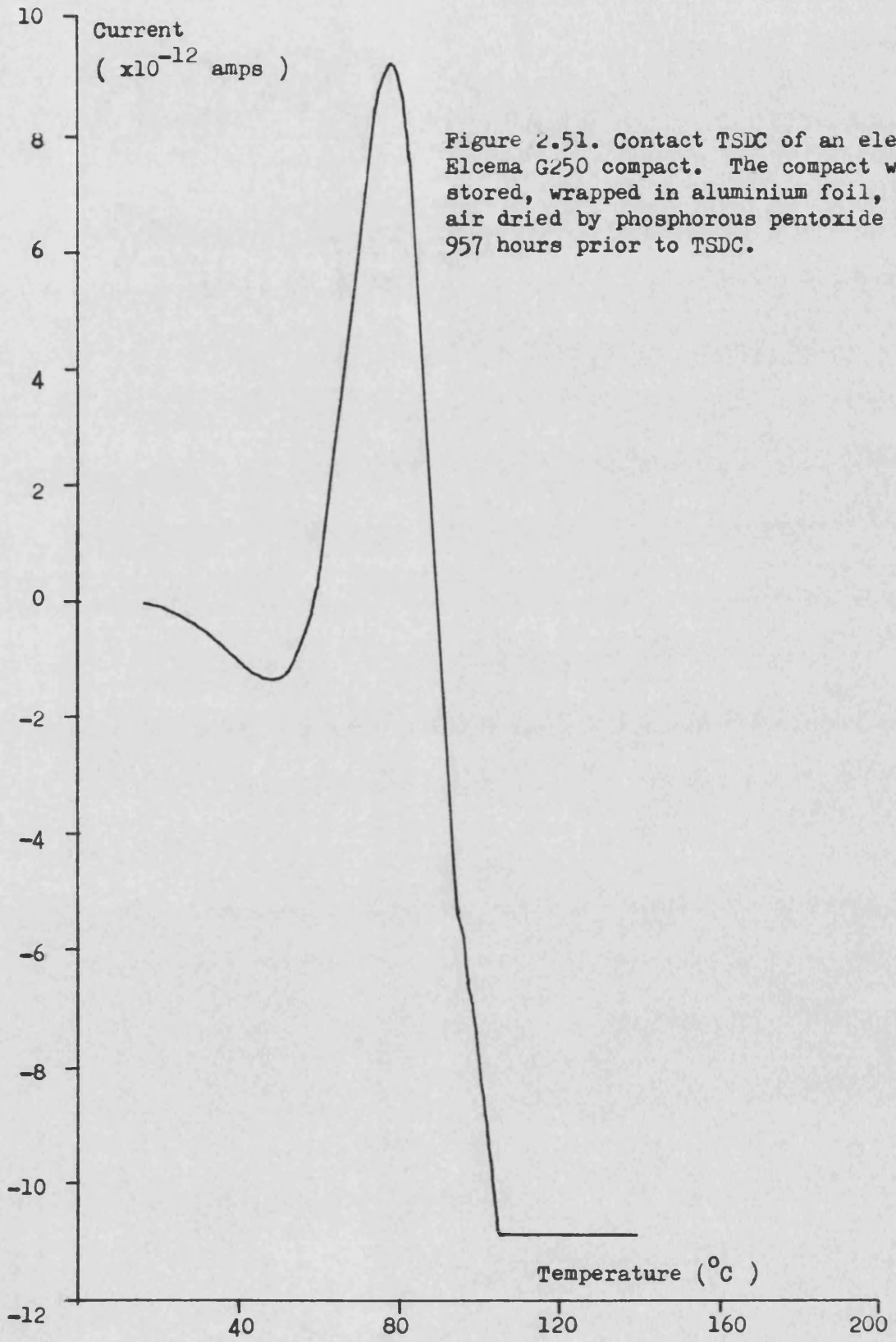

Figure 2.51. Contact TSDC of an electrised Elcema G250 compact. The compact was stored, wrapped in aluminium foil, in air dried by phosphorous pentoxide for 957 hours prior to TSDC.

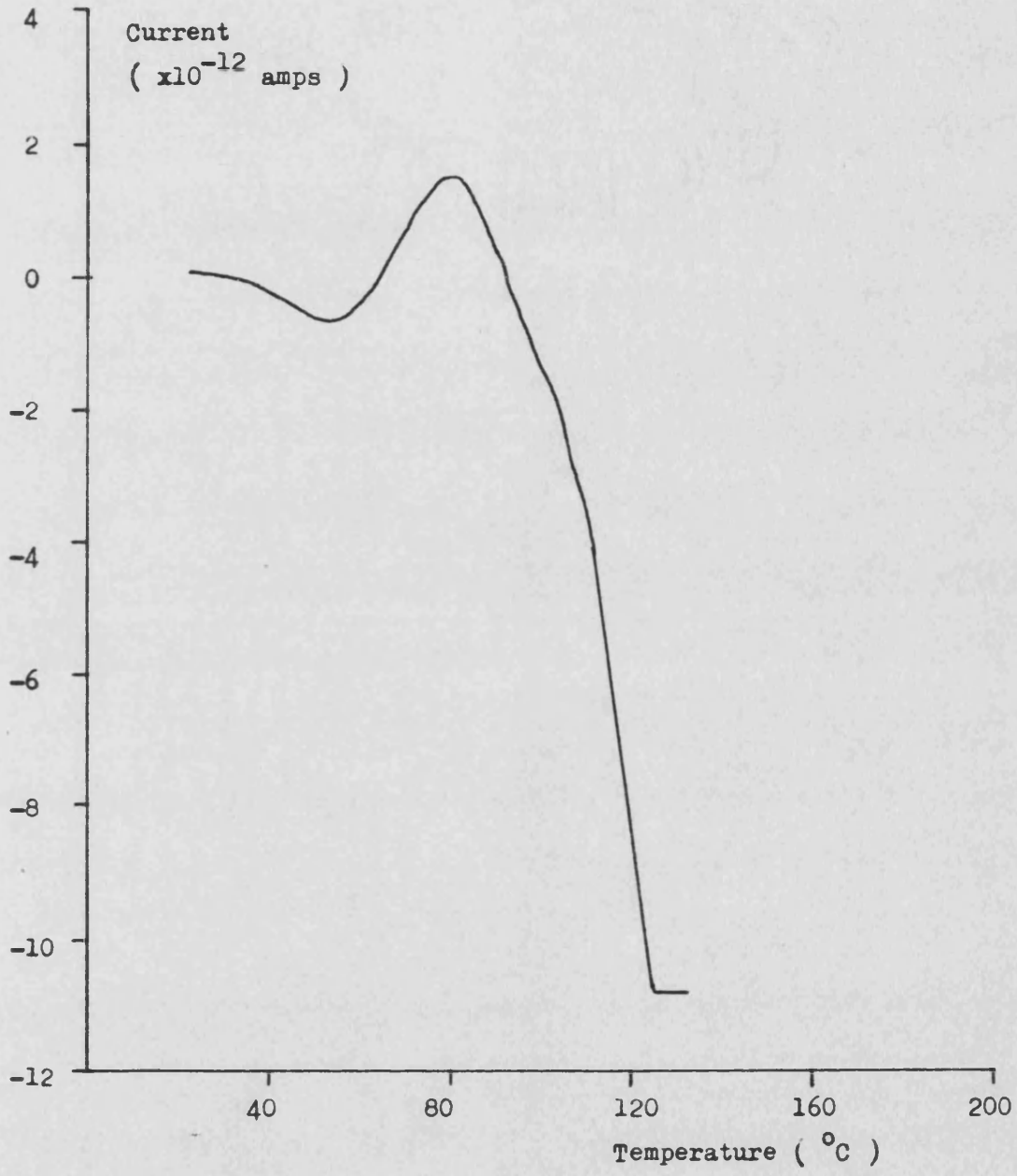

Figure 2.52. Contact TSDC of an electrised Elcema G250 compact. The compact was stored, wrapped in aluminium foil, in air dried by phosphorous pentoxide for 1370 hours prior to TSDC.

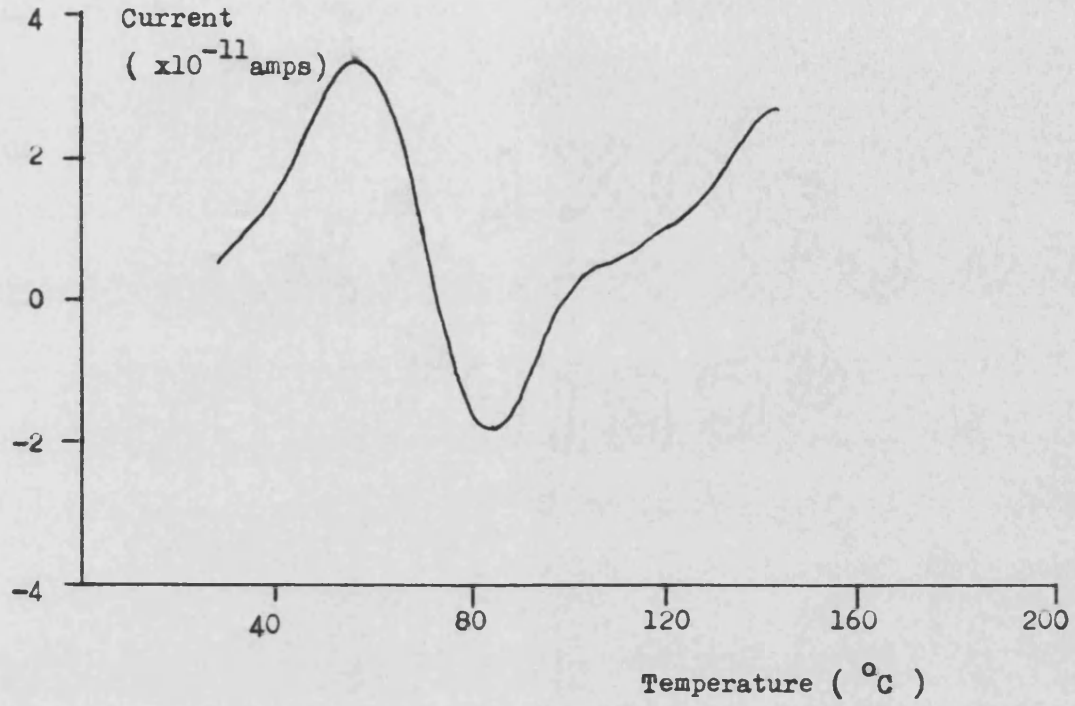

Figure 2.53. Contact TSDC of an electrised Elcema G250 compact. The compact was stored, wrapped in aluminium foil, under a vacuum for 0 hours prior to TSDC.

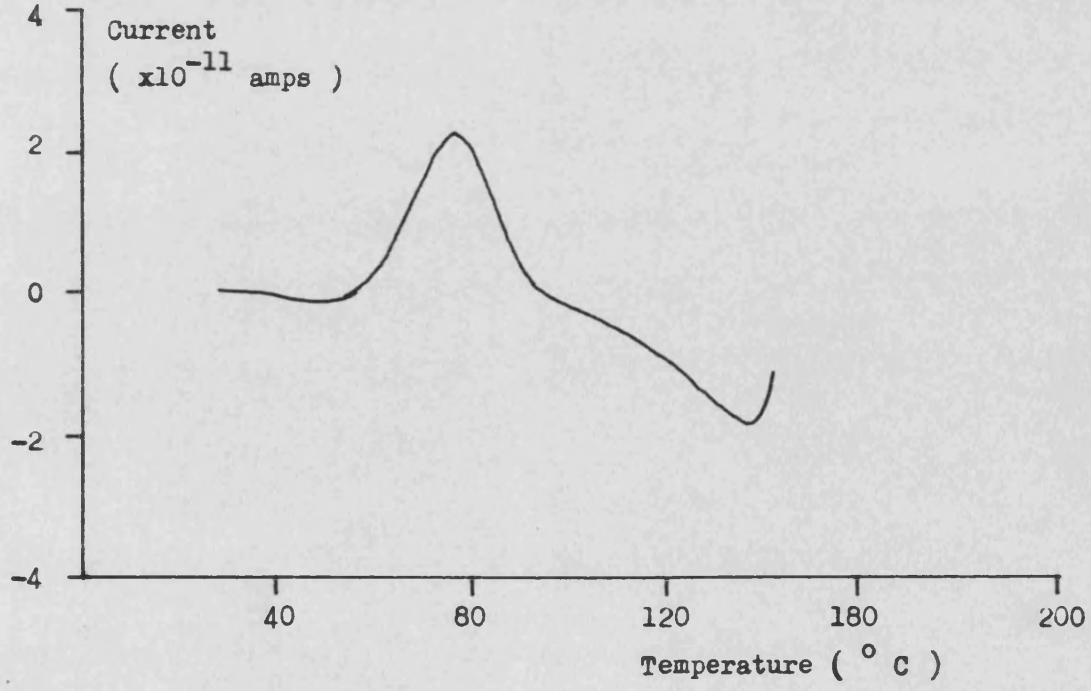

Figure 2.54, Contact TSDC of an electrised Elcema G250 compact. The compact was stored, wrapped in aluminium foil, under vacuum for 70 hours prior to TSDC.

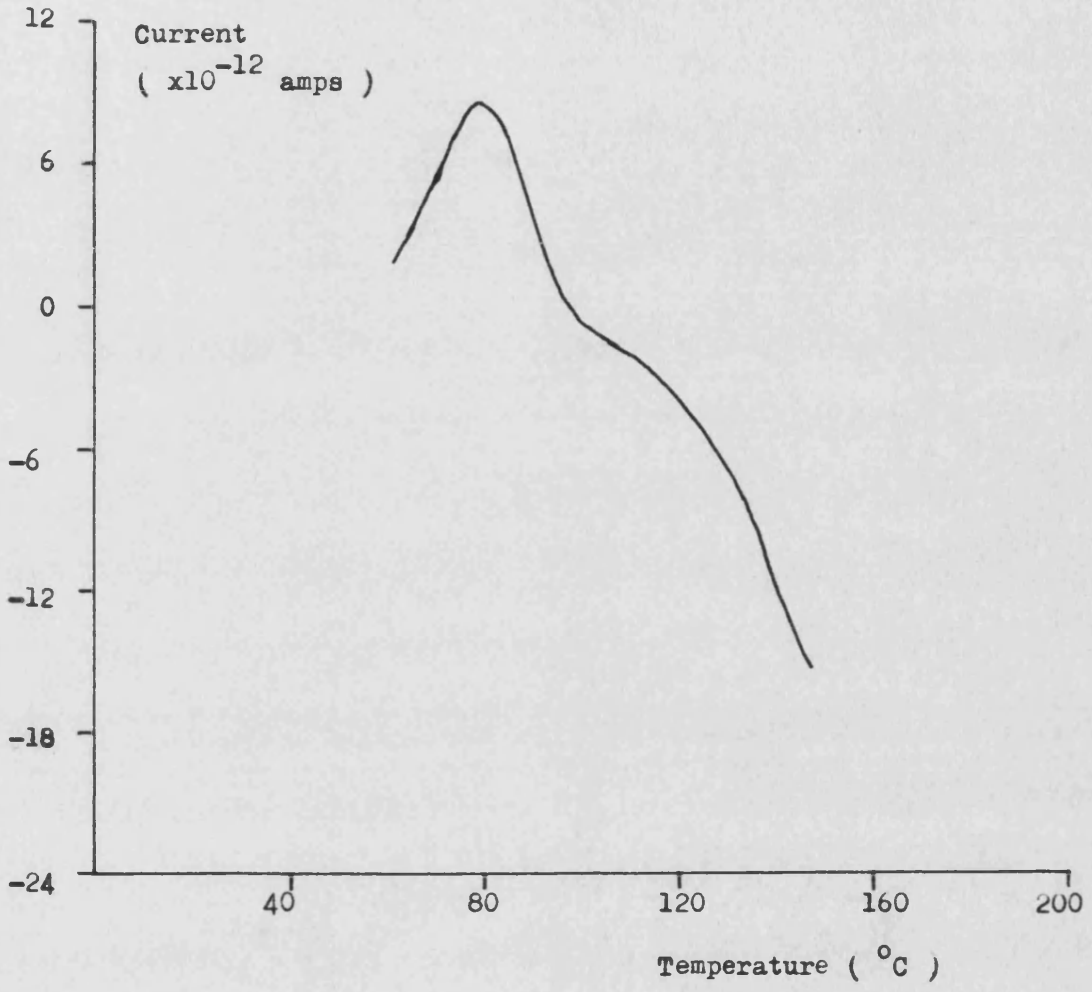

Figure 2.55. Contact TSDC of an electrised Elcema G250 compact. The compact was stored, wrapped in aluminium foil, under vacuum for 107 hours 10 minutes prior to TSDC.

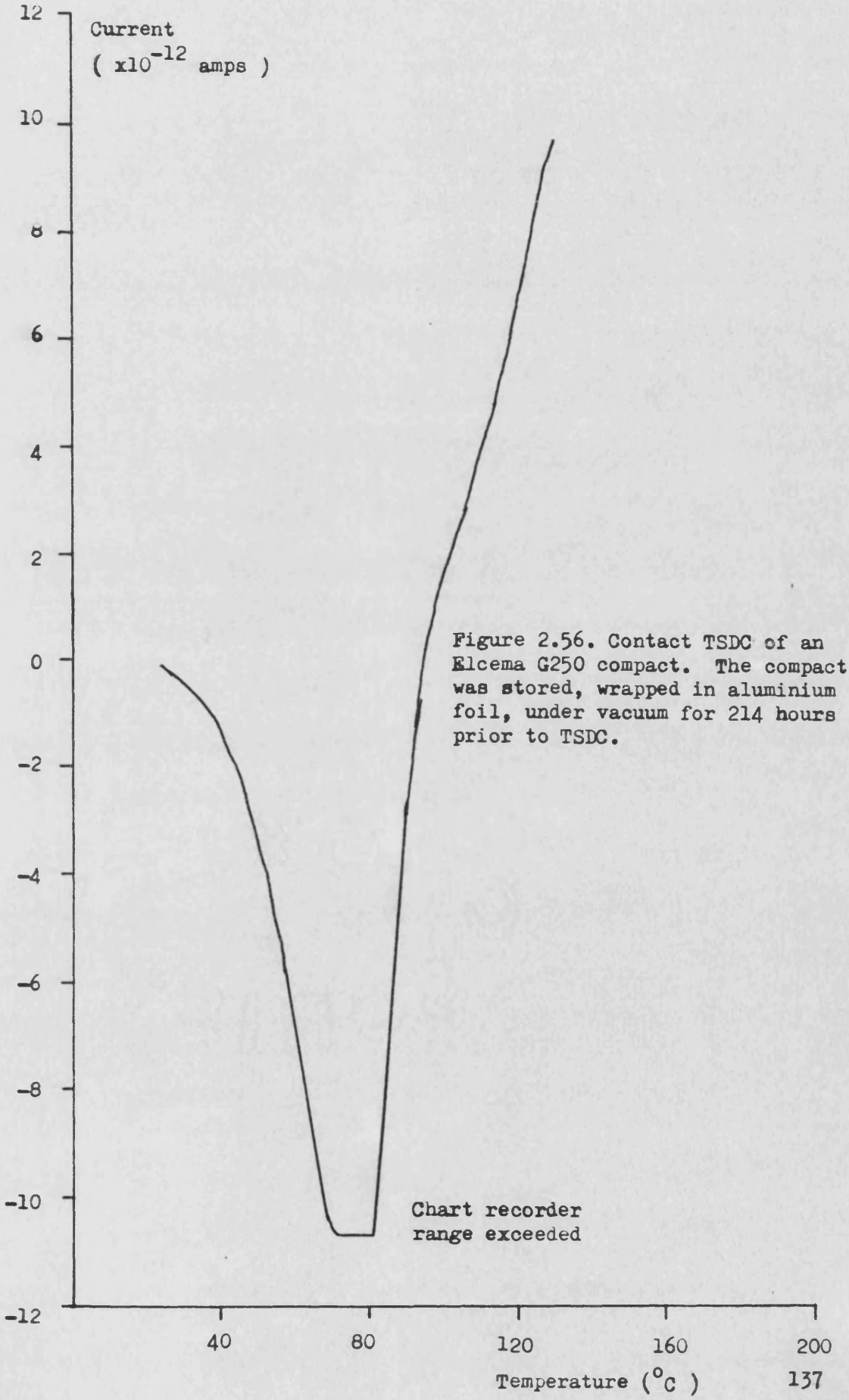

Figure 2.56. Contact TSDC of an Elcema G250 compact. The compact was stored, wrapped in aluminium foil, under vacuum for 214 hours prior to TSDC.

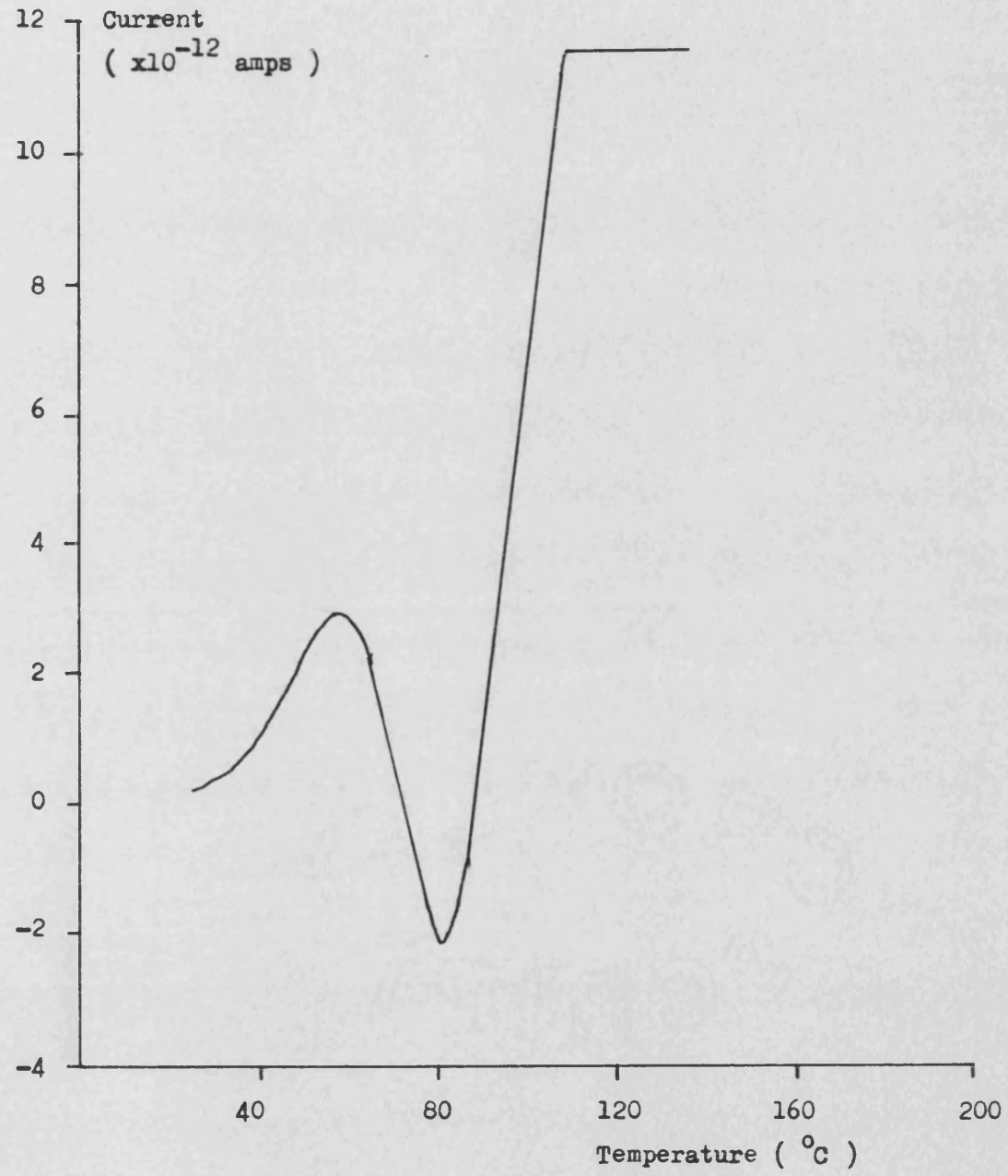

Figure 2.57. Contact TSDC of an electrised Elcema G250 compact. The compact was stored, wrapped in aluminium foil, under vacuum for 663 hours prior to TSDC.

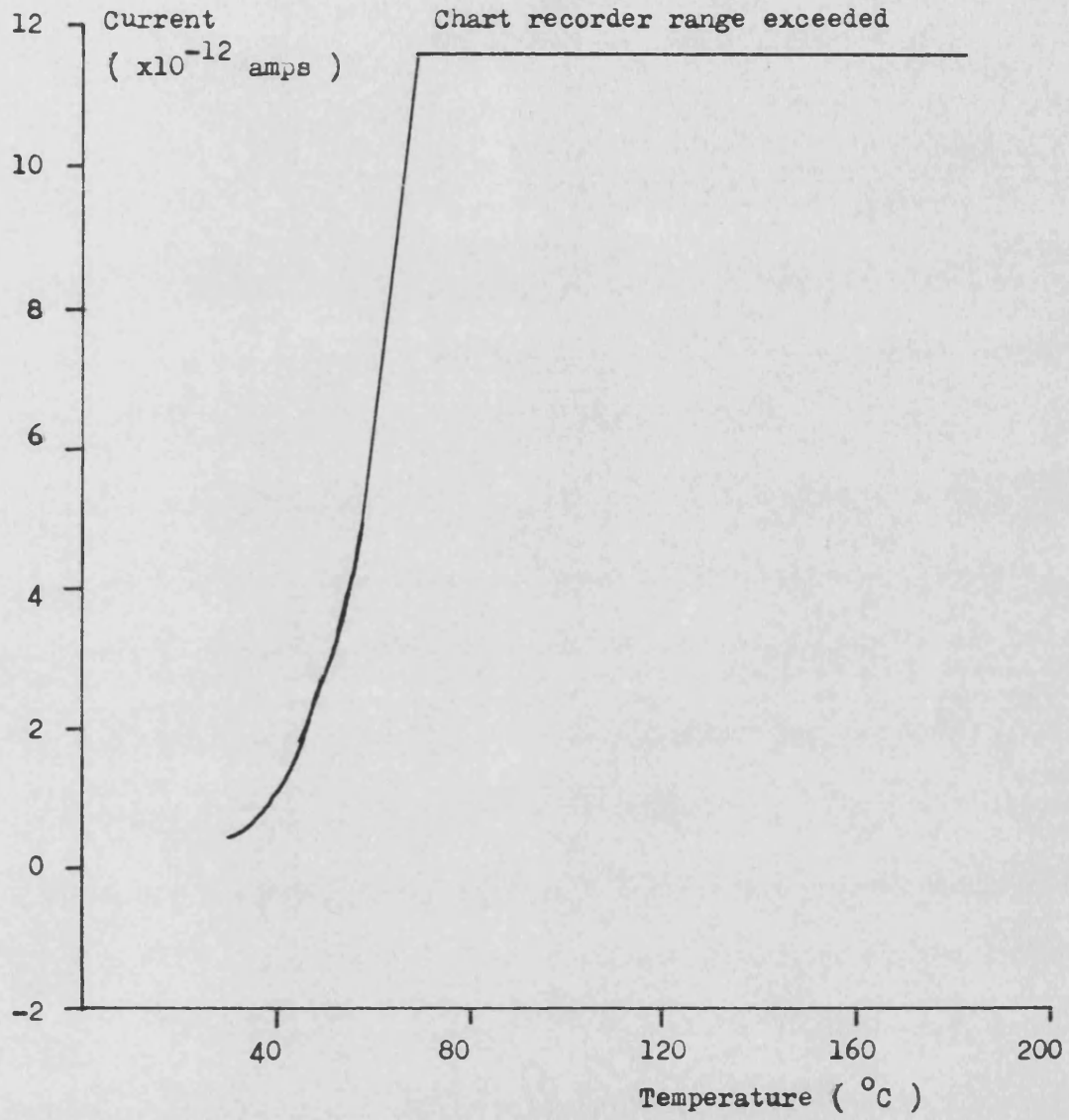

Figure 2.58. Contact TSDC of an electrised Elcema G250 compact. The compact was stored at 55% relative humidity for two hours thirty minutes prior to TSDC. Unlike compacts stored in low humidity environments, the compacts stored at 55% relative humidity were not wrapped in aluminium foil .

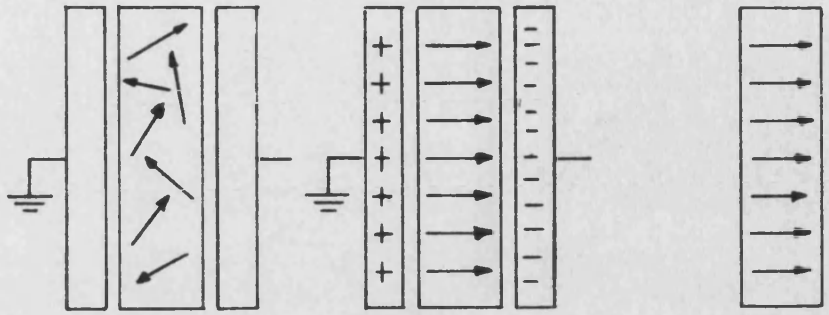

Formation of an electret due to the alignment of dipoles

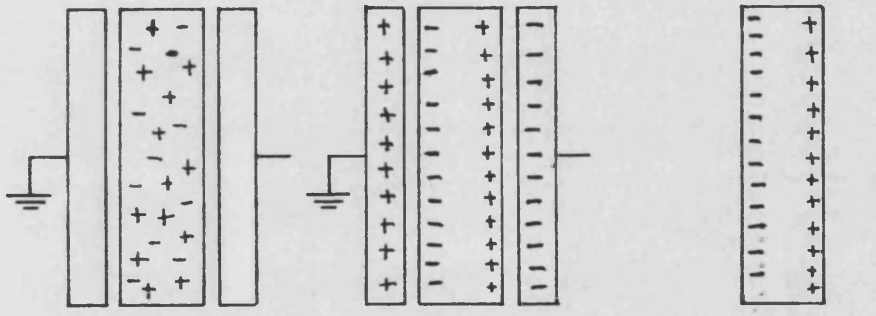

Formation of an electret due to the separation of charge carrying species.

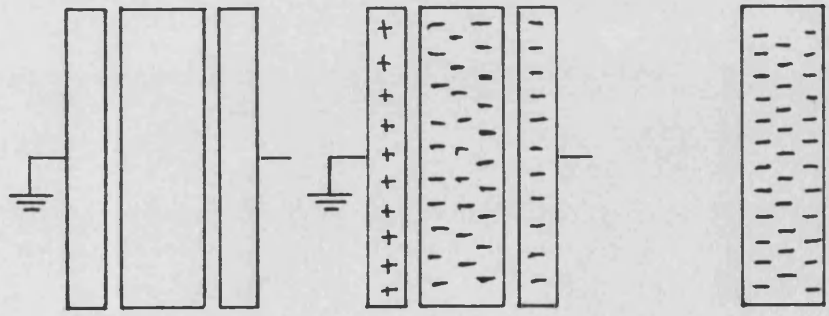

Formation of an electret by injection of a space charge.

Figure 2.59. Schematic representation of the three types of electret that can be formed due to the presence of dipoles or a charge carrying species. Note that all three types of charge storage mechanism can be present simultaneously.

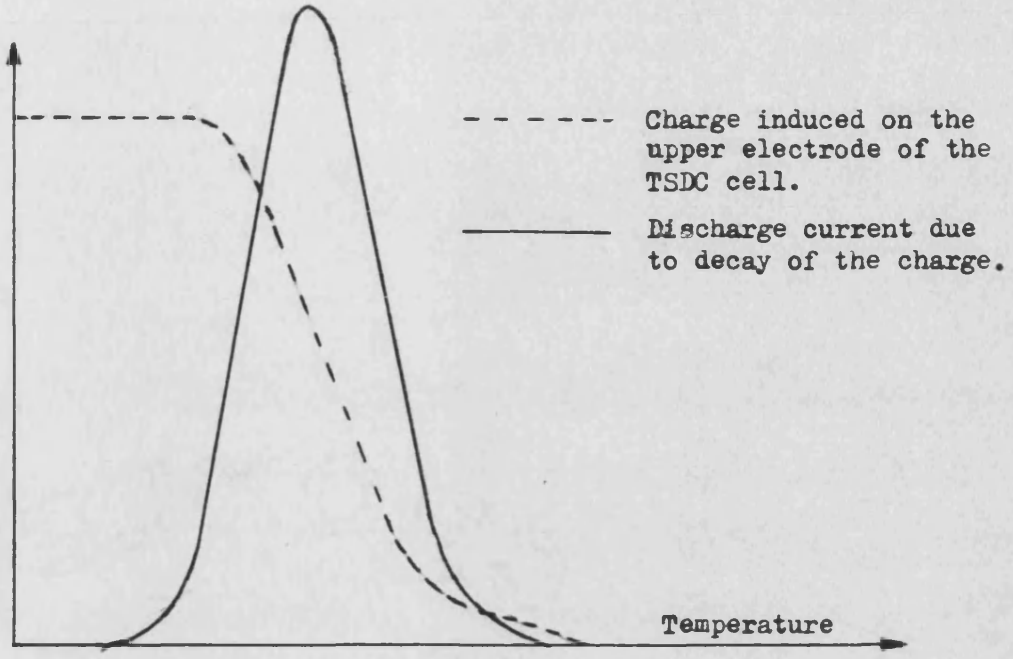

Figure 2.60. Schematic representation of the change in induced charge and the resulting discharge current for an electret with a single charging mechanism.

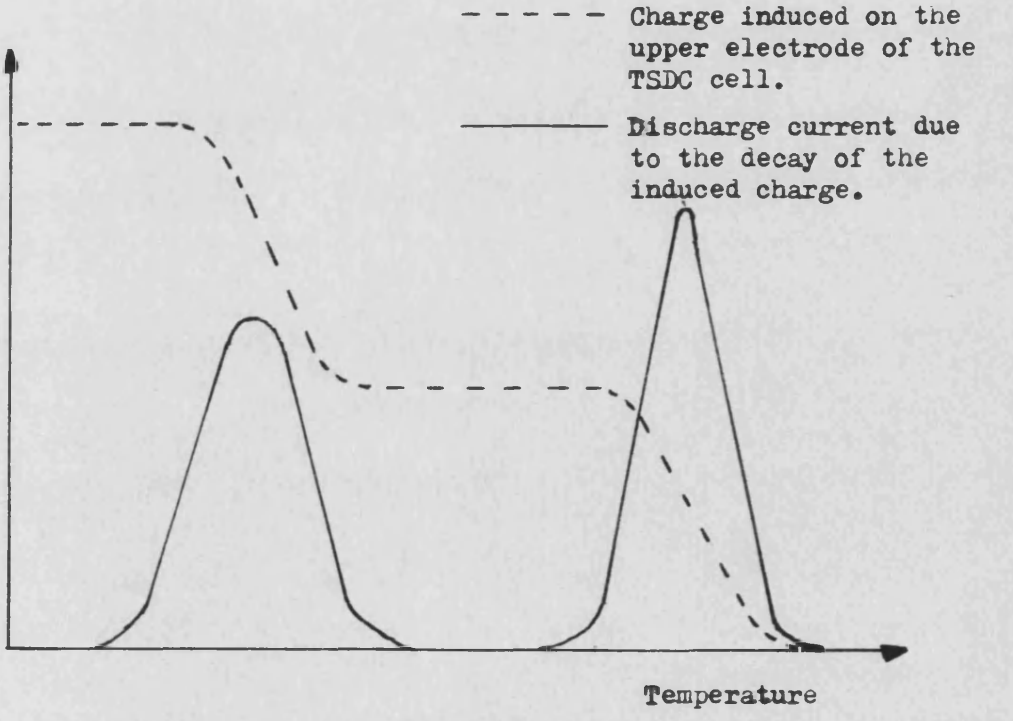

Figure 2.61. Schematic representation of the change in induced charge and the resulting discharge current for an electret with two charge storage mechanisms. The possible combinations are dipole/charge separation or two dipoles or separated charge carriers with different activation energies.

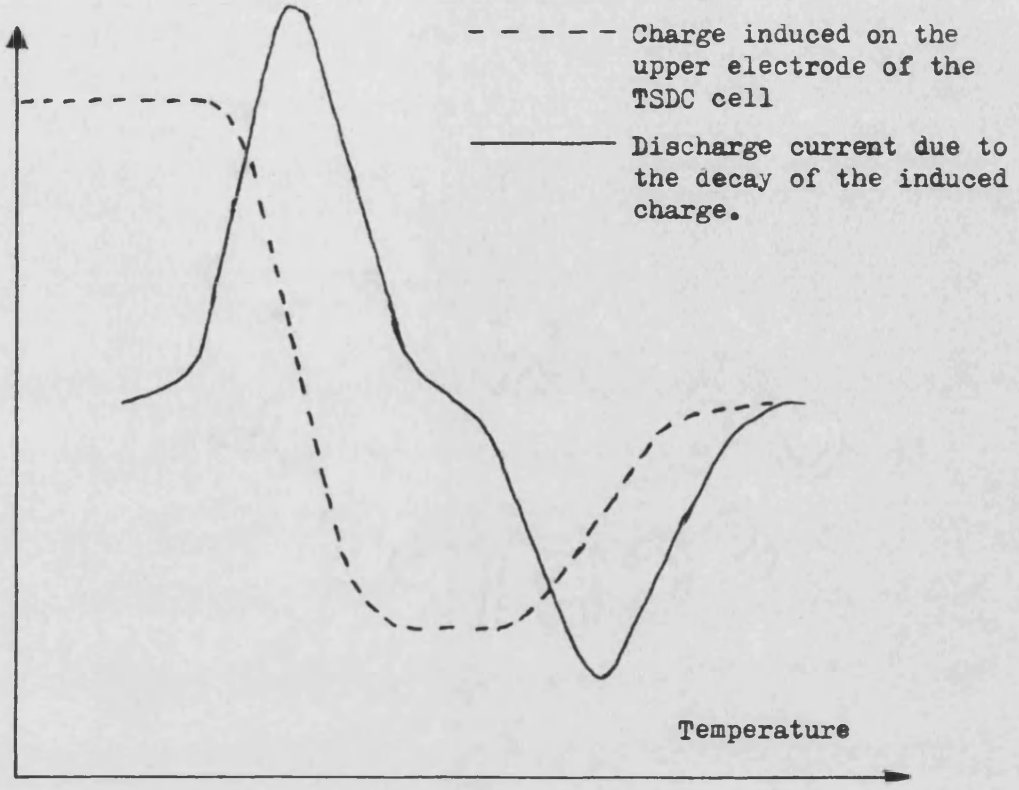

Figure 2.62. Schematic representation of the change in the induced charge and the resulting discharge current for an electret with two charge storage mechanisms. NB the presence of positive and negative charge indicates the the combinations of charge storage mechanisms possible are either dipole/space charge or charge separation/space charge.

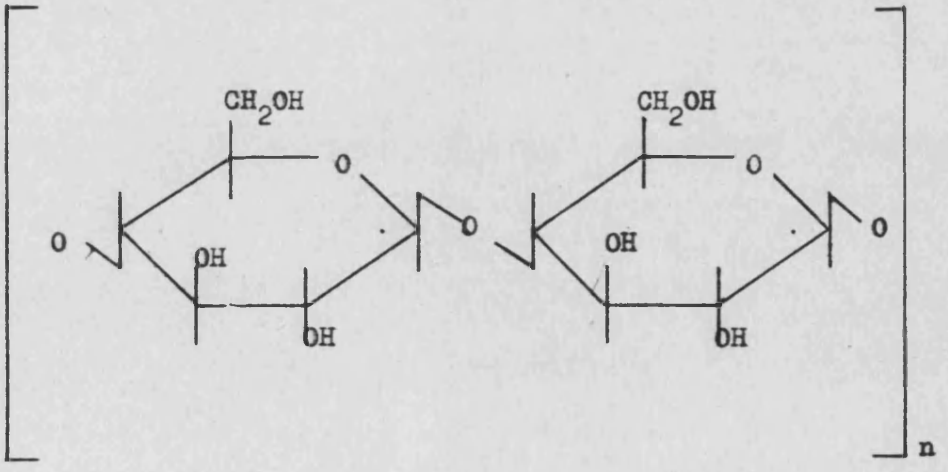

Figure 2.63. Chemical structure of the cellulose molecule.

Chapter 3.

3. Determination of the distribution of adherent particles in isolated ordered units using image analysis.

Measurement of the adhesion forces between the adherent fine particles and the carrier substrate in isolated ordered units can be performed using photomicrographic methods (96) but does suffer from several problems (104). The most significant of these problems is related to the fact that the surface to which the fine particles adhere is not flat so that wherever the plane of focus for the field of view in the microscope is placed, some of the adherent particles will always be out of focus. Attempts at extending the depth of field (96, 104) have only been partially successful because of the consequent lack of resolution in the resulting photographic image (175, 176, Chapter 1, 1.5).

The use of several photomicrographs with different planes of focus through the particle has been proposed as one method of overcoming the limitations of microscopy due to an inadequate depth of field or resolution. This approach is, however, likely to be expensive in terms of photographic film and also prone to error as subsequent analyses of the photographic images, to determine the adherent particle distribution, are likely to be dependant on examination by the naked eye (96, 104).

The technique of collecting a sequence of images at different planes of focus can be used with relative ease and precison by employing an image analyser to record the images in place of a photographic medium. Similar methods to this have already been used to determine the three dimensional structure of neurones from successive tissue sections (194, 195).

A method has been developed, using a low cost microcomputer and video digitising interface, that allowed a sequence of digitised images of an individual ordered unit to be obtained at different planes of focus and processed so that the relevant parts of each image which were determined to be in focus were combined to produce a single composite image.

3.1. Apparatus, materials and methods.

3.1.1. Materials.

The materials used to prepare ordered mixtures suitable for

image analysis were,

1. Triamterene, Supplied as a gift by Hoescht (UK) Ltd, Milton Keynes, U.K..
2. Elcema 250, BN D/409165, Degussa GmbH, Frankfurt, FRG.

Triamterene was selected for use as the fine adherent particle because of its ability to fluoresce when exposed to ultra-violet light, the peak excitation wavelength being approximately 360 nm with fluorescence at approximately 424 nm. Elcema G250 was selected for use as a carrier substrate because of its relatively large particle size and regular spheroidal shape.

3.1.2 Apparatus.

The image analyser used to obtain digitised images of individual ordered units was constructed from a British Broadcasting Corporation (BBC) model B microcomputer (Acorn Computers Ltd, Cambridge, U.K.), a dual, double sided disc drive, a 128K sideways ram board (Solidisk Technology Ltd, Southend-on-sea, U.K.) a Microeye video digitising interface (Digithurst Ltd, Royston, Herts., U.K.) a Vidicon video camera fitted with a standard 'C' mount lens (Digithurst Ltd, Royston, Herts., U.K.), a fluorescence microscope (Fluoval, Ziess, Oberkocken, F.R.G) and two monochrome monitors.

The BBC microcomputer was fitted with an Acorn disc interface, issue 1.0 disc filing system (DFS) ROM, issue 1.2 machine operating system (MOS) and BASIC II (copyright 1982 version). The Microeye interface was supplied with a cable for connection to the user port of the BBC microcomputer (220, 221). This provided the necessary control lines and access to the 4 most significant of the 8 bits of grey level information available from the Microeye interface. Details of the Microeye to BBC connection are shown in figure 3.1.

The fluorescence microscope was fitted with a trinocular head on which was mounted the video camera. This allowed the operator to view the particles to be examined through the microscope via the binocular eyepieces as normal whilst simultaneously displaying a video image of the field of view on a monitor. The signal from the the video camera was first passed to a monochrome monitor fitted with an auxiliary video output socket and then to the video digitising interface. This allowed the image from the camera to be viewed while being digitised.

The ability to view the true video image being passed to the

Microeye interface was considered to be important because the digitised images obtained could only be displayed using a maximum of four grey levels when using display mode 1 (320x256 pixels using four colours or grey levels) of the BBC microcomputer. The second monochrome monitor was used to display the digitised image and other computer output. A schematic diagram of the image analysis system is shown in figure 3.2.

Digitised images could be viewed using the full grey level resolution by transferring them to an experimental graphics workstation (Microprocesssor unit, University of Bath, Bath, UK) which was capable of displaying images using a palette of 256 colours selected from a possible 16.7 million and a screen resolution of 768x512 pixels. This facility was only used to obtained sample photographs of the digitised images because of the length of time required to transfer data between the two computers involved and the limited amount of access available.

Photomicrographs of ordered units were taken by mounting a Praktica LTL3 camera on one of the binocular eyepieces using a microscope adaptor. This same camera was also used to take photographs of images that were displayed on the graphics workstation.

An Epson FX80 dot matrix printer (Epson Ltd, Wembley, U.K.) was used to obtain hard copy of programs and data and also to produce isometric projections of the brightness of digitised images.

3.1.2.1. Memory addressing and allocation inside the BBC microcomputer.

Memory locations and addresses are more conveniently expressed using hexadecimal notation where the numbers 1 to 15 are written using 0 to 9, A to F. To distinguish between hexadecimal notation (commonly referred to as hex) and decimal notation, the former numbers are preceded by an ampersand (&). This is the notation used throughout the manuals for the BBC microcomputer, although the dollar sign ($) is frequently used elsewhere for the same purpose.

The BBC model B microcomputer uses a 6502 microprocessor which is capable of addressing 65536 bytes of memory (0 to &FFFF). This memory range has been split into four sections (Figure 3.3) in the BBC microcomputer (220, 221), the user random access memory (0-&7FFF), the sideways ROM area (&8000-&BFFF), and the MOS and

memory mapped input output(IO) area (&C000 -&FFFF). A further division is made into pages of 256 (&FF) bytes by the 6502 microprocessor itself.

The memory pages &FC (ie &FC00 to &FCFF), &FD and &FE are dedicated to memory mapped IO. &FC is used for controlling devices connected to the 1MHz bus, &FD is used for 64K of paged memory located on the 1MHz bus and &FE is used for internal device IO. These three pages of memory are referred to as FRED, JIM, and SHEILA respectively by the user manuals for the BBC microcomputer (220, 221), a usage which will be continued here.

The sideways ROM area of memory has been paged to allow the amount of firmware (software in ROM) to be increased. Sixteen sideways ROM areas (16x16k slots) are available although only one ROM can be in the address space of the 6502 at any given time (Figure 3.3). Access to the sideways rom pages is controlled by a paging register located at &30 in SHEILA (ie &FE30). Writing a number from 0 to &F to this paging register will select that 16K page of ROM (220, 221).

3.1.2.2. Modifications made to the BBC - Microeye connector.

The connection between the Microeye interface and the BBC microcomputer was modified to allow all 8 bits of grey level information to be utilised. This was done by connecting the data lines from the Microeye interface to the data lines of the 1MHz bus. The control lines of the Microeye interface were left connected to the user port.

The details of this modification are given in figure 3.4. The user port on the BBC microcomputer is controlled by side B of the user 6522 (versatile interface adaptor or VIA) using the IO registers at &60 and &62 in SHEILA (221).

3.1.2.3. Modifications made to the 128K ram board.

The 128K sideways ram board allowed 8x16K pages of random access memory to be located in the sideways rom area (Figure 3.3). Read control of the ram board was effected through the standard paging register at &30 in SHEILA (&FE30). This allowed the ram board to emulate rom when necessary. Write access to the sideways ram was provided by using side B of the user 6522 VIA (the user port), via internal connections, as a second paging register. This usage of the

user port was in direct conflict with the requirements of the Microeye digitising interface. The write control logic on the sideways ram board was therefore moved to the standard paging register so that both read and write access to the sideways ram were controlled by the value in &30 in SHEILA. More recent versions of this sideways ram board have resolved this complication by implementing more paging registers in the 16 bytes occupied by the single BBC microcomputer paging register.

The sideways ram was used to provide two frame buffers for use by the image analysis software, ie two 256x256 pixel images could be stored in memory simultaneously with the full 256 grey level resolution available from the Microeye interface. Frame 1 was placed in sideways ram pages 8-11 (&08-&0B) and frame 2 was placed in sideways ram pages 12-15 (&0C-&0F).

3.1.3. Methods.

3.1.3.1. Preparation of ordered units of trimaterene and Elcema G250 for photomicrography.

Ordered mixtures of trimaterene and Elcema G250 were prepared by placing 20 grammes of Elcema G250 and 0.1 grammes of triamterene in a 0.2l glass jar and then shaking by hand. This produced powder mixtures with a triamterene concentration of approximately 0.5%w/w. All weighing was carried out using a balance accurate to 0.0001 grammes.

Single ordered units were obtained for microscopy by sprinkling a small amount of the powder mixture onto a small brass plate (Chapter 4) coated with a thin layer of quick setting epoxy resin (Araldite Rapid, Ciba Geigy, Manchester, U.K.). The adhesive was first allowed to partially dry to reduce the ability of the glue to 'wick' into the body of the Elcema G250 carrier particles.

The ability of the adhesive to hold the Elcema G250 particles to a surface was tested by photographing a sample of an ordered mixture before and after applying a separation force by centrifuging at 50,000 revolutions per minute (rev min^{-1}). The apparatus used to hold the brass plate during centrifugation is described in Chapter 4.

After centrifugation the Elcema G250 particles were also examined by scanning electron microscopy. This was done to determine the extent to which the adhesive had penetrated into the Elcema G250 particles.

3.1.3.2 Collection of digitised images.

The individual ordered units of triamterene and Elcema G250 were illuminated by ultra-violet light through the objective lens of the fluorescence microscope. A suitable ordered unit was located and the plane of focus of the microscope raised until it was above the top of the ordered unit so that no adherent particles were in focus.

A digitised image was then captured, saved as a file on a floppy disc and the fine focus control advanced by 10 fine focus divisions (the markings on the fine focus control were in intervals of five). This sequence of operations was repeated until the plane of focus had passed below the ordered unit and adherent particles were no longer in focus.

The number of digitised images collected was dependent on the size of the ordered unit that had been examined and varied from 15 or less for small ordered units to 30 or more for large ordered units. The distance advanced by the plane of focus was not measured but was estimated to be approximately 2μm. This figure was obtained by dividing the estimated depth of the carrier particle above the adhesive by the number of frames required for digitisation.

3.1.3.3. Control of the Microeye interface.

The Microeye interface does not utilise a flash convertor ADC to digitise the video signal. Instead, a series of 'clocks' are used to identify a specific point on each scan line of the video frame. The voltage of the video signal at the identified point is sampled and held by the ADC and then converted to a digitial value in around 12μs. Using this system a single vertical column of data was obtained from the digitising interface for each frame of video that was scanned. A 256 x256 pixel video image was captured by digitising a single column of video data from 256 separate video frames, a process which took approximately 5 seconds.

To ensure that the data can be read correctly from the digitised interface control lines are provided (Figure 3.1, 3.3) to signal to the interface when to start digitising (MASTER RESET, EOL RESET) and to signal to the computer when valid data can be read from the interface (EOL, STROBE). The operation of the Microeye interface was as follows,

1. The input and output control lines were defined by writing a value to the data direction register (DDRB) of the B side of the

user VIA (location &62 in SHEILA). A value of &0 written to a bit in DDRB will set the corresponding line in the data IO register (IORB, &60 in SHEILA) to be used as an input line, whereas writing a value of &1 to a bit in DDRB will cause the corresponding line in IORB to be used for output. For correct use, MASTER RESET and EOL RESET were set to output by writing &0A to DDRB. STROBE and EOL were simultaneosly set to zero by this action and therefore defined as input lines (Figure 3.3).

2. The interface was reset by writing the value &02 followed by the value &A to IORB.
3. The EOL control line was then repeatedly examined to determine when it changed from a 0 to a 1. This transition indicated that the end of a scan line had been reached.
4. EOL RESET was then set high for approximately two microseconds after which both EOL RESET and MASTER RESET were pulsed (ie set high then set low).
5. STROBE was then repeatedly examined until it changed from 0 to 1 and back again 20 times.
6. STROBE was then allowed to go to from 0 to 1 and back to 0 again. After a short pause to ensure that the data was valid (recommended by Digithurst), the data lines of the Microeye interface were read. A total of 64μs were available (between the change from 1 to 0 and subsequent change from 0 to 1 of STROBE) in which the digitised value could be read and stored in RAM for later use. This was sufficient time for the BBC microcomputer to read the digitised value and to add it to a cumulative sum of previous values for a given pixel, an operation which allowed digitised images to be collected by averaging together several frames.
7. Step 6 was then repeated a further 255 times to read in a whole column of data.
8. Steps 3 to 7 were then repeated a further 255 times to read in the remaining columns of the image.

The 6502 assembler code for this operation is given in subroutine DIG1, DIG2 and DIG3 in Appendix 2 (A2.3 - A2.5).

3.1.3.4. Storage and manipulation of digitised images.

The 8 x 16k blocks of sideways ram were used in two ways to manipulate images. The method used to capture digitised images

involved averaging over a number of frames (Appendix 2, BASIC program SPR128 (A2.1), Machine code programs DIG1 (A2.3), DIG2 (A2.4) and DIG3 (A2.5). During this averaging the most significant bits of the summed images were held in frame buffer 1 and the least signifiacnt bits held in frame buffer 2. After digitisation the summed image was averaged (according to the digitisation routine being used, either DIG1, DIG2 or DIG3) and the resulting values placed in frame buffer 1.

To load or save a digitised image to disc, four files were used each 16k long. This allowed a single block of sideways ram data to be swapped with 16k of the mode 1 graphics screen memory (Appendix 2, machine code programs MOVEUP (A2.11) and MOVEDOWN (A2.12)). Once in screen memory the data could be saved to disc using the standard DFS command to save a block of memory. This operation was repeated four times to save a complete image. The reverse operation was used to load digitised images from disc into sideways ram. This procedure was necessary because the DFS ROM occupied a sideways rom slot and its sideways rom page was the one selected during any disc operation. It was therefore impossible to load or save digitised images directly into the sideways ram pages by writing directly to this area.

The protocol used when manipulating images was that frame buffer 1 (sideways ram pages &0B to &0B) always held the source or raw image and frame buffer 2 (sideways ram pages &0C to &0F) always held the destination or processed image.

A machine code subroutine (DISPLAY Appendix 2, A2.10) was written to display a digitised image using a 256x256 area of the mode 1 graphics screen where the 256 grey levels available were mapped onto the four colours available according to a user defined transformation (proc COLORS in program SUPER, Appendix 2, A2.1).

3.1.3.5. Production of isometric image plots.

Isometric plots of digitised images were produced using a Sinclair QL computer fitted with a 512K ram expansion and Cumana disc interface. Data was read from BBC format discs and resaved on QL format discs. The digitised images were then processed using a specially written program (Appendix 2, program PROFILE (A2.16) which was written in the 'C' programming language (222). The use of a compiled language, rather than BASIC, was necessary to reduce the time taken to produce the isometric plots from 2 hours to around five

minutes.

The projected isometric plots represent brightness by the height above the plane. Bright areas in an image therefore form peaks, and dark areas low plateau. Hidden line removal has been employed to prevent the projected images from becoming too confused.

The Sincair QL computer was not available at the time that the digitised images were being collected hence the reason for most of the neccessary software being written in 6502 machine code.

3.1.3.6. Production of composite images.

The production of a focused image from a sequence of partially focused digitised images was done using the BASIC control program BCOMPOS (A2.14) and the machine code program COMPOS (A2.15). BCOMPOS performed two main functions,

1. The installation of the digitised images in frame 1 buffer as they were needed by the machine code program COMPOS.
2. The floating point arithmetic used when comparing two areas to determine which fulfilled the criteria for being the most focused.

The general mechanics of operation of both BCOMPOS and COMPOS are given in Appendix 2 (A2.14, A2.15). The method used by COMPOS to obtain a composite digitised image containing only the focused images of the adherent particles proceded as follows.

The 128k of sideways ram was split into two image frames which were referred to as PIC and COMP. PIC was allocated the sideways ram blocks &08 to &0B and COMP was allocated the sideways ram blocks &0C to &0F.

The first action carried out by COMPOS (called from BCOMPOS) was to set every pixel in COMPOS to zero thereby initialising the frame buffer. A digitised image was then loaded into PIC (using MOVEUP in COMPOS, called from BCOMPOS). The first phase of analysis was then carried out (PHASE1 in COMPOS) whereby each pixel in PIC was examined in turn and set to zero if it was less than or equal to the minimum background brightness. This operation was equivalent to that demonstrated for background clipping (1.6.5).

Once PIC had been clipped it was assumed that the only non zero (non background) pixels remaining were due to the brightly fluorescing adherent particles. On this assumption each pixel in PIC was again examined until a pixel with a non zero value was found.

Once a non zero pixel was found all adjacent particles were also examined using the 'grass fire burn' area fill algorithm (209). During the determination of the extent of the non background area, several items of infomation were also collected (by the stats routines in COMPOS). These items of information were.

1. The value of the brightest non background pixel found.
2. The sum of all the non background pixels found.
3. The maximum and minimum X coordinates used for non background pixels.
4. The maximum and minimum Y coordinates used for non background pixels.
5. The total number of non background pixels.

Whilst the extent of the non background area in PIC was being determined, the same pixel coordinates in COMP were also examined to determine if a non background pixel had already been recorded there. This event only occurred during the examination of the second and subsequent digitised images because of the initial clearing of COMP. When the first non background pixel in COMP was found the X,Y coordinates were recorded and no further comparison in COMP done.

When the extent of the non background area in PIC had been determined, the same process was carried out for COMP using the first non background pixel found as the starting point for the 'grass fire burn' area determination in COMP. During the determination of the extent of the non background area in COMP the items of information detailed in 1 to 5 above were also collected.

If no non background area was detected in COMP then the area in PIC was immediately copied to COMP and then deleted from PIC. Where a non background area had been detected in COMP the information in 1 to 5 above was used to determine which of the two areas was the more focused. The rules used to determine this property were,

1. The projected area for each of the detected areas was calculated by multiplying the difference between the maximum and minimum x coordinates, the difference between the maximum and minimum y coordinates and the value π together then dividing by 4. (The actual areas were also calculated but in the event were not used).
2. The average projected brightness was calculated by dividing the value obtained in 1 into the sum of the brightness values.
3. The non background area in PIC was considered to be more focused

than the non background area in COMP if its average projected brightness was larger than that from COMP and if the maximum brightness value found in PIC was greater than the maximum brightness value in COMP minus 3. The subtraction of the value 3 from the maximum brightness in COMP allowed slight variations in brightness between different digitised images, due to variations in the UV light source, to be compensated for.

Both of the conditions above had to be satisfied before the area in PIC could be considered more focussed than the area in COMP.

If the area in PIC was more focused than the area in COMP then the area in COMP was deleted, the area in PIC copied to COMP and then the area in PIC deleted. If the area in PIC was not more focussed than the area in COMP then only the area in PIC was deleted, the area in COMP being left untouched.

This comparison procedure continued until all the non background areas in PIC had been erased either because they were copied to COMP or because they were found to be less focussed than the equivalent area in COMP.

The comparison procedure above was carried out for each digitised image in turn until a complete sequence had been examined. The composite image generated in COMP was then saved to disc for subsequent analysis (PROC ANALYSE in SPR128 version 1).

3.1.3.7. Action of PROC ANALYSE.

PROC ANALYSE in the BASIC program SPR128 (A2.1) was used to measure the position and size of the adherent particles in composite digitised images generated by COMPOS. This analysis was carried out on a screen display of the composite image (obtained using the DISPLAY option in SPR128).

The data produced by PROC ANALYSE was a count of the number of particles found, the maximum and minimum X and Y coordinate of each adherent particle, the cross sectional area of each adherent particle and the cumulative area of the adherent particles. All of these measurements were given in terms of pixels rather than true physical distances. To convert the pixel measurements to true physical distances required the use of the HCAL and VCAL procedures in SPR128 version 2 to obtain calibration factors. Although HCAL and VCAL were provided no use was made of them as measurments obtained in terms of

pixels were adequate for programming development work.

3.2. Results.

3.2.1. Preparation of ordered units of Elcema G250 and triamterene for photomicrography.

Ordered mixtures of Elcema G250 and triamterene were produced by gently shaking Elcema G250 powder (>295μm size fraction) with triamterene powder. A visual examination of the glass jar after 10 minutes of shaking showed that there was no obvious excess of triamterene.

Examination of the photographs of Elcema G250 particles that had been fixed to the brass plate with epoxy resin and then centrifuged at 50,000 rev min^{-1} showed that some of the particles had been dislodged (Plates 3.1, 3.2). Those particles that remained were examined using scanning electron microscopy. This examination showed that the epoxy resin adhesive had only penetrated into the body of the Elcema G250 particles where they were immersed in the adhesive. The degree of penetration of the adhesive could be easily seen to be sufficient only to retain the Elcema G250 carrier particles (Plates 3.3, 3.4) and would not therefore be likely to cause any of the adherent particles to be glued to the surface of the Elcema G250 particles.

Samples of the ordered mixture were placed on the surface of the adhesive by sprinkling from a small spatula. The area around the ordered units was frequently examined to determine if any of the adherent particles had been dislodged by this action. Very few adherent particles were ever seen which indicated that the ordered mix prepared was very stable as some losses would have been observed if very loosely bound adherent particles had been present.

3.2.2. Collection of digitised images.

Sequences of digitised images were captured using the DIGITISE routine in SUPER version 2 with the machine code program DIG2 (see Appendix 2, A2.4). Increments of 10 fine focus divisions (approximately 2μm) were used to spatially separate the digitised images.

Plates 3.5 to 3.27 show a typical sequence of digitised images. In each image only a small area can be observed to be in focus, as demonstrated by the presence of small bright adherent particles, the rest of the image being unfocussed to a greater or lesser degree. If

the sequence of digitised images is followed, the area of focus can be seen to change so that parts of the digitised image that were previously unfocused come into focus and then go out of focus again. It is also possible to see that when the adherent particles are focused they are small bright areas, hence the rules used to detect focused adherent particles when compiling the composite image. Close examination of the original photographs of the digitised images clearly showed that they were made of small squares with distinguishable brightness levels. This phenomenon may not be as clearly visible in plates 3.5 to 3.27.

Plates 3.29 and 3.30 show a comparison between a photomicrograph (Plate 3.30) of the ordered unit used for plates 3.5 to 3.27 and the corresponding digitised image (Plate 3.29) of the ordered unit. It can easily be seen that although the digitised image is represented by a relatively coarse brightness array (256x256 pixels) the relationship between it and the photomicrograph was good. As mentioned above, it is necessary to examine the digitised image very closely to ascertain that it does in fact consist of discrete pixels. Close examination of these two plates shows that more fine detail is visible in the photomicrograph (Plate 3.30) because it has not been divided into discrete squares over which the image brightness has been averaged. The digitised images are easier to observe than the photomicrograph because the digitisation routine has enhanced the contrast of the original image to cover the 256 grey levels available.

The images obtained in plates 3.5 to 3.29 were obtained by transferring the image data to the experimental graphics workstation. The data was then plotted over a 512 x 512 area in the central region of the 728 x 512 screen using four pixels of the graphics display (2 x 2) to represent one pixel in the original data. Two stripes were placed at each side of the screen to allow easier focusing of the graphics display during photomicrography. The displayed digitised images were coloured blue using the facilities of the graphics workstation so that they would appear similar to photomicrographs (Plate 3.30).

3.2.3. Production of isometric projection of digitised images.

The isometric projections of the digitised images in plates 3.5 to 3.28 are given in figures 3.5 to 3.28. Although this facility was

not available when the digitised images were being collected it can be seen that they can provide a useful means of comparing digitised images without the need for an expensive high resolution colour display. These images can be produced using any dot matrix printer with pin addressable graphics (ie virtually any Epson compatible dot matrix printer) or computer controlled plotter.

Examination of the projections shows that peaks grow sharper and then dissappear in the same manner as bright areas in the digitised images (plates 3.5 to 3.27). It is also possible to see that peaks in the isometric projections can be easily related to areas in the digitised images. The isometric projections also show the presence of a significant degree of background fluorescence from the Elcema G250 particle. This phenomenon is not readily observable in the digitised images as they are presented above due to the range of colour values mapped to the grey level values.

3.2.4. Production of composite images.

The digitised images in plates 3.5 to 3.27 were used to produce a composite image (plate 3.28). The total time taken to produce this composite image was approximately 14 minutes. Figure 3.28 is the isometric projection corresponding to plate 3.28.

Comparison of the composite image (plate 3.28) with the sequence of digitised images from which it was compiled (plates 3.5 to 3.27) allows the source of the adherent particles in the composite image to be identified. It is also possible to see that the composite image is not perfect, as some of the adherent particles in the composite image are incorrect (excessively large) and some adherent particles in the source sequence do not appear in the composite image.

The composite image does, however, present a reasonable represention of the size and distribution of the adherent particles on the Elcema G250 carrier particle.

3.2.5. Analysis of composite images.

The composite images produced by COMPOS and BCOMPOS (Appendix 2, A2.14, A2.15) were analysed using PROC ANALYSE in SPR128 version 1 (Appendix 2, A2.1). Table 3.1 represents the output from PROC ANALYSE when applied to the composite image shown in plate 3.28. Each particle in turn was examined and the maximum and minimum X and Y co-ordinates printed, these being the extreme left, right, top and

bottom of the particle. The total cross sectional area of each particle is also given (in pixels^2) and the cumulative measured area (in pixels^2).

3.3. Discussion.

3.3.1. Materials.

The choice of Elcema G250 and triamterene to form ordered units was made because it represented a practical binary pharmaceutical system that could be easily handled and studied.

Elcema G250, particularly the size fraction most commonly used (>295μm), was specifically chosen to provide a cellulose based material with a large particle size so that individual particles could be easily isolated. In addition Elcema G250 had also been used to demonstrate that the electret effect could be induced into cellulose based pharmaceutical excipients (Chapter 2). These facilities were desirable because the main objective of the analytical technique being developed was the measurement of adhesion force profiles for the adherent particles in individual ordered units.

Triamterene was used as an adherent particle because preliminary tests showed an affinity for forming ordered mixtures with Elcema G250 and also because it fluoresced strongly when exposed to ultra violet (UV) light. UV fluorescence was used so that any adherent particles present on the surface of a carrier particle could be detected easily due to a positive brightness change. The determination of the presence of adherent particles due to the occlusion of light transmitted through the body of the Elcema G250 carrier particle would have been significantly more difficult as a method would have had to have been developed for differentiating between dark spots in the Elcema G250 itself and the adherent particles.

Tetracycline and zinc sulphide were also assessed for their ability to both fluoresce and form ordered units with Elcema G250. Zinc sulphide could easily be detected using UV fluorescence but would not form ordered mixtures, probably due to it being an inorganic material. Tetracycline both fluoresced and formed ordered mixtures with Elcema G250. The problem encountered with tetracyline was that although the fluorescence was an orange/yellow colour and therefore easily distinguishable by eye from the blue background

autofluorescence of the cellulose carrier particle, the intensity (brightness) of the fluorescence was only equivalent to that of the autofluorescence of the Elcema G250 itself. This meant that when the fluorescing tetracycline was viewed through the monochrome video camera used on the image analysis system it was not possible to distinguish it from the Elcema G250 carrier particle. For this reason tetracycline was not used.

3.3.2. Apparatus

3.3.2.1. The digitising apparatus.

The apparatus assembled to capture and analyse digtised images worked well in that it was possible to carry out quantitative work in a reliable manner. There were, however, a number of problems associated with the system which slowed down the development of image analysis software and complicated the analysis of digitised images.

The lack of memory inherent in the design of the BBC microcomputer was not initially seen to be a problem as expansion via a powerful 32 bit second processor (Acorn computers 32016 second processor) with 512k or 1024k of memory was optionally available. The use of such a processor would have allowed digitised images to have been held in memory without resort to memory paging techniques and for analysis software to be written in a high level language such as 'C', Pascal, or FORTRAN. In the event Acorn were more than 2 years late with the release of this second processor which meant it did not become available until after the completion of experimental work. The restriction of only having 32k of user memory available on the BBC microcomputer was overcome by using a 128k sideways ram board in which to store digitised images.

The use of the 128k sideways ram board allowed image processing to be performed at the cost of an increase in the complexity of the image analysis software. This was because each digitised image was split into four paged blocks occupying the same area in the memory map of the computer. It was therefore necessary to include routines in the image analysis software to switch between these pages (or blocks) of memory. The effect of this can be seen in the routines to read or write a pixel in COMPOS (subroutine PIC_RW) where it was necessary to calculate which block of memory contained the relevant pixel, switch to that page and then to adjust the X and Y coordinate provided to take account of memory paging.

The lack of a true compiled high level language in which to write the image analysis software meant that it was necessary to use 6502 machine code for any serious image analysis software since using the BASIC interpreter would have produced code that ran too slow to be usable. The development of this software was facilitated by the fact that the BASIC interpreter on the BBC microcomputer supported an inline ASSEMBLER. This meant that software could be written and tested interactively.

Although software written in 6502 machine code offered the speed necessary for the image analysis techniques required, it was prone to a number of difficulties. Initial testing of software, even when written in a modular fashion, was very slow as logical errors in the program invariably caused the microcomputer to 'crash' (ie stop working correctly) giving no indication as to what had happened or why. Large machine code programs, such as COMPOS, became increasingly difficult to modify as their size and complexity increased and were invariably prone to subtle (ie non-crashing) bugs. Considering the machine code program COMPOS (Appendix 2), the size and complexity of the code meant that it was eventually necessary to accept a less than optimal solution to generating composite images merely because it became too difficult to continually make small modifications in an attempt to improve the results.

The difficulties in developing software were compounded by the inability to display the digitised images with the brightness resolution at which they were captured unless the data was transferred to the graphics work station in the microprocessor unit. Whilst such a transfer was possible, the graphics workstation was only available on an intermittent basis and then only overnight. Furthermore, the method used to transfer data required approximately 90 minutes for a single digitised image and was very prone to transmission errors (ie 1 in 3 transfers failed) which caused the loss of the data on the destination machine.

The lack of a facility to easily display digitised images other than on the graphics screen of the BBC microcomputer meant that it was sometimes very difficult to determine if changes to the software actually improved the quality of the composite image produced.

The ability to produce isometric projections of the digitised images would have relieved the display problem to a large extent, however, the software to do this was not developed until after the

collection and analysis of digitised images had been completed.

Despite the limitations described above it has been demonstrated that the technique developed for measuring the size and distribution of adherent particles on a single carrier particle is feasible and that a significant amount of data can be obtained from a single ordered unit rapidly, and in a reliable and consistent manner.

3.3.2.2 Hardware modifications.

As supplied, the Microeye video digitising interface was only connected to the user port of the BBC microcomputer. This connection only allowed the four most siginficant bits of grey level information available to be used. This resolution was sufficient for the software supplied with the interface but inadequate for the image processing techniques actually used. In order to gain access to the full 8 bits of grey level information it was necessary to transfer the data lines to the 1MHz bus using a second connector. This modification involved the construction of a new connecting lead between the BBC microcomputer and the digitising interface where the control lines were connected to the user port and the data lines connected to the 1MHz bus. The final cable consisted of the original cable supplied for the microeye interface which had had the 1MHz bus cable soldered to it at the plug for the microeye interface.

Once this had been done, it was possible to read the value presented on the data lines by examining any of the valid addresses in the two pages of memory allocated to the control of the 1MHz bus (ie &FC and &FD). In the event the address, &FD00 was used although any other address in the range &FC00 to &FDFF would have been satisfactory. It should however be noted that this solution was only viable because no other items of equipmemt were attached to the 1MHz bus. If this had not been the case it would have been necessary to construct the appropriate address decoding circuitry (221) to ensure that reading the address &FD00 only selected the digitising interface and not any other devices attached to the 1MHz bus.

It also proved necessary to modify the connections of the solidisk 128k sideways ram board to avoid conflicting use of the user port. It was possible to connect the sideways ram board to the standard paging register so that reading and writing were controlled together rather than independently. The only change this made to the usability of the sideways ram board was that it was no longer

possible to load files directly into the sideways ram area. This facility would only have made a marginal improvement to the image analysis software as it was still necessary to copy a sideways ram area into the standard user area of memory before it could be saved to disc.

3.3.2.3. The UV fluorescence microscope.

Two problems were encountered during fluorescence microscopy. The first was due to variations in the intensity of the UV light source. These variations were generally seen as changes of intensity over periods of several seconds and caused the resultant fluorescence of adherent particles to vary as well. These variations in UV intensity were mostly overcome by averaging successive digitised images and by allowing for a small variation in brightness when processing by BCOMPOS.

The second problem, common to fluoresence microscopy, was that the fluoresced light emitted from the adherent particles was not coherent. This meant that the carrier surface immediately adjacent to the adherent particles was illuminated by the fluorescence from the adherent particles. The effect of this was to increase the apparent size of the adherent particles slightly and also to obscure some of the detail of the perimeter of the adherent particle (Plate 3.30) as perceived by the human eye. These problems were not considered to be serious and had little or no impact on image digitisation because in the majority of cases the resolution of the microeye interface was insufficient to resolve the effects due to fluorescence.

One potential area for improvement would have been to have had the computer controlling both the stage and focus controls of the microscope. This would have allowed the carrier particles to be positioned in the same place on the stage when being re-examined after centrifugation. Computer control of the focus of the microscope would have allowed much smaller changes in the fine focus to be made during the collection of digitised images. The ability to control the focus of the microscope in such a manner would have reduced the need to store a series of digitised images on floppy disc. Instead, it would have been possible to analyse each digitised image with reference to the composite image as it was collected. This facility would have reduced any operator involvement in the

collection of digitised images and therefore reduced the possibility of any errors occurring.

3.3.3. Methods.

3.3.3.1. Preparation of ordered units of Elcema G250 and triamterene for digitisation.

Ordered units of Elcema G250 and triamterene were prepared by hand shaking in a glass jar for approximately 10 minutes. Small samples of the ordered units were then sprinkled onto a small brass plate (Chapter 4) smeared with a thin layer of a rapidly setting adhesive.

The ability of the adhesive to fix the sampled ordered units was tested by centrifuging at 50,000 rpm. Examination of plates 3.1 and 3.2 showed that some of the ordered units were totally or partially removed by this operation. The majority of the carrier particles appear to be unaffected by centrifugation although some distortion of the body of the particle must have occurred.

The ordered units remaining after centrifugation were examined using scanning electron microscopy to determine the extent of penetration of the adhesive into the Elcema G250 particles. Examination of plates 3.3 and 3.4 showed that extensive surface detail was visible indicating that the adhesive had only penetrated a small distance into the Elcema G250 particles. Using this observation it was assumed that any adherent particles present had not been glued to the surface of the carrier particle. It is inevitable however that adherent particles close to the boundary between the Elcema G250 particle and adhesive be permanently fixed in place. No attempts were made to identify such particles during the production of composite images.

Although no adherent particles appeared to be lost from the Elcema G250 carrier particles when being sprinkled onto the adhesive it is possible that very loosely bound adherent particles would have already been lost prior to removal from bulk. This possiblility cannot be very great as observation of the bulk powder after mixing, using UV fluoresence, did not show any evidence for the presence of significant amounts of unmixed triamterene particles. For practical purposes it was assumed that all the triamterene used to prepare the mixture was bound to the carrier particle and could not be dislodged

when the carrier particles were sprinkled onto the adhesive.

3.3.3.2. Collection of digitised images.

Digitised images were captured using the DIGITISE option in SPR128 (Appendix 2). This option called a machine code program (either DIG1 (A2.3), DIG2 (A2.4) or DIG3 (A2.5) if using SUPER version 2 (A2.13) which actually dealt with the interface between the image digitiser and the BBC microcomputer. As described above, the digitising interface operated on a slow scan principle, digitising one column of pixels for each video frame scanned. This meant that upto 64μs were available from when the digitised data was (theoretically) available on the 1MHz bus to when the data was invalid. This 64μs period was sufficient to allow the most recently digitised pixel value to be added to the sum of the previous values obtained for that pixel. Digitised images could therefore be sequentially summed provided that both frame buffers were used to hold the 16 bit numbers generated.

The advantage of being able to sum the data for sequential digitised images was that the quality of the image was improved as the effect of noise due to electrical spikes and low level ripple were reduced. By averaging over 8 frames the effect of any noise occurring in one image was reduced to one eighth of its value in the final averaged digital image. Three digitising routines DIG1 (A2.3), DIG2 (A2.4) and DIG3 (A2.5), representing three distinct methods for averaging the summed digitised image data, were employed during image analysis experiments.

The method used by DIG1 to produce an averaged image was to repeatedly scan the digitised image, multiplying each pixel value by two on each pass, until such an operation would caused one of the 16 bit numbers representing a pixel to overflow. When this occurred the frame buffer containing the least significant 8 bits of grey level information was discarded thereby producing an averaged image with only 8 bits of grey level data. The effect of this process was to enhance the brightness of the captured image so that at least one pixel was always set to the maximum brightness value.

The disadvantage of this process was that all images were adjusted so that the recorded grey scale always occupied the highest available grey levels. Digitised images with a narrow brightness range would therefore become 'brighter' than images with wide grey level ranges. For example an image with an original grey level range

of 1 to 16 would be processed into an image with a grey level range 8 to 128 whereas an image with an original grey level range of 1 to 64 would be processed into an image with a grey level range of 2 to 128. As can be seen this process has enhanced the contrast of the first image by a greater amount then that of the second and consequently was not used for quantitative work based on comparing different images.

The digitising routine DIG2 processed the summed image by recording the value of the brightest and least bright pixels. The value of the least bright pixel was then subtracted from the value of the brightest pixel to give the range of brightness levels that had been recorded. Finally the 16 bit pixel values for the summed image were processed by subtracting the value of the least bright pixel, dividing by the brightness range previosly calculated and then multiplying by 256. The result of this action was that the recorded range of grey levels (based on 16 bit numbers) was mapped onto the range 0 to 255 (an 8 bit grey level range).

Again, this process was not suitable for the quantitative comparison of images using brightness because the full range of 0 to 255 was always used irrespective of the grey level range in the summed digitised image. The advantage that this method did offer over DIG1 was that the full range of contrast available was always used with at least one pixel having the value 255 and one pixel having the value zero. By contrast a digitised image obtained using DIG1 only had a guaranteed maximum brightness of 128 (although higher brightness values could be obtained) and a variable minimum brightness.

The digitising routine, DIG3, differed from DIG1 and DIG2 in that no enhancement of either the brightness levels or the brightness range was attempted. Instead, the average brightness value for each pixel in the summed digitised image was calculated by dividing the value of the pixel by the number of frames used to produce the image. This method retained the benefit of summing over a number of frames to reduce the effect of spikes and low level ripple and also allowed different images to be compared on a quantitative basis using brightness.

The ability to compare images using brightness was considered to be very important because the construction of composite digitised images was based on the fact that the degree to which any individual

adherent particle was focused was related to the brightness of the image of that particle. The routines DIG1 and DIG2 modify the relationship between brightness and the degree of focus in a non linear manner because when they are applied to a summed image the final brightness of an adherent particle is dependent on either the maximum brightness or the brightness range. Digitised images obtained using DIG3 could be compared in a quantitative manner because the final image was not dependent on data obtained from within the image itself.

3.3.3.3. The use of isometric projections of digitised images.

The ability to produce isometric projections of digitised images was not developed until the collection and analysis of digitised images had been completed. The development of COMPOS was therefore carried out without any detailed visual feedback regarding the effect of minor changes to the area comparison algorithms. As a result of this, the final version of COMPOS was not fully functional (ie the wrong decision was occasionally made) as the time penalties involved in making modifications and checking the processed results had become too great.

The isometric projections (figures 3.5 to 3.28) of the digitised images (plates 3.5 to 3.28) have been drawn using the full 256x256 spatial resolution of the image and all the 256 grey level resolution available. These projections would have been extremely useful when developing COMPOS as a record of how the composite image changed as subsequent images were examined would have allowed a more comprehensive set of rules for determining focused adherent particles to be developed.

The ease with which these projections were produced effectively makes them more usable than the photographs obtained from the high resolution graphics display in the micro processor unit. The advantage of these projections is easily demonstrable because they show the significance of the background autofluorescence of the Elcema G250 particle. Had this information been available during the development of COMPOS then it is almost certain that more emphasis would have been placed on reducing this effect. This would have allowed the size of the adherent particles measured to be reduced because the side effects of clipping at a fixed level would have been reduced or fully eliminated.

3.3.3.4. Production of composite images.

The composite image shown in plate 3.28 indicates that the method used to isolate the images of the focused adherent particles operates correctly for a significant proportion of the adherent particles. However, there are incidences where an adherent particle can be identified in one of the contributing images but not in the composite image or where the image of a particle in the composite image does not represent the most focused image of that particle.

These observations are due to the use of fluorescence microscopy deficiencies in the algorithm used for detecting focused particles. When two or more adherent particles are placed very closely together then the fluoresced light which they emit can illuminate the area between them so that it appears much brighter than would be the case if only one particle were present. This effect is due to the incoherence of fluoresced light. When these particles are examined by COMPOS it is not possible to separate them and as a consequence they are treated as a single particle.

The algorithm for detecting focused particles was developed without being able to observe the effects that programming changes made to the final composite images. It was therefore expected that the algorithm would not be fully accurate and this is seen to be the case. Several changes were made to COMPOS during its development however, with each change the complexity of the program made further changes more difficult. However, the primary objective which image analysis was used to demonstrate was that the method for detecting focused adherent particles was feasible and that a significant amount of usable information could be generated and in this sense COMPOS was fully adequate for its purpose.

The detection of the adherent particles was based on the fact that they fluoresced when exposed to ultra violet light. This response is rather artificial when pharmaceutical systems in general are considered because in the majority of cases no fluorescence would occur. The use of standard light microscopy would not improve the situation because pharmaceutical materials are generally white or appear white. Consequently adherent particles would be invisible because they would appear as white objects on a white background.

One solution to the problem of detecting such adherent particles would be to use the property that different materials will absorb different wavelengths of light. It should therefore be possible to

illuminate the ordered units using a very narrow spectrum of light, such as that provided by a monochromator, so that the adherent particles appear as dark objects on a light background or light objects on a dark background. Where necessary, different digitised images could be captured using different wavelengths of light so that the differences between the adherent particles and the carrier substrate can be emphasised.

Although COMPOS was only concerned with producing images of focused particles a further development would be the generation of a three dimensional projection showing the distribution of the particles over the surface of the carrier article. The information for such a projection is already known in terms of the focus control of the microscope. In addition, if the computer were able to change objectives, it would even be possible to gain some information on the orientation of the particles on the carrier surface. This could be done by scanning a single adherent particle in a similar manner to the ordered unit and utilising the fact that an edge is in focus when the grey level transition across it is at a maximum.

Activities such as these would benefit from using a frame buffer array larger than 256x256 pixels so that the spacial resolution of the digitised images was greater and by providing the facility to view the digitised images at their full grey level resolution.

3.3.3.5. Analysis of the composite image.

Measurement of the position and size of the adherent particles in a composite image represents a simple programming task. However, the data produced by such an analysis represents a very significant increase in the knowledge of the behaviour of a single ordered unit, particlulary as similar types of knowledge have previously been virtually impossible to obtain.

Table 3.1 shows the data produced by the the use of proc ANALYSE in SPR128 on the composite image. This data can be further processed to calculate the X and Y Feret diameters of the adherent particles (Table 3.2), the ellipsoidal area of the particles (Table 3.2) and the ratio between the measured area and the ellipsoidal area, a type of shape factor (Table 3.2), the mean particle sizes (Table 3.3) and histograms of the different parameters measured (Table 3.4).

The mean X and Y Feret diameters and the mean cross sectional area indicate that the majority of the adherent particles are small

as few particles have X and Y Feret dimeters greater than 4 pixels. This observation is supported by consideration of the cross sectional areas of the particles (Table 3.4) where approximately 75% are less than 10 pixels^2. Examination of the histogram data (Table 3.4) also indicates that the measured distribution is very biased towards the smaller particles. This would suggest that a significant number of the smaller adherent particles have not been measured due to the policy of discarding areas of less than three pixels during the compilation of the composite image. This policy was adopted to prevent spurious particles being introduced due to the side effects of clipping at a fixed level in the first phase of COMPOS.

The particle data produced by proc ANALYSE can, in general, be considered to be accurate. However, it should be realised that some degree of error has been introduced because of the relatively small size of the adherent particles when compared to the size of the individual pixels in the image. For example a single pixel error in measuring an area of 16 pixels^2 is approximately 6% of the final total whereas it is 50% of an area of 2 pixels^2.

Better data could be obtained by increasing the resolution with which a digitised image was captured from 256x256 to 512x512, 1024x1024 or even (as on the Zeiss IBAS system) 4096x4096 pixels. Alternatively, as already mentioned above, each adherent particle could be examined at a higher magnification thereby increasing the number of pixels needed to measure its area. Such an analysis would require a significant degree of automation and vastly greater computing power to reduce the analysis time to a reasonable length.

Particle number	Minimum Y (pixel)	Maximum Y (pixel)	Minimum X (pixel)	Maximum X (pixel)	Area (pixels^2)	Cumulative Area (pixels^2)
1	4	5	118	119	3	3
2	9	11	133	135	7	10
3	31	34	161	163	9	19
4	33	37	186	189	16	35
5	34	35	143	144	3	38
6	45	46	164	166	6	44
7	47	49	161	163	8	52
8	58	59	69	70	4	56
9	61	62	180	182	4	60
10	62	64	72	75	10	70
11	62	67	82	85	16	86
12	63	65	114	115	5	91
13	63	65	120	122	9	100
14	68	69	66	68	5	105
15	68	70	93	96	12	117
16	70	74	11	122	19	136
17	73	76	132	135	15	151
18	76	82	54	61	42	193
19	78	81	76	77	7	200
20	81	82	145	146	4	204
21	81	83	155	156	6	210
22	82	86	89	94	27	237
23	82	83	104	105	4	241
24	85	86	50	51	3	244
25	85	87	61	63	9	253
26	86	89	99	103	16	269
27	87	88	126	127	4	273
28	88	89	91	92	4	277
29	89	94	84	89	16	293
30	90	91	97	98	4	297
31	93	94	109	110	3	300
32	94	95	177	178	3	303
33	95	97	162	163	5	308
34	96	98	68	70	9	317
35	98	99	107	108	3	320
36	98	99	186	187	3	323
37	99	104	88	91	21	344
38	100	102	111	113	5	349
39	102	103	118	119	3	352
40	103	104	75	77	5	357
41	104	107	64	65	8	365
42	105	106	112	114	5	370
43	111	113	141	143	7	377
44	117	120	145	148	14	391
45	120	123	63	64	8	399

Table 3.1. Data produced by proc ANALYSE in SPR128 version 2 (Appendix 2, A2.13) using the composite image shown in Figure 3.29.

Table continued below.

Table continued from above.

Particle number	Minimum Y (pixel)	Maximum Y (pixel)	Minimum X (pixel)	Maximum X (pixel)	Area (pixels^2)	Cumulative Area (pixels^2)
46	120	122	137	138	5	404
47	121	125	170	173	12	416
48	122	125	133	135	10	426
49	123	124	57	58	3	429
50	127	129	99	101	8	437
51	127	128	128	129	3	440
52	129	131	123	125	9	449
53	140	147	104	109	37	486
54	141	143	157	161	13	499
55	144	145	133	136	6	505
56	146	151	93	100	35	540
57	151	154	112	113	5	545
58	152	154	89	91	8	553
59	154	157	60	62	9	562
60	154	156	75	76	4	566
61	158	159	145	146	4	570
62	159	160	95	96	4	574
63	160	163	85	87	10	584
64	161	162	91	93	4	588
65	163	165	82	84	7	595
66	164	166	92	94	7	602
67	165	169	56	59	16	618
68	165	168	89	91	8	626
69	165	167	124	125	5	631
70	166	169	142	148	27	658
71	171	179	94	108	101	759
72	171	172	134	136	4	763
73	174	175	140	142	5	768
74	180	182	63	63	3	771
75	181	184	55	57	11	782
76	184	185	62	64	4	786
77	188	190	78	81	10	796
78	188	196	93	102	67	863
79	189	202	109	121	146	1009
80	190	195	68	76	28	1037
81	193	194	106	107	4	1041
82	194	195	130	131	4	1045
83	201	204	68	69	8	1053
84	203	205	105	106	6	1059
85	208	209	88	89	4	1063

Table 3.1. Data produced by proc ANALYSE in SPR128 version 2 (Appendix 2, A2.13) using the composite image shown in Figure 3.29.

Particle number	Y feret diameter (pixels)	X feret diameter (pixels)	Measured area ($pixels^2$)	Elliptical area ($pixels^2$)	Area ratio
1.00	2.00	2.00	3.00	3.14	1.05
2.00	3.00	3.00	7.00	7.07	1.01
3.00	3.00	4.00	9.00	9.42	1.05
4.00	4.00	5.00	16.00	15.71	0.98
5.00	2.00	2.00	3.00	3.14	1.05
6.00	3.00	2.00	6.00	4.71	0.79
7.00	3.00	3.00	8.00	7.07	0.88
8.00	2.00	2.00	4.00	3.14	0.79
9.00	3.00	2.00	4.00	4.71	1.18
10.00	4.00	3.00	10.00	9.42	0.94
11.00	4.00	6.00	16.00	18.85	1.18
12.00	2.00	3.00	5.00	4.71	0.94
13.00	3.00	3.00	9.00	7.07	0.79
14.00	3.00	2.00	5.00	4.71	0.94
15.00	4.00	3.00	12.00	9.42	0.79
16.00	5.00	5.00	19.00	19.63	1.03
17.00	4.00	4.00	15.00	12.57	0.84
18.00	8.00	7.00	42.00	43.98	1.05
19.00	2.00	4.00	7.00	6.28	0.90
20.00	2.00	2.00	4.00	3.14	0.79
21.00	2.00	3.00	6.00	4.71	0.79
22.00	6.00	5.00	27.00	23.56	0.87
23.00	2.00	2.00	4.00	3.14	0.79
24.00	2.00	2.00	3.00	3.14	1.05
25.00	3.00	3.00	9.00	7.07	0.79
26.00	5.00	4.00	16.00	15.71	0.98
27.00	2.00	2.00	4.00	3.14	0.79
28.00	2.00	2.00	4.00	3.14	0.79
29.00	6.00	6.00	16.00	28.27	1.77
30.00	2.00	2.00	4.00	3.14	0.79
31.00	2.00	2.00	3.00	3.14	1.05
32.00	2.00	2.00	3.00	3.14	1.05
33.00	2.00	3.00	5.00	4.71	0.94
34.00	3.00	3.00	9.00	7.07	0.79
35.00	2.00	2.00	3.00	3.14	1.05
36.00	2.00	2.00	3.00	3.14	1.05
37.00	4.00	6.00	21.00	18.85	0.90
38.00	3.00	3.00	5.00	7.07	1.41
39.00	2.00	2.00	3.00	3.14	1.05
40.00	3.00	2.00	5.00	4.71	0.94
41.00	2.00	4.00	8.00	6.28	0.79
42.00	3.00	2.00	5.00	4.71	0.94
43.00	3.00	3.00	7.00	7.07	1.01
44.00	4.00	4.00	14.00	12.57	0.90
45.00	2.00	4.00	8.00	6.28	0.79

Table 3.2. Feret dimaters, ellipsoidal area and area ratio calculated from the data presented in Table 3.1.

Table continued below.

Table continued from above.

Particle number	Y feret diameter (pixels)	X feret diameter (pixels)	Measured area (pixels^2)	Elliptical area (pixels^2)	Area ratio
46.00	2.00	3.00	5.00	4.71	0.94
47.00	4.00	5.00	12.00	15.71	1.31
48.00	3.00	4.00	10.00	9.42	0.94
49.00	2.00	2.00	3.00	3.14	1.05
50.00	3.00	3.00	8.00	7.07	0.88
51.00	2.00	2.00	3.00	3.14	1.05
52.00	3.00	3.00	9.00	7.07	0.79
53.00	6.00	8.00	37.00	37.70	1.02
54.00	5.00	3.00	13.00	11.78	0.91
55.00	4.00	2.00	6.00	6.28	1.05
56.00	8.00	6.00	35.00	37.70	1.08
57.00	2.00	4.00	5.00	6.28	1.26
58.00	3.00	3.00	8.00	7.07	0.88
59.00	3.00	4.00	9.00	9.42	1.05
60.00	2.00	3.00	4.00	4.71	1.18
61.00	2.00	2.00	4.00	3.14	0.79
62.00	2.00	2.00	4.00	3.14	0.79
63.00	3.00	4.00	10.00	9.42	0.94
64.00	3.00	2.00	4.00	4.71	1.18
65.00	3.00	3.00	7.00	7.07	1.01
66.00	3.00	3.00	7.00	7.07	1.01
67.00	4.00	5.00	16.00	15.71	0.98
68.00	3.00	4.00	8.00	9.42	1.18
69.00	2.00	3.00	5.00	4.71	0.94
70.00	7.00	4.00	27.00	21.99	0.81
71.00	15.00	9.00	101.00	106.03	1.05
72.00	3.00	2.00	4.00	4.71	1.18
73.00	3.00	2.00	5.00	4.71	0.94
74.00	1.00	3.00	3.00	2.36	0.79
75.00	3.00	4.00	11.00	9.42	0.86
76.00	3.00	2.00	4.00	4.71	1.18
77.00	4.00	3.00	10.00	9.42	0.94
78.00	10.00	9.00	67.00	70.69	1.06
79.00	13.00	14.00	146.00	142.94	0.98
80.00	9.00	6.00	28.00	42.41	1.51
81.00	2.00	2.00	4.00	3.14	0.79
82.00	2.00	2.00	4.00	3.14	0.79
83.00	2.00	4.00	8.00	6.28	0.79
84.00	2.00	3.00	6.00	4.71	0.79
85.00	2.00	2.00	4.00	3.14	0.79

Table 3.2. Feret dimaters, ellipsoidal area and area ratio calculated from the data presented in Table 3.1.

	Y feret diameter (pixels)	X feret diameter (pixels)	Measured area (pixels^2)	Elliptical area (pixels^2)	Area ratio
mean	3.4706	3.4824	12.5059	12.5109	0.9691
Standard Deviation	2.3343	1.9560	20.2110	20.7286	0.1766
number of particles	85	85	85	85	85
Standard Error of mean	0.2353	0.2122	2.1922	2.2483	0.0192
Coefficient of Variation	67.2593	56.1682	161.6117	165.6843	18.2231

Table 3.3. Statistical summary of the particle size data presented in Table 3.2.

X feret diameter		Y feret diameter		Measured area		Elliptical area		Area ratio	
size	number	size	number	size	number	size	number	size	number
1	1	1	-	3	11	2.36	1	0.79	23
2	33	2	31	4	16	3.14	21	0.81	1
3	27	3	24	5	10	4.71	16	0.84	1
4	11	4	15	6	4	6.28	6	0.86	1
5	3	5	5	7	5	7.07	12	0.87	1
6	3	6	5	8	7	9.42	12	0.88	3
7	1	7	1	9	6	11.78	1	0.90	3
8	2	8	1	10	4	12.57	2	0.91	1
9	1	9	2	11	1	15.71	4	0.94	12
10	1	10	-	12	2	18.85	2	0.98	4
13	1	13	-	13	1	19.63	1	1.01	4
14	-	1	1	14	1	21.99	1	1.02	1
15	1	15	-	15	1	23.56	1	1.03	1
				16	4	28.27	1	1.05	15
				19	1	37.7	1	1.06	1
				21	1	42.41	1	1.08	1
				27	1	43.98	1	1.18	7
				28	1	70.69	1	1.26	1
				35	1	106.03	1	1.31	1
				37	1	142.94	1	1.41	1
				42	1			1.51	1
				67	1			1.77	1
				101	1				
				146	1				

Table 3.4. Frequency summary of the particle size data presented in Table 3.2.

Microeye interface pin labels	Microeye interface pin numbers	BBC user port pin labels	Data direction
STROBE	1	PB0	INPUT
EOL RESET	2	PB2	OUTPUT
EOL	3	PB1	INPUT
MASTER RESET	4	PB3	OUTPUT
DATA 0 (2^7)	5	PB7	INPUT
DATA 1 (2^6)	6	PB6	INPUT
DATA 2 (2^5)	7	PB5	INPUT
DATA 3 (2^4)	8	PB4	INPUT
DATA 4 (2^3)	9	NOT USED	
DATA 5 (2^2)	10	NOT USED	
DATA 6 (2^1)	11	NOT USED	
DATA 7 (2^0)	12	NOT USED	
GND	13 (15)	SIGNAL GND	

Figure 3.1. Connection details for the Microeye interface to BBC user port using the supplied software. The supplied cable could only be fitted one way round due to the different plug fittings used at each end of the cable.

Microeye interface pin labels	Microeye interface pin numbers	BBC user port pin labels	Data direction
STROBE	1	PB0	INPUT
EOL RESET	2	PB2	OUTPUT
EOL	3	PB1	INPUT
MASTER RESET	4	PB3	OUTPUT
GND	13(15)	SIGNAL GND	
		1MHz bus pin labels	
DATA 0 (2^7)	5	D7	INPUT
DATA 1 (2^6)	6	D6	INPUT
DATA 2 (2^5)	7	D5	INPUT
DATA 3 (2^4)	8	D4	INPUT
DATA 4 (2^3)	9	D3	INPUT
DATA 5 (2^2)	10	D2	INPUT
DATA 6 (2^1)	11	D1	INPUT
DATA 7 (2^0)	12	D0	INPUT

Figure 3.4. Modified connection details for the Microeye interface to BBC user port and 1MHz bus. This modification was made to allow all 8 bits of the digitised grey level to be read into the BBC computer. The modified cable was made by soldering a second ribbon cable, fitted with a 1MHz bus socket, to the microeye connector. This modification was only possible because no other devices were connected to the 1MHz bus.

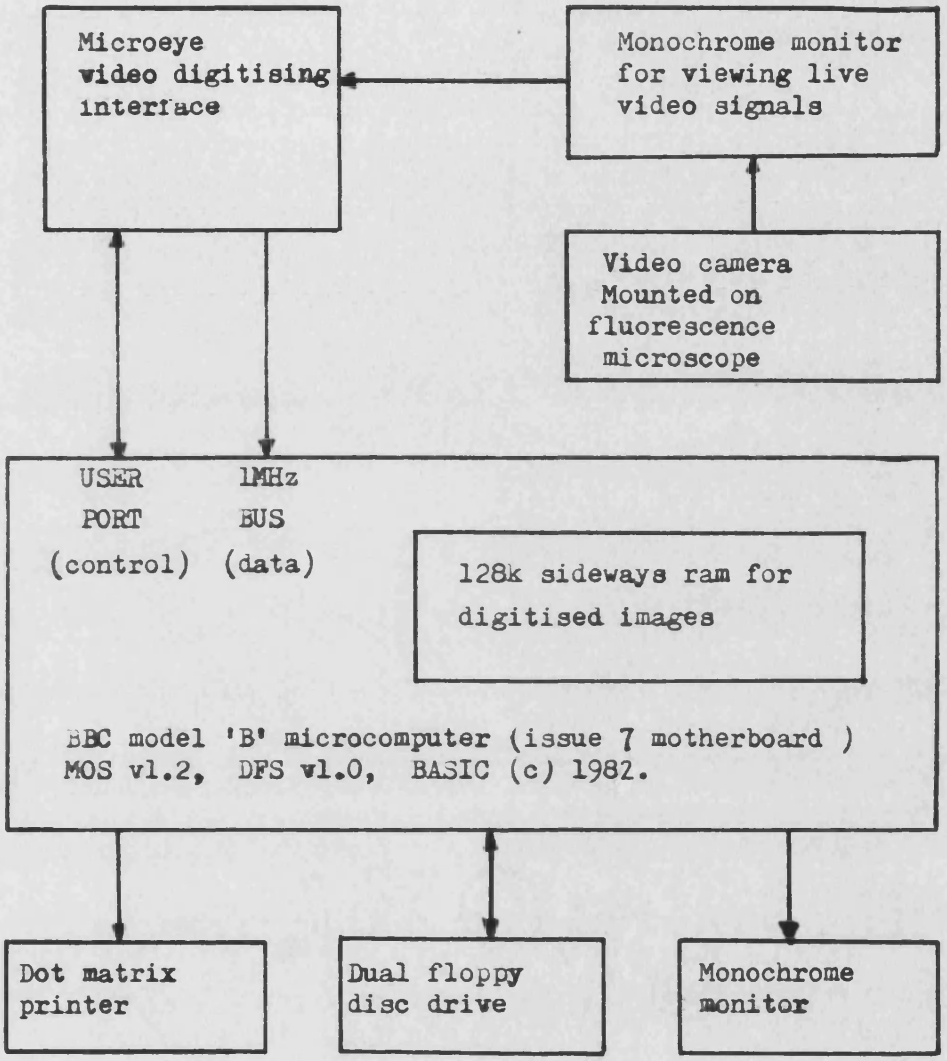

Figure 3.2. Schematic representation of the image analysis system used to process digitised images. The arrows denote the direction of data flow.

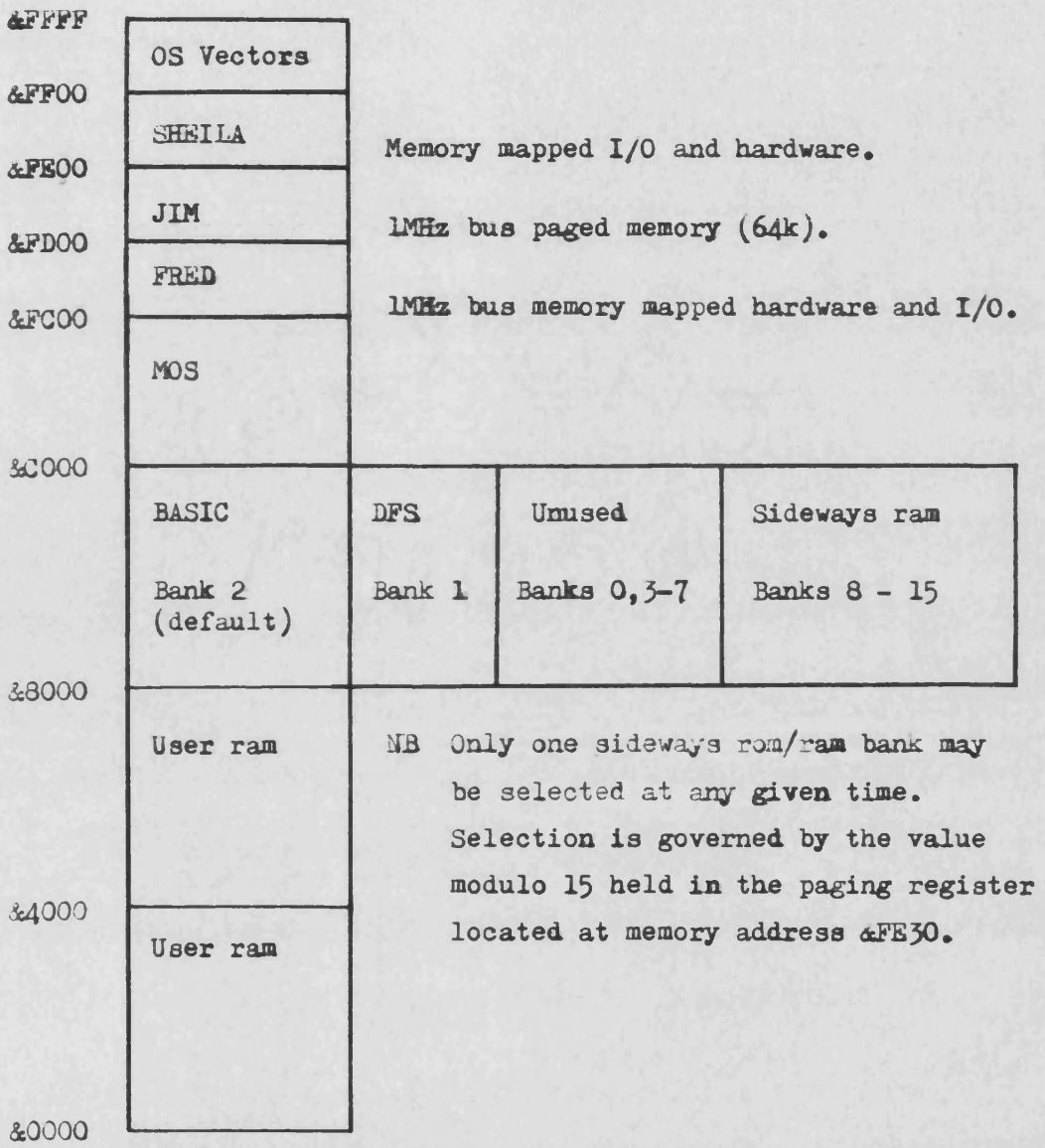

Figure 3.3. Memory map of the BBC model 'B' microcomputer showing allocation of sideways memory for roms and ram.

Figure 3.4. See page 174.

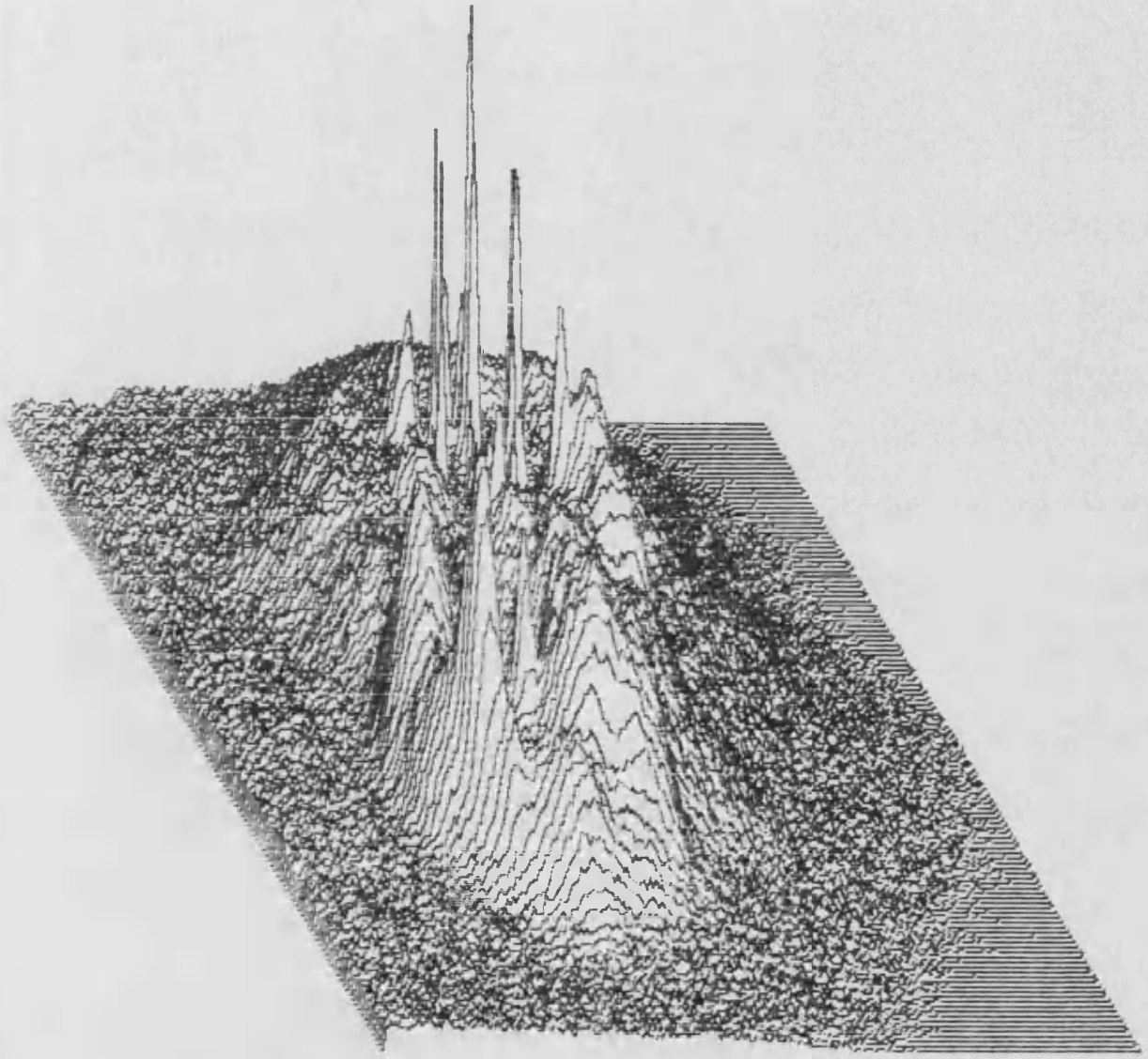

Figure 3.5. Isometric projection of the brightness of the digitised image of an Elcema G250 particle with adherent Triamterene particles shown in plate 3.5. Focus position at 00 fine focus divisions.

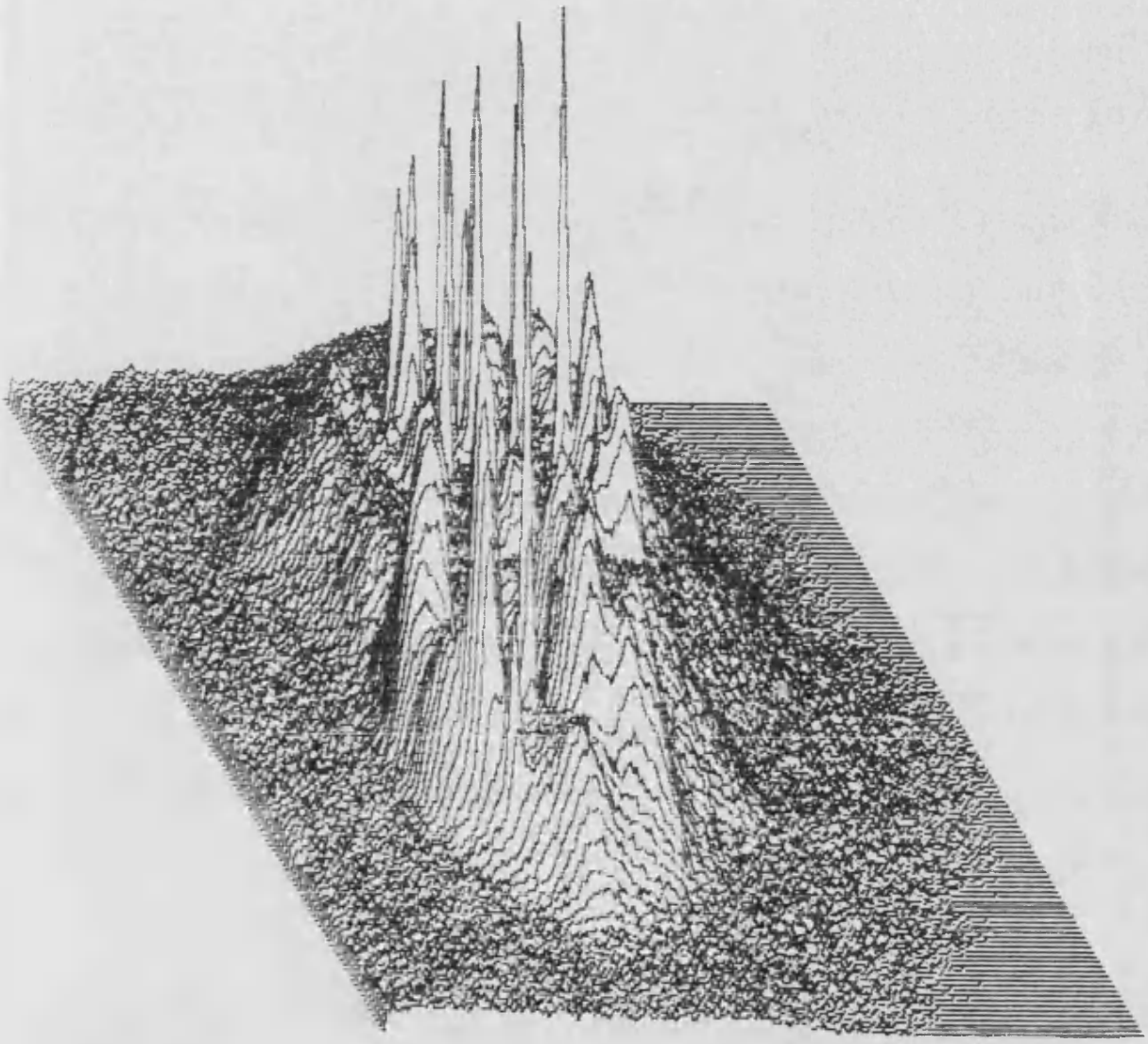

Figure 3.6. Isometric projection of the brightness of the digitised image of an Elcema G250 particle with adherent Triamterene particles shown in plate 3.6. Focus position at 10 fine focus divisions.

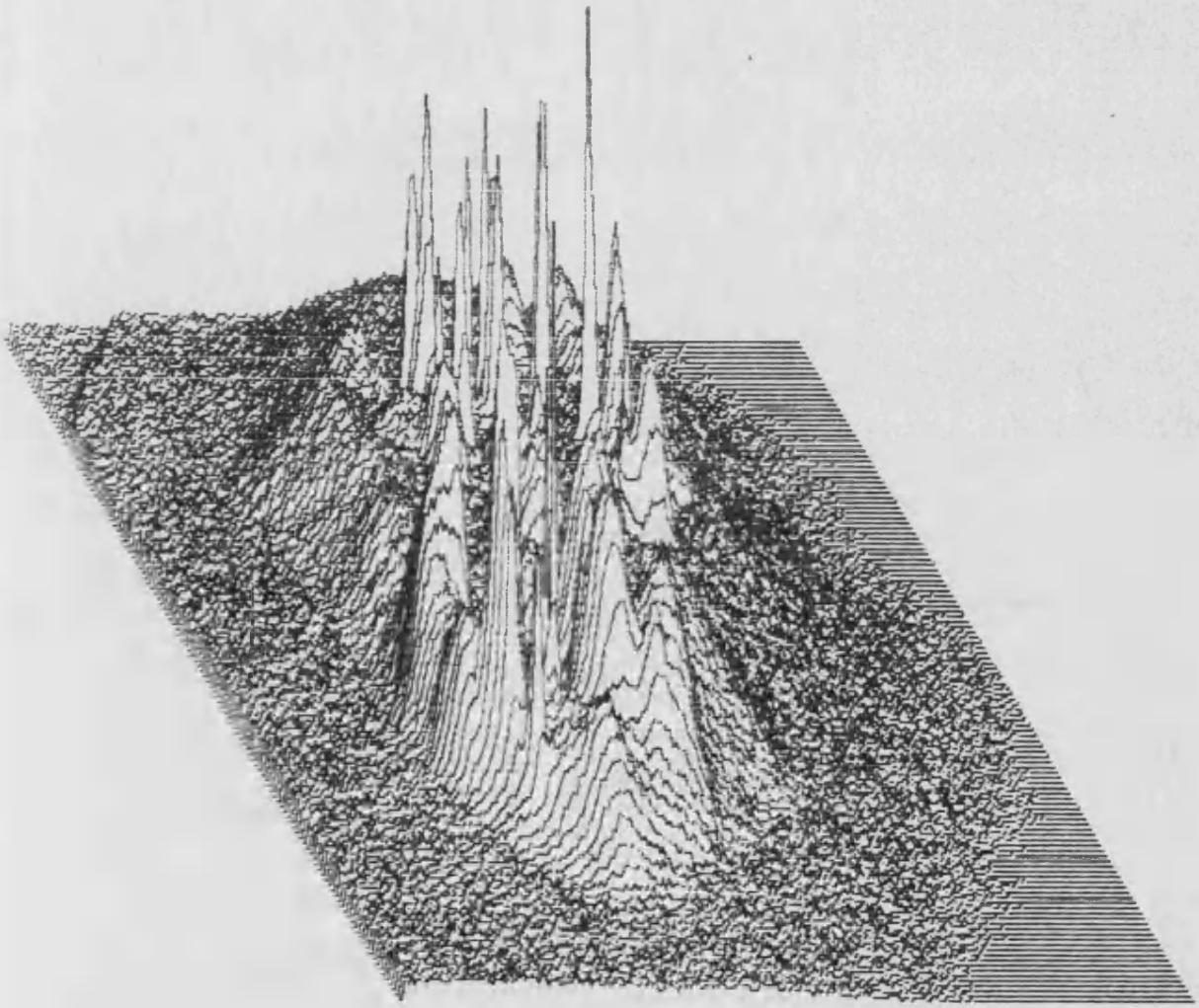

Figure 3.7. Isometric projection of the brightness of the digitised image of the Elcema G250 particle with adherent Triamterene particles shown in plate 3.7. Focus position at 20 fine focus divisions.

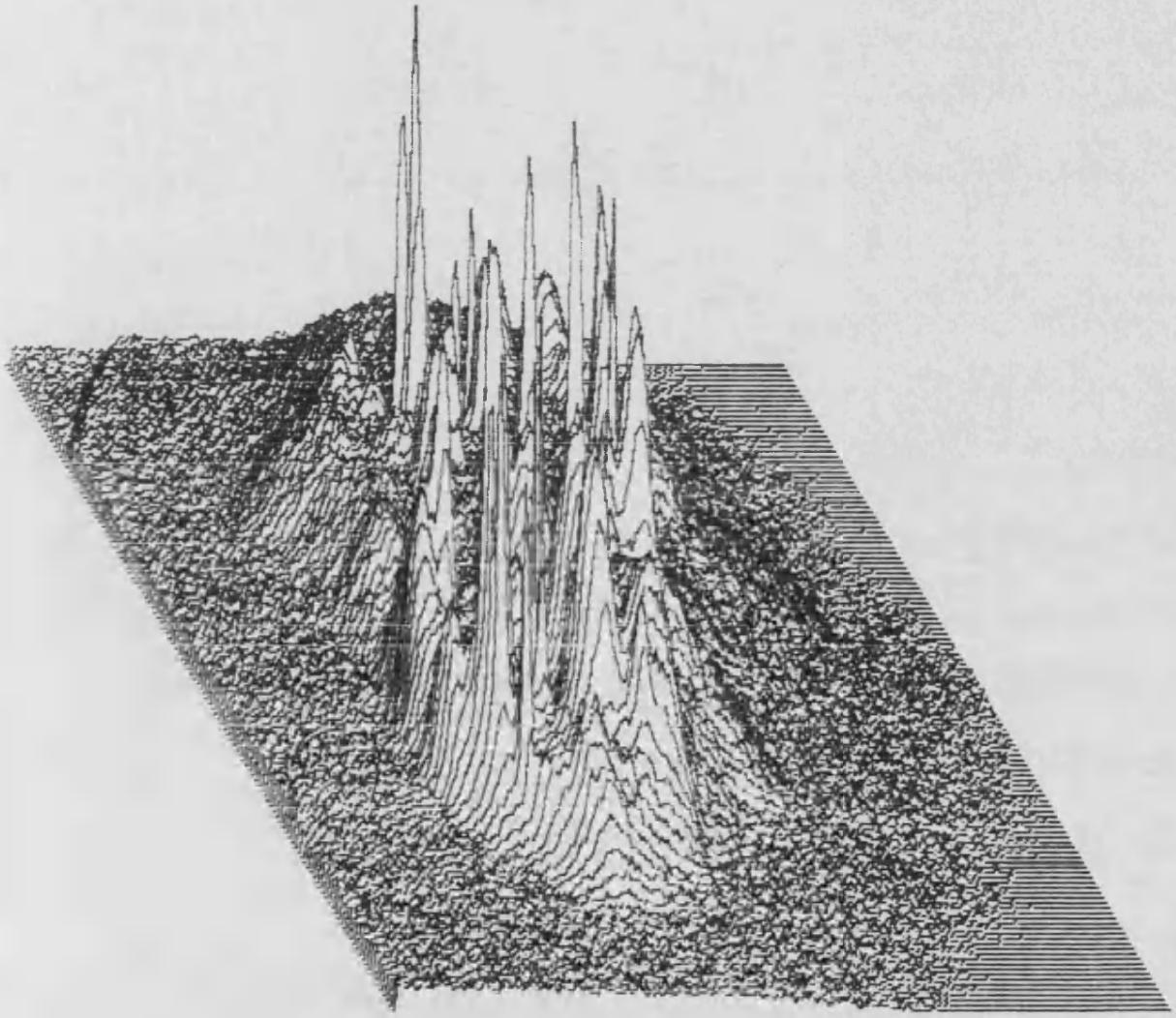

Figure 3.8. Isometric projection of the brightness of the digitised image of an Elcema G250 particle with adherent Triamterene particles shown in plate 3.8. Focus position at 30 fine focus divisions.

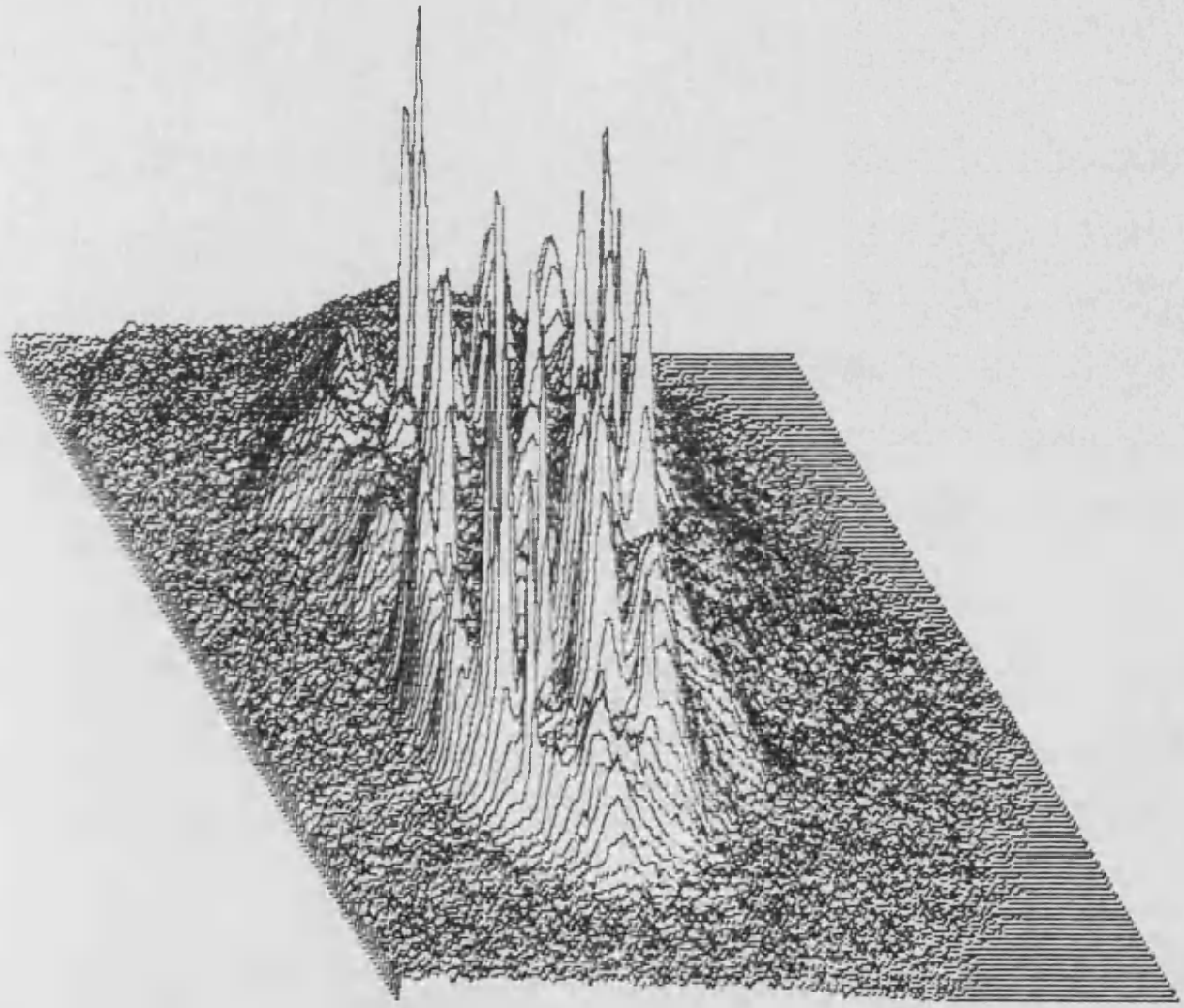

Figure 3.9. Isometric projection of the brightness of the digitised image of an Elcema G250 particle with adherent Triamterene particles shown in plate 3.9. Focus position at 40 fine focus divisions.

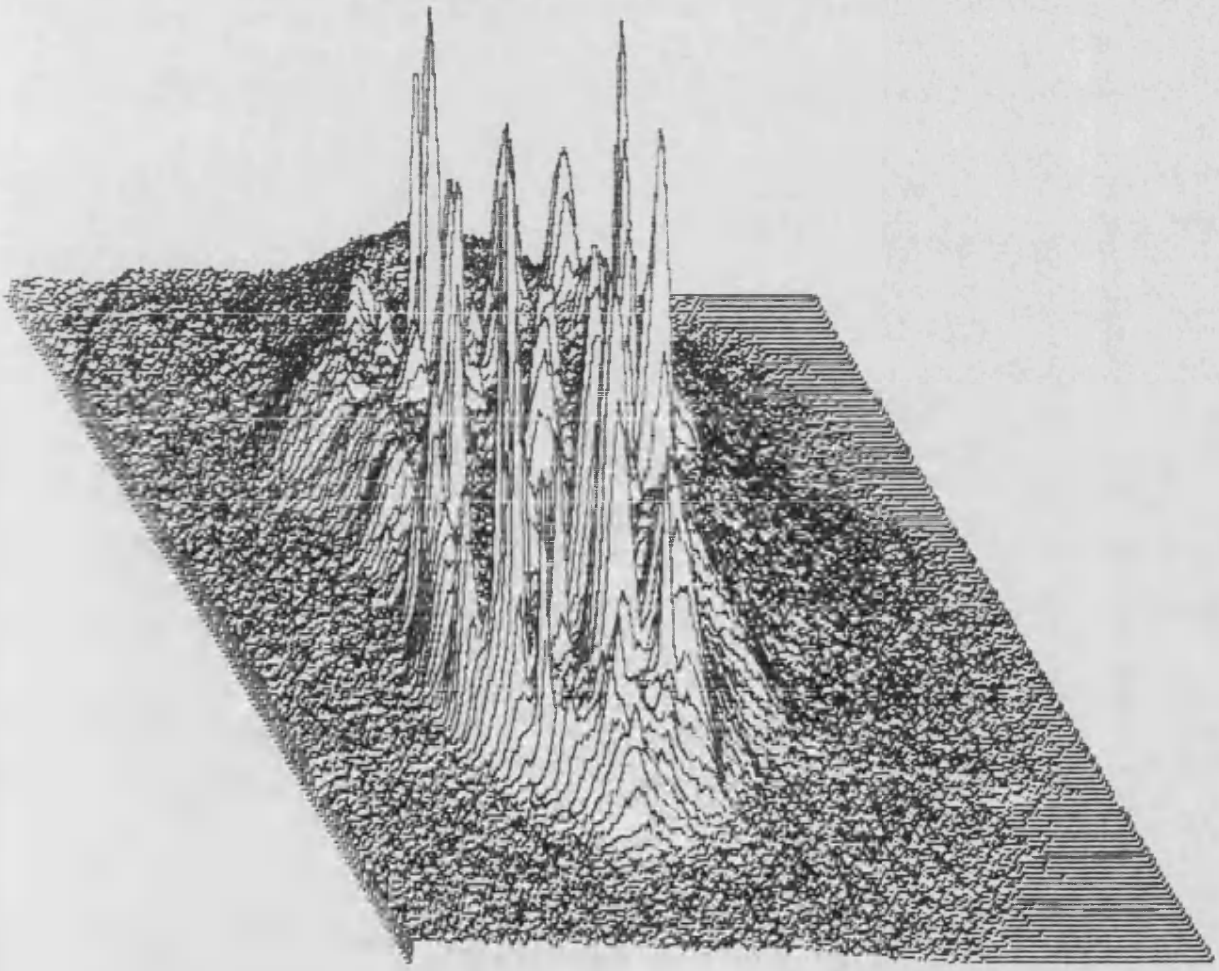

Figure 3.10. Isometric projection of the brightness of the digitised image of an Elcema G250 particle with adherent Triamterene particles shown in plate 3.10. Focus position at 50 fine focus divisions.

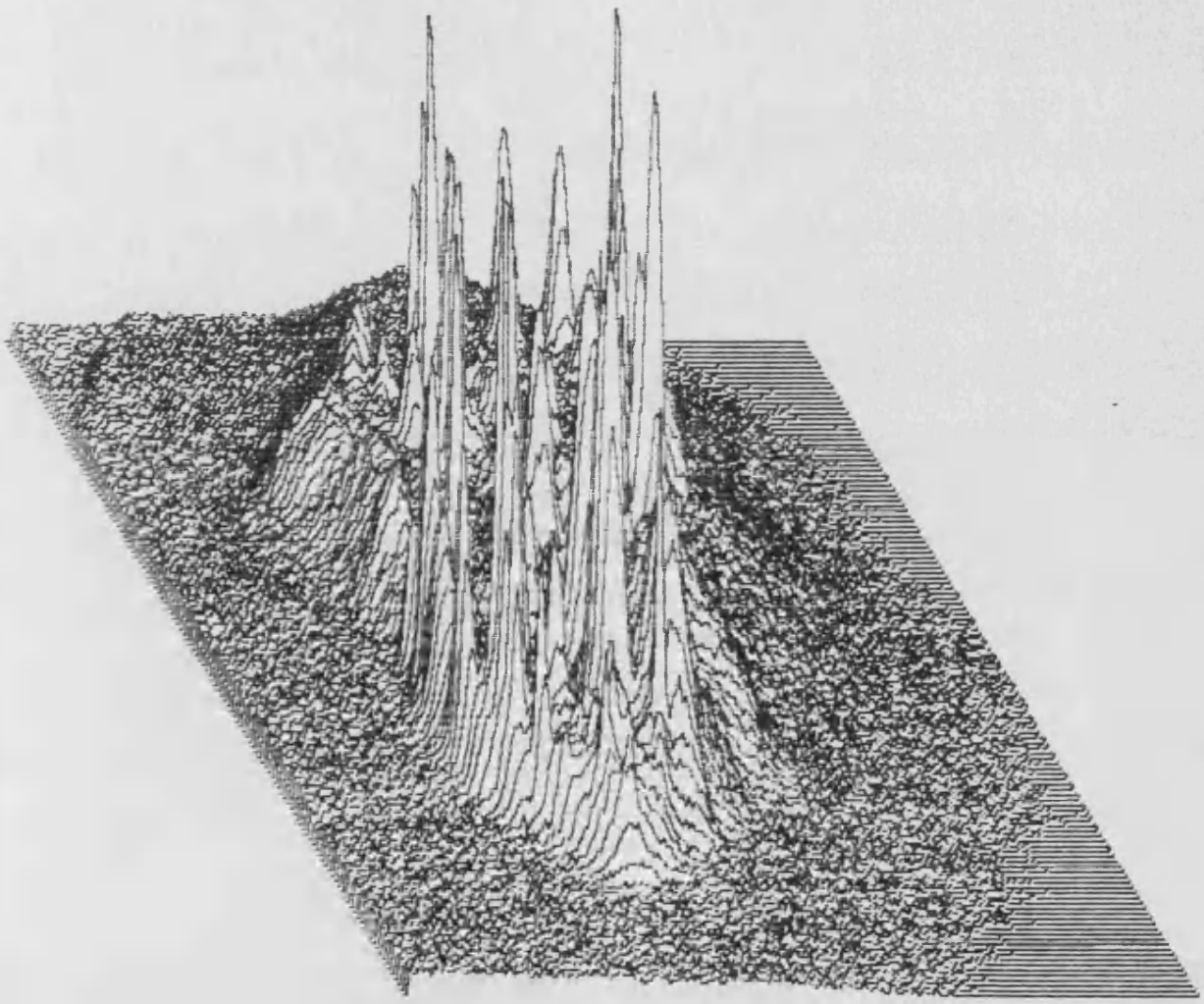

Figure 3.11. Isometric projection of the brightness of the digitised image of an Elcema G250 particle with adherent Triamterene particles shown in plate 3.11. Focus position at 60 fine focus divisions.

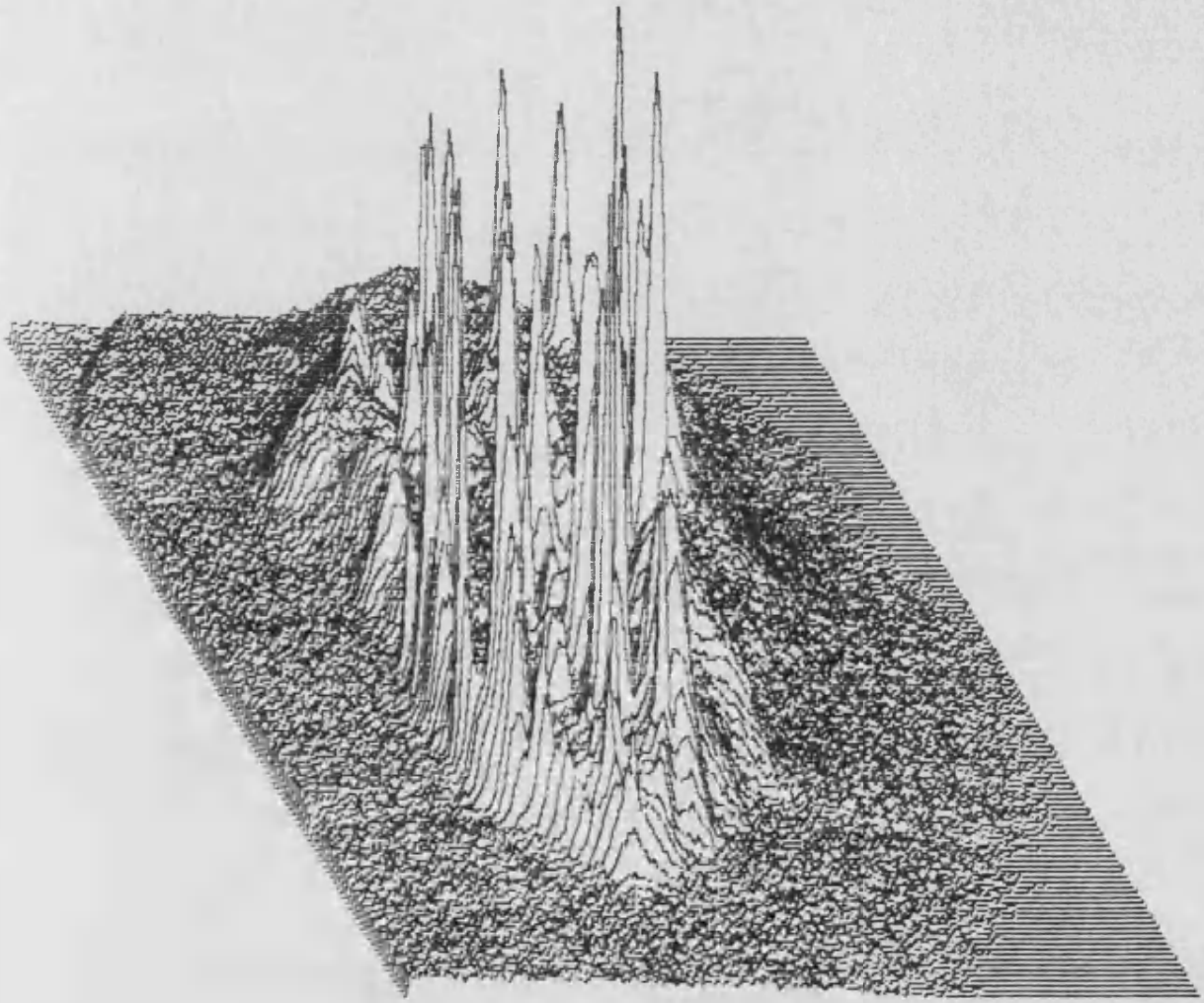

Figure 3.12. Isometric projection of the brightness of the digitised image of an Elcema G250 particle with adherent Triamterene particles shown in plate 3.12. Focus position at 70 fine focus divisions.

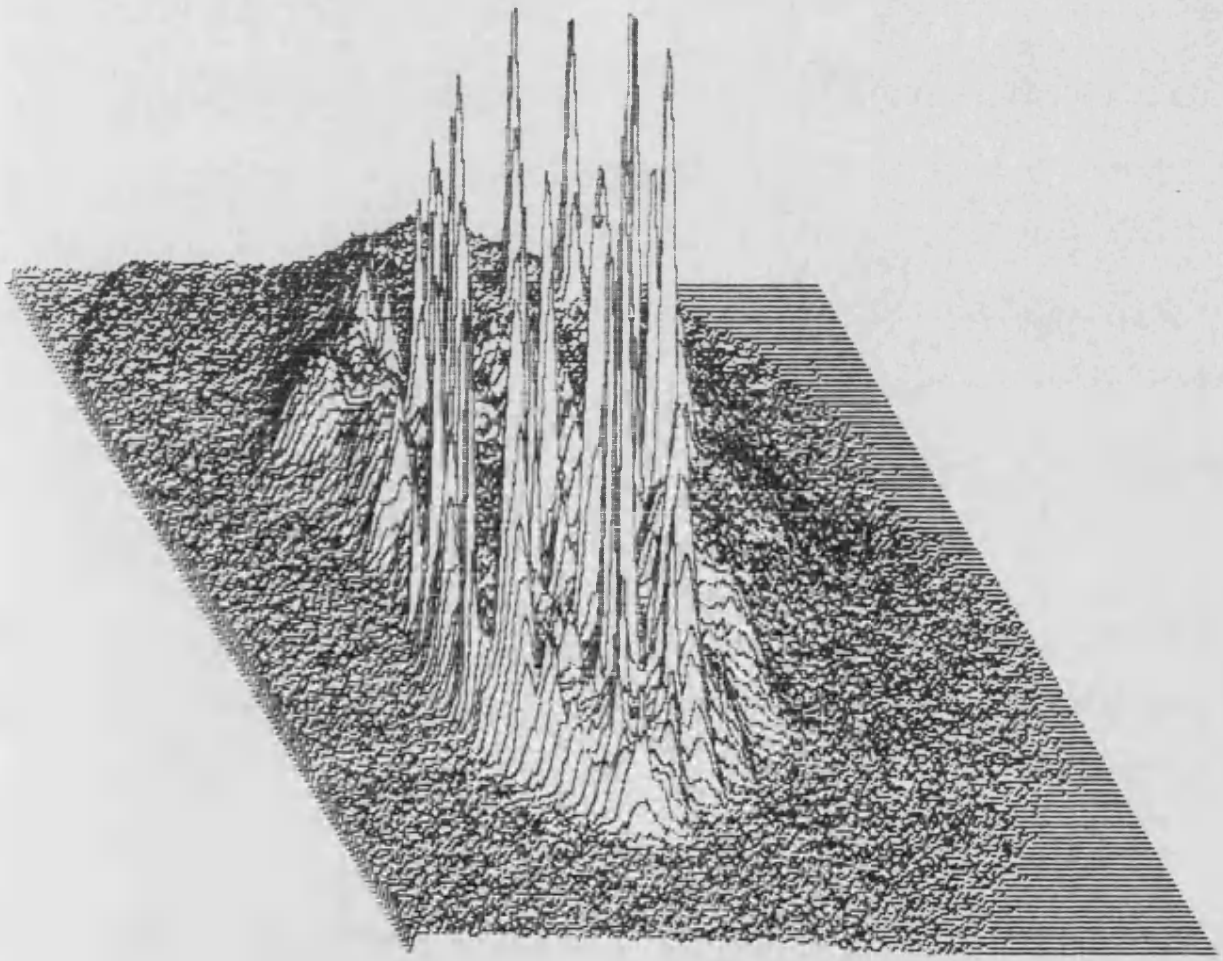

Figure 3.13. Isometric projection of the brightness of the digitised image of an Elcema G250 particle with adherent Triamterene particles shown in plate 3.13. Focus position at 80 fine focus divisions.

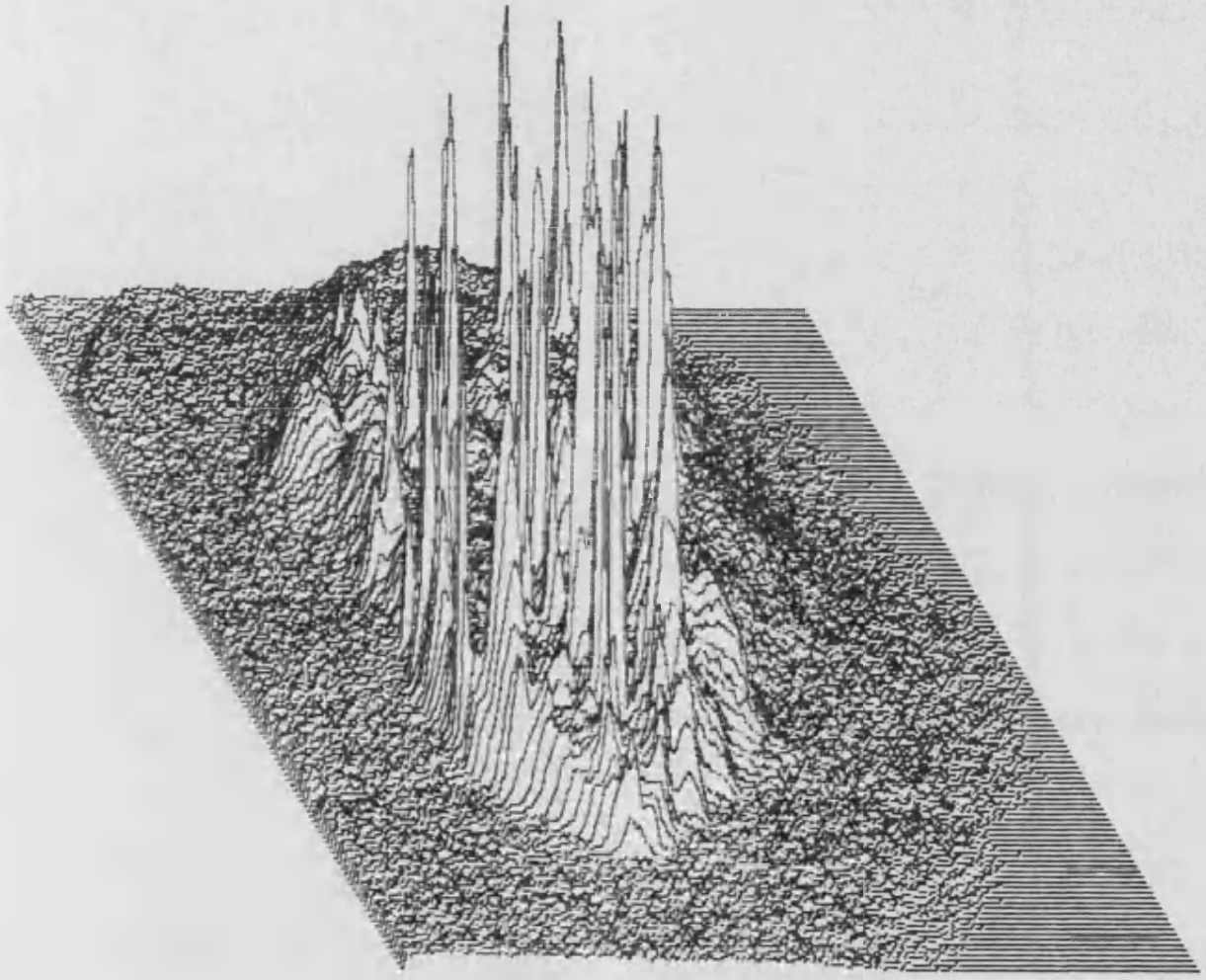

Figure 3.14. Isometric projection of the brightness of the digitised image of an Elcema G250 particle with adherent Triamterene particles shown in plate 3.14. Focus position at 90 fine focus divisions.

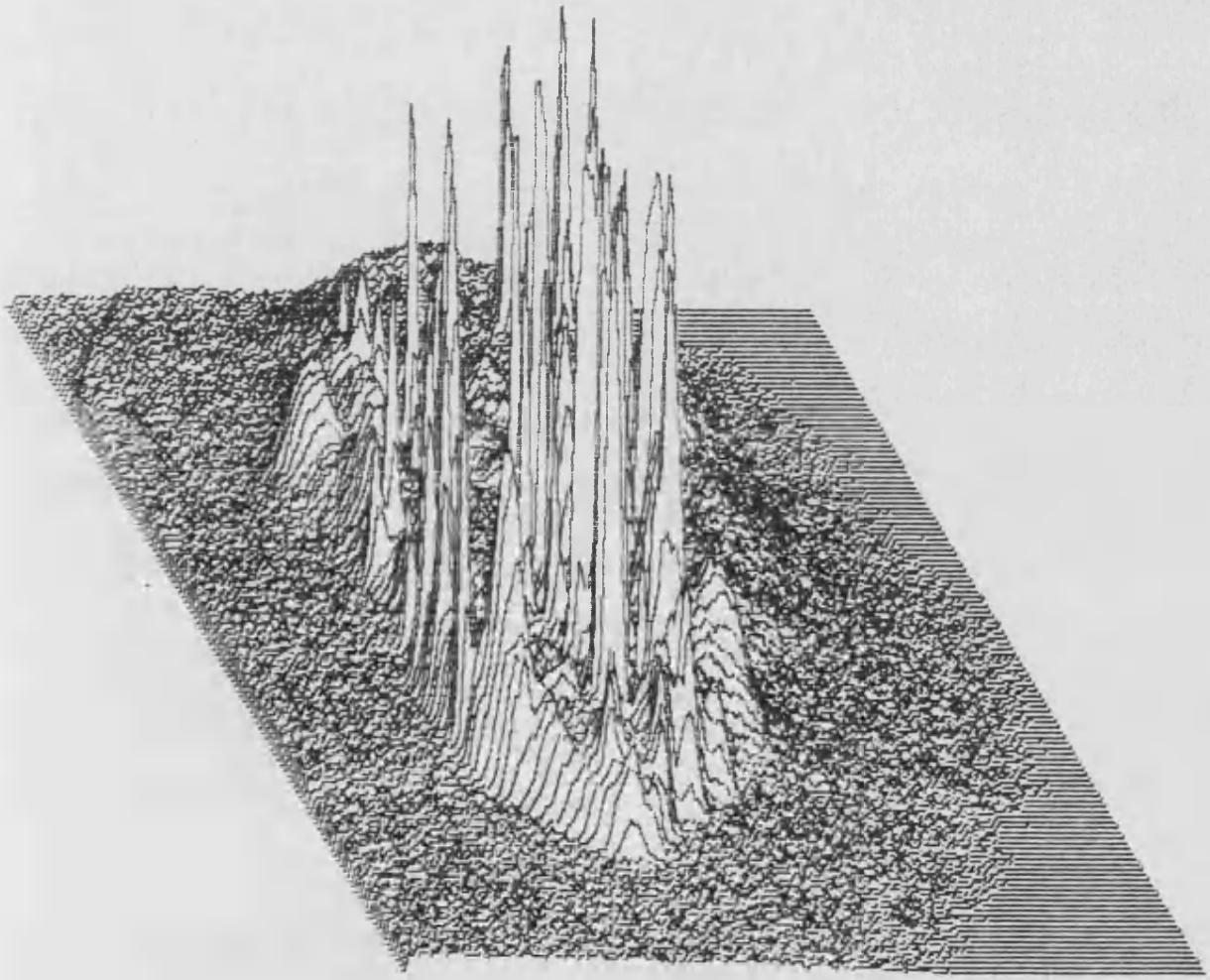

Figure 3.15. Isometric projection of the brightness of the digitised image of an Elcema G250 particle with adherent Triamterene particles shown in plate 3.15. Focus position at 100 fine focus divisions.

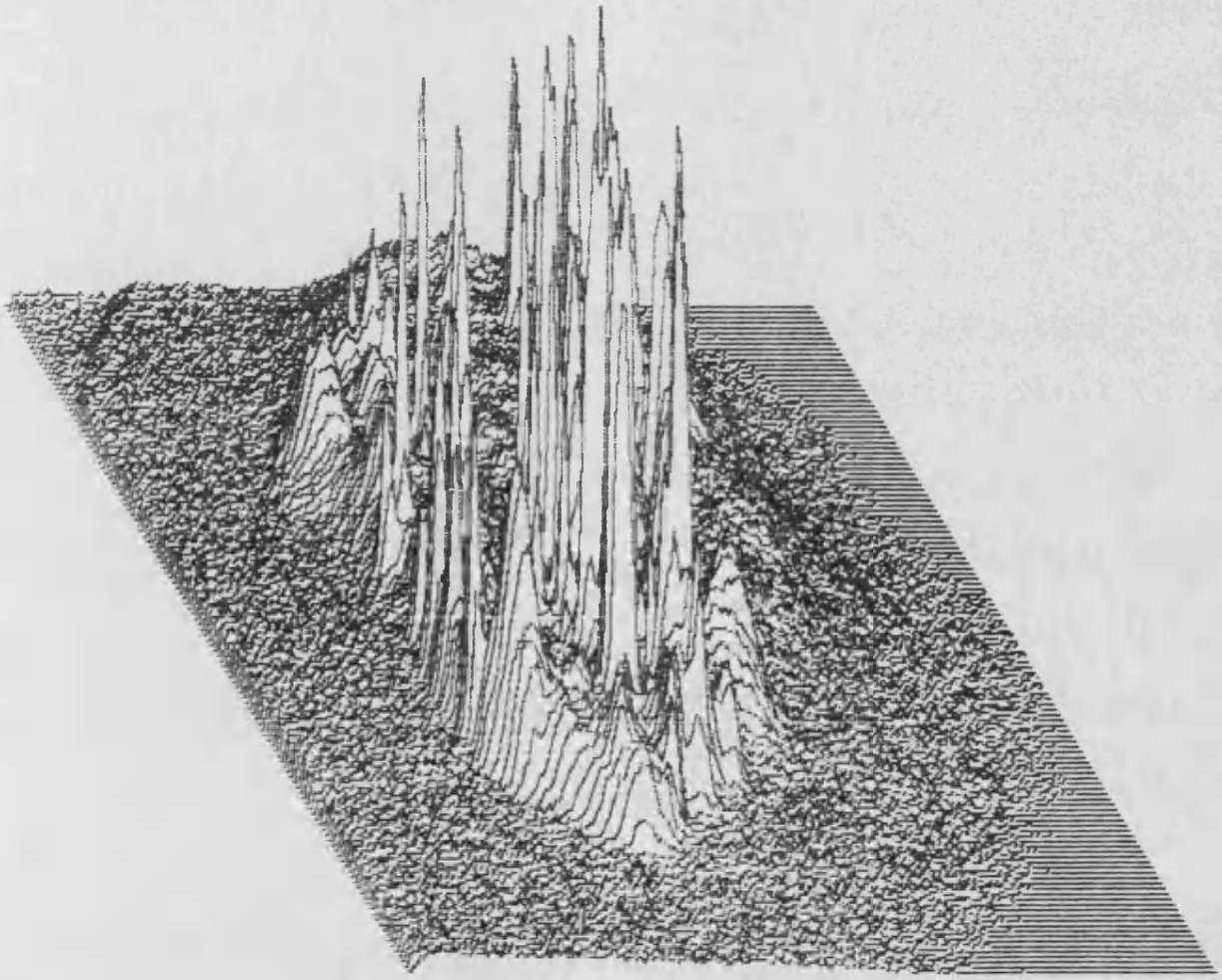

Figure 3.16. Isometric projection of the brightness of the digitised image of an Elcema G250 particle with adherent Triamterene particles shown in plate 3.16. Focus position at 110 fine focus divisions.

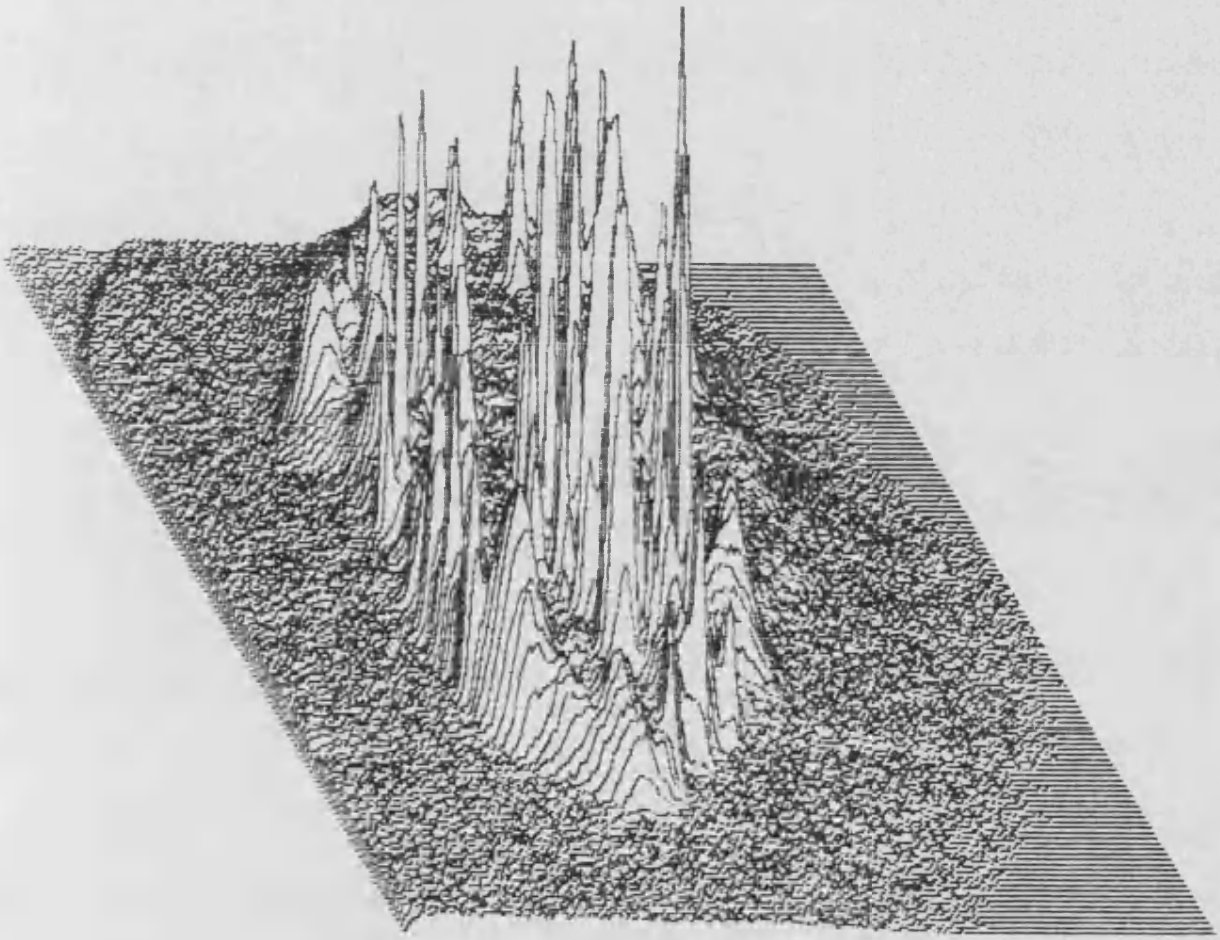

Figure 3.17. Isometric projection of the brightness of the digitised image of an Elcema G250 particle with adherent Triamterene particles shown in plate 3.17. Focus position at 120 fine focus divisions.

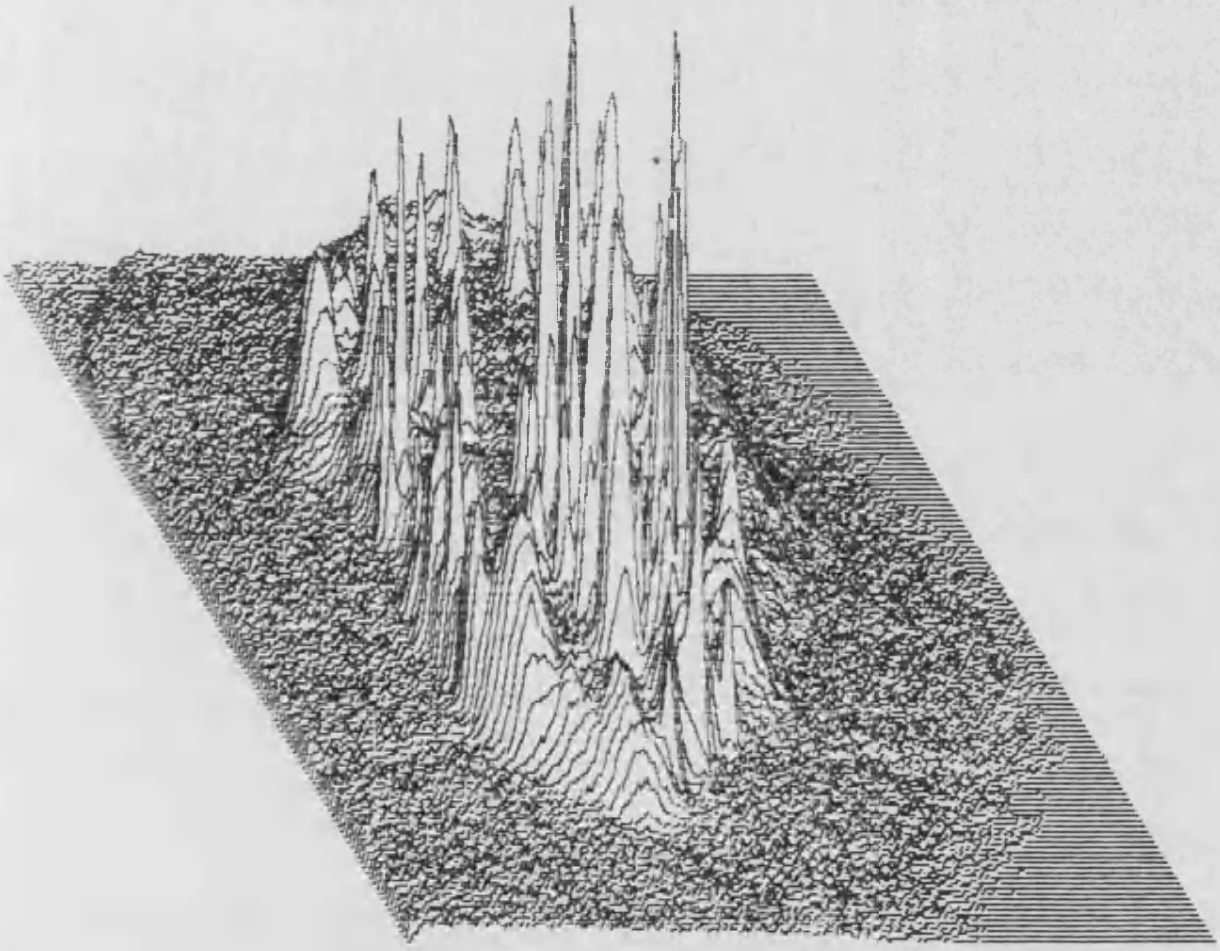

Figure 3.18. Isometric projection of the brightness of the digitised image of an Elcema G250 particle with adherent Triamterene particles shown in plate 3.18. Focus position at 130 fine focus divisions.

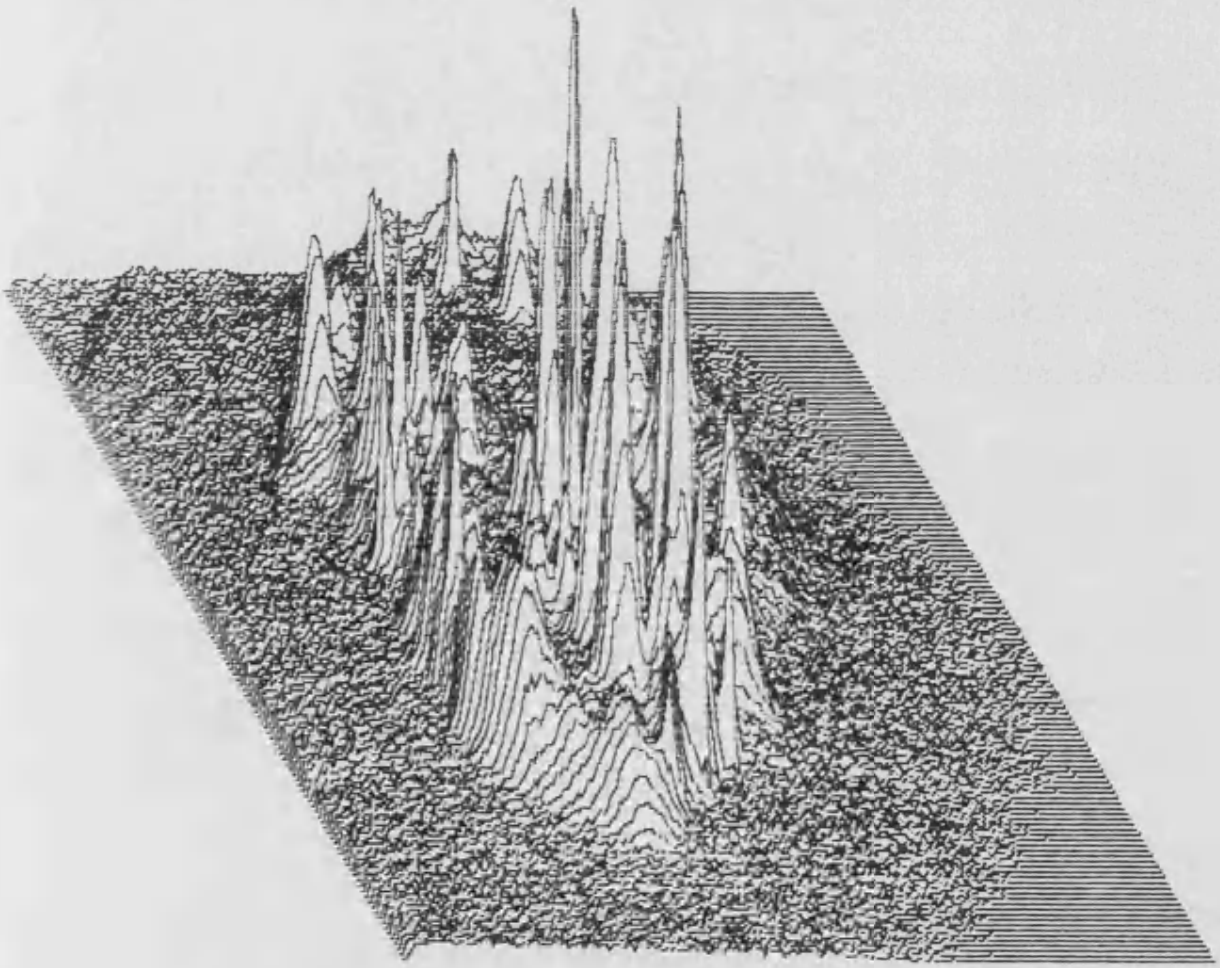

Figure 3.19. Isometric projection of the brightness of the digitised image of an Elcema G250 particle with adherent Triamterene particles shown in plate 3.19. Focus position at 140 fine focus divisions.

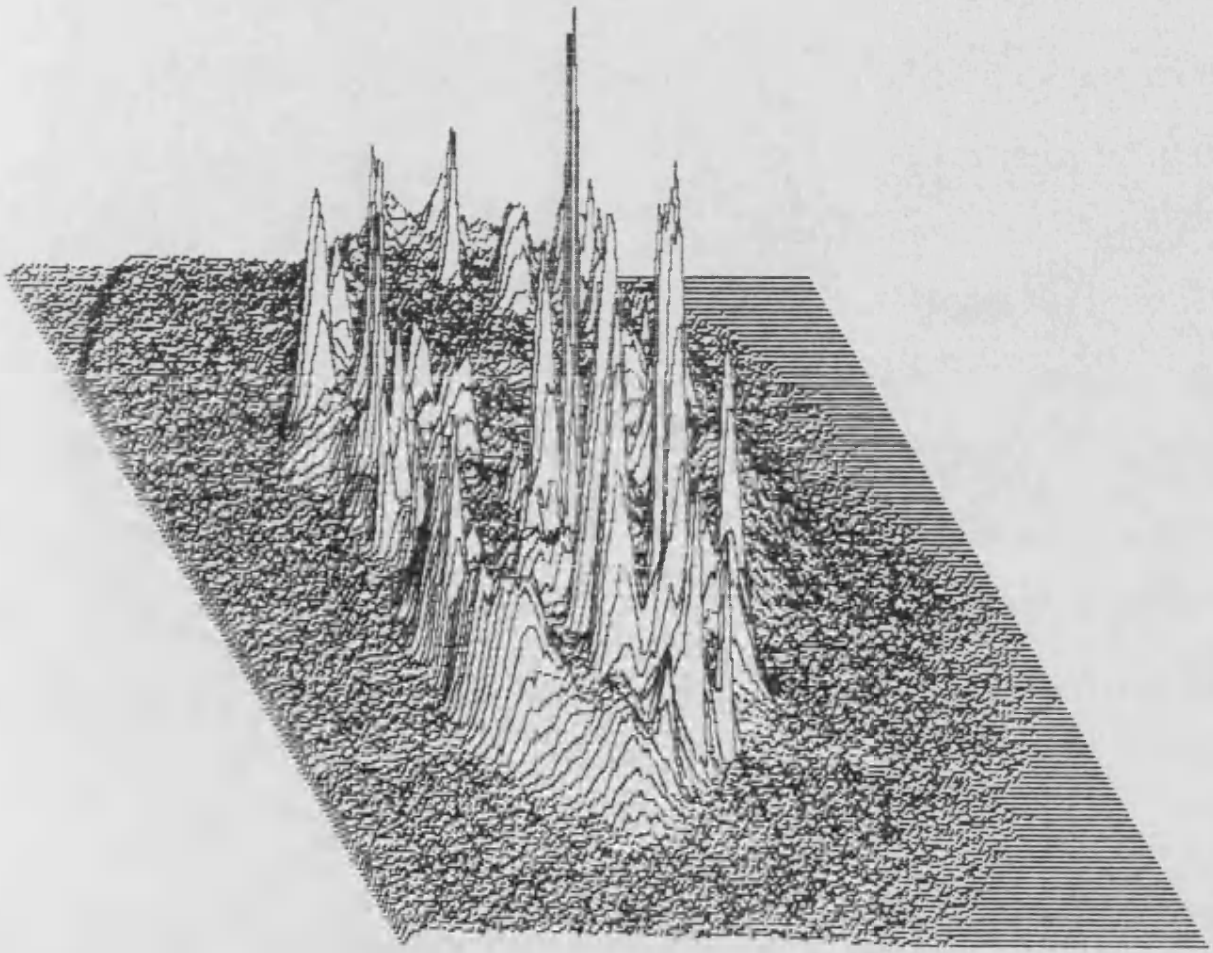

Figure 3.20. Isometric projection of the brightness of the digitised image of an Elcema G250 particle with adherent Triamterene particles shown in plate 3.20. Focus position at 150 fine focus divisions.

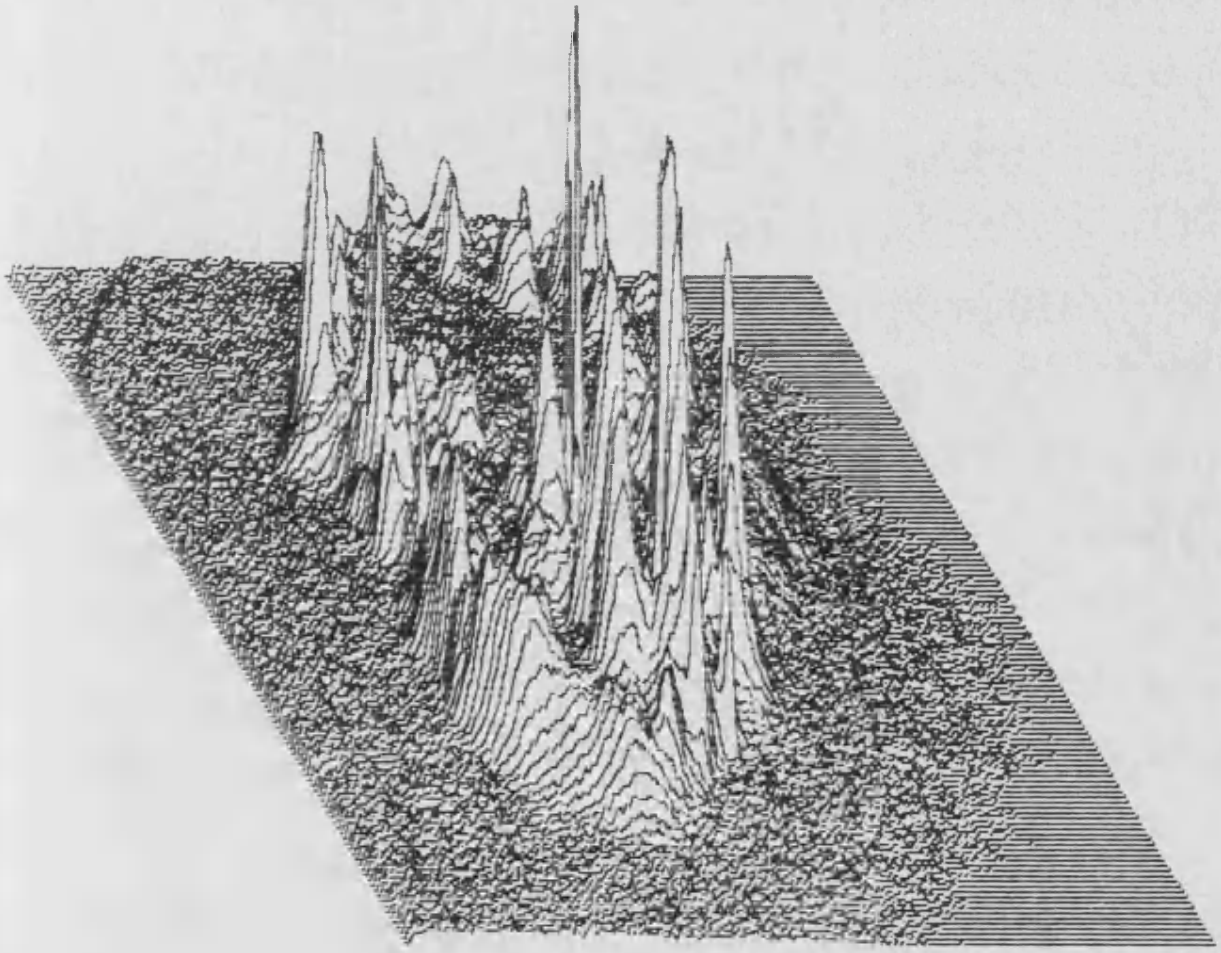

Figure 3.21. Isometric projection of the brightness of the digitised image of an Elcema G250 particle with adherent Triamterene particles shown in plate 3.21. Focus position at 160 fine focus divisions.

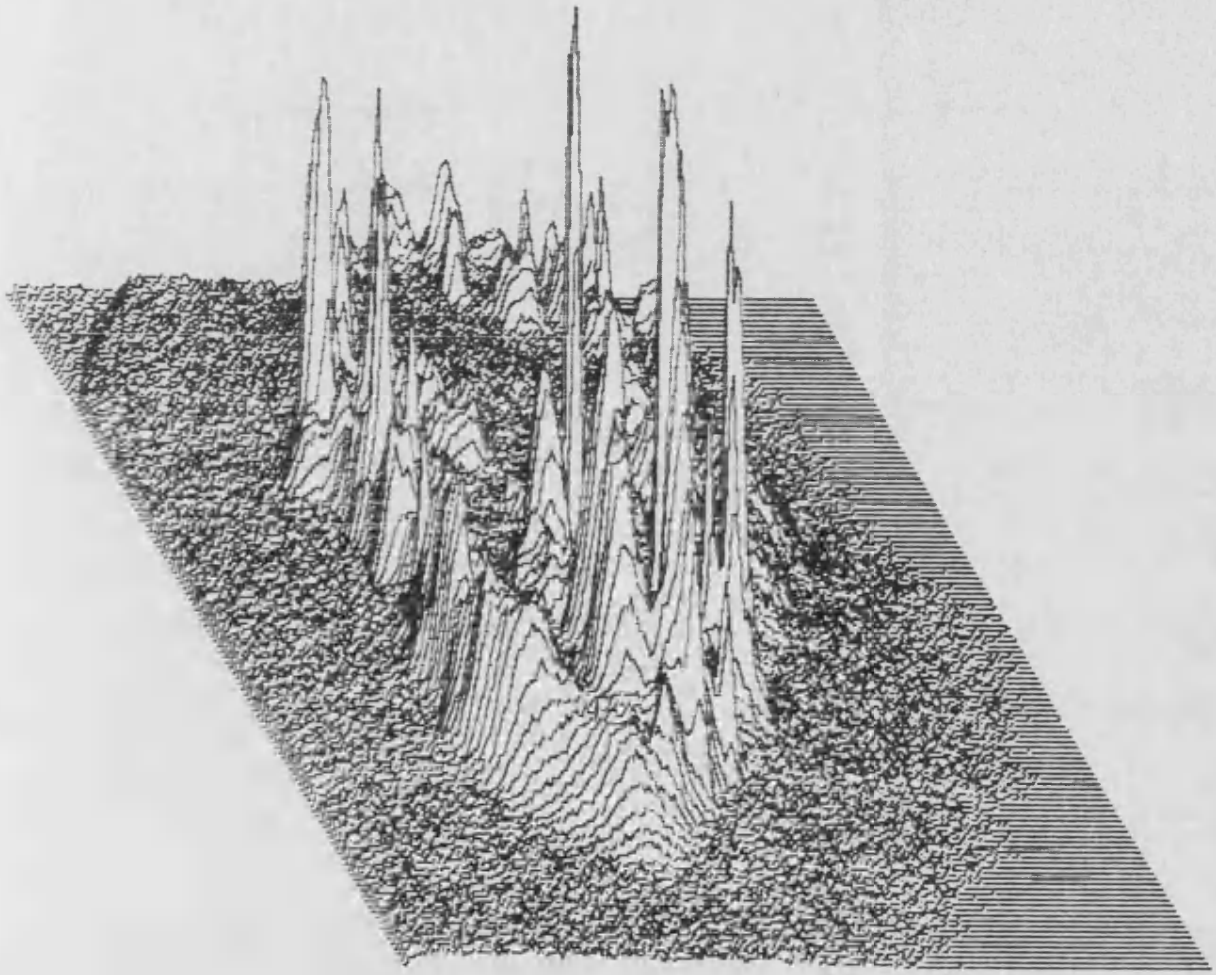

Figure 3.22. Isometric projection of the brightness of the digitised image of an Elcema G250 particle with adherent Triamterene particles as shown in plate 3.22. Focus position at 170 fine focus divisions.

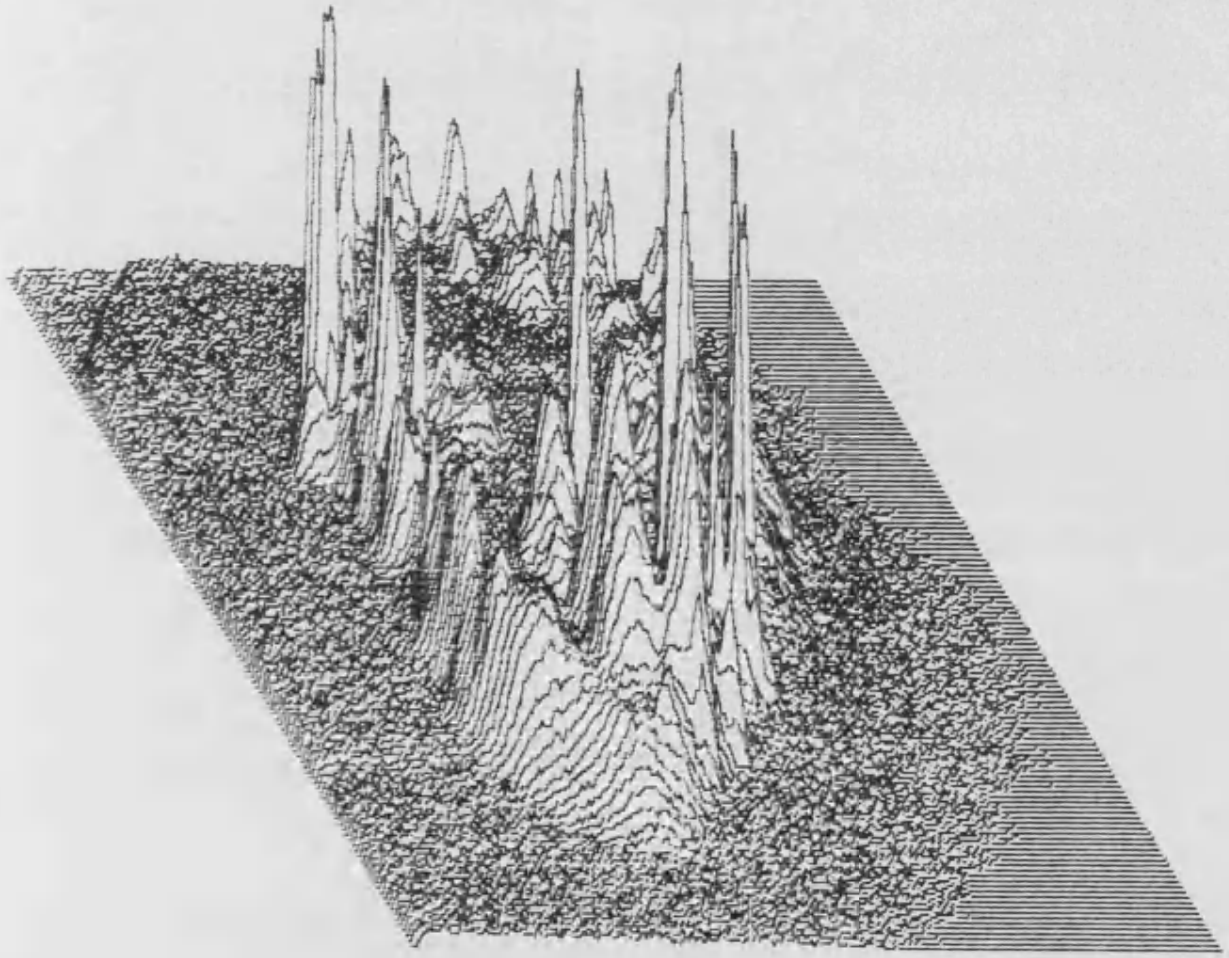

Figure 3.23. Isometric projection of the brightness of the digitised image of an Elcema G250 particle with adherent Triamterene particles as shown in plate 3.23. Focus position at 180 fine focus divisions.

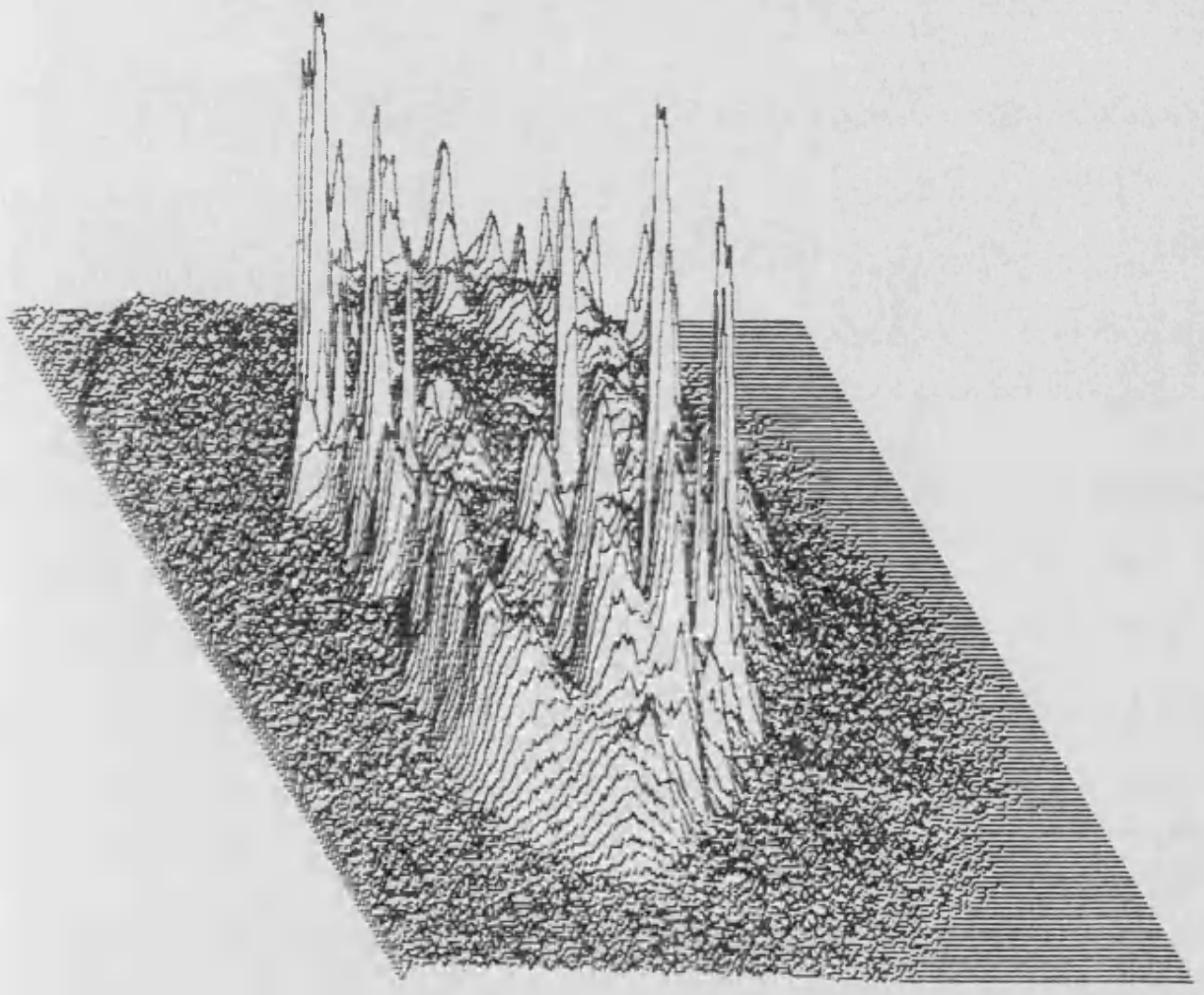

Figure 3.24. Isometric projection of the brightness of the digitised image of an Elcema G250 particle with adherent Triamterene particles as shown in plate 3.24. Focus position at 190 fine focus divisions.

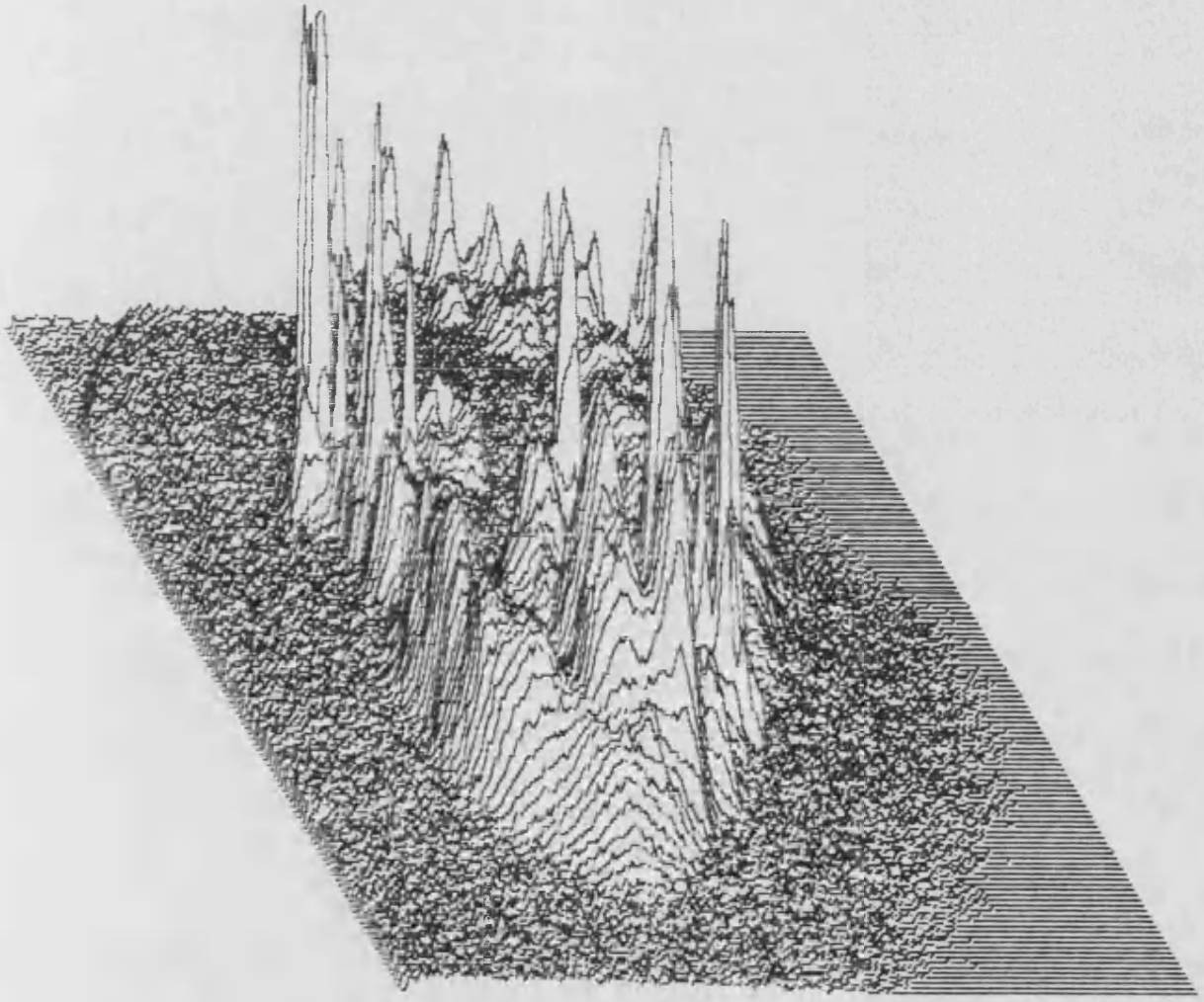

Figure 3.25. Isometric projection of the brightness of the digitised image of an Elcema G250 particle with adherent Triamterene particles as shown in plate 3.25. Focus position at 200 fine focus divisions.

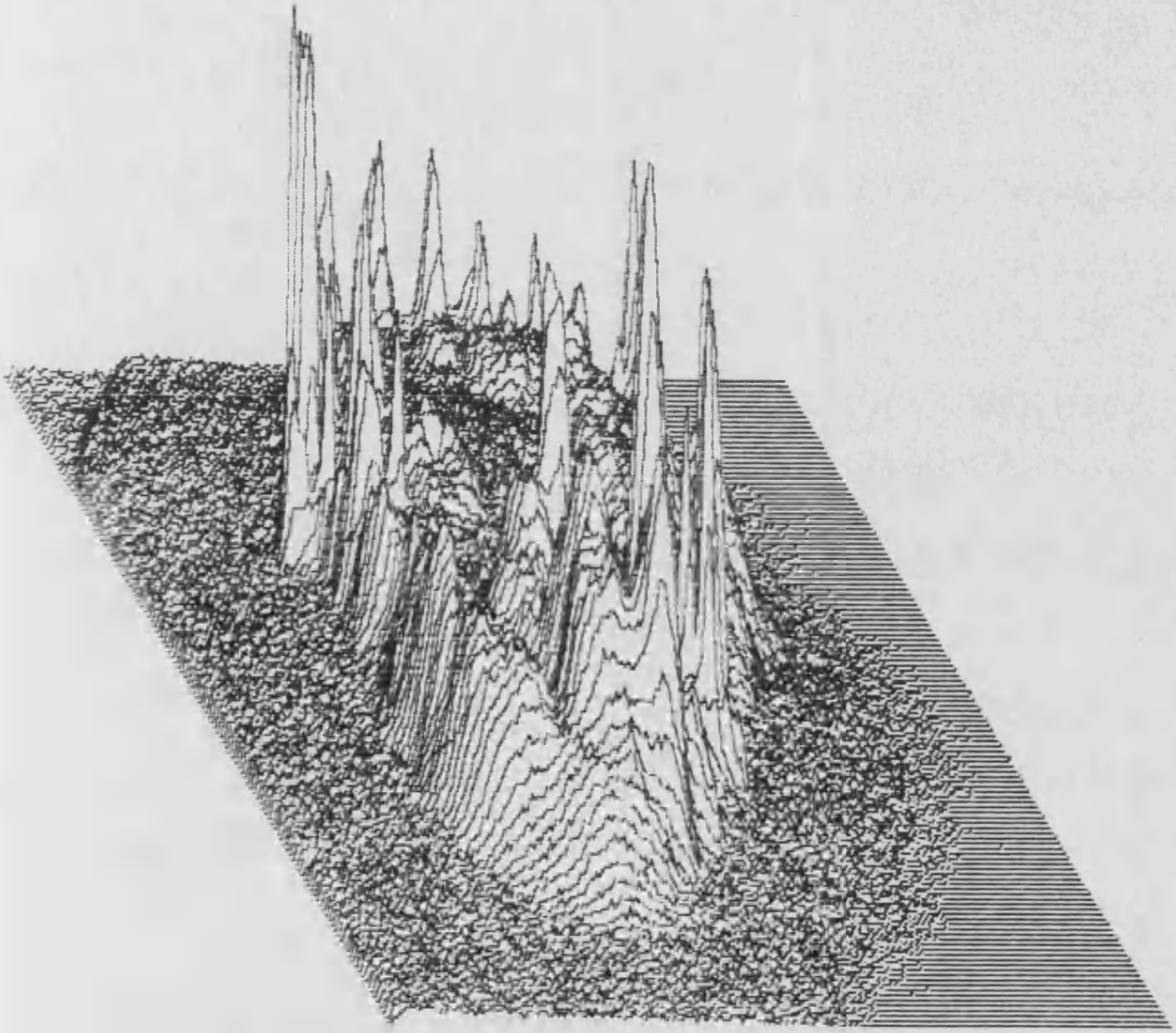

Figure 3.26. Isometric projection of the brightness of the digitised image of an Elcema G250 particle with adherent Triamterene particles as shown in plate 3.26. Focus position at 240 fine focus divisions.

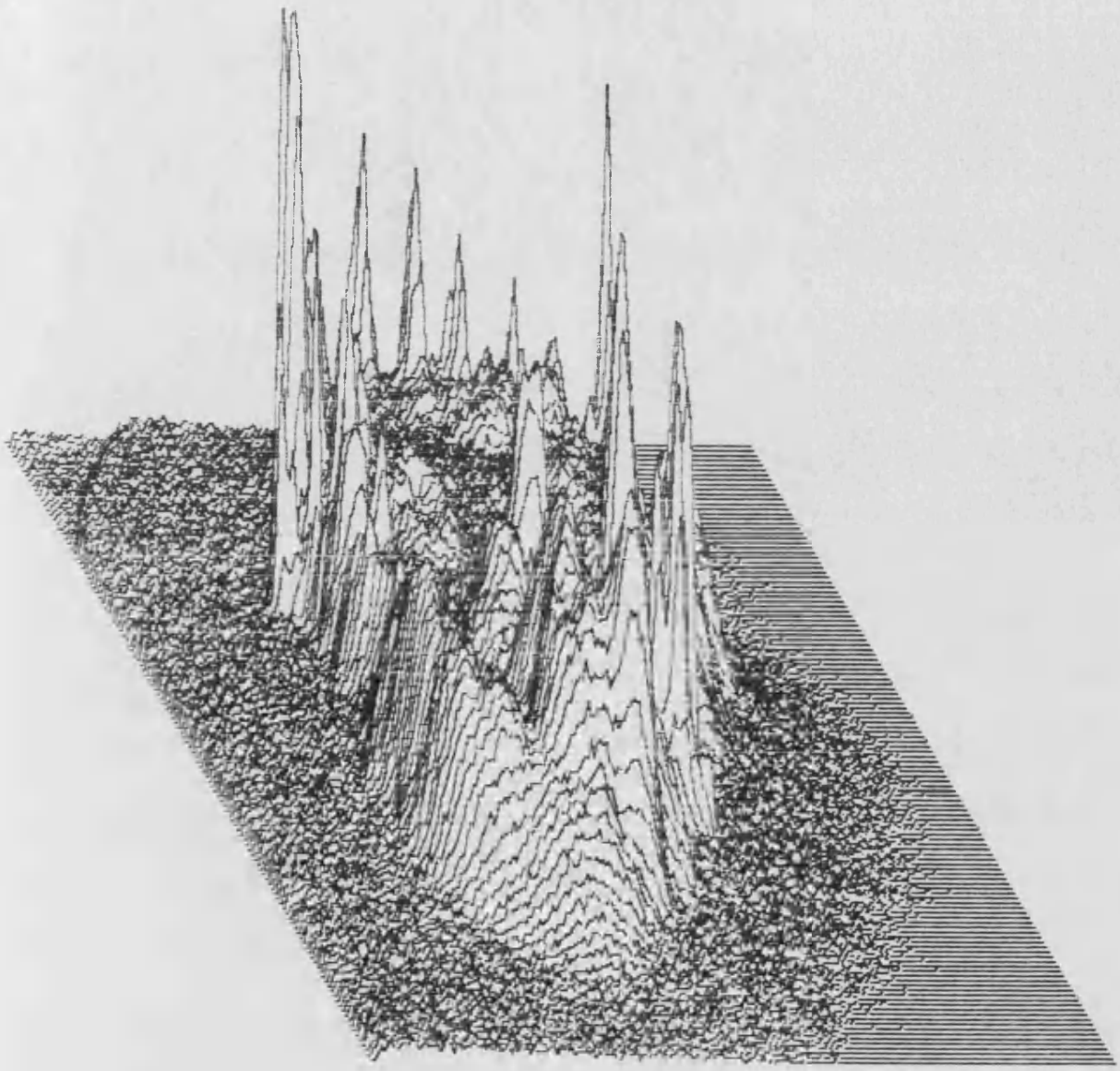

Figure 3.27. Isometric projection of the brightness of the digitised image of an Elcema G250 particle with adherent Triamterene particles as shown in plate 3.27. Focus position at 220 fine focus divisions.

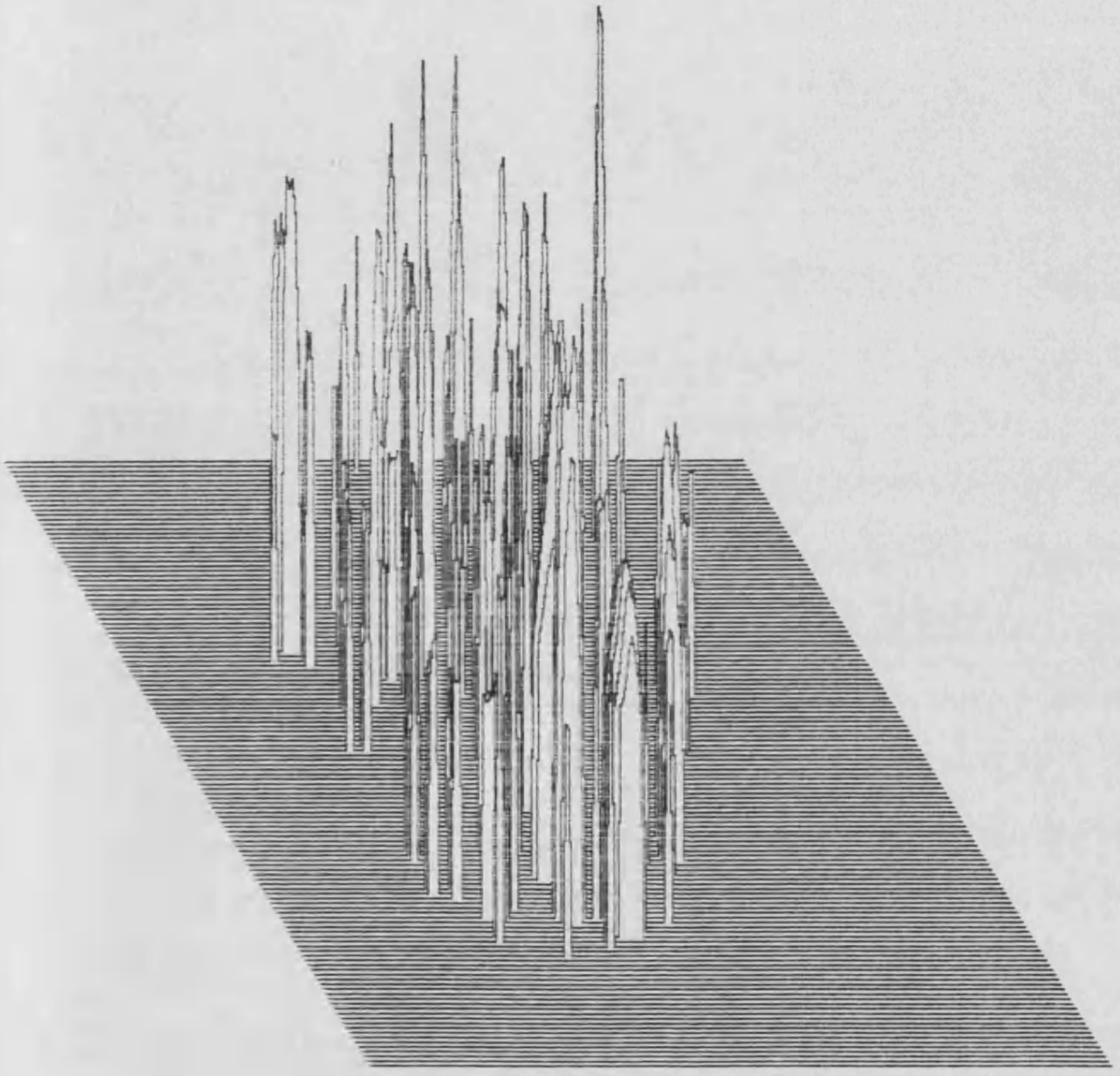

Figure 3.28. Isometric projection of the brightness of the composite digitised image of an Elcema G250 particle with adherent Triamterene particles as shown in plate 3.28. The peaks correspond to focussed adherent Triamterene particles as determined by the BASIC program BCOMPOS and the 6502 machine code program COMPOS (Appendix 2).

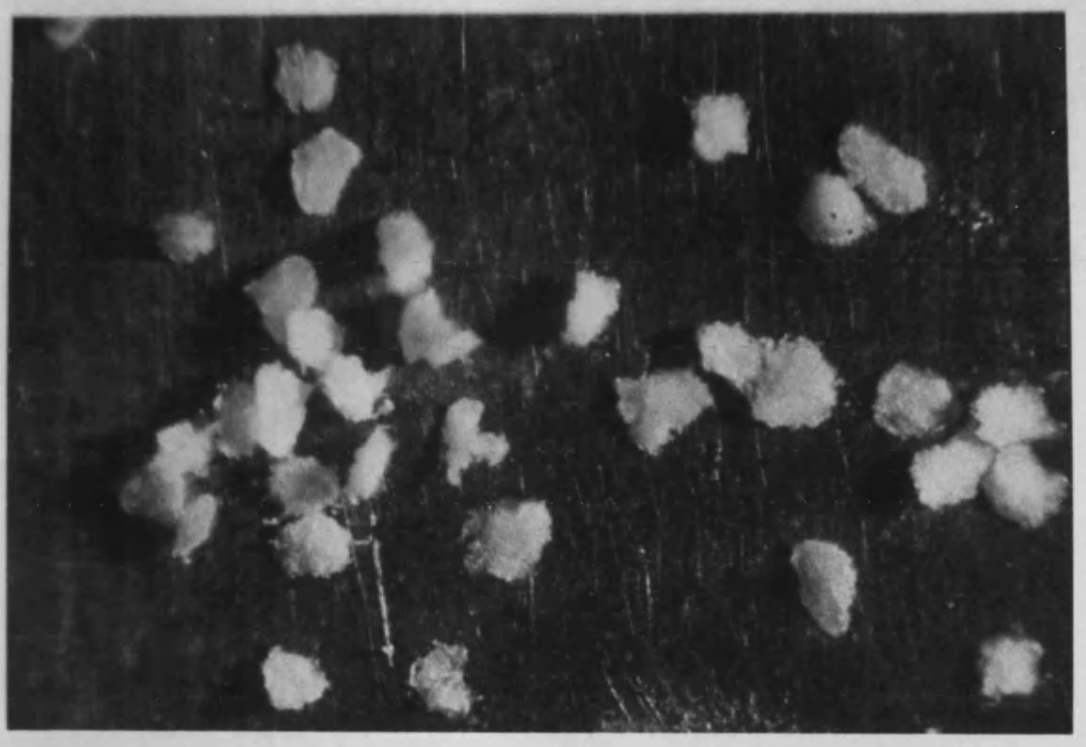

Plate 3.1. Elcema G250 particles fixed to the brass plate with epoxy resin prior to centrifugation at 50,000 rev min^{-1}.

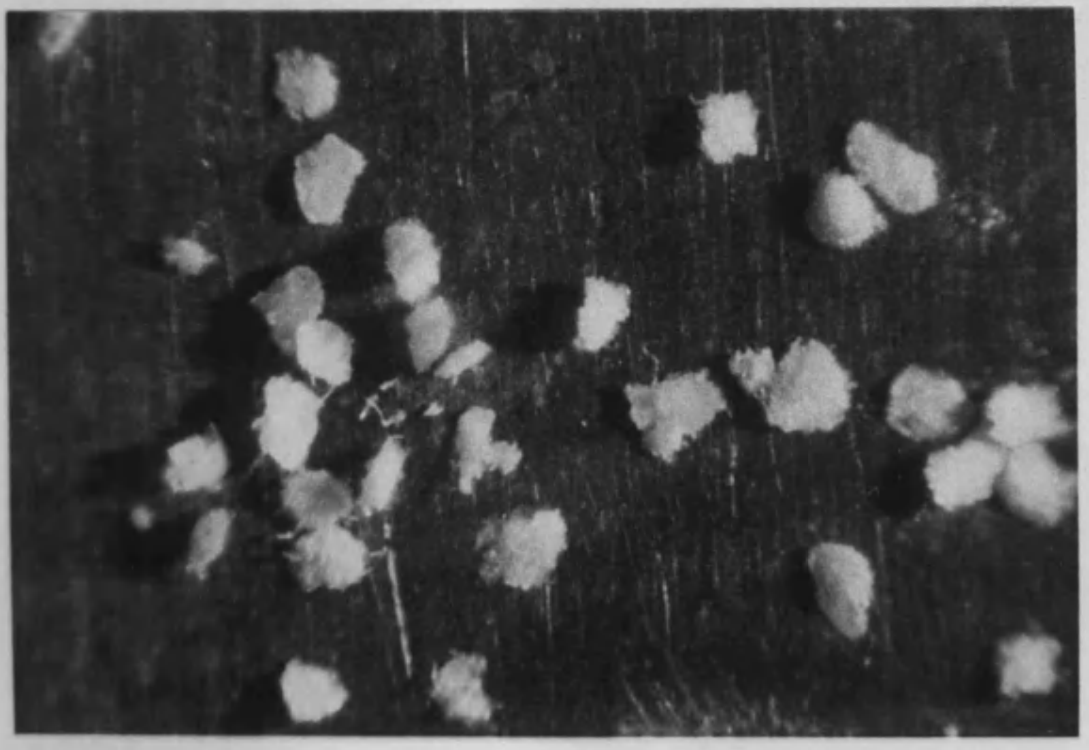

Plate 3.2. Elcema G250 particles fixed to the brass plate with epoxy resin after centrigugation at 50,000 rev min^{-1}. Note that some particles have been detatched.

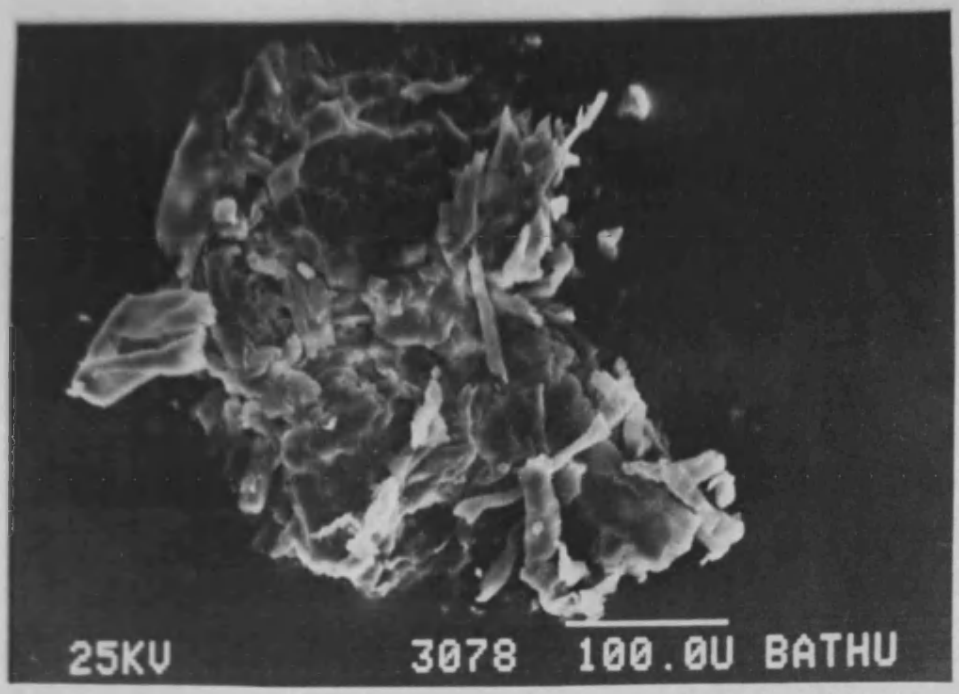

Plate 3.3. Scanning electron micrograph of an Elcema G250 particle fixed to the brass plate with epoxy resin. The surface detail present indicates that no 'wicking' of the adhesive through to the particle surface has occurred.

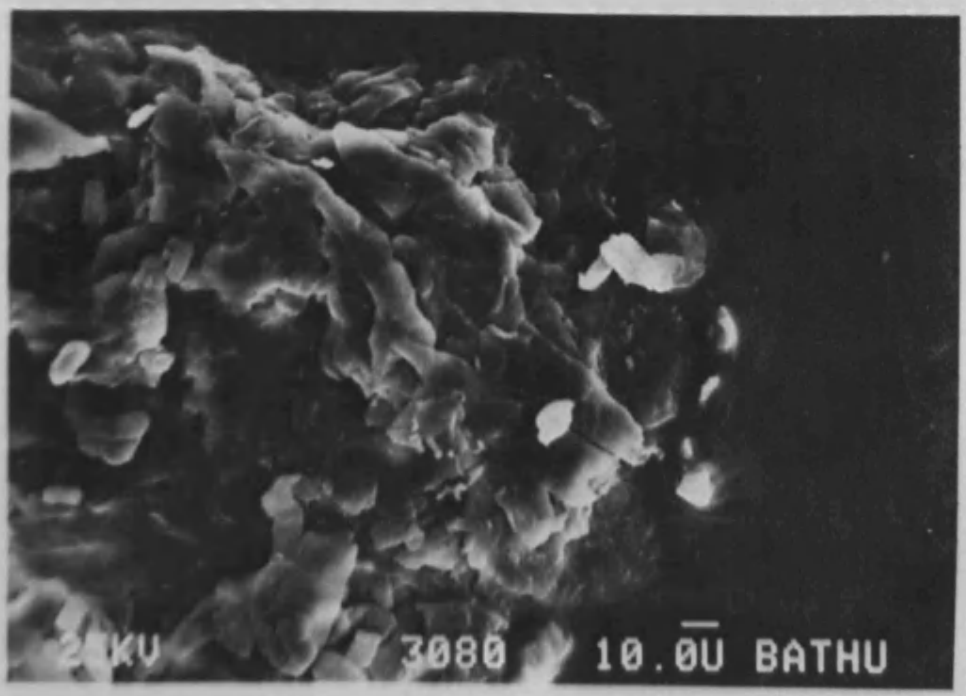

Plate 3.4. Scanning electron micrograph of an Elcema G250 particle fixed to the brass plate with epoxy resin showing that the penetration of the resin is limited, even at the periphery of the particle.

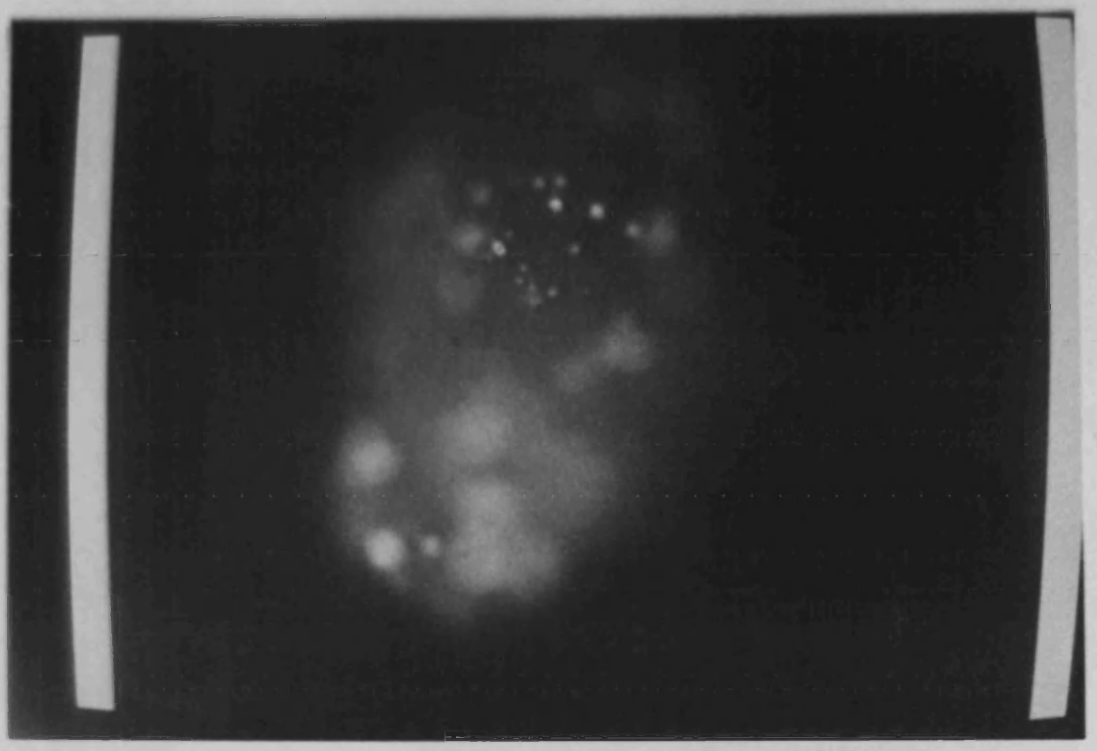

Plate 3.5. Digitised image of an Elcema G250 particle with adherent Triamterene particles. Focus position at 00 fine focus divisions.

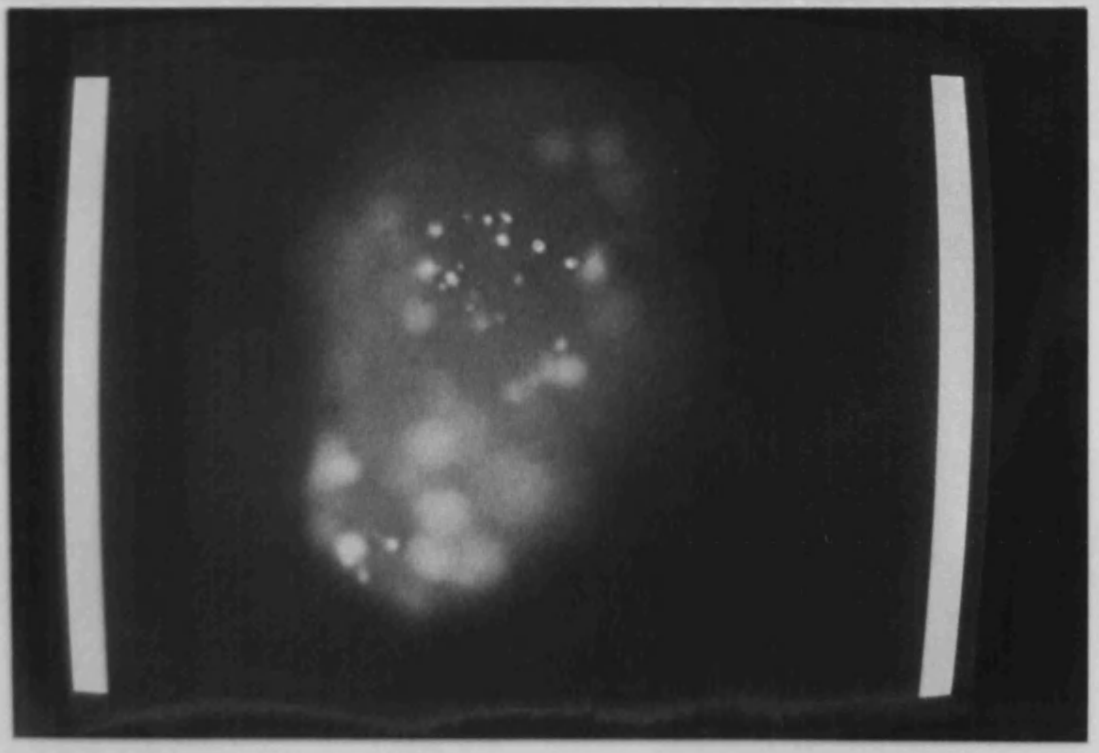

Plate 3.6. Digitised image of an Elcema G250 particle with adherent Triamterene particles. Focus position at 10 fine focus divisions.

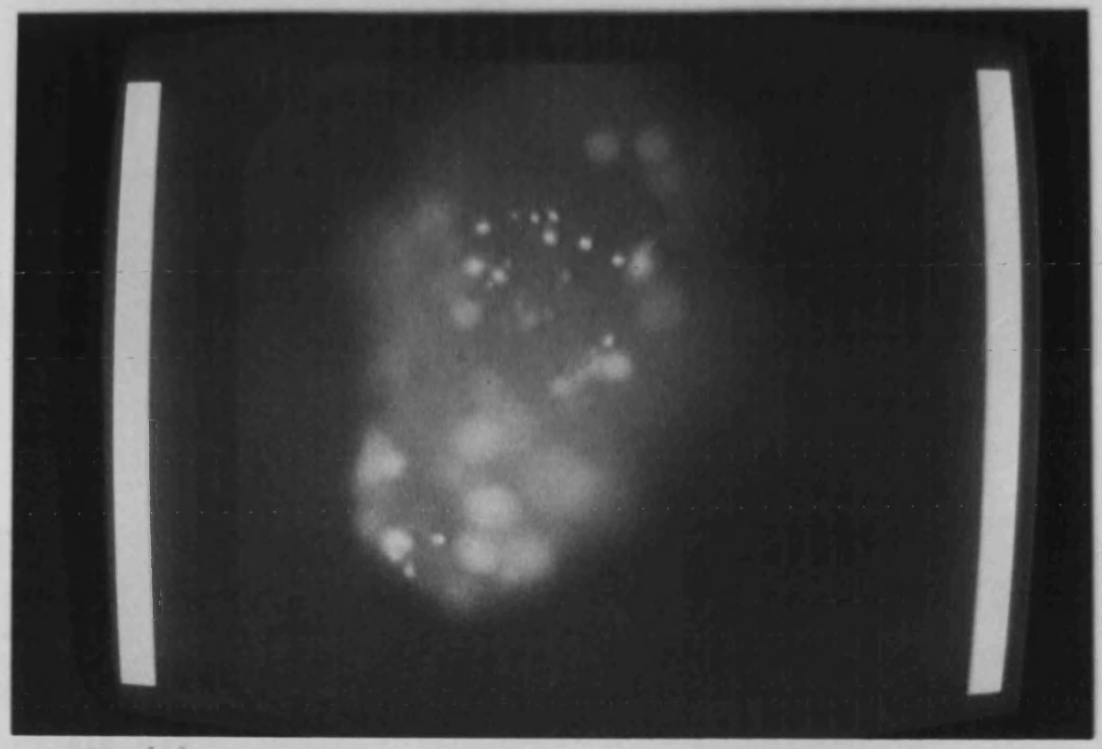

Plate 3.7. Digitised image of an Elcema G250 particle with adherent Triamterene particles. Focus position at 20 fine focus divisions.

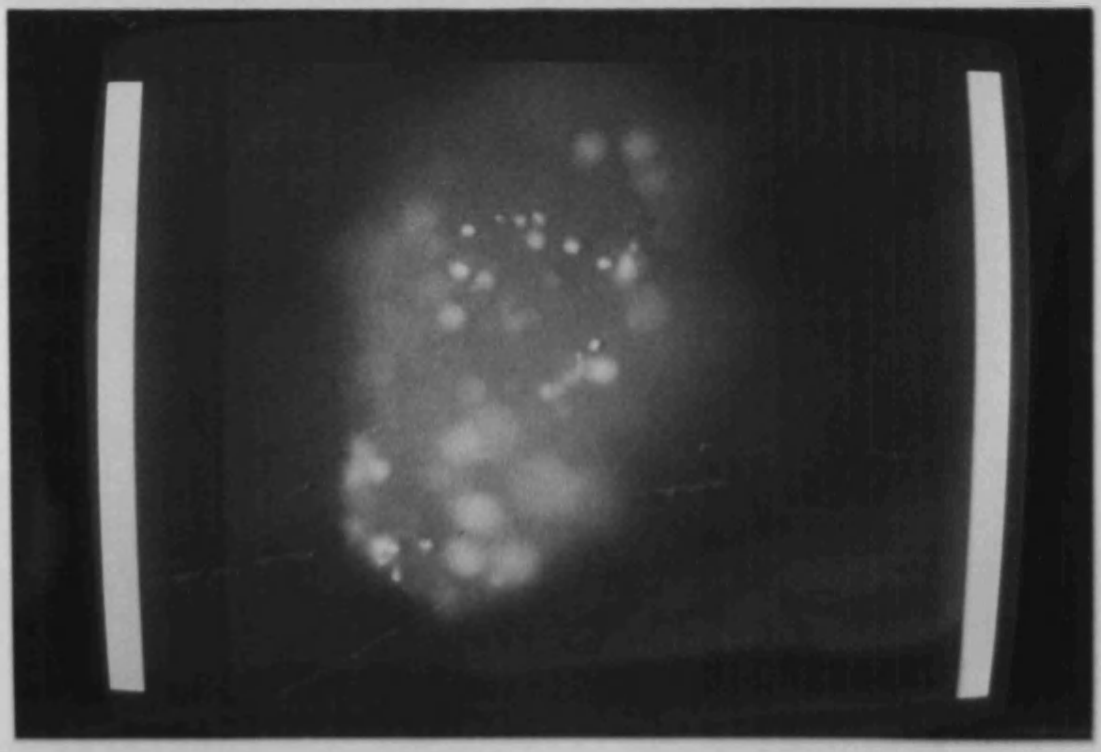

Plate 3.8. Digitised image of an Elcema G250 particle with adherent Triamterene particles. Focus position at 30 fine focus divisions.

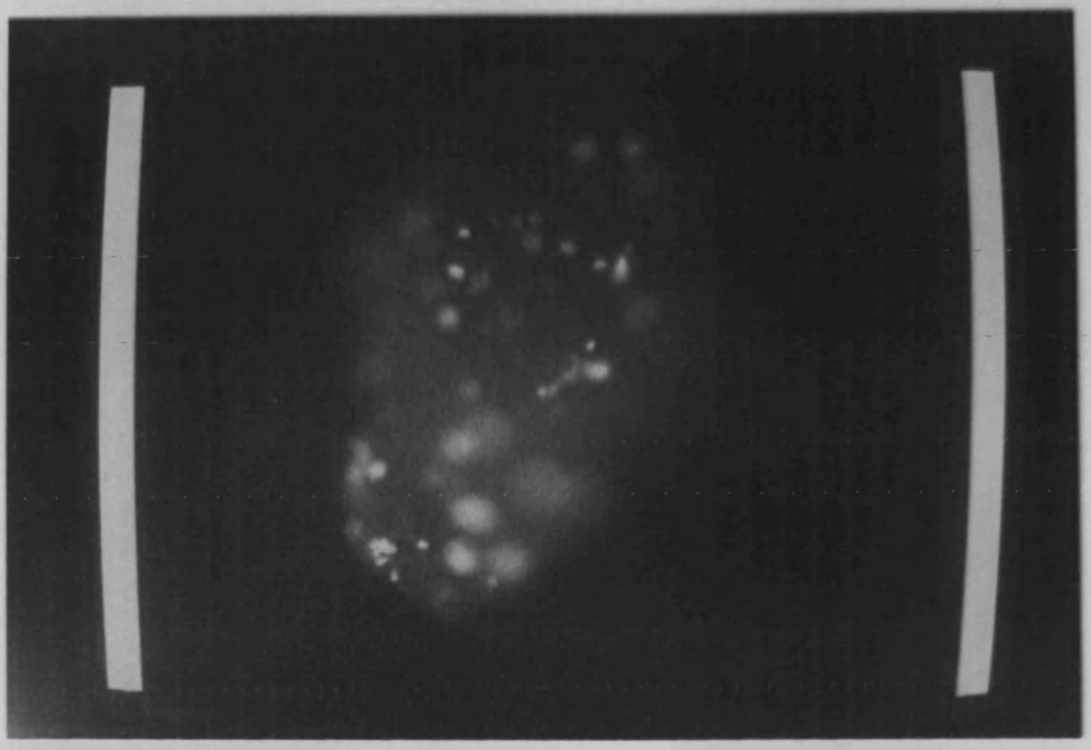

Plate 3.9. Digitised image of an Elcema G250 particle with adherent Triamterene particles. Focus position at 40 fine focus divisions.

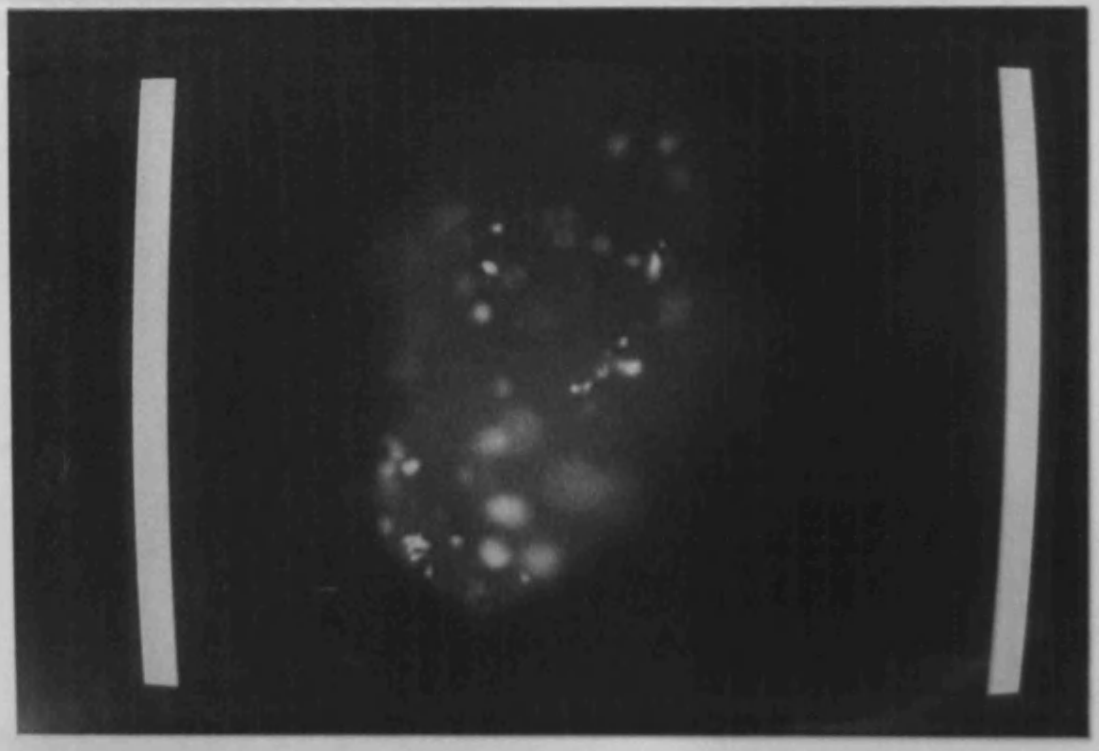

Plate 3.10. Digitised image of an Elcema G250 particle with adherent Triamterene particles. Focus position at 50 fine focus divisions.

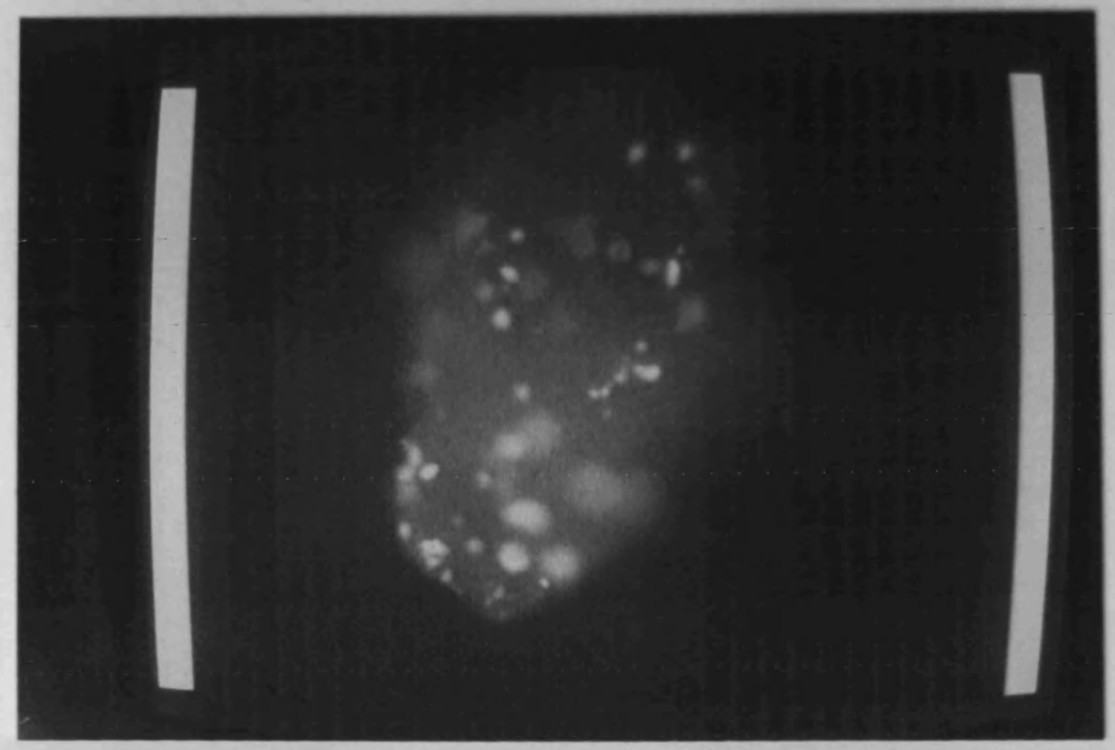

Plate 3.11. Digitised image of an Elcema G250 particle with adherent Triamterene particles. Focus position at 60 fine focus divisions.

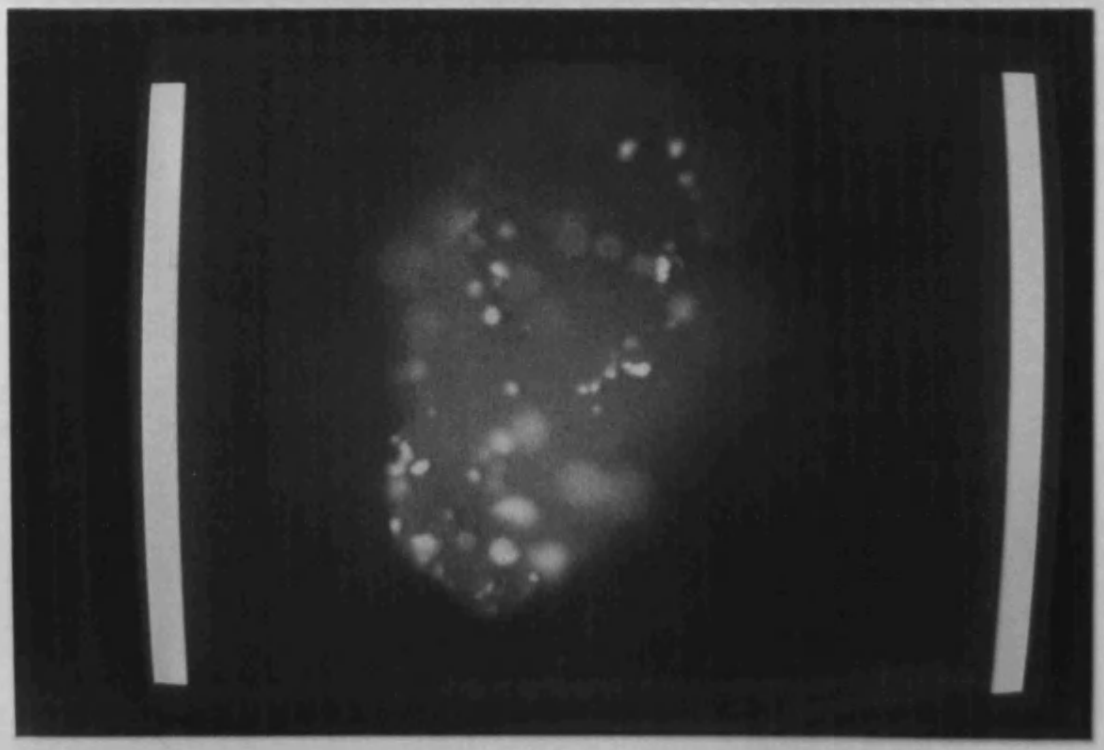

Plate 3.12. Digitised image of an Elcema G250 particle with adherent Triamterene particles. Focus position at 70 fine focus divisions.

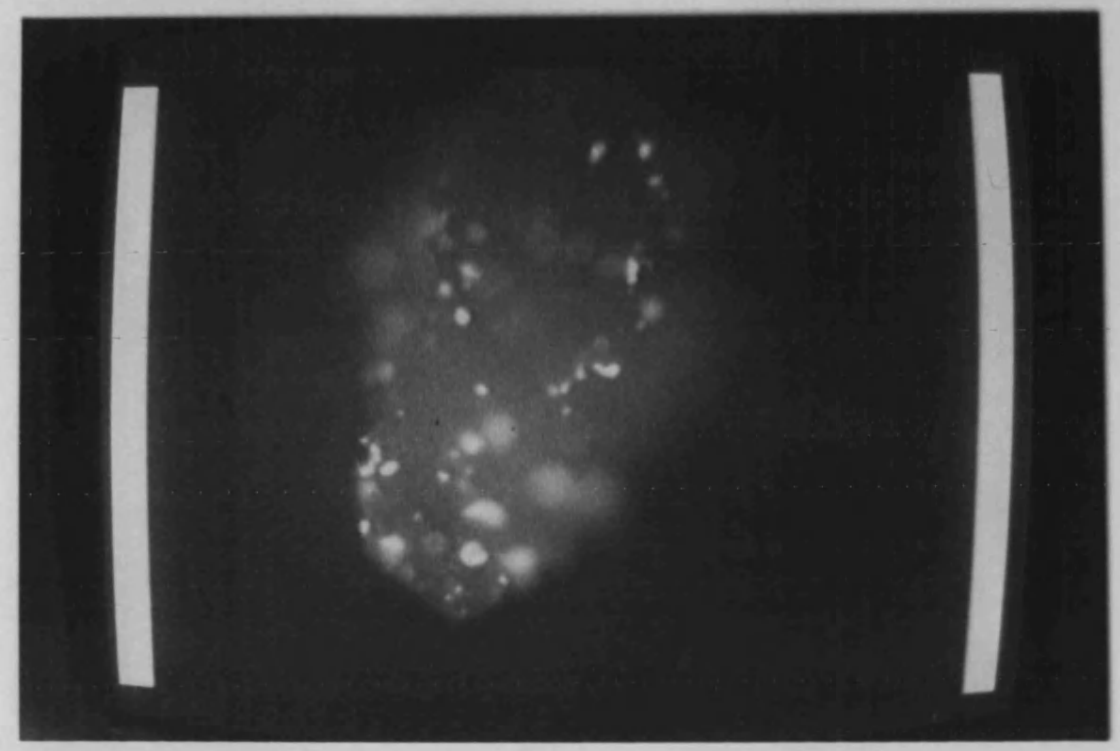

Plate 3.13. Digitised image of an Elcema G250 particle with adherent Triamterene particles. Focus position at 80 fine focus divisions.

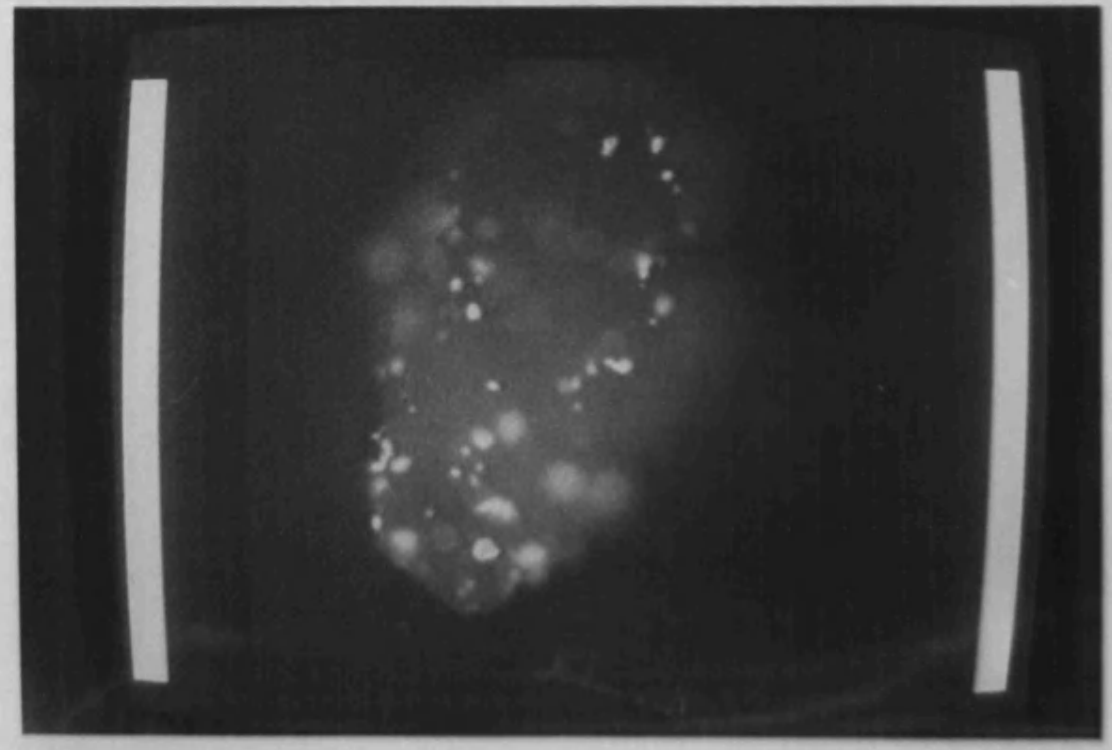

Plate 3.14. Digitised image of an Elcema G250 particle with adherent Triamterene particles. Focus position at 90 fine focus positions.

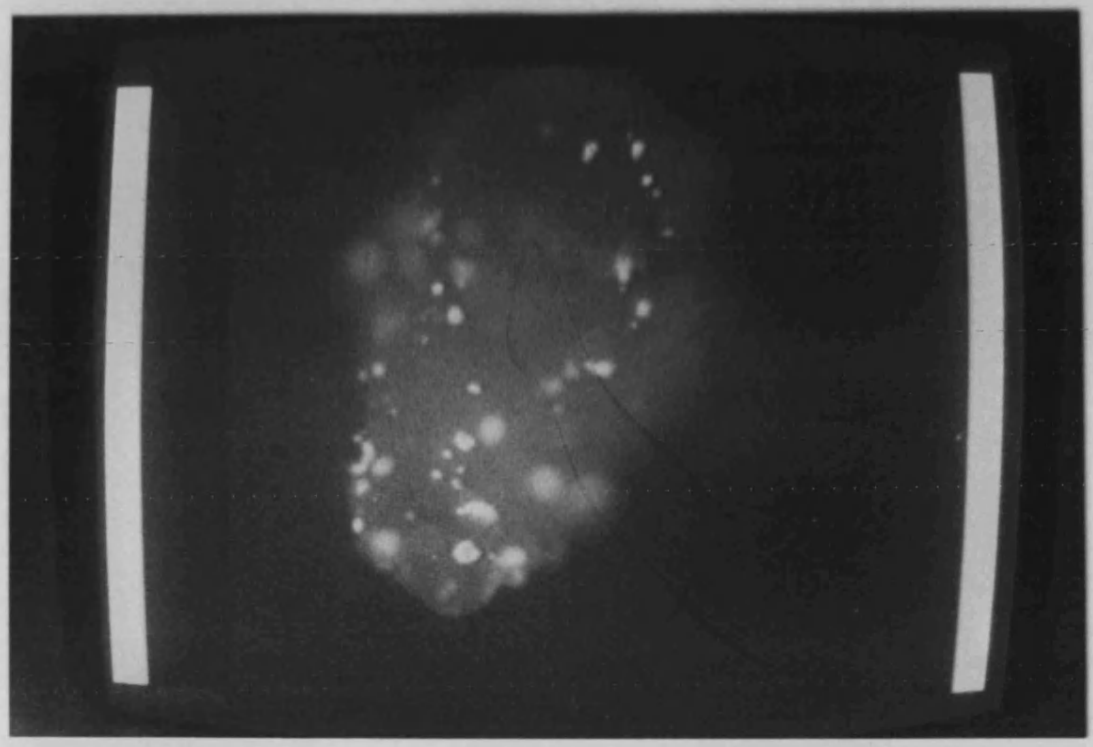

Plate 3.15. Digitised image of an Elcema G250 particle with adherent Triamterene particles. Focus position at 100 fine focus divisions.

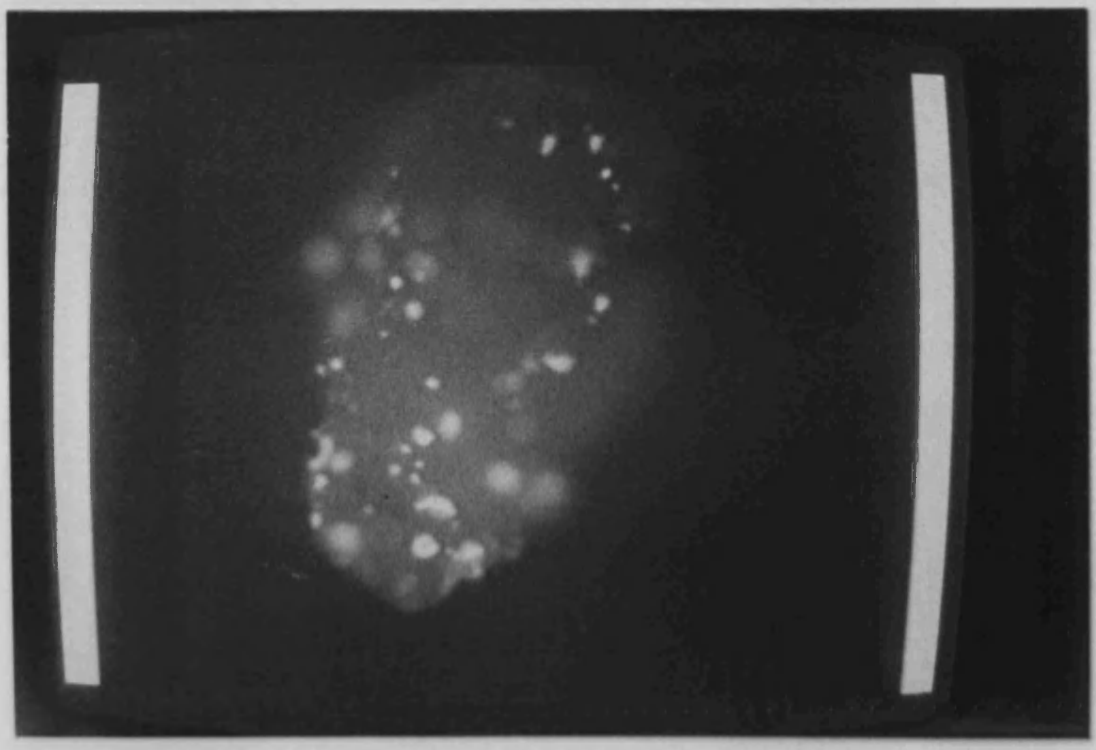

Plate 3.16. Digitised image of an Elcema G250 particle with adherent Triamterene particles. Focus position at 110 fine focus positions.

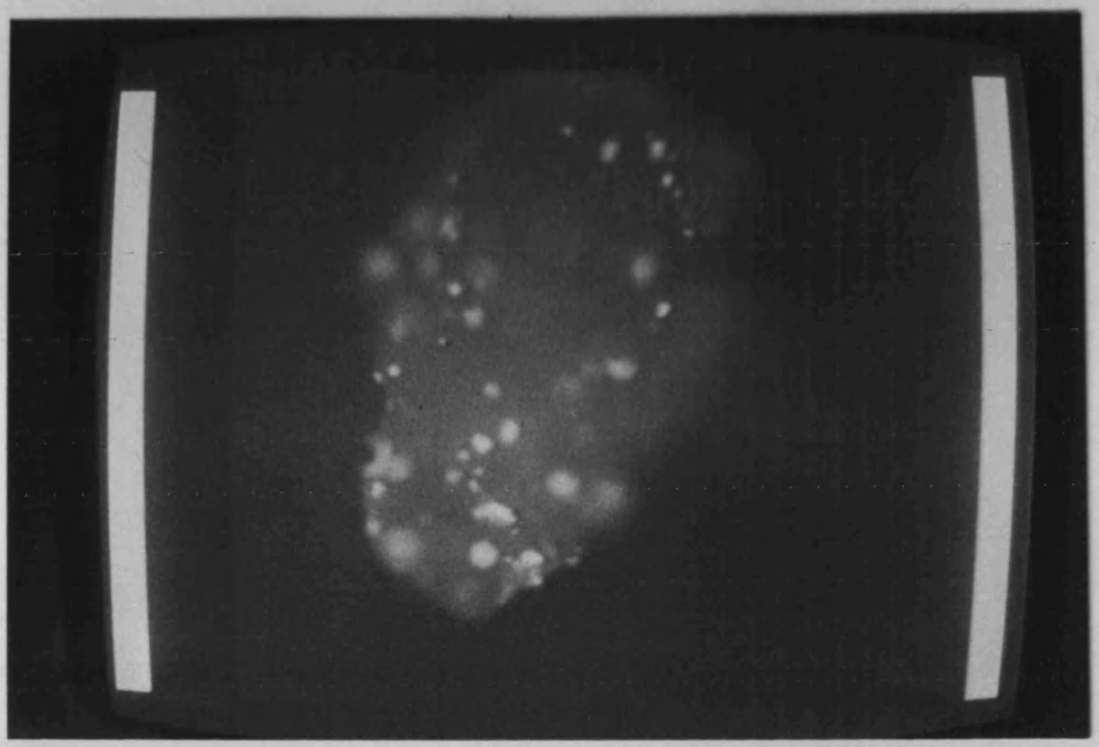

Plate 3.17. Digitised image of an Elcema G250 particle with adherent Triamterene particles. Focus position at 120 fine focus divisions.

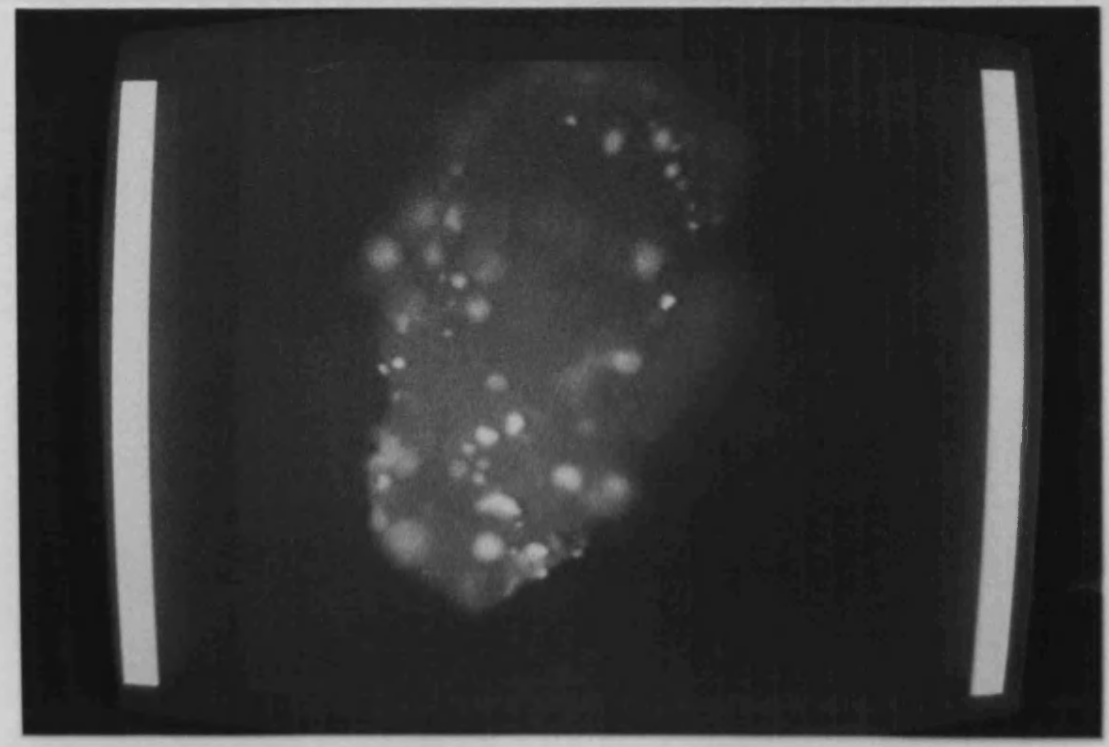

Plate 3.18. Digitised image of an Elcema G250 particle with adherent Triamterene particles. Focus position at 130 fine focus divisions.

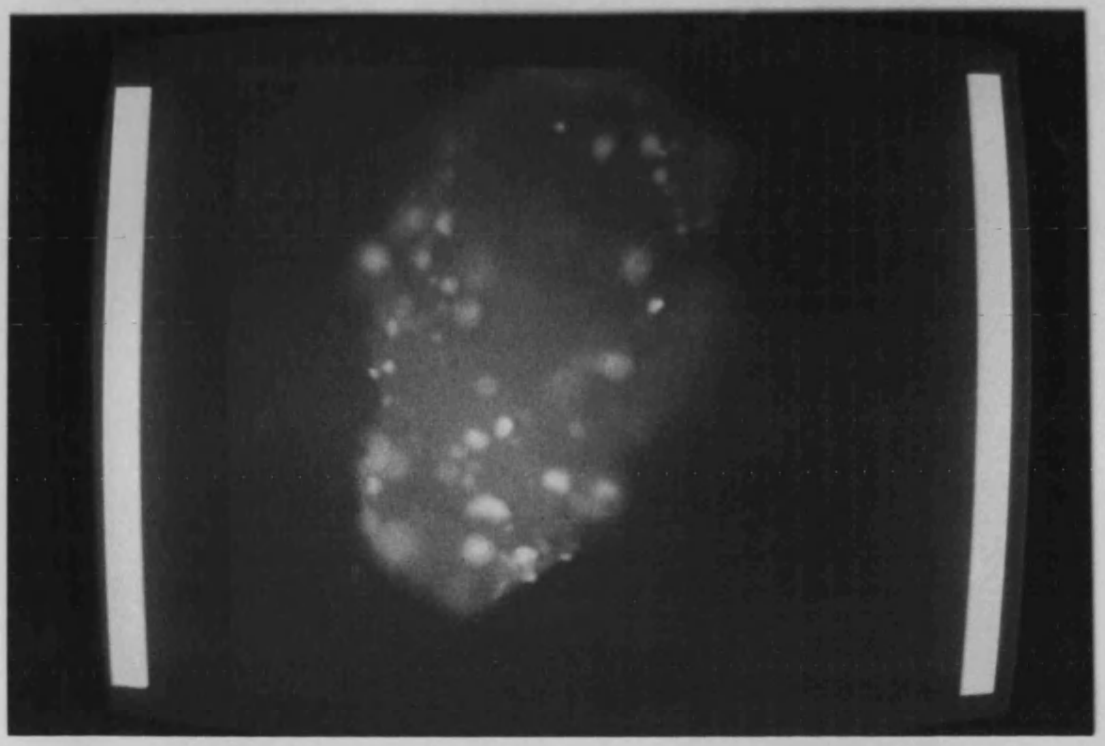

Plate 3.19. Digitised image of an Elcema G250 particle with adherent Triamterene particles. Focus position at 140 fine focus divisions.

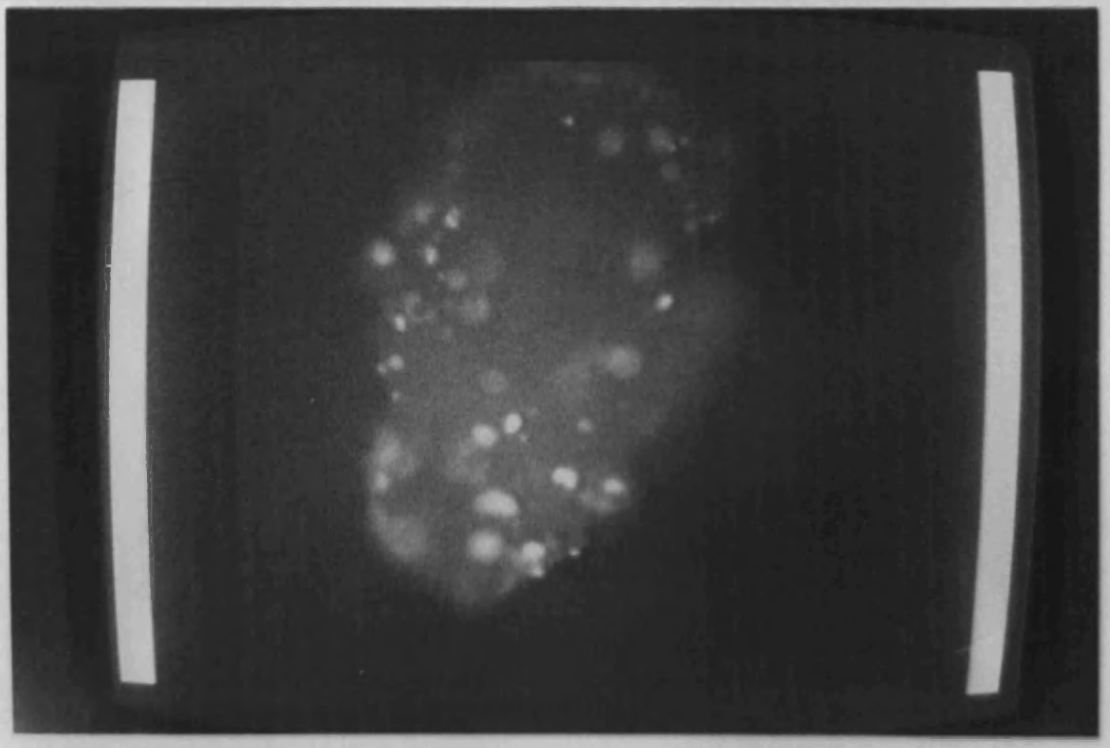

Plate 3.20. Digitised image of an Elcema G250 particle with adherent Triamterene particles. Focus position at 150 fine focus positions.

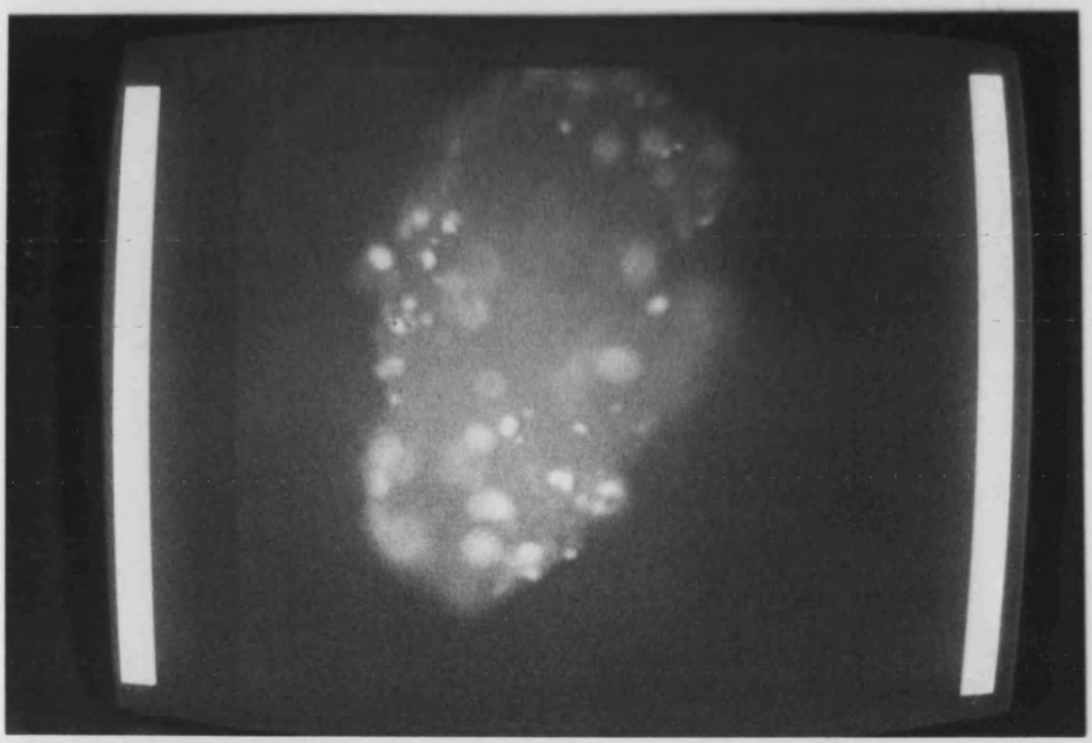

Plate 3.21. Digitised image of an Elcema G250 particle with adherent Triamterene particles. Focus position at 160 fine focus divisions.

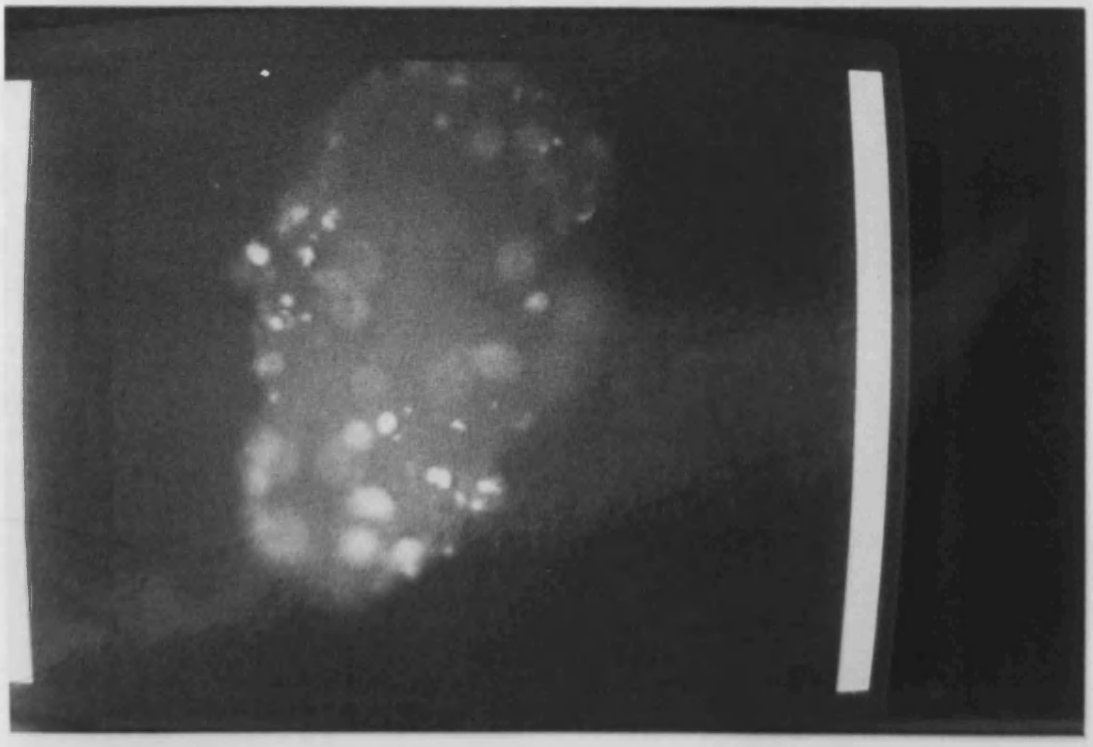

Plate 3.22. Digitised image of an Elcema G250 particle with adherent Triamterene particles. Focus position at 170 fine focus divisions.

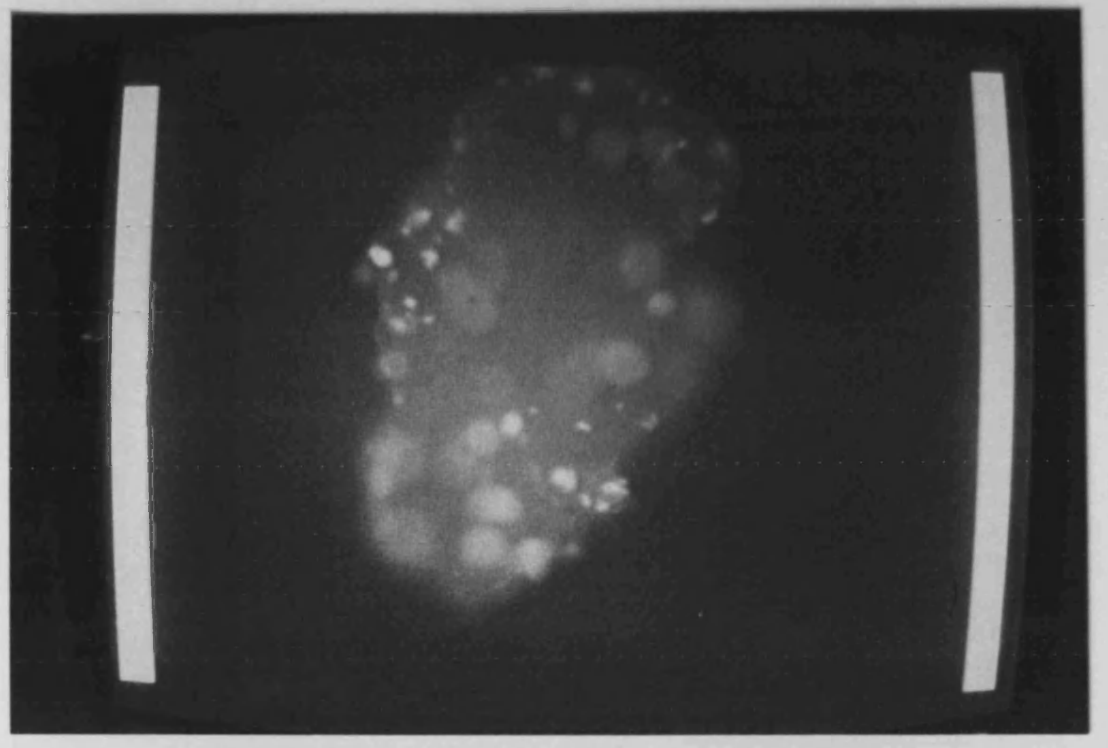

Plate 3.23. Digitised image of an Elcema G250 particle with adherent Triamterene particles. Focus position at 180 fine focus divisions.

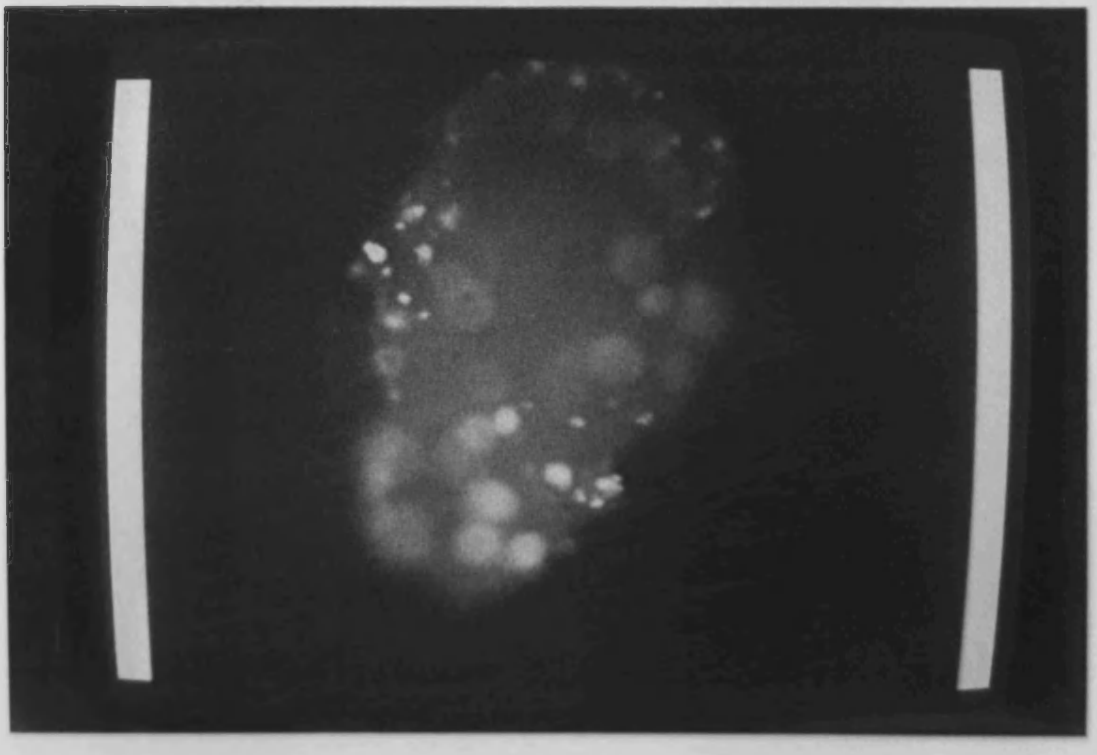

Plate 3.24. Digitised image of an Elcema G250 particle with adherent Triamterene particles. Focus position at 190 fine focus divisions.

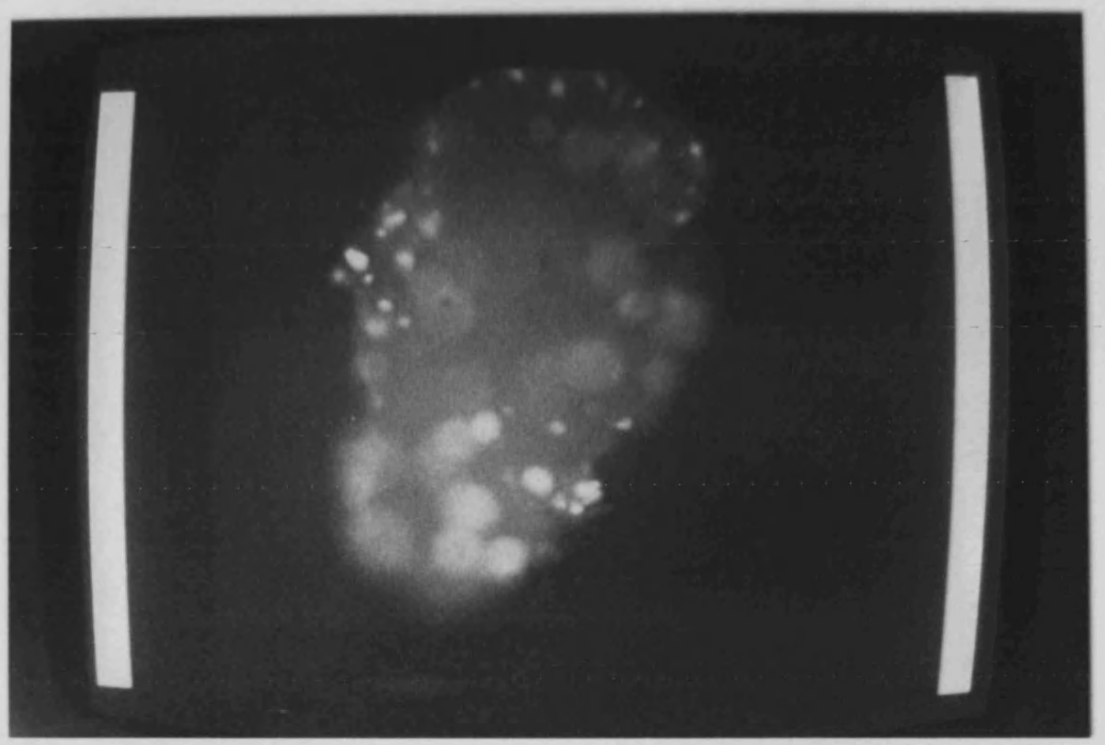

Plate 3.25. Digitised image of an Elcema G250 particle with adherent Triamterene particles. Focus position at 200 fine focus divisions.

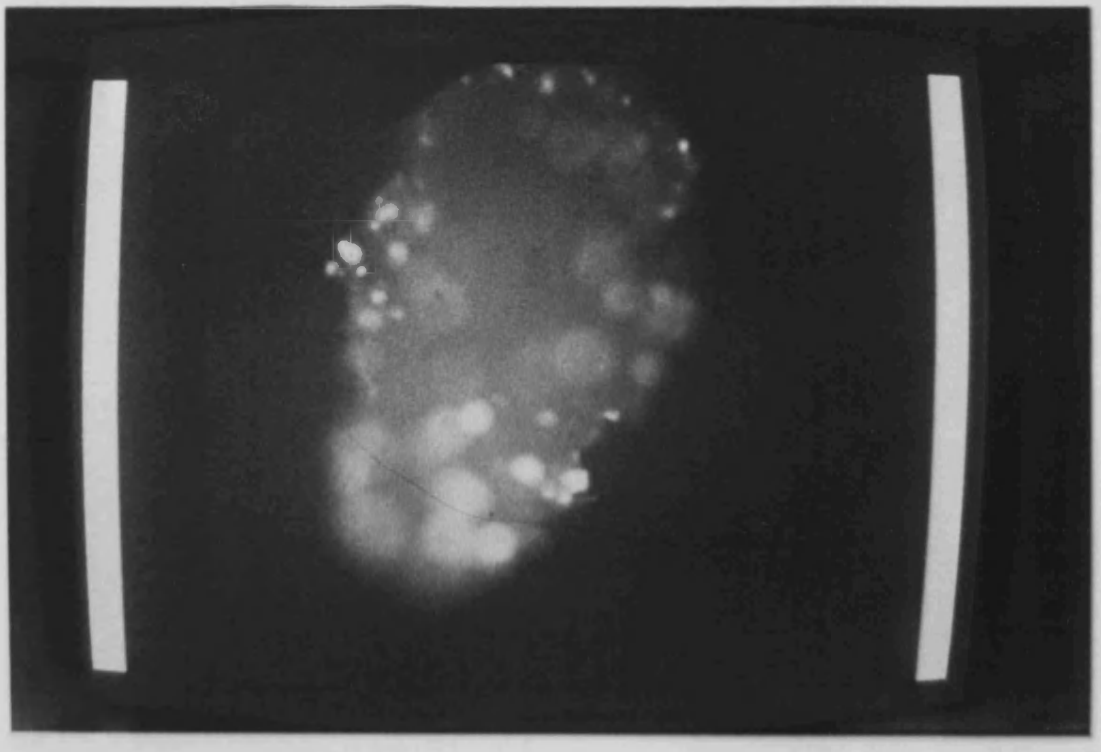

Plate 3.26. Digitised image of an Elcema G250 particle with adherent Triamterene particles. Focus position at 210 fine focus divisions.

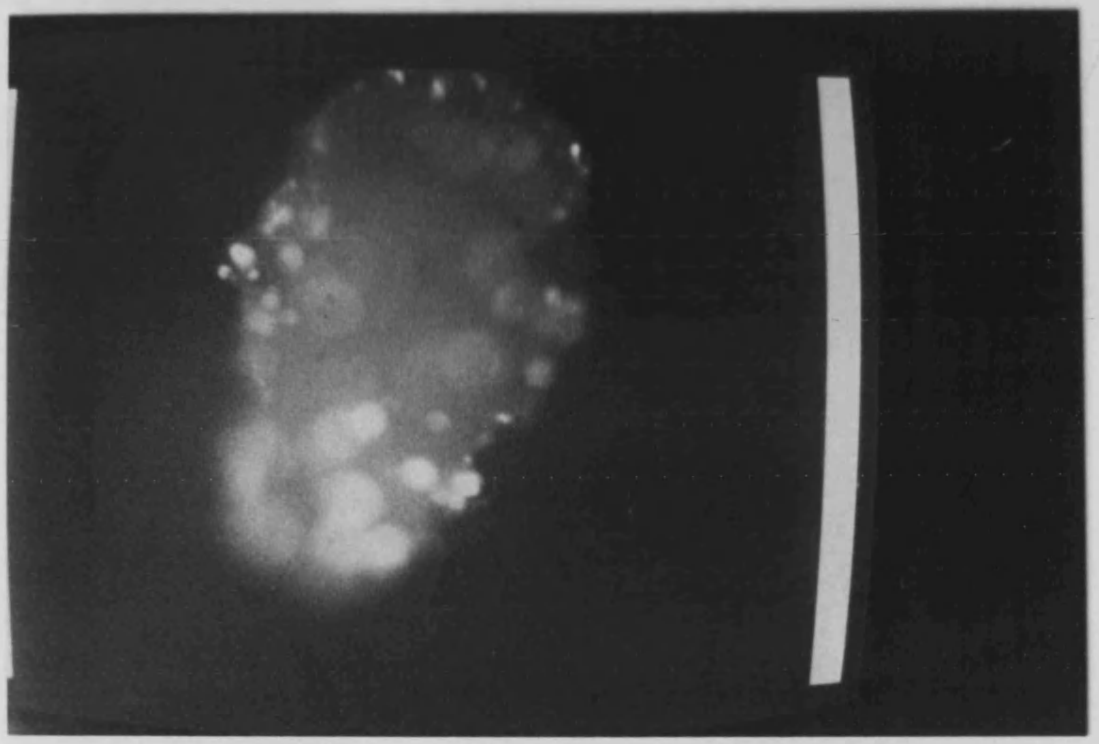

Plate 3.27. Digitised image of an Elcema G250 particle with adherent Triamterene particles. Focus position at 220 fine focus divisions.

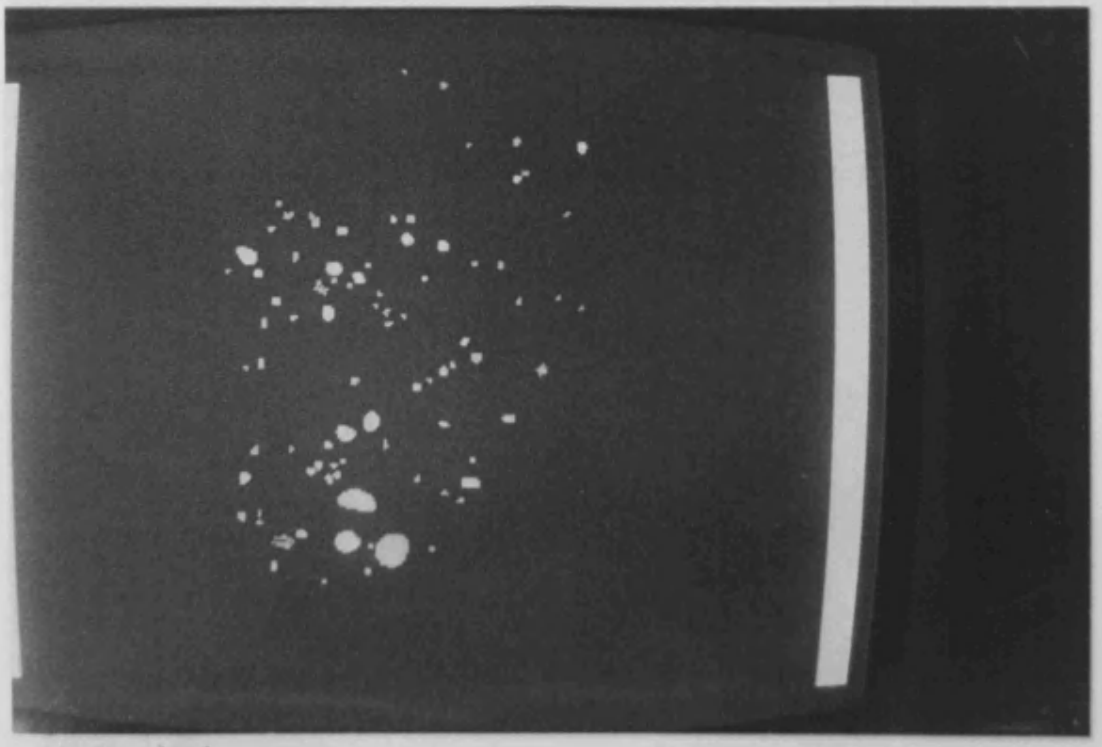

Plate 3.28. Composite digitised image derived from the digitised images in plates 3.5 to 3.27, using the BASIC program BCOMPOS and the 6502 machine code program COMPOS.

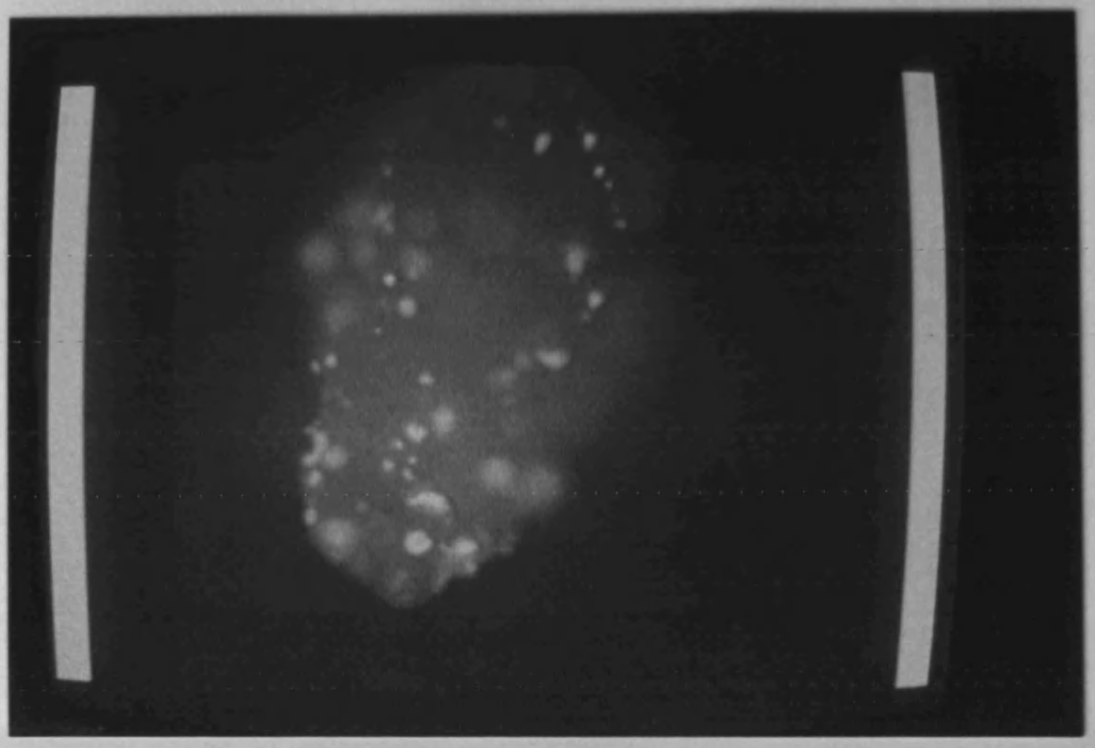

Plate 3.29. Digitised image of an Elcema G250 particle with adherent Triamterene particles.

Plate 3.30. Photomicrograph of an Elcema G250 particle with adherent Triamterene particles taken at the same time as the digitised image in Plate 3.29. Note the higher degree of resolution compared to the digitised image above.

Chapter 4.

4. Measurment of interparticle adhesion forces in single ordered units.

The measurement of the force of adhesion between particles and plane surfaces has been investigated by a number of workers (73, 74, 81, 97-99, 101-103, 109). Several aspects of this work have shown that magnitude of the interparticle adhesion forces measured can be be affected by atmospheric conditions, for example the presence of atmospheric moisture (101, 102, 109, 110) or the lack of it (98). The presence of electrostatic forces have also been found to affect the magnitude of interparticle adhesion forces (73, 103).

The most common method used to apply a separating force to particles adhering to a surface has been centrifugation (73, 74, 81, 97-99, 101-103, 110) usually preceded and followed by photomicrography to allow the distribution of particles on the surface to be recorded. This method has the advantage that the applied force is non invasive and can be readily controlled. Centrifugation has also been applied to the determination of adhesion forces in ordered mixtures (69, 95, 96, 104, 105).

One method of measuring the adhesion forces between adherent particles and the carrier substrate allowed the behaviour of the bulk powder to be investigated by centrifuging small samples of an ordered mixture supported by a steel mesh (69, 95, 105). Another, more refined method, allowed the measurement of the adhesion force between individual adherent particles and the carrier substrate by trapping the ordered units at one end of a small hole drilled through a brass plate (96). This method was potentially useful as it allowed the applied separating force to be related to the number of adherent particles and their size. It was, however, found to be very difficult to produce good quality photomicrographs of the surfaces to be examined as these were deeper than the depth of field of the microscope (104). This limitation, inherent in the photomicrography of deep surfaces, meant that the method descibed above method could not be applied to any great extent (104) because of the problems associated with the interpretation of the photomicrographs obtained. The development of the image analysis method described in Chapter 3 effectively eliminates the depth of field limitation of conventional photomicrography making it possible to measure particles adhering to

a deep surface.

A method has therefore been developed, using the image analysis techniques described in Chapter 3, which allows the magnitude of the adhesion force between the individual adherent particles and the carrier substrate of isolated ordered units to be determined.

4.1. Materials, apparatus and methods.

4.1.1. Materials. The materials used to prepare ordered mixtures suitable for the measurement of the adhesion forces between the adherent particles and carrier substrate of single ordered units were as follows.

1. Triamterene, supplied as a gift by Hoechst (UK) Ltd, Milton Keynes, U.K..
2. Elcema G250, BN D/409165, Degussa GmBH, Frankfurt, FRG.

The reasons for the use of triamterene and Elcema G250 are given above in section 3.1.1 of Chapter 3.

4.1.2. Apparatus.

4.1.2.1. Supporting mount for ordered units.

Ordered units of Elcema G250 and triamterene were fixed to a brass plate (Figure 4.1) measuring 11.0mm x 14.7mm x 0.8mm. The brass plate was supported by two specially constructed perspex holders which were designed to fit inside a $10cm^3$ volume ultracentrifuge tube (Figure 4.2). The holders for the brass plate were designed so that when the ultracentrifuge tube was inserted in the rotor and correctly aligned, the plane of the brass plate would be parallel to the axis of rotation (Figure 4.3).

The outside of the ultracentrifuge tube was threaded so that it could be sealed using an aluminium screw cap. This facility was necessary because the rotor chamber of the ultracentrifuge was evacuated above rotational speeds of 20,000rpm to reduce aerodynamic drag and eliminate heating due to friction between the air in the rotor chamber and the rotor. The distance of the brass plate from the axis of rotation was 63mm. During centrifugation the rotor was balanced using an equivalent tube filled with fine sand.

4.1.2.2. Fluorescence microscopy.

The distribution of the adherent trimaterene particles on the surface of an Elcema G250 carrier particle was determined using a

fluorescence microscope (Fluovar, Zeiss, Oberkochen, F.R.G.). This microscope was fitted with a trinocular head which allowed simultaneous viewing by the operator and either a video camera or photographic camera. The carrier particles to be examined were illuminated using incident ultraviolet light and the position of the adherent triamterene particles determined by virtue of their blue fluorescence. The magnification of the microscope was adjusted so that a single carrier particle occupied most of the field of view when observed through the video camera.

The peak fluorescence of triamterene occurred at an excitation wavelength of approximately 365 nm, the fluoresced light had a wavelength of 450nm.

4.1.2.3. The image analysis equipment.

The image analyser used to measure the distribution of the adherent triamterene particles is described in section 3.1.2 of Chapter 3.

4.1.2.4. The ultracentrifuge.

The ultracentrifuge used to apply a separating force to the adherent Triamterene particles was capable attaining a rotational speed of 60,000 revolutions per minute (rev min^{-1}). When the rotational speed exceeded 20,000 rev min^{-1} the rotor chamber was automatically evacuated to reduce the effect of drag from the surrounding air. The temperature of the rotor chamber could be thermostatically controlled, however, this facility was not used because samples of ordered units were only centrifuged for short time periods.

4.1.3. Methods

4.1.3.1. Preparation of ordered mixtures of Elcema G250 and triamterene.

Ordered mixtures of Elcema G250 and triamterene were prepared by placing 20 grammes of Elcema G250 together with 0.1 grammes of triamterene in a 0.2l amber glass jar and then shaking by hand for a minimum of 5 minutes. The size fraction of Elcema G250 used was that which passed through a 405μm aperture sieve but was retained on a 295μm aperture sieve.

Four different ordered mixtures were investigated using samples

of Elcema G250 that had been processed using four distinct methods.

1. Elcema G250, as received from the manufacturer, was exposed to ambient atmospheric conditions for a minimum period of 24 hours before being used to prepare an ordered mixture.
2. Elcema G250 was stored in a closed desiccator over distilled water at a temperature of 30°C for a minimum period of 72 hours before being used to prepare an ordered mixture.
3. Elcema G250 was formed into a loosely pressed powder bed and subjected to the temperature program used in the electret forming procedure described in Chapter 2 (2.1.3.6). The processed power was used to prepare an ordered mixture as soon as it had cooled to room temperature. It should be noted that the Elcema G250 processed in this manner was not exposed to an electric field at any time during the heating period.
4. Elcema G250 was formed into a loosely pressed powder bed and subjected to the electret forming procedure described in Chapter 2 (2.1.3.6). The processed powder was used to prepare an ordered mixture as soon as it had cooled to room temperature and the electric field removed.

With all four forms of the Elcema G250 used above, the adhesion forces between the trimaterene and the processed Elcema G250 carrier particles were measured using single ordered unit samples of the mixture. These samples were taken as soon as the mixing process was complete and the adhesion force profiles determined with the minimum of delay.

During centrifugation and subsequent microscopy no attempt was made to preserve the processing state of the Elcema G250.

4.1.3.2. Method for fixing ordered units to the brass plate.

Ordered units of triamterene and Elcema G250 were secured to the one surface of the brass plate described above using a rapidly setting epoxy resin adhesive. A thin film of the adhesive was smeared onto the brass plate and allowed to partially dry. A small sample of the ordered mixture was then sprinkled onto the adhesive and then left undisturbed for approximately 10 minutes for the adhesive to set. This procedure was found to secure the Elcema G250 particles to the brass plate without the adhesive wicking into the body of the Elcema G250 carrier particle (Chapter 3, 3.2.1).

4.1.3.3. Application of separating force.

A separating force was applied to the adherent triamterene particles by centrifuging the brass plate, to which the carrier Elcema G250 particles were attached, in the mount described above. A sequence of increasing separating forces was applied to the adherent triamterene particles by centrifuging at 0 rev min^{-1}, 2500 rev min^{-1}, 5000 rev min^{-1}, 10000 rev min^{-1}, 20000 rev min^{-1}, 30000 rev min^{-1}, 40000 rev min^{-1} and 50000 rev min^{-1}. Ordered units were exposed to each rotor speed for a five minute period to allow the effects of time dependent bonding to be overcome and to ensure that the maximum number of particles were removed for any given separating force. The centripetal acceleration for the above rotor speeds and the separation force exerted on a 1μm particle and a 10μm particle of density 1000 kgm^{-3} are shown in Table 4.1.

During centrifugation the time to reach maximum speed and the number of rotations (rounded to the nearest 10,000) were noted.

4.1.3.4 Collection and analysis of composite images.

Prior to each period of centrifugation and after the final period of centrifugation the distribution of the adherent particles was recorded by collecting a series of digitised images similar to those shown in Chapter 3 (Plates 3.5 to 3.27). Each series of digitised images was then used to produce a composite digitised image as described in Chapter 3.

The videomicrography used to generate the digitised images meant that it was necessary to remove the brass plate, and hence the ordered units under examination, from the closed centrifuge tube. This in turn meant that the ordered units were exposed to ambient atmospheric conditions. During videomicrography no attempt was made to maintain the initial processing state of the Elcema G250.

The composite images generated were analysed using proc ANALYSE (Chapter 3, Appendix 2, A2.1). The data collected consisted of the total number of detected particles, measured as the distinct bright fluorescing areas greater than 3 pixels in extent, and the total number of detected pixels. These data were used to calculate the average size of the adherent particles that remained after each period of centrifugation by dividing the total number of detected pixels by the total number of detected areas. The total number of detected pixels, total number of detected particles and mean particle

size (in pixels) were plotted against rotor speed, in rev min^{-1}, for all four Elcema G250 processing methods.

4.1.3.5. Determination of the cross sectional area of the Elcema G250 carrier particle.

The cross sectional area of the Elcema G250 carrier particles in the ordered units examined was measured by employing proc ANALYSE in SPR128. One of the sequence of digitised images used to generate the composite image from which particle size data was obtained was displayed so that all grey levels above a predetermined grey level value (usually 5 or 10) were displayed as white. This was done using proc COLOURS in SPR128. The size of the displayed area was then measured using proc ANALYSE. The value generated for the area of the Elcema G250 carrier particle was then used to adjust the number of adherent particles to account for differences in size between different ordered units. The reference used here for comparison was the size of the ordered unit prepared from Elcema G250 stored under ambient laboratory conditions.

4.2. Results.

4.2.1. Centrifugation.

The time to reach the maximum rotor speed were 1 minute for 2,500 rev min^{-1}, 1 minute for 5,000 rev min^{-1}, 2 minutes for 10,000 rev min^{-1}, 4 minutes for 20,000 rev min^{-1}, 7 minutes for 30,000 rev min^{-1}, 10 minutes for 40,000 rev min^{-1} and 12.5 minutes for 50,000 rev min^{-1}. The total number of revolutions, to the nearest 10,000, for each of the rotor speeds used were 10,000, 10,000, 30,000, 70,000, 180,000, 330,000 and 530,000 revolutions respectively. These figures were found to be similar for all centrifugations at the corresponding rotor speeds.

Observation of the carrier particles indicated that minimal distortion had occurred during centrifugation. In addition no carrier particles were detached from the adhesive during centrifugation.

4.2.2. Measurement of particle adhesion using composite digitised images.

Prior to each period of ultracentrifugation and after the final period of ultrcentrifugation a sequence of digitised images was

collected and a composite image produced. The composite images were then examined to determine the number of detected non background areas (ie adherent particles), the size of each of the non background areas and the total number of non background pixels.

For each Elcema G250 processing method it was found that the trend was for the number of detected particles and the total number of detected pixels to decrease with increasing speed of rotation (Tables 4.2, 4.3, Figures 4.4, 4.5). The mean cross sectional area of the adherent particles remaining after each period of centrifugation was also found to follow a similar trend, decreasing with increasing speed of rotation (Tables 4.4 to 4.7, Figure 4.6). There were however several anomalous observations for this data where the mean cross sectional area increased with increasing rotor speed or did not fall as sharply as expected.

Examination of the data obtained for the four processes used to prepare Elcema G250 carrier particles showed that they could be ranked according to their ability to retain adherent triamterene particles and that this ranking was Electrised > Ambient > Dried > Humid. This ranking did not change when the number of adherent particles and total number of detected pixels was adjusted to account for differences in the size of the carrier particles (Tables 4.7, 4.8, Figures 4.7, 4.8).

The effect demonstrated by these results is that electrising the Elcema G250 has increased the degree of particle interaction between the adherent Trimaterene particles and the Elcema G250 substrate. The interparticle adhesion forces for Elcema G250 exposed to very humid conditions were significantly reduced compared to the Elcema G250 stored under ambient conditions and almost equivalent to the dried Elcema G250. This result is contrary to that expected by consideration of other particle adhesion experiments (101, 102, 109, 110) where high levels of humidity were found to increase interparticle adhesion forces.

4.2.3. Measurement of the Cross sectional area of the Elcema G250 carrier particles.

The cross sectional area of the Elcema G250 carrier particles were measured as described. For the four ordered units examined, one for each of the storage environments used to condition the Elcema G250, the cross sectional areas were 19661 pixels (ambient), 26986

pixels (humid), 26031 pixels (dried) and 20544 pixels (electrised). Where data was adjusted to account for differences in the size of the carrier particle the area obtained for the ambient ordered unit was used as a standard (unit carrier particle area). The multiplying factors obtained by this operation were 1.0 (ambient), 0.7286 (humid), 0.7553 (dried) and 0.9570 (electrised).

The measurement of the cross sectional area was carried out after centrifugation at 50,000 rev min^{-1}. This meant that it was not possible to assess the change, if any, in the cross sectional area of the carrier particles due to centrifugation.

4.3. Discussion.

4.3.1. Exposure of processed Elcema G250 to ambient atmospheric conditions.

Four processes, exposure at ambient atmospheric conditions, high humidity, severe drying and electrisation, were used to prepare samples of Elcema G250 for the series of adhesion force measurements made. These processing conditions were maintained until the processed Elcema G250 was mixed with the triamterene. From that point onwards the ordered mixtures were exposed to ambient atmospheric conditions whilst being mounted on the brass plate, during centrifugation and finally during videomicrography.

The exposure to ambient atmospheric conditions is very likely to have affected the adhesion forces that were being measured. The most probable cause of changes in particle adhesion would have been due to the adsorption or loss of moisture as the addition or removal of moisture was a key part of the processes used to prepare the Elcema G250 used. When exposed to ambient atmospheric conditions the reverse of these processes would have occurred, the dried and electrised Elcema G250 adsorbing atmospheric moisture and the saturated Elcema G250 losing moisture to the atmosphere.

Moisture adsorption has been found to cause significant reductions in the stored charge in Elcema G250 electrets (Chapter 2) over relatively short time periods. Exposure of the electrised Elcema G250 to atmospheric moisture is therefore likely to reduce the electret contribution to particle adhesion as the measurement of the adhesion force profiles are measured. Particles remaining after centrifugation at 50,000 rev min^{-1} will therefore be bound by mechanisms other than excess electrostatic charge. In a similar

manner the loss of surface moisture from the saturated Elcema G250 will lead to a reduction of the adhesion forces (Chapter 1, 1.2.2.3) as the size of the meniscus of the liquid bridge will be reduced.

The effect of exposure to atmospheric conditions can be examined by expressing the number of adherent particles and total cross sectional areas, adjusted for unit carrier particle area, as a percentage of the value obtained under ambient conditions. This will show if the rate of loss of particles after centrifugation is greater or less than that occurring for adherent particles under ambient conditions (Tables 4.9, 4.10, Figures 4.9, 4.10.). In Figures 4.9 and 4.10 it can be seen that the rate of loss of adherent particles remains relatively constant for the Elcema G250 substrate exposed to humid conditions. The relative loss of adherent particles for the dried Elcema G250 and the electrised Elcema G250 decreases with increasing rotor speed (ie particles are not being lost as rapidly). This phenomena would suggest that electrising the Elcema G250 increases the initial interparticle adhesion forces however it is not the sole effect causing the interparticle adhesion.

The loss or adsorption of water from the Elcema G250 particles may also have other side effects because water can act as a plasticiser for cellulose (218). It is therefore possible that the size of the contact area between the adherent particle and the carrier substrate will change as water is lost or adsorbed. This is particularly true if the contact area is dependent on any elastic and/or plastic deformation of the cellulose substrate. Application of this hypothesis to the relative adhesion force profiles (Figures 4.9, 4.10) would explain why the number of particles lost are not as great as for Elcema G250 mixed under ambient conditions. The contact area has increased because the adsorption of moisture has increased the plasticity of the cellulose substrate and hence the penetration of the adherent particles into the substrate.

Some evidence to support this hypothesis can be gained from Figures 4.9 and 4.10 because the rate of particle loss of the electrised Elcema G250 is less than that of the dried Elcema G250. The adsorption of atmospheric moisture would inevitably occur at the surface of the carrier particles. Initially any increase in the plasticity of the Elcema G250 substrate would occur at the surface. This would allow the electrostatic attraction due to any electret charge relatively distant from the surface to continue acting and

promote the creation of an increased contact area. Consequently the contact area would be greater than that obtained for dried Elcema G250 even though the same quantities of moisture are involved.

Consideration of the forces involved for hypothetical 1μm diameter and 10μm diameter particles (Table 4.1) shows that at 50,000 rev min^{-1} the separating force being applied are $\approx 90 \times 10^{-9}$ N and $\approx 90 \times 10^{-6}$N respectively. If it is assumed that the area of contact between the adherent particles and the carrier substrate is equivalent to one tenth of the cross sectional area of the particles then the pressures exerted between the carrier particles and their carrier substrate are $\approx 1 \times 10^{-6}$ Nm^{-2} and $\approx 10 \times 10^{-6}$ Nm^{-2} These pressures, even if overestimated by a factor of 10, are certainly sufficient to cause the deformation of the surfaces involved. Consequently, the mechanism proposed above for the retention of the adherent particles after the adsorption of atmospheric moisture is very likely to occur.

The exposure to ambient atmospheric conditions can be avoided although this would require changes to the equipment and methodology described above. Mixing in a dry atmosphere could be arranged by using dried nitrogen so that moisture could be excluded where it were not required. The centrifuge tube could be redesigned so that the brass plate could be observed without the need for disassembling the perspex supports. This task has been made easier by the arrival of microscope objective lenses with working distances upto 2cm (as used in the semiconductor industry).

4.3.2. Assessment of the particle adhesion data.

The data obtained for the number of adherent particles remaining after centrifugation and the mean adherent particle size show evidence of anomalous results. These anomalous results consist of an apparent increase in the number of adherent particles (Table 4.2) or an increase in the mean particle size (Table 4.4) with increasing rotor speed. The electrisation of Elcema G250 appears to have increased the degree of particle interaction as desired. This increase, however, appears to persist even when sufficient atmospheric moisture had been adsorbed to destroy the electret charge. In contrast, the degree of particle adhesion observed for the Elcema G250 exposed to very humid conditions was reduced compared to the Elcema G250 exposed to ambient atmospheric conditions. This result was the opposite of that expected

(101, 102, 109, 110).

4.3.2.1. Effect of image resolution and particle agglomeration on the particle adhesion profiles measured.

The apparent increase in the number of particles remaining after centrifugation noted on several occasions and the anomalies in the mean particle areas, can be explained by consideration of the resolution of the digitised image and by close packing of the adherent particles. The analysis of the adherent particles remaining after centrifugation is based upon the assumption that any non background area occurring in the composite image relates to a single adherent particle. This assumption was not correct for the composite digitised images produced by COMPOS.

When a number of adherent particles were placed very close together the resolution of the digitised image is insufficient to separate them and as a consequence they appear as a single particle. If such a group of particles are subjected to centrifugation then several events can occur. One possibility is that all the adherent particles could be detached at the same time. This is effectively the same as if the group of particles were a single particle. Another possibility is that one of the group of particles would be removed. This would have the effect of reducing the total cross sectional area of the adherent particle whilst maintaining the number of particles. Consequently the mean cross sectional area would decrease although the number of adherent particles remains the same.

A variation on the loss of one particle in a group is the movement of one of the particles across the carrier particle surface. This is a phenomenon that has been observed in other particle adhesion experiments (97). If such movement meant that the particle could be resolved in its own right then the effect would be to increase the number of particles present whilst maintaining the total cross sectional area. Again, this would lead to a decrease in the mean adherent particle size. The apparent increase observed for the mean adherent particle size requires the presence of a group of closely packed adherent particles and some other single particles which can be individually resolved. If after centrifugation some of the single particles were removed but the group of particles maintained intact then it would appear as though only the smaller particles had been removed. Consequently the mean adherent particle

size would appear to have increased after centrifugation rather than being decreased as would be expected.

Examination of the particle size and area data for the four types of processed Elcema G250 powder examined shows that all of the above mechanisms must be taking place in the prepared ordered units. The confusion brought about by these effects could be reduced by comparing images before and after centrifugation to determine where any changes had taken place. This would allow the identification of areas which have 'shrunk', particles that have moved or been newly created, thereby allowing a profile to be generated which related the size of the detached particles to the separating force applied. This type of analysis was that originally intended for use here, however, the complexity of the software involved when written in machine code meant that it had to be dropped in favour of the methods used in COMPOS.

4.3.2.2. Effect of electrisation on particle adhesion.

The examination of the electret effect in cellulose based tableting ecipients (Chapter 2) was performed in order to determine the feasibility of using electrised materials to enhance particle interaction without the danger of powder explosions inherent with the use of conventional electrostatic charging. Examination of the adhesion force profiles in Figures 4.7 and 4.8. indicate that electrisation increased the degree of interparticle adhesion compared to Elcema G250 exposed to ambient atmospheric conditions. The total effect of the electret charge is, however, far more pronounced when it is compared to a material which has been subjected to the same process without the electrisation step, that is the dried Elcema G250. In this case it can be seen that the degree of particle interaction is increased to an even greater extent, there being approximately 50% more adherent particles per unit area or a minimum of 100% more cross sectional area for the electrised material than the dried material.

It was initially thought that the increase in interparticle adhesion due to the electret effect would be lost when the material was exposed to ambient atmospheric conditions due to the adsorption of moisture. However, consideration of the effect of water on dried cellulose (218) and Figure 4.9 and 4.10 would indicate that this is not the case. The observed effects are that the dried and electrised

material lose their adherent particles less easily as they adsorb moisture. This effect is thought to be due to the softening of the cellulose substrate due to the plasticising effect of water. In addition, the presence of the electret charge, although destroyed by the adsorption of water, is sufficient to increase the interparticle contact area compared to the dried Elcema G250, during the initial stages of moisture adsorption.

The effect of electrisation and drying have, however, only been examined here using a single ordered unit from each batch of material. The results obtained indicate that electrisation does significantly increase particle interaction and that the adsorption of moisture does not destroy the degree of particle interaction but merely replaces one adhesion mechanism for another. This latter point does require further investigation to determine the exact mechanisms involved.

4.3.2.3. Explanation for the reduced interparticle adhesion forces between Triamterene and Elcema G250.

The particle adhesion data obtained for the Elcema G250 exposed to very high levels of humidity was expected to be comparable to, or greater than, the particle adhesion observed for the electrised Elcema G250. In practise the degree of particle adhesion was the lowest observed, being lower even than the dried Elcema G250. This apparent anomaly can be explained by consideration of the molecular structure of triamterene (Figure 4.11) and the nature of the hydrogen bond (Chapter 1, 1.2.2.4).

An initial consideration of the molecular structure of triamterene reveals that it contains seven nitrogen atoms each of which has a lone pair of electrons suitable for hydrogen bonding. It would therefore be expected that hydrogen bonding between triamterene and water would be extensive, the hydrogen molecules in the water molecules associating with the lone pair electrons of the nitrogen atoms. The nature of the hydrogen bond, however, requires that both electrons of the lone pair are involved in the bond. A more detailed consideration of triamterene reveals that it is a molecule which can undergo a substantial degree of resonance and that the resonance structures formed would almost certainly involve the delocalisation of electrons from the lone pairs due to their involvement in resonance hybrids of triamterene. As a result of this the lone pairs

of electrons on the nitrogen atoms are prevented from being involved in hydrogen bonding so that the actual degree of interaction between water and triamterene is actually very small. Triamterene is in fact only slightly soluble in water which tends to support this hypothesis.

It would therefore appear that, although in general, the presence of surface moisture leads to an increase in particle interaction, as indicated by literature references (101, 102, 109, 110), the nature of the Triamterene molecule is such that the main mechanism for the increase in particle adhesion cannot be utilised.

This observation also means that the adsorption of water by the cellulose substrate of Elcema G250 will not affect any particle adhesion due to hydrogen bonding between it and the adherent triamterene particles because little or none would occur. The interparticle forces between triamterene and Elcema G250 are therefore likely to be due solely to electrostatic effects (excess charge, electric double layer etc) and true van der Waals-London forces.

4.3.3. Advantages and limitations of image analysis.

The use of image analysis to measure the number of particles adhered to a carrier particle has been successful. The techniques developed, although not perfect, have allowed the generation of particle adhesion data based on individual adherent particles. This type of data has not previously been available in such detail. However, despite the success of the image analysis techniques developed above it has not been possible to take full advantage of all the information available due to lack of time and difficulties involved in developing software in 6502 machine code. The analysis of successive composite images has demonstrated that several significant deficiencies exist in the image analysis software developed above. These deficiencies are the inability to resolve groups of closely packed particles due to the resolution of the digitised image, the failure to correctly identify adherent particles when they are correctly focused, the failure to take the cross sectional area of the adherent particle into account automati caly when analysing composite images. Less serious are the lack of a three dimensional reconstruction of the carrier particle surface and the ability to identify which adherent particles have been detatched

from the carrier particle surface.

These deficiencies are not difficult to overcome but would require a more advanced image analysis system than that used here.

Rotor speed (rev min^{-1})	Angular acceleration ($x10^{3}$ mrad s^{-2})	($x10^{3}$ g)	Separating force 1μm ($x10^{-9}$ N)	10μm ($x10^{-6}$ N)
0	0	0	0	0
2500	4.3180	0.4403	0·22614	0·22614
5000	17.2718	1.7612	0·90437	0·90437
10000	69.0872	7.0449	3·62817	3·62817
20000	276.3849	26.9818	13·85454	13·85454
30000	621.7851	63.4044	32·55661	32·55661
40000	1105.3957	112.7190	57·86115	57·86115
50000	1727.7181	176.1234	90·43496	90·43496

Table 4.1. Rotor speeds, angular accelerations and separating forces experienced by adherent spherical particles, of unit density material, 1μm and 10μm in diameter.

Rotor speed (rev min^{-1})	Elcema 6250 storage conditions			
	Ambient	Humid	Dried	Electrised
0	110.00	108.00	109.00	134.00
2500	104.00	66.00	87.00	126.00
5000	87.00	59.00	77.00	116.00
10000	81.00	58.00	70.00	113.00
20000	70.00	48.00	65.00	98.00
30000	45.00	37.00	60.00	93.00
40000	50.00	33.00	58.00	82.00
50000	43.00	33.00	49.00	75.00

Table 4.2. Number of adherent particles remaining after centrifugation as determined from the composite image using Proc ANALYSE in SPR128 version 2 (Appendix 1).

Rotor speed (rev min^{-1})	Elcema 6250 storage conditions			
	Ambient	Humid	Dried	Electrised
0	2366.00	1573.00	1283.00	2862.00
2500	1128.00	979.00	832.00	1948.00
5000	866.00	929.00	713.00	1306.00
10000	652.00	691.00	523.00	1004.00
20000	597.00	419.00	436.00	960.00
30000	314.00	358.00	406.00	766.00
40000	275.00	248.00	364.00	541.00
50000	211.00	205.00	289.00	452.00

Table 4.3. Total cross sectional area (in pixels) of particles remaining after centrifugation as measured by Proc ANALYSE in SPR128 version 2 (Appendix 2 ,A2.13)

Rotor speed (rev min^{-1})	Elcema G250 storage conditions			
	Ambient	Humid	Dried	Electrised
0	21.51	14.56	11.77	21.36
2500	10.85	14.83	9.56	15.46
5000	9.95	15.75	9.26	11.26
10000	8.05	11.91	7.47	8.88
20000	8.53	8.73	6.71	9.80
30000	6.98	9.68	6.77	8.24
40000	5.50	7.52	6.28	6.60
50000	4.91	6.21	5.90	6.03

Table 4.4. Mean cross sectional area (measured in pixels) of adherent particles remaining after centrifugation.

Rotor speed (rev min^{-1})	Elcema G250 storage conditions			
	Ambient	Humid	Dried	Electrised
0	31.90	30.32	14.38	63.57
2500	15.96	24.20	11.69	29.62
5000	15.28	21.36	8.35	18.69
10000	8.39	14.53	7.33	10.31
20000	9.02	8.89	4.22	12.64
30000	6.81	11.36	5.94	9.42
40000	4.99	7.27	6.19	6.91
50000	3.34	5.48	4.79	5.55

Table 4.5. Standard deviation of the mean cross sectional area of adherent particles remaining after centrifugation.

Rotor speed (rev min^{-1})	Elcema G250 storage conditions			
	Ambient	Humid	Dried	Electrised
0	148.31	208.17	122.17	297.64
2500	147.15	163.15	122.24	191.59
5000	153.51	135.66	90.18	166.01
10000	104.23	121.96	98.11	116.04
20000	105.76	101.84	62.91	129.03
30000	97.60	117.41	87.78	114.37
40000	90.72	96.74	98.63	104.74
50000	68.02	88.21	81.21	92.09

Table 4.6. Coefficient of variation of the mean cross sectional area of adherent particles remaining after centrifugation.

Rotor speed (rev min^{-1})	Elcema G250 storage conditions			
	Ambient	Humid	Dried	Electrised
0	110.00	78.68	82.33	120.53
2500	104.00	48.09	65.71	113.34
5000	87.00	42.99	58.16	104.34
10000	81.00	42.26	52.87	101.64
20000	70.00	34.97	49.09	88.15
30000	45.00	26.96	45.32	83.65
40000	50.00	24.04	43.81	73.76
50000	43.00	24.04	37.01	67.46

Table 4.7. Number of adherent particles remaining after centrifugation. Adjusted for differences in the cross sectional area of the Elcema G250 carrier particles using the ambient carrier particle as unit reference.

Rotor speed (rev min^{-1})	Elcema G250 storage conditions			
	Ambient	Humid	Dried	Electrised
0	2366.00	1146.03	969.04	2574.30
2500	1128.00	713.26	628.40	1752.20
5000	866.00	676.83	538.52	1174.73
10000	652.00	503.44	395.02	903.09
20000	597.00	305.27	329.31	863.51
30000	314.00	260.83	306.65	689.01
40000	275.00	180.68	274.93	486.62
50000	211.00	149.36	218.28	406.57

Table 4.8. Total cross sectional area (measured in pixels) of adherent particles remaining after centrifugation. Adjusted for differences in the cross sectional area of the Elcema G250 carrier particles.

Rotor speed (rev min^{-1})	Elcema G250 storage conditions			
	Ambient	Humid	Dried	Electrised
0	100	71.53	74.85	109.57
2500	100	46.24	63.18	108.98
5000	100	49.41	66.85	119.93
10000	100	52.17	65.27	125.48
20000	100	49.96	70.13	125.93
30000	100	59.91	100.71	185.89
40000	100	48.08	87.62	147.52
50000	100	55.91	86.07	156.88

Table 4.9. Number of adherent particle remanining after centrifugation vs rotor speed. Values have been expressed as a percentage of the number of ambient adherent particles at each rotor speed.

Rotor speed (rev min^{-1})	Elcema G250 storage conditions			
	Ambient	Humid	Dried	Electrised
0	100	48.44	40.96	108.80
2500	100	63.23	55.71	155.34
5000	100	78.16	62.18	135.65
10000	100	77.21	60.59	138.51
20000	100	51.13	55.16	144.64
30000	100	83.07	97.65	219.01
40000	100	65.70	99.97	176.95
50000	100	70.79	103.45	192.69

Table 4.10. Total cross sectional area of adherent particles remanining after centrifugation vs rotor speed. Values have been expressed as a percentage of the total cross sectional area of the ambient adherent particles at each rotor speed.

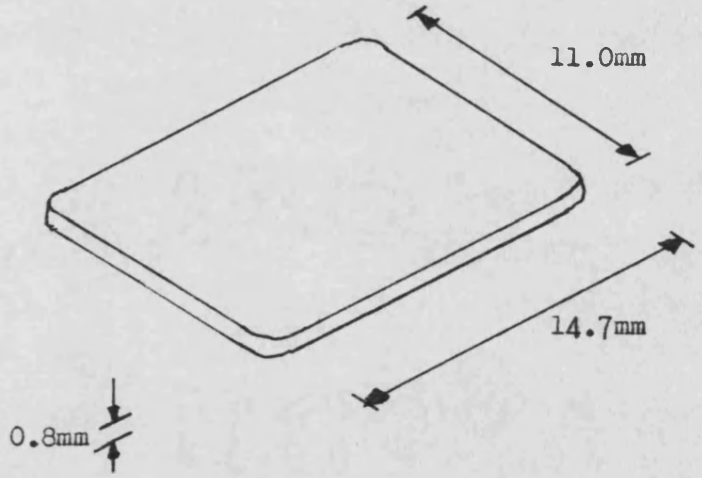

Figure 4.1. Dimensions of the brass plate used to support ordered units during centrifugation. The plate was prepared by smearing a thin layer of a rapidly setting epoxy resin on on side, waiting for a few minutes and sprinkling on a few ordered units from a small spatula.

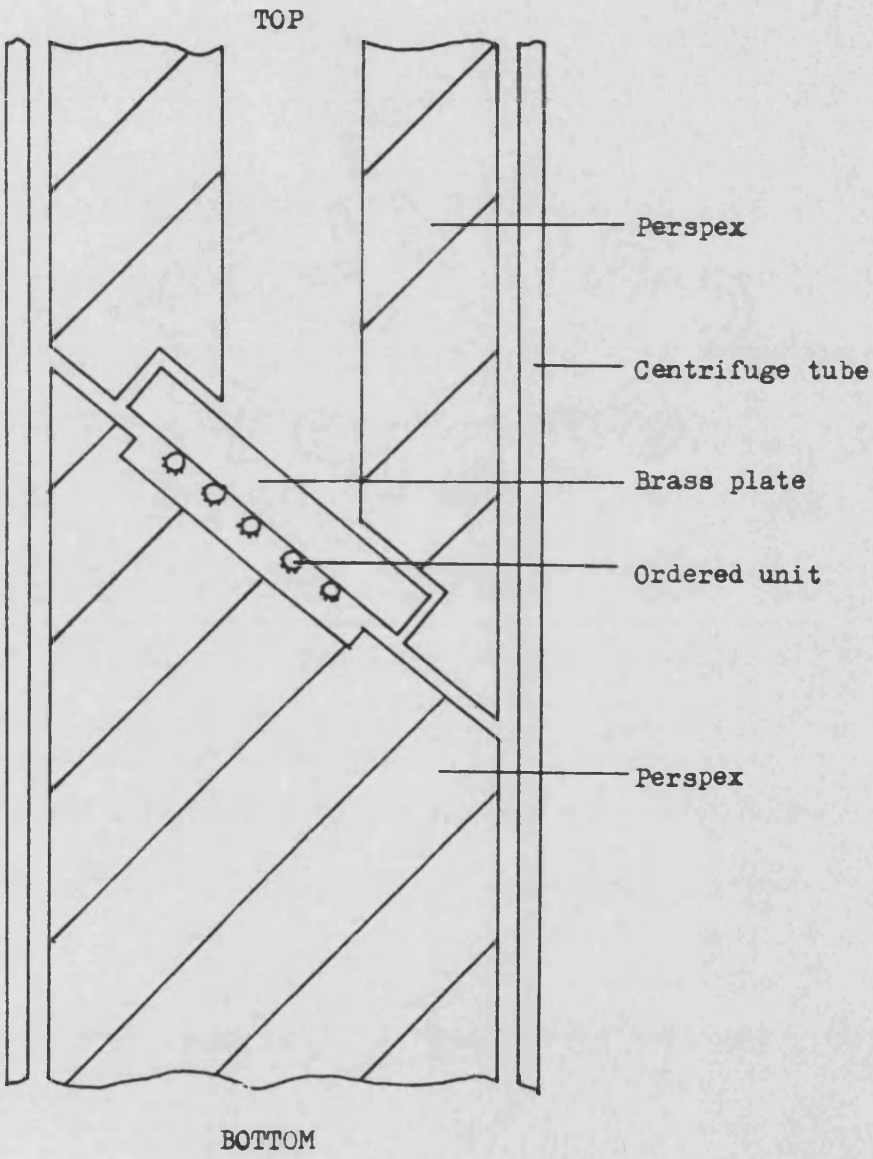

Figure 4.2 Schematic representation of the brass plate mounted between the perspex holders and the position of the ordered units fixed to the plate.

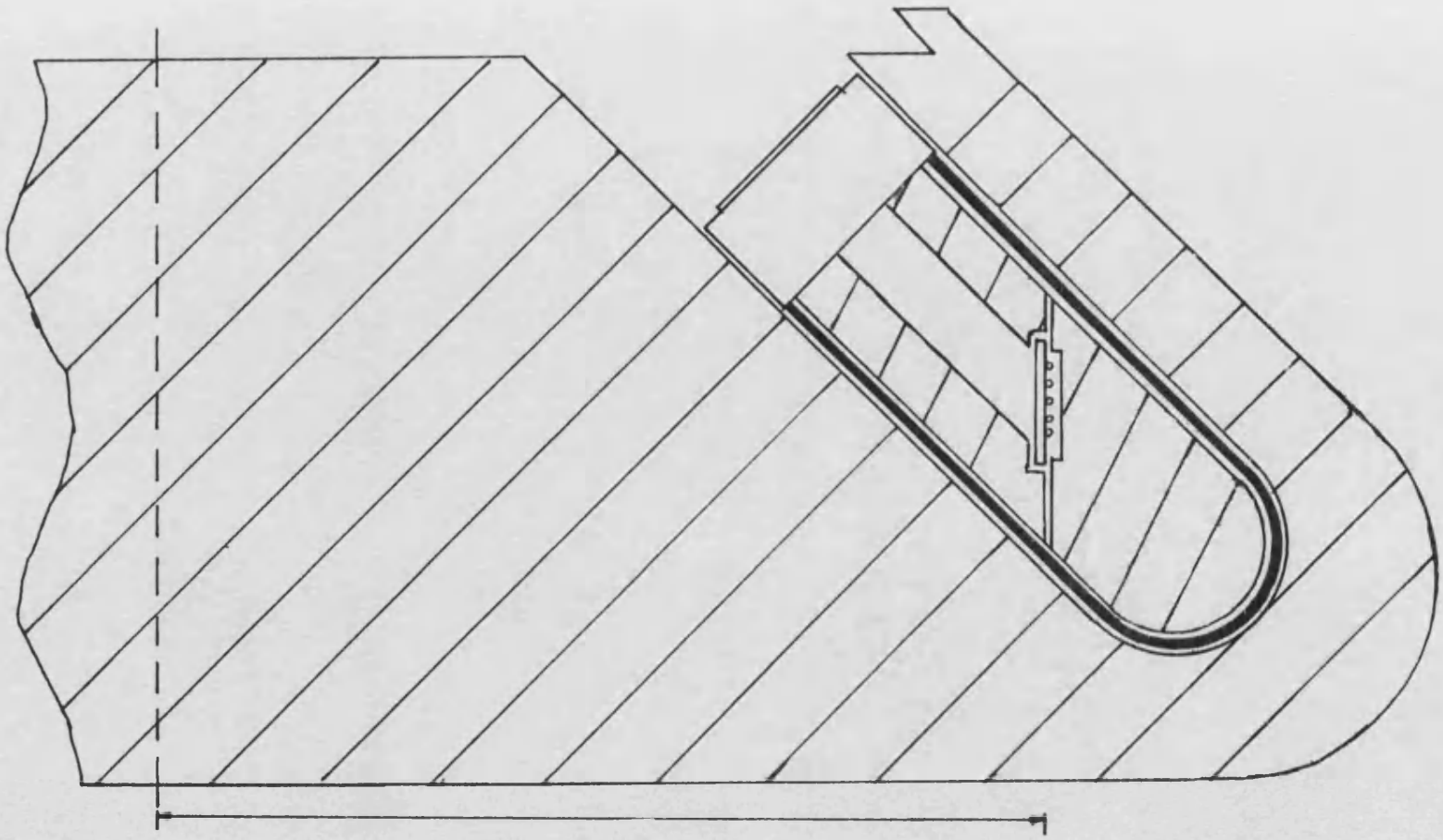

Figure 4.3. Centrifuge tube mounted in rotor showing the position of the brass plate carrying ordered units

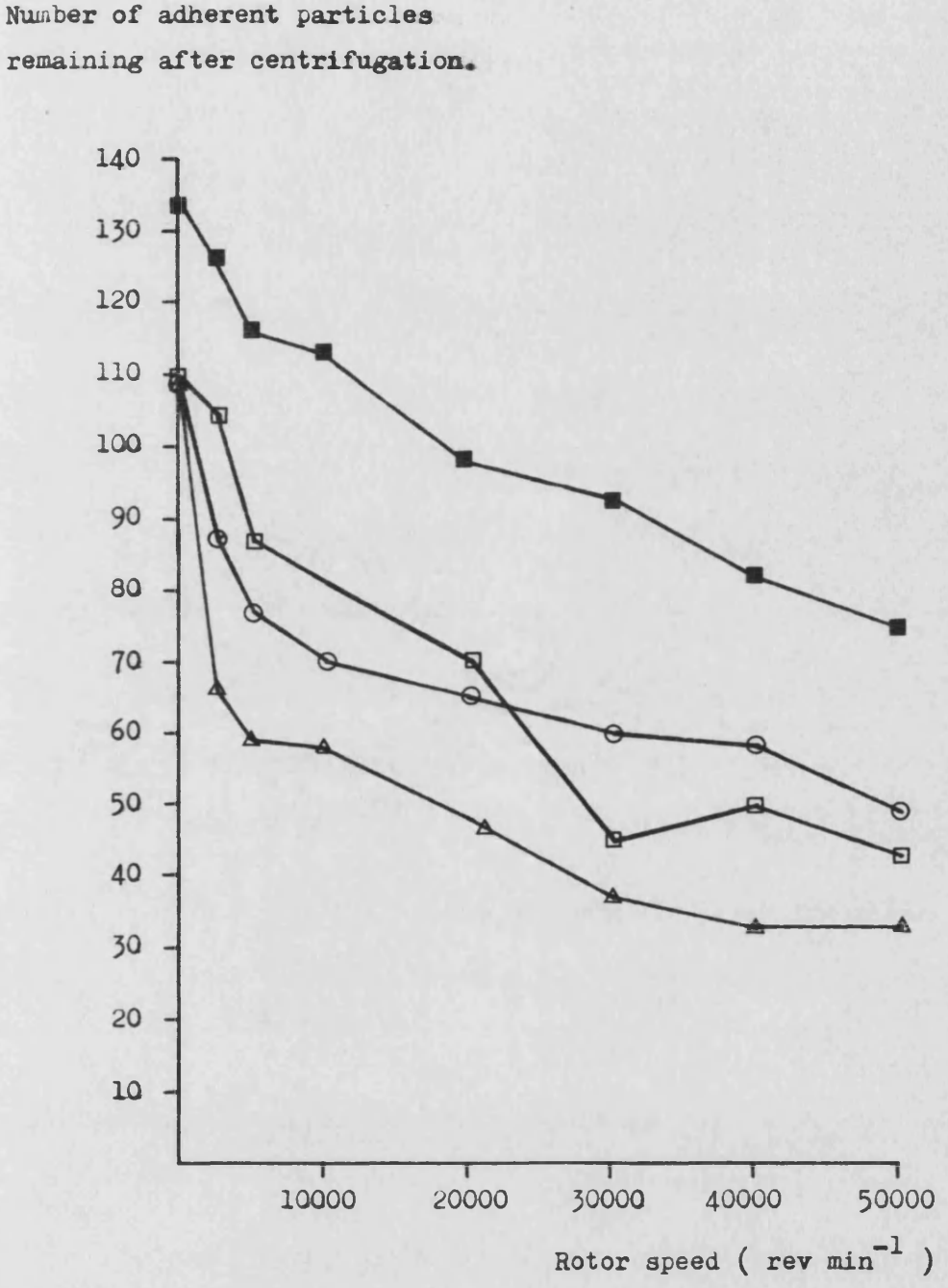

Figure 4.4. Number of adherent particles remaining after centrifugation as determined using proc ANALYSE in SPR128 version 2 (Appendix 2, A2.13).
□ Ambient, ▲ Humid, ○ Dried, ■ Electrised

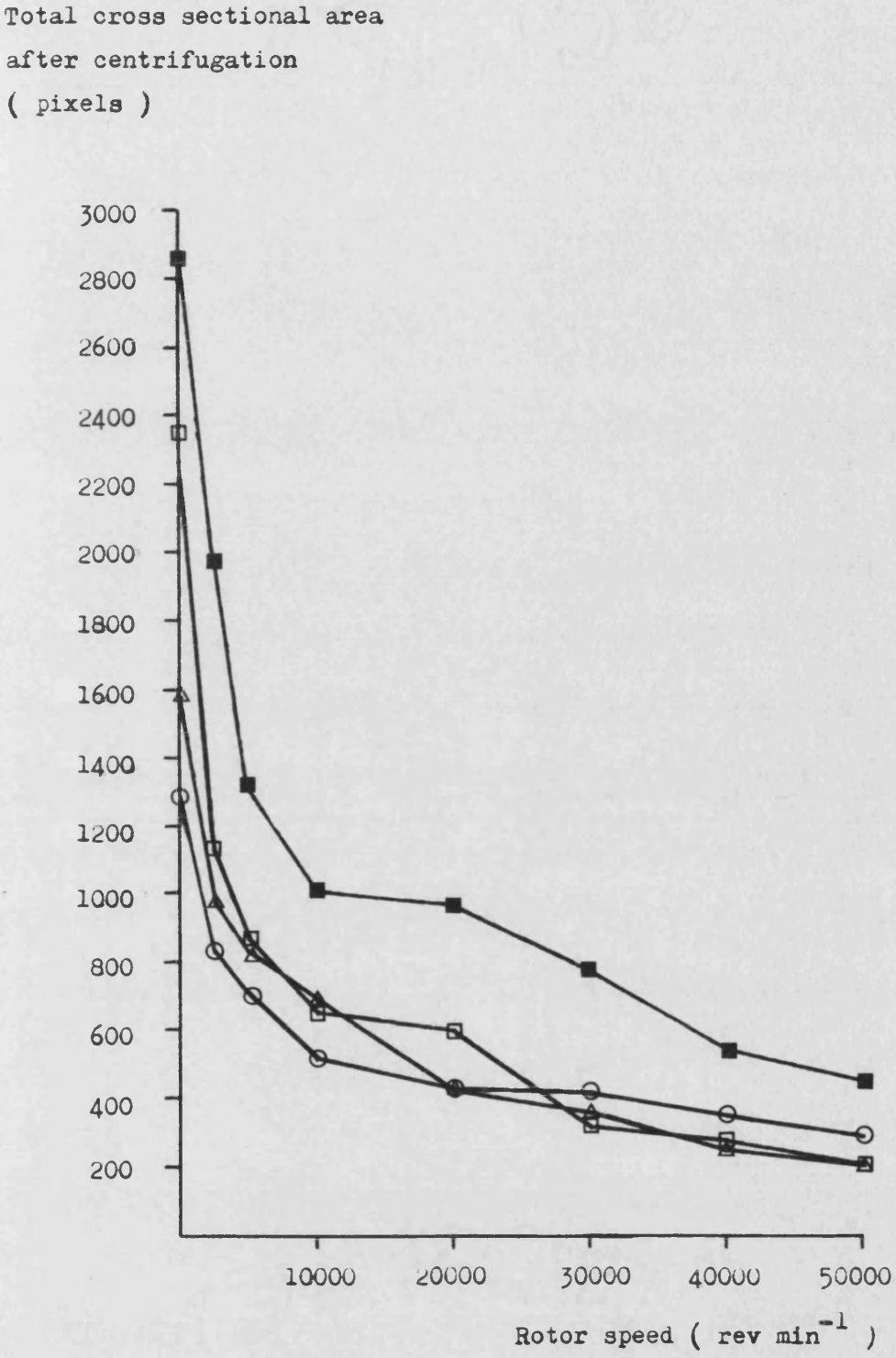

Figure 4.5. Total cross sectional area, measured in pixels, after centrifugation as determined using proc ANALYSE in SPR128 version 2 (Appendix 2, A2.13).
□ Ambient, △ Humid, ○ Dried, ■ Electrised.

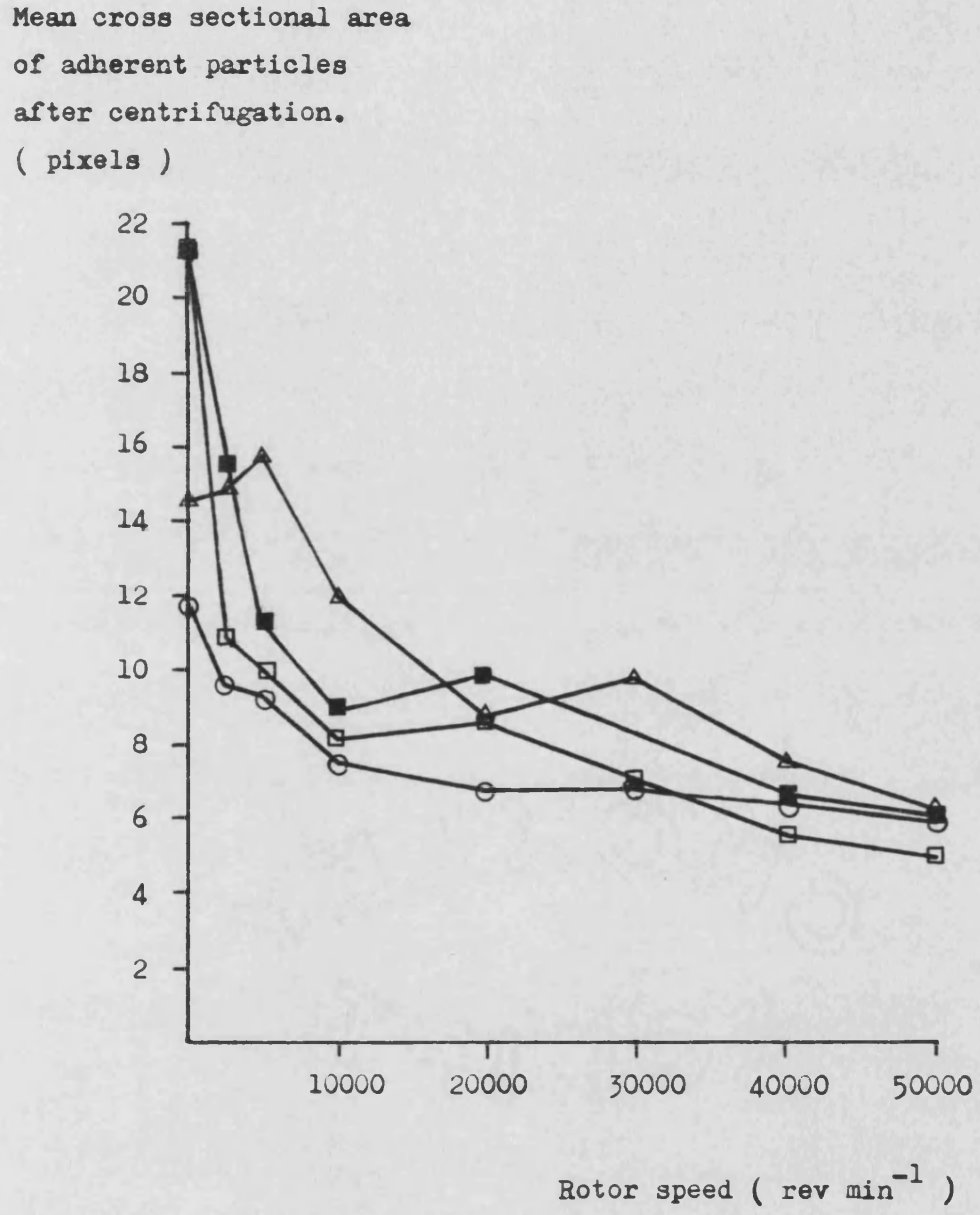

Figure 4.6. Mean cross sectional area, measured in pixels, of adherent particles remaining after centrifugation. □ Ambient, Δ Humid, ○ Dried, ■ Electrised.

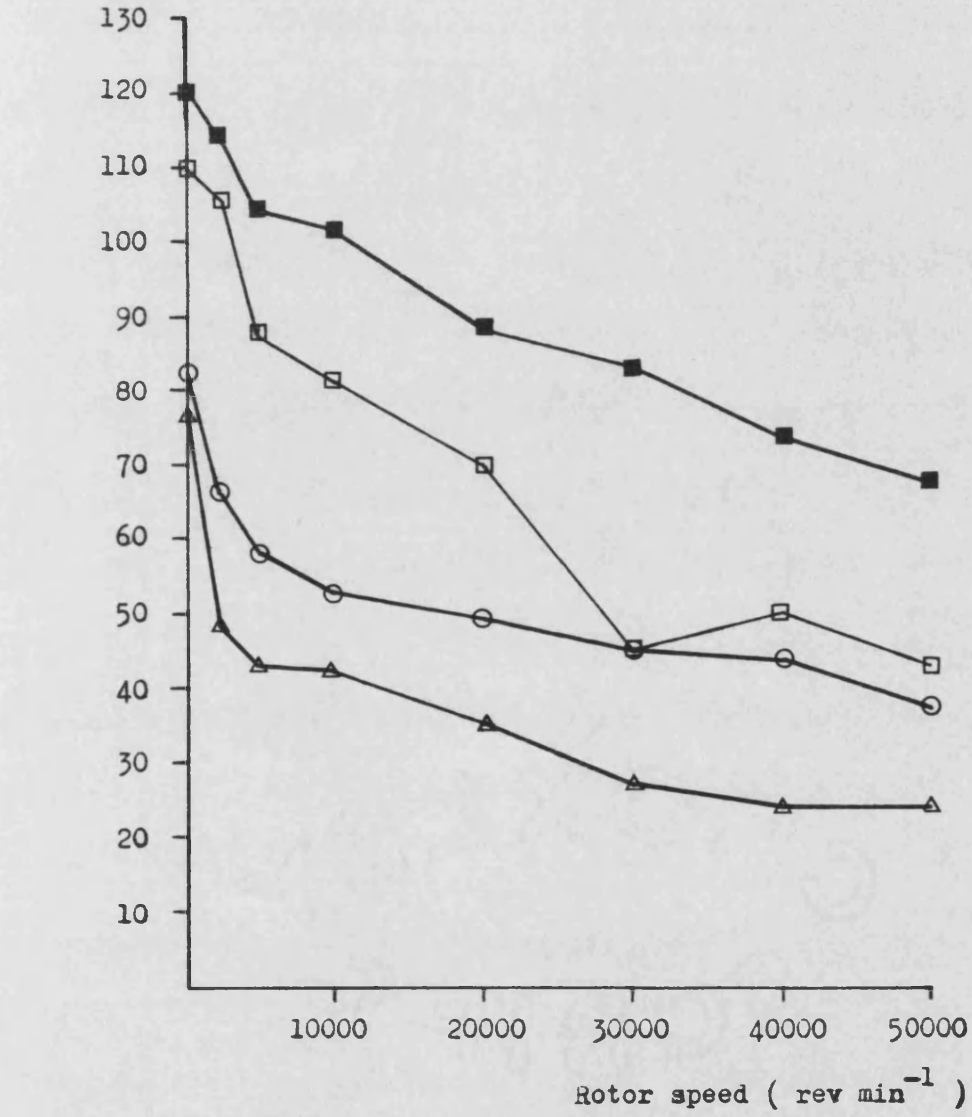

Figure 4.7. Number of adherent particles remaining after centrifugation, adjusted for differences in cross sectional area of the carrier particle.
□ Ambient, △ Humid, ○ Dried, ■ Electrised.

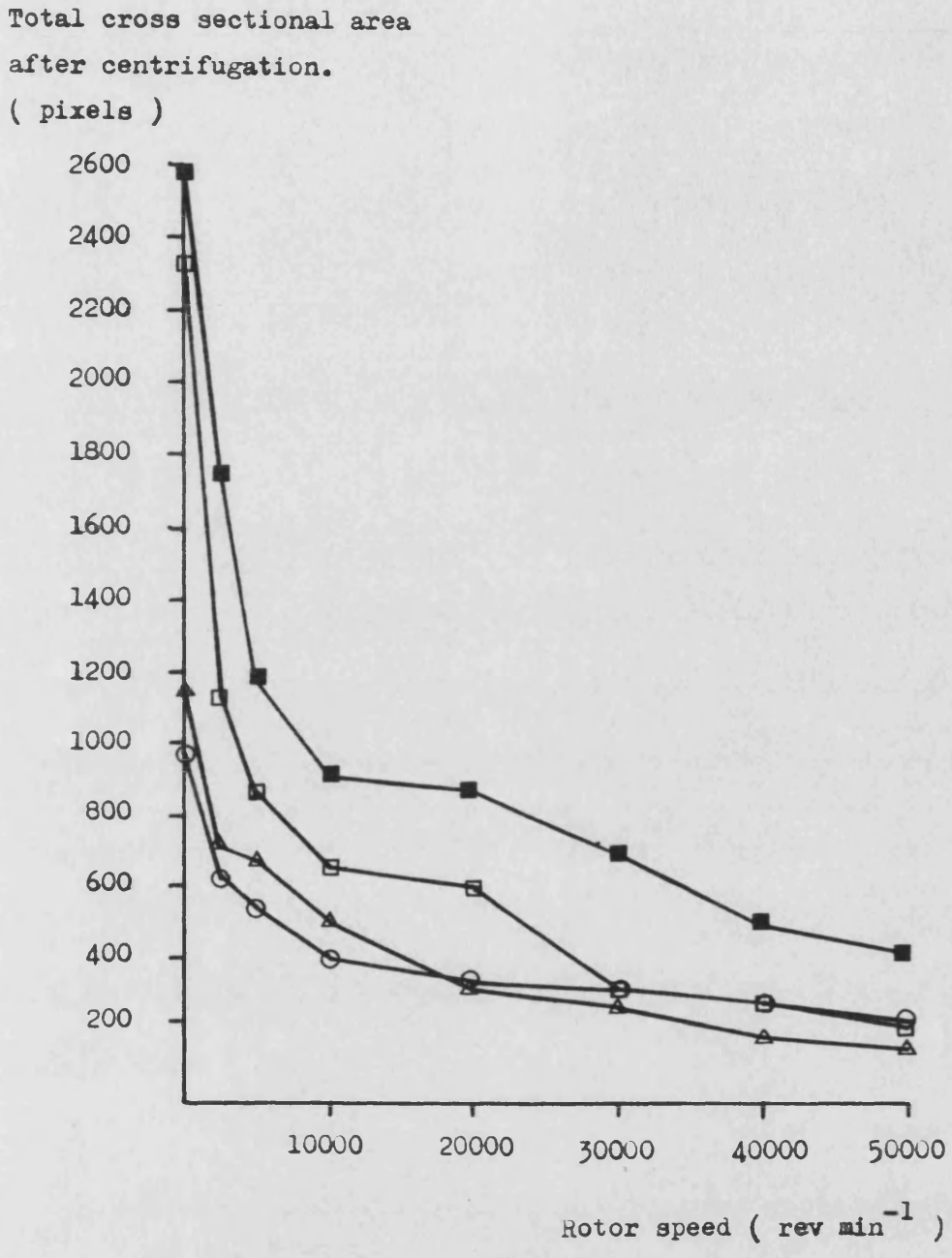

Figure 4.8. Total cross sectional area, measured in pixels, after centrifugation, adjusted for differences in cross cectional area of the carrier particles. □ Ambient, △ Humid, ○ Dried, ■ Electrised.

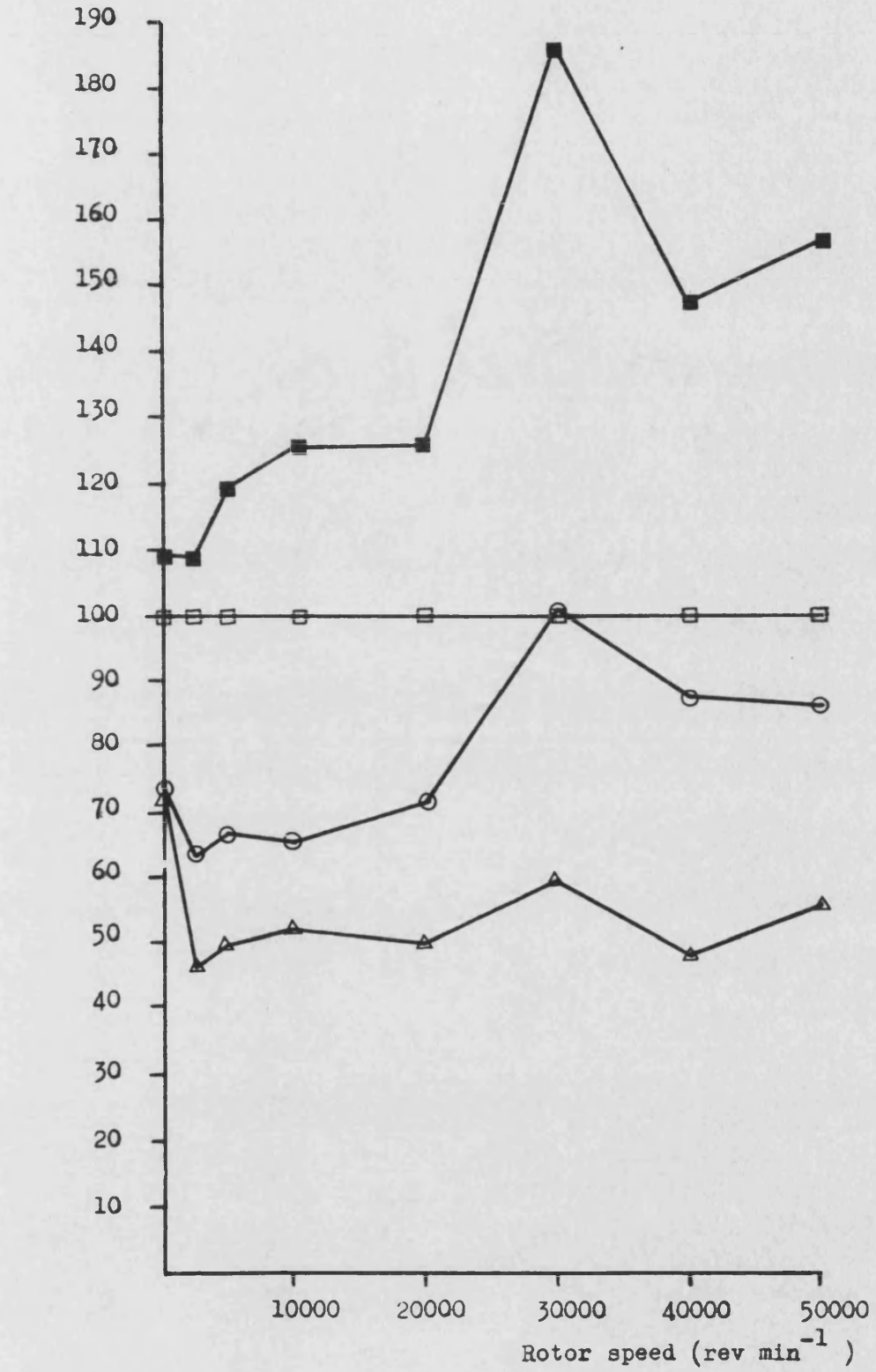

Figure 4.9. Number of particles remaining after centrifugation verses rotor speed. Number of particles expressed as a percentage of the number of ambient particles remaining at that rotor speed.
□ Ambient, △ Humid, ○ Dried, ■ Electrised.

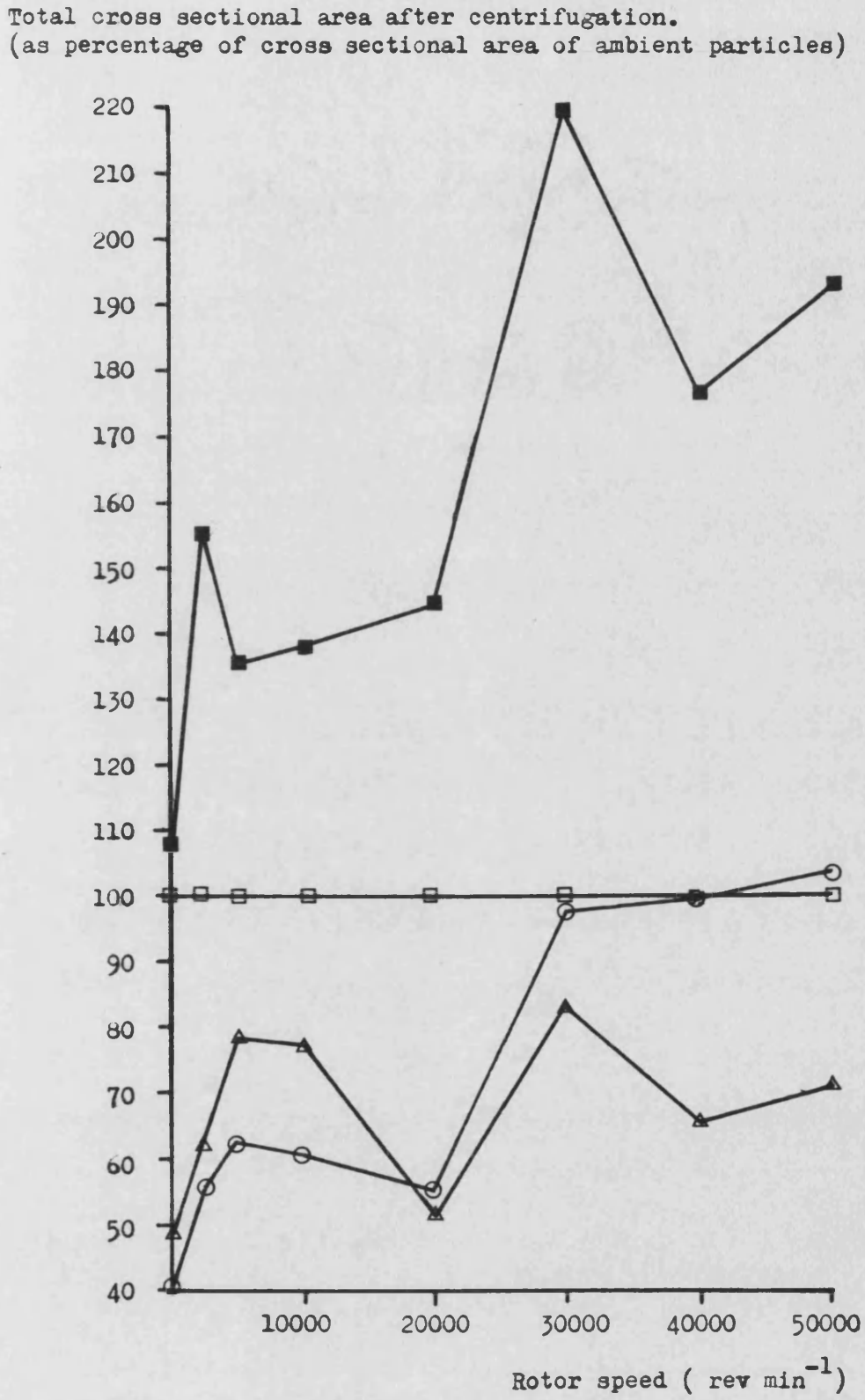

Figure 4.10. Total cross sectional area remaining after centrifugation vs rotor speed. Cross sectional area expressed as a percentage of the cross sectional area of the ambient particles at that rotor speed.
□ Ambient, △ Humid, ○ Dried, ■ Electrised.

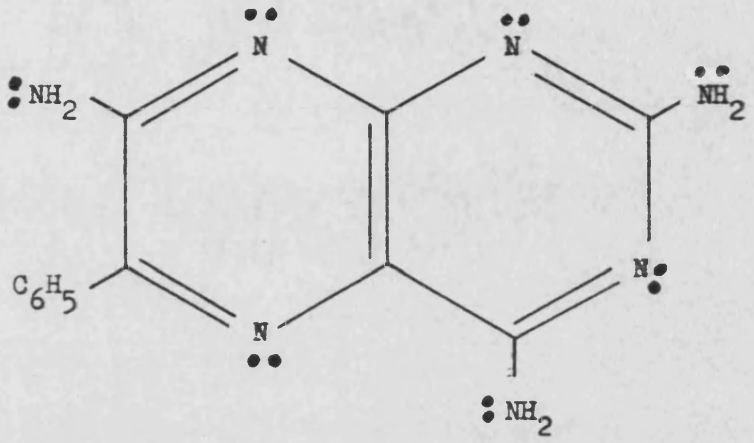

Figure 4.11. Molecular structure of Triamterene. Note the lone pair electrons on the nitrogen atoms.

Chapter 5.

5. General Discussion.

The results presented in this thesis have shown that it is possible to induce an electret charge in cellulose based tableting excipients and that such an effect can significantly enhance the degree of interparticle adhesion occurring in an ordered mixture. In addition, it has also been possible to demonstrate that image analysis can be used to overcome some of the basic physical limitations of optical microscopy, so that it becomes feasible to measure the numbers of adherent particles in individual ordered units and even calculate the separation force of individual adherent particles.

The image analysis techniques developed have been simple due to the limitations of the equipment used and the requirement for developing software in 6502 machine code. As a result, the particle adhesion measurements that were made were also simple. The use of more sophisticated image analysis equipment would, however, allow significant progress to be made in the study of particle interactions in ordered powder mixtures.

5.1. Formation of electrets.

The results presented in Chapter 2 have demonstrated that it is possible to produce thermoelectrets using cellulose based tableting excipients such as Avicel PH102 and Elcema G250. The electret effect was shown to be stable over periods of up to two months, albeit with a reduced charge, provided that the electrets were stored in an environment free from atmospheric moisture. When Avicel PH102 or Elcema G250 electrets were exposed to atmospheric moisture it was found that the electret effect deteriorated rapidly and could be lost completely within two and a half hours.

The electret charge in cellulose has been attributed to the alignment of dipoles due to hydrogen bonding and also due to a space charge which is possibly located at the interface between crystalline and amorphous regions of cellulose. These two mechanisms are necessary to explain the presence of two peaks, of opposite sign, during TSDC. The evidence for hydrogen bonding being involved in the alignment of dipoles is based on the significant effect of the adsorption of atmospheric moisture on the stability of the electret

charge.

The magnitude of the charge stored in Avicel PH102 and Elcema G250 was examined by using TSDC (thermally stimulated discharge current) with either contacting electrodes or airgap electrodes. These two techniques produced traces which were very similar, the only significant difference being the appearance of a tailing peak when contact electrodes were used during TSDC, and some moisture was present in the cellulose. The similarity of the air gap and contact electrode TSDC traces does, however, present some problems when interpreting the data.

Conventionally, TSDC performed with both electrodes in contact will not detect a charge component due to a space charge because when the charges are detrapped they can flow out of the electret through both the electrodes therby producing a zero current. To overcome this problem, TSDC with contacting electrodes is often done with a voltage applied across the sample to force free charge carriers to move through only one of the electrodes thereby producing a measurable discharge current (174). Consequently the two peaks observed for the contact electrode TSDC should not have been observed. Instead, TSDC traces similar to those obtained for electrets stored in ambient atmospheric conditions whilst wrapped in aluminium foil (Figures 2.39, 2.40) should have been obtained.

One possible explanation for the dual peaks observed for contact electrode TSDC is that the electrometer used had an offset current (less than $5x10^{-15}$ amps). This small amount of current would have been sufficient to produce an electric potential across the electret thereby producing an effect similar to contact TSDC with a deliberately applied voltage bias. This mechanism does not, however, explain the fact that the discharge peaks were sensitive to the orientation of the electret in the cell (Figures 2.37, 2.38). If the offset current had been responsible for forcing the direction of movement of detrapped charge carriers then the peak produced would not be sensitive to the orientation of the eletret but on the polarity of the two electrodes. This is obviously not the case so that the above hypothesis can be discarded.

The cause of the dual peak observed during contact electrode TSDC must therefore be due to the space charge component of the electret charge being located on one side of the electret only. This would allow the TSDC trace to be sensitive to the orientation of the

electret in the discharge cell. In addition to the localisation of the space charge to one surface of the electret, it is also necessary to realise that the flow of the space charge through only one electode is due to it being easier to move in this direction than it is to move through the body of the electret to the other electrode.

Another feature of contact electrode TSDC that was initially difficult to explain was the presence of a tailing peak that was dependent on the level of moisture adsorbed by the cellulose. It was discovered, however, that at elevated temperatures the presence of adsorbed moisture in cellulose could give rise to ionic conduction effects (174, 214). This phemonenon would explain why the tailing peak increased in proportion to the amount of atmospheric moisture adsorbed by stored electrets and why the unprocessed material produced such large peaks during TSDC.

The examination of the charge storage mechanism in cellulose requires further investigation because the results from Chapter 2 do not describe the charging and discharging behaviour of the cellulose elecrets completely. For example, an X-ray diffraction study of dried and electrised material may show that there is a change in the internal structure of the cellulose substrate as in the case of carnauba wax (167). The application of differential scanning calorimetry may also produce some useful data concerning charge storage as it would be possible to relate the effect of adsorbed water and loss of electret charge to physical changes in the structure of the cellulose molecule itself.

Future work on TSDC of cellulose almost certainly requires that the discharge cell be redesigned so that the upper or both electrodes can be placed known distances from the surfaces of the electret being examined. This would allow the use of air gap TSDC which is free of the large tailing peak found for contact electrode TSDC. It is also necessary to carry out further work to confirm the charge contribution thought to be due to hydrogen bonding between molecules is actually due to this phenomenon and not due to the separation of charge across boundaries between crystalline and amorphous phases of the cellulose. This could be done by using celluloses where the hydroxyl groups have been modified to non hydrogen bonding groups such as the acetate (224).

Once the mechanism of charge storage in cellulose is better

understood it would be possible to process cellulose to enhance the electret effect thereby further increasing the particle adhesion effects observed.

5.2. Image analysis.

The image analysis techniques developed in Chapter 3 were designed to overcome some of the physical limitations of conventional light microscopy, namely, that the depth of field was insufficient to view the whole surface of a carrier particle in focus simultaneously (Chapter 1, 1.5). It was demonstrated that, provided the adherent particle can be distinguished from the background, a series of digitised images through a carrier particle could be used to generate an image in which all the adherent particles were in focus (Figures 3.5 to 3.28). The composite image generated by COMPOS was found to be deficient in some areas because occasionally some adherent particles were omitted and others were incorrectly focused. These deficiencies were due, however, to the limitations of the equipment used to perform the image analysis.

Although it was possible to store two digitised images in the 128k sideways memory board it was then necessary to write all the software which accessed this memory in 6502 machine code. This had the advantage that image analysis programs could be run at reasonable speed, however, the development time for the more complex progrms was extremely lengthy. As a result of this, ideas which could have been tried out were not considered because it would have taken too long to write and debug the programs involved.

This problem can be illustrated by consideration of the COMPOS program, written using the 6502 assembler of BBC BASIC and the program PROFILE, which was written in 'C'. The former program was developed over a minimum period of six months and when used to produce data for this thesis, was still not fully functional. This is despite the ideas used in COMPOS being very simple in programming terms. PROFILE however, was written in approximately four days starting with no prior knowledge of the 'C' programming language. Profile was written to demonstrate simple image analysis functions using isometric projections of the brightness of the digitised image (Chapter 1, Section 1.6).

A serious restriction imposed by the BBC based image analysis system was that it was not possible to view the digitised image in

the grey scale resolution with which it was digitised unless the digitised data was transferred to an experimental graphics workstation. The inability to view digitised images meant that any software developed could not be assessed fully. This deficiency was one of the major contributors to the problems associated with COMPOS.

The production of the composite images only used part of the information available from the digitised images collected for analysis. As each digitised image was associated with a known level of focus it would have been possible to have produced a three dimensional representation of the surface of the carrier particle showing the distribution of the adherent particles. Had the microscope been controlled by the BBC computer it would have been possible, having identified the position of the adherent particles, to change to a higher magnification and reassess the size of the adherent particle using techniques similar to that used to produce a composite image. This type of analysis would have allowed the orientation of the adherent particle to be measured and consequently a better three dimensional reconstruction of the carrier particle and adherent particles.

5.3. Measurement of particle adhesion.

The results obtained in Chapter 4 demonstrated that it ws possible to use the composite images produced using the image analysis techniques described in Chapter 3 to accurately measure particle adhesion in single ordered units using individual adherent particles.

The use of centrifugation to provide a separating force has been used by a number of authors (73, 74, 81, 97-99, 101-103) as a means of removing particles from plane or nearly plane surfaces. The ability to use the same technique with single ordered units and to be able to measure the size of the adherent carrier particles means that it is now possible to carry out fundamental adhesion studies for pharmaceutical powder mixtures. The feasibility of this possibility was demonstrated by measuring the adhesion force profile of an Elcema G250/triamterene powder mixture where the Elcema G250 had been processed in four different ways.

The adhesion force profiles generated showed that electrising Elcema G250 increased the interparticle adhesion forces by a significant amount whereas exposing the Elcema G250 to humid

atmospheric conditions prior to mixing reduced the particle adhesion measured. This latter result was contrary to that expected but was satisfactorily explained by consideraton of the molecular structure of the triamterene molecule.

A further anomaly was noted when the rate at which particles were lost was considered (Figures 4.9, 4.10). It was thought that as the electret charge was destroyed by exposure to atmospheric moisture, adherent particles would be lost more rapidly from the electrised Elcema G250 than from the Elcema G250 prepared by exposure to ambient atmospheric conditions. In the event, this proved not to be the case as the adherent particles on the electrised and dried Elceam G250 became more difficult to dislodge as atmospheric moisture was adsorbed. This effect was finally attributed to the fact that water acts as a plastisicer for cellulose (218) and that its adsorption by dried cellulose caused the cellulose to soften and become more plastic (from the surface inwards) thereby allowing greater plastic deformation at the point of contact between adherent particle and the carrier surface. The presence of the electret charge was found to incease this effect as the charge would not be instantly destroyed as moisture was adsorbed.

This observation has significant implications as it means that electrised powder mixtures (at least those based on Elcema G250) will tend to become more stable when exposed to ambient atmospheric conditions rather than less stable as originally thought. This implies that such mixtures may be resistant to component particle segregation caused by the addition of lubricants or other excipients, provided that sufficient time was allowed for equilibration with atmospheric moisture.

The general quality of the particle adhesion data was good, particularly as the data is impossible or very difficult to obtain in any other way and when the problems associated with the method are considered. However, it should be noted that no account was taken of the curvature of the surface of the Elcema G250 carrier particle and that the results obtained will therefore contain some error due to this.

The particle adhesion measurements made for the Elcema G250/triamterene mixtures could also be used to assess the effect of adding a ternary component, such as a lubricant, to a powder mixture. Used in this way the methods described above would provide a way of

assessing the impact of adding a lubricant to an otherwise stable mixture, a process which currently involves cumbersome analysis of bulk powder samples. Such applications would require a significant increase in processing power, image resolution, automation and display facilities of the image analysis sytem, to be used as a routine tool for the examination of powder samples.

6. Conclusions.

Thermoelectrets can be manufactured using cellulose based tableting excipients such as Avicel PH102 and Elcema G250. The electret charge measured in Elcema G250 is stable over a period of several months provided that the adsorption of moisture is prevented. The adsorption of atmoshperic moisture destroys the electret effect within several hours of exposure.

The charge storage mechanism in cellulose thermoelectrets is thought to be associated with a space charge component trapped at the junction between the crystalline cellulose/amorphous cellulose boundaries of long micelle like structures, and aligned dipoles due to the presence of inter molecular hydrogen bonding. The tailing peak observed during TSDC using contact electrodes has been attributed to ionic conduction in cellulose at elevated temperature.

Further investigation of the charge storage mechanism in cellulose is required. This should be performed using techniques such as differential scanning calorimetry so that changes in the phsical structure of the cellulose molecule can be related to the loss of the electret charge.

The image analysis techniques developed in Chapter 3 were able to produce images where the adherent particles were all in focus thereby overcoming the depth of field limitation of conventional light microscopy. The image analysis equipment was thought to be the minimum that could be easily used.

A limitation of the image analyser that was built was its inability to view digitised images with the grey level resolution with which they were digitised. This was a significant problem when developing the image analysis software that was used. The actual development of the image analysis software was also a problem because of the necessity for writing programs in machine code to obtain adequate processing speed. However, there is no reason why the image analysis techniques used in this thesis could not be implemented on other, more sophisticted image analysers.

The image analysis methods developed in Chapter 3 allowed adhesion force profiles of the adherent particle in binary ordered powder mixtures based on Elcema G250 and triamterene to be generated with relative ease. The particle adhesion data obtained showed that

electrising Elcema G250 significantly increased the degree of interparticle adhesion as predicted. The degree of interparticle adhesion between triamterene and cellulose in the presence of high levels of adsorbed moisture was significantly reduced. This was attributed to the inability of triamterene to promote hydrogen bonding.

Appendix 1.

A1. Electrets

Although descriptions of electret formation and charge measurement are available in the literature (135-137, 174), it is thought that a background to the theoretical considerations involved in this work is useful. For this reason, this appendix has been included as a means of introducing the fundamental electrostatic and quantum mechanical aspects of materials that are involved in the formation of an electret.

The discussion below does not attempt to present a comprehensive treatment of the theory of electrets. Instead, information readily available in textbooks (75, 76, 80), has been assembled in a manner which emphasises those aspects of classical electrostatic and quantum mechanics relevant to the formation of electrets and the measurement of the charge stored in them.

A1.1. Definition of an electret.

The original definition of an electret was made by Heaviside (131, 132) during a discussion on the behaviour of a dielectric material in an electric field. Heaviside stated that a dielectric or insulator which exhibited a residual electric field after being exposed to an external electric field could be regarded as being 'permanently' electrised. In this state the dielectric or insulator could be considered as the electrical equivalent of a permanent magnet and could therefore be called an electret.

A more practical definition of an electret (159) is any dielectric which retains a residual electrostatic charge for a time period several orders of magnitude larger than that which was originally used to induce the charge. Using this definition, a dielectric which was exposed to an electric field for one second and which still exhibited a residual electric field 100 seconds after the electric field had been removed could be considered to be an electret.

It should be stressed that this definition of an electret requires that the exposure of the dielectric to an electric field is done in a way that prevents the transfer of charge from or to the body of the dielectric. The electric field thus generated is due solely to the electronic response of the dielectric and not the

transfer of charge to or from it.

A1.2. Contributary factors to electret formation.

The mechanisms by which an electric charge may be stored in a dielectric for long periods of time are the result of a number of complex interactions. However, in the immediate case, it is only necessary to consider the main mechanisms of electret formation, the alignment of permanent dipoles found within the dielectric, separation of charge and the induction of space charge due to the presence of holes or excess electrons.

Dipolar charge storage occurs in materials which have permanent dipole moments, eg long chain carboxylic acids, which can be forced into alignment by an external electric field. Electrets formed from dielectrics with permanent dipoles exhibit opposite charges on opposite faces and are therefore referred to as dipolar electrets. The same effect can be achieved where charge can be separated across a physical boundary within the body of the dielectric, for example at the junction of crystalline and amorphous regions. The induction of a space charge within a dielectric is dependent on the presence of sites within the dielectric where it is possible for an electron to be injected into or removed from a shallow energy well. Electrets formed from material where electrons have been removed or trapped generally show only one electrostatic charge on both sides of the dielectric and are therefore referred to as monopolar electrets.

The formation of dipolar electrets can be explained using classical electrostatic theory (75, 80) whereas monopolar electrets require the application of quantum mechanics (76, 80) to the electronic nature of materials for their explanation.

A1.3. Classical electrostatic theory.

The aim of this section is to introduce the fundamental concepts of classical electrostatics and has been included for two reasons. An appreciation of electrostatic charge and the behaviour of bodies with such charges will show how electrostatic charge can be used to increase particle interaction in ordered mixtures. In addition, an appreciation of how electrostatic charge can be induced in a dielectric and how dipolar molecules behave when exposed to an external electric field and temperature will show how it is possible to form dipolar thermoelectrets. The molecular basis for this

explanation will also show that thermoelectrets are an inevitable consequence of the properties of the molecules themselves and not a special case.

A1.3.1. Positive and negative charges.

For the purposes of classical electrostatic theory it is only necessary to consider atoms as consisting of protons, electrons and neutrons. Electrostatic charge (negative or positive) is only carried by the electron and the proton repectively. The neutron does not carry a measurable electric charge.

The electric charge of an electron has been measured and found to be -1.602×10^{-19} Coulomb (q). The electric charge on the proton has the same magnitude as that of the electron but is opposite in sign ($+1.602 \times 10^{-19}$ q). Atoms consist of a nucleus, made up of protons and neutrons, which is surrounded by electrons. Atoms which are not ionised and are isolated have an equal number of protons and electrons and are therefore electrically neutral. An atom retains its electrons by virtue of the electrostatic attraction between the electric charge on the protons and electrons although it should be noted that several other forces are also present that are much weaker than the electrostatic force and whose origin and effect are outside the scope of this discussion.

A1.3.2. Lines of force.

The main effect of the proton and electron having an electric charge is that they can exert a force on other protons and electrons without the need for physical contact. Electric charge behaves in an analagous manner to magnetic poles where opposite fields attract and like fields repel. Thus electrons and protons are attracted to each other whilst the converse is true for electron-electron and proton-proton interactions.

If a point charge of magnitude +q is formed by removing a charge of -q from a neutral body and moving it to infinity, an attractive force between the two charges will be created. This force can be visualised by imagining lines which originate on the positive charge and terminate on the negative charge (Figure A1.1). These lines are referred to as lines of force (or flux).

The forces acting in the region of +q can be examined by placing a test charge $+q_1$ near +q and observing its subsequent motion. No

matter where $+q_1$ is placed it will be subjected to a repulsion acting along the line of force connecting the two charges (Figure A1.2). This effect is taken to mean that the charge -q at infinity can be considered as being distributed over a sphere of infinite radius rather than being located at a single point.

Replacing the charge +q with a charge of -q will change the direction of the force lines acting on $+q_1$ so that they are directed radially inwards rather than outwards indicating that there is a force of attraction between -q and $+q_1$.

A1.3.3. Coulombs's law.

Coulomb's Law states that if a charge q_1 is located at a distance r from a point charge +q, then the magnitude of the force, F, acting along the line of force joining the centres of the charges is given by equation A1.1,

$$F = \frac{qq_1}{4\pi\epsilon_0\epsilon_r r^2} \qquad (A1.1)$$

where r = Distance between the two charges (m).

ϵ_0 = Permittivity of free space (vacuum).
= 8.85×10^{-12} farad m^{-1} (Fm^{-1}).

ϵ_r = Relative permittivity or dielectric constant of the medium in which the electric charges are located.
= 1 for vacuum, 3.8 for cellulose acetate (80), no units.

$\epsilon = \epsilon_0\epsilon_r$ = Permittivity.

NB. The product $\epsilon_0\epsilon_r$ is conventionally used rather than absolute permittivity as the relative permittivity of a medium to free space is relatively easy to measure. The term ϵ_0 is therefore used as a proportionality constant. The force , in Newtons (N), is directed towards +q if the two charges are of opposite sign and away from +q if the charges are of similar sign.

A1.3.4. Electric field and potential.

The force exerted by one charge on another is repesented by an electric field which is defined as the force acting on a unit positive charge located at the point which is being considered. From equation A1.1 (substituting 1 for $+q_1$) the electric field, $\xi(r)$ Vm^{-1}, at a distance r from the charge q is given by equation A1.2,

$$\mathcal{E}(r) = \frac{q}{4\pi\epsilon r^2} \qquad (A1.2)$$

If the point charge +q (Figure A1.2) is at the centre of an imaginary sphere then equation A1.2 will give the magnitude of the electric field at all points on the surface of that sphere. This enables the density of the lines of force or displacement, D(r) qm^{-2}, at the surface of this imaginary sphere to be calculated using equation A1.3,

$$D(r) = \frac{q}{4\pi r^2} \qquad (A1.3)$$

The relationship between the electric field and the displacement can be seen to be,

$$D(r) = \epsilon\mathcal{E}(r) \qquad (A1.4)$$

The effect of equation A1.4 is to show that displacement is directly proportional to the electric field intensity and that changing the permittivity of the medium through which lines of force pass effectively changes the density of those lines of force. Alternatively, for a given density of lines of force, the force exerted on a unit charge is proportional to the permittivity of the medium in which the unit charge is placed.

Referring to equation A1.1 it can be seen that if a test charge $+q_1$ at distance , r, from a point charge +q, is moved a distance δr, then work, W, must have been done on or by $+q_1$, by virtue of the force existing between the two charges,

$$W = F.\delta r = \frac{qq_1}{4\pi\epsilon r^2}.\delta r \qquad (A1.5)$$

Any charge in an electric field must therefore possess energy and consequently have the potential to do work. The potential for work, V(r) Volts, at a distance, r, can therefore be defined as the work done in bringing a unit positive charge from infinity to a distance r from the charge +q.

$$V(r) = -\int_{\infty}^{r} \frac{q}{4\pi\epsilon r^2}\,\delta r = \frac{q}{4\pi\epsilon r} \qquad (A1.6)$$

V(r) is a measure of the potential energy, U, of the unit charge in the field of +q. The potential , U(r) Joules (J), of a charge of $+q_1$ at a distance r from +q can be calculated using equation A1.7.

$$U(r) = q_1V(r) = -\frac{qq_1}{4\pi\epsilon r} \qquad (A1.7)$$

If equations A1.2 and A1.6 are combined

$$\mathcal{E}(r) = - \frac{\delta}{\delta r} V(r) \qquad \text{(A1.8)}$$

Equation A1.8 is a statement of the fact that the magnitude of the electric field due to charge +q at any point is equal to the rate of change of potential (voltage gradient) at that point.

A1.3.5. Boundaries between dielectrics.

Thus far only electric fields in a single medium have been considered. Electric fields, however, may often pass through more than one medium. The result of such a transition does have implications when attempting to increase the degree of particle interaction due to the presence of an electrostatic force. Maxwell developed a number of equations which are particularly relevant when dealing with electric fields at the interface between two dielectrics. Whilst the proof of the equations given below is beyond the scope of this discussion they can be shown to be reasonable statements on the basis of the ideas already discussed.

When lines of force cross the boundary between two different dielectrics (Figure A1.4) two statements can be made.

1. The change in the density of lines of force, D, normal to the interface of area, A, between two dielectrics is equal to the charge density at that interface. This can be represented by equation A1.9.

$$D_1 \sin(\theta_1) - D_2 \sin(\theta_2) = Q/A \qquad \text{(A1.9)}$$

2. The magnitude of the component of the electric field parallel to the interface between two dielectrics does not change on crossing the interface. This is expressed by equation (A1.10).

$$\mathcal{E}_1 \cos(\theta_1) = \mathcal{E}_2 \cos(\theta_2) \qquad \text{(A1.10)}$$

The significance of equation A1.9 is that it states that lines of force normal to the interface between the two dielectrics must either propagate across the interface or terminate on charges of appropriate sign at the interface. This statement can be seen to be true because lines of force were defined as always starting at a positive charge and ending at a negative charge.

Equation A1.10 can be seen to be true by considering two points, P and S, on the interface. The potentials, V_p and V_s, of these two points will be uniquely defined by virtue of their being located at the interface. The work done in moving a unit charge from P to S or

vice versa will be independent of the side the interface on which the unit charge is moved. That is, in the vicinity of the interface, the electric field parallel to the boundary must be the same in both dielectrics.

The implications of A1.9 are particularly relevant to the formation of electrets. Where an electric field crosses a boundary defined by a change in the dielectric constant of a material there must, by virtue of the above, be a layer of charge associated with that boundary. The separation of such charge across boundaries due to transitions from crystalline to amorphous, or one crystalline arrangement to another crystal to phase 2 crystal must inevitably produce an electrostatic charge which may be orientated to facilitate the formation of an electret.

A1.3.6. Force on a point charge near an earthed plane.

When an isolated charge, +q, is placed a distance, d, from an earthed conducting plane (Figure A1.4) the presence of an electric field will cause free electrons in the conductor to be attracted to the surface. This movement of free charge results in a distribution of negative charge which can interact with the positive charge +q. The charge +q will therefore experience a force directed towards the surface of the conductor.

With reference to equations A1.9 and A1.10 the following observations can be made.

1. The electric field parallel to the surface of the conductor must be the same inside the conducting plane as outside, and, since the potential of any earthed conductor is zero, must also tend to zero near the surface of the conductor.
2. The force lines from the charge +q will all terminate normal to the surface of the conductor due to the presence of free electrons. Again, the potential of an earthed conductor is zero. This means that the electric field due to the charge +q cannot penetrate into the conducting plane.

Using symmetry, the negative charge at the surface of the conductor could, in theory, be replaced by a negative charge of equal magnitude, -q, at a distance d_1 from the surface of the conducting plane (Figure A1.4). This negative charge would be placed in such a manner that the distribution of the lines of force emanating from it would match exactly those from the positive charge. Thus the charge

+q 'sees' an image charge, -q, in the conducting plane and therefore experieces a force of attraction due to it. Applying Coulomb's Law the magnitude of the attractive force, F_{im}, due to the image charge can be calculated.

$$F_{im} = - \frac{qq}{4\pi\epsilon(2d)^2} = - \frac{qq}{16\pi\epsilon d^2} \qquad (A1.11)$$

The force due to the presence of an electric charge near an earthed conducting plane always drives the charge towards the conducting surface because the image charge is always of the opposite sign.

The induction of an image charge in an uncharged dielectric will always occur in the same manner as above although not to the same degree so that uncharged particles will always experience a force driving them towards the charged surface. The magnitude of the force will however greatly depend on the number of free electrons in the uncharged dielectric particle that are able to move to the surface in response to the external electric field.

It is precisely this effect which is used in electrostatic precipitators and filters and which makes them more efficient than similar equipment that does not employ electrostatic charging. Furthermore, because electrostatic forces are effective over significantly greater distances than other types of physical forces involved in interparticle adhesion the above effect can be expected to dramatically increase the number of interparticle collisions when an electrically charged and uncharged powder are mixed. This aspect of electrostatic charging of particles has been discussed more fully in Chapter 1 (1.2).

Any increase in interparticle collision would provide greater opportunity for interparticle bonds to form so that it should be expected that such mixtures would form better ordered mixtures than totally uncharged mixtures. This is, in fact, the effect observed with electrised Elcema G250 and uncharged triamterene (Chapter 4).

A1.3.7. Capacitance.

A conductor is a body which allows free passage of electric charge through it. A pair of isolated conductors, A and B, can store charge to an extent determined by the capacitance of the system. The capacitance of such a system is determined by the geometry and shape of the conductors and of the dielectric properties of the medium

between them.

If an amount of charge, +q, is transferred from conductor A to conductor B, a potential difference between the two conductors is generated. If the capacitance of the system is defined as the amount of charge that must be moved from conductor A to conductor B to produce a change of unity in the potential of conductor B with respect to conductor A then the relationship between the charge difference and the capacitance can be calculated using equation A1.12,

$$C = \frac{Q}{V} \qquad \text{(A1.12)}$$

where C = Capacitance of the system (qV^{-1} or F).

Q = Charge transferred (q).

V = Potential difference generated due to the transfer of the charge (V).

For a parallel plate capacitor (Figure A1.5) with conductors of area, A, and separation ,d, the movement of an amount of charge, Q, from the earthed lower plate to the electrically isolated upper plate would cause a potential difference, V, to exist between the two plates. The lines of force between the two conductors would be parallel, apart from those at the edges of the plates where some distortion would occur. If the area of the conductors is large in comparison to the distance between the conductors, edge effects can be ignored, and the electric field between the plates can be regarded as being constant at every point.

The density of force lines, D, between two such conductors can be calculated as Q/A. Thus from equation A1.2 and A1.6 the capacitance of the conductors can be expressed as in equation A1.13.

$$C = \frac{Q}{V} = \frac{DA}{V} = \frac{\varepsilon \mathcal{E} A}{V} = \frac{\varepsilon A}{d} \qquad \text{(A1.13)}$$

The capacitance of a parallel plate capacitor is therefore proportional to the cross sectional area of the conductors and the permittivity of the medium between conductors, and inversely proportional to the distance between the conductors.

A1.3.8. Polarisation density.

Equation A1.13 shows that the presence of a dielectric between the plates of a capacitor changes its capacitance and that this change is proportional to the permittivity of the medium between the

conductors. This permittivity, however, is a product of the permittivity of free space, ε_0, which is constant, and the relative permittivity of the medium, ε_r. The relative permittivity of a dielectric is the ratio of the absolute permittivity of the medium to that of free space (and is therefore a dimensionless number). Thus the presence of a dielectric between the conductors of a capacitor generally serves only to increase the capacitance and not to decrease it.

The increase in the capacitance of a capacitor due to the presence of a dielectric occurs because there is a reduction in the number of flux lines within the dielectric (A1.3.5) and hence a reduction in the electric field between the plates of conductors of the capacitor. The decrease in the electric field in the dielectric is a consequence of lines of force terminating at the surface of the dielectric due to the presence of an image charge induced by the presence of an external electric field.

If the assumption is made that the dielectric in the capacitor is a neutral body, ie contains no free charge, then the image charge in the dielectric must be due to the electric field caused by the alignment of permanent dipoles. The orientation of the induced electric field due to the alignment of dipoles will be opposite to that of the external electric field (Figure A1.6) and as a result it will appear as though some of the charge on the capacitor has disappeared.

The polarisation density, P, can therefore be defined as the total dipole moment induced in a unit volume of the dielectric. This can be represented as the apparent reduction in the amount of charge stored in the capacitor due to the presence of the dielectric.

$$P = C_{vac}V - CV$$

$$P = (C_{vac} - C)V$$

$$P = \left(\frac{\varepsilon_0 A}{d} - \frac{\varepsilon_0 \varepsilon_r A}{d}\right)V$$

$$P = (1 - \varepsilon_r)\frac{\varepsilon_0 AV}{d} \qquad \text{(A1.14)}$$

where P = polaristion density (Cm^{-2}).

C_{vac} = capacitance with vacuum between the conductors.

C = capacitance with dielectric between the condictors.

A = cross sectional area common to both conductors.

d = distance between the conductors.

For a unit volume of dielectric, A=1 and ℓ=V/d, therefore

$$P = (1 - \varepsilon_r)\varepsilon_0 \ell \qquad (A1.15)$$

rearranging to isolate ε_r,

$$\varepsilon_r = 1 + \frac{P}{\varepsilon_0 \ell} \qquad (A1.16)$$

Equation A1.16 states that the relative permittivity of a dielectric is dependent upon the degree of polarisation per unit electric field. This relationship is more commonly expressed as,

$$\varepsilon_r = 1 + \chi_e \qquad (A1.17)$$

where χ_e is referred to as the the electrical susceptibility of the dielectric. The electrical susceptibility of a dielectric is a measure of the degree to which polarisation will occur when it is exposed to an external electric field.

A1.3.9. Contributors to dielectric polarisation.

The strength of the internal polarisation of a dielectric, when exposed to an external electric field, is determined by the contributions from three different charge sources.

1. The electronic polarisation, α_e, produced by the opposite displacements of the electrons and protons within the same atoms.
2. The ionic polarisability, α_i, produced by the opposite displacements of positive and negative ions in the dielectric.
3. The contribution from permanent dipole moments, μ, due to the presence of complex ions or molecules.

The electronic polarisability of a dielectric arises from the fact that electrons do not occupy a precisely defined orbit around the nucleus. Instead the position of an electron at any given time is defined by a probability function which can be used to predict the most likely region that will be occupied by an electron. The application of an external electric field will provide a bias to the electron's probability function so that it becomes more probable for the electron to be on one side of the atom than the other. This changed distribution of the position of the electron creates an electric field in the dielectric in response to the applied external electric field. However, because of the nature of the charge separation, the induced electric field is lost very rapidly once the external field is removed.

The ionic polarisability of a dielectric depends upon the

presence of a regular atomic array of positive and negative atoms, as in a crystal of sodium chloride. The application of an external electric field will exert a force on these ions and cause them to be displaced slightly from their natural lattice positions. Although the ions are firmly fixed in the lattice the small amount of displacement caused by the presence of an external electric field is sufficient to produce an induced electric field in the dielectric. Again, as with electronic polarisability, the induced electric field will disappear rapidly once the external electric field is removed.

Many organic compounds are naturally polarised as a result of the relative electronegativities of the different functional groups within the molecule. Such molecules therefore have permanent dipoles associated with them. When an external electric field is applied to such molecules the dipoles will try to align themselves with the electric field. However, because of the nature of the molecules it may not be possible for dipoles to align fully in response to an external electric field. Alternatively the inertia of the molecule and the steric restraints imposed by the neighbouring molecules may mean that the dipoles present may only align themselves slowly with the external electric field. Correspondingly, the electric field induced by the external field may take some time to decay after the external field is removed. Thus, unlike electronic and ionic polarisability, the polarisation due to the presence of molecular dipoles may be time dependent.

The contribution to the polarisation density from these three sources above can be quantified. If the number of atoms or molecules per unit volume is N, then the polarisation density, P, can be represented as the sum of the three types of polarisation multiplied by N.

$$P = N(\alpha_e + \alpha_i + f(\mu)) \qquad \text{(A1.18)}$$

This relationship can also be expressed in terms of electronic susceptibility.

$$\chi_e = \frac{P}{\epsilon_0 \mathcal{E}}$$

$$\chi_e = \frac{N\,(\alpha_e + \alpha_i + f(\mu))}{\epsilon_0 \mathcal{E}} \qquad \text{(A1.19)}$$

As stated above the contribution of permanent dipoles to the polarisation of a dielectric is dependent on their ability to align themselves with the applied electric field. For example, a highly

polarised long chain acid would have dipoles on the carbonyl group and the molecule itself. When exposed to an external electric field the carbonyl group would be able to align more quickly, by rotating on its carbon link, than the molecule as a whole.

A1.3.10. Temperature dependence of permanent dipoles.

When an electric field is applied to a dielectric the permanent dipoles present experience a force causing them to try and align themselves with the direction of the field. However dipoles in a solid are not free to rotate so as to fully align themselves with the applied electric field due to the restriction of neighbouring molecules. Furthermore, the molecules are also subject to random movements due to thermal agitation which tends to disorder any alignment due to the applied electric field. Thus the contribution of polarisation due to permanent dipoles may not only be time dependent but also affected by temperature.

For any freely moveable permanent dipole of moment, μ, at an angle, θ, with the direction of the applied electric field the contribution of the dipole to the total polarisation in the dielectric will be $\mu\cos(\theta)$. The probability that δN of the dipoles are at an angle between θ and $\theta+\delta\theta$ can be calculated using Boltzmann statistics (75) and is given by

$$2\pi\sin(\theta)\delta\theta e^{-\mu\xi\cos(\theta)/kT} \qquad \text{(A1.20)}$$

The total effect of all the dipoles can be calculated by considering all possible cases, from $\theta=0$, when the dipoles are parallel to the applied electric field, to $\theta=\pi$, when the dipoles are antiparallel to the applied electric field. Thus, integrating over all the angles from parallel to antiparallel alignment, the total dipole moment, $\bar{\mu}$, can be obtained.

$$\bar{\mu} = \frac{\int_0^{\pi} \mu\cos(\theta)2\pi\sin(\theta)e^{-\mu\xi\cos(\theta)/kT}\,\delta\theta}{\int_0^{\pi} 2\pi\sin(\theta)e^{-u\xi\cos(\theta)/kT}\,\delta\theta} \qquad \text{(A1.21)}$$

This expression can be simplified as follows by cancelling the 2π terms and making the substitutions

$$a = \frac{\pi \ell}{kT} \tag{A1.22}$$

$$x = a\cos(\theta) \tag{A1.23}$$

$$x = a\sin(\theta)\,\delta\theta \tag{A1.24}$$

$$\bar{\mu} = \frac{\int_0^{\pi} \mu\cos(\theta)\sin(\theta)e^{-a\cos(\theta)}\,\delta\theta}{\int_0^{\pi} \sin(\theta)e^{-a\cos(\theta)}\,\delta\theta} \tag{A1.25}$$

$$\bar{\mu} = \frac{\int_0^{\pi} \mu\cos(\theta)\sin(\theta)e^{-x}\,\delta\theta}{\int_0^{\pi} \sin(\theta)e^{-x}\,\delta\theta} \tag{A1.26}$$

from equations A1.23 and A1.24

$$\cos(\theta) = \frac{x}{a} \quad \text{and} \quad \delta\theta = \frac{1}{a\sin(\theta)}$$

$$\bar{\mu} = \frac{\int_0^{\pi} \mu \frac{x}{a} e^{-x}\sin(\theta)\frac{1}{a\sin(\theta)}\,\delta x}{\int_0^{\pi} e^{-x}\sin(\theta)\frac{1}{a\sin(\theta)}\,\delta x} \tag{A1.27}$$

$$\bar{\mu} = \frac{\mu\int_0^{\pi} xe^{-x}\,\delta x}{a\int_0^{\pi} e^{-x}\,\delta x} \tag{A1.28}$$

for the integration limits, from equation A1.23, when $\theta=0$ then $x=a$ and when $\theta=\pi$ then $x=-a$.

$$\bar{\mu} = \frac{\mu \int_{a}^{-a} x e^{-x}\, \delta x}{a \int_{a}^{-a} e^{-x}\, \delta x} \qquad \text{(A1.29)}$$

which finally gives

$$\frac{\bar{\mu}}{\mu} = \frac{(e^{a} + e^{-a})}{(e^{a} - e^{-a})} - \frac{1}{a} \qquad \text{(A1.30)}$$

Equation A1.30 is an expression of the ratio of the average moment to the true moment of a perfect assembly of dipoles. This ratio is more conventionally referred to as the Langevin function, L(a), and expressed as equation A1.31.

$$L(a) = \coth(a) - \frac{1}{a} \qquad \text{(A1.31)}$$

The Langevin function, when applied to a dielectric, gives a measure of the degree to which the material will polarise under the prevailing conditions of electric field and temperature.

If L(a) is plotted against 'a' (Figure A1.7) it can be seen that at very low temperatures or very high electric fields the function approaches a limiting value. This indicates that under these conditions the alignment of the dipoles in response to the electric field is very nearly perfect.

For a freely rotating dipole, when 'a' is much less than 1, L(A) has a slope which approaches 1/3. Under these conditions it is possible to write,

$$L(a) = \frac{a}{3} \qquad \text{(A1.32)}$$

At room temperature, very high electric fields (in the order of 10^{9} Vm^{-1}) are required to saturate the dielectric. Thus, if the temperature and applied electric field are not too large equation A1.32 can be written as

$$\bar{\mu} = \frac{\mu^{2} \ell}{3kT} \qquad \text{(A1.33)}$$

Using equation A1.33 it is possible to replace the dipole moment function, $f(\mu)$ in equations A1.18 and A1.19 with $\bar{\mu}$. Thus equation A1.18 becomes,

$$P = N(\alpha_e + \alpha_i + \frac{\mu^2 \ell}{3kT}) \qquad (A1.34)$$

equation A1.19 becomes,

$$\chi_e = \frac{N}{\epsilon_0 \ell} (\alpha_e + \alpha_i + \frac{\mu^2 \ell}{3kT}) \qquad (A1.35)$$

and equation A1.17 becomes

$$\epsilon_r = 1 + \frac{N}{\epsilon_0 \ell} (\alpha_e + \alpha_i + \frac{\mu^2 \ell}{3kT}) \qquad (A1.36)$$

These three equations state that for a dielectric which contains freely moveable permanent dipoles the polarisation due to an applied electric field, electronic susceptibility and relative permittivity are all proportional to the number of dipoles present and to the magnitude of the electric field but inversely proportional to the temperature.

A1.3.11. Implications of temperature dependent polarista ion in solid dielectrics.

The above relationships were obtained for dipoles which were free to align themselves with an applied electric field. In solids however, this is not always the case, as an energy barrier may have to be overcome before the dipole can move. This energy is referred to as the activation energy and one of the simplest ways it can be provided is by heating.

When a solid dielectric containing permanent dipoles is heated, the plot of L(a) against a will show a sudden increase when the increase in thermal energy equals the activation energy necessary to allow free movement of the dipoles. This phenomenon has a significant implication for the formation of electrets. When the solid is in its heated state the dipoles present will be aligned with the applied electric field although some disorder will be present due to random thermal agitation. If in this state the temperature is slowly reduced, thermal agitation will be less and less able to disorder the alignment of the dipoles. Eventually the temperature will be such that there will be insufficient thermal energy to allow free movement of the dipoles so that any alignment present will persist even when the applied electric field is completely removed. A dielectric that has been exposed to an electric field and temperature will produce a measurable (dipolar) electric field and will in fact be a classical thermoelectret.

A1.4. Quantum Aspects of Electret Formation.

The application of classical elecrostatic theory cannot adequately explain all of the charge storage effects observed in electrets. It has been demonstrated above that the application of an external electric field to a dielectric containing permanent dipoles can produce an electret that exhibits both positive and negative electric fields on opposite surfaces. Using the same conditions on a dielectric that does not contain permanent dipoles it is possible to obtain an electret that exhibits only a single type of electric field on both faces, ie a monopolar electret. The existence of this type of electret can only be explained by consideration of the electronic structure of the dielectric itself, or to be more precise the electronic behaviour of collections of atoms or molecules.

A1.4.1. Fundamental concepts: Wave particle duality.

Modern physics can be considered to be based upon two fundamental concepts.

1. The quantum hypothesis of Planck which states that energy is not infinitely divisible but exists as very small discrete units or packets called quanta.
2. Mass-energy equivalence relation of Einstein who showed that mass is a form of energy and that the relationship between the mass of a body and the energy to which it was equivalent could be described by equation (A1.37).

$$E = mc^2 \qquad \text{(A1.37)}$$

where E = energy.

m = mass of body.

c = velocity of light.

The energy content of a quantum particle is not free to vary continuously but changes by discrete amounts which are dependent on the frequency of the absorbed or emitted energy (light). This property of quantum particles is aptly demonstrated by considering photoelectric emission. Einstein showed that the emitted radiations (NB not reflected) of an illuminated body were of a fixed wavelength that was independent of the intensity of the incident illumination. Futhermore, the emitted radiations were not observed until the incident radiation was greater than a certain minimum threshold frequency. Einsteins observations were empirically expressed by Planck's hypothesis which relates the energy of an emitted photon to

its frequency, ν.

$$E = h\nu \qquad (A1.38)$$

where h = Planck's constant.

The total amount of energy of a photon can be decribed in two different ways using either Planck's or Einstein's relationship. The total energies of equations (A1.37) and (A1.38) are obviously equal as they refer to the same photon thus,

$$E = mc^2 = h\nu \qquad (A1.39)$$

The relationship between the frequency, ν, and wavelength, λ, allows the velocity of the wave to be calculated, using $\nu\lambda$. Substituting this value for that of c, the velocity of light, in A1.39 gives

$$mc = \frac{h}{\lambda} \qquad (A1.40)$$

Equation (A1.40) is only valid fom quantum particles but is extremely important as it gives the relationship between the mass of a body and its wavelength and allows the body being considered to be described as a wave or a particle.

Equation (A1.40) was derived for a photon, thus photons must have both wavelength and mass. The left hand side of (A1.40) is a product of mass and velocity and can therefore be rewritten as momentum, P.

$$P = m_p c = \frac{h}{\lambda} \qquad (A1.41)$$

where m_p = mass of a photon.

This relationship is known as the de Broglie hypothesis, or concept of wave particle duality. The hypothesis is applicable to all quantum particles so that it is also possible to consider an electron as having both a mass and wavelength.

$$m_e v = \frac{h}{\lambda} \qquad (A1.42)$$

where m_e = mass of the electron.

v = velocity of the electron.

A1.4.2. The Bohr hydrogen atom.

The concept of an electron having both mass and wavelength was extended by Bohr to explain some of the spectroscopic properties observed for the element hydrogen. If is assumed that the electron in a hydrogen atom is moving in a circular orbit (Figure A1.8) of

radius, r, around the proton the electrostatic attraction between the proton and the electron must be balanced by the centripetal acceleration of the electron. This equilibrium can be written as

$$\frac{m_e v^2}{r} = \frac{q_e q_p}{4\pi\varepsilon_0 r^2} \qquad (A1.43)$$

where m_e = Mass of the electron.

q_e = electric charge of an electron = $-q_p$.

q_p = electric charge of a proton.

r = radius of the electrons orbit.

v = speed of the electron.

ε_0 = permittivity of free space.

which in terms of the speed of the electron is

$$v = \frac{q_e}{\sqrt{4\pi\varepsilon_0 r^2}} \qquad (A1.44)$$

If, however, the electron is treated as a wave moving in a circular orbit then the only orbits possible are those which correspond to integer numbers of wavelengths (Figure A1.9). If this were not the case the waveform of the electron would be superimposed on itself when it was out of phase and as a result of the ensuing interference would soon cease to exist. The possible orbits for the electron in a Bohr hydrogen atom can be described by the relationship,

$$n\lambda = 2\pi r \qquad (A1.45)$$

where n = number of wavelengths in the orbit (1,2,3 etc).

Eliminating λ using equation A1.42 and combining the result with equation A1.44 gives

$$\frac{nh}{m_e} = \frac{2\pi r q_e}{\sqrt{4\pi\varepsilon_0 m_e r}} \qquad (A1.46)$$

and on rearranging gives

$$r_n = \frac{\varepsilon_0 n^2 h^2}{\pi m_e q_e^2} \qquad (A1.47)$$

The subscript n in r_n is used to denote that there is an orbit for each interger value of n. This value of n is known as the principle quantum number because it uniquely defines the size of the orbit of the electron.

A1.4.3. Energy levels in the Bohr hydrogen atom.

The result of limiting the orbits of the electron in the Bohr atom to those defined by the principle quantum number, n, is that the

energy of each of these orbits is also as precisely defined as the size of the orbit itself. The total energy of the electron is defined as the sum of its kinetic energy, E_k, due to its movement around the nucleus and its potential energy E_p due to its electrostatic potential V(r). Thus,

$$E_k = \frac{m_e v^2}{2} = \frac{q_e^2}{8\pi\varepsilon_0 r} \qquad \text{(A1.48)}$$

and

$$E_p = \frac{-q_e^2}{4\pi\varepsilon_0 r} \qquad \text{(A1.49)}$$

The total energy, E_t, of the electron is therefore

$$E_t = E_k + E_p \qquad \text{(A1.50)}$$

$$E_t = \frac{-q_e^2}{8\pi\varepsilon_0 r} \qquad \text{(A1.51)}$$

Substituting r_n for r using equation (A1.47) allows the calculation of the permitted energy levels for the electron in a Bohr hydrogen atom.

$$E_t = \frac{-m_e q_e^4}{8\varepsilon_0^2 h^2 n^2} \qquad \text{where n=1,2,3..etc} \qquad \text{(A1.52)}$$

The energy levels given by this relationship and the size of the orbitals to which they correspond are given in Table A1.1. The reference level for the system is taken to be the point where $n = \infty$ because the total energy of the electron approaches zero at this point.

It should be noted that because the charge on the electron is such a small fraction of a coulomb, the energy of an electron is usually discussed in terms of electron volts, eV, rather than joules. An electron volt is defined as the energy required to move an electron through a potential difference of 1 volt and has the magnitude 1.602×10^{-19} J. Conversion from joules to electron volts is done by dividing the energy of the elecron by 1.602×10^{-19}.

A1.4.4. The Schrodinger wave function and its consequences.

The Bohr hydrogen atom represents one method for predicting the properties of electrons. An alternative approach to predicting the properties of an electron was presented by Schrodinger who showed that a wave equation, derived from that used to describe standing waves in a vibrating string, could be used to characterise the behaviour of electrons in a similar manner to that described by the

Bohr theory. Schrodinger's wave theory is an exact description of the atom in that it contains no approximations in its formulation. Furthermore, Schrodinger's theory has been found to agree with experimental results when the Bohr theory does not.

Whilst the detail of Schrodingers theory is beyond the scope of this discussion, some of the consequences of the theory are of great value when considering the further development of the ideas presented with the Bohr hydrogen atom.

Schrodingers theory requires the existence of three quantum numbers. The principle quantum number, which describes the total energy of an electron, performs the same function in both Bohr's and Schrodinger's theories. The remaining two numbers are the azimuthal or angular momentum quantum number, l, which determines the orbital angular momentum of the electron and the magnetic quantum number, m, which determines the orientation of the orbit of the electron when exposed to an external magnetic field. These two quantum numbers are again integer values and have their limits set by the principle quantum number, n. The angular momentum quantum number is able to take integer values from 0 to n-1 and the magnetic quantum number is able to take on integer values from -l to +l. Orbitals in the Schrodinger theory are distinguished by their having a unique set of quantum numbers.

The result of using three quantum numbers to describe each orbit is that for values of the principle quantum number greater than 1 the principal orbit is split into a number of sub orbitals each of which is able to contain two electrons.

Another consquence of Schrodinger's wave theory is that the electron is described in terms of a probability density. This means that the exact position of an electron at any moment in time cannot be determined, although it is possible to define a region in space for which there is a high probability of finding the electron. These regions of high probability correspond to the orbitals defined by the quantum numbers n, l and m, and can be represented by a charge density since the more probable it is that an electron will be found in a particular region then the greater the apparent electrostatic charge in that region.

A1.4.5. The Pauli exclusion principle.

If a collection of isolated Bohr hydrogen atoms are excited

with sufficient energy to enable the electrons to move from the n=1 orbit to the n=2 orbit with lowest energy then, according to Planck's relationship, it would be possible to measure a single wavelength of light due to the quanta of energy emitted when the electrons moved back from the n=2 orbit to the n=1 orbit.

If these atoms were then placed in a strong magnetic field under the same conditions, then, instead of a single wavelength of light being emitted there would be two, a small amount above and below the wavelength observed without the magnetic field. This effect is accounted for by allocating a fourth quantum number, the spin number, m_s, to each orbital. This quantum number refers to the spin of the electron and its associated electric field as it moves in its orbit around the nucleus and can have values of +1/2 or -1/2.

The reason for the appearance of the dual wavelength in the presence of an applied magnetic field is because a spinning electron has a spinning electric field which in turn generates a magnetic field. As the electron can only spin in a clockwise or anti-clockwise direction this magnetic field will either be aligned or opposed to the externally applied field. If the electron has a magnetic field which is aligned with the external field it will require less energy than if its magnetic field were opposed to the applied magnetic field. This difference in the energy requirements for the two possible alignments is the cause of the appearance of two wavelengths.

The difference in the energy requirements due to electron spin are much less than the energy differences due to electrons having different l and m quantum numbers within the same principal orbit. Whilst the splitting of the single energy levels of isolated atoms is only observed under the influence of an applied magnetic field it establishes the important fact that electrons have the property of spin and that this spin can have one of two possible directions. The idea introduced by Schrodinger's theory, that each orbital is described by a unique set of quantum numbers, can be extended to include the spin quantum number. Such an extension was expressed by Pauli in his exclusion priciple which states that no two electrons in an atom may have the same set of four quantum numbers.

The exclusion principle is a means of saying that each orbital is described by a unique set of n, m, and l quantum numbers and that this orbital can contain two electrons only if they have different

spin numbers. Whilst the spin of an electron may seem to be inconsequential it proves to be of major concern when considering the distribution of electrons in more complicated atoms and the changes in energy levels that occur when atoms combine to form crystals or molecules.

A1.4.6. Splitting of energy levels due to electron interaction.

If two of the Bohr hydrogen atoms considered above are allowed to approach each other so that the orbitals of the electrons overlap two possible interactions are possible depending on the spin of the two electrons involved. If the spins of the electrons are parallel they cannot occupy the same orbital by virtue of the Pauli exclusion principle. This is known as the anti-bonding state. However, if the spins of the electrons are anti-parallel then both the electrons are able to occupy the same orbital. This is known as the bonding state.

In both of the above cases a molecule of hydrogen will be formed although it is only in the latter case that a stable entity is achieved. The hydrogen molecule corresponding to the former case will be much less stable than that in the latter case and will therefore be much more likely to revert to its hydrogen atoms.

The explanation for this behaviour can be seen if the electron is examined in terms of charge density. When the orbitals of the electrons overlap the probability density describing the electrons will be different to that of the isolated atom. This difference is reflected by a redistribution of the charge density around the nuclei. Where the electrons have parallel spins the charge density of each of the electrons will tend to move so as to be as far apart as possible from the charge density of the other electron (Figure A1.10). This results in the nuclei of the two atoms being exposed to each other and as a result electrostatic repulsion occurs.

If the interacting electrons have anti-parallel spins they can both occupy the same orbital. The two electrons will therefore move to a position that gives the maximum increase in stability for both atoms. In practice it is found that the charge density of the two electrons moves so as to occupy the space between the two nuclei (Figure A1.10). In this position each of the atoms behaves as though it has a monopoly on the two electrons available and the stability of each atom is therefore increased. The increase in electrostatic

attraction that occurs as a result of this charge redistribution helps to further stabilise the atomic bond. This type of association, where the sharing of the outer electrons gives each nucleus the appearance of having a fully occupied outer orbital, is called a covalent bond.

The possibility for two different types of interaction when the electrons of a Bohr hydrogen atom overlap has an effect on the energy levels available for the electrons of the two atoms in a molecule. In the case of anti-parallel spins the additional electrostatic attraction results in a slight decrease in the size of the n=1 orbital and as a consequence the potential energy of the electron is decreased. It should be noted that because of the way in which the potential energy of an orbiting electron is defined, decreasing its value means that it becomes more negative and so the electron has more potential energy than previously hence the reason for the increase in stability. For parallel spins there is an increase in the size of the orbitals and hence an increase in the potential energy of the electron (using the argument above, the electron now has less potential energy).

The energy level of the isolated atom has therefore been split due to the formation of a hydrogen molecule (Figure A1.11). However, for isolated atoms, the probability function that describes the outer electron theoretically allows the electron to be anywhere and not just restricted to areas of very high probability. Under these circumstances it is possible for the outer electrons of two Bohr hydrogen atoms to interact in the manner described above even though a hydrogen molecule has not been formed. The degree to which the energy level of the outer electrons are split will be dependent on the distance between the two atoms. It is therefore reasonable to assume that energy differences between the parallel and anti-parallel interaction can vary in a continuous manner from 0, when the two atoms are separated by an infinite distance to the maximum when a molecule is formed.

If a large group of hydrogen atoms are considered it is possible to see that the the outer electron of any one atom can interact with the outer electron of any other hydrogen atom, although , because of the Pauli exculsion principle, only one such interaction may occur at any point in time for any given electron. The result of this is that the outer electron of a Bohr hydrogen atom can reside in any one of a

large number of closely spaced energy levels. Thus, in a group of atoms the single energy levels of the outer electron becomes a band (Figure A.11) within which the electron is relatively free to move. It should be noted that this splitting of the energy level occurs only in the presence of other atoms and does not require the application of an external magnetic field.

A1.4.7. Splitting of energy levels of electrons in crystals.

When a number of Bohr hydrogen atoms are brought together to form a crystal the number of quantum states available, as defined by the four quantum numbers, is not changed. For example, in the hydrogen molecule each atom still only has the same number of n=1 orbitals as the isolated atom. However, in a hydrogen crystal containing N atoms the single energy level will be split into N energy levels each of which is able to contain two electrons in accordance with the Pauli exclusion principle and which is closely related to the original energy level. The quasi-continuous bands that are formed are known as the allowed energy bands and the gaps that separate them, the forbidden energy bands (Figure A1.12). In addition, the outermost occupied allowed energy band is known as the valence band as this is where the valence electrons of an atom reside. The empty, allowed energy band above the valence band is known as the conduction band. Interaction between atoms occurs when the orbits of the electrons in the valence band overlap with orbitals of an equivalent energy in other atoms or molecules.

If a hypothetical hydrogen crystal is cooled to absolute zero, 0K, the electrons will lose energy and occupy the lowest energy levels available in the n=1 energy band (Figure A1.13). However, because only one electron is contributed by each hydrogen atom half of the available sublevels in the n=1 energy band will be empty. If a small electric potential, 6V, is applied across the ends of a metre long crystal the energy available to any electron will be approximately $6x10^{-10}$ eV (from 6V/m across a distance of 10 nanometres). This small amount of energy is sufficient to move the electron into a higher energy level within the allowed band where it can move under the influence of the applied electric field. The hydrogen crystal can therefore be considered as a conductor scince electrons can flow in the crystal when an electic field is applied.

If, instead of hydrogen, the crystal was composed of helium then all the sublevels in the lowest energy band would be fully occupied because each electron would have contributed two electrons (Figure A1.13). The application of the 6V electric field cannot therefore promote any electron into a higher energy level within the band as they are all occupied. The energy gap between the lowest band where n=1 and the next highest energy band where n=2 is of the order of 10eV so that the applied electric field cannot impart sufficient energy to move an electron from the n=1 allowed band to the n=2 allowed band. In these conditions no electron can move under the influence of the applied electric field and the helium crystal is therefore an insulator. A crystal of Lithium (Figure A1.13) has three electrons so that the first n=2 sublevel would be occupied although only half full. Lithium would therefore be a conductor in the same manner as hydrogen.

If the crystal above were composed of beryllium (Figure A1.13) then the n=2 suborbital would be completely filled with electrons and consequently it would be expected that beryllium, like helium, would be an insulator. This , however, is not the case as beryllium does conduct electricity. The reason for this apparant contradiction is that the three n=2 orbitals have overlapped (Figure A1.14) when their corresponding atomic energy level was split into a band on formation of the crystal. This overlap allows electrons to freely move between the three n=2 energy levels available. This overlapping of the energy bands of the n=2 suborbitals means that the next insulator is neon where the gap between the n=2 and n=3 orbits is wide enough to prevent the relevant energy bands from overlapping.

1.4.8. Energy levels in impure crystals.

Thus far the discussion has been limited to identical atoms and crystals of identical atoms. However, in practical terms such purity is very rare and crystals always have some foreign atoms present. These foreign atoms have a very important role to play in the mechanism for charge storage in monopolar electrets.

The effect of foreign atoms is best examined when considering a crystal of an insulator where the valence band has a full complement of electrons and the conduction band is unoccupied. The introduction of foreign atoms into this crystal will introduce energy levels into the crystal that were previously in a forbidden band. There are now

two possibilities of interest. The first occurs when the valence band of the foreign atom lies just above the valence band of the insulator and the second when the valence band of the foreign atom lies just below that of the conduction band of the insulator (Figure A1.15).

In both cases the application of a small electric field will fail to produce any movement of electrons. However, as the magnitude of the electric field is increased a point will be reached where an electrical current will flow. The magnitude of this field will be much less than that required to promtote an electron in the valence band of the insulator to the conduction band of the insulator.

In the first case above, the electric field was sufficient to promote an electron from the valence band of the insulator into the valence band of one of the foreign atoms. The valence band of the insulator was no longer full and as a consequence electrons were able to move under the influence of the applied electric field. Such a material is known as a semiconductor because under normal conditions it behaves as an insulator but if an electric field above a specific value is applied it becomes a conductor. In this case the foreign atoms are known as acceptor atoms because they acccept an electron from the valence band of the insulator.

In the second case above it was not possible for the electrons in the valence band of the conductor to be promoted into the valence band of the foreign atom because the energy gap was too wide. However, it was possible for electrons in the valence band of the foreign atom to be promoted into the conduction band of the insulator. Once promoted electrons were free to move under the influence of the electric field and the crystal was able to conduct elecricity. In this case the foreign atoms are known as donor atom because they donate an electron to the conduction band of the insulator.

In both of these cases it is not possible for conduction to occur purely as a result of movement in the valence band of the foreign atoms because the distance between individual atoms is too great to form a continuous energy level.

Using the properties of a semiconductor it is possible to explain how a monopolar electret can store charge. The classical method for forming an electret is to place a sample on an earthed surface and then to expose it to heat and a relatively strong

electric field ($\xi > 50 kV\ m^{-1}$) usually by placing a charged electrode above, but not in contact with, the sample to be charged. After a period of time the sample is allowed to cool whilst still under the influence of the electric field. For a semiconducter this has two interesting consequences.

If the semiconducter contains donor atoms and the electric field causes a net loss of charge in the semiconductor crystal then the donor levels will be depleted. Eventually an equilibrium will be reached where the loss of electrons from the semiconductor will be balanced by the injection of free electrons into the body of the sample. If in this state the semiconductor is cooled there will be insufficient electrons present in the conduction band to fill all the vacated donor atoms. As a result there will be a net positive charge left on the semiconductor.

In a similar manner if the semiconductor contains acceptor atoms and the electric field causes a net increase in charge in the semiconductor the all the acceptor atoms will become filled. The vacant sites in the valence band will then be occupied by the incoming electrons until there are no longer any unoccupied energy levels in the valence band. If in this state the semiconductor is cooled the excess electrons at the acceptor sites will not be able to move back to the valence band. As a result there will be a net negative charge left on the semiconductor.

It should be noted that in both these cases it has been assumed that electrons can move freely into and out of the semiconductor at an elevated temperature but not when cool. This type of behaviour is possible and can be predicted by consideration of the discussion above.

Principle quantum number	Radius of orbital (x 10^{-12} m)	Energy level of orbital (x10^{-15} J)	Energy level of orbital (eV)
1	52.9266	-2179.5388	-13.6035
2	211.7065	-544.8847	-3.4009
3	476.3397	-242.1710	-1.5115
4	846.8262	-136.2212	-0.8502
5	1323.1659	-87.1816	-0.5441
6	1905.3589	-60.5427	-0.3779
7	2593.4051	-44.4804	-0.2776
8	3387.3047	-34.0553	-0.2126
9	4287.0575	-26.9079	-0.1679
10	5292.6636	-21.7954	-0.1360

Table A1.1. Radius of the orbital and the corresponding energy levels (in Joules and electron Volts) for the electron in the hypothetical Bohr hydrogen atom.

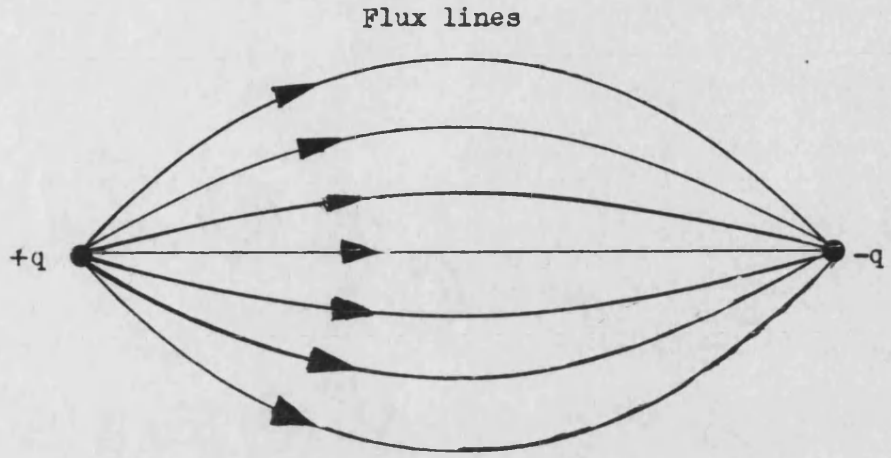

Figure A1.1. Lines of force between charges of opposite sign. The direction of the force is indicated by the arrowheads.

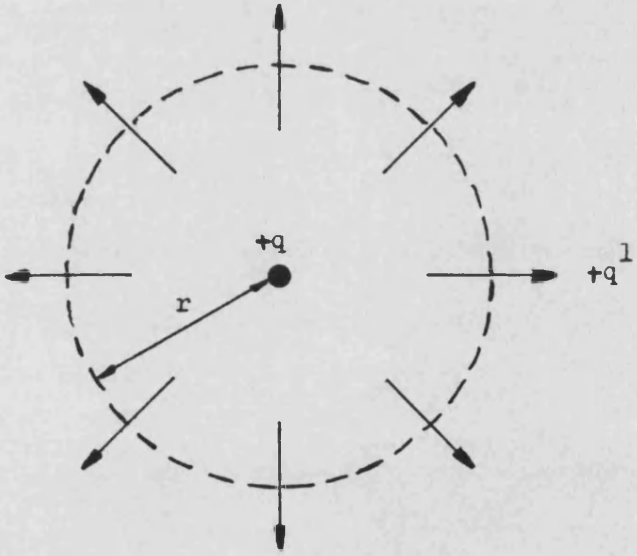

Figure A1.2. Lines of force acting between to charges of the same sign. Placing the charge $+q'$ anywhere on the circle of radius, r, will cause it to experience a force pushing it away from +q.

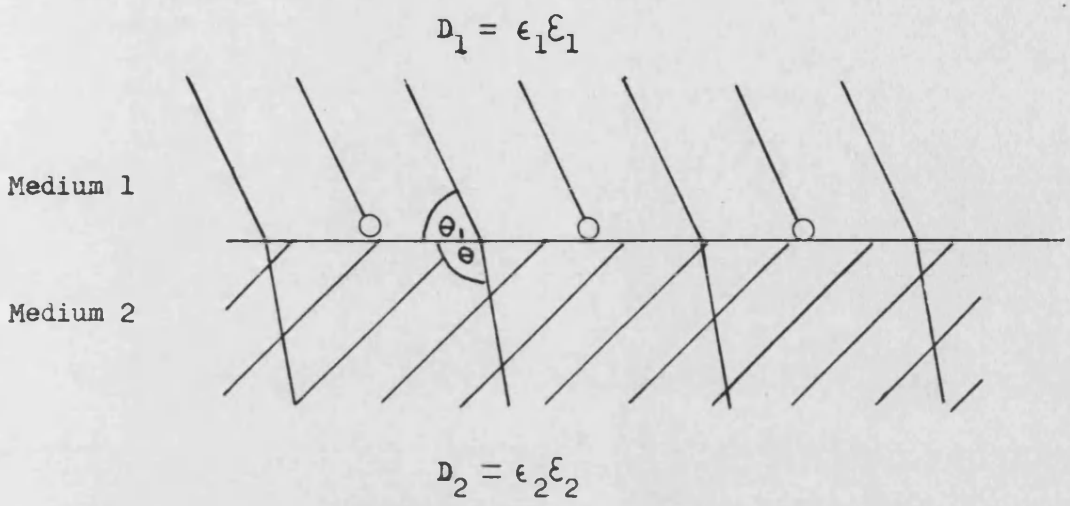

Figure A1.3. Change in the displacement, D, across the boundary between two dielectrics and the layer of charge, O, associated with it.

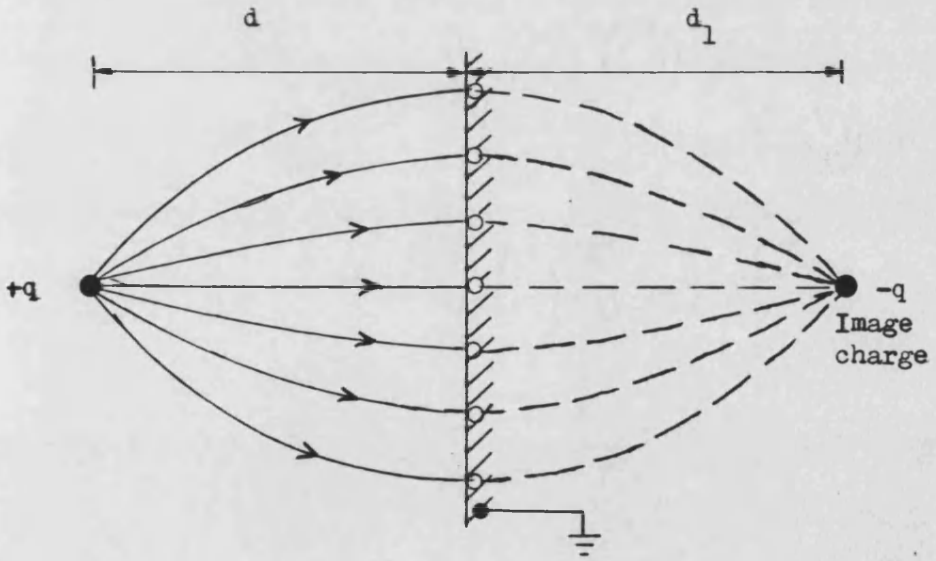

Figure A1.4. Image charge induced in an earthed conducting plane due to presence of a real charge.

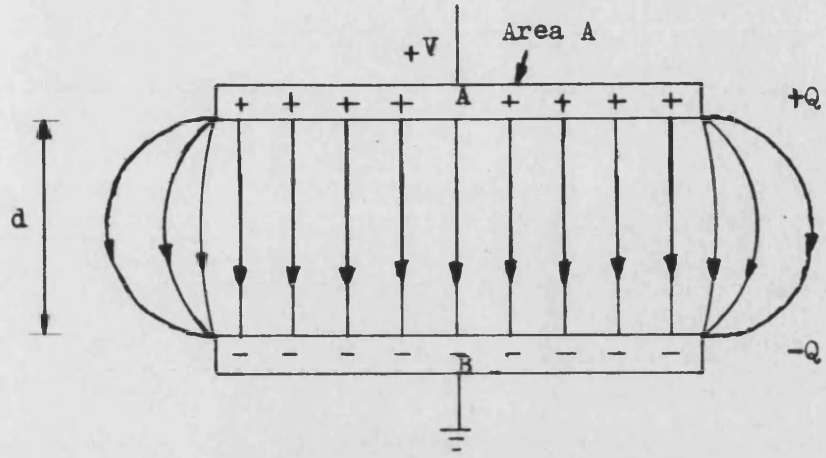

Figure A1.5. The parallel plate capacitor showing the lines of flux between the two plates

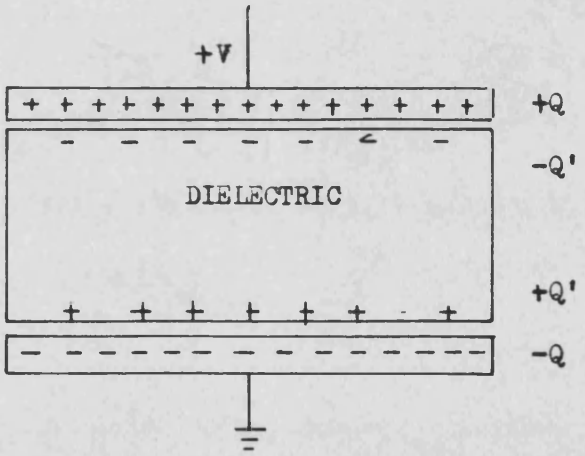

Figure A1.6. Effect of inserting a dielectric between the plates of atne capacitor illustrated in Figure A1.4.

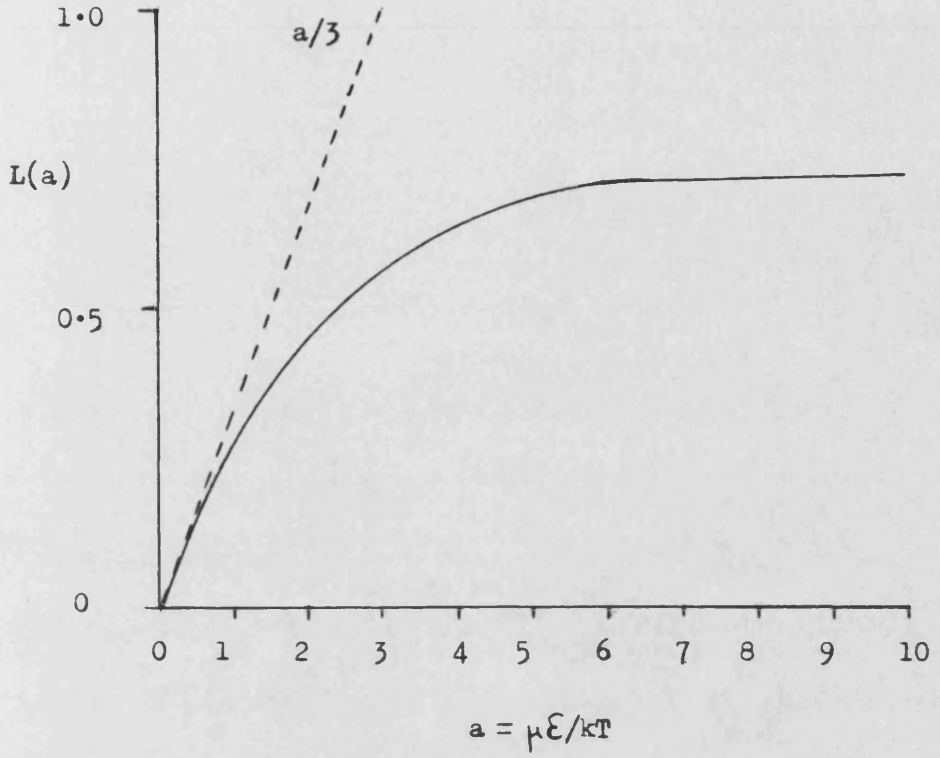

Figure A1.7. Response of a perfect dipole gas to an electric field as determined by the Langevin function. Note that when a is less than 1 the slope of the curve approaches 1/3.

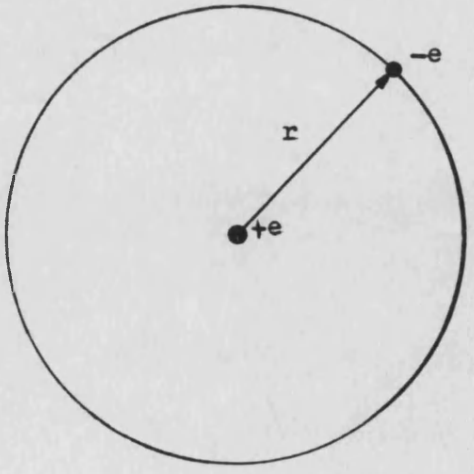

Figure A1.8. Simplified representation of the hydrogen atom.

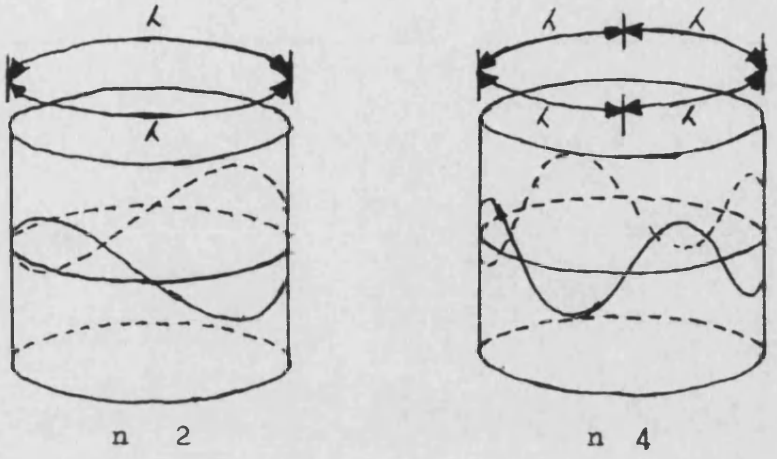

Figure A1.9. Possible orbitals for the hydrogen atom illustrated in Figure A1.8.

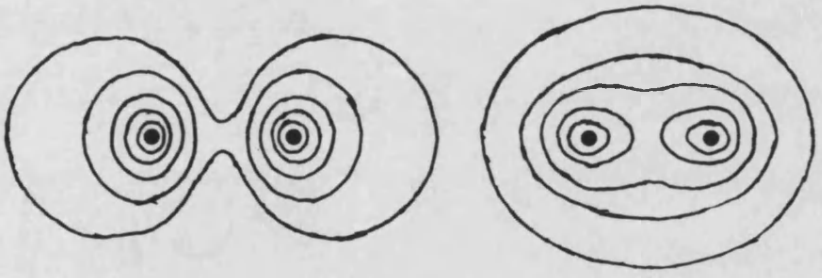

Figure A1.10. Electron densities around hydrgen atoms where the spins on the electron are parallel and antiparallel.

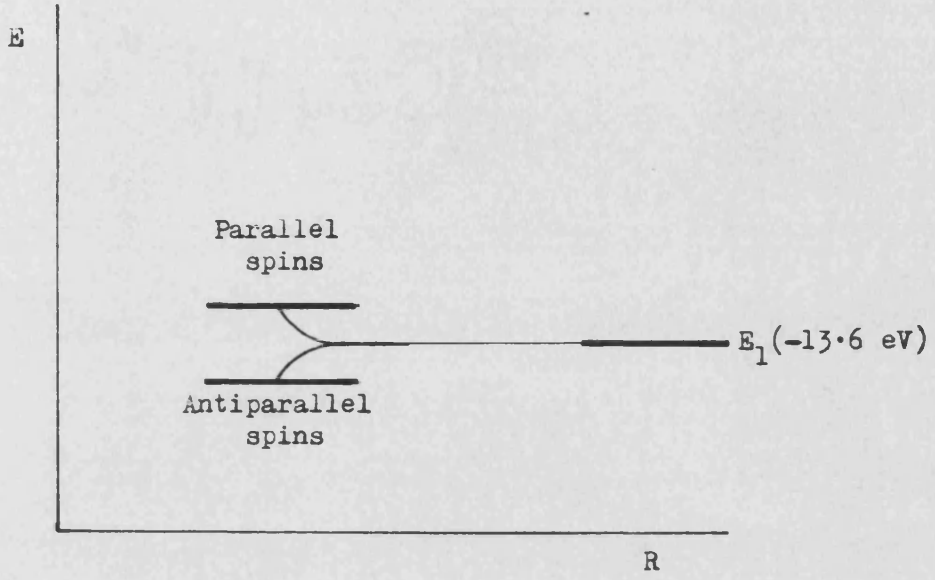

Figure A1.11. The splitting of the lowest energy level in the hydrogen atom due to the formation of a parallel or antiparallel hydrogen bond.

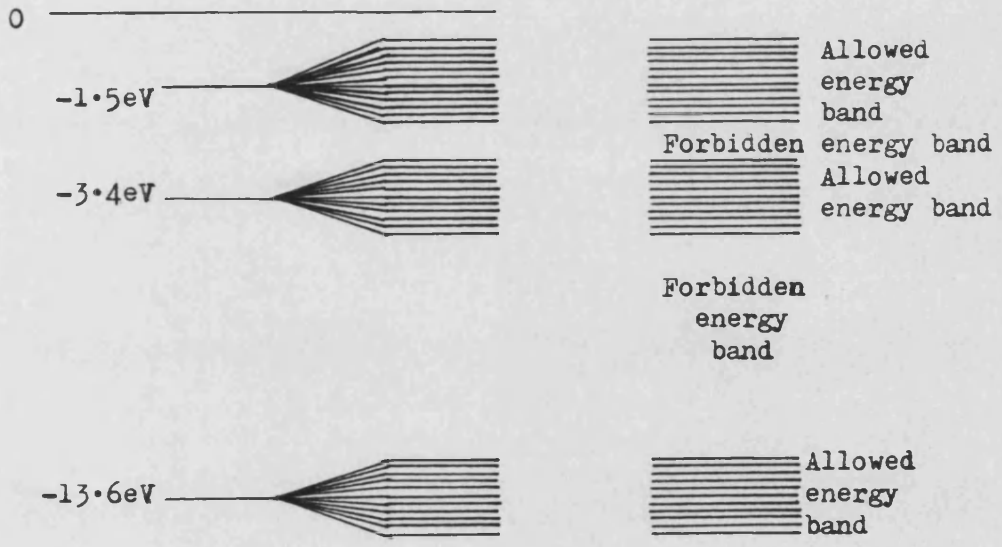

Figure A1.12. The energy bands for a hypothetical crystal of hydrogen atoms and energy band terminology.

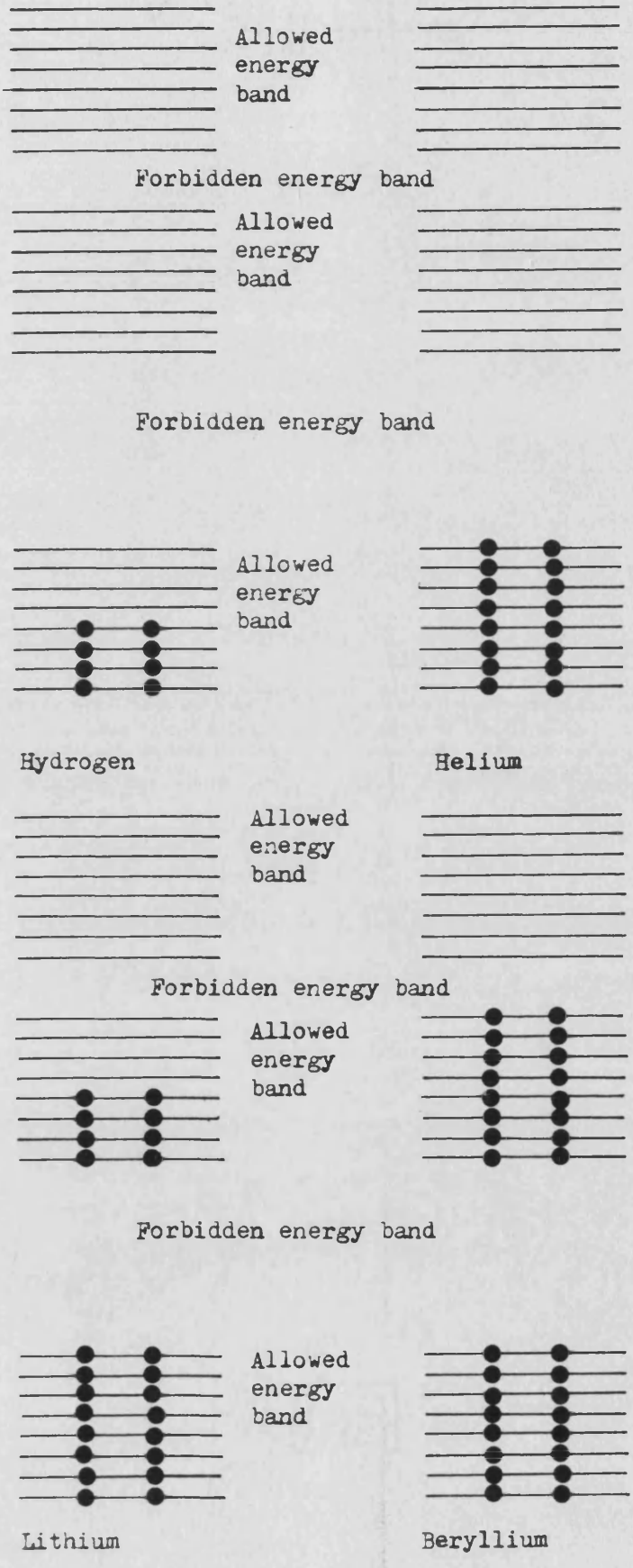

Figure A1.13. Filling of the energy levels for hypothetical crystals at $0^{\circ}K$

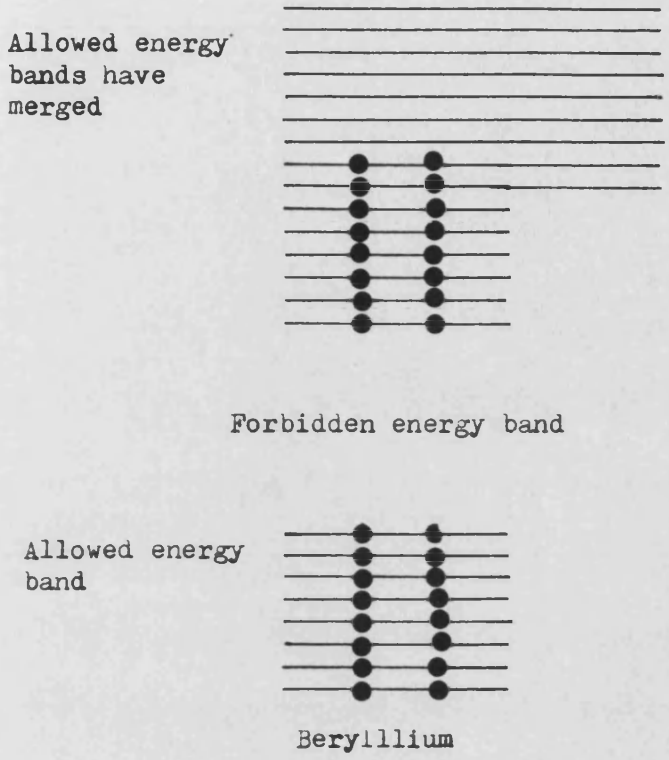

Figure A1.14. Actual filling of the energy levels for the beryllium crystal. Beryllium is a conductor because the three $n = 2$ suborbitals have merged to form a continuous energy level.

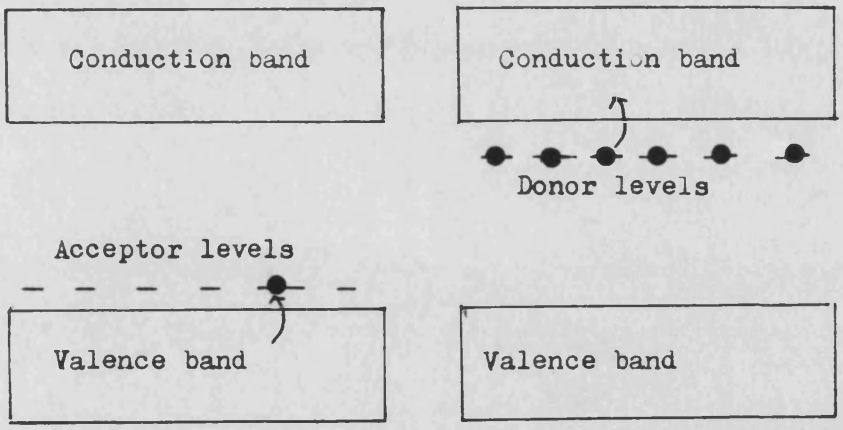

Figure A1.15. The presence of acceptor levels above a full valence band will allow conduction by 'holes' if an electron is promoted. The presence of donor levels below an empty conduction band will allow conduction if an electron is promoted. Note it is possible to have both donor and acceptor sites present simultaneously. Deep traps are acceptor levels which have a large energy diffrence between them and the valence band.

Appendix 2.

A2. Image analysis software source code listings.

The source code listings below represent the software written to perform image analysis on the BBC microcomputer using a sideways ram board and a video digitising interface. The final program to produce isometric drawings of digitised images was written in the 'C' programming language (222) on a Sinclair QL microcomputer fitted with a 512k memory expansion card (giving a total of 640k memory) and disc interface.

In general, the image analysis software consists of programs written in BBC BASIC with specific routines written in 6502 machine code (221, 223) using the resident assembler of BBC BASIC where speed or critical timing were necessary. To conserve space the machine code sections were written as independent modules which could be loaded into a specific area of memory and run. The area of memory utilised for this purpose was the unused disc buffer area located from &1200 to &18FF. Page &12 was allocated for variables used by the machine code routines and &1300 to &18FF used for the actual program code.

All the code reproduced below has been transferred directly from disc to minimise transcription errors. The condensed text of this appendix has been employed deliberately to prevent problems arising when long code lines are wrapped onto the next line. In addition sufficient space is available to comment the machine code programs without breaking the flow of the program.

All programs were run using a mode 1 graphics screen in a disc based BBC system. This arrangement left approximately 5.75k of memory for all the BASIC programming tasks required. For this reason several of the BASIC programs are very similar apart from one or two procedures.

A2.1 and A2.2. BASIC program SPR128.

This BASIC program was written to perform general purpose image analysis. It is highly dependent on a number of machine code routines described below. It allows digitised images to be collected, saved or loaded from disc, limited arithmetical manipulation, binary screen dumps, access to the operating system command line interpreter and several other basic functions. This program (in a slightly modified form) was used to obtain digitised images for later processing by COMPOS. Earlier versions of this program were called SUPER, short for supervisor program, and this name may be referred to in some comment lines. Where this is the case program SPR128 should be referred to instead.

```
IF PAGE<>&1900 THEN PAGE=&1900:CHAIN"":0.B.SPR12B"
MODE 1
PROC_init
REPEAT:PROC_menu1:UNTIL an$="e"
END

DEF PROC_init
@%=0:DIM qx(30),qy(30),f$(10):op$="":lastop$="null"
bank1$="null":bank2$="null"
FOR L%=0 TO 10: f$(L%)="null":NEXT
FOR L%=0 TO 16:L%?&1290=255:NEXT
?&1290=20:?&1291=40:?&1292=60:PROC_win
ENDPROC

DEF PROC_win
VDU 22,1,24,0;0;1023;10 3;28,32,31,39,0
ENDPROC

DEF PROC_menu1
LOCAL used:REPEAT
```

```
*FX 15,0
*DISC
VDU 24,0;0;1023;1023;28,32,31,39,0
used=NOT TRUE
CLS
PRINTTAB(0,3)"Analyse"TAB(0,4)"View"TAB(0,5)"Oscli"
PRINTTAB(0,7)"Load"TAB(0,8)"Save"TAB(0,9)"Colours"
PRINTTAB(0,10)"Quit"TAB(0,24)"bank1"TAB(0,25)bank1$
PRINTTAB(0,28)"bank 2"TAB(0,29)bank2
REPEAT
an$=GET$
UNTIL INSTR("AVOSQLC",a$)>0
IF an$="Q" THEN END
IF an$="A" THEN PROC_analyse :used=TRUE:VDU 22,1
IF an$="V" THEN PROC_view :used=TRUE
IF an$="O" THEN PROC_oscli :used=TRUE
IF an$="L" THEN PROC_filer :used=TRUE:VDU 22,1
IF an$="S" THEN PROC_filer :used=TRUE:VDU 22,1
IF an$="C" THEN PROC_colours :used=TRUE
UNTIL used
ENDPROC

DEF PROC_view
LOCAL an$:REPEAT
*FX 15,0
VDU 28,32,20,39, 6,12
PRINTTAB(0,1)"Bank 1"TAB(0,2)"Bank 2"
an$=GET$
UNTIL INSTR("12E",a$)>0
IF an$="E" THEN ENDPROC
IF an$="1" THEN ?&1200=8 ELSE ?&1200=12
?&1270=4:?&1272=3:?&1273=&FF:?&1280=0:?&1281=1
?&1282=16:?&1283=17
*:0.6.DISPLAY
VDU 28,32,31,39,0,12
ENDPROC

DEF PROC_oscli
LOCAL cl$:VDU 22,0
PRINT"Operating System Command Line Interpreter"
VDU 28,0,31,79,2
REPEAT
*FX 15,0
INPUTLINE">>>>"cl$:CLS:OSCLI(cl$)
UNTIL cl$="":PROC_win:*FX 15,0
ENDPROC

DEF PROC_colours
LOCAL L%,K%,VLUE%
VDU 22,0
PRINTTAB(3,2)"Colour assignments"
VDU 28,0,31,79,4
REPEAT
CLS
FOR L%=0 TO 16
PRINTTAB(0,L%+3)"Logical colour ";L%
PRINTTAB(20,L%+3)"old grey level = ";L%?&1290
PRINTTAB(50,L%+3)"new grey level ="
```

```
NEXT
L%=-1
REPEAT
L%=L%+1
REPEAT
PRINTTAB(68,L%+3)" "
*FX 15,
INPUTTAB(68,L%+3)VLUE%
UNTIL VLUE%)=0 AND VLUE%<=255
IF VLUE%=0 PRINTTAB(68,L%+3)L%?&C90 ELSE L%?&1290=VLUE%
UNTIL L%?&1290=255
FOR L%=0 TO 16:PRINTTAB(68,L%+3)L%?&1290:NEXT
PRINTTAB(10,25)"Are these colour definitions O.K.";
PRINT" 'Y' or 'N'"
UNTIL GET$="Y"
PROC_win
ENDPROC

DEF PROC_filer
LOCAL action$,op$
REPEAT:VDU 22,0:
PRINTTAB(20,0)"Procedure filer"
PRINTTAB(5,2)"Last operation was"TAB(40,2)lastop$
REPEAT:REPEAT:VDU28,0,10,79,3,12
PRINTTAB(0,5)"Load" TAB(10,5)"Save" TAB(20,5)"Exit":an$=GET$
UNTIL INSTR("LSE",a$)>0
IF an$="E" THEN UNTIL TRUE:UNTIL TRUE:PROC_win:ENDPROC
op$=an$
IF op$="L" THEN file$=FN_filename:bank=FN_bank
IF op$="S" THEN bank=FN_bank:file$=FN_filename
CLS
IF op$="L" THEN action$="LOAD files "+file$+" to bank "+STR$(bank)
IF op$="S" THE action$="SAVE bank "+STR$(bank)+" to files "+file$
IF bank=1 THEN bank1$=file$ ELSE bank2$=file$
PRINTTAB(5,1) "Curret operation is" TAB(40,1) action$
REPEAT
PRINTTAB(0,5) "Go" TAB(10,5)"New name/bank" TAB(30,5)"Exit"
an$=GET$
UNTIL an$="G" OR an$="N" OR an$="E"
IF an$="E" THEN UNTIL TRUE:UNTIL TRUE:ENDPROC
UNTIL an$="G"
IF bank=1 THEN bank=8 ELSE bank=12
IF op$="L" THEN OSCLI("*LOAD :0.6.MOVEUP") ELSE OSCLI("*LOAD :0.6.MOVDWN")
FOR loop=1 TO 4
IF op$="L" THEN OSCLI("*LOAD "+file$+STR$(loop)+" 4000"):?&1200=loop+bank-1:CALL &1300
IF op$="S" THEN ?&1200=bank+loop-1:CALL &1300:OSCLI("*SAVE"+file$+STR$(loop)+"4000+4000")
NEXT
lastop$=action$
UNTIL FALSE
ENDPROC

DEF FN_bank
LOCAL ans
VDU 28,0,15,79,8:REPEAT:CLS
PRINTTAB(0,1)"Bank 1" TAB(10,1)"Bank 2":ans=GET-48
UNTIL ans=1 OR ans=2
CLS:VDU 28,0,10,79,3
=ans
```

```
DEF FN_filename
LOCAL name$,loop,ans,an$
REPEAT
VDU 28,0,23,79,16
CLS
FOR loop=0 TO 4
PRINTTAB(5,loop)"f";loop TAB(9,loop)f$(loop)
PRINTTAB(40,loop)"f";loop+5 TAB(49,loop)f$(loop+5)
NEXT
REPEAT
PRINT AB(10,6)"Press function key for file, return for user defined"
*FX 225,48
ans=GET
UNTIL ans>=48 AND ans<=57 OR ans=13
IF ans=13 THEN name$=FN_filename2 ELSE name$=f$(ans-48)
REPEAT
CLS
PRINTTAB(10,3)"Current name is " TAB(40,3)name$
PRINTTAB(0,6)SPC(70)TAB(10,6)"Yes" TAB(20,6) "No"
an$=GET$
UNTIL an$="N" OR an$="Y"
UNTIL an$="Y"
CLS
VDU 28,0,10,79,3
=name$

DEF FN_filename2
LOCAL name$,drive$,dir$
REPEAT
CLS
VDU 28,0,24,79,31
PRINTTAB(20,0)"User defined filename"
INPUTTAB(10,2)"Drive is ",drive$
INPUTTAB(10,3)"Directory is ",dir$
INPUTTAB(10,4)"Generic name is ",name$
PRINTTAB(5,6)"Press function key to attach name else RETURN"
ans=GET
UNTIL ans>=48 AND ans<=57 OR ans=13
name$=":"+LEFT$(drive$,1)+"."+LEFT$(dir$,1)+"."+LEFT$(name$,7)
IF ans>13 f$(ans-48)=name$
=name$

DEF PROC_analyse
LOCAL coords,y%:tfnd=0
FOR y%=0 TO 1023 STEP 4
MOVE 0,y%
PLOT 76,0,y%
coords=FN_read_xy
IF coords MOD &FFFF<1023 THEN PROC_area((coords MOD &FFFF)+4,coords DIV &FFFF)
NEXT y%
ENDPROC

DEF FN_read_xy
X%=&70:Y%=&00:A% &0D:K%=USR(&FFF1):=!&74

DEF PROC_q(tx%,ty%)
IF (qt+1) MOD 30=qh THEN ENDPROC
```

```
qx(qt)=tx%:qy(qt)=ty%
qt=(qt+1) MOD 30
ENDPROC

DEF PROC_uq
IF (qh+1) MOD 30=qt THEN ENDPROC
cx%=qx(qh):cy%=qy(qh)
qh=(qh+1) MOD 30
ENDPROC

DEF PROC_area(startx,starty)
qh=0:qy 0:fnd=0:mxx=0:mxy=0:mnx=&FF:mny=&FF:cx%=0:cy%=0:ctr=0
PROC_q(startx,starty)
REPEAT
PROC_test(cx%+4,cy%)
PROC_test(cx%-4,cy%)
PROC_test(cx%,cy%+4)
PROC_test(cx%,cy%-4)
UNTIL (qh+1) MOD 30=qt
PROC_pdata
ENDPROC

DEF PROC_test(x,y)
IF POINT(x,y)<=0 THEN ENDPROC
GCOL0,0:PLOT 69,x,y:fnd=fnd+1:tfnd=tfnd+1
IF cx>mxx THEN mxx=cx
IF cx<mnx THEN mnx=cx
IF cy>mxy THEN mxy=cy
IF cy<mny THEN mny=cy
PROC_q(x,y)
ENDPROC

DEF PROC_pdata
@%=&00020208:ctr=ctr+1
*fx 3,2
VDU 2
PRINT ctr,mnx,mxx,mny,mxy,fnd,tfnd,CHR$(13)
VDU 3 *FX 3,0
ENDPROC
```

A2.3. Machine code program DI61.

This is the 6502 Assembler listing of the machine code routine used by SPR128 to digitise an image over a specified number of frames. In order to do this the summed values corresponding to each pixel must be held as 16 bit numbers. This is done by utilising both image frames, frame 1 (&0B to &0B) holding the most significant byte of the 16 bit number and frame 2 (&0C to &0F) holding the least significant byte.

When called, the program expects to find the total number of frames to digitise at location &1200. As each frame is captured it is added to the sum of the previous frames. When all frames have been captured and summed, each pixel value is repeatedly multiplied by 2 until a pixel, anywhere in the digitised frame, has had its most significant bit set to 1. The most significant 8 bits of the summed values will then be in frame 1(ram blocks 8 to &B) and this is the data saved as the digitised image.

This method of digitising an image ensures that the brightest end of the total average grey scale is used and that it is mapped onto the available grey scale resolution in a linear manner.

```
REM variables declaration

framectr=&1200
pagectr=&1201
blockctr=&1202
lowptr=&1203
highptr=&1204
shiftctr=&1205
temp=&1206

paging_reg=&FE30

iop=&FE60
via=&FE62

bus1mhz=&FD00

dataptr=&70

FOR LX=0 TO 3 STEP 3
P%=&1300
[OPT LX

.entry_point
        JSR wipe_sideways_ram
.entry1
        JSR digitise_one_frame
        DEC fram ctr
        BNE entry1
        JSR get_shift
        JSR select8msbits
        LDA #&02
        STA paging_reg
        CLI
        RTS

.wipe_sideways_ram
        LDX #&08
        LDA #&00
        STA dataptr
.wipe1
        LDA #&80
        STA dataptr+1
        LDA #&40
        STA pagectr
        LDA #&00
        LDY #&00
        STX paging_reg
.wipe2
        STA (dataptr),Y
        INY
        BNE wipe2
        INC dataptr+1
        DEC pagectr
        BNE wipe2
        INX
        CPX #&10
```

```
        BNE wipe1
        RTS

.digitise_one_frame
        SEI
        LDA #&04
        STA blockctr
        LDA #&08
        STA lowptr
        LDA #&0C
        STA highptr
        JSR setout
        JSR masset
        JSR frameset
        LDA #&00
        STA dataptr
        LDA #&FF
        STA shiftctr
.digitise1
        LDA #&80
        STA dataptr+1
        LDA #&40
        STA pagectr
        LDY #&00
.toplins
        LDA iop
        AND #&04
        BEQ toplins
        JSR frameset
        JSR frameset
        JSR frameset
        JSR frameset
        LDX shiftctr
        BEQ toplins1
        LDA #&00
        STA shiftctr
        JMP toplins
.toplins1
        LDX #&14
.pixh1
        LDA iop
        AND #&01
        BNE pixh1
.pixl1
        LDA iop
        AND #&01
        BEQ pixl1
        DEX
        BNE pixh1
.pixh2
        LDA iop
        AND #&01
        BNE pixh2
.pixl2
        LDA iop
        AND #&01
        BEQ pixl2
        LDA highptr
```

```
        STA paging_reg
        LDA (dataptr),Y
        STA temp
        LDA lowptr
        STA paging_reg
        LDA (dataptr),Y
        CLC
        ADC busimhz
        STA (dataptr),Y
        LDA temp
        ADC #&00
        LDX highptr
        STX paging_reg
        STA (dataptr),Y
        INY
        BNE pixh2
        INC dataptr+1
        DEC pagectr
        BNE toplins
        INC lowptr
        INC highptr
        DEC blockctr
        BEQ digitise2
        JMP digitise1
.digitise2
        RTS

.get_shift
        LDX #12
        LDA #&00
        STA dataptr
        STA temp
.get1
        LDA #&80
        STA dataptr+1
        LDA #&40
        STA pagectr
        LDY #&00
        STX paging_reg
.get2
        LDA (dataptr),Y
        ORA temp
        STA temp
        INY
        BNE get2
        INC dataptr+1
        DEC pagectr
        BNE get2
        INX
        CPX #16
        BNE get1
        LDX #0
        LDA temp
        BMI get4
.get3
        INX
        ASL temp
        BPL get3
```

```
.get4
        STX shiftctr
        RTS

.select8msbits
        LDA #&04
        STA blockctr
        LDA #&08
        STA lowptr
        LDA #&0C
        STA highptr
        LDA #&00
        STA dataptr
.select1
        LDA #&80
        STA dataptr+1
        LDA #&40
        STA pagectr
.select2
        LDA lowptr
        STA paging_reg
        LDA (dataptr),Y
        STA temp
        LDA highptr
        STA paging_reg
        LDA (dataptr),Y
        LDX shiftctr
.select3
        ASL temp
        ROL A
        DEX
        BNE select3
        STA (dataptr),Y
        INY
        BNE select2
        INC dataptr+1
        DEC pagectr
        BNE select2
        INC highptr
        INC lowptr
        DEC blockctr
        BNE select1
        LDA #&02
        STA paging_reg
        RTS

.setout
        LDA #10
        STA via
        STA iop
        RTS

.masset
        LDA #2
        STA iop
        LDA #10
        STA iop
        RTS
```

```
.frameset
        LDX #10
.frameset1
        LDA #8
        STA iop
        DEX
        BNE frameset1
        LDA #10
        STA iop
        RTS
]
NEXT
*SAVE :0.6.DIG1 1300 17FF 1300
END
```

A2.4. Machine code program DIG2.

This is a second version of the image digitising routine demonstrated in DIG1. The only difference between DIG2 and DIG1 is in the method used to process the summed pixel values. In this case, once the summed pixel values have been collected, the digitised image is searched to ascertain the maximum and minimum brightness levels. The minimum value is then subtracted from the maximum value to give the range of grey levels recorded. This range of grey levels is then mapped onto the 256 grey levels available by subtracting the minimum brightness value from each pixel, multiplying the resulting value by 256 and then dividing by the recorded range of brightness values. This method of digitisation expands or compresses, as appropriate, the recorded grey level range so that it always occupies the full grey level range that can be represented by a single frame buffer.

To avoid unnecessary repetition, the source listing for DIG2 has only been given where it differs from DIG1.

```
REM variables declaration

framectr=&1200
pagectr=&1201
blockctr=&1202
lowptr=&1203
highptr=&1204
shiftctr=&1205
temp1=&1206
divend1=&1206
temph=&1207
divendh=&1207
maxh=&1208
divisorh=&1208
max1=&1209
divisor1=&1209
minh=&120A
min1=&120B
quotient1=&120E
quotienth=&120F
counter=&1210

paging_reg=&FE30

iop=&FE60
via=&FE62
```

```
bus1mhz=&FD00

dataptr=&70

FOR L%=0 TO 3 STEP 3
P%=&1300
[OPT L%

.entry_point

/These two subroutine calls should be used in place of select8msbits in DIG1

        JSR maxmin
        JSR scale

.maxmin
        LDA #&00
        STA maxl
        STA maxh
        LDA #&FF
        STA minh
        STA minl
        LDA #&08
        STA lowptr
        LDA #&0C
        STA highptr
        LDA #&00
        STA dataptr
.maxmin1
        LDA #&80
        STA dataptr+1
        LDA #&40
        STA pagectr
        LDY #&00
.maxmin2
        LDA lowptr
        STA paging_reg
        LDA (dataptr),Y
        STA templ
        LDA highptr
        STA paging_reg
        LDA (dataptr),Y
        STA temph
        LDA temph
        CMP maxh
        BCC maxmin3
        LDA templ
        CMP maxl
        BEQ maxmin3
        BCC maxmin3
        LDA temph
        STA maxh
        LDA templ
        STA maxl
.maxmin3
        LDA temph
        CMP minh
        BEQ maxmin3a
```

```
        BCS maxmin4
.maxmin3a
        LDA templ
        CMP minl
        BCS maxmin4
        LDA temph
        STA minh
        LDA templ
        STA minl
.maxmin4
        INY
        BNE maxmin2
        INC dataptr+1
        DEC pagectr
        BNE maxmin2
        INC lowptr
        INC highptr
        LDA highptr
        CMP #&10
        BEQ maxmin5
        JMP maxmin1
.maxmin5
        SEC
        LDA maxl
        SBC minl
        STA maxl
        LDA maxh
        SBC minh
        STA maxh
        RTS

.scale
        LDA #&0C
        STA highptr
        LDA #&08
        STA lowptr
        LDA #&00
        STA dataptr
.scale1
        LDA #&80
        STA dataptr+1
        LDA #&40
        STA pagectr
        LDY #&00
.scale2
        LDA lowptr
        STA paging_reg
        LDA (dataptr),Y
        STA divendl
        LDA highptr
        STA paging_reg
        LDA (dataptr),Y
        STA divendh
        SEC
        LDA divendl
        SBC minl
        STA divendl
        LDA divendh
```

```
        SBC minh
        STA divendh
        LDA #00
        STA quotientl
        STA quotienth
        LDA #16
        STA counter
.scale3
        LDA divendh
        CMP divisorh
        BCC shiftleft
        BEQ scale3a
        BCS scale3b
.scale3a
        LDA divendl
        CMP divisorl
        BCC shiftleft
.scale3b
        SEC
        LDA divendl
        SBC divisorl
        STA divendl
        LDA divendh
        SBC divisorh
        STA divendh
        INC quotientl
        BNE scale3
        INC quotienth
        BNE scale3
        LDA #%FF
        STA quotienth
        JMP scale3
.shiftleft
        DEC counter
        BEQ scale4
        ASL quotientl
        ROL quotienth
        ASL divendl
        ROL divendh
        JMP scale3
.scale4
        LDA highptr
        STA paging_reg
        LDA quotienth
        STA (dataptr),Y
        INY
        BEQ scale4a
        JMP scale2
.scale4a
        INC dataptr+1
        DEC pagectr
        BEQ scale5
        JMP scale2
.scale5
        INC lowptr
        INC highptr
        LDA highptr
        CMP #%10
```

```
        BEQ scale6
        JMP scale1
.scale6
        RTS

]
NEXT
*SAVE :0.6.DIG2 1300 17FF 1300
END
```

A2.5. Machine code program DIG3.

This program is another variant of the digitise routine. In this case the summed pixel values are divided by the nuber of frames that have been digitised. This action effectively calculates the average brightness value for each pixel and thereby helps to reduce the effect of any low level flutter that may be present. No grey scale enhancement is performed which means that this routine can be used to collect digitised images for processing by COMPOS.

Again, to avoid uneccessary repetition, only those sections of code that differ from DIG1 are given below.

```
REM variables declaration

framectr=&1200
pagectr=&1201
blockctr=&1202
lowptr=&1203
highptr=&1204
shiftctr=&1205
templ=&1206
divendl=&1206
temph=&1207
divendh=&1207
maxh=&120B
maxl=&1209
minh=&120A
minl=&120B
quotient=&120E
counter=&120F
divisor=&1210


paging_reg=&FE30

iop=&FE60
via=&FE62

buslmhz=&FD00

dataptr=&70

FOR L%=0 TO 3 STEP 3
P%=&1300
[OPT L%

.entry_point
        LDA framectr
        STA divisor
```

```
        JSR wipe_sideways_ram
.entry1
        JSR digitise_one_frame
        DEC framectr
        BNE entry1
        JSR scale
        LDA #&02
        STA paging_reg
        CLI
        RTS

.scale
        LDA #&0C
        STA highptr
        LDA #&08
        STA lowptr
        LDA #&00
        STA dataptr
.scale1
        LDA #&B0
        STA dataptr+1
        LDA #&40
        STA pagectr
        LDY #&00
.scale2
        LDA lowptr
        STA paging_reg
        LDA (dataptr),Y
        STA divendl
        LDA highptr
        STA paging_reg
        LDA (dataptr),Y
        STA divendh
        LDA #00
        STA quotient
        LDA #&08
        STA counter
.scale3
        SEC
        LDA divendh
        CMP divisor
        BCC shiftleft
        SEC
        LDA divendh
        SBC divisor
        STA divendh
        INC quotient
        JMP scale3
.shiftleft
        DEC counter
        BEQ scale4
        ASL quotient
        ASL divendl
        ROL divendh
        JMP scale3
.scale4
        LDA quotient
        LDX highptr
```

```
        STX paging_reg
        STA (dataptr),Y
        INY
        BEQ scale4a
        JMP scale2
.scale4a
        INC dataptr+1
        DEC pagectr
        BEQ scale5
        JMP scale2
.scale5
        INC lowptr
        INC highptr
        LDA highptr
        CMP #&10
        BEQ scale6
        JMP scale1
.scale6
        RTS
]
NEXT
*SAVE :0.6.DIG3 1300 17FF 1300
END
```

A2.6. Machine code program SUMMATE.

This program operates on two digitised images that have been stored on disc. The two images are added together and then divided by two to produce a third digitised image. All the necessary variables for this program must be supplied by the calling BASIC program i.e. SUPER.

```
REM SUMMATE... TAKES TWO DIGITISED PICTURES AND ADDS
REM THEM TOGETHER PLACING THE RESULT IN A
REM THIRD FILE

SOURCE=&70
DEST =&72
DPTR1 =&74
DPTR2 =&76

OSCOLI=&FFF7
PAGING_REG=&FE30

SFILE=&C00
DFILE=&C20
OFILE=&C40
SFILE_NO=&C60
DFILE_NO=&C61
FILE_NO=&C62

FOR L%=0 TO 3 STEP 3
P%=&1250
[OPT L%
.MAIN_PROG
        LDA #&00
        STA PAGING_REG
.MAIN1
```

```
        LDA #&00
        STA PAGING_REG
        LDX #&80
        LDY #&40
        JSR BLOCK_WRITE
        JSR WREAD_FILES
        LDA #&00
        STA PAGING_REG
        INC SFILE,X
        LDX DFILE_NO
        INC DFILE,X
        LDX OFILE_NO
        INC OFILE,X
        LDA OFILE,X
        CMP #ASC"5"
        BNE MAIN1
        LDA #&03
        STA PAGING_REG
        RTS

.ADD_THEM
        LDA #&00
        STA DPTR1
        STA DPTR2
        LDA #&40
        STA DPTR1+1
        LDA #&80
        STA DPTR2+1
        LDY #&00
        LDX #&40
.ADD_THEM1
        LDA (DPTR2),Y
        CLC
        ADC (DPTR1),Y
        ROR A
        STA (DPTR1),Y
        INY
        BNE ADD_THEM1
        INC DPTR1+1
        INC DPTR2+1
        DEX
        BNE ADD_THEM1
        RTS

.BLOCK_WRITE
        STY DEST+1
        LDY #&00
        STY DEST
.BLOCK_WRITE
        STA (DEST),Y
        INY
        BNE BLOCK_WRITE1
        INC DEST+1
        DEX
        BNE BLOCK_WRITE1
        RTS

.BLOCK_MOVE
```

```
        STX SOURCE+1
        STY DEST+1
        TAX
        LDY #0
        STY SOURCE
        STY DEST
.BLOCK_MOVE1
        LDA (SOURCE),Y
        STA (DEST),Y
        INY
        BNE BLOCK_MOVE1
        INC SOURCE+1
        INC DEST+1
        DEX
        BNE BLOCK_MOVE1
        RTS

.WREAD_FILES
        LDX #SFILE MOD 256
        LDY #SFILE DIV 256
        JSR OSCOLI
        LDA #&00
        STA PAGING_REG
        LDA #&40
        LDX #&40
        LDY #&80
        JSR BLOCK_MOVE
        LDX #DFILE MOD 256
        LDY #DFILE DIV 256
        JSR OSCOLI
        RTS

.WRITE_FILE

        LDX #OFILE MOD 256
        LDY #OFILE DIV 256
        JSR OSCOLI
RTS

]
NEXT
*SAVE :0.6.SUMMATE 1250 13FF 1250
REM This is an example of how the routine should be used.
$&C00="*L. :3.S.TEMP1 4000"
$&C20="*L. :1.S.DIFF1 4000"
$&C40="*S. :1.S.SUM1 4000 +4000"
?&C60=13
?&C61=13
?&C62=12
MODE1
REPEAT UNTIL GET$<>""
CALL &1250
```

A2.7. Machine code program DIFFER.

This program differentiates a digitised image. The function of this operation is to produce an image where the brightest pixels correspond to those areas where the grey levels are changing

rapidly in the original image. It is most often used to determine the position of edges in the original image.

The routine scans the original image twice, the first pass being horizontal and the second vertical. When scanning along or down a line of pixels the program compares adjacent pixels. If the difference between them is positive then this value is written to the position corresponding to the highest value pixel but in a second picture frame. Where the difference is negative the absolute value of the difference is written to the position corresponding to the smallest value but in the second picture frame. When performing the second pass the difference between the two pixels is compared to that obtained during the previous pass and the larger of the two values used.

```
REM PROGRAM TO DIFFER A DIGITIZED PICTURE

BASE_PIX=&70
XPIX= &72
YPIX =&74
DBASE_PIX=&76
DXPIX=&78
DYPIX=&7A
SOURCE=&7C
DEST=&7E
COLMPTR=&80

SFILE=&C00
DFILE=&C20
SFILE_NO=&C60
DFILE_NO=&C61

OSCOLI=&FFF7
PAGING_REG=&FE30

FOR LX=0 TO 3 STEP 3
PX=&1250
[OPT LX
.MAIN_PROG
        LDA #&00
        LDX #&50
        LDY #&30
        JSR BLOCK_WRITE
        JSR EDGES
.MAIN1
        LDA #0
        STA PAGING_REG
        JSR WREAD_FILES
        LDA #&00
        STA PAGING_REG
        LDA #&40
        LDX #&40
        LDY #&3E
        JSR BLOCK_MOVE
        LDA #&01
        LDX #&BF
        LDY #&7F
        JSR BLOCK_MOVE
        LDA #&00
        LDX #&40
        LDY #&80
        JSR BLOCK_WRITE
```

```
        LDA #&01
        LDX COLMPTR
        LDY #&7E
        JSR BLOCK_MOVE
        INC COLMPTR
        JSR INIT_PIXEL_PTRS
        JSR DIFFER_BLOCK
        LDA #&40
        LDX #&7F
        LDY #&40
        JSR BLOCK_MOVE
        JSR LOW_FILTER
        JSR WRITE_FILES
        LDX SFILE_NO
        INC SFILE,X
        LDX DFILE_NO
        INC DFILE,X
        LDA DFILE,X
        CMP #ASC"5"
        BNE MAIN1
        LDA #&03
        STA PAGING_REG
        RTS

.DIFFER_BLOCK
        LDY #0
        LDX #&40
.DIFFERX
        LDA (BASE_PIX),Y
        CMP (XPIX),Y
        BEQ DIFFERY
        BCC DIFFERX1
\DO ACCUM_MEM
        SEC
        SBC (XPIX),Y
        CMP (DBASE_PIX),Y
        BCC DIFFERY
        STA (DBASE_PIX),Y
        JMP DIFFERY
.DIFFER1
        LDA (XPIX),Y
        SEC
        SBC (BASE_PIX),Y
        CMP (DXPIX),Y
        BCC DIFFERY
        STA (DXPIX),Y
.DIFFERY
        CPY #&FF
        BEQ DIFFERY2
        LDA (BASE_PIX),Y
        CMP (YPIX),Y
        BEQ DIFFERY2
        BCC DIFFERY1
        SEC
        SBC (YPIX),Y
        CMP (DBASE_PIX),Y
        BCC DIFFERY2
        STA (DBASE_PIX),Y
```

```
        JMP DIFFERY2
.DIFFERY1
        LDA (YPIX),Y
        SEC
        SBC (BASE_PIX),Y
        CMP (DYPIX),Y
        BCC DIFFERY2
        STA (DYPIX),Y
.DIFFERY2
        INY
        BNE DIFFERX
        INC BASE_PIX+1
        INC XPIX+1
        INC YPIX+1
        INC DBASE_PIX+1
        INC DXPIX+1
        INC DYPIX+1
        DEX
        BNE DIFFERX
        RTS


.EDGES
        LDA #&30
        STA COLMPTR
.EDGES1
        LDX SFILE_NO
        INC SFILE,X
        LDA SFILE,X
        CMP #ASC"5"
        BEQ EDGES2
        JSR WREAD_FILES
        LDA #&01
        LDX #&40
        LDY COLMPTR
        JSR BLOCK_MOVE
        INC COLMPTR
        JMP EDGES1
.EDGES2
        LDA #&01
        LDX #&7F
        LDY COLMPTR
        JSR BLOCK_MOVE
        LDX SFILE_NO
        LDA #ASC"1"
        STA SFILE,X
        LDA #&30
        STA COLMPTR
RTS

.INIT_PIXEL_PTRS
        LDA #&00
        STA BASE_PIX
        STA XPIX
        STA DBASE_PIX
        STA DXPIX
        LDA #&01
        STA DYPIX
```

```
        STA YPIX
        LDX #&7F
        STX DBASE_PIX+1
        STX DYPIX+1
        INX
        STX DXPIX+1
        LDX #&3E
        STX BASE_PIX+1
        STX YPIX+1
        INX
        STX XPIX+1
        RTS

.BLOCK_WRITE
        STY DEST+1
        LDY #0
        STY DEST
        BLOCK_WRITE1
        STA (DEST),Y
        INY
        BNE BLOCK_WRITE1
        INC DEST+1
        DEX
        BNE BLOCK_WRITE1
        RTS

.BLOCK_MOVE
        STX SOURCE+1
        STY DEST+1
        TAX
        LDY #0
        STY SOURCE
        STY DEST
.BLOCK_MOVE1
        LDA (SOURCE),Y
        STA (DEST),Y
        INY
        BNE BLOCK_MOVE1
        INC SOURCE+1
        INC DEST+1
        DEX
        BNE BLOCK_MOVE1
        RTS

.WRITE_FILES
        LDX #DFILE MOD 256
        LDY #DFILE DIV 256
        JSR OSCOLI
        RTS

.WREAD_FILES
        LDX #SFILE MOD 256
        LDY #SFILE DIV 256
        JSR OSCOLI
        RTS

.LOW_FILTER
        LDA #&40
```

```
        STA SOURCE+1
        LDY #&00
        STY SOURCE
        LDX #&40
.LOW1
        LDA (SOURCE),Y
        CMP &C70
        BCS LOW2
        LDA #0
        STA (SOURCE),Y
.LOW2
        INY
        BNE LOW1
        INC SOURCE+1
        DEX
        BNE LOW1
        RTS
]
NEXT
*SAVE :0.6.DIFFER 1250 13FF 1250
```

A2.8. Machine code program FRQHIST.

This program scans a digitised image and compiles a frequency histogram of how many times each grey level has occurred. This information is passed back to SPR128 so that the histogram can be plotted on the screen. The main function of this routine was to allow the grey level to screen colour assignment to be carried in a determined manner rather than by guesswork.

```
REM PRODUCES HISTOGRAM DATA FROM RAW DATA
OSCOLI=&FFF7
SFILE=&C00
SFILE_NO=&C60
RAW_PTR=&70

SOURCE=&72

MSB=&A00
LSB=&900

FOR L%=0 TO 3 STEP 3
P%=&1250
[OPT L%
.MAIN_PROG
        LDA #&00
        LDX #&02
        LDY #&09
        JSR BLOCK_WRITE
.MAIN1
        JSR WREAD_FILE
        LDA #&40
        STA RAW_PTR+1
        LDA #&00
        STA RAW_PTR
.MAIN2
        LDA (RAW_PTR),Y
        TAX
```

```
        INC LSB,X
        BNE MAIN3
        INC MSB,X
.MAIN3
        INY
        BNE MAIN2
        INC RAW_PTR+1
        LDA RAW_PTR+1
        CMP #&80
        BNE MAIN2
        LDX SFILE_NO
        INC SFILE,X
        LDA SFILE,X
        CMP #ASC"5"
        BNE MAIN1
        RTS

.BLOCK_WRITE
        STY SOURCE+1
        LDY #&00
        STY SOURCE
.BLOCK_WRITE1
        STA (SOURCE),Y
        INY
        BNE BLOCK_WRITE1
        INC SOURCE+1
        DEX
        BNE BLOCK_WRITE1
        RTS

.WREAD_FILE
        LDX #SFILE MOD 256
        LDY #SFILE DIV 256
        JSR OSCOLI
        RTS
]
NEXT
*SAVE :0.6.FRQHIST 1250 13FF 1250
```

A2.9. Machine code program DUMPER.

This program scans a digitised image and produces a binary image (black on white) using an FX80 dot matrix printer. During the scan, each pixel is compared with the value in BACK, if it is less than this value then the corresponding pixel in the binary printed image will be white otherwise it will be printed black.

```
REM a high density bit mapped screen dump using the 128K sideways ram
rawp=&70
blockctr=&72
back=&73
ramptr=&74
passctr=&75
bstore=&1200
osbyte=&FFF4
oswrch=&FFEE
pr1=&FE30
pr2=&FE60
```

```
bddr=&FE62
FOR L%=0 TO 3 STEP 2
P%=&1300
[OPT L%
        LDA #&FF
        STA bddr
        LDA #3
        LDX #10
        JSR osbyte
        LDA #27
        JSR oswrch
        LDA #ASC"3"
        JSR oswrch
        LDA #23
        JSR oswr h
        LDA #&80
        STA rawp+1
        LDA #&00
        STA rawp
        LDA ramptr
        STA pr1
        STA pr2
        LDA #4
        STA blockctr
.sdump1
        JSR buffer
        JSR send
        LDA blockctr
        BNE sdump1
        LDA #2
        STA pr1
        STA pr2
        LDA #12
        JSR oswrch
        LDA #3
        LDX #0
        JSR osbyte
        RTS

.buffer
        LDX #4
        STX passctr
.buffer1
        LDX #0
.buffer2
        ASL bstore,X
        ASL bstore,X
        INX
        BNE buffer2
        LDY #0
        LDX #&FF
.buffer3
        LDA (rawp),Y
        CMP back
        BCC buffer4
        BEQ buffer4
        LDA bstore,X
        ORA #&3
```

```
        STA bstore,X
.buffer4
        DEX
        INY
        BNE buffer3
        INC rawp+1
        DEC passctr
        BNE buffer1
        LDA rawp+1
        CMP #&C0
        BCC buffer5
        INC ramptr
        LDA ramptr
        STA pr1
        STA pr2
        LDA #&80
        STA rawp+1
        DEC blockctr
.buffer5
        RTS

.send
        LDA #27
        JSR oswrch
        LDA #ASC"Z"
        JSR oswrch
        LDA #0
        JSR oswrch
        LDA #6
        JSR oswrch
        LDY #0
.send1
        LDX #6
.send2
        LDA bstore,Y
        JSR oswrch
        DEX
        BNE send2
        INY
        BNE send1
        LDA #13
        JSR oswrch
        RTS
]
NEXT
*SAVE :0.6.DUMPER 1300 +100 1300
```

A2.10 Machine code program DISPLAY.

This routine scans over a digitised image and copies it to a 256x256 pixel area in the screen display (using mode 1 graphics). During this copying the 256 grey levels of the digitised image are mapped into four grey levels according to a colour table previously defined from SPR128 via the COLOURS option. This is a very fast display routine and is necessary to patially compensate for the fact that the BBC microcomputer cannot display the full 256 grey level resolution used to represent the digitised images.

```
spmem=&1278
```

```
sp=&72
rawp=&74
rawindex=&1276
ramptr=&76
ctr8=&77
byte=&78
ramptrend=&79
pixelctr=&1270
cmask0=&1280
colour0=&1290

pr1=&FE30

FOR L%=0 to 3 step 3
P%=&1300
[OPT L%
        LDA &1200
        CLC
        ADC #4
        STA ramptrend
        LDA #&30
        STA spmem+1
        LDA #&00
        STA spmem
        STA rawindex
.doy1
        LDA #&08
        STA ctr8
.doy2
        JSR dox
        INC pmem
        INC rawindex
        BEQ doy3
        DEC ctr8
        BNE doy2
        LDA spmem
        AND #&F0
        CLC
        ADC #&80
        STA spmem
        LDA spmem+1
        ADC #2
        STA spmem+1
        JMP doy1
.doy3
        LDA #2
        STA pr1
        RTS

.dox
        LDA &1200
        STA ramptr
        STA pr1
        LDA spmem+1
        STA sp+1
        LDA spmem
        STA sp
        LDA # 80
```

```
        STA rawp+1
        LDA #&00
        STA rawp
.dox1
        JSR dobyte
        LDA sp
        CLC
        ADC #8
        STA sp
        LDA sp+1
        ADC #0
        STA sp+1
        LDA rawp+1
        CMP #&C0
        BCC dox2
        INC ramptr
        LDA ramptr
        STA pr1
        LDA #&80
        STA rawp+1
.dox2
        LDA ramptr
        CMP ramptrend
        BNE dox1
        RTS

.dobyte
        LDA #0
        STA byte
        LDA #4
        STA pixelctr
.dobyte1
        LDY rawindex
        LDA (rawp),Y
        LDX #&FF
.dobyte2
        INX
        CMP colour0,X
        BEQ P%+4
        BCS dobyte2
        LDA byte
        ASL A
        ORA cmask0,X
        STA byte
        INC rawp+1
        DEC pixelctr
        BNE dobyte1
        LDA byte
        LDY #&00
        STA (sp),y
        RTS
] NEXT
*SAVE :0.6.DISPLAY 1300 +200 1300
```

A2.11. Machine code program MOVEUP.

The memory organisation of the BBC microcomputer is such that it is not possible to

load data directly into the sideways ram area. To overcome this problem digitised images were split into four files, each 16k long. These files could then be loaded into the screen area of memory (SPR12B uses mode 1 graphics and therefore requires 20k of memory) initially and then moved to the destination block of sideways ram using the routine below. The program expects to find the paging register value for the appropriate sideways ram block in memory location &1200.

```
lowptr=&70
highptr=&72
paging_reg=&FE30

FOR 1%=0 TO 3 STEP 3
P%=&1300
[OPT 1%

        LDA &1200
        STA paging_reg
        LDA #&80
        STA highptr+1
        LDA #&40
        STA lowptr+1
        TAX
        LDA #&00
        STA highptr
        STA lowptr
        TAY
.loop
        LDA (lowptr),Y
        STA (highptr),Y
        INY
        BNE loop
        INC lowptr+1
        INC highptr+1
        DEX
        BNE loop
        LDA #&02
        STA paging_reg
        RTS
]
NEXT
*SAVE :0.6.MOVEUP 1300 +100 1300
```

A2.12. Machine code program MOVEDOWN.

This program performs the opposite of MOVEUP and moves the sideways ram block specified by &1200 into the screen memory so that it can be saved to disc.

```
lowptr=&70
highptr=&72
paging_reg=&FE30

FOR 1%=0 TO 3 STEP 3
P%=&1300
[OPT 1%
        LDA &1200
        STA paging_reg
        LDA #&80
```

```
        STA highptr+1
        LDA #&40
        STA lowptr+1
        TAX
        LDA #&00
        STA highptr
        STA lowptr
        TAY
.loop
        LDA (highptr),Y
        STA (lowptr),Y
        INY
        BNE loop
        INC lowptr+1
        INC highptr+1
        DEX
        BNE loop
        LDA #&02
        STA paging_reg
        RTS
]
NEXT
*SAVE :0.6.MOVDOWN 1300 +100 1300
```

A2.13. BASIC program SUPER version 2.

This version of SUPER differs from that originally presented in that it allows the display of the digitised image to be calibrated. This is done using the options HCAL and VCAL. The calibration factors obtained are used to convert measurements made in terms of screen pixels into physical measurements such as millimeters or micrometers.

```
IF PAGE<>&1900 THEN PAGE=&1900:CHAIN":0.B.SUPER"
MODE 1
PROC_init
REPEAT:PROC_menu1:UNTIL an$="e"
END

DEF PROC_init:@%=&00020208:DIM qx(30),qy(30)
bank1$="null":bank2$="null":xcal=2.330508474:ycl=2.347417841
sum=0:sqsum=0:num=0
FOR L%=0 TO 16:L%?&1290=255:NEXT
?&1290=20:?&1291=40:?&1292=60:PROC_win
ENDPROC

DEF PROC_win
VDU 22,1,24,0;0;1023;1023;28,32,31,39,0
ENDPROC

DEF PROC_menu1
LOCAL used:REPEAT
*FX 15,0
*DISC
GCOL 0,3
VDU 24,0;0;1023;1023;28,32,31,39,0:used=NOT TRUE:CLS
PRINTTAB(0,3)"Analyse"TAB(0,4)"View"TAB(0,5)"Oscli"
PRINTTAB(0,6)"Digitis"TAB(0,7)"Vcal"TAB(0,8)"Hcal"
PRINTTAB(0,9)"Colours"TAB(0,10)"Quit"TAB(0,24)"bank 1"
```

```
PRINTTAB(0,25)bank1$TAB(0,28)"bank 2"TAB(0,29)bank2$
REPEAT
an$=GET$
UNTIL INSTR("ADVOQCUH",an$)>0
an$="Q" THEN END
IF an$="H" THEN PROC_hcal :used=TRUE:REM horizontal calibration
IF an$="U" THEN PROC_vcal :used=TRUE:REM vertical claibration
IF an$="D" THEN PROC_digitise:used=TRUE
IF an$="A" THEN PROC_analyse :used=TRUE:VDU 22,1
IF an$="V" THEN PROC_view :used=TRUE
IF an$="O" THEN PROC_oscli :used=TRUE
IF an$="C" THEN PROC_colours :used=TRUE
UNTIL used
ENDPROC

DEF PROC_digitise
LOCAL frames
*FX 15,0
REPEAT
VDU 22,0
PRINTTAB(22,0)"Procedure digitise"
VDU 28,0,31,79,2,12
INPUTTAB(5,3)"Number of frames to digitise "frames
UNTIL frames>=1 AND frames<=255
PRINTTAB(5,5)"Make sure your picture is ready for digitising"
PRINTTAB(0,7)"Method 1" TAB(10,7)"Method 2"TAB(20,7)"Method 3"
PRINTTAB(30,7)"Exit"
PRINTTAB(0,9)"Method 1 is shift left "
PRINTTAB(0,10)"Method 2 is -min,/max,*255"
PRINTTAB(0,11)"Method 3 is /frames"
REPEAT
an$=GET$
UNTIL an$="1" OR an$="2" OR an$="3" OR an$="E"
IF an$="E" THEN ENDPROC
?&1200=frames
PRINTTAB(5,20)"Currently digitising ";frames;" frames."
PRINTTAB(5,21)"Please wait about ";frames*6+60;" seconds"
IF an$="1" THEN *:0.6.dig1
IF an$="2" THEN *:0.6.dig2
IF an$="3" THEN *:0.6.dig3
bank2$="new digitised"
bank1$="rubbish"
PROC_win
*FX 15,0
ENDPROC

DEF PROC_view:LOCAL an$:REPEAT:*FX 15,0
VDU 28,32,20,39,16,12
PRINTTAB(0,1)"Bank 1"TAB(0,2)"Bank 2"
an$=GET$
UNTIL INSTR("12E",a$)>0
IF an$="E" THEN ENDPROC
IF an$="1" THEN ?&1200=0 ELSE ?&1200=12
?&1270=4:?&1272=3:?&1273=&FF:?&1280=0:?&1281=1
?&1282=16:?&1283=17
*:0.6.DISPLAY
VDU 8,32,31,39,0,12
ENDPROC
```

```
DEF PROC_oscli:LOCAL cl$:VDU 22,0
PRINT"Operating System Command Line Interpreter"
VDU 28,0,31,79,2
REPEAT
*FX 15,0
INPUTLINE">>>>"cl$:CLS:OSCLI(cl$)
UNTIL cl$=""
PROC_win:*FX 15,0
ENDPROC

DEF PROC_colours:LOCAL L%,K%,VLUE%
VDU 22,0:PRINTTAB(3,2)"Colour assignments"
VDU 28,0,31,79,4
REPEAT:CLS
FOR L%=0 TO 16
PRINTTAB(0,L%+3)"Logical colour";L%
PRINTTAB(20,L%+3)"old grey level = ";L%?&1290
PRINTTAB(50,L%+3)"new grey level ="
NEXT
L%=-1
REPEAT
L%=L%+1
REPEAT:PRINTTAB(68,L%+3)" ":*FX 15,0
INPUTTAB(68,L%+3)VLUE%
UNTIL VLUE%>=0 AND VLUE%<=255
IF VLUE%=0 PRINTTAB(68,L%+3)L%?&C90 ELSE L%?&1290=VLUE%
UNTIL L%?&1290=255
FOR L%=0 TO 16:PRINTTAB(68,L%+3)L%?&1290:NEXT
PRINTTAB(10, 5)"Are these colour definitions O.K. 'Y'or  'N'"
UNTIL GET$="Y":PROC_win
ENDPROC

DEF PROC_analyse
LOCAL coords,y%
FOR y%=0 TO 1023 STEP 4
REPEAT
MOVE 0,y%
PLOT 76,0,y%
coords=FN_read_xy:
PROC_area((? 74+256*?&75),(?&76+256*?&77))
UNTIL (?&74+256*?&75)+4>1023
NEXT y%
ENDPROC
DEF FN_read_xy
X%=&70
Y%=&00
A%=&0D
K%=USR(&FFF1)
=!&74

DEF PROC_q(tx%,ty%)
IF (qt+1) MOD 30=qh THEN ENDPROC
qx(qt)=tx%:qy(qt)=ty%:qt=(qt+1) MOD 30:ENDPROC

DEF PROC_uq:IF qh=qt THEN ENDPROC
cx%=qx(qh):cy%=qy(qh):qh=(qh+1) MOD 30:ENDPROC
```

```
DEF PROC_area(startx,starty)
qh=0:qt=0:fnd=0:nouse=FALSE
PROC_q(startx,starty)
REPEAT
PROC_uq
PROC_test(cx%+4,cy%)
PROC_test(cx%-4,cy%)
PROC_test(cx%,cy%+4)
PROC_test(cx%,cy%-4)
UNTIL qh=qt
IF fnd>0 AND nouse=FALSE THEN fnd=fnd*xcal*ycal:VDU2:PRINT fnd;:VDU 3:
?? continued from above ?? sum=sum+fnd:sqsum=sqsum+(fnd*fnd):num=num+1
IF COUNT>75 THEN VDU 1,13
ENDPROC

DEF PROC_test(x,y)
IF x>1023 OR x<0 THEN nouse=TRUE:ENDPROC
IF y>1023 OR y<0 THEN nouse=TRUE:ENDPROC
IF POINT(x,y)<1 THEN ENDPROC
GCOL0,0:PLOT 69,x,y:fnd=fnd+1
PROC_q(x,y)
ENDPROC

DEF PROC_ycal
LOCAL yl,yh,y,inc
yl=0:yh=0:yh=0:inc=0
REPEAT
MOVE 0,y:GCOL 3,3:DRAW 1023,y
y=y+inc:inc=0
MOVE 0,y:GCOL 3,3:DRAW 1023,y
IF INKEY(-58) inc=-4*(y<1023)
IF INKEY(-42) inc= 4*(y>0)
IF INKEY(-87) AND yl=0 yl=y:MOVE 0,y:GCOL 3,1:DRAW 1023,y:GCOL 3,3
IF INKEY(-54) AND yh=0 yh=y:MOVE 0,y:GCOL 3,1:DRAW 1023,y:GCOL 3,3
UNTIL INKEY(-17)
INPUT TAB(0,12)"distance in um ="dist
ycal=dist*4/(yh-yl)
PRINT'"Y calibration is ";ycal;" physical units per pixel"
ENDPROC

DEF PROC_hcal
LOCAL xl,xh,x,inc
xl=0:xh=0:xh=0:inc=0
REPEAT
MOVE x,0:GCOL 3,3:DRAW x,1023
x=x+inc:inc=0
MOVE x,0:GCOL 3,3:DRAW x,1023
IF INKEY(-122) inc=-4*(x<1023)
IF INKEY(-26) inc= 4*(x>0)
IF INKEY(-87) AND xl=0 xl=x:MOVE x,0:GCOL 3,1:DRAW x,1023:GCOL 3,3
IF INKEY(-54) AND xh=0 xh=x:MOVE x,0:GCOL 3,1:DRAW x,1023:GCOL 3,3
UNTIL INKEY(-17)
INPUT TAB(0,12)"distance in um ="dist
xcal=dist*4/(xh-xl)
PRINT'"X calibration is ";xcal;" physical units per pixel"
ENDPROC
```

A2.14. BASIC program BCOMPOS.

This BASIC program is the interface to the machine code program that produces a composite image from a sequence of digitised images. Two functions are performed. The program feeds the digitised images to the machine code routine COMPOS, prompting for a new disc when necessary, and finally saves the composite image to disc. The second function, during phase2 in procedure ANALYSE, is to the floating point calculations that would be too complicated to code in assembler.

```
code=&1200
scanx=code+3
scany=code+4
tscanx=code+5
tscany=code+6
pscanx=code+7
pscany=code+8
cscanx=code+9
cscany=code+10
genx=code+11
geny=code+12
tmpx=code+13
tmpy=code+14
pic=code+15
comp=code+16
audit=code+17
back=code+18
mask=code+19
route=code+20
totalp=code+21
totalc=code+23
sump=code+25
sumc=code+29
maxpx=code+33
maxpy=code+34
maxcx=code+35
maxcy=code+36
minpx=code+37
minpy=code+38
mincy=code+39
mincy=code+40
qflag=code+41
cflag=code+43
ramptr=code+44
auditptr=code+45
maxbp=code+47
maxbc=code+48

genptr=&70
queuex=&72
queuey=&74

paging_reg=&FE30

oswrch=&FFEE
osword=&FFF1
table=&1300
phase1=table
phase2=table+3
```

```
wipe_comp=table+9
comp_down=table+12
move_up=table+15

MODE 0
*LOAD :0.6.COMPOS
CLS
INPUT" What is the generic file name "gname$
INPUT" Number of files to process"max
INPUT" Maximum grey level for background eleimination "mback
PRINT"Please insert the disc containing files ";gnames; 1 to 6 in drive 1/3"
PRINT''"then press the space bar to continue"
PROC noisy
?queuex=0
queuex?1=&30
?queuey=0
queuey?1=&31
?back=mback
CALL wipe_comp
FOR files=1 to max
IF files MOD 6=1 AND files>1 PRINT''Please insert disc with files "gnames$;" ";files;" TO
?? continued from above ?? ";files+6;" into drive 1/3"
IF files MOD 6=1 AND files>1 THEN PROC_noisy
IF files MOD 6=4 or files MOD 6=5 or files MOD 6=0 then dr$="3" ELSE dr$="1"
FOR block=1 to 4
block$=STR$(block)
?route=7+block
OSCLI("*L. :"+dr$+"."+gname$+STR$(files)+block$+" 4000")
CALL move_up
NEXT block
CLS
PROC_analyse
NEXT files
FOR block=1 TO 4
block$=STR$(block)
?route=block+&B
CALL comp_down
OSCLI("*S. :2.S.COMP"+block$+" 4000 +4000")
NEXT
END

DEF PROC_noisy
REPEAT
SOUND 1,-15,100,10
SOUND 1,-15,150,10
UNTIL INKEY$(0)=" "
*fx 15,0
ENDPROC

DEF PROC_analyse
CALL phase1
CLS
?scanx=0
?scany=0
REPEAT
CALL phase2
IF ?scanx=&00 AND ?scany=&00 THEN UNTIL ?scanx=0:CLS:ENDPROC
tp=?totalp+256*(totalp?1)
```

```
tc=?totalc+256*(totalc?1)
ap=((?maxpx-?minpx)/2+(?maxpy-?minpy)/2)^2*PI
ac=((?maxcx-?mincx)/2+(?maxcy-?mincy)/2)^2*PI
IF ap>0 THEN tiap=(!sump)/ap ELSE tiap=0
IF ac>0 THEN tiac=(!sumc)/ac ELSE tiac=0
IF ?maxbp>=(?maxbc)-3 AND tiap<=tiac AND tiap>0 AND tiac>0 THEN ?route=2
IF ?route=2 then call_copypc
UNTIL ?route=&00 or ?scanx=&00
CLS
ENDPROC
```

A2.15. Machine code program COMPOS.

This program performs the task of examining a sequence of digitised images and constructing a composite image which shows all the adherent particles in focus. As Triamterene fluoresces when exposed to ultra violet light the composite image is formed using a number of simple rules relating to the brightness, total area and perimeter of non background areas that are discovered. A more comlete discussion of the rules used to define an area in focus can be found in Chapter 3 (3.1.3.6).

```
REM a basic program to assemble
REM the machine code for COMPOS.
code=&1200
qheadptr=code
qtailptr=code+1
scanx=code+3
scany=code+4
tscanx=code+5
tscany=code+6
pscan =code+7
pscany=code+8
cscanx=code+9
cscany=code+10
genx=code+11
geny=code+12
tmpx=code+13
tmpy=code+14
pic=code+15
comp=code+16
audit=code+17
back=code+18
mask=code+19
route=code+20
totalp=code+21
totalc=code+23
sump=code+25
sumc=code+29
maxpx=code 33
maxpy=code+34
maxcx=code+35
maxcy=code+36
minpx=code+37
minpy=code+38
mincx=code+39
mincy=code+40
qflag=code+41
cflag=code+43
ramptr=code+44
auditptr=code+45

genptr=&70
queuex=&72
queuey=&74
dptr_low=&80
dptr_high=&82

paging_reg=&FE30

oswrch=&FFEE
```

```
osword=&FFF1

FOR L%=0 TO 3 STEP 2
P%=code+&100
[ OPT L%

\a table of basic entry points

.basic_entry_points
.table
.phase1
      JMP phase1_1
.phase2
      JMP phase2_1
.copypc
      JMP copy_pic_to_comp
.wipe_comp
      JMP wipe_comp1
.comp_down
      JMP comp_down1
.mov_up
      JMP mov_up1
.table_end
      RTS


.mov_up1

      This routine is equivalent to the machine code program MOVEUP given above.

      LDA route
      STA paging_reg
      LDA #0
      STA dptr_low
      STA dptr_high
      LDA #&40
      STA dptr_low+1
      LDA #&80
      STA dptr_high+1
      LDX #&40
      LDY #0
.mov_up2
      LDA (dptr_low),Y
      STA (dptr_high),Y
      INY
      BNE mov_up2
      INC dptr_low+1
      INC dptr_high+1
      DEX
      BNE mov_up2
      LDA #&02
      STA paging_reg
      RTS


.queue

      This  routine pushes the x and y values of a non background pixel onto the x and y queues.
```

The actual values to be pushed onto the x and y queues are passed to the routine in the variables genx and geny. The queue routine (and its converse unqueue) is intimately involved in the 'grass fire burn' algorithm (209) used to determine the extent of an area of non background pixels.

The X and Y coordinate queues are only 256 bytes (ie 1 page) long so that if an unusually large or convoluted area of non background pixels is examined they may become full. There is, however, sufficient redundancy of information in the queue (ie X,Y coordinate pairs appearing more than once) that X,Y coordinate pairs can freely be discarded when this occurs.

```
        LDX qtailptr
        INX
        CPX qheadptr
        BEQ queue1
        LDY qtailptr
        LDA genx
        STA (queuex),Y
        LDA geny
        STA (queuey),Y
        INC qtailptr
.queue1
        RTS
```

.unqueue

This routine performs the reverse of QUEUE as it pulls two values off the X and Y coordinate queues and assigns them to genx and geny respectively. If the queue is empty (ie an attempt is made to pull off more data than was pushed onto the queue) then qflag is set to &FF so that the calling routine can easily test for a queue underflow.

```
        LDX qheadptr
        CPX qtailptr
        BEQ unqueue1
        LDY qheadptr
        LDA (queuex),Y
        STA genx
        LDA (queuey),Y
        STA geny
        LDA #&00
        STA (queuex),Y
        STA (queuey),Y
        INC qheadptr
        RTS
.unqueue1
        LDA #&FF
        STA qflag
        RTS
```

.pic_rw

This routine allows a pixel value to be read from, or written to, a digitised image using x and y coordinates that vary between 0 and 255. Generally, the current digitised image (referred to as PIC) will be stored in sideways ram pages 8 to &0B and the composite image (referred to as COMP) will be stored in sideways ram pages &0C to &0F. Using this information the main section of the routine, swram_rw, can be used to calculate the memory address of an x,y coordinate relative to the start of a frame buffer area. Once this has been done adding the correct frame buffer address (set by calling either pic_rw or comp_rw) will access the appropriate pixel in either PIC or COMP.

If the carry flag is set, the value passed in the A register will be written to the appropriate pixel otherwise the value of the pixel will be read and returned in the A register.

```
        PHP
        PHA
        LDX #&08
        STX ramptr
        JMP sram_rw
.comp_rw
        PHP
        PHA
        LDX #&0C
        STX ramptr
.sram_rw
        LDA genx
        AND #&3F
        CLC
        ADC #&80
        STA genptr+1
        LDA #&00
        STA genptr
        LDA genx
        AND #&C0 \top two bits
        CLC
        ROL A
        ROL A
        ROL A
        CLC
        ADC ramptr
        LDX #&FF
        STA paging_reg
        LDY geny
        PLA
        PLP
        BCS sram_rw1
        LDA (genptr),Y
        JMP sram_rw2
.sram_rw1
        STA (genptr),Y
.sram_rw2
        LDX #&02
        STX paging_reg
        RTS


.paudit_rw
```

When a non background area is being examined to determine its extent it is necessary to mark each pixel in some way to show that it has been examined to prevent the 'grass fire burn' algorithm from becoming locked into an endless loop. In COMPOS this is done by using two 256x256 bit arrays located in screen memory. When a pixel in a frame buffer has been examined the corresponding bit in the bit array is set to 1. In view of their function these bit arrays are known as audit trails. Paudit_rw and caudit_rw perform exactly the same function as pic_rw or comp_rw above except that they read or write a single bit value.

```
        PHP
        PHA
        LDA #&60
```

```
        STA auditptr
        JMP audit_rw
.caudit_rw
        PHP
        PHA
        LDA #&40
        STA auditptr
.audit_rw
        LDA genx
        AND #&07
        TAX
        LDA #&01
        STA mask
.audit_rw1
        DEX
        BMI audit_rw2
        ASL mask
        BPL audit_rw1
.audit_rw2
        LDA genx
        LSR A
        LSR A
        LSR A
        CLC
        ADC auditptr
        STA genptr+1
        LDA #0
        STA genptr
        LDY geny
        PLA
        PLP
        BCS audit_rw3
        LDA mask
        AND (genptr),Y
        RTS

.audit_rw3
        CMP#&00
        BEQ audit_rw4
        LDA mask
        ORA (genptr),Y
        STA (genptr),Y
        RTS

.audit_rw4
        LDA mask
        EOR #&FF
        AND (genptr),Y
        STA (genptr),Y
        RTS


.phase1_1
```

This routine is effectively a preprocessor for phase2. Its only function is to examine the current digitised picture (PIC) and set any pixel whose value is less than or equal to the value in BACK to zero. This clipping operation is necessary to isolate the bright areas of the image from each other.

```
        LDA #8
        STA route       \Used as a temporary variable
.phase1_1a
        LDA route
        STA paging_reg
        LDA #0
        STA genptr
        LDA ##80
        STA genptr+1
        LDX ##40
        LDY ##00
.phase1_2
        LDA (genptr),Y
        CMP back
        BEQ phase1_3
        BCS phase1_4
.phase1_3
        LDA ##00
        STA (genptr),Y
.phase1_4
        INY
        BNE phase1_2
        INC genptr+1
        DEX
        BNE phase1_2
        INC route
        LDA route
        CMP #12
        BNE phase1_1a
        LDA #2
        STA paging_reg
        RTS
```

.phase2_1

This routine scans the current digitised image (PIC) until it finds a non background pixel. The extent of this area is then determined and statistics relating to the brightness, area and perimeter collected. During this search the same area in the composite image (COMP)is also searched. If a non background pixel is found in COMP then cflag is set to a non zero value. When the area in PIC has been examined and cflag is found to be non zero then the same procedure is carried out for the non background area in comp. Once the relevant statistics for the areas in PIC and COMP have been collected the routine exits to BASIC where the floating point calculations necessary to determine which area is more 'focussed' are carried out.

Any area discovered in PIC which is less than 2 pixels in size is deleted from pic as it is assumed that it is an artefact of the clipping operation carried out in phase1.

```
        LDA scanx
        STA genx
        LDA scany
        STA geny

        CLC
        JSR pic_rw
        BEQ phase2_4
        CLC
        JSR paudit_rw
```

```
        BNE phase2_4
        LDA #&00
        STA cflag
        JSR pic_area
        LDA totalp+1
        CMP #2
        BCS phase2_4
.phase2_2
        LDA cflag
        BEQ phase2_3
        JSR comp_area
        RTS             \exit to BASIC at this point to test degree of focus

.phase2_3
        LDA #&04
        STA route
        JSR examine_from
.phase2_4
        INC scany
        BNE phase2_1
        INC scanx
        BNE phase2_1
        RTS


.init_examine

      This routine initialises  the variables used when  the extent of a  non background area is
being determined in either PIC or COMP.

        LDA #&00
        STA qflag
        STA qheadptr
        STA qtailptr
        LDA scanx
        STA genx
        LDA scany
        STA geny
        RTS


 .examine_from

      This routine is part of the area determination.  It examinines the eight pixels around the
pixel specified by genx and geny to determine their status and is called from pic_area.

        JSR init_examine
        JSR router
.examine1
        JSR unqueue
        LDA qflag
        BEQ examine2
        RTS

.examine2
        LDA genx
        STA tmpx
        LDA geny
```

```
        STA tmpy
        LDA tmpx
        CMP #&FF
        BEQ examine3
        INC genx
        JSR router
.examine3
        LDX tmpx
        DEX
        STX genx
        LDA tmpx
        BEQ examine4
        JSR router
.examine4
        LDA tmpx
        STA genx
        INC geny
        LDA tmpy
        CMP #&FF
        BEQ examine5
        JSR router
.examine5
        LDX tmpy
        DEX
        STX geny
        LDA tmpy
        BEQ examine6
        JSR router
.examine6
        JMP examine1
        RTS


.router
```

This routine is effectively a multiple branch (similar to the swith command in 'C'). The actual subroutine called is determined by the value in route.

```
        LDA route
        CMP #&00
        BNE router1
        JMP pointpc
.router1
        CMP #&01
        BNE router2
        JMP pointcp
.router2
        CMP #&02
        BNE router3
        JMP wipe_pica
.router3
        CMP #&03
        BNE router4
        JMP wipe_compa
.router4
        CMP #&04
        BNE router5
        JMP copypc1
```

```
.router5
        RTS
```

.pic_area

This routine initialises the variables used to collect the statistics relating to the non background area about to be determined in PIC. The value of route is set such that routine pointpc is called during subsequent calls to examine_from.

```
        LDA genx
        STA pscanx
        LDA geny
        STA pscany
        LDA #&00
        STA totalp
        STA totalp+1
        STA sump
        STA sump+1
        STA sump+2
        STA sump+3
        STA maxpx
        STA maxpy
        LDA #&FF
        STA minpx
        STA minpy
        LDA #&00
        STA route
        JSR examine_from
        RTS
```

.pointpc

This routine determines the extent of the non background area in PIC updating the appropriate statistics as it progresses. When a non background pixel is examined here, the equivalent pixel in COMP is also examined. The first occurrence of a non background pixel in comp causes the variable cflag to be set to &FF and the X,Y coordinate of that pixel to be placed in cscanx and cscany. Once a non background pixel has been found in COMP no further examinination of COMP is made during the determination of the non background area in PIC.

```
        CLC
        JSR paudit_rw
        BNE pointpc1
        CLC
        JSR pic_rw
        BEQ pointpc1
        JSR statsp
        JSR queue
        LDA #&FF
        SEC
        JSR paudit_rw
        LDA cflag
        BMI pointpc1
        CLC
        JSR comp_rw
        BEQ pointpc1
        LDA #&FF
```

```
        STA cflag       \found 1st
        LDA genx
        STA cscanx
        LDA geny
        STA cscan
.pointpc1
        RTS
```

.comp_area

This routine performs the same function for COMP as pic_area did for PIC above.

```
        LDA scanx
        STA tscanx
        LDA scany
        STA tscany
        LDA cscanx
        STA scanx
        LDA cscany
        STA scany
        LDA #&00
        STA totalc
        STA totalc+1
        STA sumc
        STA sumc+1
        STA sumc+2
        STA sumc+3
        STA maxcx
        STA maxcy
        LDA #&FF
        STA mincx
        STA mincy
        LDA #&01
        STA route
        JSR examine_from
        LDA tscanx
        STA scanx
        LDA tscany
        STA scany
        RTS
```

.pointcp

This routine essentially performs the same action as pointpc except that it is not necessary to examine pixels in PIC from COMP.

```
        CLC
        JSR caudit_rw
        BNE pointcp1
        CLC
        JSR comp_rw
        BEQ pointcp1
        JSR statsc
        JSR queue
        LDA #&FF
        SEC
```

```
        JSR caudit_rw
 .pointcp1
        RTS


.statsp

      This  routine is called during the determination of  the extent of the non background area
in PIC and is reponsible for updating the relevant area and brightness statistics.

        CLC
        ADC sump
        STA sump
        LDY #&01
.statsp1
        LDA sump,Y
        ADC #0
        STA sump,Y
        INY
        CPY #4
        BNE statsp1
        LDA genx
        CMP minpx
        BCS statsp2
        STA minpx
.statsp2
        CMP maxpx
        BCC statsp3
        BEQ statsp3
        STA maxpx
.statsp3
        LDA geny
        CMP minpy
        BCS statsp4
        STA minpy
.statsp4
        CMP maxpy
        BCC statsp5
        BEQ statsp5
        STA maxpy
.statsp5
        INC totalp
        BNE statsp6
        INC totalp+1
.statsp6
        RTS


.statsc

        This routine performs the same functions for COMP as statsp performed for PIC above.

        CLC
        ADC sumc
        STA sumc
        LDY #&01
.statsc1
        LDA sumc,Y
```

```
        ADC #0
        STA sumc,Y
        INY
        CPY #4
        BNE statsc1
        LDA genx
        CMP mincx
        BCS sta sc2
        STA mincx
.statsc2
        CMP maxcx
        BCC statsc3
        BEQ statsc3
        STA maxcx
.statsc3
        LDA geny
        CMP mincy
        BCS statsc4
        STA mincy
.statsc4
        CMP maxcy
        BCC statsc5
        BEQ statsc5
        STA maxcy
.statsc5
        INC totalc
        BNE statsc6
        INC totalc+1
.statsc6
        RTS


.copy_pic_to_comp

      This  routine erases the audit trail and current area in COMP in readiness for the current
area in PIC to be copied to COMP.

        LDA scanx
        STA tscanx
        LDA scany
        LDA tscany
        LDA cscanx
        STA scanx
        LDA cscany
        STA scany
        LDA #&03
        STA route
        JSR examine_from
        LDA pscanx
        STA scanx
        LDA pscany
        STA scany
        LDA #&04
        STA route
        JSR examine_from
        LDA tscanx
        STA scanx
        LDA tscany
```

```
        STA scany
        RTS


.copypc1

      This  routine copies the current non background area in  PIC to COMP.  The area in PIC and
its audit trail is deleted as this is done.

        CLC
        JSR paudit_rw
        BEQ copypc2
        CLC
        JSR pic_rw
        SEC
        JSR comp_rw
        JSR queue
        LDA #&00
        SEC
        JSR pic_rw
        LDA #&00
        SEC
        JSR paudit_rw
        LDA #&FF
        SEC
        JSR caudit_rw
.copypc2
        RTS


.wipe_pica

        This routine erases the current PIC audit area and the corresponding area in PIC.

        CLC
        JSR paudit_rw
        BEQ wipe_pica1
        JSR queue
        LDA #&00
        SEC
        JSR paudit_rw
        LDA #&00
        SEC
        JSR pic_rw
.wipe_pica1
        RTS


.wipe_compa
        This routine erases the current audit trail for COMP and the corresponding area in COMP.

        CLC
        JSR caudit_rw
        BEQ wipe_compa1
        JSR queue
        LDA #&00
        SEC
        JSR caudit_rw
```

```
        LDA #&00
        SEC
        JSR comp_rw
.wipe_compa1
        RTS


.wipe_comp1
```

This routine clears the sideways ram area allocated for the composite picture (ie area COMP) in preparation for the compilation of the composite digitised image. This routine is only called once at the beggining of COMPOS.

```
        LDA #12
        STA route
.wipe_comp1a
        LDA route
        STA paging_reg
        LDA #&80
        STA genptr+1
        LDA #&00
        STA genptr
        LDY #&00
        LDX #&40
        LDA #&00
.wipe_comp2
        STA (genptr),Y
        INY
        BNE wipe_comp2
        INC genptr+1
        DEX
        BNE wipe_comp2
        INC route
        LDA route
        CMP #16
        BNE wipe_comp1a
        LDA #2
        STA paging_reg
        RTS


.comp_down1
```

This routine moves the contents of a 16k sideways ram block in the COMP frame buffer into screen memory ready for saving to disc. It is directly comparable to the machine code routine MOVEDOWN described above.

```
        LDA route
        STA paging_reg
        LDA #&00
        STA queuex
        STA queuey
        LDA #&80
        STA queuex+1
        LSR A
        STA queuey+1
        LDY #&00
        LDX #&40
```

```
.comp_down2
        LDA (queuex),Y
        STA (queuey),Y
        INY
        BNE comp_down2
        INC queuex+1
        INC queuey+1
        DEX
        BNE comp_down2
        LDA #&02
        STA paging_reg
        RTS
 ]
NEXT
*SAVE :0.6.COMPOS 1200 18FF 1300
```

A2.16. 'C' program PROFILE.

This is the program used to produce the isometric projections of the digitised images shown in Chapter 1 and Chapter 3. The program is written in the 'Lattice' version of the 'C' programming language (222) distributed by Metacomco for the Sinclair QL. This facility was not available until several months after collection of digitised images was complete.

The program requires a QL with a minimum of 256k expansion memory to function and allows several operations to be performed on a digitised image besides the production of an isometric plot. Most of these routines were used to produce the isometric images used in Chapter 1 to demonstrate the various properties of digitised images and to demostrate how they can be manipulated.

It should be noted that this program was written in approximately two weeks (starting with no knowledge of 'C') whereas the COMPOS routine above was still being perfected after 6 months.

```
#include "ram1_stdio_h"
#include "ram1_qdos_h"
#include "ram1_ctype_h"
#include "ram1_math_h"
#include "ram1_limits_h"

#define newline 10
#define formfeed 12
#define esc 27
#define picmax 256
#define profxmax 768
#define profymax 64

FILE *infile_fp,*serp,*fopen();

char serial_out[7]= "ser1hr";
char infile[] = "flp1_filename_extension_etc";

unsigned char (*s_pic)[picmax][picmax];
unsigned char (*d_pic)[picmax][picmax];
unsigned char (*prof_pic)[profxmax][profymax];

char choice = '=';
main()
{
```

```
   init_printer();
   s_pic = (unsigned char (*)[picmax][picmax]) getmem(65536);
   d_pic = (unsigned char (*)[picmax][picmax]) getmem(65536);
   prof_pic = (unsigned char (*)[profxmax][profymax]) getmem(49152);
   init_arrays();
   while (choice!='q')
   {
      action_menu();
      choice = (char) getc(stdin);
      if (isalpha( choice ) == 0 ) continue;
      select_action();
   }
}

init_arrays()
{
   setmem(s_pic, 65536, 0);
   setmem(d_pic, 65536, 0);
   setmem(prof_pic, 49152, 0);
}

white_noise()
{
   unsigned short i,j;
   for (i=0; i<=255; i++)
   {
      for (j=0; j<=255; j++)
      {
         (*s_pic)[i][j] += (unsigned char) (drand48()* 4.0 );
      }
   }
}

mean32()
{
   unsigned short i, j, k;
   int nsum;
   for (i=0; i<=255; i++)
   {
      for (j=0; j<=255; j++)
      {
         nsum = 0;
         for (k=1; k<=32; k++)
         {
           nsum += (int) ( drand48()* 4.0 );
         }
         (*s_pic)[i][j] = (unsigned char) ((nsum + 32 * (int)(*s_pic)[i][j])/32);
      }
   }
}

clip()
{
   unsigned short i,j;
   int below;
   cls();
   printf("\n\nPlease enter the value to clip at \n\n ----> ");
   scanf(" %d",&below);
```

```
   for (i=0; i<=255; i++)
   {
      for (j=0; j<=255; j++)
      {
         (*s_pic)[i][j] = ((*s_pic)[i][j] <= below) ? 0 : (*s_pic)[i][j] ;
      }
   }
}

reduce_contrast()
{
   unsigned short i,j;
   int newmax, temp;
   cls();
   printf("\n\nPlease enter the new maximum value \n\n ----)  ");
   scanf(" %d", &newmax);
   printf(" Newmax is %d\n\n", newmax);
   for (i=0; i<=255; i++)
   {
      for (j=0; j<=255; j++)
      {
         temp = (int) (newmax * (*s_pic)[i][j]);
         (*s_pic)[i][j] = (unsigned char) (temp>>8);
      }
   }
}

Enhance_contrast()
{
   int biggest = 0;
   int smallest = 500;
   unsigned short i,j;
   for (i=0; i<=255; i++)
   {
      for (j=0; j<=255; j++)
      {
         biggest = max((*s_pic)[i][j], biggest);
         smallest = min((*s_pic)[i][j], smallest);
      }
   }
   biggest-=smallest;
   for (i=0; i<=255; i++)
   {
     for (j=0; j<=255; j++)
     {
        (*s_pic)[i][j]=(unsigned char)(((*s_pic)[i][j]-smallest)*256/biggest);
      }
   }
}

smoothing_filter()
{
   unsigned int temp;
   unsigned short i,j;
   for (i=1; i<=254; i++)
   {
      for (j=1; j<=254; j++)
      {
```

```
         temp= (*s_pic)[i][j];
         temp*=8;
         temp+=(*s_pic)[i-1][j-1]+(*s_pic)[i-1][j]+(*s_pic)[i-1][j+1];
         temp+=(*s_pic)[i][j-1]+(*s_pic)[i][j+1];
         temp+=(*s_pic)[i+1][j-1]+(*s_pic)[i+1][j]+(*s_pic)[i+1][j+1];
         (*d_pic)[i][j] = (unsigned char) (temp>>4);
      }
   }
   swap_em();
}

laplace_sharpening()
{
   int i,j,k;
   for (i=0; i<picmax-1; i++)
   {
      for (j=0; j<picmax-1; j++)
      {
         k=(*s_pic)[i][j]*5-(*s_pic)[i+1][j]-(*s_pic)[i-1][j]-(*s_pic)[i][j+1]-(*s_pic)[i][j-1];
         k=(k>255) ? 255 : k;
         k=(k<0) ? 0 : k;
         (*d_pic)[i][j]=k;
      }
   }
   swap_em();
}

swap_em()
{
   unsigned char (*temp)[picmax][picmax];
   temp =  s_pic;
   s_pic = d_pic;
   d_pic = (unsigned char (*)[picmax][picmax]) temp;
}

get_infile_name()
{
   cls();
   printf("The current file name is --> %s",infile);
   printf("\n\nPlease enter new name or 'CR'.\n\n-->");
   scanf("%s", infile);
}

dump_it()
{
   int i,j;
   fprintf(serp,"%c%c%c%c%c",esc,51,24,13,10);
   for (j=profymax-1; j>=0; j--)
   {
      fprintf(serp,"%s%c%c%c%c%c","          ",esc,42,1,0,3);
      for (i=0; i<=profxmax-1; i++)
      {
        putc((*prof_pic)[i][j],serp);
      }
      fprintf(serp,"%c%c",13,10);
   }
   fprintf(serp,"%c%c%c",13,13,formfeed);
   i=fclose(serp);
```

```
   init_printer();
}

cls()
{
   struct REGS in,out;
   in.D0 = 0x20;
   in.D3 = -1;
   in.A0 = (char *) fgetchid(stdout);
   qdos3(&in,&out);
}

blankline( x,yl,yh)
int x,yl,yh;
{
   int loopctr,ychar,ybit,flag;
   for ( loopctr=yl; loopctr<yh; loopctr++)
   {
      ychar=loopctr>>3;
      ybit=loopctr&7;
      switch (ybit)
      {
         case 0 : flag=254;break;
         case 1 : flag=253;break;
         case 2 : flag=251;break;
         case 3 : flag=247;break;
         case 4 : flag=239;break;
         case 5 : flag=223;break;
         case 6 : flag=191;break;
         case 7 : flag=127;break;
      }
      (*prof_pic)[x][ychar]&=flag;
   }
}

drawline(x,yl,yh)
int x,yl,yh;
{
   int loopctr,ybit,ychar,flag;
   for (loopctr=yl; loopctr<=yh; loopctr++)
   {
      ychar=loopctr>>3;
      ybit=loopctr & 7;
      switch (ybit)
      {
         case 0 : flag=1;break;
         case 1 : flag=2;break;
         case 2 : flag=4;break;
         case 3 : flag=8;break;
         case 4 : flag=16;break;
         case 5 : flag=32;break;
         case 6 : flag=64;break;
         case 7 : flag=128;break;
      }
      (*prof_pic)[x][ychar]|=flag;
   }
}
```

```
profile()
{
   int xbase,ybase,ytop,oldy,hwy;
   int i,j;
   for (i=0; i<=profxmax-1; i++)
      for (j=0; j<=profymax-1;j++)
         (*prof_pic)[i][j]=0;
   for (j=254; j>=0; j-=2)
   {
      oldy=j;
      for (i=0; i<=255; i++)
      {
         xbase=255+i*2-j;
         ybase=j;
         ytop=j+(*s_pic)[i][j];
         hwy=(ytop-oldy)/2+oldy;
         if (hwy>=oldy)
         {
            blankline(xbase,ybase,oldy);
            blankline(xbase+1,ybase,hwy);
            drawline(xbase,oldy,hwy);
            drawline(xbase+1,hwy,ytop);
         }
         else
         {
            blankline(xbase,ybase,hwy);
            blankline(xbase+1,ybase,oldy);
            drawline(xbase,hwy,oldy);
            drawline(xbase+1,ytop,hwy);
         }
         oldy=ytop;
      }
   }
}

loadfile()
{
   int retcode,i,j;
   if  ( (infile_fp=fopen(infile,"r") ) == NULL)
   {
      printf("\File %s does not exist\n\n", infile);
      return(0);
   }
   for (i=255; i>=0; i--)
   {
      for (j=255; j>=0; j--)
      {
         (*s_pic)[i][j]=(unsigned char) getc(infile_fp);
      }
   }
   retcode=fclose(infile_fp);
   if (retcode != 0)
   {
      printf(" Problems closing %s\n", infile);
      return(0);
   }
}
```

```
trim_edges()
{
   int i;
   for ( i=0; i<=255; i++)
   {
      (*s_pic)[i][0] = 0;
      (*s_pic)[i][picmax] = 0;
      (*s_pic)[0][i] = 0;
      (*s_pic)[picmax][i] = 0;
   }
}

action_menu()
/* presents a list of possible actions to do to *(*s_pic)[ */
{
   cls();
   printf("\n  Current file name is --> %s",infile);
   printf("\n\n  Action menu: use first letter to indicate choice.");
   printf("\n     F)ilename.");
   printf("\n     S)moothing filter.");
   printf("\n     E)nhance contrast.");
   printf("\n     R)educe contrast.");
   printf("\n     C)lip.");
   printf("\n     P)rofile. ");
   printf("\n     M)ean of 32 frames with white noise added. ");
   printf("\n     D)ump profile to printer.");
   printf("\n     L)oad current specified file.");
   printf("\n     W)hite noise added.");
   printf("\n     LA)placian sharpening filter.");
   printf("\n     T)rim edges to zero");
   printf("\n     Q)uit the program.");
   printf("\n\n Input is --->");
}

init_printer()
{
   serp=fopen(serial_out,"w");
}

select_action()
{
   switch (choice)
   {
      case 'f':
         get_infile_name(); /* get name of file to operate on */
         break;
      case 't':
         trim_edges(); /*Set the 1 pixel border at the edge of an image to zero */
         break;
      case 's':
         smoothing_filter(); /* 3x3 smoothing filter */
         break;
      case 'e':
         enhance_contrast(); /* contrast enhancement grey range -> 0 to 255 */
         break;
      case 'c':
         clip(); /* set anything <= clipval to zero */
         break;
```

```
      case 'p':
         profile(); /* hidden line removal plot of *s_pi into pic */
         break;
      case 'd':
         dump_it();/* dump profile to printer */
         break;
      case 'l':
         loadfile(); /* load the file specified by infile */
         break;
      case 'm':
         mean32(); /* average of 32 frames of an image with white noise */
         break;
      case 'w':
         white_noise();
         break;
      case 'a':
         laplace_sharpening();
         break;
      case 'r' :
         reduce_contrast();
         break;
      default :
         printf("\nNo such option ???????");
         break;
   }
}
```

Chapter 7.

7. References.

1. Pharmaceutical dosage forms: Tablets. Volume 2, Ed H. A. Lieberman, L. Lachman, Marcel Dekker Inc, New York, (1981), ISBN 0-8247-1269-2.

2. J. E. Rees, Characterisation of Pharmaceutical Particulate Materials, *Boll. Chim. Farm.*, **116**, (1977), 125-141.

3. Standards for content of active ingredient in tablets. *British Pharmacopoeia*, Her Majesty's Stationary Office, SBN 11320426, (1973), 460.

4. Monograph on Content Uniformity, *United States Pharmacopoeia, National Formulary*, United States Pharmacopoeial Convention INC, **20th Revision**, (1980), ISBN 0195-7996, 955-957.

5. D. Train, Pharmaceutical Aspects of Mixing Solids, *Pharm. J.*, **185**, 6th August, (1960), 129-134.

6. R. E. Moskalyk, L. G. Chatten, C. E. Cox, M. Pernarowski, Uniformity of drug dosage in compressed tablets., *J. Pharm. Sci.*, **50**, (1961), 650-657.

7. Monograph on Dexamathasone tablets., *British Pharmacopoeia*, Her Majesty's Stationary Office, SBN 11320426, (1973), 146.

8. Monograph on Digoxin tablets., *British Pharmacopoeia*, Her Majesty's Stationary Office, SBN 11320426, (1973), 163-164.

9. J. Cooper, "Inert" Components of Pharmaceutical Preparations., *Drug Dev. and Industrial Pharmacy*, **5**, (1979), 293-334.

10. Homogeneous, In: The Concise Oxford Dictionary, Ed J. B. Sykes, 6th Edition, Clarendon Press, Oxford, ISBN 0-19-861121-8, (1976), 514-515.

11. P. M. C. Lacey, The mixing of solid particles, *Trans. Inst. Chem. Eng.*, **21**, (1943), 53-59.

12. P. M. C. Lacey, Developments in the theory of particle mixing, *J. Appl. Chem.*, **4**, (1954), 257-268.

13. J. Bridgewater, Fundamental powder mixing mechanisms.,*Powder Technol,*, **15**, (1976), 215-236.

14. K. Sommer, Powder mixing mechanisms., *Journal of Powder & Bulk Solids Technology.*, **3(4)**, (1979), 2-9.

15. J. N. Staniforth, Advances in powder mixing and segregation in relation to pharmaceutical processing., *Int. J. Pharm. Tech. & Prod. Mfr.*, **3(Suppl)**, (1982), 1-12.

16. J. C. Williams, The mixing of dry powders., *Powder Technol.*, **2**, (1968/69), 13-20.

17. D. Buslik, Mixing and sampling with special reference to multisize granular materials., *ASTM Bull.*, **165**, (1950), 66-73.

18. S. S. Weidenbaum, C. F. Bonilla, A fundamental study of the mixing of particulate solids., *Chem. Eng. Progr.*, **51**, (1955), 27J-36J.

19. K. R. Poole, R. F. Taylor, G. P. Wall, Mixing powders to fine scale homogeneity: Studies of batch mixing., *Trans. Instn. Chem. Engrs.*, **42**, (1964), T305-T315.

20. D.S. Cahn, D. W. Fuerstenau, A probablistic model of the diffusional mixing of particlulate solids., *Powder Technol.*, **2**, (1968/69), 215-222.

21. R. Hogg, G. Mempel, D. W. Fuerstenau, The mixing of trace quantities into particlulate solids, *Powder Technol.*, **2**, (1968/69), 223-228.

22. M. C. R. Johnson, Particle size distributions of the active ingredient for solid dosage forms of low dosage., *Pharm. Acta. Helv.*, **47**, (1972), 546-559.

23. H. Gjelstrup Kristensen, Statistical properties of random and non-random mixtures of dry solids. Part 1: A general expression for the variance of the composition of samples., *Powder Technol.*, **7**, (1983), 249-257.

24. H. Gjelstrup Kristensen, Statistical properties of random and non-random mixtures of dry solids. Part 2: Variance-sample size relationships derived by autocorrelation theories., *Powder Technol.*, **8**, (1983), 149-157.

25. K. Sommer, H. Rumpf, The variance of stochastic homogeneity of multicomponent powders with highly different particle sizes and its practical application., CHISA 75 (Prague), *Mixing of Particluate Solids*, **C1.3.**, 25-29 Aug., (1975), 17pp.

26. K. Sommer, Statistics of mixedness with unequal particle sizes., *Journal of Powder & Bulk Solids Technology.*, **3(4)**, (1979), 10-14.

27. Z. T. Chowhan, E. E. Linn, Li-Hua Chi, Mixing of pharmaceutical solids II: Evaluation of multicomponent mixing of cohesive powders in cylindrical shear mixer., *J. Pharm. Sci.*, **70(3)**, (1981), 243-247.

28. Z. T. Chowhan, Li-Hua Chi, Mixing of pharmaceutical solids III: Multivariate statistical analysis of multicomponent mixing., *J. Pharm. Sci.*, **70(3)**, (1981), 247-251.

29. D. S. Cahn, D. W. Fuerstenau, Simulation of diffusional mixing of particulate solids by Monte Carlo techniques., *Powder Technol.*, **1**, (1967), 174-182.

30. R. S. C. Rogers, R. P. Gardner, A Monte Carlo method for simulating dispersion and transport through horizontal rotating cylinders., *Powder Technol.*, **23**, (1979), 159-167.

31. M. D. Faiman, E. G. Rippie, Segregation kinetics of particulate solid systems III: Dependence on agitation intesity., *J. Pharm. Sci.*, **54**, (1965), 719-722.

32. J. C. Williams, M. I. Khan, The mixing and segregation of particulate solids of different particle size., *The Chemical Engineer.*, **January**, (1973), 19-25.

33. J. C. Williams, The segregation of particulate materials. A review., *Powder Technol.*, **15**, (1976), 245-251.

34. Z. T. Chowhan, E. E. Linn, Mixing of pharmaceutical solids. I. Effect of particle size on mixing in cylindrical shear and V-shaped tumbling mixers., *Powder Technol.*, **24**, (1979), 237-244.

35. Z. T. Chowhan, Lu-Hua Chi, I-Chang Yang, Mixing of Pharmaceutical Solids. IV. Effects of concentration and material properties on multicomponent mixing of cohesive powders., *Powder Technol.*, **29**, (1981), 251-256.

36. W. B. Pietsch, Adhesion and agglomeration of solids during storage, flow and handling-A survey., *Transactions of the ASME Journal of Engineering for Industry.*, **May**, (1969), 435-449.

37. N. A. Orr, E. Shotton, The mixing of cohesive powders., *The Chemical Engineer*, **January**, (1973), 12-18.

38. S. Varthalis, N. Pilpel, Anomalies in some properties of powder mixtures., *J. Pharm. Pharmac.*, **28**, (1976), 415-419.

39. D. F. Bagster, M. J. Crooks, Evaluation of some properties of powder mixtures., *Drug Development and Industrial Pharmacy*, **4(5)**, (1978), 413-425.

40. J. Klein, J. D. Wilcox, The effect of blending on the properties of powders treated with a hydrophobic Silica., *Powder Technol.*, **6**, (1972), 25-31.

41. N. Pilpel, Metal stearates in pharmaceuticals and cosmetics., *Manuf. Chem. Aerosol News*, **42**, (1971), 37-40.

42. M. Peleg, C. H. Mannehiem, Effect of condtioners on the flow properties of powdered Sucrose., *Powder Technol.*, **7**, (1973), 45-50.

43. P. York, The use of glidants to improve the flowability of fine Lactose powder., *Powder Technol.*, **11(2)**, (1975), 197-198.

44. S. Varthalis, N. Pilpel, The action of colloidal silicon dioxide as a glidant for lactose, paracetamol, oxytetracycline and their mixtures., *J. Pharm. Pharmac.*, **29**, (1977), 37-40.

45. J. Cibrowski, A. Wolny, The effects of moisture content of loose materials on the dynamics of their mixing., *Int. Chem. Eng.*, **8(2)**, (1968), 199-204.

46. V. K. Karra, D. W. Fuerstenau, The effects of humidity on the trace mixing kinetics in fine powders., *Powder Technol.*, **16(1)**, (1977), 97-105.

47. M. C. Coelho, N. Harnby. The effect of moisture on the equilibrium mixture quality of powders., *Powder Technol.*, **23(2)**, (1979), 209-217.

48. P. L. Stephenson, W. J. Theil, The effect of humidity on the production of ordered mixtures., *Powder Technol.*, **25(1)**, (1980), 115-119.

49. J. A. Hersey, Ordered Mixing: A New Concept in Powder Mixing Practise., *Powder Technol.*, **11**, (1975), 41-44.

50. J. A. Hersey, The development and applicability of powder mixing theory., *Int. J. Phar. Tech & Prod. Mfr.*, **1(1)**, (1979), 6-13.

51. D. N. Travers, Some observations on the ordered mixing of micronised Sodium Bicarbonate with Sucrose crystals., *Powder Technol.*, **12(2)**, (1975), 189-190.

52. M. J. Crooks, R. Ho, Ordered mixing in direct compression of tablets., *Powder Technol.*, **14**, (1976), 161-167.

53. H. Egermann, I. Kemptner, E. Pichler, Effects of interparticulate interactions on mixing homogeneity., *Drug Development and Industrial Pharmacy*, **11(2 & 3)**, (1985), 663-676.

54. F. K. Y. Lai, J. A. Hersey, Simulated ordered powder mixture, *International Journal of Pharmaceutics.*, **36**, (1987), 157-164.

55. C. W. Yip and J. A. Hersey, Perfect powder mixtures., *Powder Technol.*, **16(2)**, (1977), 189-192.

56. J. E. Rees and J. N. Staniforth, Charcterisation of ordered mixes using X-ray microanalysis, *Powder Technol.*, **23**, (1979), 135-138.

57. C. C. Yeung, J. A. Hersey, Ordered powder mixing of coarse and fine particlulate systems., *Powder Technol.*, **22(1)**, (1979), 127-131.

58. J. E. Rees, J. N. Staniforth, The segregation of perfect powder mixes, *J. Pharm. Pharacol.*, **30(Suppl)**, (1978), 24P.

59. N. Orr, Assessment of an ordered mix., *Powder Technol.*, **24**, (1979), 105-106.

60. H. Egermann, Effects of adhesion on mixing homogeneity. Part1: Ordered adhesion-random adhesion, *Powder Technol.*, **27**, (1980), 203-206.

61. F. Lai, J. A. Hersey, The variance-sample size relationship and the effects of magnesium stearate on ordered powder mixtures. *Chem. Eng. Sci.*, **36(7)**, (1981), 1133-1137.

62. D. Bryan, Y. Rungvejhavattivittaya, P.J.Stewart, Mixing and demixing of microdose quantities of Sodium Salicylate in a direct compression vehicle., *Powder Technol.*, **22**, (1979), 147-151.

63. M. Wayer, M. Kata, The mixing of powders with very low active content., *Acta Pharmaceutica Technologica*, **23(1)**, (1977), 63-68.

64. P. J. Stewart, Influence of Magnesium Stearate on the homogeneity of a Prednisone-granule Ordered Mix., *Drug Dev. Ind. Pharm.*, **7(5)**, (1981), 485-495.

65. C. W. Yip, J. A. Hersey, Segregation in Ordered Powder Mixtures., *Powder Technol.*, **16(1)**, (1977), 149-150.

66. F. Lai, J. A. Hersey, J. N. Staniforth, Segregation and mixing of fine particles in an ordered mixture., *Powder Technol.*, **28(1)**, (1981), 17-23.

67. F. Lai, J. A. Hersey, Mixing performance of a V-Blender, *Inst. Chem. Eng. Symp. Ser.*, **65**, (1981), S1/C/1-S1/C/6.

68. J. N. Staniforth, J. E. Rees, J. B. Kayes, Relation between mixing time and segregation of ordered mixes., *J. Pharm. Pharmacol.*, **23(3)**, (1982), 175-176.

69. J. N. Staniforth, J. E. Rees, F. K. Lai, J. A. Hersey, Interparticle forces in binary and ternary ordered powder mixes., *J. Pharm. Pharmacol.*, **34**, (1982), 141-145.

70. J. N. Staniforth, Determination and handling of total mixes in pharmaceutical systems., *Powder Technol.*, **33**, (1982), 147-159.

71. J. Verraes, R. Kinget, Ordered powder mixing: Theory and practise, *Int. J. Pharm. Tech. and Prod. Manuf.*, **1(3)**, (1980), 36-41.

72. A. G. Bailey, Electrostatic phenomena during powder handling, *Powder Technol.*, **37**, (1984), 71-85.

73. D. K. Donald, Contribution of charge to powder particle adhesion, *J. Adhesion*, **4**, (1972), 223-245.

74. H. Krupp, Particle adhesion and theory., *Advan. Colloid Interface Sci.*, **1**, (1967), 111-239.

75. L. V. Azaroff, J. J. Brophy, Electronic processes in materials, McGraw-Hill Book Company, INC., Library of Congress Catalog Card Number 62-2156602669, (1963), 462pp.

76. A. Nussbaum, Electronic and magnetic properties of materials, Ed J. Dorn, Prentice Hall series in Materials Science, Prentice-Hall Inc, New Jersey, Library of Congress Catalog Card Number 67-23371, (1967), 155pp.

77. J. H. de Boer, Atomic Forces and Adsorption, 1-64, Unattributable source. Alternative source J. H. de Boer, *Trans. Faraday Soc.*, **32**, (1936), 10.

78. H. C. Hamaker, The London-Van der Waals Attraction between spherical particles., *Physica*, **4**, 23rd November, (1937), 1058-1072.

79. E. M. Lifschitz, The theory of molecular attractive forces between solids., *Soviet Physics J.E.T.P*, **2**, (1956), 78-83.

80. A. D. Moore (Editor), Electrostatics and its applications, John Wiley and Sons, ISBN 0-471-61450-5, (1973), 481pp.

81. J. C. McClure, D. V. Keller, Adhesion of micron sized Coal Particles to a massive Coal substrate., *J. Adhesion*, **5**, (1973), 17-27.

82. P. J. Sherrington, R. Oliver, Fundamentals of particle size enlargement by granulation., In: Granulation, Heyden, London, (1980), 7-21.

83. J. Visser, Colloid and other forces on particle adhesion and particle removal.(A review)., *Deposition Filtr. Part. Gases. Liq. Symp.*, (1978), 121-141.

84. R. E. Press, The chemical electron., Concepts in chemistry, Longman Group Ltd, London, ISBN 0-582-32149-2, (1969), 114pp.

85. A. N. Martin, J. Swarbrick, A. Cammarata, Intermolecular forces and states of matter., In: Physical Pharmacy, Lea and Febiger, Philadelphia, 2nd Edition, ISBN0-8121-0163-4, (1969), 66-101.

86. V. M. Muller, B. V. Deryaguin, Yu. P. Toporov, Effect of elastic contact deformation on the adhesion of particles., *Colloid J. USSR*, **38(1)**, (1976), 41-47.

87. B. V. Deryaguin, V. M. Muller, Yu, P. Toporov, Influence of contact deformations on particle adhesion. 2. Macroscopic calculation of adhesive force with allowance for contact deformations in spherical elastic particles., *Colloid J. USSR*, **37(6)**, (1975), 962-969.

88. D. Tabor, Surface forces and surface interactions., *Journal of Colloid and interface Science.*, **58(1)**, (1977), 2-13.

89. B. V. Deryaguin, V. M. Muller, Yu. P. Toporov, I. N. Aleinikova, The role of the pressing-on in the adhesion of elastic particles., *Powder Technology*, **37**, (1984), 87-93.

90. K. Malmqvist, C. Nystrom, Studies on direct compression of tablets VII: Sieve methods for the charaacterisation of the adhesion tendency in ordered mixing., *Acta. Pharm. Suecica.*, **19**, (1982), 437-446.

91. C. Nystrom, K. Malmkvist, Studies on direct compression of tablets. 1: The effect of particle size in mixing finely divided powders with granules., *Acta. Pharm. Suec.*, **17**, (1980), 282-287.

92. J. N. Staniforth, Relationship between vibration produced during handling and segregation of pharmaceutical powder mixes., Powder and Bulk Solids Handling and Processing; Int. Prog., Cahners Exposition Group., (1982), 203A-203N.

93. P. L. Stephenson, W. J. Thiel, The mechanical stability of ordered mixtures when fluidized and their pharmaceutical application.Powder Technol. 26, 225, (1980).

94. H. G. Kristensen, Homogeneity of low dose tablet formulations., *Acta. Pharm. Suec.*, **18**, 81, 1981.

95. J. N. Staniforth, J. E. Rees, F. K. Lai, J.A. Hersey, Determination of interparticle forces in ordered powder mixes., *J. Pharm. Pharmacol.*, **33**, (1981), 485-490.

96. S. Laycock, J. N. Staniforth, A method for determining interparticle forces in ordered mixes., *Labo. Pharma. Probl. Tech.*, **32**, (1984), 185-189.

97. D. F. St. John, D. J. Montgomery, Adhesion of small metal spheres to plane metal substrates. *Journal of Applied Physics*, **42(2)**, (1971), 663-668.

98. G. Bohme, P.Hohn, H. Krupp, H. Rabenhorst, W. Schnabel, G. Walter, Adhesion of gold particles to silicon and gold substrates in ultrahigh vacuum., *J. Appl. Phys.*, **44(9)**, (1973), 3914-3918.

99. B. M. Bozorg, G. E. Klinzing, Adhesion of Alumina powder to glass surfaces., *The Canadian Journal of Chemical Engineering*, **57**, (1979), 655-658.

100. J. N. Staniforth, J. E. Rees, Electrostatic charge interactions in ordered powder mixes., *J. Pharm. Pharmacol.*, **34**, (1982), 69-76.

101. A. B. Ketkar, D. V. Keller, Adhesion of micron sized limestone particles to a massive coal substrate., *J. Adhesion*, **7**, (1975), 235-251.

102. W. Schutz, Influence of pressing forces and of atmospheric humidity on particle adhesion., *Deposition Filtr. Part. Gases Liq. Symp. Soc. Chem. Ind.*, London(England), (1978), 199-210.

103. J. A. Cross, A. Cetronio, Electrostatic forces and adheson of particles. *Deposition Filtr. Part. Gases Liq. Symp. Soc. Chem. Ind.*, London(England), (1978), 227-239.

104. S. Laycock, J. N. Staniforth, Problems encountered in accurate determination of interparticle forces in ordered mixes., *Particulate Science and Technology*, **1**, (1983), 259-268.

105. J. N. Staniforth, Interparticle forces in ordered mixes., *J. Pharm. Pharmacol. (Suppl)*, (1980), 23P.

106. J. N. Staniforth, Ordered mixing of drugs with particulate excipients, Ph.D. Thesis, University of Aston in Birmingham, 1980.

107. P. York, Solid-state properties of powders in the formulation and processing of solid dosage forms, *Int. J. Pharm.*, **14**, (1983), 1-28.

108. R. Huttenrauch, I. Keiner, Influence of lattice defects upon mixing processes., *Powder Technol.*, **22**, (1979), 289-290.

109. R. S. Bradley, The cohesive force between solid surfaces and the surface energy of solids., *Phil. Mag.*, **13**, (1932), 853-862.

110. W. J. Whitfield, A study of the effects of relative humidity on small particle adhesion to surfaces, *Surf. Contam.: Genesis, Detect., Control, [Proc Symp]*, **1**, (1978) Pub. 1979, 73-81.

111. G. T. Dzodziev, V. E. Grakov, A. A. Kal'kov, L. I. Klyachko, S. A. Alekseev., Vacuum mixing of powders., *Powder Metallurgy Industry, Economics, and Organisation of Production.*, **14(A) Sept**, (1975), 764-767.

112. K. H. Ludde, Formation of excess electrical charge of pharmaceutical solids and influence to powdertechnology., In:*Mixing of particulate solids, CHISA 75 (Prague)*, **C1.8**, (25-29 August 1975), 2-17.

113. J. N. Staniforth, The effect of frictional charges on flow properties of direct compression tableting excipients, *Int. J. Pharm.*, **11**, (1982), 109-117.

114. I. Krycer, J. A. Hersey, Fine powder mixing in a vibratory ball mill., *Int. J. Pharm.*, **6(2)**, (1980), 119-129.

115. J. A. Cross, Electrostatic charging and ignition of dusts, *Proc. I. Chem. E. Symposium Series*, **58**, (1980), 1-10.

116. C. L. Tucker III and Nam P. Suh, Electrostatic powder mixing., *Polym. Eng. and Sci.*, **16(10)**, (1976), 657-663.

117. G. G. Enstad, A theoretical investigation of electrostatic mixing of a coarse and a fine powder, *J. Electrostatics*, **10**, (1981), 183-188.

118. G. G. Enstad, Electrostatic mixing of powders, *I. Chem. E. Symposium Series*, **No. 65**, (1981), S3/1/1-S3/L/8.

119. J. N. Staniforth, J. E. Rees, Powder mixing by triboelectrification, *Powder Technol.*, **30**, (1981), 255-256, (1981).

120. Morio Jido, Method for blending by combining fine particles, US Pat 4383767, 17 May 1983.

121. J. A. Cross, Applications of electrostatics, *Phys. Technol.*, **12**, (1981), 54-59.

122. J. Hughes, Electrostatics and applications to industrial processes, In:Lecture notes for Summer School In Electrostatics, Industrial Development Bangor Ltd., University College of North Wales, Bangor, 16-18 September, (1981), 73-111.

123. W. H. Walton, Summary of Porton Report No. 2465: First report on the electrical characteristics of resin impregnated filters, Porton Report No 2465, Chemical Defence Establishment, Porton Down, (1940).

124. D. F. Sherony, Packing of binary granular mixtures which triboelectrically interact, *Powder Technol.*, **11**, (1975), 85-86, (1975).

125. F. J. Feltham, Second thoughts on the Hansen electrostatic filter, *Filtration and Separation*, **Sept/Oct**, (1976), 467-469.

126. M. J. Pearse, A. D. Read, Triboelectric separation - A dry process for separating particulate mixtures. Warren Spring Laboroatory Report, LR 223 [MP], (1976).

127. G. W. Penney, Using electrostatic forces to reduce pressure drop in fabric filters., *Powder Technol.*, **18**, (1977), 111-116.

128. M. Carta, G. Alfano, P. Carbini, R. Ciccu, C. Del Fa, Triboelectric phenomena in mineral processing: Theoretic Fundamentals and Applications., *Journal of Electrostatics*, **10**, (1981), 177-182.

129. G. A. Kallio, P. W. Dietz, Image charge collection of fine particles in granular beds. *Gas Born Particles, Conf., Mech. Eng. Publ.*, **C73**, (1981), 101-110.

130. S. Mukherjee, K. a. Nielsen, J. C. Hill, Effect of electrical forces on particle collection by spheres and spheroids., *Journal of Powder and Bulk Solids Technology*, **2**, (1978), 29-37.

131. O. Heaviside, Electromagnetic induction and its propagation, *The Electrician*, August 7, (1885), 230-231.

132. O. Heaviside, Electrical Papers, Volume 1, Macmillan (London), (1982), 488-493.

133. B. Gross, Charge storage in solid dielectrics., Elselvier (Amsterdam), (1964).

134. G. M. Sessler (Editor), Electrets: Topics in applied physics., Volume 33, Springer-Verlag (Berlin, Heidelburg), 1980, ISBN 3-540-09570-5 or ISBN 0-387-09570-5.

135. H. J. Wintle, Introduction to electrets, *The Journal of the Acoustical Society of America*, **53(6)**, (1973), 1578-1588.

136. R. N. Varney, H. T. Hahn, Electrets and electrostatic measurement. *American Journal of Physics*, **43(6)**, (1975), 509-513.

137. G. M. Sessler, Physical principles of electrets., In Electrets: Topics in applied physics, Volume 33, G. M. Sessler (Editor), Springer-Verlag (Berlin, Heidelburg), ISBN 3-540-09570-5 or ISBN 0-387-09570-5, (1980), 13-80.

138. J. van Turnhout, W. J. Hoenveld, J. Willem, C. Adamse, L. M. van Rossen, Electret filters for high efficiency and high flow air cleaning, *IEEE Transactions on Industry Applications*, **1A-17(2)**, (1981), 240-248.

139. L. C. Wadsworth, P. Hersh, Method of making fibrous electrets, US Pat. 4-375-718, 4p, March 8, (1983).

140. G. M. Sessler, J. E. West, Applications., In Electrets: Topics in applied physics, Volume 33, G. M. Sessler (Editor), Springer-Verlag (Berlin, Heidelburg), ISBN 3-540-09570-5 or ISBN 0-387-09570-5, (1980), 347-382.

141. B. Gross, Radiation-induced charge storage and polarisation effects., In Electrets: Topics in applied physics, G. M. Sessler (Editor), Springer-Verlag (Berlin, Heidelburg), ISBN 3-540-09570-5 or ISBN 0-387-09570-5, (1980), 217-284.

142. G. A. Baum, Thermal depolaristion currents of regenerated cellulose films., *J. Appl. Polym. Sci.*, **17**, (1973), 2855-2866.

143. Masami Fushitani, Thermally stimulated currents in wood electrets., *Mokuzai Gakkaishi*, **24(1)**, (1978), 7-11. (Japanese, English abstract)

144. Atsushi Sawatari, Thermally stimulated current of cellulose electrets., *Charge Storage, Charge Transp. Electrost. Their Appl. Stud. Electr. Electron. Eng.*, **2**, (1979), 347-351.

145. A. Sawatari, H. Kurihara, T. Takashima, Thermally stimulated current of cellulose powder., *Mokuzai Gakkaishi*, **24(4)**, (1978), 224-9.
(Japanese, English abstract)

146. P. K. C. Pillai, M. Mollah, Thermo-induced electrical current from paper cellulose sandwiched between metal electrodes., *Charge Storage, Charge Transp. Electrost. Their Appl. Stud. Electr. Electron. Eng.*, **2**, (1979), 352-356.

147. P. K. C. Pillai, M. Mollah, Polarisation and thermally stimuated discharge current studies in cellophane thermoelectrets., *J. Macromol. Sci. Phys.*, **B17(1)**, (1980), 69-81.

148. K. K. Saini, I. M. Talwar, N. Lal, K. Mahash, K. K. Nagapaul, Thermally stimulated depolarization studies of cellulose nitrate. *Acta Polym.*, **34(1)**, (1983), 16-18.

149. I. M. Talwar, D. I. Sharma, Dielectric relaxation studies of cellulose, *Journal of Electrostatics*, **9**, (1980), 49-58.

150. C. I. Simionescu, E. Neagu, M. Leanca, C. Chelaru, Thermally stimulated studies in cellulose hydrate film electrets, *Cellulose Chem. Technol.*, **18**, (1984), 389-393.

151. M. Eguchi, Variation of electrical conductivity of oils and waxes., *Proc. Phys.-Math. Soc. Japan*, **1**, (1919), 320.
(Abstract IV/2/2 in reference 133)

152. M. Eguchi, On dielectric polarisation., *Proc. Phys.-Math. Soc. Japan*, **1**, (1919), 326.
(Abstract IV/2/3 in reference 133)

153. M. Eguchi, Further researches on permanently polarized dielectric., *Proc. Phys.-Math. Soc. Japan*, **2**, (1920), 169.
(Abstract IV/2/4 in reference 133)

154. M. Eguchi, On the temporary destruction of the apparent charges of permanently charged dielectrics by X-rays., *Proc. Phys.-Math. Soc. Japan*, **2**, (1920), 45.
(Abstract IV/2/5 in reference 133)

155. M. Eguchi, On the intensity of polarization or dielectric displacement of a permanent electret., *Proc. Phys.-Math. Soc. Japan*, **3**, (1921), 2.
(Abstract IV/2/6 in reference 133)

156. M. Eguchi, Effects of electric force on a permanent electret., *Proc. Phys.-Math. Soc. Japan*, **3**, (1921), 110.
(Abstract IV/2/7 in reference 133)

157. M. Eguchi, Some experimental studies on the nature of the internal electrical charge of the electret., *Proc. Phys.-Math. Soc. Japan*, **5**, (1923), 107.
(Abstract IV/2/8 in reference 133)

158. M. Eguchi, On the permanent electret., *Phil. Mag.*, **49**, (1925), 178-192.

159. G. M. Sessler, Introduction., In Electrets: Topics In Applied Physics, Volume 33., G. M. Sessler (Editor), Springer-Verlag (Berlin, Heidelburg), ISBN 3-540-09570-5 or ISBN 0-387-09570-5, (1980), 1-10.

160. B. Gross, On permanent charges in solid dielectrics. II: Surface charges and transient charges in Carnauba wax., *J. Chem. Phys.*, **17**, (1949), 866.
(Abstract IV/3/1 in 133)

161. B. Gross, L. F. Denhard, On permanent charges in solid dielectrics. I: Dielectric absorption and temperature effects in Carnauba wax., *Phys. Rev.*, **67**, (1945), 253.
(Abstract IV/5/6 in reference 133)

162. A. I. Froiman, V. M. Fridkin, Investigation of the heterocharges of electrets in Carnuaba wax., *Kristallografiya*, **1**, (1956), 342.
(Abstract IV/5/11 in reference 133)

163. J. Van Calker, W. Frohlich, Investigations on Carnauba wax electrets and the origin of their heterocharge., *Ann. Phys.*, **4**, (1959), 216.
(Abstract IV/5/13 in reference 133)

164. B. Gross, Polarization of the electret., *J. Chem. Phys.*, **37**, (1962), 710.
(Abstract IV/7/6 in reference 133)

165. R. Gerson, Some experiments on Carnauba wax electrets., Baltimore, Md., John Hopkins University, Thesis (Ph. D.), 1953.

166. Toshiaki Takamatsu, Eiichi Fukada, Electric charge in thermal electret of Carnauba wax and Rosin studied by thermally stimulated current., *Charge Storage, Charge transport and electrostatics with their applications, Stud. Electr. Electron. Eng.*, **2**, (1979), 292-296.

167. N. R. Pan, Change in lattice parameters of Carnauba wax thermoelectrets at elevated temperatures., *Indian Journal of Pure & Applied Physics*, **17**, (1979), 211-214.

168. Toshiaki Takamatsu, Eiichi Fukada, Surface charge, depolarization and piezoelectricity in electrets., *Electrets: Charge storage and transport in dielectrics.*, (1973), 128-140.

169. B. Gross, R. J. de Moraes, Polaristation of the electret, *The Journal of Chemical Physics*, **37(4)**, (1962), 710-713.

170. P. I. Kuindersama, R. M. Van der Heij, Dynamic methods for determination of charge density on unipolar electrets., *Annu. Rep. Conf. Elect. Insul. Dielectr. Phenom.*, (1979), 325-333.

171. R. E. Collins, Measurement of charge distribution in Electrets., *Rev. Sci. Instrum.*, **48(1)**, (1977), 83-91.

172. C. Bucci, R. Fieschi, *Phys. Rev. Lett*, **12**, (1964), 16.

173. C. Bucci, R. Fieschi, G. Guido, Ionic thermocurrents in dielectrics., *Phys. Rev.*, **148**, (1966), 816-823.

174. J. van Turnhout, Thermally stimulated discharge of electrets., In Electrets: Topics in Applied Physics, G. M. Sessler (Editor), Springer-Verlag (Berlin, Hiedelburg), ISBN 3-540-09570-5 or ISBN 0-387-09570-5, (1980), 81-216.

175. S. Bradbury, An introduction to the optical microscope, Royal Microscopical Society, Microscopy Handbooks 1, Oxford University Press, ISBN 0-19-856401-5, (1984), 85pp.

176. Photography through the microscope., 7th Edition, G. Delly, Eastman Kodak Company, 96p (1980), Library of congess catalog number 79-54858.

177. V. Wilke, Optical scanning microscopy - The laser scan microscope, *Scanning*, **Vol 7**, (1985), 88-96.

178. J. G. White, W. B. Amox, Confocal microscopy comes of age, *Nature*, **Vol 328(9 July)**, (1987), 183-184.

179. P. Gregory, Advances in automatic image analysis., *International Laborarory*, **April**, (1983), 56-65.

180. G. W. Jenkinson, An Advanced image analysis system., *Internaltional Laboratory*, **September**, (1983), 74-81.

181. G. W. Jenkinson, The solution of problems in science and technology by image analysis, *International Laboratory*, **January/February**, (1984), 36-45.

182. R. A. Swenson, J. R. Attle, Counting, measuring, and classifying with image analysis., *American Laboratory*, **11(4)**, (1979), 50-68.

183. J. R. Attle, D. Oney, R. A. Swenson, Applications of image analysis., *American Laboratory*, **12(4)**, (1980), 85-99.

184. S. P. Azen, J. B. Marbolick, R. P. Sherwin, An experimental model and automated methodology of the analysis of the effects of ambient levels of air pollutants on the lung., *Applied Math. Comp.*, 3, (1977), 95-102.

185. A. F. Bush, J. P. Burke, E. S. C. Bowler., Role of submicron particles in air pollution., *Proceedings, 30th Annual Proc. Electron Microscopy Society of America*, Los Angeles, (1972).

186. B. Clements, R. Swenson, Automated microscopy for contamination control., *Pharm. Tech.*, **2(1)**, (1978), 42-62.

187. S. J. Findlay, Image analysis and cytogenetics: developments in chromosome analysis using the Magiscan 2A image analysis system., *Optical and Electron Microscopy*, **Issue 20**, 6-8, (1986).

188. J. Philip, C. Lundsteen, Semi-automated karyotyping system for chromosome analysis. A clinical test., *Clinical Genetics*, **27**, (1985), 140-146.

189. J. Piper, Interactive image enhancement and analysis of prometaphase chromosomes and their band patterns., *Analytical and Quantitative Cytology*, **4**, (1982), 233-240.

190. I. B. Monk, J. F. Malone, D. A. Smith, J. S. Orr, The use of a television image analysis system to determine the number and size distribution of mammalian cell clones., *Brit. J. Radiology*, **46**, (1973), 388-391.

191. R. S. Poulsen, L. H. Oliver, R. L. Cahn, C. Louis, G. Toussaint, High resolution analysis of cervical cells: A progress report, *J. Histochem. Cytochem.*, **25(7)**, (1977), 689-695.

192. J. Rowinski, M. Pienkowski, J. Abramczuk, Area representaation of optical density and chromatin in resting and stimulated lymphocytes as measured by means of Quantimet., *Histochemie*, **32(7)**, (1972), 75-80.

193. M. Mertz, R. Hinrichsen, Recognition of morphological features of cell nuclei using image analysis: The calibration of the Quantimet as a densitometer., *Prac. Metallogr.*, **6(11)**, (1969), 676-688.

194. J. Houchin, An automatic focus algorithm used in 3-D reconstruction of Neurones., *Journal of Physiology*, **319**, (1981), 26-27.

195. J. Houchin, Tracing neuronal Structures in 3-D. *Prceedings of Physiological Society*, **D18**, (1983), 19.

196. S. Caiazza, C. Fanizza, M. Ferrari, Rapid dimensional characterisation of Perfluorocarbon (PFC) particles by means of EM and automatic image analysis methods., *Micron and Microscopica Acta*, **14(4)**, (1983), 357-360.

197. J. M. Vleeskens, Optical image analysis of fine coal particles as an aid to optimising combustion in a fluidised bed., *Powder Technol.*, **40(N1-3)**, (1983), 232-330.

198. H. E. Exner, E. Linck, Image analysis for characterisation of size distribution ond shape distribution of lead powders., *Powder Metallurgy Internaltional*, **9(3)**, (1977), 131-133.

199. F. G. Yost, Image analysis of particle perimeters., *Metallography*, **16(1)**, (1983), 99-106.

200. E. E. Sims, R. Withington, Description and evaluation of a semi-automatic system for particle size analysis by microscopy., *International Journal of Pharmaceutics*, **17**, (1983), 167-181.

201. L. C. Lenny, Accurate location of particle boundaries in a digitised image from the optical microscope. *Particle Size Analysis 1985*, Editor P. J. Lloyd, John Wiley and Sons LTD, (1987) Published, 247-259.

202. A. Rosenfeld, Picture processing by computer. Computer science and applied mathematics., W. Rheinboldt (Editor), Academic Press, New York, Library of Congress Catalog Card Number 78-84255, (1969), 196pp.

203. A. Rosenfeld and A. C. Kak, Digital Picture Processing, Computer Science and Applied Mathematics, W. Rheinboldt (Editor), Academic Press, New York, 457 (1976), ISBN 0-12-597360-8, (1976), 457pp.

204. E. L. Hall, Computer image processing and recognition, Computer Science and Applied Mathematics, W. Rheinboldt (Editor), Academic Press, New York, ISBN 0-12-318850-4, (1979), 584pp.

205. H. C. Andrews, B. R. Hunt, Digital image restoration., Prentice-Hall signal processing series, Prentice-Hall, New Jersey, 238p (1977). ISBN 0-13-214213-9, (1977), 238pp.

206. M. Bradthorpe, Pictures via video., *Acorn User*, **Issue 40(November)**, (1985), 73-76.

207. A. Bangham, Micro-Robotic's Snap., *Personal Computer World*, **7(11)**, (1984), 186-188 & 334.

208. S. Applebaum, Pluto II, *Personal Computer World*, **8(11)**, (1985), 158-159.

209. J. McGregor, A. Watt, Colour-fill graphics, *Acorn User*, **August**, (1983), 53-58.

210. Calibration tables for thermocouples, Chromel-Alumel Thermocouples. *Handbook of Chemistry and Physics*, Editor R. C. West, 60th Edition, (1979-80), CRC Press, Boca Ration, Florida, ISBN 0-8493-0460-8, E-108.

211. G. Zografi, M. J. Kantry, A. Y. S. Yang, G. S. Brenner, Surface area and water sorption of microcrystalline cellulose., *Int. J. Pharm.*, **18**, 99-116, (1984).

212. M. M. Tang, R. Bacon, Carbonization of cellulose fibres- 1. Low temperature pyrolysis., *Carbon*, **2**, 211-220, (1964).

213. Constant humidity., *Handbook of Chemistry and Physics*, Editor R. C. West, 60th Edition, (1979-80), CRC Press, Boca Ration, Florida, ISBN 0-8493-0460-8, E-46.

214. E. J. Murphy, High field conduction in native cellulose and its structural implications, *Journal of Colloid and Interface Science*, **Vol. 49(3)**, (1974), 442-452.

215. A. H. Piekara, Polarization reversal in electrets and hydrogen bonding, *Journal of Electrostatics*, **1** (1975), 209-216.

216. W. A. Frey, *Fortsch. Chem. Org. Naturst.*, **27**, (1969), 1. (Reference 33 in 149)

217. J. R. Clovin, *J. Polym. Sci. Chem. Ed.*, **14**, (1976), 2377.

218. N. L. Salmen, E. L. Beck, The influence of water on the glass transition temperature of cellulose, *Tappi*, **60(12)**, (1977), 137-140.

219. A. D. Tavares, The Costa Redeiro effect and the thermodielectric electret, *Proc. Int. Sym. on Electrets & Dielectrics*, Ed M. Soares de Compos, (1975), Published 1977, 413-445.

220. J. Coll, The BBC Microcomputer User Guide., Editor D. Allen, British Broadcasting Corporation, London, (1982), ISBN 0-563-16558-8, pp519.

221. A. C. Bray, A. C. Dickens, M. A. Holmes, The advanced user guide for the BBC microcomputer, Cambridge Computer Center, Cambridge, England, ISBN 0-946827-00-1, (1983), 510pp.

222. B. W. Kernighan, D. M. Ritchie, The C programming language, Prentice-Hall Inc, 1978, New Jersey, ISBN 0-13-110163-3, 228pp.

223. R. Zaks(1978), Programming the 6502, Sybex INC, ISBN 0-89588-046-6, (1980), 386pp.

224. J. L. Kice, E. N. Marvell, Cellulose, in *Modern Principles of Organic Chemistry, An Introduction.*, Second Edition, Macmillan Publishing Co., Inc., New York, (1974), ISBN 0-02-362890-2, 435-437.